MODELING AND SIMULATION OF PCM-ENHANCED FAÇADE SYSTEMS

By

Saleh Nasser Al-Saadi

B.E., Sultan Qaboos University, l997

M.S., King Fahd University of Petroleum and Minerals, 2006

A thesis submitted to the

Faculty of the Graduate School of the

University of Colorado in partial fulfillment

of the requirement for the degree of

Doctor of Philosophy

Department of Civil, Environmental and Architectural Engineering

2014

This thesis entitled:

Modeling and Simulation of PCM-Enhanced Façade Systems

written by Saleh Nasser Al-Saadi

has been approved for the Department of Civil, Environmental and Architectural Engineering

Zhiqiang (John) Zhai

Moncef Krarti

Michael J. Brandemuehl

Harihar Rajaram

Kurt Maute

Date_____

The final copy of this thesis has been examined by the signatories, and we find that both the content and the form meet acceptable presentation standards of scholarly work in the above mentioned discipline.

ABSTRACT

Saleh Nasser Al-Saadi (Ph.D., Department of Civil, Environmental and Architectural Engineering)

Modeling and Simulation of PCM-Enhanced Façade Systems

Thesis directed by Associate Professor Zhiqiang (John) Zhai

Building façade contributes to the overall architectural aesthetic but can be utilized for heat storage when proper systems are incorporated. Latent heat storage such as using a phase change material (PCM) gains growing attentions recently due to its ability of storing significant thermal energy within a small volume, making it one of most promising technologies for developing energy efficient buildings.

This research is focused on modeling and simulation of PCM when integrated into advanced façade systems. The study first reviews the different mathematical modeling methods generally used for PCM's simulations. It categorizes the PCM's numerical models that are implemented for standalone facade systems. The study then evaluates the PCM's models that are integrated into whole building simulation tools such as EnergyPlus, TRNSYS, ESPr etc. It is revealed that the heat capacity method is mostly used in programs, despite its limitations on time and spatial resolutions. Therefore, alternative numerical models are investigated to overcome the above constrains and limitations in current PCM's simulation practice.

Eight potential computational models based on a fully implicit finite volume method are developed in MATLAB/SIMULINK environment, validated using experimental results from the literature and verified against well-known building simulation programs. A linearized enthalpy method with hybrid correction scheme is proposed and validated in this work as an improvement

to the existing numerical schemes for implementation into building simulation tools. Through sensitivity analysis achieved by varying the PCM thermal properties, the models have been analyzed for their computational efficiency and prediction accuracy. Some models are found sensitive to melting range of PCM, for example heat capacity method, but less sensitive to the variations of latent heat. Among the correction schemes, the non-iterative scheme is inaccurate due to the significant temperature spikes when PCM changes a state. The iterative and the hybrid correction schemes are computationally efficient and less sensitive to variations of PCM's thermal properties. Hence, these two schemes can potentially be implemented for modeling PCM instead of existing slow and unstable numerical algorithms. Based on this conclusion, a library of modules capable of modeling Advanced Façade Systems, entitled "AdvFacSy" toolbox, is developed in SIMULINK GUI environment. The toolbox can be easily used to evaluate innovative advanced façade systems with and without PCM. Using this toolbox, two PCM-enhanced façade designs are evaluated and general conclusions have been drawn.

Using a novel coupling methodology, several modules from the toolbox are then fully integrated into TRNSYS; a whole-building simulation tool. In addition, a standard TRNSYS module, Type-285, is specifically developed under this research work for modeling multilayer wall with/without PCM. A typical residential building with PCM-embedded walls is analyzed under representative US climates. It is concluded that PCM poorly performs when it is exposed to natural environmental conditions. However, the performance of PCM has indeed been enhanced when activated using other passive strategies.

DEDICATION

To the soul of my Dad
To my Family

ACKNOWLEDGMENT

All praise and thanks are due to my Lord: ALLAH Almighty for giving me the health, knowledge and patience to complete this work. I acknowledge the financial support from Sultan Qaboos University, Oman. My sincerest gratitude goes to my advisor Prof. John Zhai who guided me with his dedicated attention, expertise, and knowledge throughout the process of this research work. I'm grateful to him for being a member in his team of NSF project "EFRI-SEED #1038305: Living Wall Materials and Systems for Automatic Building Thermo-Regulation". I'm also grateful to my committee members, Prof. Krarti, Prof. Brandemuehl, Prof. Harihar and Prof. Kurt for their constructive guidance and support in the course of this work.

My thanks go to the colleagues and friends in the Building System Program at the University of Colorado Boulder for their supports, open discussions, sharing ideas, and motivations during the course of this work. In particular, James McNeill, Haidong Wang, Knud Hermansen, Dr. Quan Zhang (a visiting scholar from Hunan University, China). I thank my Korean friend; YoonSuk Kang for sharing his MATLAB code that I modified for TRNSYS parametric study. I appreciate the friendly chat and discussion with Alaa Alaidroos and Rayyan Alsamadani (from Saudi Arabia), Baqer Ameer (from Kuwait), Benjamin Park and Hyunwoo Lim (from Korea) and all other colleagues in ECCE150, the BSP's office. I acknowledge the support of our graduate coordinator; Pamela Williamson. Thanks are also due to all members of the department of Civil, Environmental and Architectural Engineering who has helped me directly or indirectly during this work.

Special thanks go to Prof. Amer Al-Rawas, Prof. Ali Al-Harthi and Prof. Khalifa Al-Jabri at Sultan Qaboos University (SQU) for their moral support and motivations throughout the course of this research. I'm grateful to my colleagues at the Department of Civil and

Architectural Engineering, SQU, Oman for their support. I would like to thank my friends and colleagues in Oman for their moral support and encouragements.

My heartfelt gratitude is given to my beloved mother, my wife *Mariam* and my kids; Zaizafoon, Nassar, Mohammad and Hossam who always support me with their love, patience, encouragement and constant prayers. I would like to thank my grandmothers, brothers, sisters, and mother-in-law, brothers- and sisters' in-law and all members of my family in Oman for their emotional and moral support throughout my study.

Table of Content

List of Figures

List of Tables

CHAPTER 1: INTRODUCTION

1.1 Background

There is a clear relationship between the economic growth in a country and energy use. In United States, 41% of primary energy is consumed by building sector [1]. The same report stated that 74% of this energy comes from fossil fuels, 16% from nuclear sources, and only 9% from renewables. The bulk of this energy is used by mechanical and electrical systems to achieve acceptable indoor environmental quality such as thermal and visual comfort, and air quality. On the other hand, it is interesting to note that U.S. buildings emissions are approximately equivalent to those produced by Russia and Canada altogether [1]. Therefore, reducing energy consumption and improving efficiency in buildings is of high importance. Many strategies do exist to improve energy efficiency such as incorporating new and advanced envelope designs, improving the efficiency of mechanical and electrical systems, and adopting appropriate control strategies.

For skin-load dominant buildings such as residential and light commercial buildings, advanced façade systems become an attractive candidate to reduce the energy consumption and consequently improve the building performance. For this particular building typology, energy use is characterized by heat loss or gain through exterior envelope. For instance, the thermal load of building envelope (i.e., walls, roof and windows) in a typical harsh climate is responsible for more than 70% of the total thermal load in residential buildings [2, 3]. Since the system is exposed to outside aggressive environment, it is imperative to consider the thermal characteristics. Thermal characteristics are the principle properties of building materials such as heat transmission, thermal heat storage, solar heat gain and air infiltration [4]. Givoni [5] has

identified these characteristics as thermo-physical properties of building envelope which include thermal conductivity and subsequently thermal resistance, thermal heat storage capacity, transparency to radiation of different wavelengths, surface convective coefficient, and surface radiation properties: absorptivity, reflectivity, and emmisivity.

An important and exciting element that influences the dynamic behavior of buildings is the thermal energy storage. Thermal energy storage (TES) or thermal mass is a property of materials that describes its ability to absorb, store and release heat depending on the surrounding environmental conditions. Traditional architecture, for example, is distinguished with its heavy weight and thermally massive construction elements to moderate the indoor environment extremes experienced in hot or cold days. The thermal properties of construction elements have significantly improved thermal comfort by manipulating the indoor air temperature without the need of mechanical air conditioning systems [5]. On the other hand, light weight buildings are characterized by its lower thermal mass and thus expose to significant temperature swings, demanding high cooling and heating energy. A dynamic thermal mass such as phase change materials (PCMs) has been considered as a promising technology to reduce the inherited climatic deficiency in light weight buildings. The apparent advantage of using PCMs lies on the amount of latent heat a thin PCM layer can store compared to that in a sensible heat storage material such as concrete. For instance, a wall of 25 mm thickness with PCM could store an equivalent amount of thermal energy as a 420 mm thick concrete wall [6]. As a result, the use of PCMs has recently attracted great attentions for improving thermal and energy performance of buildings [7-12].

1.2 Design Paradigm using Phase Change Materials (PCMs)

PCMs refer to substances that are used to store or release thermal energy associated with phase change process. Based on environmental conditions, PCMs can store significant latent heat energy when phase state changes from solid to liquid and releases an equivalent heat when phase state changes from liquid to solid. The thermal performance of PCMs is characterized by their Enthalpy-Temperature (h-T) curve as shown in **Figure 1.1**. The figure shows how the ideal PCMs melts/solidifies at isothermal temperature, the common PCMs undergo the phase change over a temperature range at which the state is a mixture of solid and liquid (i.e., mushy region). The figure also shows the behavior of sensible heat storage materials.

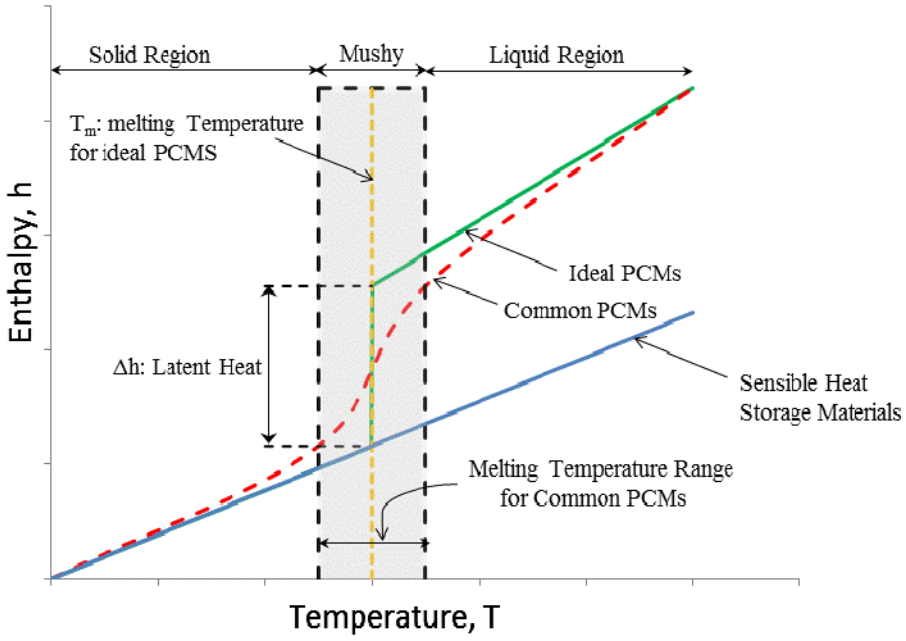

Figure 1.1 Enthalpy-Temperature performance curve for ideal and common PCMs

1.2.1 Classification of PCMs

PCMs can be classified into organic, inorganic and eutectics (i.e. mixtures) as shown in **Figure 1.2** [13]. The most common PCMs used in buildings are paraffin wax and salt hydrates [14]. For practical applications in buildings, Hawes [15] has divided the temperature ranges for thermal storage into five principle categories:

1. Hydronic heating: 75-90˚C
2. Hot water heating: 60-75˚C
3. Hot air heating: 35-60˚C
4. Space heating: 17-25˚C
5. Cold storage: 5-20˚C

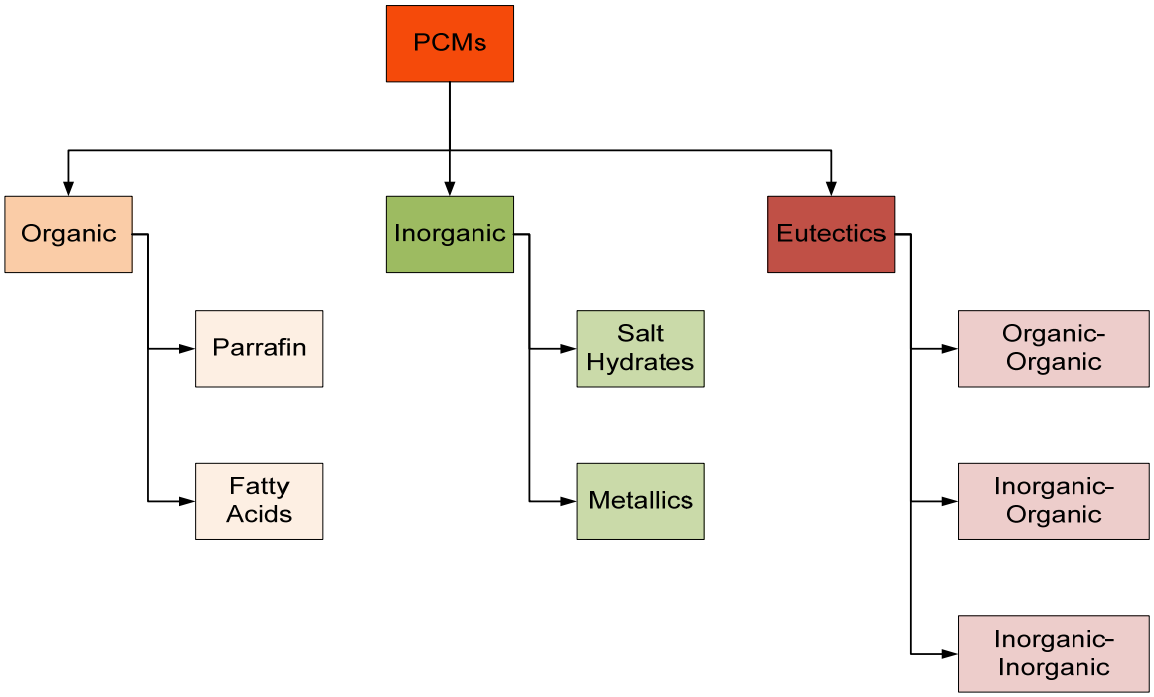

Figure 1.2 Generic classification of PCMs

1.2.2 PCMs for Building Applications

Sensible energy storage such as water, rock, adobe or ground has been known for centuries but latent heat storage using PCMs can be considered new. Maria Telkes, a Hungarian-American scientist, is the first who used PCMs for passive heating systems in buildings [16]. In 1948, *Maria* used Glauber's salts, an earlier PCM type, to store solar energy for an experimental solar-heated house *"Dover Sun House'* in Dover, Massachusetts at MIT. The salts were enclosed in drums where solar energy is stored and a ventilated air was allowed to discharge the stored heat in winter [17].

PCMs can be integrated into different building envelope designs. Common applications are when PCMs used with walls, roof, floors, ceiling and windows. Literature shows numerous examples on how PCMs are integrated into buildings. Recent studies that review PCMs in building applications are described in [13, 18-26]. Zhang et al. [20] reviewed different PCMs applications in buildings enclosure as shown in **Figure 1.3**.

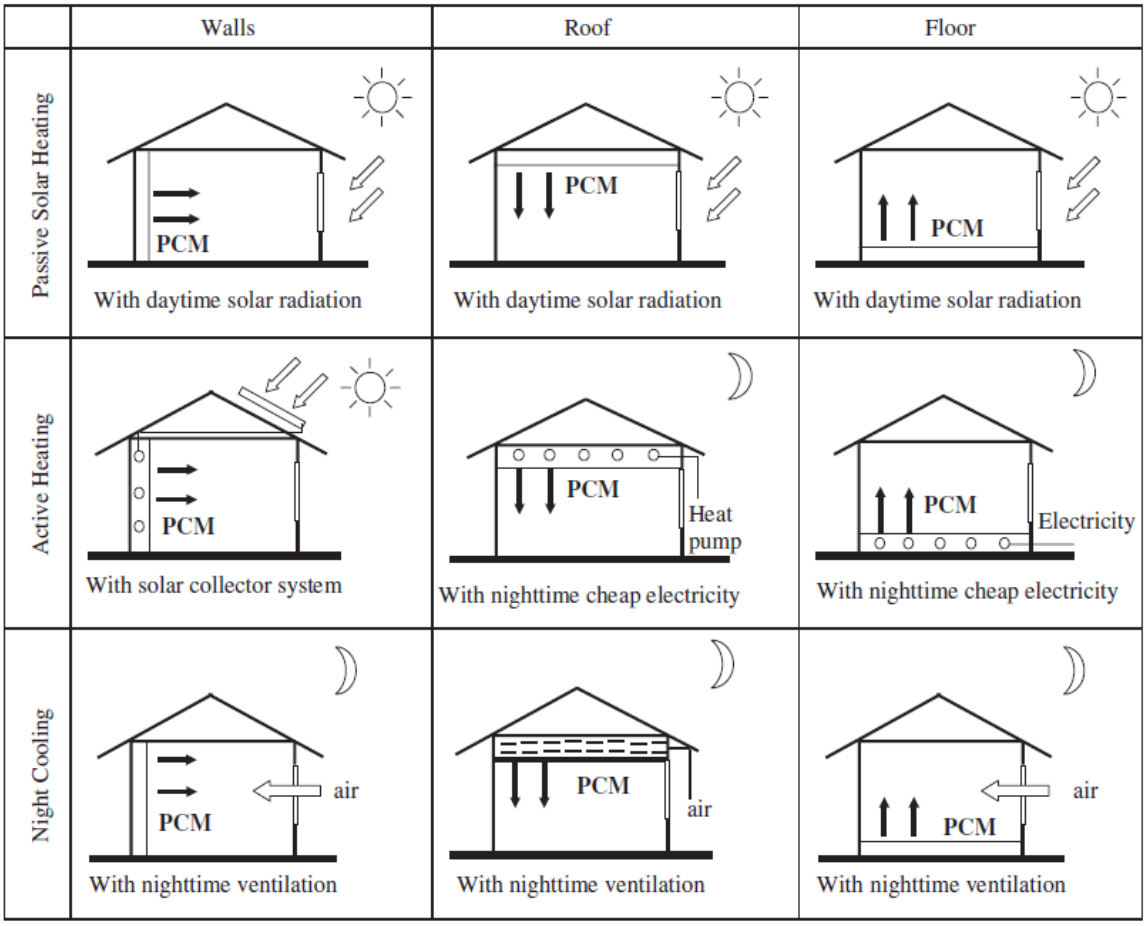

Figure 1.3 PCMs integrated within different building enclosures [20]

In addition to above design examples, advanced façade systems can be used to store solar energy for passive and active heating and cooling [27-30]. Although many applications are suggested for sensible thermal storage, they can potentially be used with latent thermal storage such as PCMs. For example, classical TROMBE walls and TROMBE-MITCHEL walls are kind of façade systems developed in 70s and used for solar heating as schematically shown in **Figure 1.4**. Solar energy from sun charges the thermal storage medium during the day and air is used to discharge the stored energy for direct space heating use. These particular design configurations use concrete for thermal storage. Alternatively, PCMs can be used as a thermal storage medium.

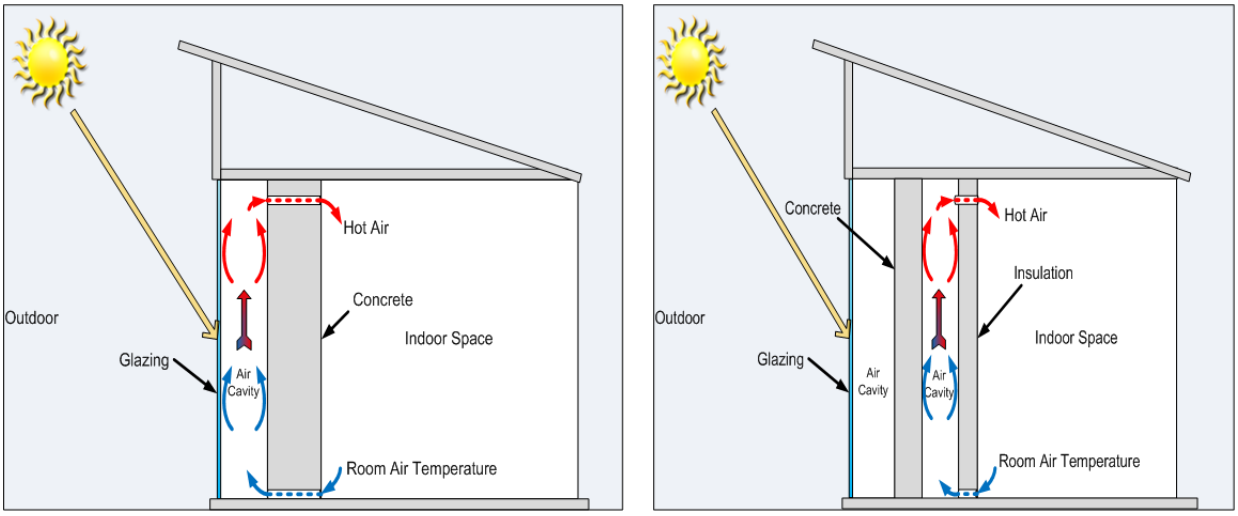

(a) Classical TROMBE Wall (b) TROMBE-MICHEL Wall

Figure 1.4 Classical TROMBE wall and composite TROMBE wall

Another class of thermal storage wall designs is when water is used as a storage medium or as a heat transfer medium. For example, **Figure 1.5** shows the water TROMBE wall design used in Odeillo house, France [31]. The cold water is heated by solar radiation and naturally driven by thermo-siphoning to hot water storage tank. Many thermal storage wall systems are however suggested in literature such as those described by Anderson [32].

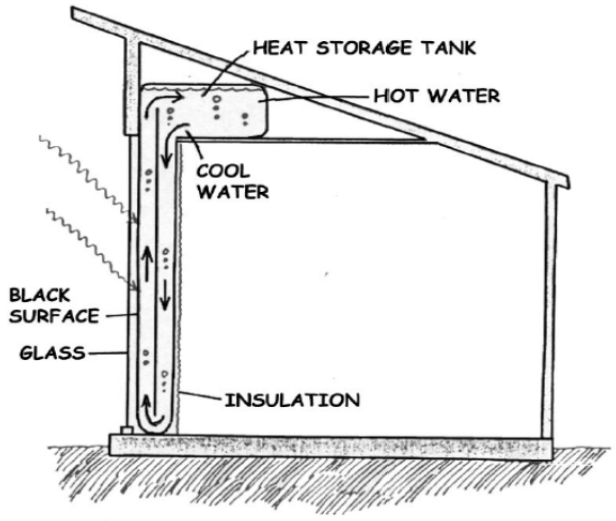

Figure 1.5 Water -TROMBE wall design built in Odeillo house, France [31]

Recently, new designs using bio-mimicry concepts are emerging. Examples of 100 climate adaptive building shells are fully described by Loonen [33]. A recent research proposed by a team of scholars at the University of Colorado Boulder has contributed to this paradigm using bio-mimicry of living body's thermo-regulation systems (i.e., respiratory and circulatory systems)[34]. The living wall design and operational concept is schematically shown in **Figure 1.6**.

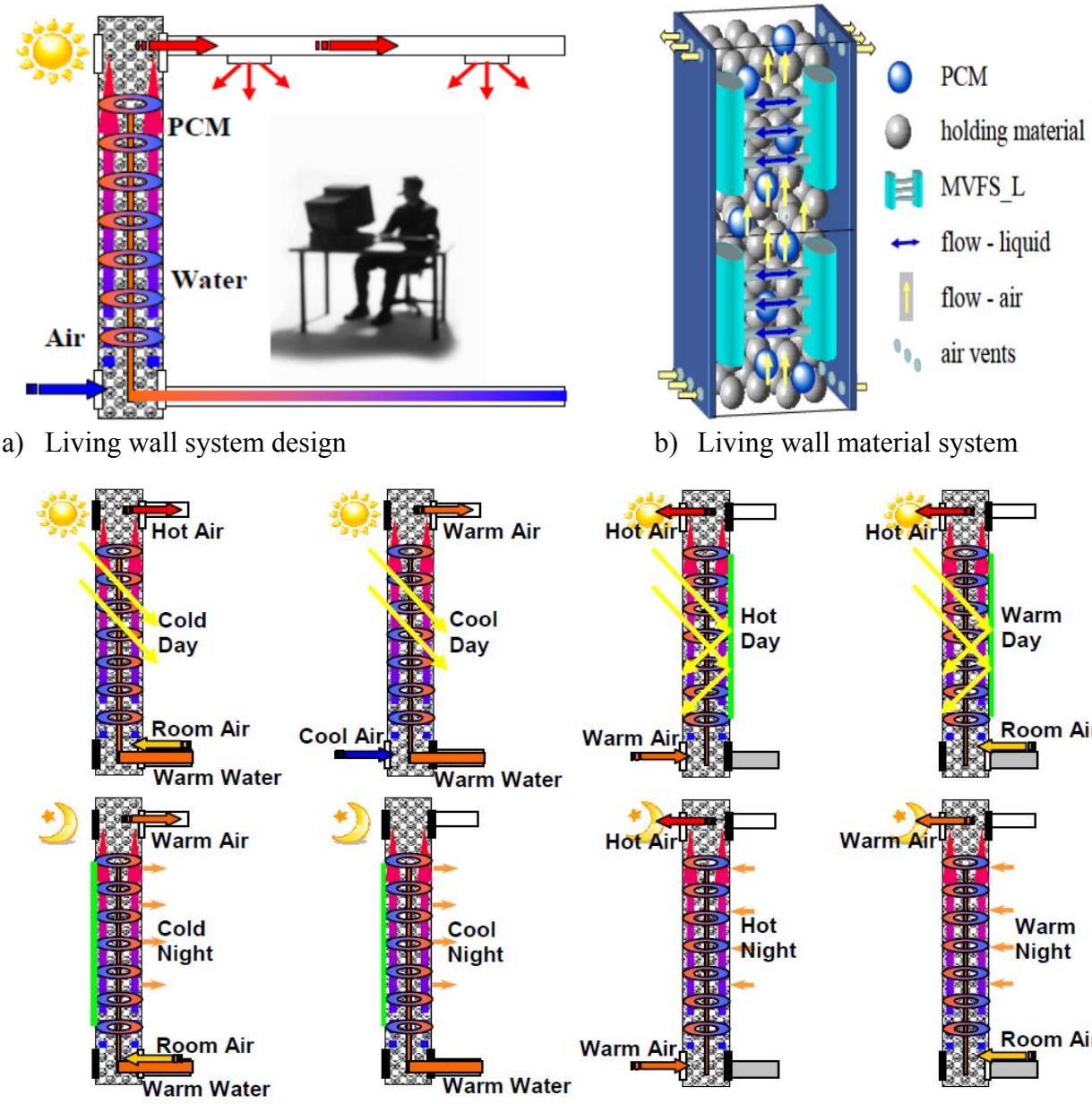

a) Living wall system design

b) Living wall material system

c) Environmental and system operating conditions for the living wall

Figure 1.6 Conceptual design and operating conditions of living wall [34]

1.3 Research Motivation

Complex façade systems have become an integral part of modern architecture. This is partly due to their architectural aesthetic but also pertained to their capability of achieving multi-purpose functions. For example and in addition to the architectural flavor, appealing façade

systems can be used to provide free heating, store heat, or direct surplus heat to other heat storage system or discard heat to the outside environment. In such designs, PCMs can be considered as an attractive thermal energy storage material that can be integrated without complication. The previous section shows prototype designs where PCMs can be used in building enclosures. It is apparent that various innovative advanced façade designs and different integration concepts can be engendered with PCMs. When this strategy is embraced as is the case of living wall, the abundant solar energy is captured by charging the PCMs and heat transfer medium such as air or water can then be utilized to discharge the stored energy. The whole system acts like a living environment where fluid (i.e. air, water or both), building materials (i.e. PCMs, or other layers), and energy source (i.e. sun, or internal building load) or energy sink (i.e., sky or ground) are interacting with each other in a sequential or simultaneous manner to transport and utilize energy.

Various challenges are, however, arisen when using PCMs in such buildings design, including the variety of available materials, material's liability and safety, cost and economic feasibility, design configurations, integration with other sustainable energy technologies, impact on thermal and energy performance. The problem can then be considered as an optimization dilemma where all these counterparts' challenges are becoming critical in the design process. As a result, computational modeling is often used as an effective tool to quantitatively understand and help resolving this complex system. When compared to field studies, modeling offers inexpensive alternative for analyzing, optimizing and fine tuning the final designs. Although whole building simulation tools such as EnergyPlus, TRNSYS, ESP-r etc. are capable of simulating dynamic systems, they still lack algorithms that are fast, accurate and numerically stable for modeling PCMs. A recent study pointed out limitations and provided guidelines when

simulating PCMs using EnergyPlus [35]. Similar limitations exist for other building simulation tools such as TRNSYS[36] and ESPr [37]. These shortcomings have been identified recently by a group of experts among the International Energy Agency's (IEA) Annex 23 team members who concluded, based on their comprehensive review on the PCM modeling, that the confidence in PCM models is too low to use for future building's behavior[38]. Moreover, the reviewed models are not tested in a very stringent or exhaustive way.

In addition, current algorithms used for PCMs modeling are limited to conventional envelope designs and therefore modeling advanced façade system such as PCMs-embedded living wall and fluid interactions is inadequate. The need to develop new models arises today for better understanding, utilization, optimization and dissemination of PCMs-embedded designs, not only for a conventional building design but also for an advanced and complex system design. This particular need has been emphasized in a report published by International Energy Agency (IEA) concerning the responsive building elements [39].

1.4 Research Objectives

The main goal of this research is to develop a generic numerical heat transfer model that is able to model the phase change process encountered in typical building envelope systems. The numerical model is developed to simulate air ventilated façade systems where cavities are integrated. In cavities, the air is driven naturally due to thermal forces (i.e., buoyancy) or forced using mechanical systems to transport and distribute energy. The developed model is a standalone and a self-sustained tool to quickly evaluate the thermal performance of traditional (i.e., single or multilayer walls), PCMs-embedded walls and ventilated façade system. In addition, the developed tool is integrated using established co-simulation approaches into an

existing energy simulation program to evaluate the thermal and energy performance of complex building systems. In particular, the objectives of this research work are to:

1. Evaluate existing mathematical models for simulating phase change materials in building applications.
2. Verify, validate the models using the standard validation protocols and subsequently propose a suitable model for building enclosure considering accuracy, computational efficiency and ability to capture phase change process.
3. Develop a stand-alone framework model for simulating advanced façade systems including ventilated façade systems where air can be used to transport and distribute stored energy.
4. Integrate the developed models into existing whole building simulation program to evaluate the thermal and energy performance of PCM-enhanced façade systems in whole building system context.
5. Develop design guidelines for using phase change materials in typical residential building.

1.5 Research Contributions and Challenges

In recent years, the use of phase change materials (PCMs) in buildings has gain significant attention in research community. While few use lab or field experiments to evaluate the thermal performance of PCMs, simulation programs are becoming attractive design tools. However, many existing simulation tools lack accurate and quick algorithm for modeling PCMs. This is vital since design decisions may be based on inaccurate results.

The conventional way of tackling this topic would be to use a mathematical model that is commonly used for simulating PCMs. Literature has indicated that a particular mathematical model is selected based on preference or experience instead of performance. However, the selection approach may result in a model that is not suitable for the PCM in hand. This is pertained to the wide variation of thermal properties of PCM such as the melting temperature, melting range and latent heat. Therefore, the rational for selecting a model should be based on actual testing and screening. This may look trivial but impose a challenge for selecting a suitable model. Therefore and after rigorous verification and validation efforts, this research work has explored the performance of common mathematical forms and several numerical schemes for modeling PCMs for a potential application in building simulation tools. The outcome from this exercise has given clear insights into the limitations and capabilities of each mathematical model and the corresponding numerical scheme. For building application, the conclusion uncovers many facts and provides guidelines for selecting a numerical model for simulating PCMs. Additionally, a new scheme called *"hybrid correction scheme"* based on linearized enthalpy method is proposed and validated. This enhancement is particularly developed for implementation into whole-building simulation tools. For a typical wall model with PCM, the scheme can save simulation time and yet provides results at comparable level of accuracy.

Without workarounds, advanced façade systems are difficult to evaluate with existing simulation tools. This research has focused mainly on developing standalone and self-sustained framework models for modeling façade systems with and without PCMs. The **Adv**anced **Faç**ade **Sy**stems "*AdvFacSy*" toolbox is developed under SIMULINK environment, a GUI add-on to MATLAB. From a list of library modules, the user can drag, drop and link an advanced façade system design in a single screen with few input parameters. Furthermore, several modules from

the toolbox have been fully integrated into whole-building simulation tool "TRNSYS". The coupling efforts have extended the flexibility and application of the toolbox for modeling advanced façade systems with and without PCM within the whole-building systems context. The developed models have been used to thoroughly study the performance of PCM in residential buildings. The set of simulation results are used to develop new design guidelines for using PCMs in residential buildings in representative US climates.

1.6 Outline of the Dissertation

The dissertation is divided into eight chapters. Chapter 1 describes the background information about the research, the motivation to do this research, objectives and research contributions.

Chapter 2 provides a state-of-art literature review on general mathematical modeling of phase change materials, standalone models developed in literature, and existing PCM modeling algorithms integrated into whole-building simulation tools. Additionally, studies that show the energy performance of PCM-enhanced enclosures have been identified. Throughout this chapter, the shortcomings have been identified. The outcome from this chapter was a base for further investigations of the modeling techniques of PCMs.

Chapter 3 details the mathematical models, numerical discretization, and calculation procedure for modeling PCM using various methods. This chapter further describes the verification and experimental validation efforts. The performance of the developed models is evaluated, numerical guidelines are developed and finally models are proposed for further utilization in the standalone toolbox.

Chapter 4 presents the standalone toolbox "AdvFacSy" developed under this research work. It explains the fundamentals, rational, concept, and structure of the toolbox. Verification cases for different modules are also discussed in this chapter.

Chapter 5 describes the utilization of the AdvFacSy toolbox for evaluation of multilayer wall systems with PCMs when placed at different locations. Ventilated cavity design is also modeled in this chapter. As a result, design guidelines are developed.

Chapter 6 outlines the coupling approaches between the AdvFacSy and TRNSYS that have been tested in this work. The concept and procedure for direct coupling and indirect coupling are fully explored in this chapter. The advantages and disadvantages of both approaches are described. Additionally, a standard TRNSYS Type-285 for modeling multilayer wall using finite volume method is described in this chapter. Verification cases are performed and results are discussed.

Chapter 7 provides details about modeling PCM in a whole building context. Type-285 and other types from Chapter 6 are utilized for modeling PCM in a typical residential building. Sensitivity analysis is performed for different design and operation parameters. Various US representative climates are selected for modeling PCMs. Analysis includes technical feasibility and economic feasibility utilizing simplified payback period. Design guidelines for different climates are drawn from this set of simulations. Additionally, two designs are presented to demonstrate the improvement of PCM performance when complementary passive strategies are used.

Chapter 8 summarizes the results, conclusions and recommendation from this research work. It outlines the way forward and provides future direction for researching the phase change materials for building application.

CHAPTER 2: LITERATURE REVIEW

This chapter provides a state-of-art literature review on the mathematical modeling of phase change materials for building applications. A systematic review is provided for the general theories and techniques for modeling PCMs, with an emphasis on the specific models used for simulating the thermal and energy performance of PCMs embedded in building enclosures. Furthermore, it reviews and summarizes the capabilities, limitations and validations of prevalent whole building simulation programs that have been used for modeling phase change materials.

2.1 General formulation of phase change problems

The main feature of phase change problems (i.e., Stefan problems) is the moving boundary where the Stefan condition must be met. For pure materials there is a clear distinction between the solid and liquid phase separated by a sharp moving interface and hence melting occurs at isothermal temperature. For conduction-dominated heat transfer, the governing equation can be written for the solid and liquid phase, respectively, which have to be satisfied by the Stefan condition as follows [40]:

Heat transfer in the solid phase:

$$\rho . c_s . \frac{\partial T_s}{\partial t} = \frac{\partial}{\partial x}\left(k_s . \frac{\partial T_s}{\partial x}\right) \qquad \text{Equation 2-1}$$

Heat transfer in the liquid phase:

$$\rho . c_l . \frac{\partial T_l}{\partial t} = \frac{\partial}{\partial x}\left(k_l . \frac{\partial T_l}{\partial x}\right) \qquad \text{Equation 2-2}$$

The Stefan condition that enforces the heat balance at the solid-liquid interface is:

$$\frac{\partial}{\partial x}\left(k_s.\frac{\partial T_s}{\partial x}\right).n-\frac{\partial}{\partial x}\left(k_l.\frac{\partial T_l}{\partial x}\right).n=\rho.L.v.n \qquad \text{Equation 2-3}$$

Very few analytical solutions are available in a closed form for phase change problems and can be found in advanced heat transfer books such as those by Crank [41], Alexiades and Solomon [42], and Özışık [43]. Therefore, approximate numerical solutions are usually used to handle this class of problems. The numerical methods for addressing these problems have been reviewed in literature [44-47] and can be generally divided into:

1. Fixed grid method (i.e., weak solution): These methods consist of fixed space grids where the boundary is tracked by the use of an auxiliary function. Different approaches are employed to account for latent heat evolution [45, 47, 48]. This class of methods has been widely used and therefore will be the focus in this research work.
2. Deforming grid method or front tracking scheme (i.e., classical solution or strong numerical solution): These methods allow the grid nodes move along with the moving boundary layer and thus the space girds deform as the solution develops. Here the interface is explicitly tracked using the Stefan condition [42].
3. Hybrid method: these methods utilize the features of both fixed and deforming grids which uses a fixed background grid and employs local front tracking schemes to follow the movement of the boundary [44].

2.2 Numerical formulation of phase change problems using fixed grid methods

An intuitive approach in solving phase change problems is to explicitly follow the moving boundary using the front-tracking methods. However, this method needs to make a *priori* assumption that the boundary is smooth or monotonic during the period [49]. This

assumption is not always true and therefore reformulating phase change problems using the fixed grid techniques becomes an obvious alternative [41, 48, 50, 51]. The Stefan condition Equation 2-3 within the fixed grid method is implicitly treated by the reformulated governing equation and hence the position of the moving boundary is known when the solution is converged.

The fixed grid method is simple compared to the others, most versatile, convenient, adaptable and easily-programmable [42]. The latent heat evolution is accounted for in the governing equation by using either enthalpy method [52-56], heat capacity method [57-60], temperature transforming model [61-64], heat source method [56, 65-68], or other methods [45, 47, 69]. The following sections will describe the widely used methods.

2.2.1 **The enthalpy method**

In the Enthalpy method, the latent and specific heat are combined into an enthalpy term in the governing equation. The enthalpy method was proposed by Eyres [56] to deal with variations of thermal properties with respect to temperature. For conduction-dominated heat transfer, the governing Equations (2-1:3) can be reformulated into one equation where the latent heat is absorbed into the enthalpy term as follows:

$$\rho \frac{\partial h}{\partial t} = \frac{\partial}{\partial x}\left(k \frac{\partial T}{\partial x}\right) \qquad \text{Equation 2-4}$$

To demonstrate this method, a fully implicit control volume approximation of Equation 2-4 for a typical grid shown in **Figure 2.1** leads to the following discretized equation:

$$h_p^{n+1} = h_p^n + a_w^{n+1} * T_w^{n+1} + a_p^{n+1} * T_p^{n+1} + a_e^{n+1} * T_e^{n+1} \qquad \text{Equation 2-5}$$

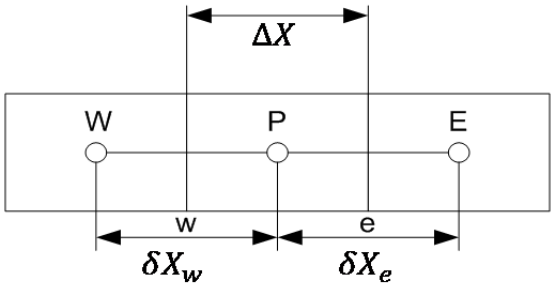

Figure 2.1 Typical control volume grid

According to Equation 2-5, it is clear that the current enthalpy (h_p^{n+1}) is dependent on the current value of temperature (T_p^{n+1}) and therefore the enthalpy term is nonlinear. The equation cannot be solved without using proper numerical techniques to handle this nonlinearity. This has to be solved either by nonlinear solvers such as the Newton's method or by linearizing the nonlinear terms and utilizing iterative methods as fully explained by [42, 48, 49, 52, 53, 70-74]. If a non-linear solver is selected, an auxiliary temperature-enthalpy function is required for Equation 2-5 and can be written for materials that change phases at specific temperature range as follows [40]:

$$T_p = \begin{cases} \frac{h_p}{C_s} & , \quad h_p \le C_s * (T_m - \in) \\ \frac{h_p + \left[\frac{C_l - C_s}{2} + \frac{L}{2*\in}\right] * (T_m - \in)}{\left[\frac{C_l - C_s}{2} + \frac{L}{2*\in}\right]} & , \quad C_S * (T_m - \in) < h_p < C_l * (T_m + \in) + L \\ \frac{h_p - (C_s - C_l) * T_m - L}{C_l} & , \quad h_p \ge C_l * (T_m + \in) + L \end{cases} \qquad \text{Equation 2-6}$$

Alexiades and Solomon [42] have outlined numerical schemes for solving phase change problems with the enthalpy method using both linear and nonlinear approaches. Knoll on the other hand reviewed various approaches utilizing nonlinear solvers to resolve the Stefan problem [73]. He, in particular, developed an algorithm to solve the Stefan problem using the Jacobian-free Newton-Krylove method and applied for two scenarios: (1) pure materials where melting

occurs at isothermal temperature and (2) non-isothermal case where phase change occurs at a range of melting temperature.

An alternative approach to solving the discretized Equation 2-5 is to linearize the nonlinear term, $h_p^{n+1}(T)$, using the methods explained by Patankar [75]. The discretized nonlinear equation becomes linear with one primary dependent variable "Temperature" that can be iteratively solved with enthalpy using common linear solvers such as direct methods (e.g., Gauss elimination or Tri-diagonal algorithm) or iterative methods (e.g., Gauss–Seidel method). Shamsunder [52], for example, proposed a Gauss-Seidel iterative scheme where the solution sweeps from west to east to determine the state of phase change and subsequently determine the new nodal enthalpy. The nodal temperatures are then determined based on the discrete form of the enthalpy-temperature relationship. To avoid excessive iterations, the scheme was later improved by introducing an over-relaxation parameter that is used at nodes where no phase change occurs [76]. The scheme was however intended for phase change that occurs at isothermal temperature. An iterative Newton linearization scheme was introduced by Furzeland [49]. The solution process is the same as that of Shamsunder except that the over-relaxation parameter can be applied at all nodes.

Iterative methods such as Gauss-Seidel are inherently slow and computationally inefficient. Therefore, fast numerical schemes have been introduced to improve the computational efficiency [53, 60, 66]. Pham [60] proposed a method that combines the features of the enthalpy and heat capacity methods. The method consists of two steps: a prediction step followed by a correction step as shown in **Figure 2.2**. Based on guessed values, the new nodal temperatures are predicted (point (2) on the graph). The enthalpy is determined based on the predicted temperature values. The predicted temperatures are subsequently corrected to be

consistent with the enthalpy-temperature curve (point (3) on the graph). This temperature correction step is the key of this method. This method is later known to be the *"Quasi-Enthalpy"* method [77].

Voller pointed out that this method might not conserve energy at every time step [40] and a better conservative iterative scheme was proposed by Swaminathan and Voller as illustrated in **Figure 2.3** [53]. The method iterates the predicted and corrected intermediate values until the convergence is achieved. The method has been recently investigated as an alternative to overcome the limitations of the PCM simulation algorithm implemented in ESP-r [37].

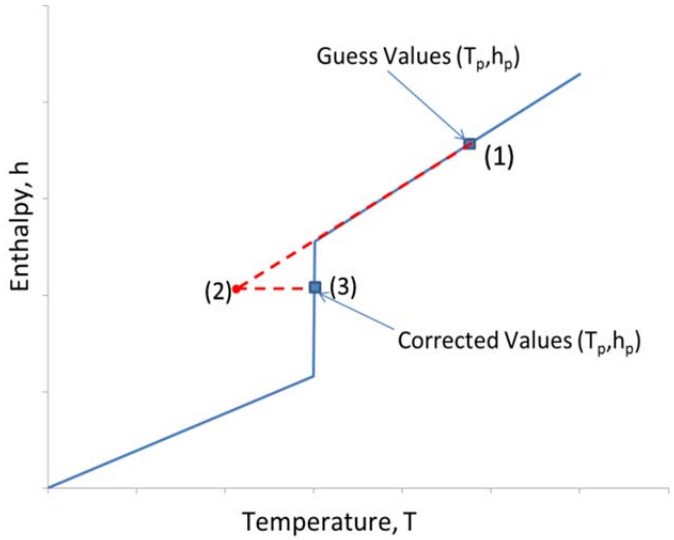

Figure 2.2 Corrective non-iterative scheme in the Quasi-Enthalpy method at a node during one time step

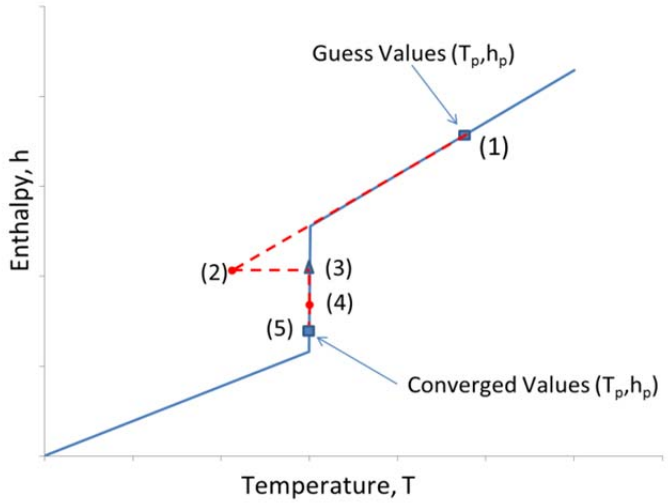

Figure 2.3 Corrective iterative scheme in the Enthalpy method at a node during one time step

2.2.2 The heat capacity method

The heat capacity term in the governing equation imitates the effect of enthalpy (sensible and latent heat) by increasing the heat capacity value during the phase changing stage. Two approaches are generally used to account for the latent heat liberation: the apparent heat capacity [40, 45, 47] and the effective heat capacity [78, 79]. Although the two approaches differ in the heat capacity approximation, recent literatures, however, use the terminologies interchangeably. More details on the effective heat capacity concept are explained by Poirier [80].

The apparent heat capacity method was introduced by Hashemi and Sliepcevich [81] to solve a one-dimensional heat transfer with phase change in a mushy region. The conduction-dominated one-dimensional heat transfer equation using the apparent heat capacity can be written as:

$$\rho * C^A(T) * \frac{\partial T}{\partial t} = \frac{\partial}{\partial x}\left(k \frac{\partial T}{\partial x}\right) \qquad \text{Equation 2-7}$$

The method receives the popularity because the temperature is the only prime variable that needs to be solved in the discretized form. The key in this approach lies in the heat capacity approximation. Two methods are commonly used to approximate the apparent heat capacity term in Equation 2-7: the analytical/empirical relationships and the numerical approximations.

2.2.2.1 The analytical/empirical relationships

The heat capacity of a PCM can be determined from the testing data with differential scanning calorimeters (DSC). Manufacturers of PCMs normally provide limited data pertained to their products such as melting temperature, heat of fusion and heat capacity at solid and liquid states. Such minimal data can be used to approximate the heat capacity of a PCM using a simple direct relationship with an introduction of fictitious melting temperature range ($2 * \in$) [40, 61]:

$$C^A = \begin{cases} C_s, & T \leq T_m - \in \quad \text{(Solid region)} \\ \frac{C_s + C_l}{2} + \frac{L}{2\in}, & T_m - \in < T < T_m + \in \quad \text{(Mushy region)} \\ C_l, & T \geq T_m + \in \quad \text{(Liquid region)} \end{cases} \qquad \text{Equation 2-8}$$

Convergence might be an issue when solving Equation 2-7, if the half phase change range ($\in$) is set too small or the time step is too large. There is a possible risk of missing the latent heat contribution in a large time step. Hence, DSC testing results can be used to form an empirical expression to approximate the heat capacity. Fang [14], for instance, proposed a mathematical expression for the heat capacity of paraffin–based PCM obtained from DSC. Others have suggested and used alternative forms to approximate the heat capacity [82-85].

2.2.2.2 The numerical approximations

Numerical approximation is an alternative when detailed information about PCM's thermal behaviors is available. Many numerical approximations have been proposed in literature [59, 86-91]. For example, Comini [86] applied a numerical technique in the finite element method where the heat capacity was determined using a derivative of enthalpy with respect to temperature. Later, Morgan [87] has improved the relationship to avoid the convergence problems. When using an iterative scheme, the heat capacity can be approximated using the successive temperature and enthalpy solutions. The temporal averaging proposed by Morgan [87] is illustrated in **Figure 2.4** and is represented by the following equation :

$$C^A = \frac{\Delta h}{\Delta T} = \frac{h^n - h^{n-1}}{T^n - T^{n-1}} \qquad \text{Equation 2-9}$$

On the other hand, Lemmon [89] proposed an approximation based on the space average rather than the time average approach. The temporal and space average approximations are, however, prone to convergence issues unless some precautions are taken [92]. Solutions to the limitations of the apparent heat capacity method have been proposed in literature [51, 78, 93-95]. Voller [40] found that the apparent heat capacity approximation based on the direct relationships are more accurate than the Morgan approximation used for the cases he studied.

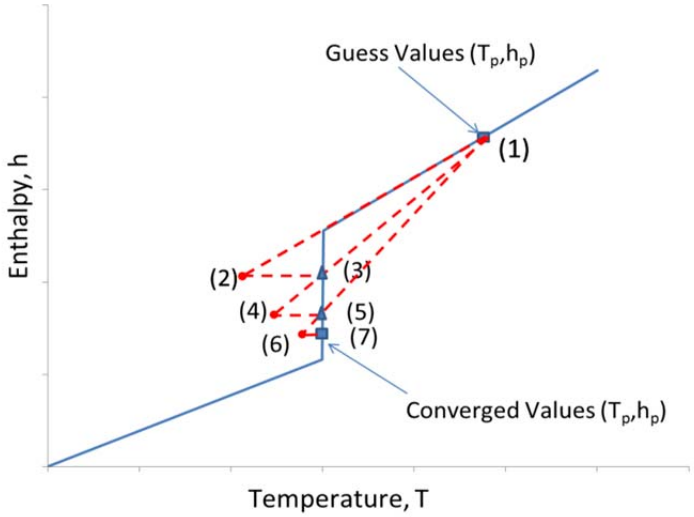

Figure 2.4 Apparent heat capacity approximation at a node during one time step using iterative methods

2.2.3 The temperature transforming model

The temperature transforming model was developed by Cao and Faghri [96] to overcome the time and spatial limitations in the heat capacity method. The model has been used by Faghri and his co-workers for many applications [62, 63, 97]. The method is also called as "the improved temperature-based equivalent heat capacity method" [98]. While the method was tested against several benchmark examples, it has been reported to produce inconsistent results especially when mass transfer through PCM is considered. Corrections were proposed to improve the accuracy [97, 98]. The key of this method is that the energy Equation 2-4 is transformed into a nonlinear Equation 2-10 with a single dependent variable "Temperature" [61].

$$\rho * C_{eff}(T) * \frac{\partial T}{\partial t} = \frac{\partial}{\partial x}\left(k\ \frac{\partial T}{\partial x}\right) - \rho * \frac{\partial S}{\partial t} \qquad \text{Equation 2-10}$$

This source term is represented by the following equation [61]:

$$S(T) = \begin{cases} C_s * \epsilon & , \quad T < T_m - \epsilon \\ \left(\frac{C_s + C_l}{2}\right) * \epsilon + \frac{L}{2}, & T_m - \epsilon < T < T_m + \epsilon \\ C_l * \epsilon + L & , \quad T > T_m + \epsilon \end{cases}$$ Equation 2-11

The latent heat during the phase change stage is represented by a source term in the governing equation with the heat capacity term similar to the apparent heat capacity method. The method is, however, not commonly used but offers an alternative solution when compared to the apparent heat capacity method.

2.2.4 The heat source method

Using the heat source method, the total enthalpy in the governing Equation 2-4 is split into the specific heat and latent heat where the latent heat acts as a source term [41, 65]. Equation 2-4 thus becomes:

$$\rho * C_{avg} * \frac{\partial T}{\partial t} = \frac{\partial}{\partial x}\left(k \frac{\partial T}{\partial x}\right) - \rho * L * \frac{\partial f_l}{\partial t}$$ Equation 2-12

The method was alluded by Eyres [56] in the middle 40s. In popular schemes, the phase change front is tracked by the evaluation of a nodal liquid fraction field which takes a value of 0 for solid , 1 for liquid, and a value in the range of [0-1] for the mushy region [41, 67]. With this approach, the fluid fraction is linearized and the equation can be solved iteratively with temperature. The liquid fraction can be approximated using the following auxiliary equation [67]:

$$f_l = \begin{cases} 0, & if\ T \leq T_m - \epsilon \\ \frac{(T - T_s)}{(T_L - T_s)}, & if\ T_m - \epsilon < T < T_m + \epsilon \\ 1, & if\ T \geq T_m + \epsilon \end{cases}$$ Equation 2-13

When discretizing Equation 2-12 with a fully implicit scheme and linearizing the source term "liquid fraction" at the current time step, the discretized equation becomes linear and needs to be solved for temperature in an iterative manner with the liquid fraction. Costa [68] has used this method to numerically simulate the latent heat thermal storage.

2.2.5 **Summary**

Different mathematical models and methods have been suggested in literature to deal with phase change problems using the fixed grids method: enthalpy, heat capacity, temperature transforming method, and heat source method. Every method has its main distinct feature for the latent heat liberation with advantages and disadvantages. **Table 2-1** summarizes these methods, and highlights the main feature and their advantages and disadvantages. For many reasons including computational efficiency, modeling accuracy and flexibility in selecting solution schemes, the enthalpy method is merited to be an attractive mathematical model over others for simulating phase change problems. In particular, it becomes appealing when the corrective iterative scheme (i.e., a fast and energy conservative approach), or non-iterative scheme (i.e., a quick but conservative approach at low time steps) are implemented. To further exploit these two features for large time steps, a quick but energy conservative approach is envisioned.

Table 2-1 Feature, Advantages and Disadvantages of Mathematical Methods used for Phase Change Problems

Mathematical Model for Latent Heat Evolution	Main Feature	Advantages	Disadvantages	Possible Solution Schemes	Reference
Enthalpy Method	Enthalpy accounts for sensible and latent heat	• Fast if proper scheme is selected • Deal with sharp as well as gradual phase change	• Difficult to handle supercooling problems • The temperature at a typical grid point may oscillate with time	Iterative scheme with Non-linear solvers (e.g. Newton's methods) Linearized-Enthalpy: Corrective iterative scheme Quasi-Enthalpy: Non-iterative Temperature correction scheme	[42, 73] [40, 53] [60]
Heat Capacity Method	Heat capacity accounts for both sensible and latent heat	• Intuitive since dealing with one dependent variable "Temperature" • Easy to program • Suitable for gradual phase change	• Lack of computational efficiency • Small time step and fine grids are required for accuracy • Difficult in handling cases where the phase-change temperature range is small • Difficult to obtain convergence with this technique, and there is always a chance that the latent heat is underestimated • Not applicable for cases where phase change occurs at fixed temperature	Iterative Scheme (e.g. Gauss-Seidel iterative scheme) if a proper heat capacity approximation is selected	[40, 45, 47, 78, 80, 81]
Temperature Transforming Method	Heat capacity and source term are used to account for sensible and latent heat	• Deal with sharp and gradual phase change • Handle large time step and course grids	• Not a common method and therefore not tested to evaluate the pros and cons	Iterative Scheme (e.g. Gauss-Seidel iterative scheme) after linearizing the source term	[61-64, 96, 97]
Heat Source Method	Latent heat is treated as a source term	• Intuitive due to separating the latent heat from sensible • Deal with sharp and gradual phase change	• Requires under-relaxation and therefore extra efforts is needed to determine the optimum relaxation factor • Lack of computational efficiency • Problems with round off errors if melting occurs over temperature range	Iterative Scheme (e.g. Gauss-Seidel iterative scheme) after linearizing the source term	[41, 56, 65, 67]

2.3 Models for building enclosures with PCM

A few models have been developed to solve phase change problems on the basis of the general mathematical methods described above. A list of the models for various engineering fields including building applications was reviewed recently by these studies [99-104]. This section, however, provides a more concentrated and in-depth review on the models that are proposed and used for simulating PCM integrated within building enclosures.

A few innovative and sustainable designs have been proposed by integrating PCM within building construction elements. These designs demand different levels of model complexity to evaluate the thermal performance of such elements. The computational models are classified hereafter as the simplified, intermediate and sophisticated models. Within this context, the simplified models are rough approximations of the physics in the phase change process but offers quick results. The intermediate models are a tradeoff between the speed of the simplified models and the accuracy and flexibility of the sophisticated models. The sophisticated models are created using well validated numerical packages that offer a choice of established and optimized numerical methods. This class offers a high level of accuracy and modeling flexibility but is computationally expensive.

2.3.1 The simplified models

Detailed models for simulating PCM within building enclosures may capture more physics of heat transfer process. However, simplified models are sometimes preferred to provide a quick estimation of PCM's thermal performance. Some simplified models have been developed with this intention [105-109].

A steady-state analytical model for evaluating the benefits of PCM in walls and roofs has been proposed by Kaushik [105]. The model used the heat capacity method to represent the dynamic thermal storage of PCM. The model was utilized to analyze the dynamic thermal performance of a free floating building with PCM embedded in a south wall façade [106]. The result for a typical mild winter day in New-Delhi showed that the wall with PCM outperformed that of an ordinary wall. A rough model utilizing the heat capacity method was developed to characterize the heat transfer process and subsequently estimate the temperature trend in a PCM mixed with gypsum plaster board [107]. The simplified model was able to capture the overall trend of air temperature in the conditioned room. Another simplified physical model using the R-C network method was developed and validated for three wall types: light, medium and heavy with shaped-stabilized phase change material [108]. The model, however, had to use a genetic algorithm to identify the key model parameters: resistances and capacitances of the wall layers to reach an optimal node distribution. When the optimal parameters are identified, the model can be used to simulate the heat transfer process in a wall unit that has a PCM layer. Although the model is intended to be simple, multiple procedures are necessary for practical applications. The model was however implemented to evaluate the energy performance of an office building with shaped-stabilized phase change material embedded in a wall unit [109].

2.3.2 **The intermediate models**

A variety of intermediate models using, respectively, the enthalpy method, heat capacity method and heat source methods have been developed for one, two and three dimensional cases for building enclosures.

2.3.2.1 The enthalpy method

In the enthalpy method, the enthalpy may be solved by nonlinear solvers with an auxiliary function (e.g. temperature-enthalpy relationship) or implicitly in the governing equation using linearization techniques. A theoretical analysis based on the enthalpy method was presented in a study evaluating a PCM in a wallboard for solar energy storage [110]. A semi-implicit Crank-Nicolson method was used for numerical discretization, which was subsequently solved using the Newton's method. A more sophisticated two dimensional finite volume heat transfer model based on the enthalpy method was developed and validated to explore the behaviors of phase change materials incorporated into building-integrated photovoltaic (BIPV) system [111, 112]. The heat equation is solved with an auxiliary temperature-enthalpy function. The model was utilized to perform an optimization study of commercially available PCM products embedded into cavity-wall systems with different wall-PCM configurations [113]. In addition to simulating heat transfer process, the model has the capability to solve the Navier–Stokes equation (i.e., the momentum and mass equations). The model was expanded later to evaluate a three dimensional heat transfer process with PCM [114]. It was found that the 3D model does not offer additional accuracy when compared to the previously validated 2D model. Another example of a validated finite element 3D numerical model based on the enthalpy method has been suggested to simulate the PCM mixed with common mortars for wall plaster [115].

Using the enthalpy linearization approach, a model was recently presented as an alternative method for a PCM algorithm in ESP-r, a whole building simulation program [37, 116]. The MATLAB simulation environment was used to develop a one dimensional numerical model using a corrective iterative scheme proposed by Swaminathan and Voller [53] based on

the enthalpy linearization. The customized model in MATLAB uses the finite volume method with a Crank Nicholson scheme to produce a fair comparison to ESP-r. The model has proven to be accurate and fast when compared to the ESP-r results for a BESTEST Case 600 model configured with PCM.

2.3.2.2 The heat capacity method

Phase change materials for building applications such as Paraffin melt or freeze over a temperature range compared to pure materials where phase change occurs at fixed temperature [13, 24, 25, 101]. This property makes the heat capacity method an attractive approach to simulating PCM in building applications. Utilizing MATLAB package, a research group has developed an implicit one dimensional finite difference model for PCM in inner wallboard, ceiling and floor with the heat capacity method [117]. The discretized equation was solved using the Gauss-Seidel iterative method. Although the lab experiments were limited and simulation program was incomplete at that stage, the overall benefits from PCM in wallboard were evident.
A semi-implicit one dimensional finite volume heat transfer model for simulating PCM in a ceiling of a room using the heat capacity method was developed and validated by Pasupathy [118, 119]. The model was solved using the tri-diagonal matrix algorithm (TDMA) with very small time step. Although the overall trend of indoor air temperature was captured by the model, the numerical results were not in a good agreement with the experiments due to many limitations of the model. The same model was later used for evaluating the PCM integrated into a roof system [120].

The heat capacity method has also been implemented in a one dimensional numerical model to evaluate shape-stabilized phase change materials embedded with a floor heating system

[121]. The specific heat capacity was used to account for the enthalpy of PCM at different temperature regimes. The model gave good agreement results when compared to experimental data. The model was also used for PCM evaluations under different climates and various system configurations [9, 122, 123]. A variety of modeling applications of PCM embedded in floor system for different purposes using the heat capacity method have been reported in literature [124-126].

PCMs have also been integrated in transparent building envelopes such as glazed windows. An explicit one dimensional finite-difference model based on the heat capacity method was extended to evaluate PCM performance when integrated into a double glazing system [127, 128]. The developed model was validated with experimental data and then subsequently utilized to evaluate the impact of PCM on heat loss and gains.

While models developed for building envelope are typical for one dimensional geometry, two and three dimensional heat transfer approaches have also been suggested for modeling PCM using the heat capacity method. In early 90s, a numerical code "WALL88" was proposed for modeling two dimensional transient thermal transport and storage of both sensible and latent heat [129]. The model was validated against analytical solution and experimental lab results. The model was found to give an excellent agreement with experimental results only after allowing the PCM to melt over a temperature range rather than at isothermal temperature. A three dimensional finite-difference heat transfer model using the heat capacity method was developed to study the thermal performance of randomly mixed PCM and laminated PCM-wallboard systems [130, 131]. Although the numerical model was not validated in these papers, the simulation results were helpful to conclude that laminated PCM-wallboard performs thermally better than the randomly PCM-wallboard. This model was later validated against an experiment

and found a maximum of 3% deviation from the average experimental results [132]. The model was further used to evaluate the PCM applications in the drywall in a passive solar building [133]. The results confirmed the conclusions from previous studies for the application of laminated PCM-wallboard. Optimizing the PCM distribution within building envelope is the overall goal of an energy efficient design. The heat capacity method was adopted by an in-house software "CODYMUR", developed by a team from France, to optimize the use of a PCM wallboard for building energy use [134].

2.3.2.3 The heat source method

The heat source method is an intuitive approach due to the separation of specific and latent heat. An explicit one dimensional finite-difference heat transfer model for a wall with PCM was developed using the heat source method by Athienitis [135] and validated against a full-scale outdoor test-room with PCM gypsum board at interior side. The model showed a reasonable agreement with experimental results. A heat transfer model of a newly developed hybrid thermal energy storage system (HTESS) using PCM capsules in a wall-unit was developed and validated for managing solar and electric energy [136]. The numerical model uses the heat source method similar to that proposed by Voller [66] where the latent heat evolution is represented by a source term in the governing equation. The fluid fraction is the key to track the latent heat process.

Phase change materials incorporated within floor systems was evaluated using a one dimensional finite volume heat transfer model based on the heat source method [137]. The numerical model was validated with a benchmark analytical solution of Stefan problem explained by Hu [47]. After optimizing the grid and the time resolution, the developed model

together with an optimization algorithm was used to perform an optimization analysis on PCM-floor designs. A two dimensional numerical model was developed based on the heat source method to simulate the effect of PCM in the design of a solar passive wall [138]. The model has been verified using benchmark cases documented in literature. The model was later validated using experimental data performed in the Lab and found to be unsatisfactory due to the limitation of handling the super-cooling effect inherited in the tested PCM [139].

2.3.3 **The sophisticated models**

Developing a numerical model in two or three dimensional domain is complicated and difficult to be generalized for different geometries, applications and physics; hence existing simulation packages such as COMSOL (formerly known as *FEMLAB*) [140], ANSYS-FLUENT [141], HEATING [142] and others are used as convenient design tools. Although, these models offer high level of flexibility, they are not fully explored for heat transfer process with phase change.

One study has used a commercial package FEMLAB (later *COMSOL multiphysics*) to develop a wall model with phase change materials using the enthalpy method and heat capacity method [143]. COMSOL is a finite element simulation package that allows multi-physics modeling for many engineering applications. Utilizing this package, the created model was validated against experimental results. It was found that both numerical methods give good estimation of latent heat evolution process. However, the heat capacity method found to be more precise with the experimental results when a narrow melting temperature range of 2˚C was selected. COMSOL has also been used to study envelope systems with PCM [144]. The numerical results from COMSOL were successfully compared with another well-established

numerical model “WUFI-5”. COMSOL is flexible in modeling multi-physics within irregular and complex geometries. For example, an innovative honeycomb wallboards with PCM have been modeled in a 3D domain using the heat capacity method [145]. The simulation results showed a very good agreement with the experimental results.

A computational fluid dynamics (CFD) simulation package “FLUENT” can also be utilized to evaluate a heat source method when using user-defined functions for heating and cooling cycles of PCM rather than using one idealized function to represent both phenomena [146]. The results of a PCM box model utilizing the two functions showed very small error (in root mean square (RMS) values) when compared with a case of using an ideal function for phase change. Another example of using FLUENT is reported for PCM integration into a wall cavity system[147].

Heat Engineering And Transfer In Nine Geometries (HEATING) is a multidimensional, general-purpose heat transfer code that has been extensively validated under ASHRAE project RP-1145 [148]. The code can also be used to model the phase change using the heat capacity method. Ahmad [149] has used the program to study the behaviors of PCM in wallboard of a test cell. The model was validated using experimental test results and found to agree well with experiments. The PCM research program at Oak Ridge National Laboratory (ORNL) has used this program to study the thermal behaviors of PCM in complex two and three geometries in building envelope [150]. Lab tests using a heat flow meter apparatus (HFMA) have been conducted to validate the model in HEATING. HEATING has also been used as a standard benchmark numerical package to validate the finite-difference algorithm used for PCM modeling in EnergyPlus [151].

2.3.4 **Summary**

A variety of models for different building enclosures have been developed using various simple, intermediate and sophisticated approaches. **Table 2-2** summarizes the models, application usages, and validations. It is obvious that very few simplified models have been suggested due to the complexity of approximating the heat transfer process associated with phase change. The intermediate models are commonly used but are developed for specific applications and to investigate explicit envelope designs. Hence, they lack flexibility in analyzing complex and advanced design alternatives which becomes norms for selecting optimal or near optimal designs. Sophisticated models offer flexibility in solving complex and multi-physics problems but are not fully explored for modeling PCMs. This is partly due to the computational inefficiency. They additionally demand considerable amount of detailed data inputs, lengthy model setup and validations, and limited access to the source codes.

Generally, all models that adopt the heat capacity or heat source methods must be, however, used with small time steps to attain acceptable accuracy and therefore slow for whole year simulation which is typical for building's thermal performance evaluation. In addition, many existing models ignore inherited characteristics of some PCMs such as hysteresis or subcooling and therefore cannot be used for this particular application.

Table 2-2 Modeling Approaches for Latent Heat Evolution in Building Enclosure

Complexity Level	Latent Heat Evolution's Approach	Building Enclosure Case Studied	Modeling Formulation	Solution Strategy	Validation	References
Simplified Models						
	Heat Capacity Method	Wall and Roof	Steady-State Analytical Model			[105, 106]
		Wallboard			Experimental	[107]
	Optimum nodes for Heat Capacity distribution using Genetic Algorithm	Wall	R-C Network		N/A	[108, 109]
Intermediate Models						
	Enthalpy Method	Wall	FVM: 1D	Newton's method		[110]
		BIPV	FVM: 2D & 3D	Non-linear solver	Experimental	[111, 113, 114]
		Wall	FVM: 1D	Iterative Corrective Scheme	Comparative	[37, 116]
	Heat Capacity Method	Wall	FDM: 1D	G-S	Experimental	[117]
		Ceiling/Roof	FVM: 1D	TDMA	Experimental	[118-120]
		Floor	FDM: 1D	G-S	Experimental	[9, 121-123]
		Glazed-Windows	FDM: 1D	EM	Experimental	[127, 128]
		Wallboard	FDM:2D		Analytical and Experimental	[129]
		Wallboard	FDM: 3D		Experimental	[130-133]
	Heat Source Method	Wall	FDM: 1D	EM	Experimental	[135]
		Wall	FDM: 1D	TDMA	Experimental	[136]
		Wall	FVM: 1D	Iterative scheme	Analytical	[137]
		Wall	FVM: 2D	TDMA	Analytical, Comparative and Experimental	[138]
Sophisticated Numerical Packages						

COMSOL	Heat Capacity Method and Heat Source Method	Wall	FEM: 2D		Experimental	[143]
	Heat Capacity Method	Wall	FEM		Comparative	[144]
	Heat Capacity Method	Wall	FEM: 3D		Experimental	[145]
FLUENT	Heat Source Method	Wall	FVM: 3D	SIMPLE algorithm	Experimental	[146]
	Heat Source Method	Wall	FVM: 2D		Experimental	[147]
HEATING	Heat Capacity Method	Wall and Roof	FDM: 1D, 2D and 3D	Point-successive over-relaxation iteration	Experimental	[149-151]

FVM: Finite Volume Method, FDM: Finite Difference Method, FEM: Finite Element Method, G-S: Gauss-Seidel iterative method, TDMA: Tridiagonal Matrix Algorithm, EM: Explicit Time Stepping Marching, R-C: Resistance-Capacitance

2.4 PCM models integrated into whole building simulation programs

Many detailed simulation programs are nowadays available to assist designers, researchers, manufacturing companies to implement new technologies and evaluate innovative ideas that improve the energy and thermal performance of buildings. Detailed simulation tools perform computations on an hourly or sub-hourly bases for accurate considerations of the dynamic interactions between all thermal-based elements associated with comfort and energy consumption, including building envelope, HVAC systems, lighting and control devices [152]. Many building simulation tools are listed at the U.S. Department of Energy (DOE) web directory [153]. The twenty prevalent whole building energy simulation programs that are considered accurate and capable of handling the dynamic behaviors of a building and its systems are reviewed by Crawley et al. [154]. Few whole building simulation programs can handle the thermal performance of building envelope with phase change materials such as EnergyPlus, TRNSYS, ESP-r, and BSim. In addition, some other programs with limited capabilities are available for modeling phase change in buildings. The following paragraphs brief and compare the conditions of these programs.

2.4.1 EnergyPlus

EnergyPlus uses the Conduction Transfer Functions (CTF) to approximate heat transfer in building envelope. Since the CTF method uses the historical values of heat flux in the computation, Barbour [155] has studied the possibility of using this method in EnergyPlus to approximate the latent heat evolution in building envelope. The study developed multiple sets of CTFs based on the temperature of phase change materials. A switching mechanism was proposed

to exchange between these sets during the simulation. The CTF-switching algorithm was found to be within 20% accuracy for a range of conditions typically encountered in buildings.

The capability of modeling PCMs has been facilitated in EnergyPlus program Version 2.0 released in April 2007 by adding a conduction finite difference (CondFD) solution algorithm [156]. The algorithm uses a semi-implicit finite difference scheme based on the heat capacity method with an auxiliary enthalpy-temperature dataset to account for latent heat evolution [157]. Using this dataset, the heat capacity is approximated using a temporal averaging approach similar to that proposed by Morgan [87]. While the previous versions of EnergyPlus had a semi-implicit scheme for modeling PCMs, a fully implicit scheme has been recently added to Version 7 of the program with more numerical flexibility [158]. For both schemes, it is however recommended to use a small time step for accurate results.

Experimental validations have been conducted for this algorithm with mixed feelings of accuracy. Castell, for example [159], found that EnergyPlus simulation results did not show a good agreement with the experiments when phase change materials were implemented in concrete blocks. The study concluded that the simulation results did not reflect the thermal improvement of PCM observed in the test cells. However, the study highlighted that the weather data used in this simulation was not representative of the actual weather data.

An experimental test shed with a commercial PCM product has been used to validate EnergyPlus (Version 5) simulation results under the climatic conditions of Phoenix, Arizona [160]. It was found that the predicted energy consumptions were half during winter and slightly greater for the summer months. In addition, the time shift was observed for a very short time span during the month of April (3 min) and October (9 min).

Under the climatic conditions of Auckland New-Zealand, an experimental study using PCM in gypsum board has been compared to the simulation results of EnergyPlus using both historical weather data and actual measured weather data [161]. Although EnergyPlus model using actual weather data has captured the overall trend of indoor air temperature but failed to accurately predict the actual indoor air temperature from measurements. The study highlighted that due to many parameters including air infiltration, the simulation results might deviate from the actual measurement.

An early successful validation of the CondFD solution algorithm used for PCM modeling has been reported by Zhuang [162] using two envelope systems with PCM: envelope "A" (one layer of PCM: melting Temperature at 40℃) and envelope "B" (two layers of PCM: one melting Temperature at 40℃ and another at 33℃). The study shows that the largest relative difference in indoor temperature is 12.41% and the least is 0.71% between the simulation and testing results in a sequential 36h period on envelope "A" condition. For envelope "B" condition, the largest relative difference is 8.33% and the least is 0.33% in a sequential 72h. It was concluded that the most important factors in reducing the discrepancies between the simulation and the test results are to use proper actual weather data as well as using proper material thermal characteristics. Other successful validations of EnergyPlus algorithm for PCM have been conducted by Campbell [163] and Chan [164] using published experimental data by Kuznik [165]. For both validation studies, the indoor air temperature was found to agree well with the experimental results.

A field test house was used to study the impacts of PCMs in building envelope and consequently used to validate the CondFD algorithm in EnergyPlus [166]. The test house used the cellulose insulation mixed with 20% PCM by mass. The study reported that simulated daily

average heat flux through walls was within 9% of the field measurements. In addition, simulation results for temperature distribution through envelope compared fairly well with the experimental data apart from some delayed response compared to the measurement. However, EnergyPlus has given unreasonable results for heat fluxes and temperature distributions in the attic floor of the experimental house.

In addition to the validations above, the EnergyPlus's developer team has performed rigorous validation and verification studies for general heat transfer calculations as well as the CondFD solution algorithm [35, 151, 167]. These validation studies used analytical benchmark solutions, comparative tests with well-established program "HEATING", and experimental results. The studies concluded that versions prior Version 7 contains two bugs and subsequently will be fixed in later versions. It is also recommended to follow guidelines and bear in mind limitations in using Version 7:

- The time step should be shorter than 3 minutes.
- For an accurate hourly thermal performance, 1/3 of the default node space should be used.
- Hysteresis in PCM is not modeled in EnergyPlus and therefore inaccurate results may be produced.

2.4.2 **TRNSYS**

TRNSYS is a modular program where components modules "TYPES" are linked together in which output of one type can be an input to another in the model. It has been widely used for modeling building and its complex systems. Due to its modularity, users can either utilize available types in the simulation package or develop new modules and easily integrate to

the TRNSYS simulation package. Many features have been introduced in Version 16, including a graphical user interface “Simulation studio” and the possibility to call external programs such as MATLAB, FLUENT and many others [168].

Many models have been proposed in TRNSYS for modeling phase change heat transfer in building envelope but majority are proprietary research modules. Ghoneim for example used a modified type of the thermal storage wall “TYPE36” where the use of PCM has been tested for thermal storage in a wall system [169, 170]. The model was based on the enthalpy method and solved using an explicit scheme. Despite the numerical problems encountered when modeling PCM due to the smaller time step required for the stability of the explicit scheme, the model was successfully integrated into TRNSYS and validated against published data for a concrete storage wall. Another explicit numerical scheme using the enthalpy method was developed for modeling the effects of integrating PCM into a solar wall [171, 172]. The module “TYPE58” was integrated into TRNSYS to explore the significance of heating outside air for ventilation purposes in the experimental house.

Modeling PCM in TRNSYS is recently provided through “TYPE204” by a team of researchers from Helsinki University of Technology [173]. The model simulates heat transfer through a wall in a three dimensional domain using the Crank-Nicolson scheme with 729 nodes. The model can indeed use a fully implicit or explicit scheme with an appropriate selection of a parameter that switches between different schemes. The model uses the heat capacity to account for latent heat evolution in the wall. Although this type has not been validated in its 3D form due to its poor computational efficiency, Ahmad [174] has converted the 3D model into a 1D module “TYPE101” and validated the modified code. The simulation results were compared to experimental results from two test cells: one without PCM and another with PCM. While the

model without PCM works well when compared to the experimental results, the model with PCM overestimates the daily peak indoor temperature in the cell. The authors outlined several reasons for this discrepancy including: i) evaluation of the energy transmitted through the window, (ii) imprecision in the melting temperature range taken in the heat capacity definition, (iii) values of the convective heat transfer coefficient between wall surfaces and ambient air and (iv) existence of cold bridges. Out of these reasons, it was found that correcting cold bridges by introducing extra term for resistance improved the simulation results significantly when compared to the experimental results.

A study reported a simplified approach of simulating PCM in walls/ceiling and floor in TRNSYS [175]. The approach is to use the existing capability of TRSNYS to simulate a standard active wall in "TYPE56" (i.e., building module in TRNSYS). The key in this approach is a user input of equivalent heat transfer coefficients introduced in each time step of the simulation that characterizes the thermal behaviors of the wall with PCM. The model does not evaluate the real heat transfer behaviors in PCM but accurate enough for modeling PCM thermal behaviors. The model has been validated under laboratory setting conditions.

On the other hand, Schranzhofer [176] has developed a PCM module "TYPE241" where PCM was modeled as an internal layer based on the heat source method. TRNSYS capability was utilized to model other envelope layers using the transfer function method by creating dummy contact zones between the PCM layer and the remaining layers. In this type, the PCM is modeled using external code based on finite different method with other layers modeled through CTF algorithm available internally in TRNSYS "TYPE56". One advantage of this approach is the short computational time needed for numerical solution but the physics might not be captured

well because of assumptions involved in the dummy contact zones. The model however was not validated due to a lack of appropriate experimental data.

Kuznik et al. have recently developed a new model "TYPE260' in TRNSYS utilizing the heat capacity method [177]. The model is semi-implicit since the physical properties of PCM used in the computations are calculated from previous time step. This type has been validated with two lab tests conducted by authors: one when the outdoor temperature was increased in two steps and the second where it was a sinusoidal behavior. The heating heat capacity curve was used for the numerical modeling. For both validations, the simulation results showed good agreement with the test results.

A newly developed one-dimensional heat transfer model using the heat capacity method was applied to a dividing wall with 16 glass bricks filled with PCM in TRNSYS [36]. The model has been validated and showed fair agreement with experimental results. In addition, a simplified PCM module "TYPE1270" has been recently developed by Thermal Energy System Specialists (TESS) and added to its commercially available individual components [178]. The module simulates PCM as an internal layer within an envelope system. The model is currently limited to materials that melt/freeze at isothermal temperature and with constant specific heat at solid and liquid. In the transition state, the PCM layer temperature is constant and the model tracks the energy absorption and release. The tracking methodology is similar to the heat source method and therefore can be identified as "Quasi-Heat Source Method".

2.4.3 **ESP-r**

ESP-r is a dynamic energy simulation tool of UK, used for modeling thermal, visual and acoustic performance of buildings [179]. With many features suitable to model advance

sustainable energy technologies, ESP-r has the capability to model phase change materials using two methods: the effective heat capacity method and the additional heat source method [79, 180, 181]. ESP-r uses four models for PCM simulation, with one that accounts for sub-cooling, using special materials function. However, it is necessary to use a small time step to obtain accurate results for these two methods. While simulation results using ESP-r have been found in literature, none showed any substantial validations for these two algorithms in ESP-r [182-185].

2.4.4 **BSim**

BSim is a dynamic simulation program originated from Denmark that offers an easy user graphical interface [186]. Using the quasi-steady state in building modeling, the program models phase change using the heat capacity method [187]. The simulation time step has to be small, too, for accurate prediction. Lab test results from literature were used to validate the model on three cases: continuous heating, continuous cooling, and heating but with initial temperature below melting point of PCM. The simulation model captures the overall trend of actual thermal behaviors of PCM but with small deviations.

2.4.5 **Other building simulation programs**

Some other building simulation programs have been developed for specific research purposes of modeling phase change materials, such as RADCOOL [188], ESim [189], and CoDyBa [82]. Few have been proposed and developed to simulate simple building configurations, such as PCMExpress [190] or the one using Engineering Equation Solver (EES) [124]. Due to limited literature available for these programs, only few will be discussed hereafter.

2.4.5.1 RADCOOL

RADCOOL is a design tool for cooling and heating system developed at the Lawrence Berkeley National Laboratory of the US [191]. The program was created using the Simulation Problem Analysis and Research Kernel (SPARK) [192]. A one dimensional finite-difference model for a wall with PCM was added to this validated thermal building simulation program [188]. The model was then used to study the capability of a double PCM-wallboard to achieve thermal comfort without using mechanical cooling system under a typical climatic condition of Sunnyvale, California [193].

2.4.5.2 ESim

ESim was developed at University of Dayton for building energy simulation and can be downloaded from the developer website [194]. The simulation program was expanded and validated to model PCM-wallboards using an explicit finite-difference approach [195]. A list of template files are available for use but with limited capability to model complex buildings and systems.

2.4.5.3 PCMexpress

PCMExpress is a planning and simulation program for buildings using phase change materials [190], which was developed by a German company, in collaboration with the Fraunhofer Institute for Solar Energy (ISE) in Freiburg and partners from industry [196]. The program simulates a free floating building with a library data for weather and various construction materials including PCM and the flexibility to add new materials. It is an effective

tool to evaluate the economic and technical feasibility of PCM usage during an early design stage. The mathematical model of the heat transfer process in PCM is not available. The model has been tested by Castell [159] who found that the simulations deviate significantly from the experiments. As commented by Castell, the discrepancy could be attributed to the lack of accurate infiltration model in the program. The program however has been used to demonstrate the impact of using PCM in residential and commercial buildings [196, 197].

2.4.6 **Summary**

Whole building simulation programs play an important role for studying the economic and technical feasibility of PCMs. This section reviews the capability of various whole building simulation programs as summarized in **Table 2-3**. It is noted that most PCM models integrated into whole building simulation programs are based on the heat capacity method. Hence, it becomes necessary to reduce the typical one hour time step to a very small time step (i.e., in order of minutes) to achieve acceptable level of accuracy. For one year thermal performance evaluation, building simulation programs become computationally inefficient since iterative methods are used in each time step. Additionally, the convergence may not be achieved due to numerical instability especially when PCM enters or leaves the phase change region. With all constraints and limitations above, none of whole building simulation programs are currently implementing efficient mathematical models that are quick, accurate and numerically stable at realistic time step. It becomes important to thoroughly investigate different mathematical models with various numerical approaches for modeling PCMs in whole building simulation programs.

Table 2-3 Numerical Methods for Latent Heat Evolution in Building Simulation Programs

Building Simulation	Module Identification	Numerical Formulation	Numerical Method used for Latent Heat Evolution	Time Stepping Scheme	Limitations/ Constrains	Validation	Reference
EnergyPlus	CondFD	FDM: 1D	Heat Capacity Method	1. Implicit 2. Semi-implicit	• Time step < 3min • Small grids • Hysteresis in PCM is not modeled • Phase Change at isothermal temperature is not modeled	Analytical, Comparative and Experimental	[35, 151, 162-164, 166, 167]
TRNSYS	Modified "TYPE36"	FDM: 1D	Enthalpy Method	Explicit	• Low time step • No access to the code	Limited validation using Experimental results for concrete	[169, 170]
	"TYPE58"	FDM: 2D	Enthalpy Method	Explicit	No access to the code	Experimental	[171]
	"TYPE204"	FDM: 3D	Heat Capacity Method	Select an appropriate factor for Implicit, semi-implicit or explicit	Computationally inefficient	N/A	[173]
	"TYPE101"	FDM: 1D	Heat Capacity Method	Semi-implicit (Crank-Nicolson)	• A correction factor to account for cold bridges has to be used for model accuracy	Experimental	[174]
	TRNSYS "Active Wall"	Equivalent Heat Transfer Coefficients	Variable Heat Source Function mimicking PCM behavior		• Real heat transfer physics in PCM is not modeled	Experimental	[175]
	"TYPE241"	FDM: 1D	Heat Source Method		No Published data	N/A	[176]
	"TYPE260"	FDM: 1D	Heat Capacity Method	Implicit	• Thermal properties including heat capacity are based on previous time step (i.e. explicit scheme)	Experimental	[177]
	Modified "TYPE101"	FDM: 1D	Heat Capacity Method	Implicit	• Developed for Internal partition wall	Experimental	[36]
	"TYPE1270"	Lumped Method using Heat Balance	Quasi-Heat Source Method		• Very simplified model • Internal layer within an envelope	N/A	[178]

						• Based on lumped heat balance (not a finite volume), low accuracy • For phase change at fixed temperature		
ESP-r	SPMCMP53-SPMCMP56	FDM: 1D	Heat Capacity and Heat Source Method			• Low time step	N/A	[180, 181]
BSim		FVM: 1D	Heat Capacity Method		Implicit	• Low time step to avoid instability	Experimental	[187]
RADCOOL		FDM: 1D	Heat Capacity Method		Implicit			[188]
ESim		FDM: 1D	Heat Capacity Method		Explicit	• Explicit scheme requires low time step to avoid instability	Experimental	[195]

FVM: Finite Volume Method, FDM: Finite Difference Method

2.5 Energy performance of PCM-enhanced enclosures

Latent heat storage using PCM is a very effective passive technique that is used to dampen the effect of heat wave. As a result, the thermal load of the zone is reduced and delayed, and consequently reducing the energy consumption. Hence, PCM has gained great attention in the past decade or so. Literature shows numerous conceptual and real examples of PCM integration into building applications [13, 18-26]. Many studies have been conducted to evaluate the thermal and energy performance of PCM-enhanced envelopes including field testing, laboratory, and simulations. Different performance indicators have been used to evaluate the thermal performance of PCM-enhanced envelope. This section is focused on studies that consider the peak or annual heating and cooling loads.

At the University of Dayton, Kissock et. al. [195] built a testing facility solely for validating a PCM numerical model [195]. Kissock used this validated model to study the impact of PCM integration into concrete sandwiched walls [198]. The peak and annual cooling loads were reduced by 19% and 13%, respectively. When PCM is discharged using cold air via natural ventilation, the annual cooling load could be reduced by as much as 17% (a 4% enhancement).

Since 2000, a research group lead by Medina from the University of Kansas has established experimental testing facilities, a lab dynamic simulator and computer model for evaluating PCM-enhanced walls[14, 199-202]. Over a course of a decade of research, the group has published several studies evaluating a verity of PCM design configurations in different wall orientations. Several experimental studies conducted over summer or winter days revealed that PCM has significant reduction in peak and daily loads. The three common PCM integrations tried by the group into the wood assembly wall are: 1) PCM encapsulated in embedded copper

pipe, 2) Structural Insulated Panel (PCM-SIP), 3) PCM blended with cellulose insulation. Two PCM concentrations are tested throughout these studies with various latent heats: 1) 10% of PCM, and 2) 20% of PCM concentration. The average reduction in peak heating load for all walls ranges from as low as 5.7% to as high as 15% depending on the thermal properties of PCM, PCM design configurations, PCM concentrations, and the time period of the study. Similarly for the average space cooling load, the reduction ranges from 9% to 11% was reported. For particular orientations, the south and west are the best for PCM integration. In one study [200], the average reduction in peak heat transfer for 10% PCM concentration was found 37% and 20% for south and west walls, respectively. For the 20% PCM concentration, the average reduction in peak heat transfer rate was 62% and 60% for south and west walls. Recent experimental results conducted by one of the group member found that the average reduction in peak heat transfer could reach as much as 27% for the four wall's orientations [202]. Using a validated computer model, he also found that the average reduction in peak heat transfer rate of all four walls can reach 12% in coastal climate of California.

Over the last few decades, new PCM products have emerged into US market. An experimental testing facility was built at Arizona State University to evaluate one commercial PCM product [160]. The PCMs were installed on every surface of the test shed on the interior side. Over the course of many months of testing under Phoenix climate, the results show a reduction of 27% in peak cooling load and a reduction of 19% in annual cooling energy.

Using the Natural Exposure Testing facility located in Charleston in south California, two testing campaigns in summer and winter (every period lasts 30 days) have been conducted to evaluate the performance of different PCM panels (divided into two wall groups) under real climatic conditions [203]. Results from wall group-1 indicated an increase in both heat gain and

heat losses in summer and winter periods. The authors have indicated that the temperature and heat flux sensors installed in this wall category may have been jeopardized by the air gap that resulted in erroneous readings. The results from the other wall group show a reduction in heat gain that ranges between 21.8-22.9% in summer. In winter, the reduction in heat gain ranges from 5.7%-15.4% and a reduction in heat loss from 25.5-27.7% have been reported.

Validated simulation tools have also been used to evaluate the energy performance of PCM in buildings. The NREL research team has used EnergyPlus to simulate the PCM integrations into different envelope systems using a typical house as per America benchmark protocols under Phoenix, AZ weather file [35]. The results show that PCM has minor effect on reducing the peak cooling load in cooling season of Phoenix. For the best PCM application in the wall, a maximum reduction of around 8% in peak cooling was achieved in the month of May with only 4% peak cooling reduction in July.

A couple of hospital spaces including administration office space, group treatment and patient rooms have been individually simulated using EnergyPlus for Oregon State Hospital in Junction City [204]. PCM layers with different thermal properties are integrated into these spaces for three envelope options: 1) external walls only, 2) external walls and ceiling, 3) all surfaces. The charging occurs naturally during the day but discharging is performed using night flush via integrated economizer with HVAC system. Average reduction of 15%, 17% and 28% in annual cooling energy, and 9.5%, 11%, 12% reduction in peak cooling load are achieved for external walls only, external walls and ceiling deign option, and all surfaces option respectively.

A simulation study using RADCOOL found that a PCM integrated into wallboard can reduce the peak cooling load by 28% in California climate for a typical office building[205]. The claimed savings can be facilitated when PCM is coupled with mechanical night ventilation.

A simulation study using HEATING 8 has been conducted to evaluate the PCM performance for two US climates: Phoenix, AZ and Baltimore, MD[206]. The study has investigated many PCM design configurations in a base residential wall case and various thermal properties for four wall orientations individually. The study found that when PCM placed to the interior side achieves slightly better performance but is sensitive to the zonal setpoint. When PCM is blended with full insulation thickness, the performance is less sensitive. The main focus of the study was the potential in reducing the cooling energy. For PCM full thickness, the reduction in wall-related cooling electricity ranges from 6-10% and 35-62% for Phoenix and Baltimore respectively. For both climates, west and south orientations are the best for PCM integration. For Phoenix, the optimal melting temperature range is about 2°C and 1°C above cooling setpoint (i.e., 25°C) for North and East walls and about 1°C above cooling setpoint for South and West. For Baltimore climate, the optimal midpoint temperature is always the cooling setpoint temperature.

Athienitis [135] has validated a numerical model for evaluating gypsum board soaked in PCM using a testing facility built in Canada, Montreal. The savings in total heating load was predicted to be 15% under the clod climatic condition of Montreal, Canada.

A simulation study using EnergyPlus has been conducted for office space under the climate of Seol, Korea [207]. Four PCM layers with different melting temperatures integrated into insulated lightweight wall has been studied. With all PCM types, annual heating loads have marginally increased but peak loads has decreased by 3.2% for PCM with 21°C melting temperature. The maximum reduction of 1.2% in annual cooling load and a maximum reduction of 1.3% in peak cooling load were achieved. The PCMs with melting temperature close to the heating and cooling setpoints (Tclg=26°C, Thtg=22°C) are showing the highest potential. The

study further uses the natural ventilation to discharge the absorbed heat. On average for all PCM layers, a reduction of 9% and 10.5% are achieved for annual cooling and peak cooling load, respectively. However, a 7.5% reduction in annual cooling load and a reduction of 10.2% in peak cooling load are solely due to natural ventilation.

A simulation study for a residential flat in tropical climate of Hong Kong using EnergyPlus has indicated a reduction of only 2.9% in annual cooling energy[164]. The study concluded that the PCM installation in this climate is not feasible due to the long payback period.

Utilizing a self-developed computer model, a small room was modeled using Algeria weather file [208]. The study found that a maximum reduction in annual cooling energy and peak cooling load are 1% achieved with 24.5°C melting temperature and 24% achieved with 33.2°C melting temperature, respectively. In addition, a maximum reduction of 12.8% in annual heating energy and a 35.4% reduction in peak heating load are achieved using PCM with 19.8°C and 19°C melting temperature, respectively.

Table 2-4 summarizes the results from the field, laboratory and simulation studies. The various studies indicate that the PCM's performance is highly dependent on many factors including the PCM thermal properties (latent heat, melting temperature, and melting range), zonal thermostat setpoints, PCM design configurations and integration mechanism, the insulation level of the wall assembly, surface areas, exposure to internal heat and solar gains, charging and discharging strategies and the climate. The balance between these factors will lead to a better PCM performance. For example, standalone cases show high PCM performance compared to cases when internal load is considered. For standalone cases, the PCM has to deal with the climatic variation only compared to cases where internal heat gain has to be manipulated too.

Table 2-4 Summary of literature on energy performance of PCM-enhanced enclosures

Reference	Country	Study Type	Building Type	Integration Mechanism	Internal Load	PCM Type	Savings
Kissock et. al. [195] and Kissock [198]	USA, Dayton	Experimentation and simulations	Test cells and Mobile house	Walls	none	PCM(K18)-enhanced concrete sandwiched walls: L: ~60 kJ/kg Tm: 25.6°C	1) No natural ventilations: The peak and annual cooling loads were reduced by 19% and 13%. 2) Natural ventilation (0.25-4 ACH): The annual cooling load was reduced by 17%.
Zhang et. al. [199]	USA, Lawrence, KS	Experimentation	Test houses	Different wall's orientations	none	PCM encapsulated in embedded copper pipe: L: 122 kJ/kg Tm: 20-30°C	For 10% PCM concentration: ▪ The average reduction in peak heat transfer rate was 15% for all walls. ▪ The average space-cooling load was reduced by approximately 8.6%. For 20% PCM concentration: ▪ The average reduction in peak heat transfer rate was 9% for all walls. ▪ The average space-cooling load was reduced by approximately 10.8%
Medina et. al. [200]	USA, Lawrence, KS	Experimentation	Test houses	Different wall's orientations	none	PCM (RT-26) in Structural Insulated Panel (PCM-SIP): L: 131 kJ/kg Tm: 26°C	For 10% PCM concentration: The average reduction in peak heat transfer rate was 37% and 20% for south and west walls. For 20% PCM concentration: The average reduction in peak heat transfer rate was 62% and 60% for south and west walls.
Evers et. al. [201]	USA, Lawrence, KS	Experimentation	Dynamic simulator in the Lab	Box	none	PCM(RT27) -enhanced cellulose insulation: L: 179 kJ/kg Tm: 26-28°C	For 10% PCM concentration: The average reduction in peak heat transfer rate was 5.7%. Total daily heat reduction of 0.6%. For 20% PCM concentration:

Reference	Country	Study Type	Building Type	Integration Mechanism	Internal Load	PCM Type	Savings
							The average reduction in peak heat transfer rate was 9.2%. Total daily heat reduction of 1.2%.
Lee [202]	USA, Lawrence, KS	Experimentation	Test houses	Different wall's orientations	none	PCM encapsulated in embedded copper pipe: L: 175-188kJ/kg Tm: 28- 30°C	The average reduction in peak heat transfer rate of all four walls was 27%
Lee [202]	USA, California Coastal climate, CA	Simulation, In-house code	Standalone wall	Different wall's orientations	none	PCM encapsulated in embedded copper pipe: L: 175-188kJ/kg Tm: 28- 30°C	The average reduction in peak heat transfer rate of all four walls was 12%. South is 16% and west wall is 21%.
Muruganantham [160]	USA, Phoenix, AZ	Experimentation	Test houses	All surfaces	none	PCM (BioPCM) concentrated layer: L: 200 kJ/kg Tm: 29°C	27% reduction in peak cooling load 19% reduction in annual cooling energy
Biswas et. al. [203]	USA, Charleston, CA	Experimentation	Natural Exposure Test facility in Charleston CA	Wall panels	none	Wall Test-1: L: 28.2-29.3 kJ/kg Tm: 21.1-21.3°C	Increase from 2.6-9.8% in heat gain and increase from 0.7-6.6% in heat loss in winter
						Wall Test-2: L: 18.8-26.9 kJ/kg Tm: 18.9-20.9°C	Summer: Reduction from 21.8-22.9% in heat gain Winter: Reduction from 5.7-15.4% in heat gain and 25.5-27.7% in heat loss
Tabares et. al. [35]	USA, Phoenix AZ	Simulation, E+	Residential	Walls and ceiling	Typical	PCM mixed with insulation: L: 33-130 kJ/kg ΔTm: 22.5-24.5°C	4% peak cooling reduction in July
Affiliated Engineers[204]	USA, Junction city, OR	Simulation, E+	Hospital spaces	1) External Walls only 2) External walls and ceiling	Typical	BioPCM L: 200 kJ/kg Tm: 23, 25, 29°C	PCM coupled with night flushing via economizer 1) External walls only: average reduction of 15% in annual cooling energy, 9.5%

Reference	Country	Study Type	Building Type	Integration Mechanism	Internal Load	PCM Type	Savings
				3) All surfaces including interior			reduction in peak cooling load 2) External walls and ceiling: average reduction of 17% in annual cooling energy, 11% reduction in peak cooling load 3) All surfaces: average reduction of 28% in annual cooling energy, 12% reduction in peak cooling load
Corina and Feustel [205]	USA, Sunnyvale, CA	Simulation, RADCOOL	Office	Walls	Typical	L: 39 kJ/kg Tm: 25°C ΔTm: 4°C	PCM coupled with mechanical night ventilation: reduction of 28% in peak cooling load
Childs and Stovall [206]	USA, Phoenix, Az Baltimore, MD	Simulation, HEATING 8	Standalone wall	Different wall's orientations	none	PCM mixed with insulation: L: 170kJ/kg Tm:20-34°C ΔTm: 4°C	Phoenix: reduction in wall-related cooling electricity from ~6-10% Baltimore: reduction in wall-related cooling electricity ranges from ~35-62% Based on absolute savings, South and west being the best and north the least
Athienitis et. al.[135]	Canada, Montreal	Experimentation and Simulation, in-house code	Test house	External walls	Solar only	PCM gypsum board L: 30.7 kJ/kg ΔTm: 16-20.8°C	Predicted savings of approximately 15% of the total heating load
Seong and Lim[207]	Korea, Seoul	Simulation, E+	Office	Walls	Typical	PCM concentrated later: L=230-281 kJ/kg Tm: 20, 21, 24, 29°C	1) No Natural ventilation: ▪ Slight increase in annual heating load, peak loads has decreased by 3.2% ▪ 1.2% reduction in annual cooling load and a reduction of 1.3% in peak cooling load 2) with natural ventilation:

Reference	Country	Study Type	Building Type	Integration Mechanism	Internal Load	PCM Type	Savings
							▪ 9% and 10.5% are achieved for annual cooling and peak cooling load
Chan [164]	China, Hong Kong	Simulation, E+	Typical residential flat	External walls	Typical	PCM Energain from DuPont: L: 114 kJ/kg Tm: 21.7°C	▪ A reduction of 2.9% in annual energy of air-conditioning system ▪ payback period of 91 years
Diaconu and Cruceru [208]	Algeria, Béchar	Simulation, In-house code	Room	External walls	none	External and internal PCM layers with insulation sandwiched inbetween: L=57.3 kJ/kg Annual Cooling energy: Tm: 24.5°C Peak cooling load: Tm: 33.2°C Annual heating energy: Tm: 19.8°C Peak heating load: Tm: 19°C	▪ maximum reduction of 1% for annual cooling energy and 24.3% reduction in peak cooling load ▪ maximum reduction of 12.8% for annual heating energy and 35.4% reduction in peak heating load

2.6 Conclusions

Significant heat storage offered by phase change materials is promising and favorable for developing various innovative building energy technologies. To quantify the technical and economic feasibility of PCM-embedded technologies, it requires the development of proper computational models. This chapter reviews various numerical modeling approaches of phase change problems such as the enthalpy, heat capacity, temperature-transforming and heat source methods. The main features, advantages and disadvantages of each method have been discussed. The discretized form of the heat equation with PCM can either be solved with nonlinear solvers such as Newton's methods or via linearizing the nonlinear term and using linear solvers such as iterative methods. For both approaches, the numerical solutions are computationally inefficient or difficult to reach convergence. Therefore, fast numerical schemes are suggested such as the quasi enthalpy non-iterative scheme or the enthalpy conservative iterative scheme.

Using these general mathematical methods, different computational models have been developed to simulate PCMs in building enclosures. Based on the level of complexity, models are classified into three categories: simple, intermediate and sophisticated models. Majority of these models have been validated using analytical solutions, comparative testing using validated numerical models, and/or experimental results.

While many models are used to study the heat transfer in an enclosure unit, a few models have been integrated into whole building simulation programs. A variety of models are available and some are available with no cost to users such as EnergyPlus, "TYPE204" in TRNSYS or ESP-r. These particular models, however, have limitations on modeling PCM including the time and spatial resolutions, inability to model hysteresis, lack of validations of some models, and

poor computational efficiency. These modeling challenges add complexity to the already existing uncertainties in experimental results of PCM's thermal behaviors. Therefore, further research is needed to quantitatively explore the prediction performance of different models including their limitations on accuracy, parameters sensitivity, speed, and stability for modeling PCM envelopes under different climatic and operating conditions.

Finally, several studies based on field, laboratory and simulations have been reviewed to highlight the energy performance of PCM-enhanced enclosures. The various studies indicated that the PCM's performance is highly dependent on many factors including the PCM thermal properties (latent heat, melting temperature, and melting range), zonal thermostat setpoints, PCM design configurations and integration mechanism, the insulation level of the wall assembly, surface areas, exposure to internal heat and solar gains, charging and discharging and the climate. This necessitates a well balanced approach between all these factors to reach an optimized PCM performance.

CHAPTER 3: NUMERICAL MODELS FOR PCM SIMULATION: DEVELOPMENT, VERIFICATION, VALIDATION AND ANALYSIS

The literature review from Chapter 2 indicated several models and schemes for modeling phase change materials (PCMs) for building envelope. This chapter outlines the calculation procedure for eight potential numerical models/schemes implemented in MATLAB/SIMULINK environment. A hybrid correction scheme is proposed under this study as an improvement to the existing linearized enthalpy method. All models have been validated using experimental results from the literature and further verified against a well-known building simulation program "EnergyPlus". The models show good agreement with experimental data as well as with comparative results. Through extensive sensitivity analysis, the models have been analyzed for their computational efficiency and prediction accuracy using normalized root mean squared error (NRMSE) and normalized central processing unit (NCPU) time respectively. The linearized enthalpy method with correction schemes; the iterative correction scheme and the hybrid correction scheme are found computationally efficient and their numerical predictions are consistent and therefore less sensitive to PCM properties compared to other models. These two schemes are potential candidates for PCM modeling that can be implemented into whole building simulation tools instead of existing slow and unstable numerical algorithms.

3.1 Introduction

In general, four mathematical models are used to simulate heat transfer associated with phase change: enthalpy method, heat capacity method, Temperature Transforming method, and heat source method as shown in **Figure 3.1**. These methods are discussed in detail in Chapter 2.

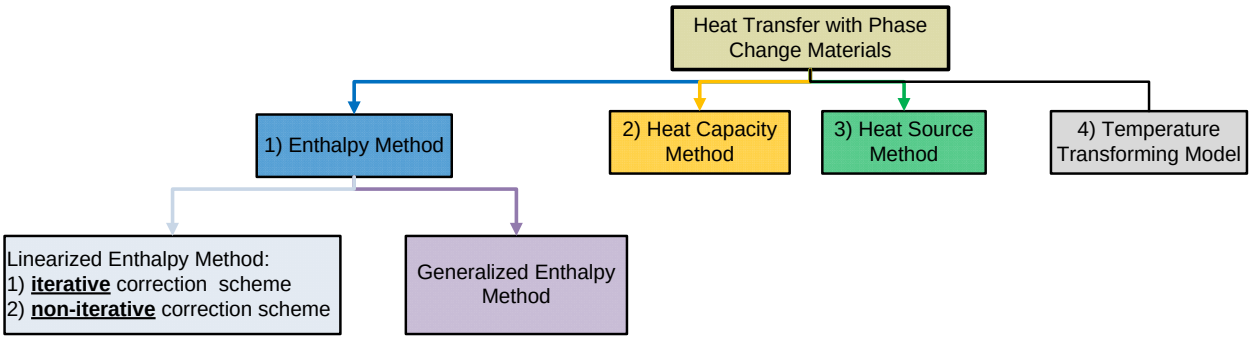

Figure 3.1 Mathematical methods used for modeling PCMs

Three common mathematical models, based on enthalpy method, heat capacity method, and heat source method, are selected for further evaluation. Using these three general models, a wide selection of numerical schemes and solvers can be utilized for solving phase change heat transfer problems. Literature research has indicated a variety of schemes and numerical solvers can be used. However, several challenges including accuracy, numerical stability and computational efficiency, are confronted when selecting a specific scheme and a suitable numerical solver. The motivation for this task is the great desire to determine a model, an associated scheme and solver that can be used for a quick yet accurate simulation of PCMs at realistic time step. This particular need is pronounced when the algorithms are integrated into whole building simulation programs that perform yearly simulations at hourly and sub-hourly time steps. Therefore, the objective of this section is to investigate common numerical schemes and the related solvers that can be used to solve the nonlinearity with PCMs in conduction-dominated heat transfer problems similar to those that are common in building application. Two numerical solvers are selected: Gauss-Seidel solver, an iterative solver, and Tri-diagonal matrix algorithm (also called Thomas algorithm or TDMA), a direct solver.

3.2 General Description and Numerical assumptions

The numerical models and schemes considered under this study are based on assumptions. Majority of building simulation programs are based on one dimensional heat transfer model and therefore the same is assumed in this work. A fully implicit time stepping scheme is utilized for all models since it is more stable regardless of the time step. The spatial discretization is based on the finite volume method and the harmonic average suggested by Patankar [75] for materials conductivity is used. Typical grid points for a system of wall layers using finite volume method are illustrated in **Figure 3.2**.

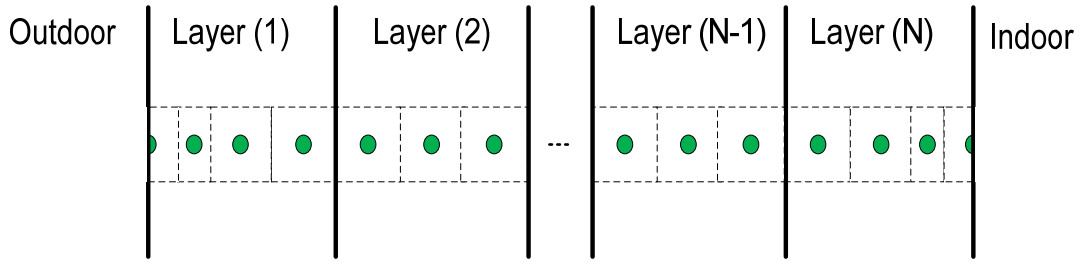

a) Grid points for a system of wall layers including internal and boundary nodes

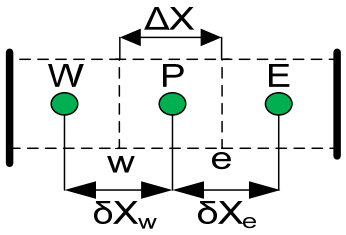

b) Typical grid points for the middle layer

Figure 3.2 Grid points location for Numerical models using Finite Volume Method

The convergence is declared using this relationship: $\text{error} = \left|\frac{\sum(T-T_{new})}{\sum(T_{new})}\right|$, where T is a vector of nodes temperature from previous iteration and T_{new} is the new results. This convergence relationship is adopted from EnergyPlus conduction finite difference solution

algorithm which was found to work satisfactory for heat capacity method. Under-relaxation is implemented for some models. For example, Voller et al. [48] recommended a value between 0.5-0.7 for heat source method. The study indicated that a factor in this range provides efficient convergence for both one- and two-dimensional cases. For all models developed in this section, the hysteresis and sub-cooling are not considered since they are negligible in common PCM used for building envelopes [209, 210].

For many PCMs, minimal design information pertained to the thermal characteristics such as melting temperature; melting range and latent heat are provided by manufactures. These design parameters are illustrated in **Figure 3.3**. Although the models described in this study can be solved with detailed h-T performance curve, a simplified h-T performance curve defined by four points is assumed. Other assumptions pertained to specific model is outlined when the scheme is described. In addition, boundary conditions will be described under each section as appropriate. The following sections outline the numerical discretization and calculation procedure using these three general methods.

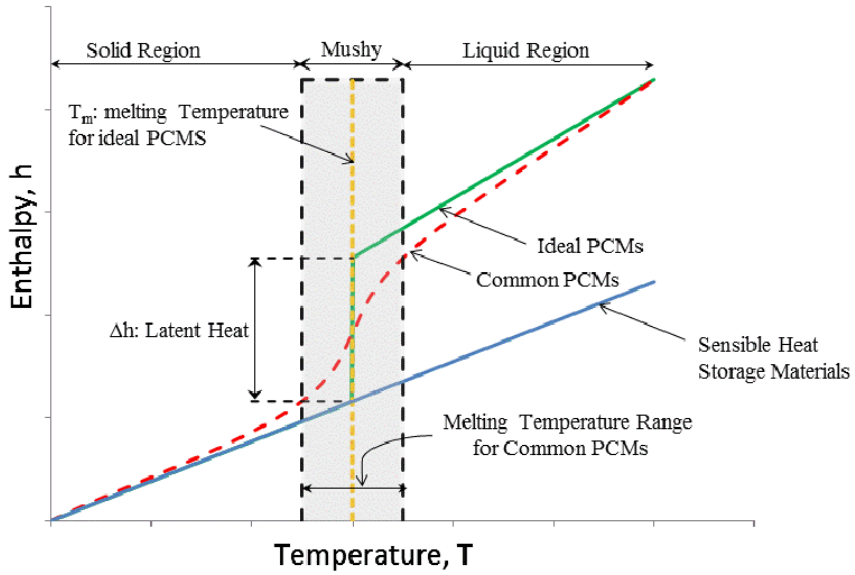

Figure 3.3 Enthalpy-Temperature (h-T) performance curve for ideal and common PCMs

3.3 Enthalpy Method

The general heat transfer model based on enthalpy method can be written as follows:

$$\rho \frac{\partial h}{\partial t} = \frac{\partial}{\partial x}\left(k \frac{\partial T}{\partial x}\right) \qquad \text{Equation 3-1}$$

Using **Figure 3.2**, a fully implicit control volume approximation is used. Therefore for internal nodes, Equation 3-1 can be discretized as follows:

$$\rho \frac{h_p^{n+1} - h_p^n}{\Delta t} = k_w \frac{T_w^{n+1} - T_p^{n+1}}{\Delta X * \delta X_w} + k_e \frac{T_e^{n+1} - T_p^{n+1}}{\Delta X * \delta X_e} \qquad \text{Equation 3-2}$$

Where:

n: indicate a time step, w: west node, p: point node, e: east node

Collecting terms and rearranges, Equation 3-2 becomes:

$$h_p^{n+1} = h_p^n + a_w * T_w^{n+1} + a_p * T_p^{n+1} + a_e * T_e^{n+1} \qquad \text{Equation 3-3}$$

Where:

$$a_w = \frac{k_w * \Delta t}{\rho * \Delta X * \delta X_w}, \quad a_e = \frac{k_e * \Delta t}{\rho * \Delta X * \delta X_e}, \quad a_p = -(a_w + a_e)$$

The discretized equation (Equation 3-3) is nonlinear since both h_p^{n+1} and T^{n+1} are unknown at this time step. Therefore, linearization technique is used to solve the equation using those techniques proposed by Patankar [75]. The h_p^{n+1} term can be expanded using Taylor series first order approximation:

$$h_p^{n+1} = h_p^n + C(T)^{n+1,m} * \left(T_p^{n+1} - T_p^n\right) \qquad \text{Equation 3-4}$$

At the start of simulation, the temperature fields are based on guess values. Hence, $\mathrm{C(T)}^{\mathrm{n+1,m}}$ (tentative values that will be updated at the beginning of the iteration) can be found using:

$$C(T) = \begin{cases} C_s & T \le T_m - \epsilon \\ \dfrac{C_s + C_l}{2} + \dfrac{L}{2\epsilon} & T_m - \epsilon < T < T_m + \epsilon \\ C_l & T \ge T_m + \epsilon \end{cases} \qquad \text{Equation 3-5}$$

When Equation 3-4 is substituted into Equation 3-3 and after rearrangement and collecting terms, the following linear discretized equation is derived:

$$a_w{}^{n+1,m} * T_w^{n+1,m+1} + a_p{}^{n+1,m} * T_p^{n+1,m+1} + a_e{}^{n+1,m} * T_e^{n+1,m+1} = R^{n+1,m} \qquad \text{Equation 3-6}$$

Where:

$$a_w{}^{n+1,m} = -\frac{k_w * \Delta t}{\rho * \Delta X * \delta X_w}, \qquad a_e{}^{n+1,m} = -\frac{k_e * \Delta t}{\rho * \Delta X * \delta X_e}$$

$$a_p{}^{n+1,m} = (C(T)^{n+1,m} + a_w{}^{n+1,m} + a_e{}^{n+1,m})$$

$$R^{n+1,m} = (h_p^n - h_p^{n+1,m} + C(T)^{n+1,m} * T_p^{n+1,m})$$

The discretized Equation 3-6 can be solved using different schemes as described in the following sections.

3.3.1 Generalized Enthalpy Method using Gauss–Seidel Solver

When no further numerical techniques are adopted, Equation 3-6 can be written in a general point form as follows:

$$T_p^{n+1,m+1} = \frac{1}{a_p{}^{n+1,m}} * [R^{n+1,m} - \sum a_w{}^{n+1,m} * T_w^{n+1,m+1} - \sum a_e{}^{n+1,m} * T_e^{n+1,m}] \qquad \text{Equation 3-7}$$

Equation 3-7 can be solved for $T^{n+1,m+1}$ using Gauss–Seidel algorithm. Once the temperature field is determined, the node enthalpies (h_p^*) are calculated using Equation 3-4. In order to avoid a numerical instability, under-relaxation factor (ω) is applied as follows:

$$h_p^{n+1,m+1} = \omega * h_p^* + (1 - \omega) * h_p^{n+1,m} \qquad \text{Equation 3-8}$$

The new node enthalpies are subsequently used in the next iteration. The iteration process continues until convergence is achieved. The iteration process is not complemented with a

correction step for this scheme compared to other schemes in the next sections. **Figure 3.4** shows how this algorithm is programmed in MATLAB/SIMULINK environment.

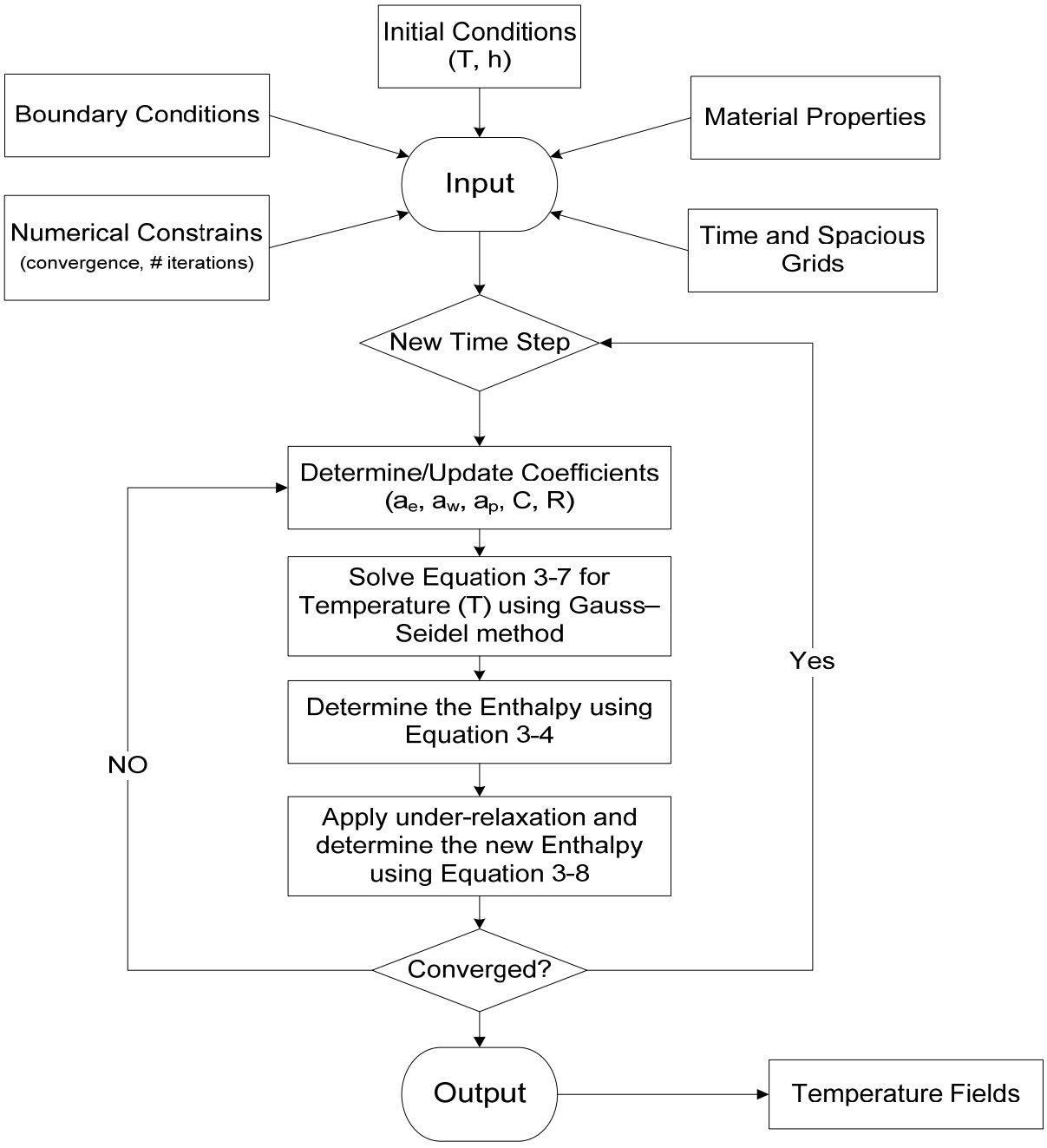

Figure 3.4 Flow chart of the calculation procedure implemented in MATLAB for the general enthalpy method using Gauss–Seidel Algorithm

3.3.2 Iterative Correction scheme using TDMA Solver

Following the generalized enthalpy method procedure above, the iterative correction scheme developed by Swaminathan and Voller [53] can be written in a matrix format to be solved by a direct solver. Equation 3-6 can then be written as:

$$[A]^{n+1,m} * T^{n+1,m+1} = R^{n+1,m} \qquad \text{Equation 3-9}$$

This equation can be solved for $T^{n+1,m+1}$ using Tri-diagonal matrix algorithm (TDMA). Once the temperature field is determined, the node enthalpies are updated based on Equation 3-4. At this iteration instant, the enthalpy is known and therefore the temperature field is corrected to be in consistent with enthalpy temperature performance curve using the following relationship[40]:

$$T_p = \begin{cases} \frac{h_p}{C_s} & , \quad h_p \le C_s * (T_m - \in) \\ \frac{h_p + \left[\frac{C_l - C_s}{2} + \frac{L}{2*\in}\right] * (T_m - \in)}{\left[\frac{C_l - C_s}{2} + \frac{L}{2*\in}\right]} & , \quad C_s * (T_m - \in) < h_p < C_l * (T_m + \in) + L \\ \frac{h_p - (C_s - C_l) * T_m - L}{C_l} & , \quad h_p \ge C_l * (T_m + \in) + L \end{cases} \qquad \text{Equation 3-10}$$

The iteration process in this prediction-correction cycle continues until convergence is achieved. **Figure 3.5** shows how this algorithm is programmed in MATLAB environment.

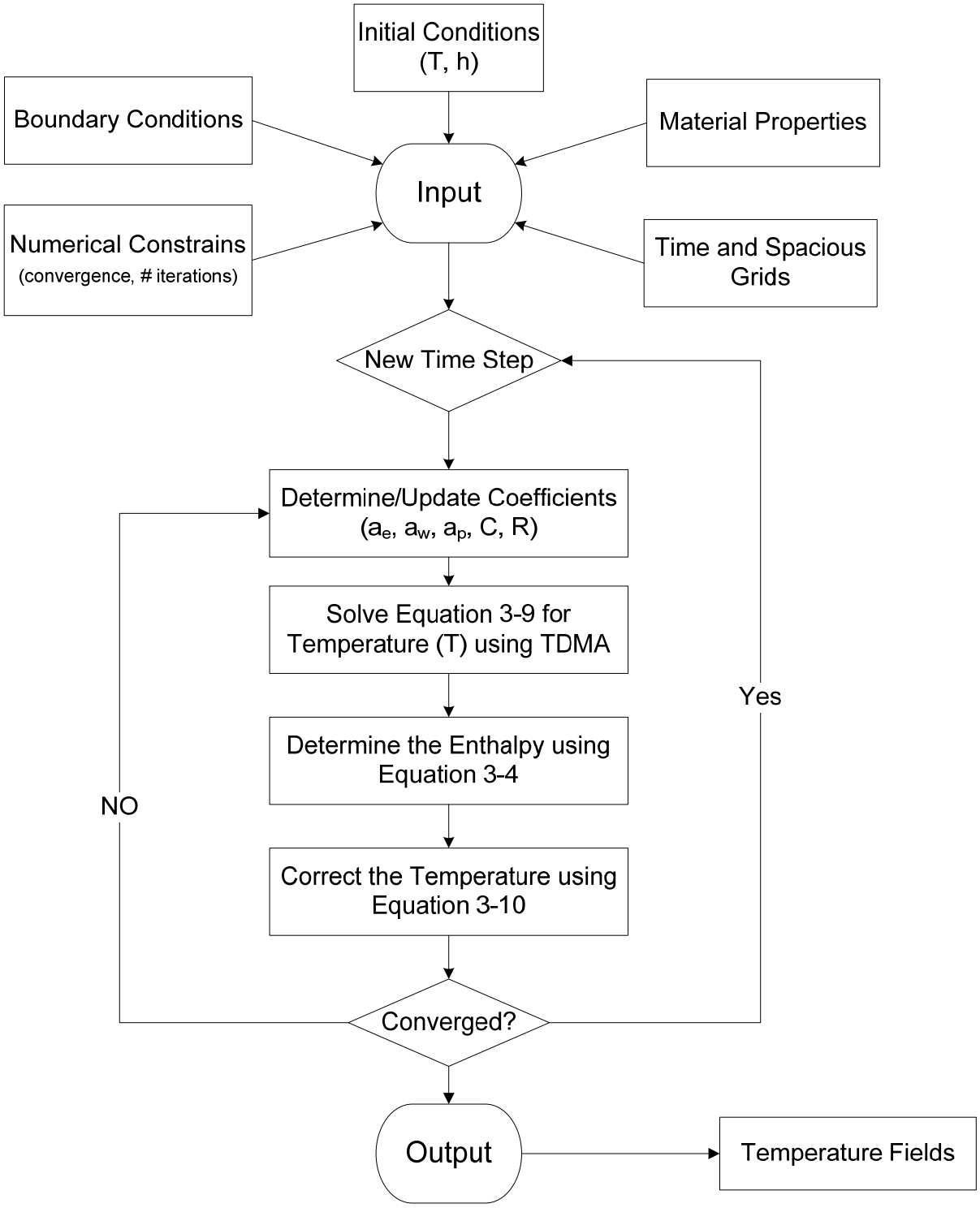

Figure 3.5 Flow chart of the calculation procedure implemented in MATLAB for the linearized enthalpy using Iterative correction scheme

3.3.3 Non-Iterative Correction scheme using TDMA Solver

The non-iterative scheme proposed by Pham [60] is similar to the previous one except that no iterations are attempted and therefore no convergence criterion is specified. The matrix coefficients are based on temperature from previous time step. For this reason, the scheme can be considered as a semi-implicit scheme. The discretized equation becomes:

$$a_w{}^n * T_w^{n+1} + a_p{}^n * T_p^{n+1} + a_e{}^n * T_e^{n+1} = R^n \qquad \text{Equation 3-11}$$

Where:

$$a_w{}^n = -\frac{k_w * \Delta t}{\rho * \Delta X * \delta X_w} \qquad a_e{}^n = -\frac{k_e * \Delta t}{\rho * \Delta X * \delta X_e} \qquad a_p{}^n = (C(T)^n + a_w{}^n + a_e{}^n)$$

$$R^n = (C(T)^n * T_p^n)$$

In a matrix format, Equation 3-11 can be written as:

$$[A]^n * T^{n+1} = R^n \qquad \text{Equation 3-12}$$

Using TDAM algorithm, the temperature field is solved and subsequently used to determine the enthalpy h_p^{n+1} using Taylor series expansion as per Equation 3-4. Once the enthalpy is determined, the temperature is corrected before proceeding to the next time step using Equation 3-10 . The matrix coefficients are subsequently updated for the next time step based on the corrected temperature field. **Figure 3.6** shows how this model is programmed in MATLAB.

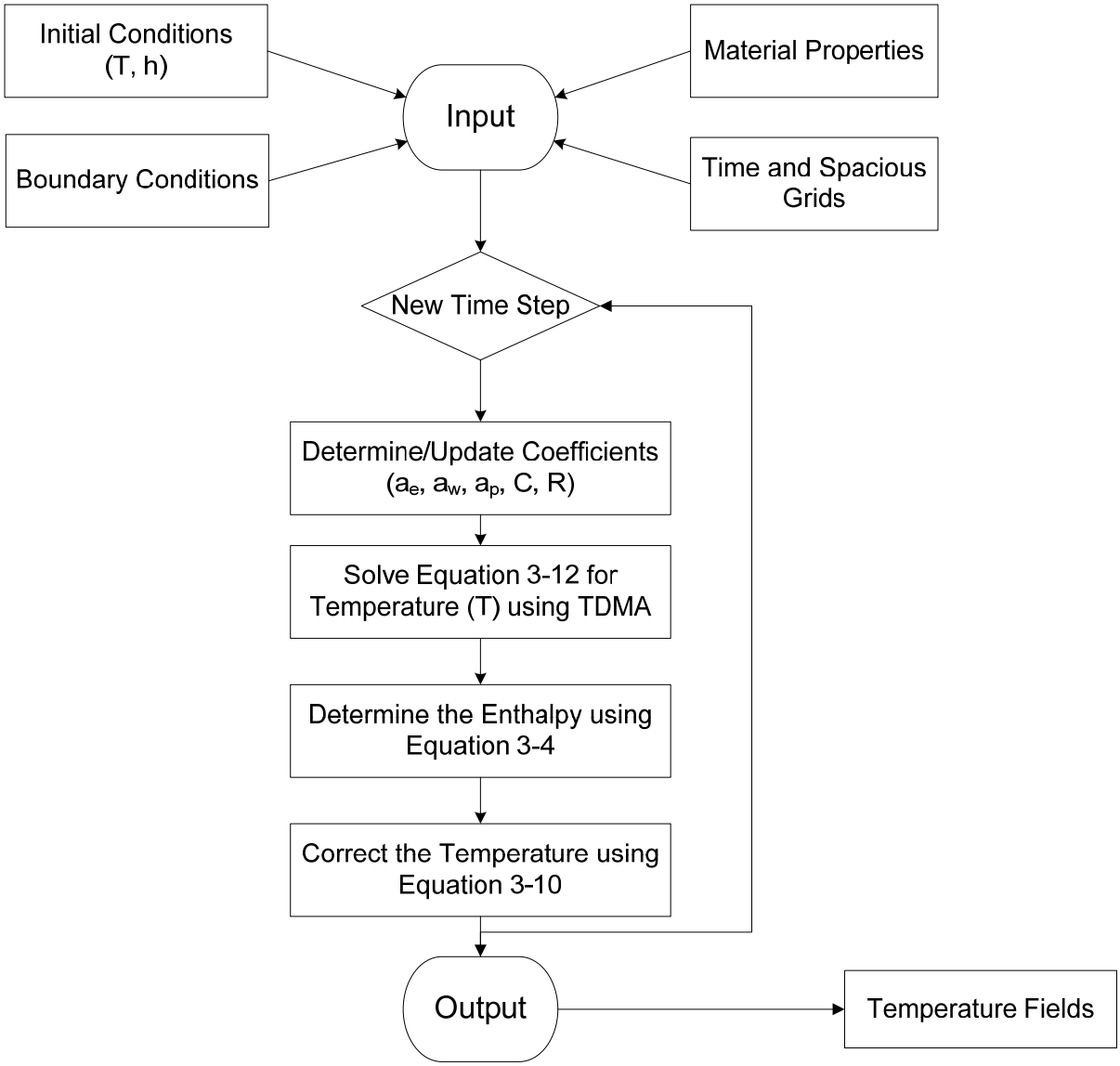

Figure 3.6 Flow chart of the calculation procedure implemented in MATLAB for the linearized enthalpy using non-Iterative correction scheme

3.3.4 **Development of Hybrid Correction Scheme using TDMA Solver**

In building simulations, energy systems are modeled on hourly bases using typical metrological weather data. When PCMs are incorporated into building systems, a sub-hourly simulation is required to accurately capture the latent heat liberation. Therefore, a quick but

energy conservative approach is highly demanded. Previous sections have outlined potential quick schemes that are commonly used to solve latent heat problems with few that fulfil the unique requirement of building simulations; the iterative correction scheme developed by Swaminathan and Voller [53] and non-iterative scheme proposed by Pham [60]. The prediction-correction cycles are demonstrated using h-T curve shown in **Figure 3.7**. **Figure 3.7** (a) shows the iterative correction scheme numerically progresses through solving the latent heat problem in two consecutive time steps when the PCM is going through solidification process. At first time step, the guess values of both temperature and enthalpy values (liquid state: point (a) in **Figure 3.7** (a)) are based on previous time step. Using this guess point for determining the matrix coefficients, the scheme predicts the new nodal temperature (point (b) in **Figure 3.7** (a)) and subsequently calculates the corresponding nodal enthalpy. Since the enthalpy is the same for any point on a horizontal line, the temperature is corrected using the h-T curve (point (c) on **Figure 3.7** (a)). This new enthalpy and temperature values are used as guess values for next time step. The scheme iterates going through the same process until convergence is achieved at this time step (point (e) on **Figure 3.7** (a)). For the next time step, the numerical solution follows the line a', b', c', d', e' in **Figure 3.7** (a) as it did in the first time step until convergence is achieved. The number of iterations depends on the convergence limit. For this scheme, it is observed that there are unnecessary iterations since the slope is the same if a PCM doesn't change a state. On the other hand, **Figure 3.7** (b) demonstrates how the non-iterative correction scheme solves the latent heat problem. The same calculation procedure as that for the iterative correction scheme is adopted except that the solution is reached in a single correction step. The matrix coefficients are based on previous time step solutions and therefore there is a risk of reaching inaccurate results. This risk is not substantial when a node is on a single state but signifies as the node's state

progresses from one state (say a liquid) to a different state (say a mushy). The correction step adopted by both schemes makes the numerical solution fast since direct solvers can be utilized. Iteration process, on the other hand, makes the solution robust and rigorous since the energy is balanced at each time step. The new scheme should therefore be based on these two features for modeling phase change materials in future generations of building simulation tools.

Figure 3.7 (c) shows the proposed improvement for a new scheme that combines the features of both schemes. The hybrid correction scheme iterates the solution when at least one PCM's node enters or leaves a state. The scheme is not iterative during the time period when all nodes are at one state (solid, liquid or mushy region). Since the slope of the simplified h-T curve doesn't change during a state, the iterations are not necessary. Therefore, a checking step is introduced to determine the current slope (the slope is the specific heat) for each node using Equation 3-5. If the slope is constant (i.e. the specific heat is the same for all PCM's nodes during a time step), then the solution advances to the next time step otherwise iterate the solution until the slope is constant between iterations. Therefore, the number of iterations decreases when compared to the iterative correction scheme since it mimics the non-iterative correction scheme feature. On the other hand, the scheme iterates the solution when a node enters or leaves a state, making it conservative as the case with the iterative correction scheme.

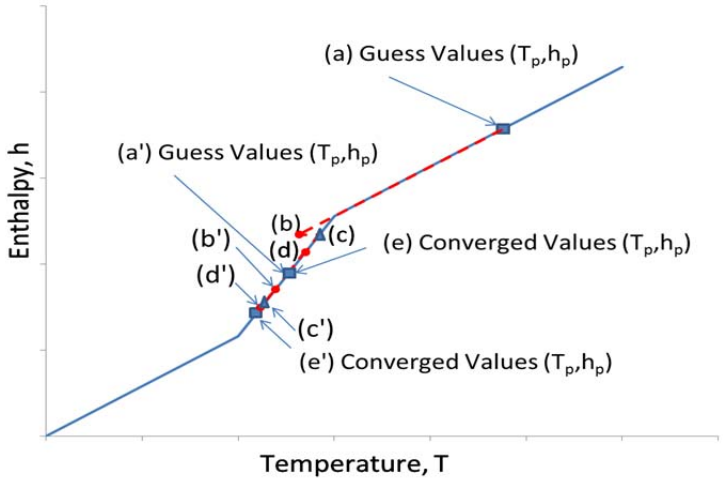

a) Iterative Correction Scheme

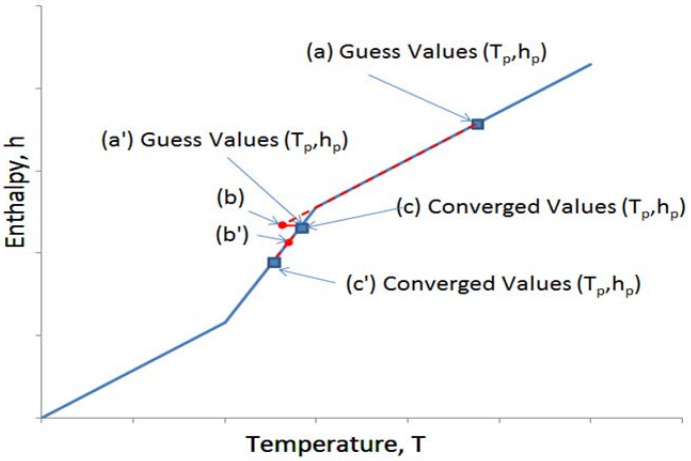

b) Non-iterative Correction Scheme

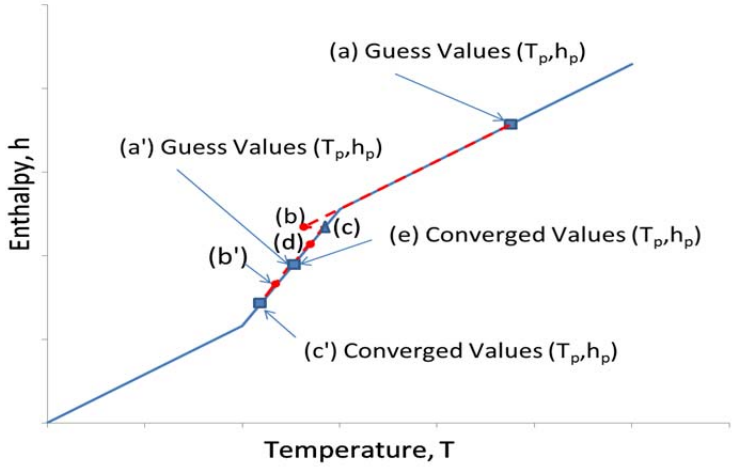

c) Hybrid Correction Scheme

Figure 3.7 Advances of numerical solutions using correction schemes during two consecutive time steps

Therefore, this approach switches between the corrective iterative and non -iterative scheme based on the state of the node. **Figure 3.8** shows the calculation procedure for this scheme in MATLAB.

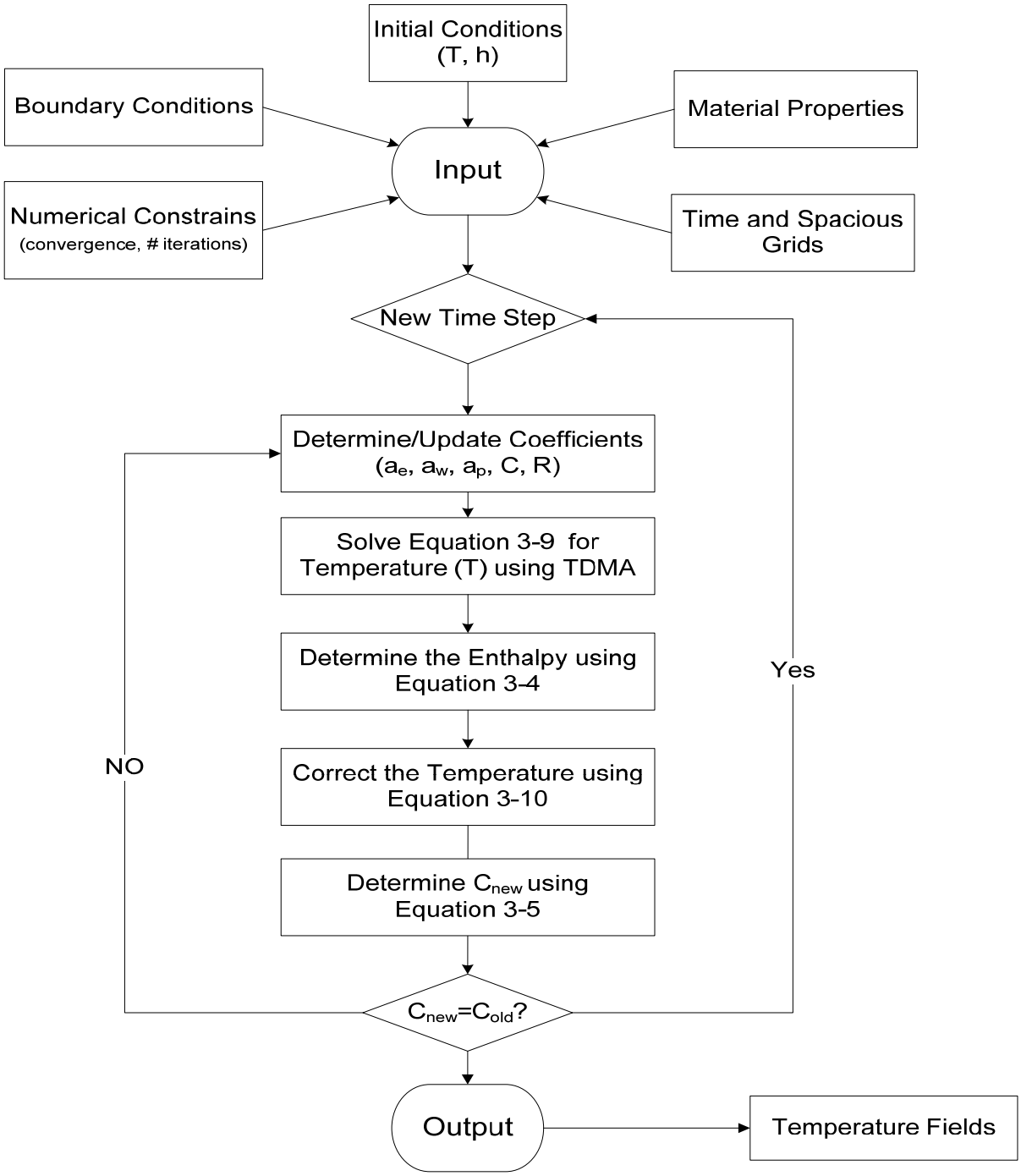

Figure 3.8 Flow chart of the calculation procedure implemented in MATLAB for the linearized enthalpy using hybrid correction scheme

3.4 Heat Capacity Method

The heat capacity term in the governing equation imitates the effect of enthalpy (sensible and latent heat) by increasing the heat capacity value during the phase changing stage. Therefore, Equation 3-1 is reformulated so that the governing equation is written in terms of a single unknown variable with a non-linear coefficient (in this case the apparent heat capacity). Hence, Equation 3-1 can be written:

$$\rho \frac{\partial h}{\partial T} * \frac{\partial T}{\partial t} = \frac{\partial}{\partial x}\left(k \frac{\partial T}{\partial x}\right) \qquad \text{Equation 3-13}$$

Where:

$\frac{\partial h}{\partial T} = C^A(T)$

In a similar fashion to the enthalpy method, Equation 3-13 is discretized and can be represented in point form using Gauss-Seidel iteration method as:

$$T_p^{n+1,m+1} = \frac{1}{{a_p}^{n+1,m}} * [R^{n+1,m} - \sum {a_w}^{n+1,m} * T_w^{n+1,m+1} - \sum {a_e}^{n+1,m} * T_e^{n+1,m}] \qquad \text{Equation 3-14}$$

Where:

$${a_w}^{n+1,m} = -\frac{k_w * \Delta t}{\rho * \Delta X * \delta X_w} \quad , \qquad {a_e}^{n+1,m} = -\frac{k_e * \Delta t}{\rho * \Delta X * \delta X_e}$$

$${a_p}^{n+1,m} = (C^A(T) + {a_w}^{n+1,m} + {a_e}^{n+1,m}) \, , \; R^{n+1,m} = \; ({C^A}^{n+1,m} * T_p^n)$$

The subscript *"n+1"* represents the current time step, *"n"* means the previous time step, *"m+1"* is the current iteration and *"m"* is the previous iteration. When using Gauss–Seidel method, the solution sweeps from west node to east node. Therefore, the solution for the point node will be based on the updated value of west node but still use an old value from previous iteration for the east node. The solution iterates until convergence is achieved. The apparent heat capacity term can be evaluated using the temporal averaging proposed by Morgan [87] and is represented by the following equation :

$$C^{A^{n+1,m}} = \frac{\Delta h}{\Delta T} = \frac{h^{n+1,m} - h^{n}}{T^{n+1,m} - T^{n} + 10^{-6}}$$ Equation 3-15

In order to avoid division by zero in Equation 3-15, a value of "10^{-6}" is added to the denominator. Alternatively, the discretized Equation 3-14 can be solved using TDMA algorithm[118]. It must be mentioned, however, that the solution might not converge at higher time step and small time step is necessary when TDMA is used. **Figure 3.9** shows the flow chart of the programmed method in MATLAB.

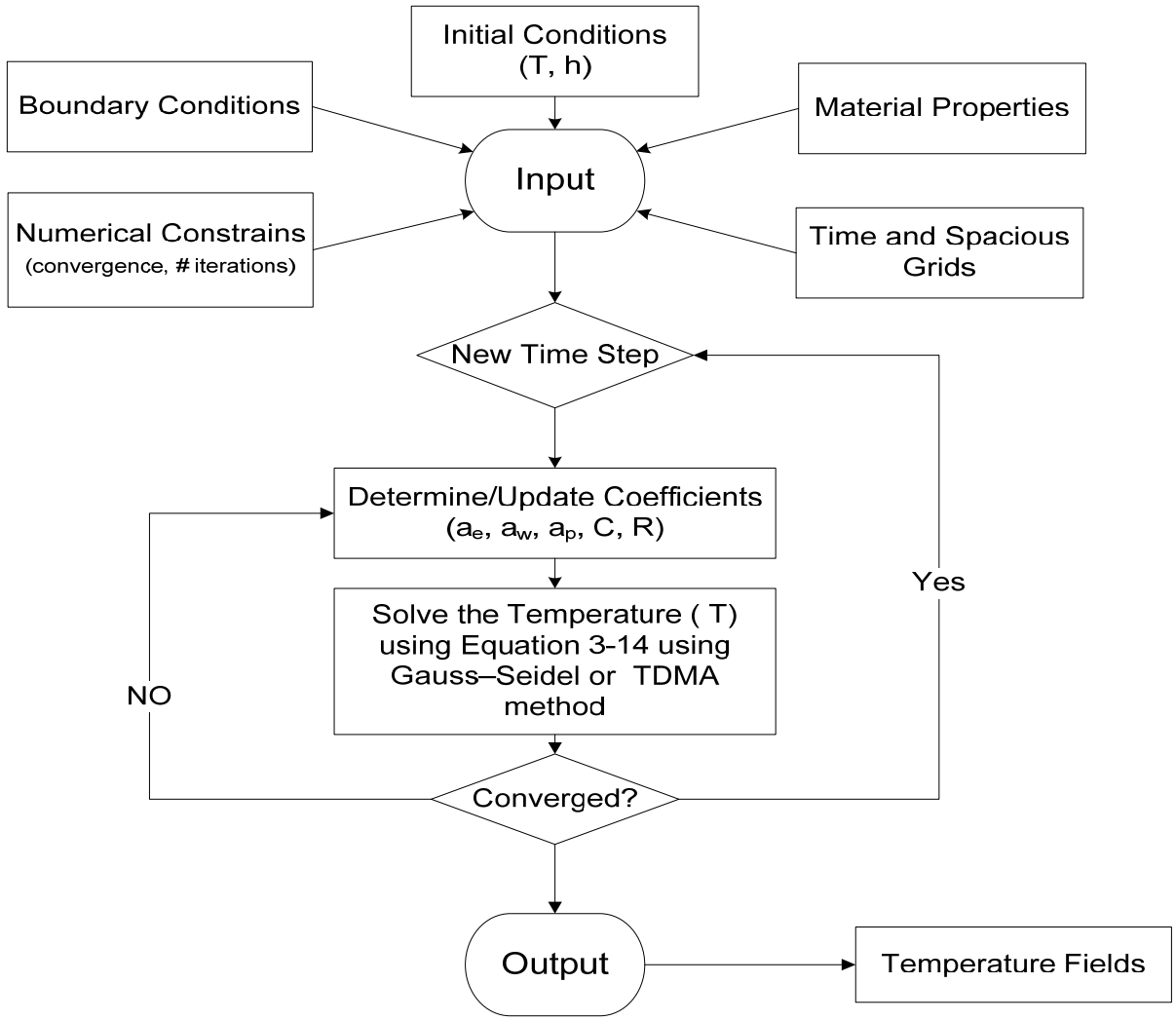

Figure 3.9 Flow chart of the calculation procedure implemented in MATLAB for the heat capacity method

3.5 Heat Source Method

In a common approach proposed by Swaminathan and Voller [48, 67] to deal with PCMs with mushy regions, the heat equation using the heat source method can be written as:

$$\rho * C_{avg} * \frac{\partial T}{\partial t} = \frac{\partial}{\partial x}\left(k\ \frac{\partial T}{\partial x}\right) - \rho * L * \frac{\partial f_l}{\partial t} \qquad \text{Equation 3-16}$$

Where:

f_l: liquid volume fraction, , C_{avg}: volume averaged specifc heat capacity, L: $latent\ heat$

Liquid fraction "f_l" can be evaluated using the following liquid fraction-temperature relationship assuming that there is a linear evolution of the latent heat over the phase change range [211]:

$$f_l = \begin{cases} 1, & \text{if } T > T_L \\ \frac{(T-T_s)}{(T_L-T_s)}, & \text{if } T_s \le T \le T_L \\ 0, & \text{if } T < T_s \end{cases} \qquad \text{Equation 3-17}$$

Where: T_s: Solidus Temperature (i. e. $T_m - \in$), T_L: Liquidus Temperature (i. e. $T_m + \in$), T_m: melting Temperature, $\in$: half phase change temperature range

Similar to Heat capacity method, when Equation 3-16 is discretized using fully implicit method, it becomes:

$$T_p^{n+1,m+1} = \frac{1}{{a_p}^{n+1,m}} * [R^{n+1,m} - \sum {a_w}^{n+1,m} * T_w^{n+1,m+1} - \sum {a_e}^{n+1,m} * T_e^{n+1,m}] \qquad \text{Equation 3-18}$$

Where:

$${a_w}^{n+1,m} = -\frac{k_w * \Delta t}{\rho * \Delta X * \delta X_w}\ ,\ {a_e}^{n+1,m} = -\frac{k_e * \Delta t}{\rho * \Delta X * \delta X_e},$$

$${a_p}^{n+1,m} = \left(C_{avg} + L * \frac{df}{dT}\Big|_{f^m} + {a_w}^{n+1,m} + {a_e}^{n+1,m}\right)\ ,$$

$$R^{n+1,m} = C_{avg} * T_p^n + L * \left(f_{l,p}^n - f_{l,p}^{n+1,m} + \left.\frac{df}{dT}\right|_{f^m} * T_p^{n+1,m}\right)$$

The term $\left.\frac{df}{dT}\right|_{f^m}$ is evaluated based on previous two iterations using the numerical approximation approach:

$$\left.\frac{df}{dT}\right|_{f^m} = \begin{cases} \frac{f_{l,p}^{n+1,m} - f_{l,p}^{n+1,m-1}}{T_p^{n+1,m} - T_p^{n+1,m-1} + 10^{-6}}, & \text{if } 0 < f_{l,p}^{n+1,m} < 1 \\ 0, & \text{if } f_{l,p}^{n+1,m} = 1 \text{ or } f_{l,p}^{n+1,m} = 0 \end{cases} \qquad \text{Equation 3-19}$$

In order to avoid division by zero in Equation 3-19, a value of "10^{-6}" is added to the denominator. After solving for temperature field at all nodes, the liquid fraction field is updated which is a key to this scheme.

$$f_{l,p}^{n+1,m+1} = f_{l,p}^{n+1,m} + \omega * SLOPE * \left(T_p^{n+1,m+1} - T_p^{n+1,m}\right) \qquad \text{Equation 3-20}$$

Where:

$$SLOPE = \begin{cases} \left.\frac{df}{dT}\right|_{f^m}, & \text{if } 0 < f_{l,p}^{n+1,m} < 1 \\ \frac{C_{avg}}{L}, & \text{if } f_{l,p}^{n+1,m} = 1 \text{ or } f_{l,p}^{n+1,m} = 0 \end{cases}$$

ω: under − relaxation factor $(0.5 - 0.7)$ [48]

Practically, the update is done for all nodes including those that don't undertake phase change. Therefore, an under-shoot/over-shoot correction is applied to ensure that fluid fraction takes values between 0 and 1 using the following relation:

$$f_{l,p}^{n+1,m+1} = \begin{cases} 0, & \text{if } f_{l,p}^{n+1,m+1} < 0 \\ 1, & \text{if } f_{l,p}^{n+1,m+1} > 1 \end{cases} \qquad \text{Equation 3-21}$$

Before proceeding to the next iterations, the temperature field must also be corrected for the case when the nodes are in the mushy region using the following relationship:

$$T_p^{*,n+1,m+1} = \begin{cases} T_p^{n+1,m+1}, & \text{if } f_{l,p}^{n+1,m+1} < 0 \text{ or } f_{l,p}^{n+1,m+1} > 1 \\ T_s + f_{l,p}^{n+1,m+1} * (T_L - T_s), & \text{if } 0 < f_{l,p}^{n+1,m+1} < 1 \end{cases}$$ Equation 3-22

Alternatively, the temperature can be corrected using Equation 3-10 after determining the enthalpy using the following equation:

$$h_p^{n+1,m+1} = C_{avg} * T_p^{n+1,m+1} + f_{l,p}^{n+1,m+1} * L$$ Equation 3-23

Then, the iteration process is repeated until convergence is attained. When arranged in a matrix format, the discretized Equation 3-18 can be solved using TDMA algorithm. Similar to the heat capacity method, the solution might not converge at higher time step and small time step is necessary when TDMA is used. **Figure 3.10** shows how this method is implemented in MATLAB.

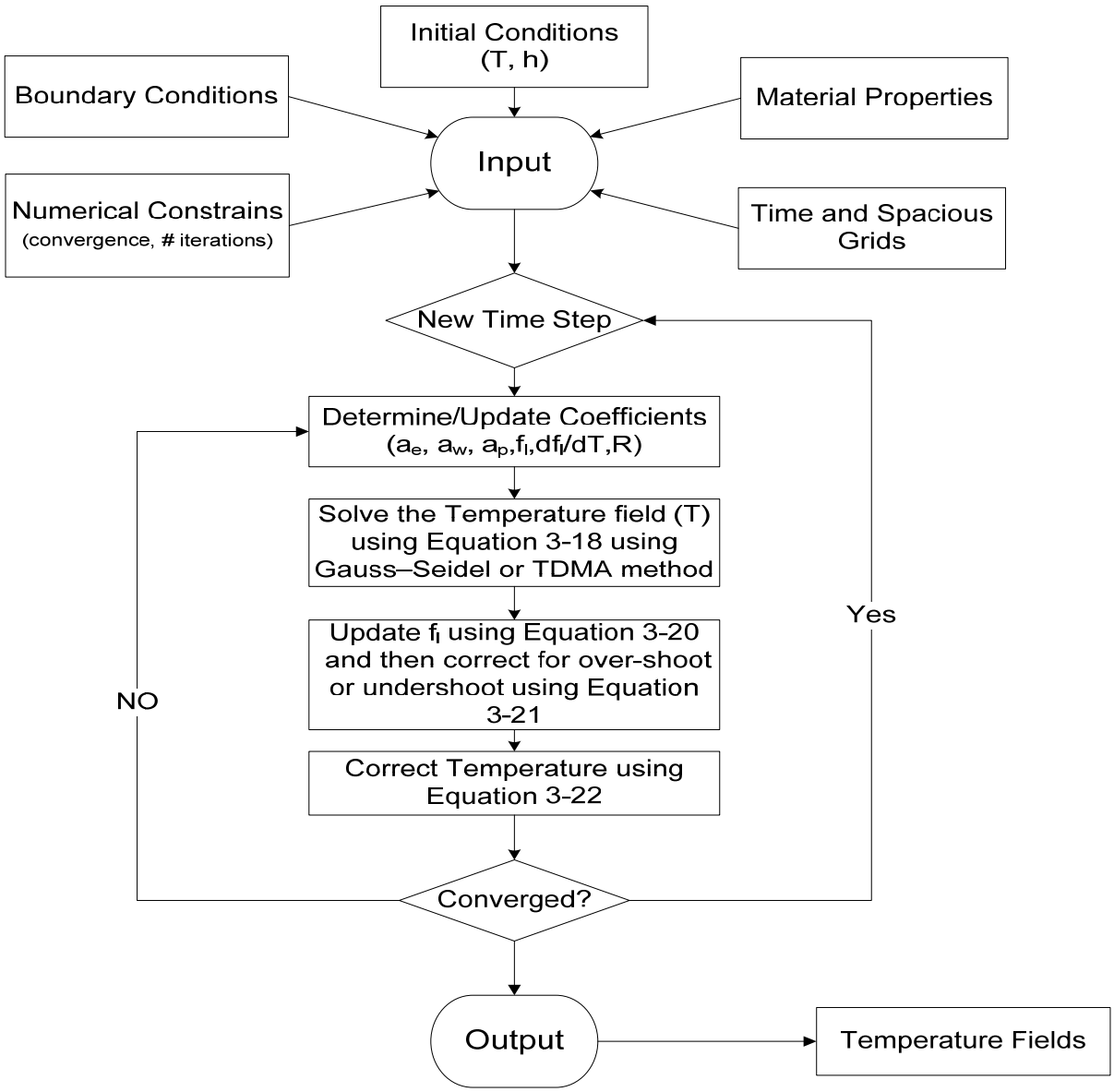

Figure 3.10 Flow chart of the calculation procedure implemented in MATLAB for the heat source method using iterative method

3.6 Verification and Validation of Numerical Models

Buildings are exposed to environmental conditions such as outside air temperature, wind, and solar radiations. The exterior envelope exchanges heat with the environment via convection heat transfer, short wave radiation and long wave radiation. Since these phenomena are nonlinear, analytical solutions are difficult to develop. In particular, there is no analytical

solution for heat transfer associated with phase change that takes into account the above variables. However, there exists a toolkit that was developed under ASHRAE 1052 research project framework [212]. The toolkit contains several analytical solutions that can be used to verify newly developed numerical models of heat transfer without the phase change for building's fabrics. Alternatively, experimental results from lab cells or field studies can be used to validate the numerical models. The accuracy of the results is however dependent on instrumentation used. In addition, software-software comparison can also be used for verification purposes. All these approaches have been used to verify and validate the models developed in this research. **Table 3-1** summarizes the characteristics of the tested numerical methods, schemes, and solvers. Although not optimized, Under-relaxation factor is used for schemes that have shown numerical instabilities.

Table 3-1 Characteristics of the tested numerical methods and schemes

Method	Solver	Scheme Identification	Correction Step	Under-relaxation
Enthalpy Method (EM)	G-S	Generic (EM_Generic_GS)	No	Yes (=0.8)
	TDMA	Iterative Correction Scheme (EM_ICS_TDMA)	Yes	No
	TDMA	Hybrid Correction Scheme (EM_HCS_TDMA)	Yes	No
	TDMA	Non-Iterative Correction Scheme (EM_NIC_TDMA)	Yes	No
Heat Capacity Method (HCM)	TDMA	HCM_TDMA	No	No
	G-S	HCM_GS	No	No
Heat Source Method (HSM)	TDMA	HSM_TDMA	Yes	Yes (=0.5)
	G-S	HSM_GS	Yes	Yes (=0.5)

G-S: Gauss-Seidel, TDMA: Tri-Diagonal Matrix Algorithm

3.6.1 Verification Case1: Transient Conduction at Step Response

For this testing, the case of *"Test TC2: Transient Conduction – Step Response"* from ASHRAE 1052 project framework [212] was selected. The case determines the response of a single wall layer in terms of its indoor and outdoor surface temperatures. The fabric is exposed to outdoor air temperature that follows a step function which changes from initial temperature at two periods (period 1: 2160-2260 hrs [90-94 days] and period 2: 4320-4420 hrs [180-184 days]) as shown in **Figure 3.11** and when the indoor temperature is kept constant. In addition, outside convection and inside convection are considered but no solar radiation is considered. **Table 3-2** summarizes the parameters used for this test case.

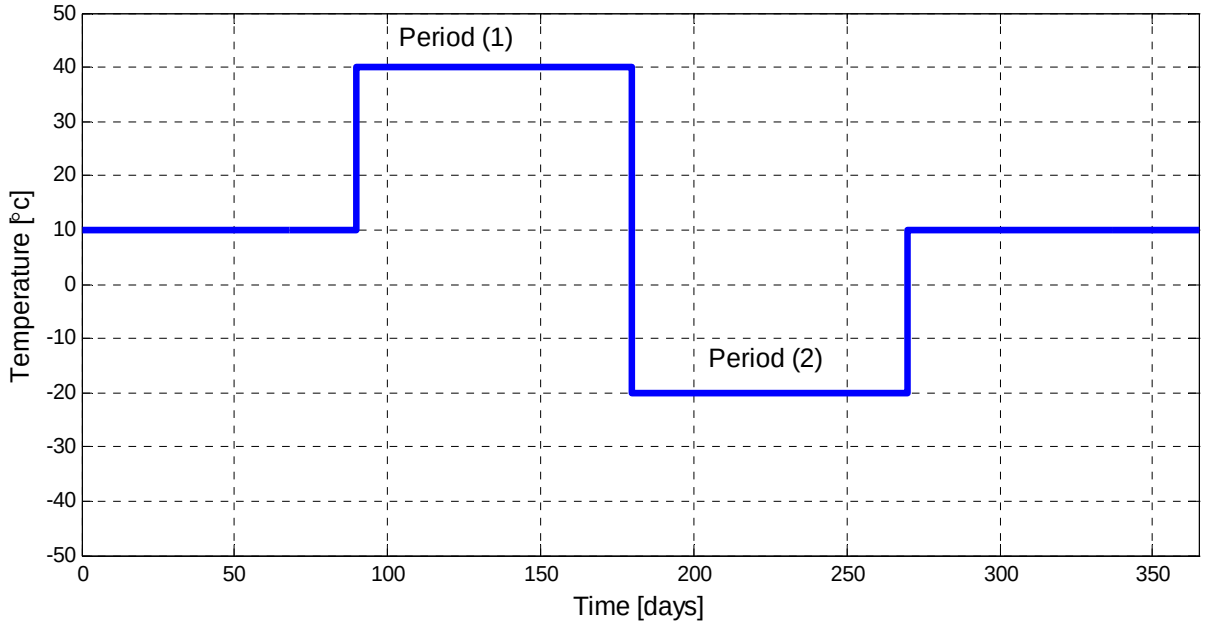

Figure 3.11 Step function of outdoor air temperature for a yearly simulation

Table 3-2 Parameters used for ASHRAE Test Case TC2 [212]

Test Parameter	Value	Units
Thermal Conductivity	0.14	W/m.K
Density	500	Kg/m^3
Specific Heat Capacity	2500	J/kg.K
Thickness	0.1	m
Initial Temperature	10	˚C
Temperature Step	30	˚C
External Convective Heat transfer Coefficient	2.607	$W/m^2.K$
Internal Convective Heat transfer Coefficient	3.18	$W/m^2.K$

At initial stage of this research, a heat transfer code based on implicit time stepping was developed and verified against this test case. This program was later used as a template file to develop other numerical schemes where phase change is considered. The main program was modified to accommodate similar parameters and boundary conditions as those used in the analytical solution. **Figure 3.12** shows the performance of the numerical solution to that of the analytical. Despite that the time step is 1 hour; the numerical solutions show a good fit to those from the analytical one.

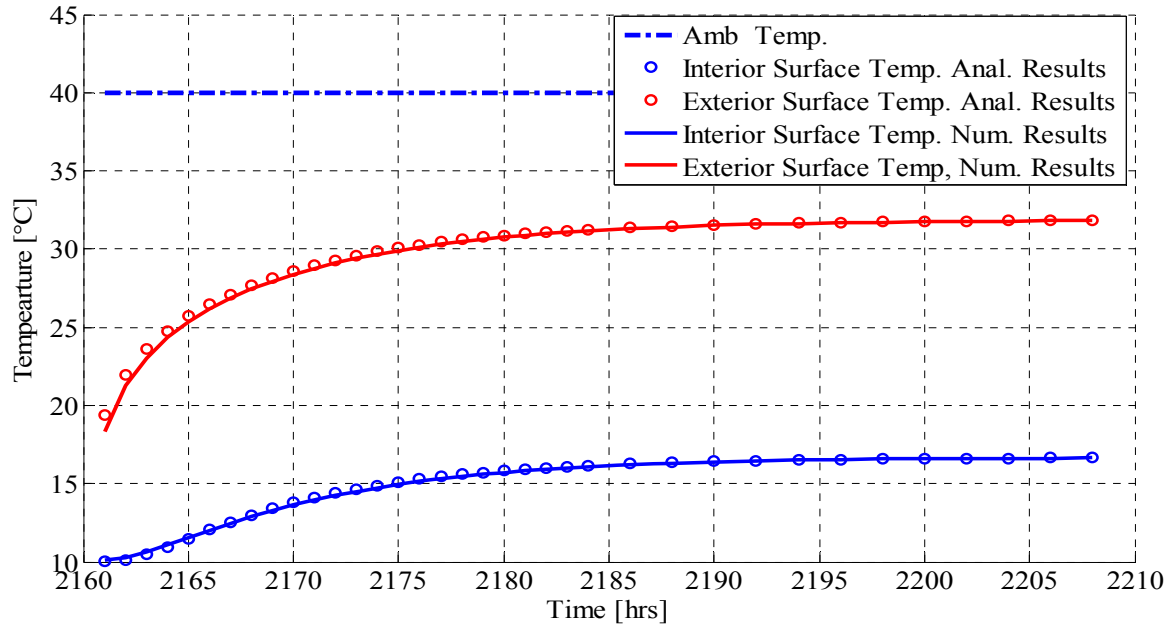

a) Numerical Results against Analytical for Period 1

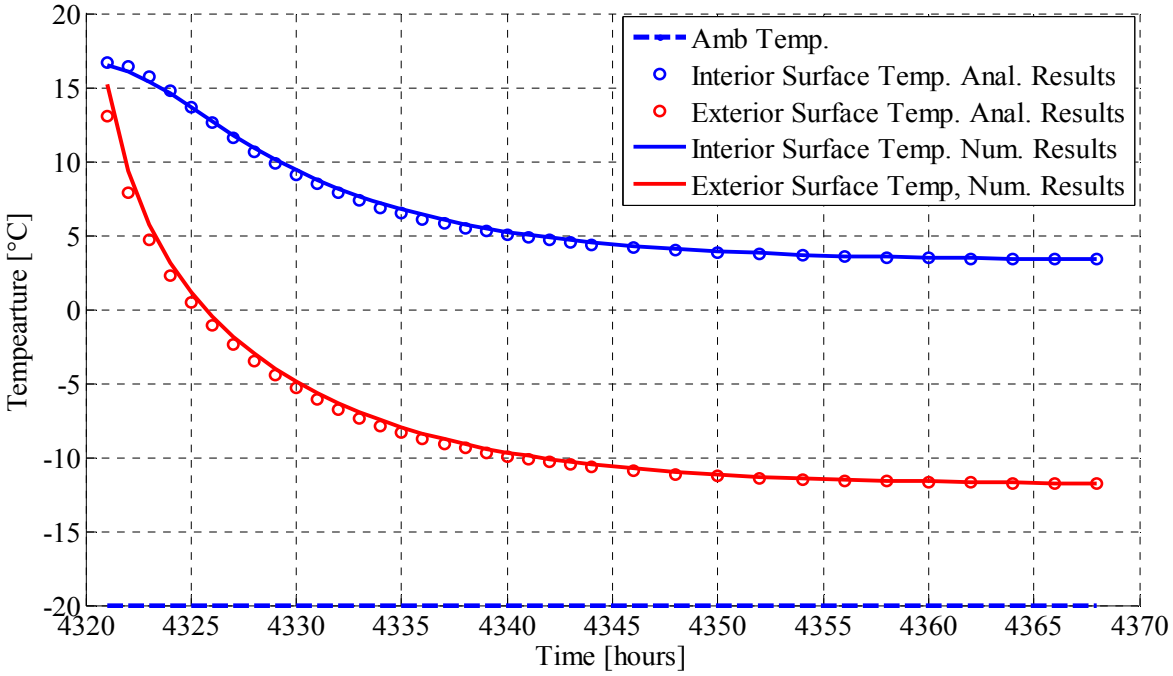

b) Numerical Results against Analytical for Period 2

Figure 3.12 Verification of the numerical solution with ASHRAE-1052 Test Case-2 for time step is 1 hr

3.6.2 Verification Case 2: Multi-layer wall under sinusoidal temperature profile

This case "*Test* TC3*: Transient Conduction – Sinusoidal Driving Temperature and Multi-layer Wall"* ASHRAE 1052 project framework [212] was used to determine the response of a multilayer wall when exposed to outside temperature that follows a steady-periodic sinusoidal function. The indoor air temperature is fixed to 20 °C, outside and inside convection is considered. **Table 3-3** summarizes the input for this case. **Figure 3.13** shows the comparison between the numerical and analytical solutions. The figure shows that the numerical solutions are close to the analytical solution. This is predictable since all the models are used for materials when no latent heat is involved.

Table 3-3 Parameters used for ASHRAE Test Case TC3 [212]

Test Parameter	Value			Units
	Layer 1 (inside)	Layer 2	Layer 3 (outside)	
Thermal Conductivity	0.14	0.1	0.2	W/m.K
Density	700	50	500	Kg/m^3
Specific Heat Capacity	500	200	800	J/kg.K
Thickness	0.1	0.05	0.1	m
Initial Temperature	20			˚C
Temperature Step	15			˚C
External Convective Heat transfer Coefficient	1.81			$W/m^2.K$
Internal Convective Heat transfer Coefficient	3.18			$W/m^2.K$

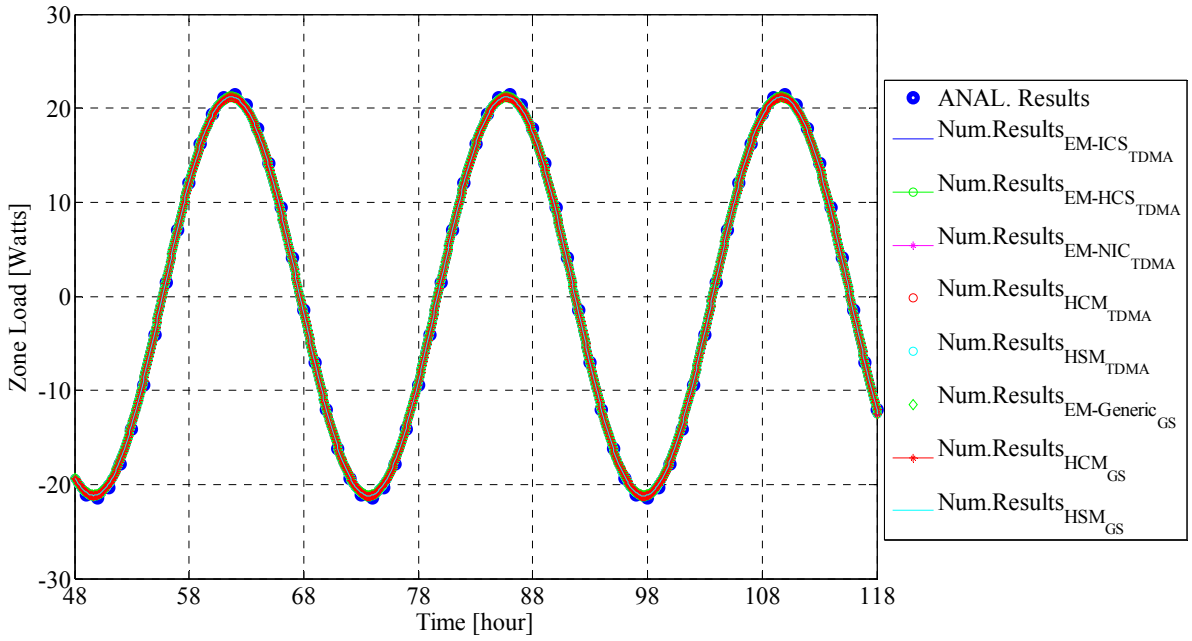

Figure 3.13 Verification of the numerical solution with ASHRAE-1052 Test Case-3

3.6.3 Validation using Experimental Results

In order to quantify the benefits of PCMs under dynamic environmental conditions, lab tests, field studies or actual implementation in large scale buildings are considered. The results from these studies can be used as bases for model's validations. For this work, experimental results from Sunliang [213] are used to validate the developed numerical models. The same experimental results have been used to validate the PCM algorithm in EnergyPlus [35]. The experimental work with the PCM integrated wall was conducted in the NTNU/SINTEF Building and Infrastructure Laboratory. **Figure 3.14** shows a schematic of the test chamber used, wall configuration and temperature sensor locations inside the wall panel. **Table 3-4** summarizes the material properties used in this validation. **Figure 3.15** shows the temperature enthalpy performance curve for the PCM product used in this experimental work. **Figure 3.16** reports the

boundary condition on both sides of the wall. The thermal properties of wall assembly are documented in these references [35, 213, 214]. The thermocouples have an accuracy of ±0.1 ºC and the data are recorded at 10 minutes time intervals.

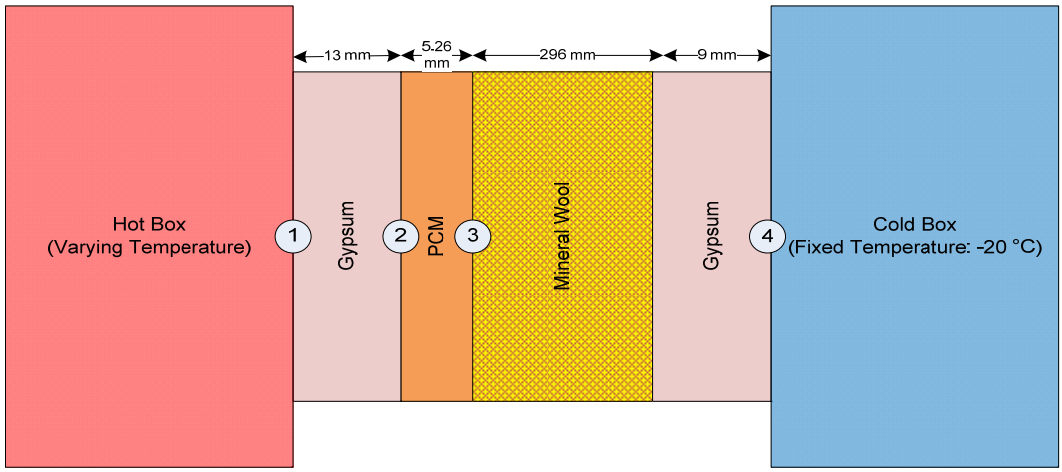

Figure 3.14 Environmental chamber with wall configurations and temperature sensors location

Table 3-4 Thermal properties of materials used in the tested PCM wall assembly

Material	Thermal Conductivity [W/(m.K)]	Density [kg/m^3]	Thickness [m]	Heat Capacity [J/(kg.K)]	Latent Heat [kJ/kg]	Ref.
Gypsum	0.21	700	0.009 at cold side 0.013 at hot side	1000		[214]
PCM,(DuPont Energain)	0.18	856	0.00526	836.8	Calculated from **Figure 3.15** using numerical approach	[35, 213]
Mineral Wool	0.037	16	0.296	1030		[214]

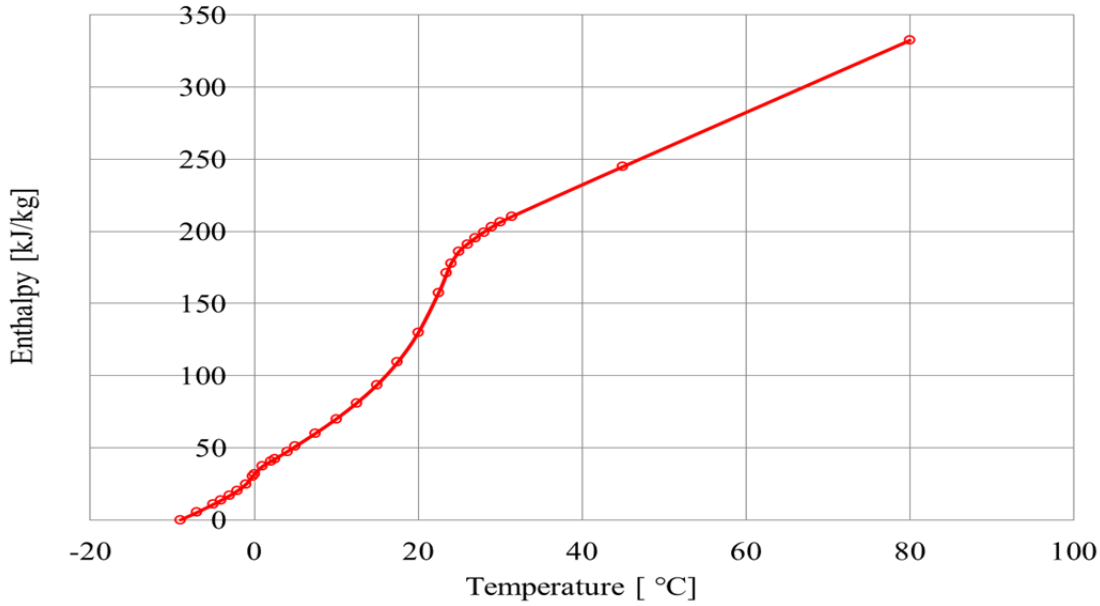

Figure 3.15 Temperature-Enthalpy performance curve for DUPont Energain PCM Panel

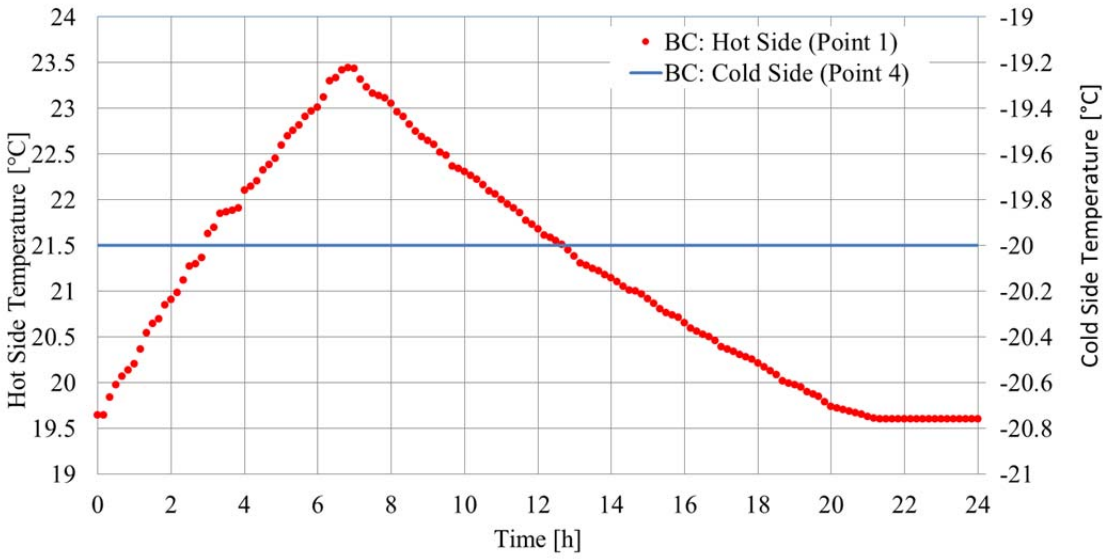

Figure 3.16 Boundary conditions applied at hot and cold sides of the wall panel

The numerical models developed for PCMs simulations (refer to **Table 3-1**) were exposed to the boundary conditions (refer to **Figure 3.16**) and using the materials properties used in the experiment. Since the experimental results are reported for 10 minutes, the simulation time

step is also similar. **Figure 3.17** shows the temperature profiles at two points where PCM layer is located (point 2 and 3 in **Figure 3.14**). All models show good agreement with the experimental results except the non-iterative correction scheme proposed by Pham. Although this method is quick, it is inaccurate at time step of 10 minutes. This drawback has been eliminated using the hybrid scheme proposed under this research.

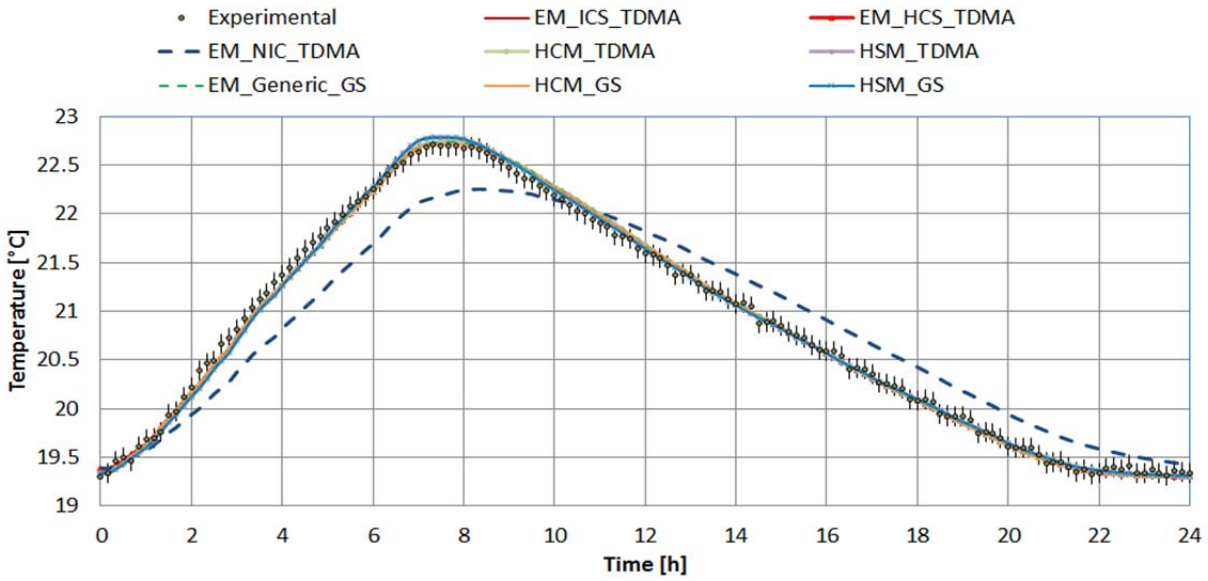

a) Temperature profile at point 2

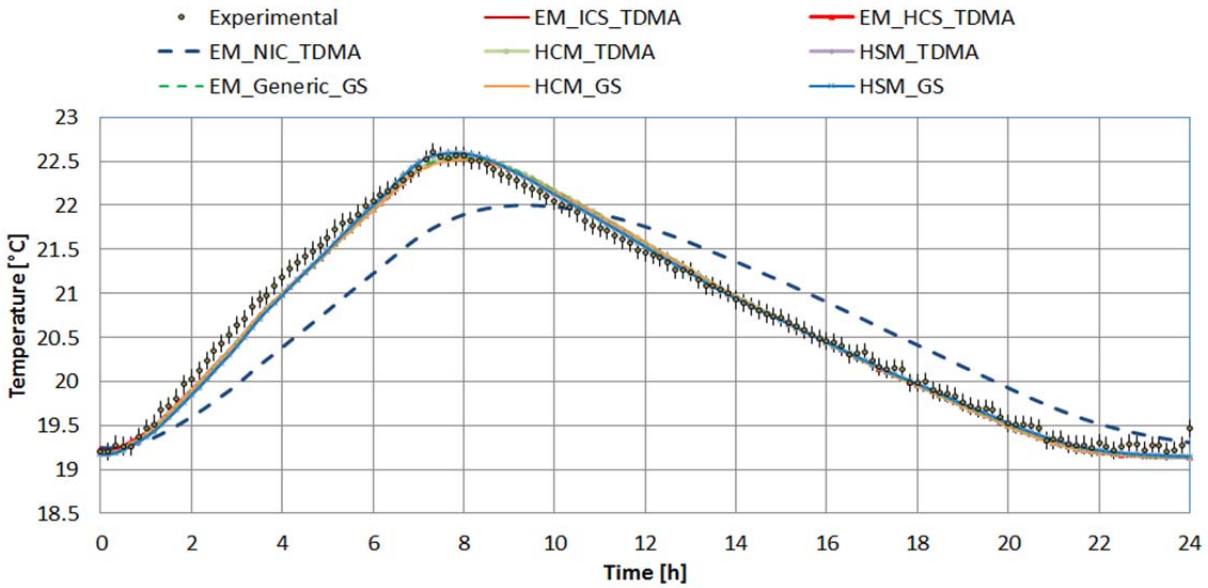

b) Temperature profile at point 3

Figure 3.17 Validation of numerical models with experimental results

The number of iterations for all models is recorded as shown in **Figure 3.18**. The schemes that use direct solvers take less iteration than iterative solvers as expected.

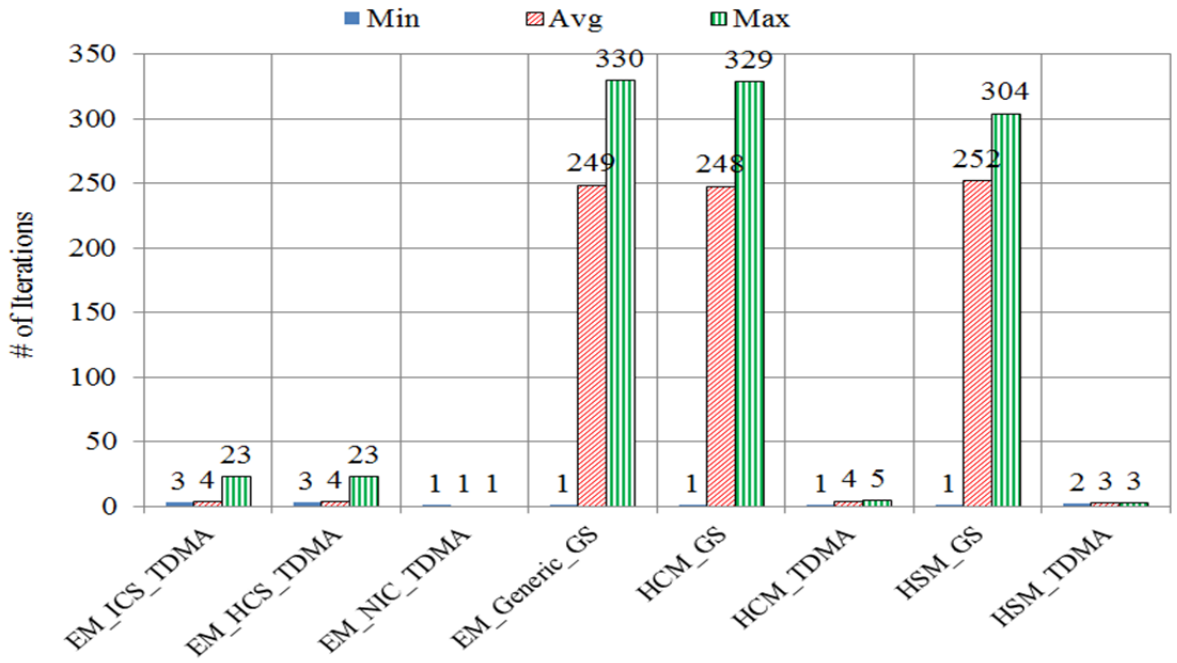

a) Min, Avg and Max number of iterations

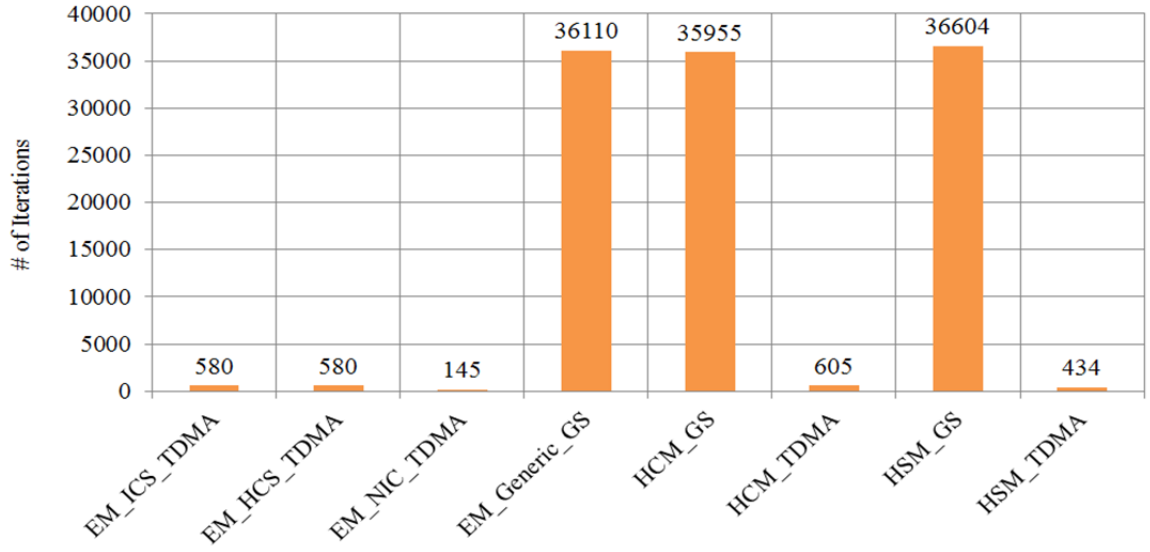

b) Total Number of Iterations

Figure 3.18 Number of Iterations for the numerical models

Further analysis of the model's predictions and errors can be evaluated using similar methods described by Polly at. al [215]. One of the accuracy metrics used is the root mean squared error (RMSE) using the following relationship:

$$\text{RMSE} = \sqrt{\frac{\sum_{i=1}^{n}(\text{Prediction}-\text{Measurement})_i^{\,2}}{n}} \qquad \text{Equation 3-24}$$

Where: n: number of data points

Figure 3.19 shows the accuracy of the models when the above metric is used. All the models except the non-iterative correction scheme model *"EM_NIC_TDMA"* show an error close or less than 0.1˚C which is within the uncertainty range of the experimental data acquisition equipment.

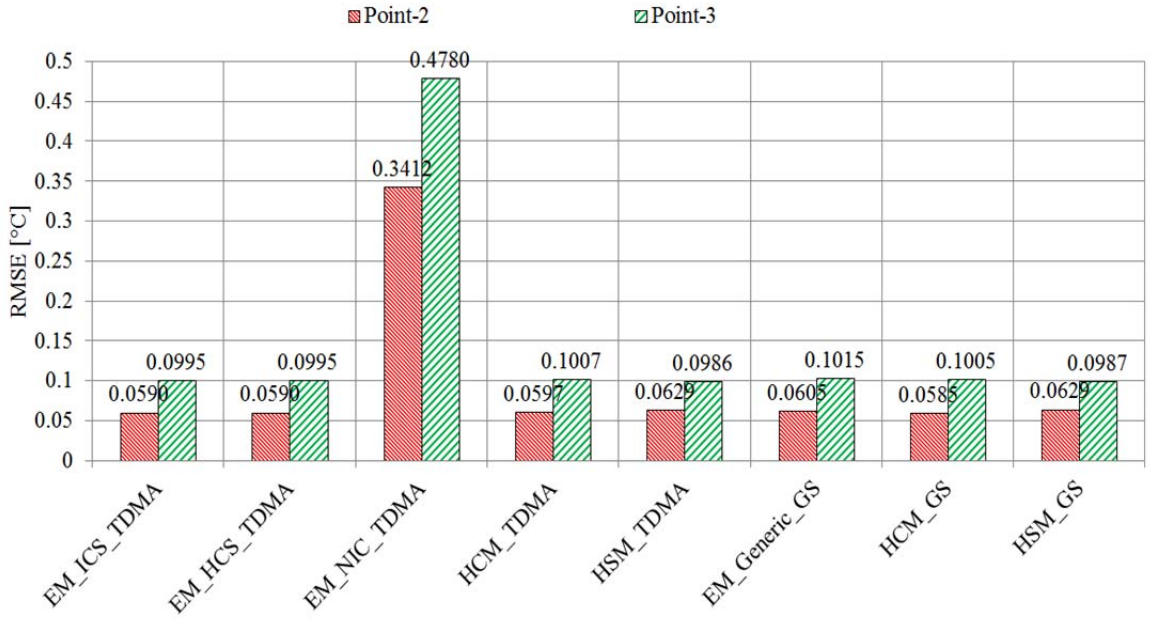

Figure 3.19 Root mean squared error for the numerical model's predictions

3.6.4 Verification using Comparative Studies

The verification and experimental validation above do not consider the long wave or short wave radiation of the envelope. Therefore, a comparative analysis can be used for this purpose. For this verification, EnergyPlus was selected for benchmark testing. EnergyPlus has recently undergone a rigorous verification and validation process [35]. This testing resulted in two bug identifications in version 6 and before: 1) variable thermal conductivity (not working properly) and 2) non convergence issue at higher time steps. The later E+ versions (v7.0 and above) can't be used with time step of 1 hour when using CondFD algorithm with PCMs. Therefore, E+ version 6 was used with precautions to avoid the two bugs: 1) materials used for testing are with constant thermal conductivity, 2) stability and convergence are important for this research to compare with other models at higher time step. A south wall is assumed to be located in Golden, Colorado. The results are assumed to converge when error falls below 10^{-7} and maximum iterations allowed are 3000. The material properties and simulation parameters are summarized in **Table 3-5**.

Figure 3.20 and **Figure 3.21** show the comparison between the developed numerical models and the EnergyPlus results. The exterior and interior surface temperatures for a typical time step of 1 hour and a sub-hourly time step of 3 minutes are selected for comparison. In addition, the root mean squared error (RMSE) for both time steps is calculated using Equation 3-24. For this calculation, the EnergyPlus results are assumed to be the reference. The calculations are performed over the time interval shown in the figures.

Table 3-5 Parameters used for South Wall

Test Parameter	Values		Units
	Concrete (Outside)	PCM Layer (Inside)	
Thermal Conductivity	0.733	0.726	W/m.K
Density	2315	1601	Kg/m^3
Specific Heat Capacity	800	836	J/kg.K
Thickness	0.15	0.019	m
Latent Heat of Fusion		13740	J/kg
Melting Temperature		22	˚C
Melting Range		0.10	˚C
Mesh Grid Points	22	22	
Indoor Temperature	24		˚C
External Convective Heat transfer Coefficient	11		$W/m^2.K$
Internal Convective Heat transfer Coefficient	3.079		$W/m^2.K$
Solar absorption	0.2		
Time Step	1 hour and 3 minutes		
Simulation Time	Selected interval where PCM is active and non-active.		

It is clear that all models show good agreement with EnergyPlus results for both exterior and interior surface temperatures. The models also show that for the first two days, PCM are not engaged but got engaged when the interior surface temperature reaches 22°C, which is the melting point of PCM. It is observed that the non-iterative correction scheme (EM_NIC_TDMA) shows significant temperature spikes for interior surface (a node in the PCM layer) and subsequently high errors when PCM node leaves the mushy region.

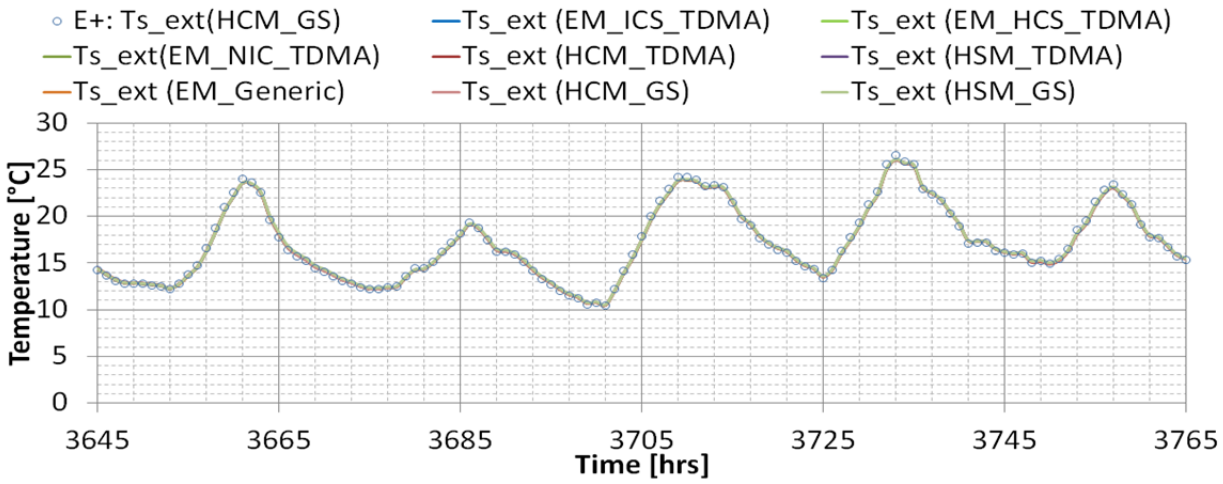

a) Exterior Surface Temperature at 1 hour time step

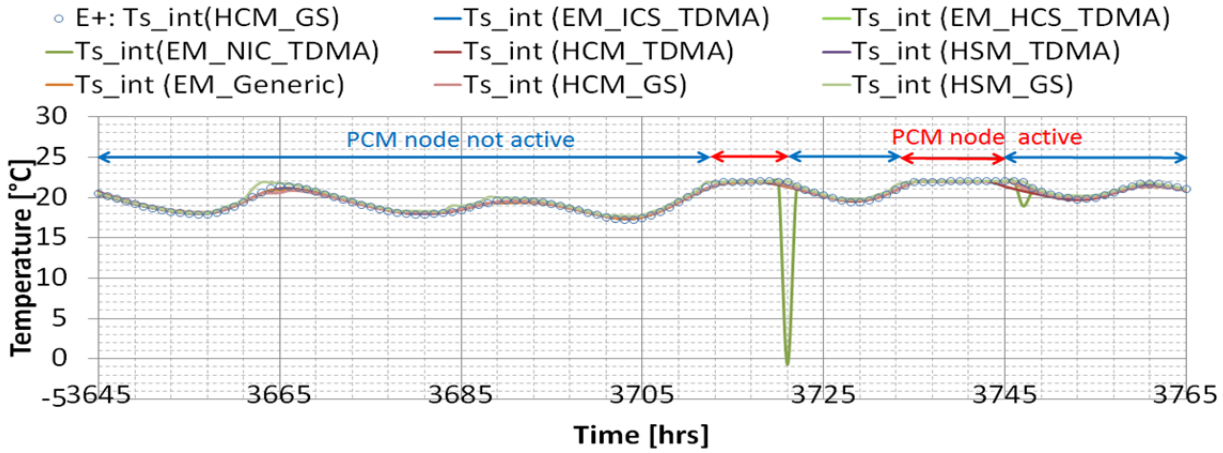

b) Interior Surface Temperature at 1 hour time step

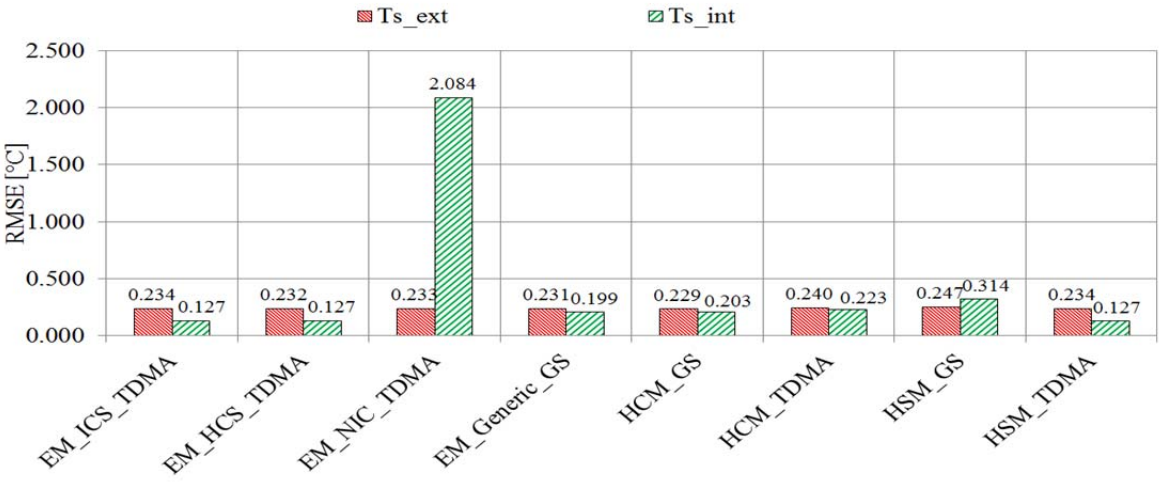

c) RMSE of the numerical models when compared with EnergyPlus

Figure 3.20 Verification of the developed numerical models against EnergyPlus for a south wall at 1 hour time step

Although less severe, the spikes can also be seen when the time step reduces to 3 minutes. Other models such as heat capacity method using TDMA solver (HCM_TDMA) and heat source methods (HSM_GS) using Gauss-Seidel solver also show a slight deviation from EnergyPlus results for a time step of 1 hour. For HCM_TDMA model, the convergence may not be reached and small time step is therefore necessary. On the other hand, HSM_GS model requires an under-relaxation factor which was not optimized for this case. The non-iterative corrective scheme shows the highest RMSE for nodes with PCM (i.e. interior nodes) among all even at smaller time step. Generally, the error for all models is less than 0.1°C for the time step of 3 minutes as demonstrated in **Figure 3.21**.

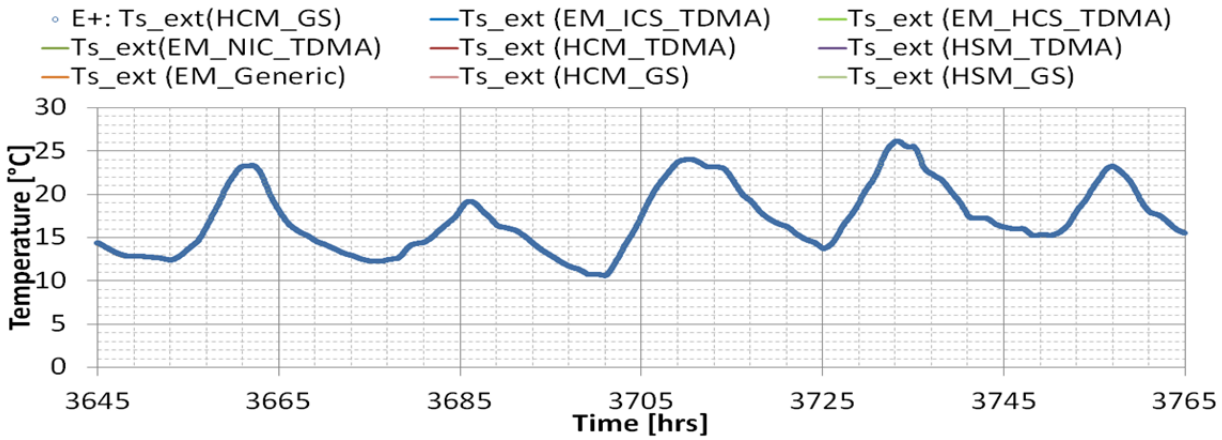

a) Exterior Surface Temperature 3 minutes time step

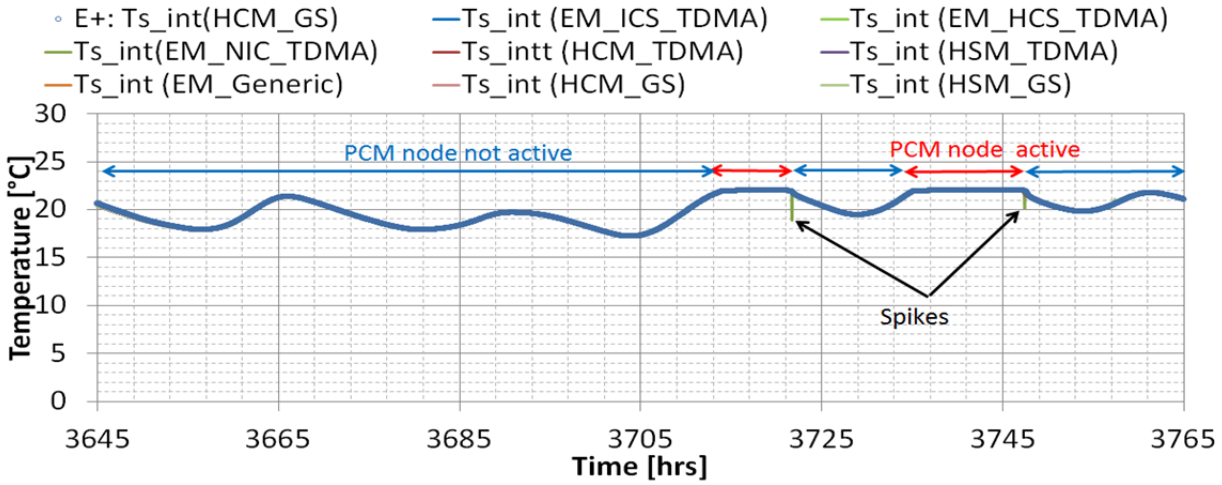

b) Interior Surface Temperature at 3 minutes time step

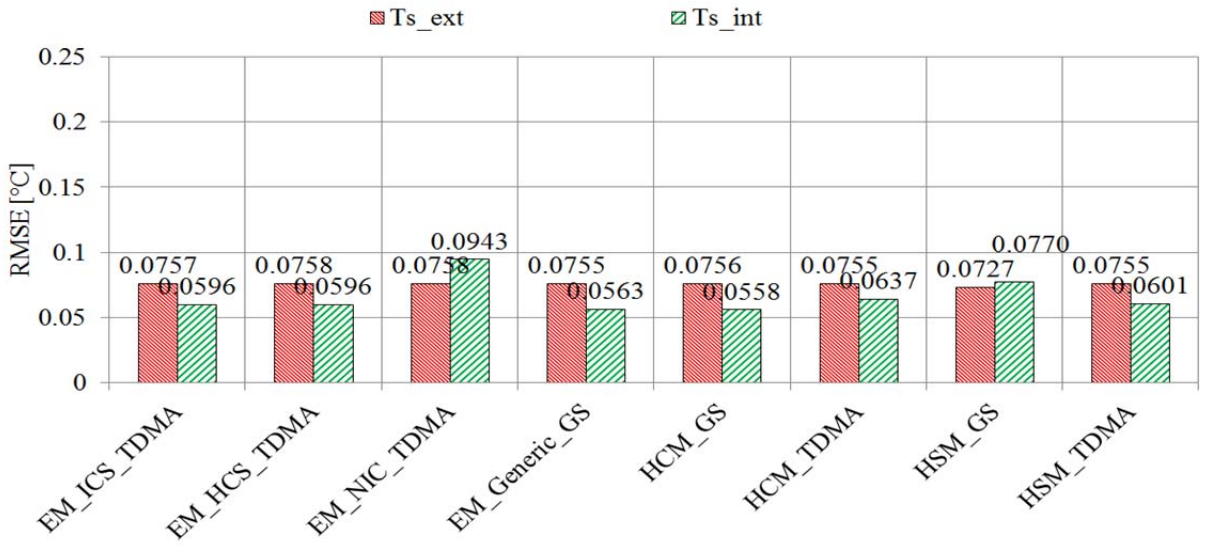

c) RMSE of the numerical models when compared to EnergyPlus results

Figure 3.21 Verification of the developed numerical models against EnergyPlus for a south wall at 3 minutes time step

3.6.5 Conclusions of Models Validations and Verifications Efforts

The developed numerical models have been validated and verified using analytical solutions, empirical results and comparative studies under typical building wall configurations and boundary conditions. The generic model without latent heat was verified against the analytical solution from ASHRAE 1052 research framework. This generic model was later modified for modeling latent heat. Eight different models were then developed and coded in MATLAB/SIMULINK environment. The developed numerical models were validated using experimental results for predicting the thermal performance of PCM using results from the literature. In addition, a comparative study was conducted using EnergyPlus for a typical time step of 1 hour and a sub-hourly time step of 3 minutes. Generally, all numerical models show good agreement with experimental results as well as with the comparative results using EnergyPlus with the exception of non-iterative correction scheme. The following sections will examine the computational efficiency, accuracy of these models under different scenarios, the models sensitivities to PCM thermal properties.

3.7 Sensitivity Analysis of Numerical Models: comparisons and discussions

Previous sections outlined the calculation procedure for different methods and schemes for simulating PCMs. This section provides a closer insight into the numerical performance of these models to solve the nonlinearity associated with PCMs in conduction-dominated heat transfer case. In particular, the followings are investigated:

1. Accuracy and numerical stability:
    a. Spatial resolution: using grid independent study
    b. Time resolution: using different time steps

2. Computational efficiency: using a normalized CPU time

3.7.1 Boundary Conditions

This study is based on a simple geometry illustrated in **Figure 3.22**. Both sides of the wall are exposed to a theoretical, yet realistic, boundary conditions considered for building applications.

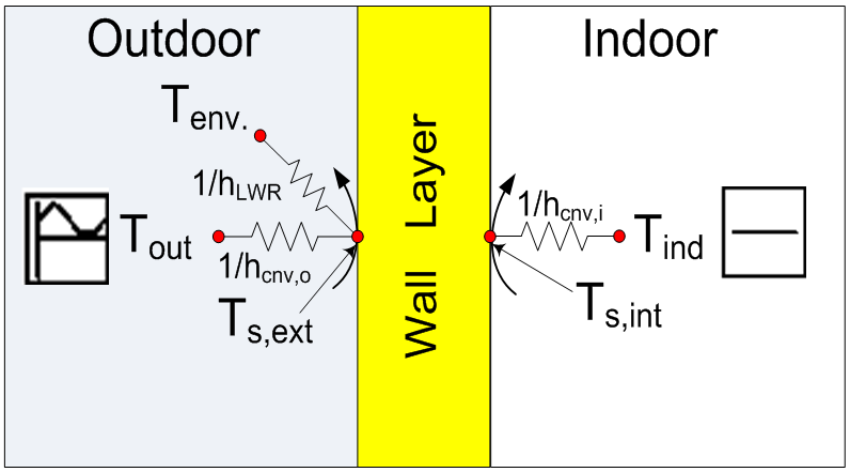

Figure 3.22 Illustration of the wall geometry and its boundary conditions

Table 3-6 provides detailed assumptions and description of the boundary conditions. The wall is exposed to a fixed air temperature at the indoor side and a sinusoidal periodic steady-state temperature profile on the exterior side. Long wave radiation is assumed to be between the exterior surface and the outside environment: sky, ground and air. The outdoor air temperature fluctuates above and below that of the indoor allowing the PCM to charge and discharge the latent heat during a course of a 24 hour time period. The outdoor air temperature is following a sinusoidal function with assumptions provided in the table below:

$$T_{out}(t) = Amp * \sin(Freq * t + Phase) + Bias \qquad \text{Equation 3-25}$$

Table 3-6 Boundary conditions parameters used for the simulation test cases

Boundary Condition					Unit
Indoor Temperature (T_{ind})	20				°C
Environmental Temperature (T_{env})	Sky Temperature	Ground Temperature	Air Temperature		°C
	10	T_{out}	T_{out}		
Outside Temperature Profile (T_{out})	Amp [°C]	Freq [rad/sec]	Phase [rad]	Bias [°C]	
	15	$\frac{2*\pi}{1*24*3600}$	$\frac{-90*\pi}{180}$	20	
External long-wave radiation Heat transfer Coefficients (h_{LWR}) [158]					
Sky	$h_{Sky} = \sigma * \varepsilon_w * F_{Sky} * \beta * \frac{((T_{sky}+273)^4 - (T_{s,ext}+273)^4)}{(T_{sky} - T_{s,ext})}$				$W/m^2.K$
Air	$h_{air} = \sigma * \varepsilon_w * F_{Sky} * (1-\beta) * \frac{((T_{amb}+273)^4 - (T_{s,ext}+273)^4)}{(T_{amb} - T_{s,ext})}$				$W/m^2.K$
Ground	$h_{grnd} = \sigma * \varepsilon_w * F_{ground} \frac{((T_{ground}+273)^4 - (T_{s,ext}+273)^4)}{(T_{ground} - T_{s,ext})}$				$W/m^2.K$
External Convective Heat transfer Coefficient ($h_{cnv,o}$)				29	$W/m^2.K$
Internal Convective Heat transfer Coefficient ($h_{cnv,i}$)				3	$W/m^2.K$

Where:

$F_{ground} = 0.5 * (1 - \cos(surfTilt))$, $F_{Sky} = 0.5 * (1 + \cos(surfTilt))$, $\beta = \sqrt{F_{Sky}}$, $\sigma = 5.67e-8$ W/m^2.K^4

3.7.2 **Grid independent Study**

Grid independent analysis is a crucial step when numerical simulation is used. It is a process of determining a grid resolution at which no improvement is attained when a grid is further refined. The main advantage of performing this task is to save computational time since unnecessary fine grid is eliminated and yet the accuracy is maintained. This task is particularly important when simulating phase change materials due to the high nonlinearity nature of the governing heat transfer equation. It is also valuable when iterative slow solvers are utilized for solving phase change problems. However, grid independent can't be generalized and therefore

has to be done for each scheme under study. Therefore, it has been performed for all numerical schemes described above. The temperature profile across the walls is predicted; utilizing a sensible heat storage wall assuming a concrete layer and a latent heat storage wall using a PCM layer. **Table 3-7** summarizes the physical and thermal properties of both cases with various grid resolutions. The grid resolutions for sensible case are 1, 2, 3, 6 nodes/cm. Additional grid points are considered for latent heat case and are 1, 2, 3, 6, 12 and 24 nodes/cm. In addition, 2 boundary nodes are located on wall exterior and interior boundary nodes.

Table 3-7 Thermal characteristics of walls used for grid independency

Test Parameter	Sensible Wall	Latent Wall	Units
	Concrete	PCM	
Thermal Conductivity	0.14	0.2	W/m.K
Density	2315	235	Kg/m^3
Specific Heat Capacity	800	1970	J/kg.K
Thickness	0.05	0.05	m
Latent Heat of Fusion		300	kJ/kg
Melting Temperature		23	°C
Melting Range		0.1	°C
Initial Temperature	20		°C
Grid resolution	Varies: 1, 2, 3, 6	Varies: 1, 2, 3, 6, 12, 24	nodes/cm

Using the above simulation parameters and assumptions, the results are extracted after the temperature field is stabilized in a sinusoidal steady state. **Figure 3.23** shows the results across the concrete wall using different numerical models under various grid resolutions. It is observed that the temperature profile across the wall doesn't improve with increasing the grid resolution. Therefore, 1 node per cm of layer thickness is considered enough for accurate results when modeling sensible heat process. **Figure 3.24**, on the other hand, shows the performance of the numerical models when latent heat is considered. It is observed that more nodes are necessary when latent heat is considered compared to the sensible case. At least 6 nodes for each 1 cm are necessary for all models. This nodes distribution is used in all subsequent analysis.

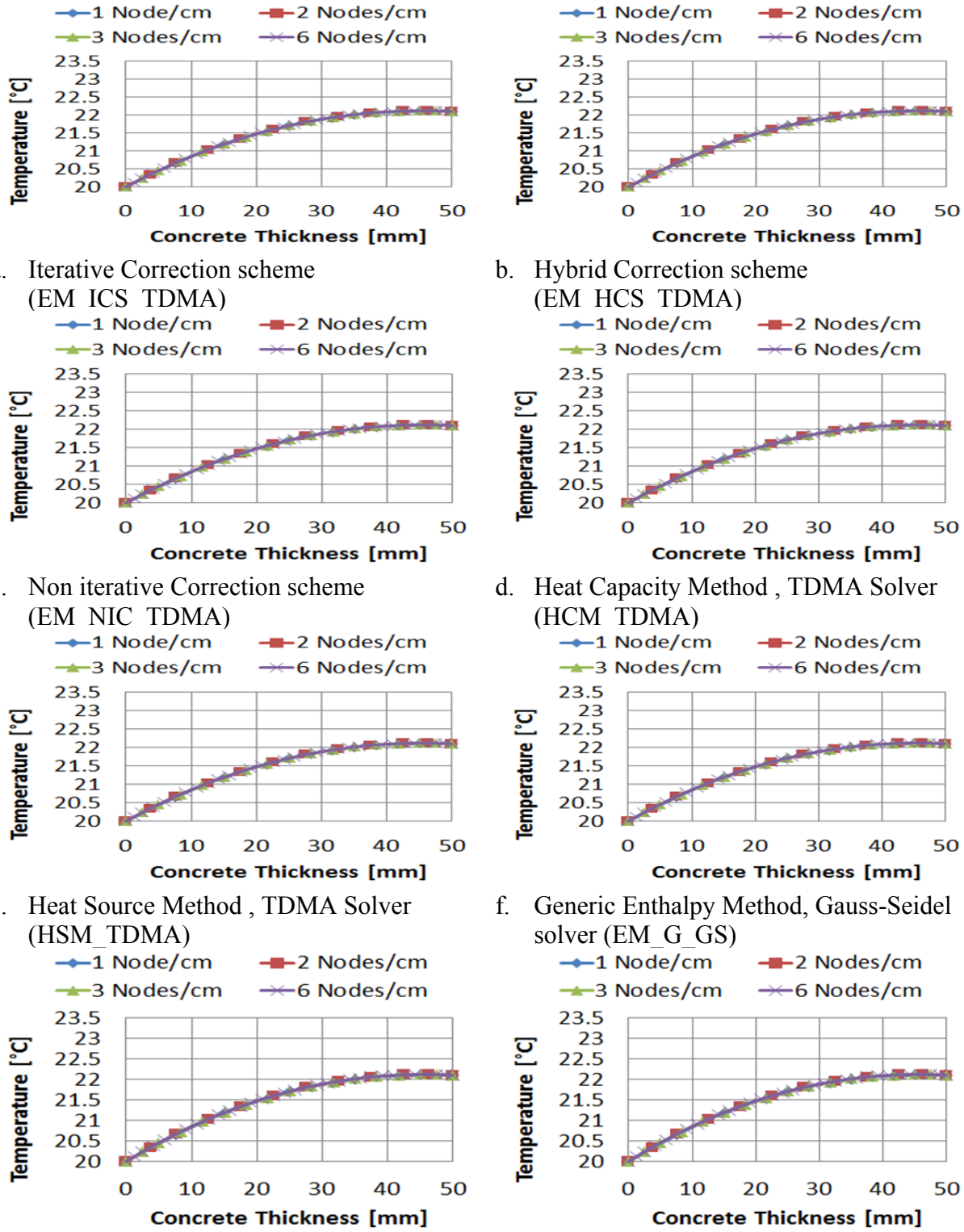

a. Iterative Correction scheme (EM_ICS_TDMA)

b. Hybrid Correction scheme (EM_HCS_TDMA)

c. Non iterative Correction scheme (EM_NIC_TDMA)

d. Heat Capacity Method , TDMA Solver (HCM_TDMA)

e. Heat Source Method , TDMA Solver (HSM_TDMA)

f. Generic Enthalpy Method, Gauss-Seidel solver (EM_G_GS)

g. Heat Capacity Method, Gauss-Seidel solver (HCM_GS)

h. Heat Source Method, Gauss-Seidel solver (HSM_GS)

Figure 3.23 Grid independent results of the tested models for a 5 cm Concrete layer

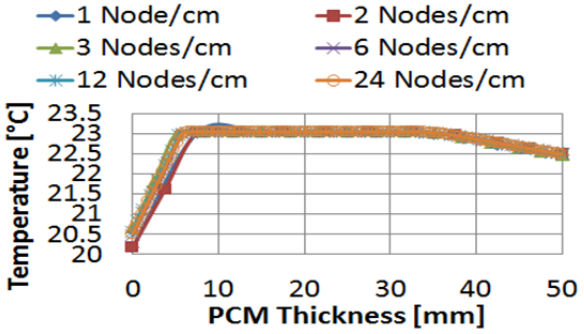

a. Iterative Correction scheme (EM_ICS_TDMA)

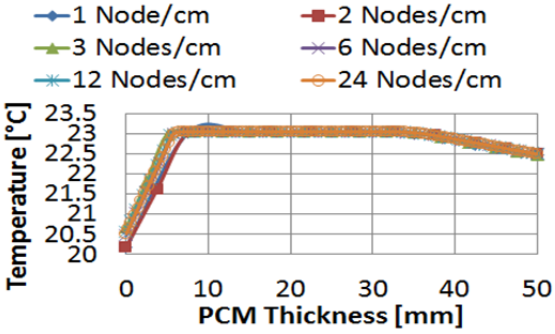

b. Hybrid Correction scheme (EM_HCS_TDMA)

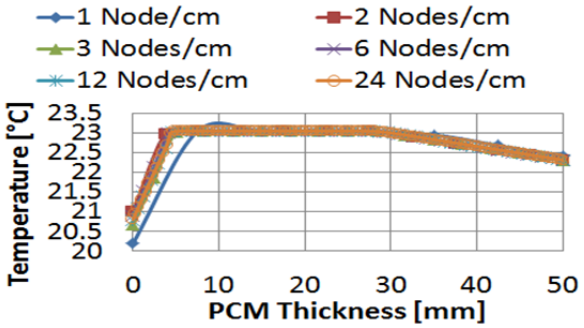

c. Non iterative Correction scheme (EM_NIC_TDMA)

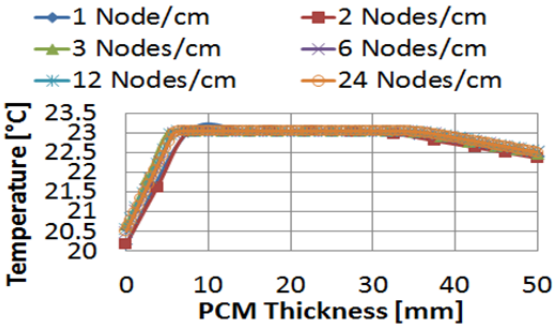

d. Heat Capacity Method , TDMA Solver (HCM_TDMA)

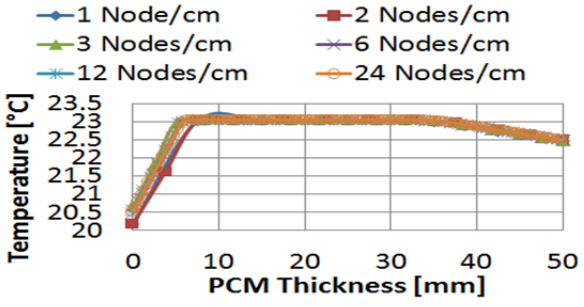

e. Heat Source Method , TDMA Solver (HSM_TDMA)

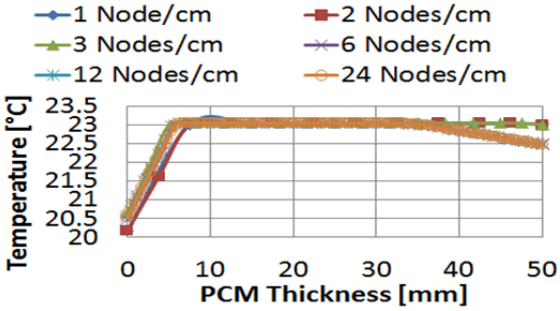

f. Generic Enthalpy Method, Gauss-Seidel solver (EM_Generic_GS)

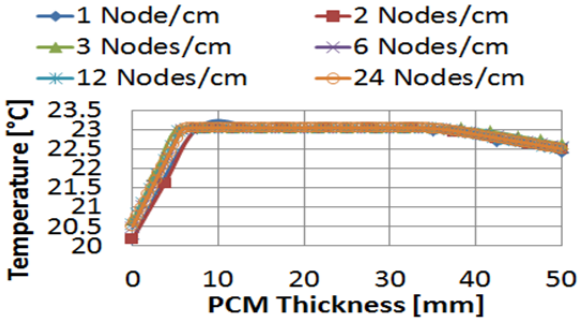

g. Heat Capacity Method, Gauss-Seidel solver (HCM_GS)

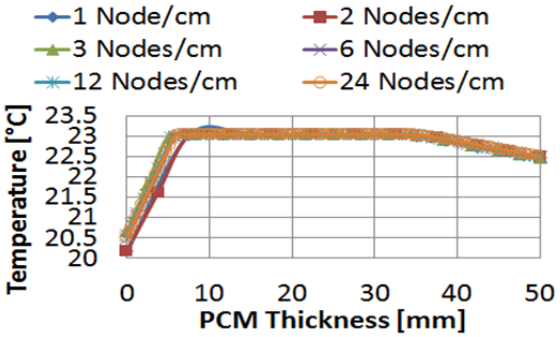

h. Heat Source Method, Gauss-Seidel solver (HSM_GS)

Figure 3.24 Grid independent results of the tested models for a 5 cm PCM layer

3.7.3 Time Resolution Study for the numerical models

All numerical models use a fully implicit scheme time stepping since it is unconditionally stable regardless of the time step. However, the accuracy will depend on the time resolution. The current state-of-the-art building simulation programs model the building envelopes with or without PCM using a time step of a 1 minute (60s) or more. For the tested cases, a time resolution of 1 minute, 5 minutes, 10 minutes, 15 minutes, 30 minutes, 60 minutes are considered. It is assumed that the result of each numerical model at a time step of 1 minute is the reference case. Therefore, each numerical model is compared to its results at a 1 minute time step. Two performance indicators are used to evaluate the results accuracy and the computational efficiency. For accuracy, the normalized root mean squared error (NRMSE) is adopted using the following relationships:

$$\mathrm{RMSE} = \sqrt{\frac{\sum_{i=1}^{n}(T_{Model} - T_{Reference})_i^2}{n}} \qquad \text{Equation 3-26}$$

$$\sigma_{Reference} = \sqrt{\frac{\sum_{i=1}^{n}(T_i - \bar{T})^2}{(n-1)}} \qquad \text{Equation 3-27}$$

$$\mathrm{NRMSE}[\%] = \frac{\mathrm{RMSE}}{\sigma_{Reference}} * 100 \qquad \text{Equation 3-28}$$

The NRMSE is determined for three nodes; exterior node, interior node and the middle node. The NRMSE is averaged for these three nodes over the simulation time period. The NRMSE value of 100% means that the RMSE is in the bound of the standard deviation [216]. If the errors are higher than these bound values the NRMSE will be above 100%.

The computational efficiency is evaluated using the normalized CPU time (NCPU), using the following equation:

$$\text{NCPU} = \frac{CPU_{Model}}{CPU_{Reference}}$$ Equation 3-29

A Quad laptop (Intel i7-2640M processor, CPU 2.8 GHz, 8G RAM) was used for this analysis. Only one processor was allowed to operate during the simulation and no other tasks, except windows overhead, were running when this study is performed. The CPU time is estimated using a MATLAB benchmarking function "TIMEIT' provided from the MATLAB FILE Exchanger web site [217]. This code runs each case three times and averaged the CPU times. Two numerical experiments are run to achieve the objective of this task:

Case 1: for this case, the melting temperature range is fixed to 0.1 °C and latent heat of fusion is varied from 0-300 kJ/kg. This case determines how rigorous the models are when melting range is fixed to a very narrow melting range.

Case 2: for this case, the latent heat of fusion is fixed at 200 kJ/kg and the melting range varies from 0.1 to 8 °C. This case determines how sensitive the models are when the melting range varies from a narrow to a wide range and the latent heat is fixed.

For both cases, the melting temperature is fixed at 23 °C and a grid resolution of 30 interior nodes and 2 for boundary nodes are assumed as a result of the grid independent study. All simulation parameters and other properties are kept unchanged as per **Table 3-6** and **Table 3-7** respectively.

3.7.3.1 Case 1: Varying the latent heat with fixed melting range

As noted earlier, each model is compared to itself at a time step of 1 minute. The results under this section should not be interpreted as a cross comparison but a self-comparison instead. **Figure 3.25** shows the results of both the NRMSE and the NCPU time for all the models under

different time steps and varying latent heat. The one minute time step is used as a reference case and therefore not shown in the figure. **Figure 3.25** (a) and (b) shows the performance of the models when no latent heat is modeled. Under this benchmark case, all models show a similar error pattern when the time step increases from 5 minutes to 60 minutes. As expected, the error increases as the time step increases since implicit time stepping (1^{st} order approximation) is adopted in this work. The NRMSE for all modes is below 1 %. This value will be later used as a threshold NRMSE for the models accuracy when PCMs are used. The NCPU time decreases as the time step increases for all models as shown in **Figure 3.25** (b). Models with iterative solvers (G-S) show high NCPU time reduction when compared to models that uses direct solvers (TDMA). This is not uncommon since direct solvers need less calculation time and therefore low savings on calculation time is expected. At 1 hour time step, the iterative solvers take less time to converge when compared to itself at 1 minute time step.

For all other tests when latent heat is modeled as the time step decreases, the NRMSE decreases too as shown in **Figure 3.25** (c, e, g, i, k). For some cases, the error is related to the inherited feature of the fully implicit time stepping scheme rather than the models' sensitivity to the latent heat process. This is true for the models that use the correction scheme (EM_ICS_TDMA, EM_HCS_TDMA, HSM_TDMA, and HSM_GS). For these particular models, the NRMSE is between 0.1 and 5 % when PCM is used compared to 0.1 and 1% when no PCM is used. The other four models (EM_NIC_TDMA, EM_Generic_GS, HCM_TDMA, and HCM_GS) show higher NRMSE especially at higher time steps due to several reasons. For example, EM_NIC_TDMA model is a semi-implicit since properties are assumed constant based on previous time step. For this method, no further iterations are attempted in a time step which resulted in high error. Therefore, lower time steps are demanded to reduce the associated

NRMSE. The EM_Generic_GS uses under-relaxation factor that has to be optimized for each time step and perhaps for each latent heat case. For this case, however, the under-relaxation factor was fixed and not optimized. Subsequently, the NRMSE is inconsistent across the cases. Heat capacity method (both versions HCM_TDMA and HCM_GS models) occasionally show higher NRMSE (refer to the cases of L= 200 and 300 kJ/kg). In particular, the HCM_TDMA is not accurate when compared to the HCM_GS even at smaller time step. The heat capacity method uses the numerical approximation for the estimation of the apparent heat capacity. This approximation requires a slow and gradual movement to the solution. This particular requirement can only be achieved using iterative solvers rather than direct solvers when melting range is very narrow. Since all these variants of Case 1 uses narrow melting range, the TDMA version of heat capacity method is not recommended under this situation.

The NCPU times for the models under different latent heat are shown in **Figure 3.25** (d, f, h, j, l). The figure shows that methods uses TDMA with correction scheme do not show major CPU time savings beyond the 5 minutes time step. It is likely due to small number of iterations at low time steps, consequently lower CPU time. The methods reach convergence quickly regardless of its time step and therefore less CPU savings are achieved. HSM_TDMA (Heat source method, TDMA version) is an exception since it shows a significant CPU time savings when compared to itself at 1 minute time step. The methods that implement G-S solvers show a steady decrease in CPU time as the time step decreases. At higher time steps, some methods that use G-S solvers show less NCPU time than those use TDMA. This does not mean that they are quicker than direct solvers, but because they are normalized to themselves at 1 minute time step. The NCPU pattern is consistent when increasing the latent heat and therefore the CPU time is not sensitive to the changes in latent heat.

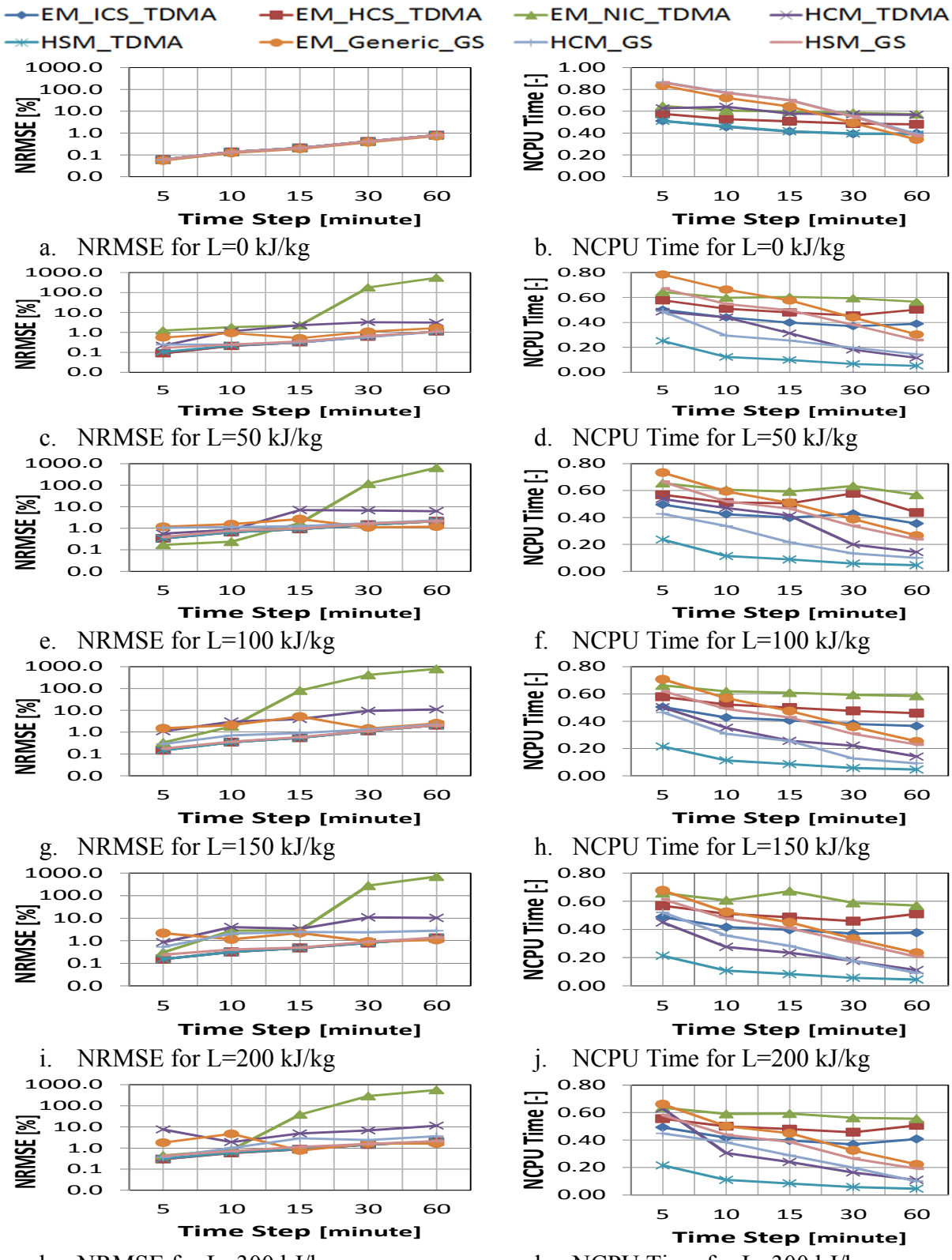

a. NRMSE for L=0 kJ/kg

b. NCPU Time for L=0 kJ/kg

c. NRMSE for L=50 kJ/kg

d. NCPU Time for L=50 kJ/kg

e. NRMSE for L=100 kJ/kg

f. NCPU Time for L=100 kJ/kg

g. NRMSE for L=150 kJ/kg

h. NCPU Time for L=150 kJ/kg

i. NRMSE for L=200 kJ/kg

j. NCPU Time for L=200 kJ/kg

k. NRMSE for L=300 kJ/kg

l. NCPU Time for L=300 kJ/kg

Figure 3.25 Performance of different models for various latent heat at fixed melting range of 0.1 °C

The overall trend from this case shows that the models are not sensitive to the amount of latent heat since no major improvement or degradation for both the NRMSE and NCPU time are observed. All models show small NRMSE when small time steps are used with an exception of the EM_Generic_GS which is likely related to un-optimized under-relaxation factor. If a threshold of 1% NRMSE is considered (a threshold NRMSE value based on a sensible case at 1 hour time step), then the models that are based on iterative solvers should be limited to a maximum of 15 minutes time step or less. This will result in a significant CPU time savings when compared to a base case of 1 minute time step. The Heat capacity method (HCM_GS), however, requires a time step of less than 5 minutes (refer to **Figure 3.25** e, i). Although high time steps can be used, quick models that are based on correction scheme (EM_ICS_TDMA, EM_HCS_TDMA, HSM_TDMA, HSM_GS) can be run at 10 or even at 5 minutes time step without significant CPU overhead.

3.7.3.2 Case 2: Varying melting range with fixed latent heat

This case is intended to evaluate the sensitivities of the numerical methods when the melting range varies from narrow to wide melting range (0.1, 1, 2, 4, and 8 °C) when latent heat is fixed at 200 kJ/kg. **Figure 3.27** (a, c, e, g, i) show that the NRMSE of all models decreases as the melting range becomes wider and eventually converge to the same results. In addition, the models that use the correction scheme (EM_ICS_TDMA, EM_HCS_TDMA, HSM_GS, HSM_TDMA) are less sensitive to the melting range compared to those which don't (HCM_TDMA, HCM_GS, EM_Generic_GS). It is noted that the heat capacity method becomes more accurate as the melting range increases above 1°C. Since the heat capacity method approximate the slope (i.e. the apparent heat capacity) numerically, the approximation becomes

smoother as the melting range is widened and therefore low error is propagated into the calculations. The numerical performance of the EM_NIC_TDMA is not improving for all the cases.

On the other hand, **Figure 3.27** (b, d, f, h, j) show that the trend in NCPU time is consistent as the melting range increases. There are no significant changes (improvement or degradation) in NCPU time as the melting range increases for all methods. However, the heat capacity method, specifically the TDMA version, shows inconsistent CPU time as the melting range increases especially for low time steps.

This case provides more insights on how the models behave as the melting range increases. It is found that the as the melting range increases, the models becomes more accurate in their predictions. In particular, the heat capacity method becomes more accurate since the apparent heat capacity becomes smoother. The models that uses correction scheme are not sensitive to the melting range.

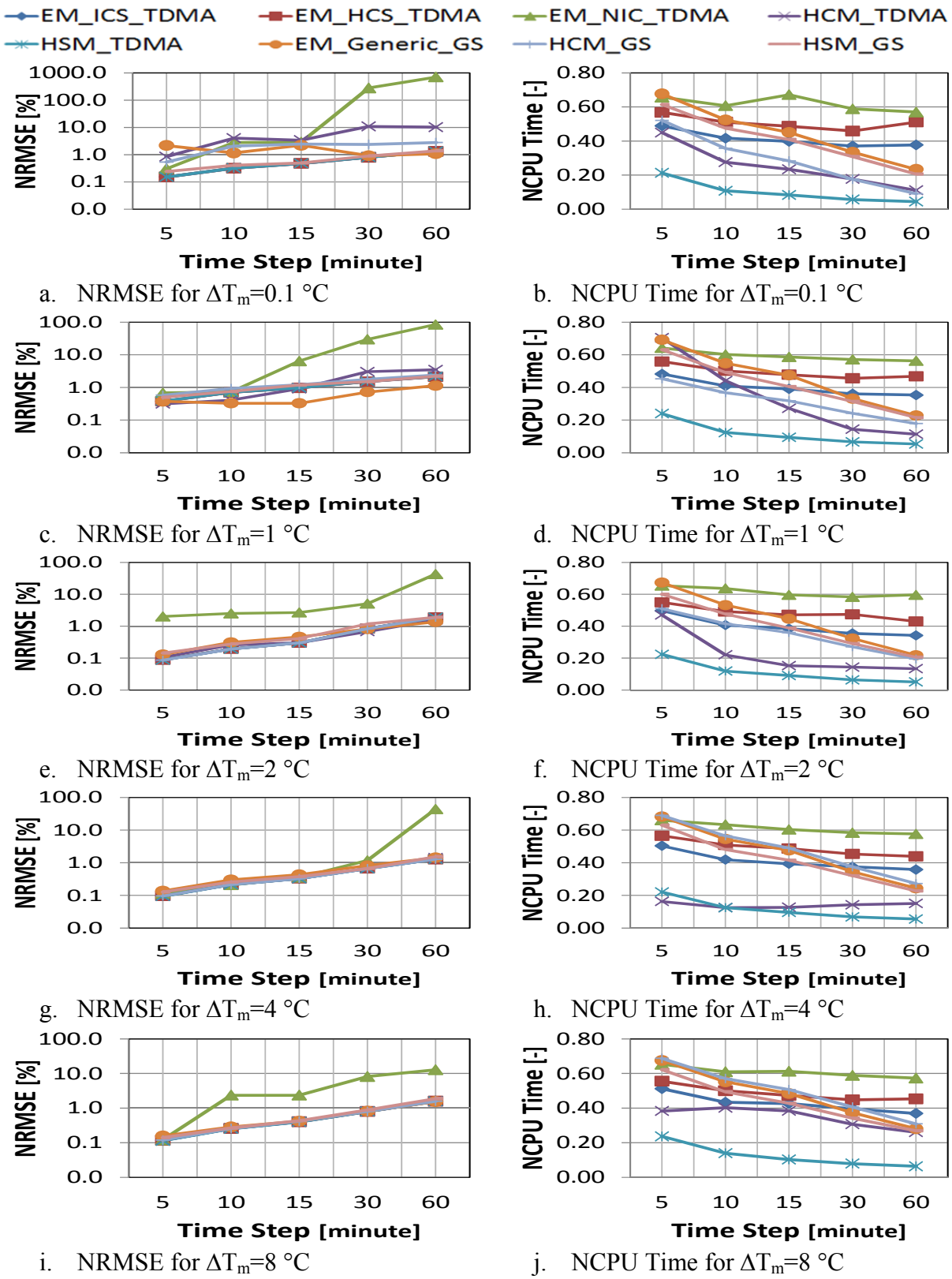

a. NRMSE for ΔT_m=0.1 °C

b. NCPU Time for ΔT_m=0.1 °C

c. NRMSE for ΔT_m=1 °C

d. NCPU Time for ΔT_m=1 °C

e. NRMSE for ΔT_m=2 °C

f. NCPU Time for ΔT_m=2 °C

g. NRMSE for ΔT_m=4 °C

h. NCPU Time for ΔT_m=4 °C

i. NRMSE for ΔT_m=8 °C

j. NCPU Time for ΔT_m=8 °C

Figure 3.26 Performance of the numerical models for various melting range at constant latent heat of 200 kJ/kg

3.7.3.3 Cross comparison

The previous two cases indicated that there are potential numerical models that could be used for modeling PCM. Models that use correction scheme are found to be less sensitive to PCM thermal properties; latent heat and melting range. However, the above two cases showed a self-comparison rather than a cross comparison. This section further highlights the accuracy and computational efficiency of these methods when one scheme is used as a reference case. The reference case selected for this comparison is the EM_ICS_TDMA. This method is found to be consistent in NCPU and provides conservative results all over the analysis. **Figure 3.27** (a) shows the NRMSE of the models when compared to this reference case. The figure shows that there are few models close to the reference case; EM_HCS_TDMA, EM_NIC_TDMA, HSM_TDMA, HSM_GS. These models show a NRMSE of less than 1% at 1 minute time step. The EM_HCS_TDMA, hybrid scheme proposed in this study, shows a NRMSE of less than 0.01%. Beyond 5 minutes time step, the models have a similar NRMSE to the reference case. **Figure 3.27** (b) shows that enthalpy methods with correction scheme (TDMA versions) are fast although no significant CPU time savings are achieved as the time step increases. All other methods are at least 10 times slower than these methods at low time steps. The HSM_TDMA shows a significant reduction in NCPU time yet maintaining the same accuracy when compared to others slow models. Its computational efficiency is comparable to the fast methods at 1 hour time step. Since they are the fastest, the enthalpy methods with correction scheme are further analyzed as shown in **Figure 3.27** (c) and (d). The figure shows that the EM_HCS_TDMA (hybrid correction scheme) is very close to the EM_ICS_TDMA (iterative correction scheme) which is deemed to be fast and conservative [66]. At 1 minute time step, the hybrid scheme is 20 % faster than the iterative correction scheme. At 5 minute time step, the hybrid scheme is 4%

faster yet have a similar error. There is no significant time savings beyond 5 minutes interval. The non-iterative correction scheme (i.e. EM_NIC_TDMA) is faster than all of the models but has high NRMSE and therefore inaccurate.

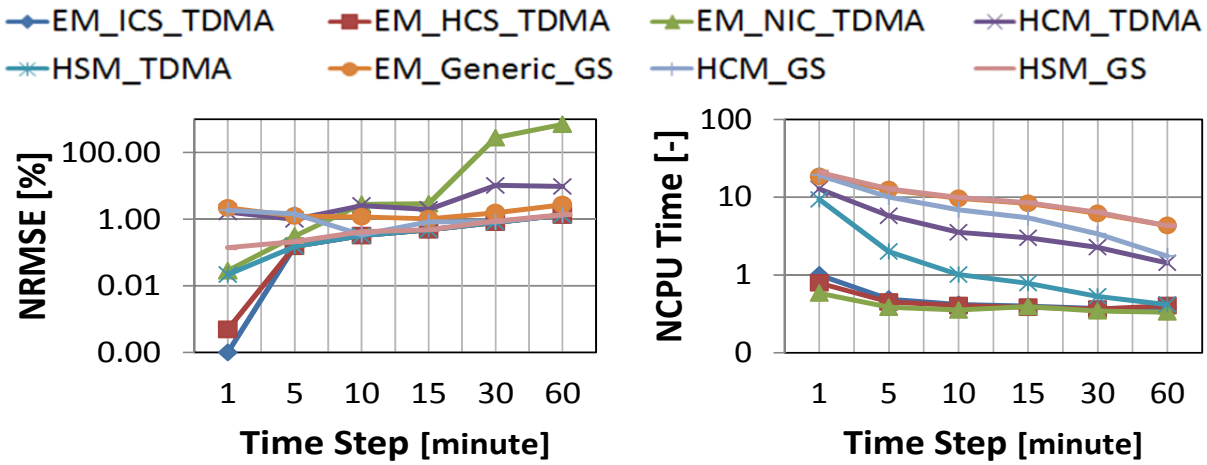

a. NRMSE for ΔT_m=0.1 °C

b. NCPU Time for ΔT_m=0.1 °C

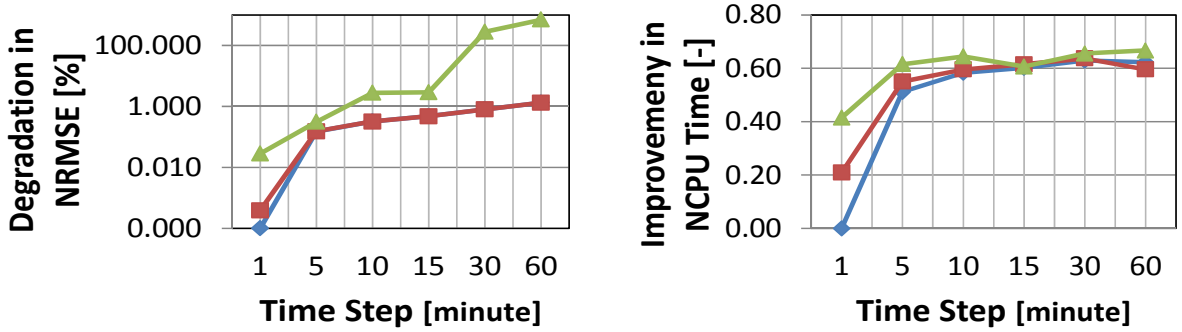

c. Degradation in NRMSE for the quick models

d. Improvement in NCPU for the quick models

Figure 3.27 Performance of different models under narrow melting range at constant latent heat of 200 kJ/kg

3.7.4 Conclusions on sensitivity analysis

According to the above results, the numerical schemes have shown to be less sensitive to the variations in latent heat of PCMs. Although some models are associated with high NRMSE, they show consistent NRMSE and NCPU regardless of varying the latent heat. Few models are, however, found to be sensitive to the melting range. In particular, the result from the heat

capacity method converges to other schemes when the melting range becomes wider. Models that use correction scheme are found to be less sensitive to the melting range. Further analysis of quick schemes indicated that the hybrid correction scheme (i.e. EM_HCS_TDMA) is faster than the iterative correction scheme's (i.e. EM_ICS_TDMA). This is a significant improvement when a numerical model is sought for building simulation programs that are run for full year simulation at sub-hourly time steps. **Table 3-8** summarizes the findings of the sensitivity study and provides recommendations for selecting a numerical model and scheme for modeling PCM.

Table 3-8 Summary of sensitivity analysis and recommendation for numerical models for simulating PCMs

Model	Melting Range	Recommended Maximum Time Step [min]*	Computational Speed	Remarks
Generic Enthalpy Method (EM_Generic_GS)	Becomes accurate with wide melting range (> 1°C)	Inconsistent results at small time steps	Slow	Optimum under-relaxation factor is needed
Iterative Correction Scheme (EM_ICS_TDMA)	Less sensitive to melting range	< 15 minutes	Fast	
Hybrid Correction Scheme (EM_HCS_TDMA)	Less sensitive to melting range	< 15 minutes	Fast	CPU savings when time step is ≤ 5 minutes
Non-Iterative Correction Scheme (EM_NIC_TDMA)	Inconsistent results	< 1 minute	Fast	Not recommended since temperature spikes always occur
Heat Capacity Method (HCM_TDMA)	Becomes accurate with wide melting range (> 1°C)	<5 minutes	Medium	Not recommended since it is highly sensitive to variations in latent heat and melting range
Heat Capacity Method (HCM_GS)	Becomes accurate with wide melting range (> 1°C)	<5 minutes	Slow	sensitive to variations in latent heat and melting range
Heat Source Method (HSM_TDMA)	Less sensitive to melting range	< 15 minutes	Medium	
Heat Source Method (HSM_GS)	Less sensitive to melting range	< 15 minutes	Slow	

G-S: Gauss-Seidel, TDMA: Tri-Diagonal Matrix Algorithm
*This is based on a threshold of 1% NRMSE

3.8 Summary

This chapter outlines the calculation procedure for several numerical models and proposes an improvement to an existing scheme for simulating PCM for integrating into whole building simulation tool. The models have been validated using experimental results from literate and verified using comparative results from EnergyPlus. All models agree well with both the experimental and comparative results except the non-iterative correction scheme. The models are then used to conduct a sensitivity study on PCM properties; latent heat and melting range at different time steps. The sensitivity study is performed to evaluate the computational efficiency and the prediction accuracy under different PCM properties. The results have given more insights on how the models perform and can be summarized as follows:

1. Models that use correction schemes are less sensitive to the latent heat and melting temperature range variations. However, the non-iterative scheme (EM_NIC_TDMA) is found to be inaccurate for all cases since PCM properties are based on previous time step. If a 1% NRMSE threshold is considered (an NRMSE value achieved with a sensible case at 1 hour time step), the time step could be as maximum as 15 minutes. However, using a 5 minute time step would not add a considerable CPU time yet having low NRMSE. The proposed improvement implemented in the hybrid correction scheme (EM_HCS_TDMA) has resulted in CPU time savings of 20% and 4% at 1 and 5 minute time step respectively when compared to the fastest and most conservative method; the iterative correction scheme (EM_ICS_TDMA). This improvement is significant when a PCM model is sought for implementation into whole building simulation tool that runs on yearly simulation at sub-hourly time step.

2. Direct solver (TDMA) is not recommended for the heat capacity method when PCM exhibits a narrow melting range (< 1 °C).
3. Generally, the heat capacity method is found to be sensitive to the melting range and its predictions gets more accurate as the melting range increases above 1 °C. This is likely due to the approximation mechanism of apparent heat capacity. The approximation becomes smoother with wide melting range. Therefore, it is recommended that this method is used for PCMs that has a wide melting range, >1 °C. In order to achieve a 1% NRMSE threshold value, the time step for this method has to be less than 5 minutes.
4. Heat source method, the TDMA and G-S version, show good results when compared to the heat capacity method and comparable results to the linearized enthalpy methods. However, the method is approximately 10 times slower than the linearized enthalpy methods, the fastest schemes at small time steps. Although the heat source method uses a correction scheme too, the method utilizes an under-relaxation factor that hindered its speed.
5. The general enthalpy method has a similar behavior as the heat capacity method but an optimum relaxation factor is required. In addition, the method is computationally intensive and doesn't offer an advantage for potential implementation into building simulation tools.

It is concluded that only two schemes out of eight developed can be considered as potential candidates for integrating into whole building simulation tool; the linearized enthalpy method with the iterative correction scheme (EM_ICSS_TDMA) and the hybrid correction scheme (EM_HCS_TDMA). These two schemes offer many advantages over others:

1) Flexibility to use with large time steps (a maximum of 15 minutes) and still with small NRMSE.
2) Based on the time step used, computational efficiency as they are 3-10 times faster than others.
3) Less sensitive to the variation of PCM properties; latent heat and melting range and hence stable in their numerical predictions.

CHAPTER 4: DEVELOPMENT OF SIMULINK TOOLBOX FOR MODELING ADVANCED FAÇADE SYSTEMS

According to Chapter 3, two numerical schemes have been selected for modeling PCMs in building envelope; enthalpy method with iterative correction scheme and the hybrid correction scheme proposed in this study. Using these two schemes, a design toolbox for modeling advanced façade system is developed in MATLAB/SIMULINK environment. This chapter presents the structure of the developed toolbox, the blocks and the background fundamentals. It further discusses verified cases by using multilayer wall and ventilated cavity wall systems. Good agreement between the developed tool and results from well-credited building simulation programs EnergyPlus and TRNSYS are observed.

4.1 MATLAB/SIMULINK and Application for modeling building performance

MATLAB is a high-performance language for technical computing [218]. It is powerful package integrated with huge functions. MATLAB is becoming a standard programming language used by various scientific groups. It is progressively improved with many toolboxes developed for many applications. In MATLAB environment, a standalone graphical user interface (GUI) based on MATLAB commands can be built. Using this approach, the GUI can be designed for a specific model. Alternatively, SIMULINK can be used. SIMULINK is an add-on to the MATLAB environment with a graphical user interface (GUI) for modeling dynamical systems. It has many built-in functions, ready-made modules and library of toolboxes as illustrated **Figure 4.1**. From a list of libraries, the user can drag, drop and link a component into

a single screen. The component represents a mathematical function where inputs are necessary for output calculation.

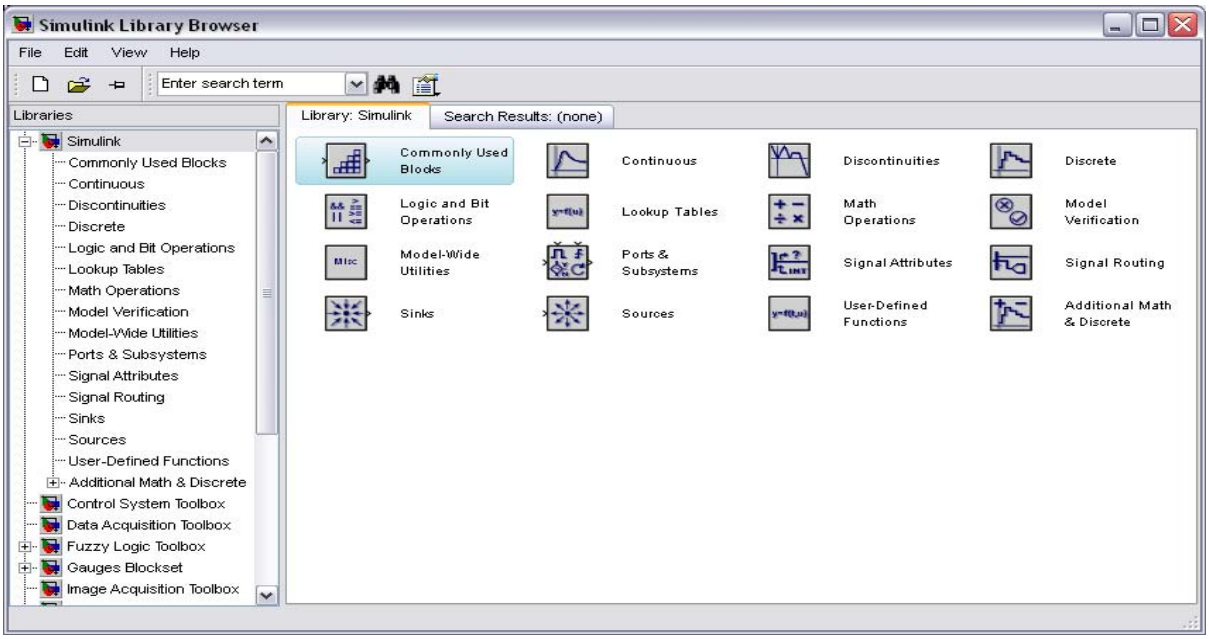

a. A sample of SIMULINK libraries

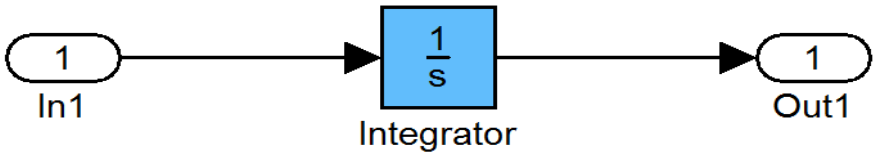

b. Component representation in SIMULINK

Figure 4.1 Libraries of SIMULINK

Many successful standalone as well as complex system models have been developed using SIMULINK. For building applications, SIMULINK is primarily used for modeling HVAC systems and controls [219-224]. Other research groups have developed comprehensive libraries for modeling energy and hygrothermal performance of full scale buildings. Examples includes HAMLab developed in Eindhoven University of Technology [225] and International Building Physics Toolbox (IBPT) developed jointly by a team from Chalmers University of Technology and Technical University of Denmark [226]. Others have developed simplified zones too [227-

230]. Therefore, SIMULINK has provided a flexible modeling framework for simulating building performance and its systems. Hence, SIMULINK is considered as a framework for this work. The package is used in this work due to many reasons such as the flexibility, graphical capabilities and data visualization. In addition, it can be used for co-simulation with many building simulation programs such as EnergyPlus, TRNSYS and ESPr.

4.2 Development of "AdvFacSy" Toolbox in SIMULINK

Advanced façade systems are becoming important architectural elements in modern buildings. While many façade systems are installed for architectural reasons, they can be utilized to perform multiple functions such as heat storage using PCM-enhanced components for example. However, there is no tool yet that helps to investigate the thermal performance of these systems. The overall goal was then to provide a framework tool or a library of modules that can be easily used to achieve this task. Advanced Façade Systems "AdvFacSy" is developed for this purpose using SIMULINK environment. In order to make it a self-sustained tool, the intended standalone models needs additional supporting utilities and modules that provide boundary conditions for the developed PCMs model. For example, weather data module that reads typical weather data files such as EnergyPlus weather format (EPW) is needed. In addition, solar radiation model is mandatory to calculate the solar radiation on tilted surfaces. **Figure 4.2** illustrates the concept of AdvFacSy in SIMULINK. The Simulink modules call MATLAB files that are located under subroutines folder. This folder contains many files necessary to provide necessary information such as materials library and weather files or performs calculations such as mesh functions, solvers and other general functions for calculating mass flow rate, convective heat transfer coefficients etc.

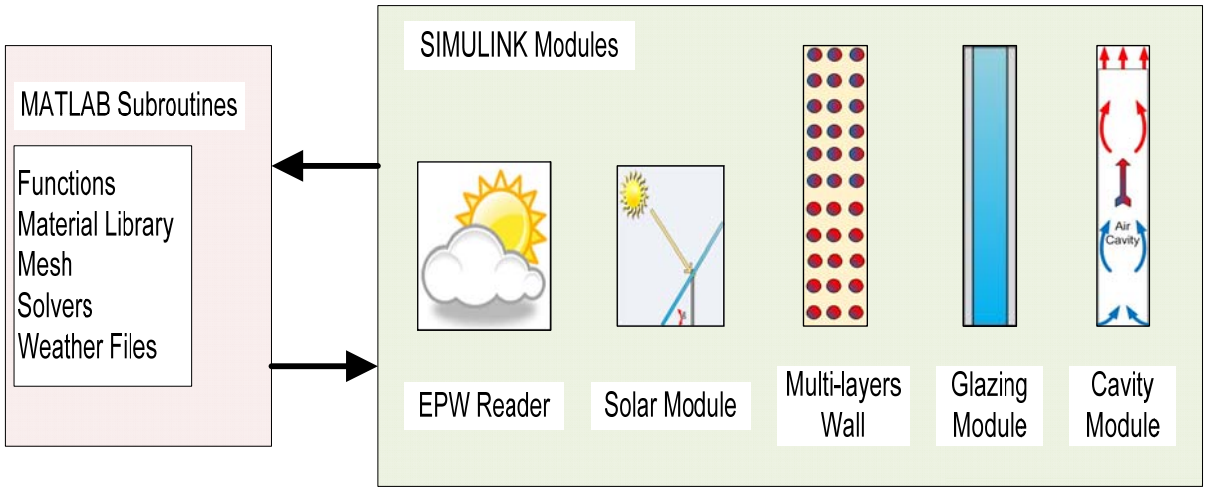

Figure 4.2 AdvFacSy Toolbox concept in SIMULINK

4.2.1 **Weather Data Reader**

The weather data is available in raw data formats for many years. The raw data is not suitable for building simulation programs. A typical weather year, representing many years of weather data, has to be selected for the energy analysis. Many typical weather data sets are internationally recognized for use in detailed energy simulation programs. Well known weather data sets are available for energy simulation such as Typical Metrological Year (TMY,TMY2 and TMY3)[231]. Simulation programs use these weather data either in their original format or change them to a format that is compatible with its calculation engine. To run EnergyPlus file for example, a weather file utility is used to convert other formats to a compatible format "EPW". AdvFacSy uses EPW format where the weather file is read and processed for solar calculations. According to **Figure 4.3**, the flexibility is given to select the simulation time period. Under the hood, the weather data block reads the weather file from the workspace of MATLAB. The module then combines all the necessary data in a vector output to be used by other components. The sky radiative temperature is calculated in this module using the following relationship[158]:

$$T_{sky} = \left(\frac{Horizontal\_IR}{\sigma}\right)^{0.25} - 273.15 \quad , [°C]$$ Equation 4-1

Where:

Horizontal_IR: Horizontal infrared radiation intensity [Wh/m^2]

σ : Stefan–Boltzmann constant [W/m^2.K^4]

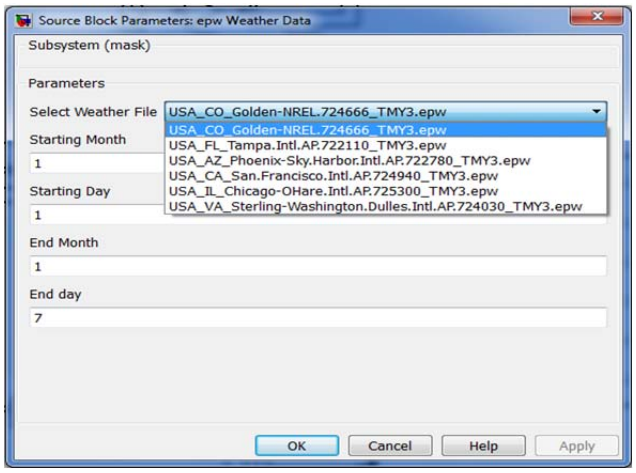

a. User interface for selecting weather file and simulation run time

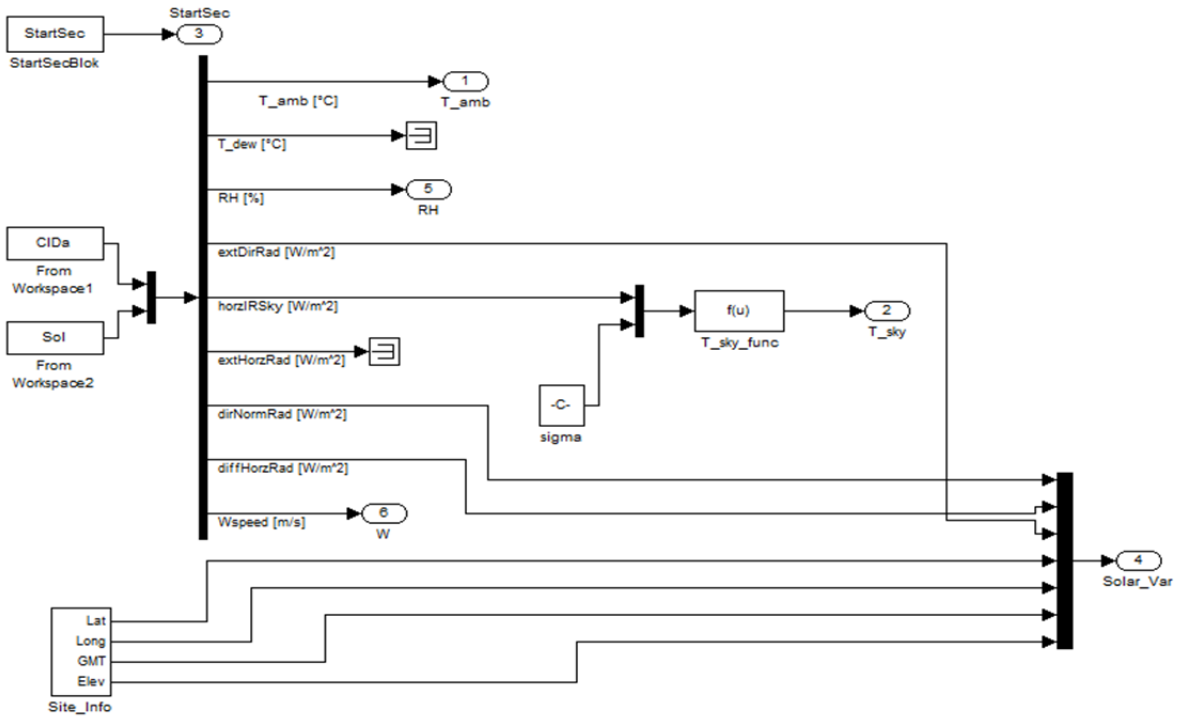

b. SIMULINK model for Weather data reader

Figure 4.3 Weather data reader and processor block in AdvFacSy

4.2.2 **Solar Radiation Model**

Solar radiation model is important since it provides boundary condition for the exterior envelope. A variety of solar models can be used to calculate the solar radiation received on tilted surfaces such as isotropic sky model and anistropic sky models [232]. While isotropic sky model is simple, it underestimates the total solar radiation received on sloped surfaces. On other hand, anistropic sky models consider individual components of diffusive part. Examples of anistropic sky models implemented in building simulation programs include those developed by Klucher [233], Hay and Davies [234], Reindl et al. [235], Muneer [236], Perez et al. [237], and improved Perez model published in 1990 [238]. A study has empirically validated the above solar models using building energy simulation programs for two periods during 25 days in October and March/April [239]. The mean absolute difference between the hourly measured and the predicted vertical irradiance were found to be:

1) isotropic sky model:
    a) 13.7% when using TRNSYS-TUD and
    b) 14.9% when using ESP-r
2) Hay–Davies model: 9.1% for TRNSYS-TUD
3) Reindl model: 9.4% using TRNSYS-TUD
4) Muneer model: 7.6% using ESP-r
5) Klucher model: 13.2% when using ESP-r
6) Improved Perez models 1990:
    a) 9.0% using EnergyPlus,
    b) 7.7% using DOE2.1e,
    c) 6.6% using TRNSYS-TUD, and

d) 7.1% using ESP-r

7) Perez model 1987: 7.9% when using ESP-r

For this research, the solar module is based on the improved Perez model 1990 [238]. This model is also used in EnergyPlus with updated coefficients [158]. The total solar radiation received on titled surface is composed of three components: beam, diffusive and reflected solar radiation from ground. Using the Perez model, the total solar radiation received on titled surface can be written as[232]:

$$I_T = I_{b,n} * Cos(\theta) + I_d * \left[(1 - F_1) * \left(\frac{1+Cos(\beta)}{2}\right) + F_1 * \frac{a}{b} + F_2 * Sin(\beta)\right] + I_h * \rho_g * \left(\frac{1-Cos(\beta)}{2}\right) \quad \text{Equation 4-2}$$

Where:

$I_{b,n}$: direct normal solar radiation, [W/m^2]
I_d: diffuse solar radiation on horizontal surface, [W/m^2]
I_h : total solar radiation on horizontal surface (=$I_{b,n} * \sin(\alpha_s) + I_d$), [W/m^2]
α_s : solar altitude angle
θ : angle of incident of beam radiation on a surface
β : surface tilt angle
ρ_g : ground reflectance (=0.2 for grass, 0.8 for snow)
$a = max(0, cos(\theta))$, $b = max(cos(85°), cos(\theta))$
F_1 : circumsolar brightness coefficient ($F_1 = max\left[0, (f_{11} + f_{12}\Delta + f_{13}\frac{\pi\theta_z}{180})\right]$)
F_2 : horizon brightness coefficients ($F_2 = f_{21} + f_{22}\Delta + f_{23}\frac{\pi\theta_z}{180}$)
θ_z :zenith angle
$\Delta = m\frac{I_d}{I_{on}}$
I_{on}: extraterrestrial normal-incidence radiation, [W/m^2]
m: air mass

The coefficients f_{11} , f_{12}, f_{13}, f_{21} , f_{22}, f_{23} are based on **Table 4-1**[158, 238].

Table 4-1 Coefficients as function of sky clearness range [158, 238]

ε Range	1.000-1.065	1.065-1.23	1.23-1.500	1.500-1.950	1.950-2.800	2.800-4.500	4.50-6.200	>6.200
f_{11}	-0.0083117	0.1299457	0.3296958	0.5682053	0.8730280	1.1326077	1.0601591	0.6777470
f_{12}	0.5877285	0.6825954	0.4868735	0.1874525	-0.3920403	-1.2367284	-1.5999137	-0.3272588
f_{13}	-0.0620636	-0.1513752	-0.2210958	-0.2951290	-0.3616149	-0.4118494	-0.3589221	-0.2504286
f_{21}	-0.0596012	-0.0189325	0.0554140	0.1088631	0.2255647	0.2877813	0.2642124	0.1561313
f_{22}	0.0721249	0.0659650	-0.0639588	-0.1519229	-0.4620442	-0.8230357	-1.1272340	-1.3765031
f_{23}	-0.0220216	-0.0288748	-0.0260542	-0.0139754	0.0012448	0.0558651	0.1310694	0.2506212

The sky clearness parameter (ε) is calculated using the following equation:

$$\varepsilon = \frac{\frac{\mathrm{I_d} + \mathrm{I_{b,n}}}{\mathrm{I_d}} + 5.535e10^{-6} * \theta_z^3}{1 + 5.535e10^{-6} * \theta_z^3} \qquad \text{Equation 4-3}$$

For a specific location (longitude, latitude) at a given time of the year (date, time), the solar geometrical angles (α_s, θ, θ_z) can be calculated. The angle of incident (θ), zenith angle (θ_z), and solar altitude angle (α_s) are calculated using the following relationships [232]:

$$cos(\theta) = \sin(\delta)\sin(\emptyset)\cos(\beta) - \sin(\delta)\cos(\emptyset)\sin(\beta)\cos(\gamma) + \cos(\delta)\cos(\emptyset)\cos(\beta)\cos(\omega) + \cos(\delta)\sin(\emptyset)\sin(\beta)\cos(\gamma)\cos(\omega) + \cos(\delta)\sin(\beta)\sin(\gamma)\sin(\omega) \qquad \text{Equation 4-4}$$

$$cos(\theta_z) = sin(\alpha_s) = \cos(\emptyset)\cos(\delta)\cos(\omega) + \sin(\emptyset)\sin(\delta) \qquad \text{Equation 4-5}$$

δ: declination angle
ω : hour angle
$\emptyset$: latitude
γ : surface azimuth angle

The declination angle(δ) and hour angle (ω) can be found using:

$$\delta = 23.45\, sin\left(360 * \frac{284 + n}{365}\right) \qquad \text{Equation 4-6}$$

$$\omega = 15 * (\mathrm{AST} - 12) \qquad \text{Equation 4-7}$$

Where:

n: day of the month, AST: actual solar time [hours]

The actual solar time (AST) can be found using the following relationship:

$$\text{AST} = \text{LST} + \text{ET}/60 - (\text{local standard merdian} * 15 - \text{longitude})/15 \quad \text{Equation 4-8}$$

Where: LST: local standard time [hrs] , ET: equation of time [minutes]

The equation of time (ET) can be determined using the following relationship:

$$\text{ET} = 9.87\sin(2\text{B}) - 7.53\cos(\text{B}) - 1.5\sin(\text{B}) \quad \text{Equation 4-9}$$

Where B is found from the following:

$$\text{B} = 360 * (\frac{\text{n}-81}{365}) \quad \text{n: day of the month} \quad \text{Equation 4-10}$$

Figure 4.4 illustrates the solar module implementation in SIMULINK. Equations above are hard coded into a MATLAB function file in SIMULINK as per **Figure 4.4** (b).

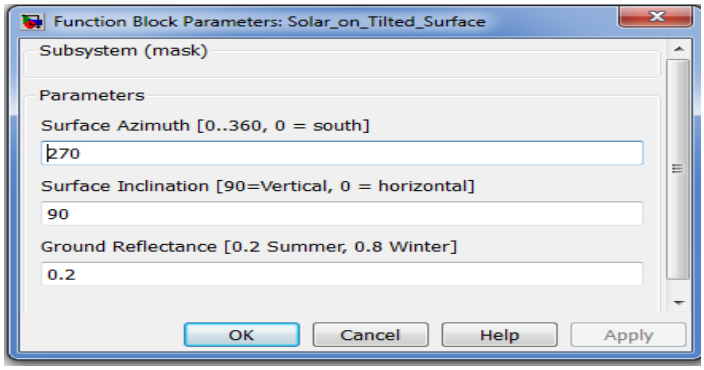

a. User interface for parameters input for calculating the solar radiation on tilted surface

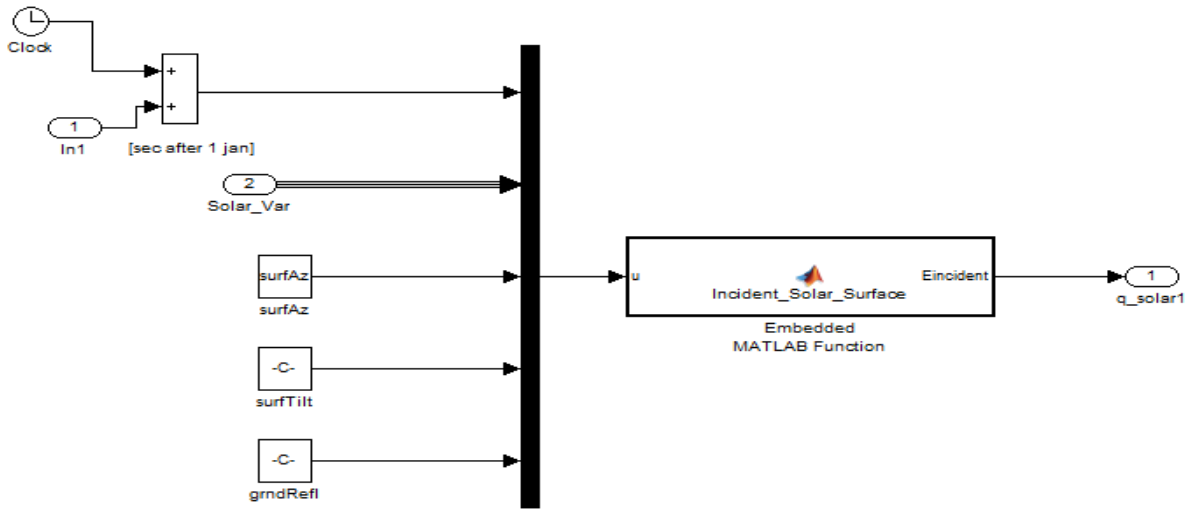

b. SIMULINK blocks calculating the solar on tilted surface

Figure 4.4 SIMULINK Module for calculating Solar in AdvFacSy

4.2.1 Verification of Weather and Solar Modules

The solar model is verified using the results from EnergyPlus hourly and sub-hourly bases as shown in **Figure 4.5**. Under different orientations, a wall located in Golden, Colorado with a solar absorption of 0.9 was simulated using EnergyPlus and the developed modules in SIMULINK. The results for both outdoor air temperature and solar radiations received on titled surfaces show that the model developed for this research is in good agreement with EnergyPlus at hourly and sub hourly time step.

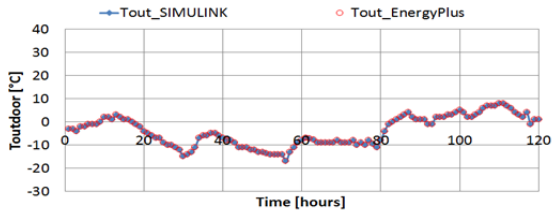

a) Outdoor air Temperature profile at 1 hour time step

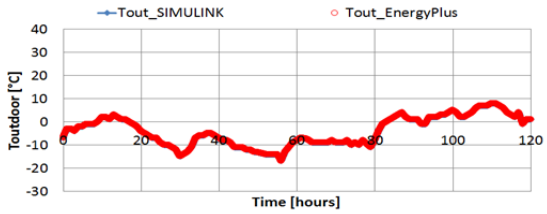

b) Outdoor air Temperature profile at 3 minutes time step

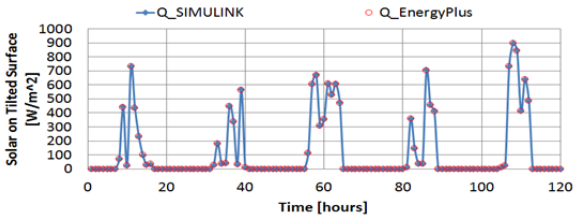

c) Solar radiation on South wall at 1 hour time step

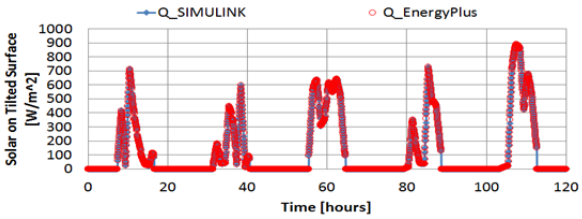

d) Solar radiation on South wall at 3 minutes time step

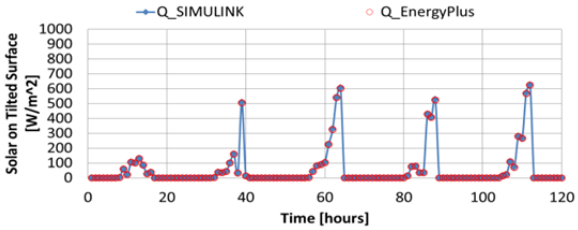

e) Solar radiation on West wall at 1 hour time step

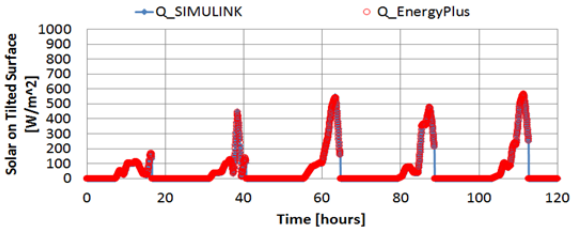

f) Solar radiation on West wall at 3 minutes time step

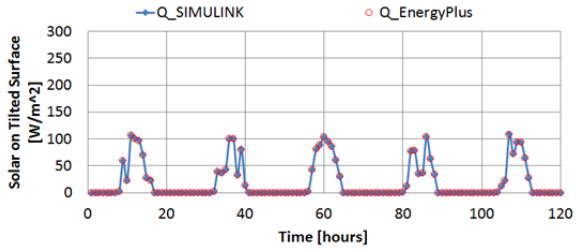

g) Solar radiation on North wall at 1 hour time step

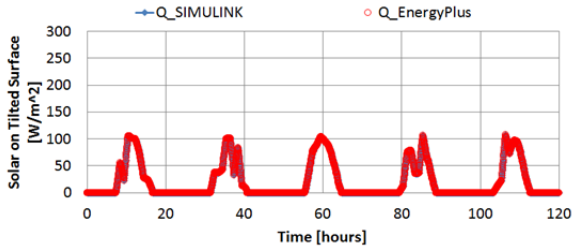

h) Solar radiation on North wall at 3 minutes time step

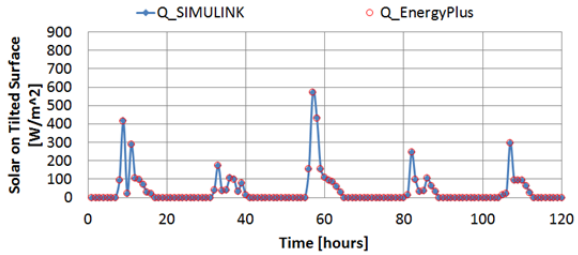

i) Solar radiation on East wall at 1 hour time step

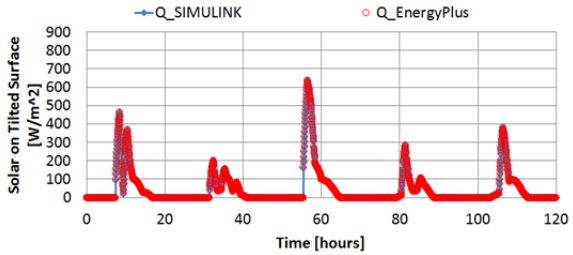

j) Solar radiation on East wall at 3 minutes time step

Figure 4.5 Verification of weather reader and solar model with hourly and sub-hourly EnergyPlus Simulation

4.1 Modeling of Wall Systems using AdvFacSy

Using the AdvFacSy toolbox, several wall designs shown in **Figure 4.6** can be easily generated and assessed under different climatic conditions. The main advantages of the developed standalone toolbox are the quick, reliable and the trouble-free evaluation of the complex façade systems by drag, drop and link blocks in one SIMULINK screen.

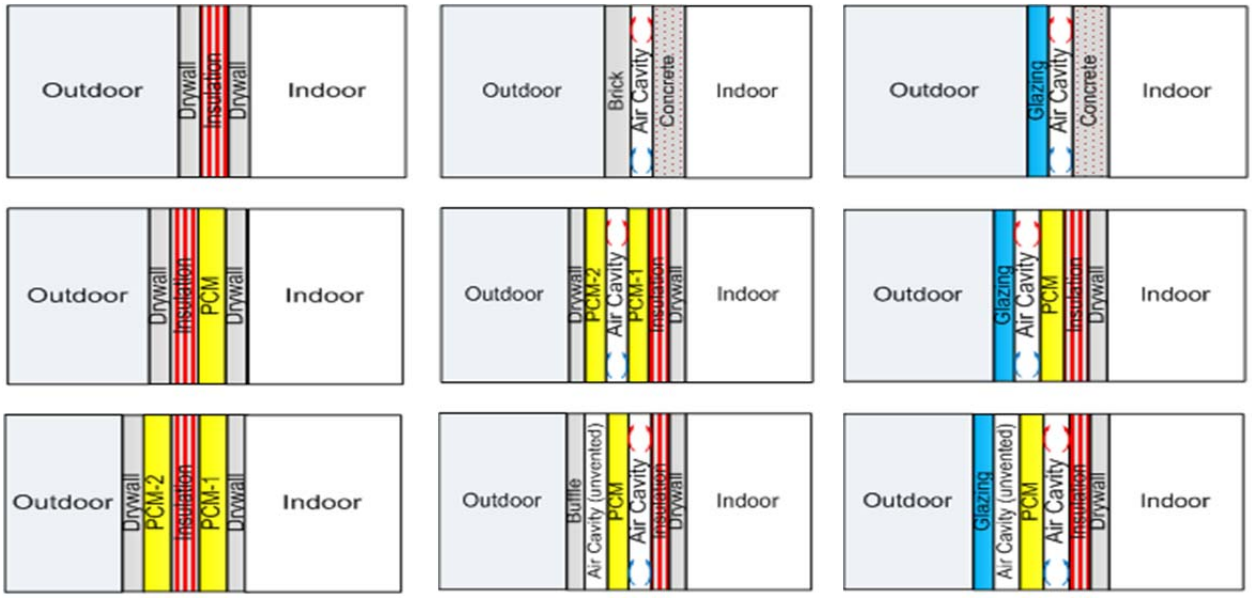

a) Multi-layers walls b) Ventilated opaque multi-layers walls c) Ventilated transparent multi-layers walls

Figure 4.6 Classical and advanced façade designs with and without PCMs in "AdvFacSy" Toolbox

In addition to envelope designs, the toolbox can be used to evaluate different operational strategies to charge and discharge energy stored in PCMs using the air in the cavity as a heat transfer medium. The air is driven by thermal buoyancy or mechanical fan. The air can be induced from the outdoor environment or indoor via air vents located at top and bottom of the façade system. The controlling mechanism facilitates the charging and discharging of PCMs in the wall unit. The recovered heat can then be directly used to meet the heat demand, or used to

preheat fresh air before treated centrally in air conditioning system, or transported to other heat storage medium for later usage.

In order to simplify the calculation procedure, the wall designs described above can be represented using the resistance-capacitance (R-C) thermal network shown in **Figure 4.7**. Using the R-C network, heat balance equation was written and numerically solved using methods explained in Chapter 3.

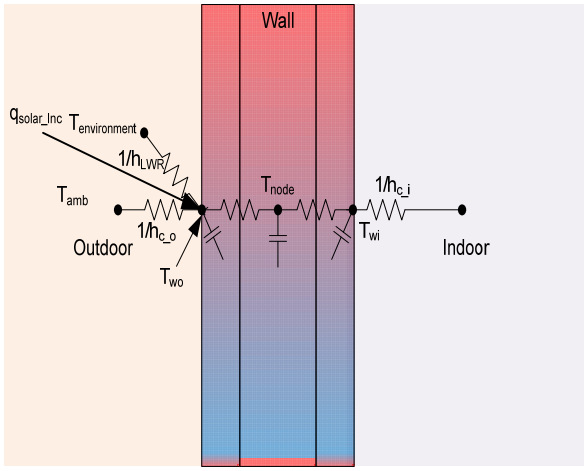

a) R-C Network for multilayer Wall

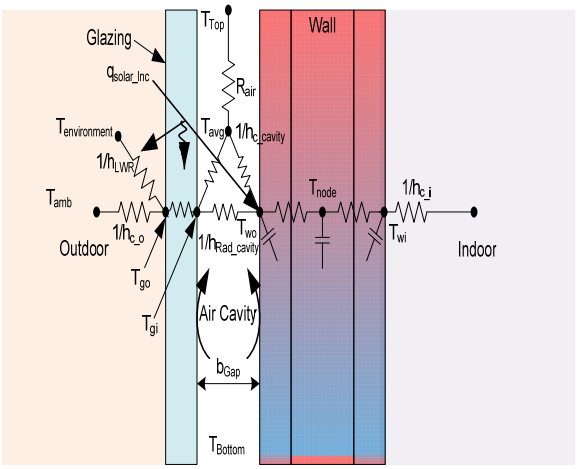

b) R-C Network for ventilated cavity multilayer Wall

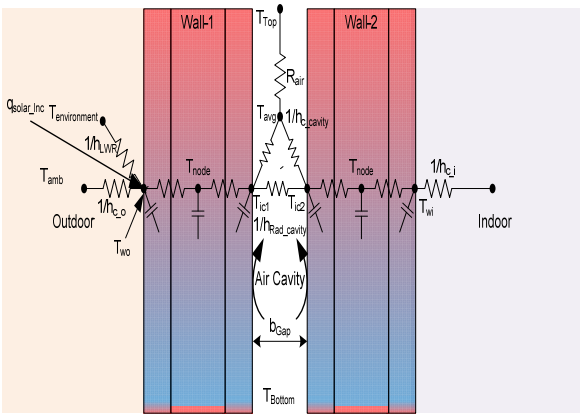

c) R-C Network for multilayer double Wall with ventilated cavity

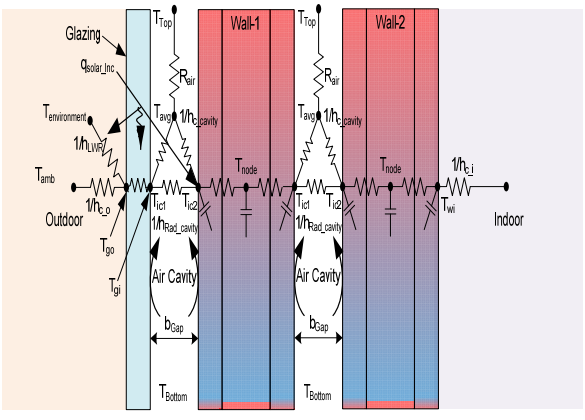

d) R-C Network for multi-cavities multilayer double Walls

Figure 4.7 R-C Network for various wall designs with and without PCMs in "AdvFacSy" Toolbox

4.2 Multilayer wall with PCM

In AdvFacSy toolbox, two numerical schemes are used to solve the multilayer walls; the iterative correction scheme suggested by Swaminathan and Voller [53] and the hybrid scheme proposed in this study. A south wall with PCM was simulated under the SIMULINK environment using Golden, CO weather file. The above weather and solar radiation model was used to provide boundary conditions. **Figure 4.8** shows an example of parameter's inputs and the SIMULINK blocks for modeling the multilayer module.

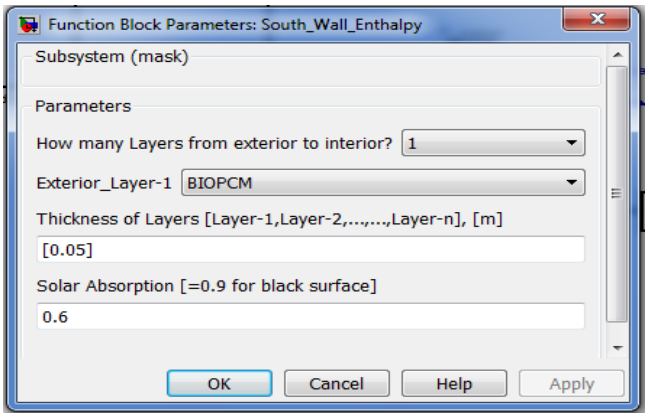

a. User interface for parameters input for multilayer wall

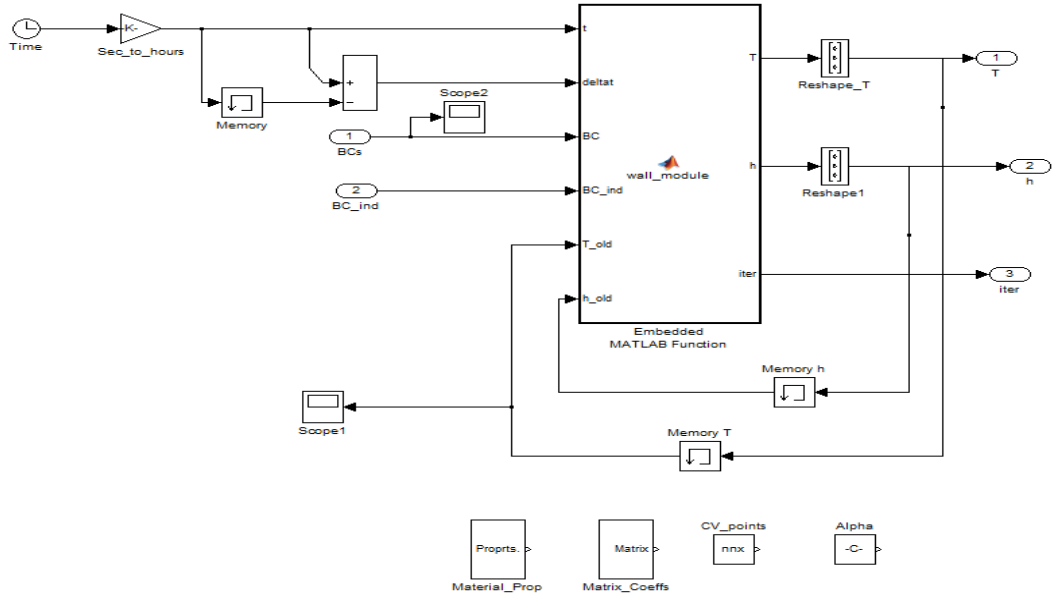

b. SIMULINK blocks solving the heat equation of phase change

Figure 4.8 SIMULINK module for solving multilayer wall in AdvFacSy

4.2.1 Verification case

A verification case was carried out using EnergyPlus at hourly and sub-hourly time steps (i.e., 3 minutes time interval). The wall configuration is similar to that described in **Table 3-5**. The surface temperatures from the SIMULINK model and EnergyPlus for this wall design are shown in **Figure 4.9**. The results for both time steps (i.e., 1 hour and 3 minutes) show good agreement with EnergyPlus results.

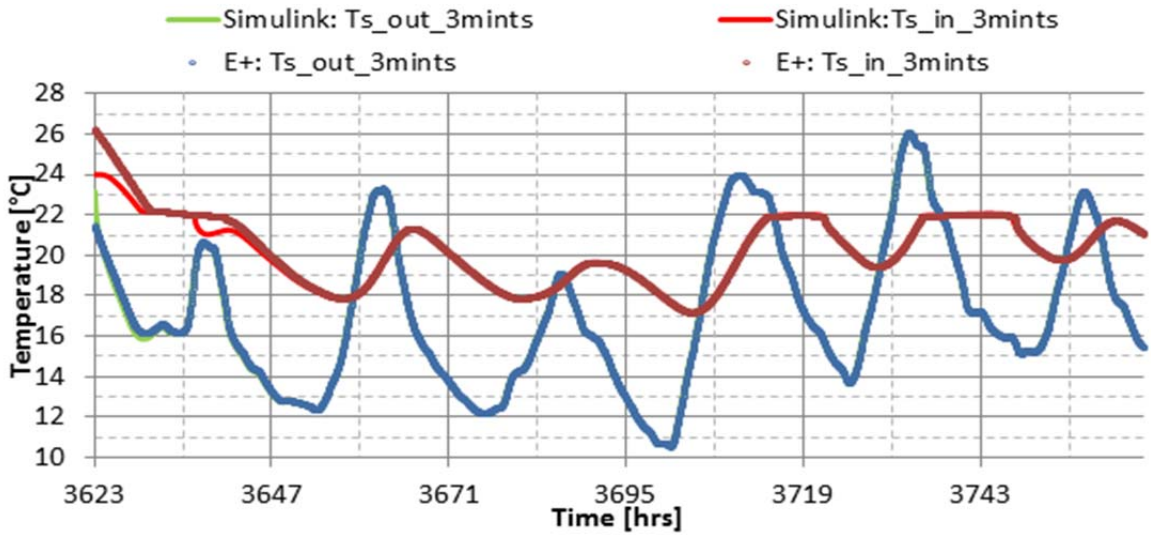

a) Interior and exterior surface Temperatures for 6 days at 3 minutes time step

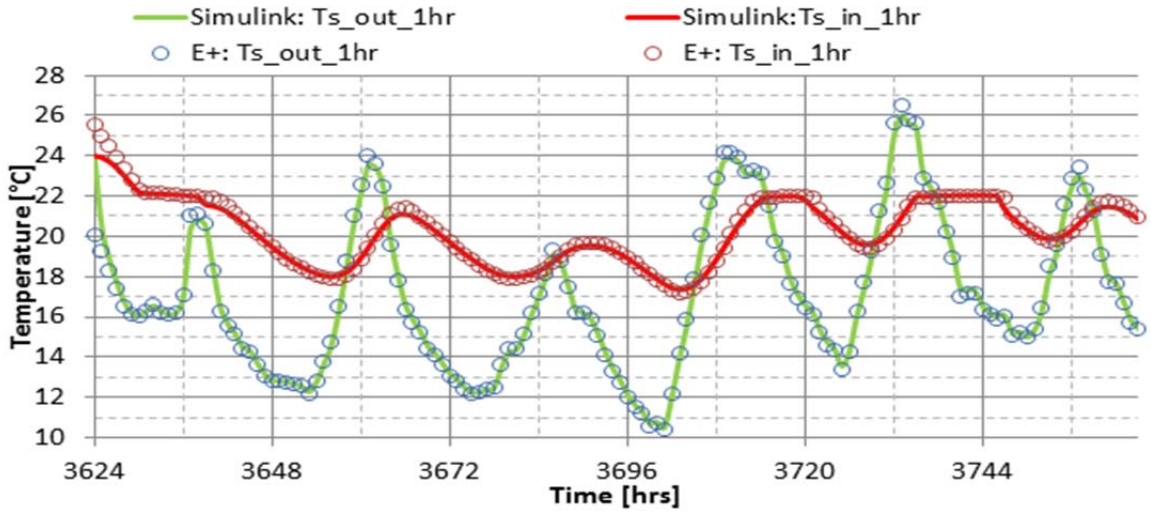

b) Interior and exterior surface Temperatures for 6 days at 1 hour time step

Figure 4.9 SIMULINK Vs EnergyPlus for south wall with PCM in Golden, CO

4.3 Ventilated Façade System

The library of "AdvFacSy" includes a cavity and a glazing module. A wall with a ventilated cavity and glazing placed to the exterior side experiences different heat transfer mechanism. This complex system can be divided into three distinguished but interconnected modules in SIMULINK: glazing, air cavity and PCM wall. The complex heat transfer between these three components is described using RC network shown in **Figure 4.7** (b). **Figure 4.10** shows the ventilated cavity module in SIMULINK.

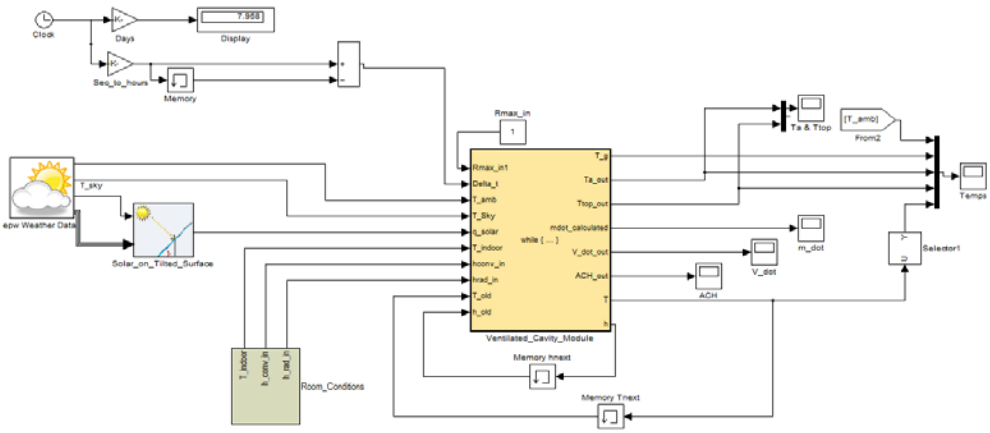

a. High level ventilated cavity wall blocks in SIMULINK

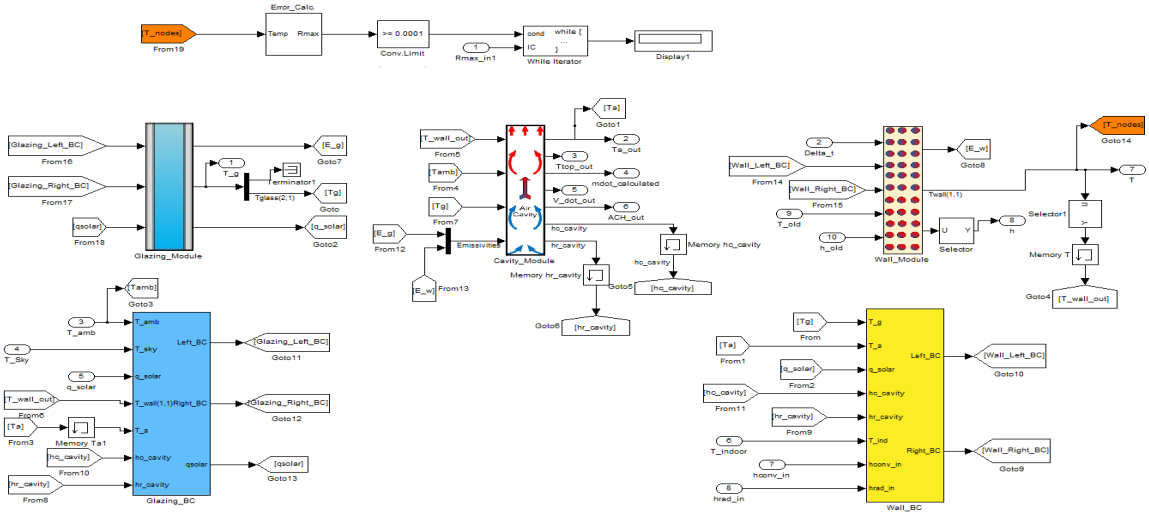

b. SIMULINK blocks for ventilated cavity wall: wall, cavity and glazing blocks

Figure 4.10 Ventilated cavity multi-layer wall in SIMULINK Tool 'AdvFacSy'

4.3.1 **Glazing Module**

The outside surface exchanges heat by convective and radiative heat transfer. For a glazing with two nodes, the outside node exchange heat with ambient air through convective heat transfer. The same node experiences long wave radiation with sky, ground and air through long wave radiation. In addition and depends on the type of glazing, part of short wave radiation from the sun may be absorbed. Interior glazing node exchanges heat with air cavity through convective heat transfer and radiative heat transfer with outside wall surface node. Neglecting the heat capacity of glazing's and performing a heat balance on these two nodes yield the following steady state equations:

$\underline{Node\,1:}$

$$q_{in} = q_{out}$$

$\underline{\underline{a)\ q_{in}}}$

$$q_{in} = q_{solar\_abs} + q_{conv} + q_{LWR}$$

$$q_{solar\_abs} = \frac{q_{absorbed}}{2}$$

$$q_{conv} = h_{c\_o} * (T_{amb} - T_{go})$$

$$q_{LWR} = h_{Sky} * (T_{sky} - T_{go}) + h_{ground} * (T_{ground} - T_{go}) + h_{air} * (T_{amb} - T_{go})$$

Radiative heat transfer coefficients between the glazing, sky (h_{Sky}) , ground (h_{ground}), and air (h_{air}) can be found using the following relationships[158]:

$$h_{grnd} = \sigma * \varepsilon_{w} * F_{ground} \frac{((T_{ground} + 273)^4 - (T_{s,ext} + 273)^4)}{(T_{ground} - T_{s,ext})}$$

$$h_{Sky} = \sigma * \varepsilon_{w} * F_{Sky} * \beta * \frac{((T_{sky} + 273)^4 - (T_{s,ext} + 273)^4)}{(T_{sky} - T_{s,ext})}$$

$$h_{air} = \sigma * \varepsilon_{w} * F_{Sky} * (1-\beta) * \frac{((T_{amb} + 273)^4 - (T_{s,ext} + 273)^4)}{(T_{amb} - T_{s,ext})}$$

Where:

$F_{ground} = 0.5*(1-\cos(surfTilt)),\ F_{Sky} = 0.5*(1+\cos(surfTilt)),\ \beta = \sqrt{F_{Sky}}, \sigma = 5.67e\text{-}8$ W/m^2.K^4

b) q_{out}

$$q_{out} = q_{conduction} = -k_g * \frac{T_{gi} - T_{go}}{d/2}$$

Collecting terms and rearranging for node 1:

$$(\frac{2*k_g}{d} + h_{c\_o} + h_{ground} + h_{sky} + h_{air}) * T_{go} - (\frac{2*k_g}{d}) * T_{gi} = \frac{\alpha\_g * q_{solar}}{2} + T_{amb} * (h_{c\_o} + h_{air}) + T_{sky} * h_{sky} + T_{ground} * h_{ground}$$

Equation 4-11

Node 2:

$q_{in} = q_{out}$

a) q_{in}

$q_{in} = q_{conduction} + q_{solar\_abs}$

$$q_{conduction} = -k_g * \frac{T_{gi} - T_{go}}{d/2}$$

$$q_{solar\_abs} = \frac{q_{solar} * \alpha\_g}{2}$$

b) q_{out}

$$q_{out} = q_{convection\_cavity} + q_{Rad\_Cavity}$$

$$q_{convection\_cavity} = -h_{c\_cavity} * (T_{avg} - T_{gi})$$

$$q_{Rad\_cavity} = -h_{Rad\_cavity}(T_{wo} - T_{gi})$$

$$h_{Rad\_cavity} = \sigma * \mathrm{F}_{glass\_wall} * \frac{((T_{wo}+273)^4 - (T_{gi}+273)^4)}{(T_{wo} - T_{gi})}$$

$$\mathrm{F}_{glass\_wall} = \frac{1}{(\frac{1}{\varepsilon_g} + \frac{1}{\varepsilon_w} - 1)}, \sigma = 5.67\text{e-}8\ \mathrm{W/m^2.K^4}$$

Collecting terms and rearranging for node 2:

$$(-\frac{2*k_g}{d}) * T_{go} + (\frac{2*k_g}{d} + h_{c\_cavity} + h_{Rad\_cavity}) * T_{gi} = \frac{\alpha_g * q_{solar}}{2} + h_{c\_cavity} * T_{avg} + h_{Rad\_cavity} * T_{wo} \qquad \text{Equation 4-12}$$

Figure 4.11 shows the user interface of the glazing module in SIMULINK toolbox.

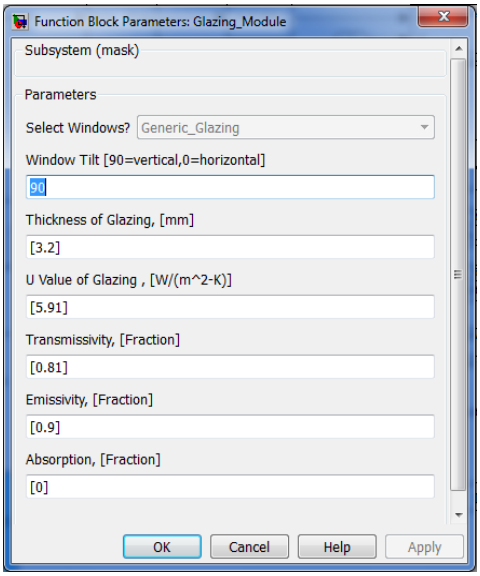

a. User interface for parameters input of glazing block

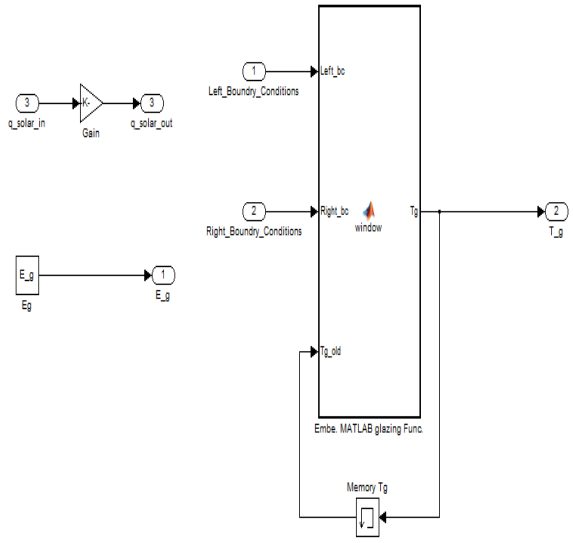

b. Glazing block representation in SIMULINK

Figure 4.11 Glazing module in 'AdvFacSy'

4.3.1 **Air Cavity Module**

This module is similar to that developed in TRNSYS, TYPE36 and fully described by Utzinger [240]. For this module, the air heat capacity is assumed to be negligible in the cavity and therefore a steady state heat balance equation is derived with only one node when air is flowing. The air exchanges heat with inside surface of glazing and outside surface of the wall by convection heat transfer. According to **Figure 4.12**, a heat balance was performed over a small height (dz) which yields the following equation:

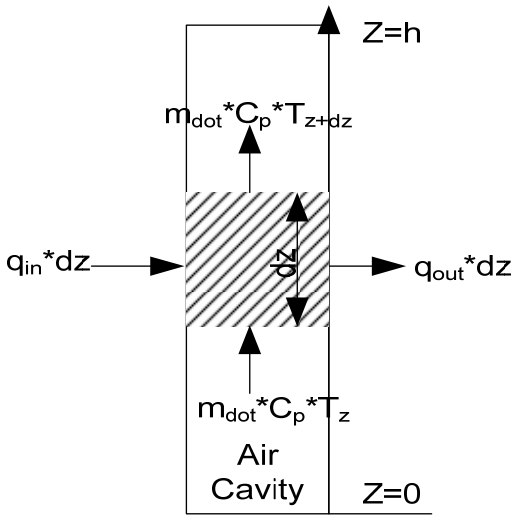

Figure 4.12 Air cavity heat balance

$$\dot{m} * c_p * T_z - \dot{m} * c_p * T_{z+dz} = q_{in} * dz - q_{out} * dz$$
$$q_{in} = h_{c\_cavity} * w * (T_z - T_{gi})$$
$$q_{out} = -h_{c\_cavity} * w * (T_z - T_{wo})$$

$$-\dot{m} * c_p * \frac{dT}{dz} = h_{c\_cavity} * w * (T_z - T_{gi}) + h_{c\_cavity} * w * (T_z - T_{wo})$$
$$w : wall \quad width$$

$$\dot{m} * c_p * \frac{dT}{dz} = h_{c\_cavity} * w * (T_{gi} - T_z) + h_{c\_cavity} * w * (T_{wo} - T_z) \quad \text{Equation 4-13}$$

Equation 4-13 can be solved analytically using separation of variables and integrating over wall height and width resulting into the following relationships [240]:

$$T_{out} = T_{in} + \frac{2 * T_{in} - T_{wo} - T_g}{2} * [\exp - (\frac{2 * h_{c\_cavity} * A}{\dot{m} * c_p}) - 1] \quad \text{Equation 4-14}$$

$$T_{avg} = T_{in} + \frac{2 * T_{in} - T_{wo} - T_g}{2} * [-\frac{\dot{m} * c_p}{2 * h_{c\_cavity} * A} * (\exp - (\frac{2 * h_{c\_cavity} * A}{\dot{m} * c_p}) - 1) - 1] \quad \text{Equation 4-15}$$

$$R_{air} = \frac{\Delta T}{\dot{q}} = \frac{A * (T_{avg} - T_{in})}{\dot{m} * c_p * (T_{top} - T_{in})} \quad \text{Equation 4-16}$$

The mass flow rate ($\dot{m}$) is derived using Bernoulli's equation which gives [232, 240]:

$$\dot{m}\ [kg/s] = \rho * C_D * A * \sqrt{\frac{g * H * (T_{avg} - T_{in})}{T_{avg}}} \quad \text{Equation 4-17}$$

$$C_D = \sqrt{\frac{2}{C_1 * (\frac{A}{A_v})^2 + C_2}}, \quad \text{Equation 4-18}$$

Where:

C_D: pressure loss of the system, A: wall area in m^2, A_v: vent area in m2, g: gravity, H: distance between vents, C_1: 8, C_2=2

Numerous studies suggested different correlations for Nusselt number that are used to determine the convective heat transfer inside the cavity "h_{c_cavity}" using the following relation:

$$h_{c\_cavity\ gi} = \frac{k * Nu}{b} \quad \text{Equation 4-19}$$

$$Nu : Nusselt\ \ number\ , k : fluid\ \ conductivi\ ty, b : cavity\ \ depth$$

Table 4-2 and **Table 4-3** summarizes the correlations proposed for ventilated wall when no flow and when air flows. TRNSYS TYP36 uses Randell et. al. [241] when there is no flow and Mercer Correlation [242] for laminar flow and Kays and Crawford [243] for turbulent flow. For this research, the same correlations are also used. **Figure 4.13** shows the user interface of the cavity module in SIMULINK.

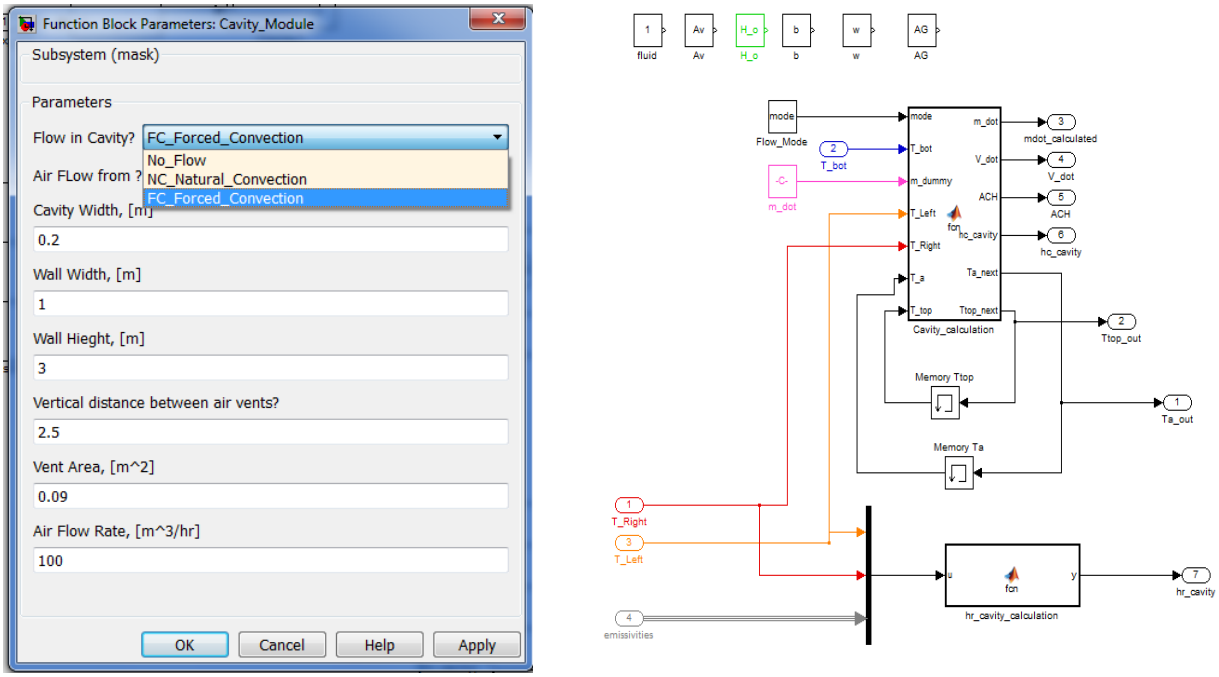

a. User interface for parameters input of ventilated cavity

b. Ventilated cavity block representation in SIMULINK

Figure 4.13 Ventilated cavity module in 'AdvFacSy'

Table 4-2 Nusselt Number correlations used for air cavity when no air flow allowed

	Correlations	Aspect Ratio (h/d)	Geometry	Application	Used or recommended
1	Randall et. al. [241]: $\overline{\mathrm{Nu}} = 0.0965 * (\mathrm{Gr.\,Pr})^{0.29}$		Parallel plates	Trombe Solar walls	TRNSYS Type 36
2	Holland et. al. [244] $\overline{\mathrm{Nu}} = \max\left[1, 0.288\left(\frac{\mathrm{Ra}}{\frac{\mathrm{h}}{\mathrm{d}}}\right)^{\frac{1}{4}}, 0.039 * (\mathrm{Ra})^{\frac{1}{3}}\right],$ $\mathrm{Ra} = \mathrm{Gr.\,Pr},\ \mathrm{Gr} = \frac{\beta * g * \rho^2 * d^3 * (T_s - T_f)}{\mu^2},\ T_f = \frac{T_{s1} + T_{s2}}{2}$		Parallel plates	composite Trombe Solar walls	[245]
3	Cane Correlation [246]: $\overline{Nu} = \left[1 + 0.89 * \cos(\beta - 60) * \left(\frac{Ra}{2420 * \left(\frac{h}{d}\right)^4}\right)^{(2.88 - 1.64 * \sin\beta}\right],$ $30 \le \beta \le 90\ and\ \frac{Ra}{\left(\frac{d}{h}\right)^4} \le 6000$	$\frac{h}{d} \ge 4\ or\ 3$	inclined square and hexagonal celled plastic honeycomb	transparent insulation system	[247]
4	ElSherbiny et al. [248]: $Nu_1 = 0.0605 * (Ra_l)^{1/3},\ \frac{h}{d} = 20,\ Ra_l < 2x10^6$ $Nu_2 = \left[1 + \left\{\frac{0.104 * (Ra_l)^{0.293}}{1 + (\frac{6310}{Ra_l})^{1.36}}\right\}^3\right]^{1/3},\ \frac{h}{d} = 40,\ Ra_l < 2x10^5$ $Nu_3 = 0.242 * \left(\frac{Ra_l}{h/d}\right)^{0.272},\ \frac{h}{d} = 80,\ Ra_l < 3x10^4$ $Nu = \max(Nu_1, Nu_2, Nu_3)$	$5 \le \frac{h}{d} \le 110$	cavities of façade elements	Comparison with other correlations and CFD study	[249]
5	Wright [250] and ISO 15099 [251]: $Nu_1 = 0.067383 * (Ra_l)^{0.3},\ 5x10^4 < Ra_l \le 10^6$ $Nu_1 = 0.028154 * (Ra_l)^{0.4134},\ 10^4 < Ra_l \le 5x\,10^6$ $Nu_1 = 1 + 1.75967\,x\,10^{-10} * (Ra_l)^{2.2984755},\ Ra_l \le 10^4$ $Nu_2 = 0.242 * (\frac{Ra_l}{\frac{h}{d}})^{0.272}$ $Nu = \max(Nu_1, Nu_2,)$	$\frac{h}{d} \ge 40$	Glazing windows	Comparison with other correlations and CFD study	[249]

Table 4-3 Nusselt Number correlations used for a ventilated cavity

	Correlation	Aspect Ratio (h/d)	Geometry	Application	Used or recommended
1	Mercer Correlation [242]: $\overline{Nu} = \left[4.9 + \frac{0.0606*(X^*)^{-1.2}}{1.0+0.0856*(X^*)^{-0.7}}\right]$, $Re < 2000\ (Laminar\ flow)\ and\ 0.1 < Pr < 10,\ X^* = \frac{L}{Re*Pr*D_H}$		Constant temperature on one side and insulated on the other side		TRNSYS Type 36
2	Kays and Crawford [243]: $\overline{\mathrm{Nu}} = [0.0158 * \mathrm{Re}^{0.8}],\ \mathrm{Re} > 2000$ (Turbulent flow)	If d/Dh=10, then increase by 16%			TRNSYS Type 36
3	Fishenden and Saunders [252] $\overline{Nu} = 0.107 * (Gr)^{1/3}$		For one plate	Used in composite Trombe Solar walls	[245, 253]
4	Tsuji and Nagano Correlation [254]: $Nu = 0.387 * (Ra)^{\frac{1}{3}}, Ra < 8x10^8$ $Nu = 0.120 * (Ra)^{\frac{1}{3}}, Ra > 3.5x10^9$		For one plate	Trombe Wall Application	[255]
5	Modified Tsuji correlation (only Turbulent) by Smolec and Thomas[256] : $Nu^{Mod} = F(Z_l) * Nu$ $where\ F(Z_l) = 1.074 * {Z_l}^2 - 5.16 * Z_l + 7.6$ Z_l: $distance\ from\ the\ bottom\ vent\ to\ the\ middle\ of\ the\ node$		For one plate	Trombe Wall Application	
6	Patt Correlation [257] $for\ K_e(loss\ coefficent)$=1: For wall: $Nu_l = 0.201 * (Gr_l)^{0.293},\ 2x10^9 < Gr_l < 8x10^9$ $Nu_l = 0.0450 * (Gr_L)^{0.358}, Gr_l > 8x10^9$, For windows: $Nu_l = 0.221 * (Gr_L)^{0.270}, 2x10^9 < Gr_l < 8x10^9$ $Nu_l = 0.0437 * (Gr_L)^{0.341}, Gr_l > 8x10^9$		For one plate	Used in Trombe Wall	[258]

7	Churchil and Chu Correlation[259]: $Nu = 0.68 + 0.67 * \frac{(Ra)^{\frac{1}{4}}}{\left[1+(\frac{0.492}{\mathrm{Pr}})^{9/16}\right]^{4/9}},\ Ra < 10^9$ $Nu^{1/2} = 0.825 + 0.387 * \frac{(Ra)^{0.17}}{\left[1+(\frac{0.492}{\mathrm{Pr}})^{\frac{9}{16}}\right]^{\frac{8}{27}}}, Ra > 10^9$	Uniform wall temperature for vertical plate	Composite Trombe-Mitchel Wall (theoretical study)	[260]
8	*Blended correlation:* $\overline{Nu} = \left[(\frac{1}{Nu_{sp}})^n + (\frac{1}{Nu_{fd}})^n\right]^{-(\frac{1}{n})}$ $Nu_{sp}: single\ plate\ , Nu_{fd}: fully\ developed\ flow$ *Churchill and Usagi correlation uses n=1.5* [261] *Bar-Cohen and Rohsenow correlation n=2* [262]		Ventilated Wall	[263]

4.3.2 **Verification case**

TRNSYS has TYPE36 that can be used for this case verification. It must be noted that there are limitations in using TYPE36:

1. Only one material layer is permitted
2. Phase change materials can't be modeled
3. Time step must be small

The developed numerical model is verified taking into considerations the above limitations. The ventilated façade system model can be used to model at least ten layers, model PCMs and can be used at high time step. For this case, a south wall is modeled as shown in **Table 4-4**. The interior, the exterior wall surface temperatures, air temperature at the top of the cavity, air mass flow rate and glazing temperatures are used for this comparison. **Figure 4.14** shows the SIMULINK results when compared to TRNSYS. The SIMULINK results are in good agreement with TRNSYS.

Table 4-4 Parameters used for a south ventilated cavity Wall

Test Parameter	Layer: Concrete	Units
Wall height	3	m
Wall width	1	m
Thermal Conductivity	0.8117	W/m.K
Density	1900	kg/m^3
Specific Heat Capacity	949	J/kg.K
Thickness	0.15	m
Mesh Grid Points	10	
Indoor Temperature	20	$^{\circ}C$
External Convective Heat transfer Coefficient	29.3	$W/m^2.K$
Internal Convective Heat transfer Coefficient	8.29	$W/m^2.K$
Solar absorption	0.9	
Emissivity of the massive wall	0.9	
Wall width	1	m
Cavity		
Depth, (b)	0.2	m
Vent Area, (A_v)	0.09	m^2
Vertical distance between two vents, (Ho)	2.5	m
Flow characteristic	Natural Convection	
Air induced	From outside	
Glazing		
Number of glazing	1	
Emissivity of the glazing	0.9	
Transmissivity of the glazing, τ	0.81	
Simulation Parameters		
Time Step	5	minutes
Weather file	EPW for Golden, Colorado	

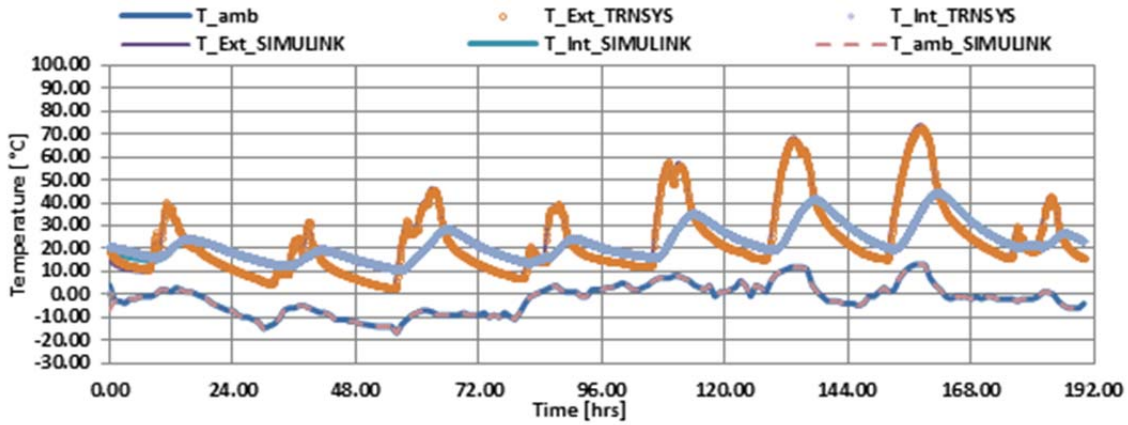

a) Interior and Exterior Surface Temperatures

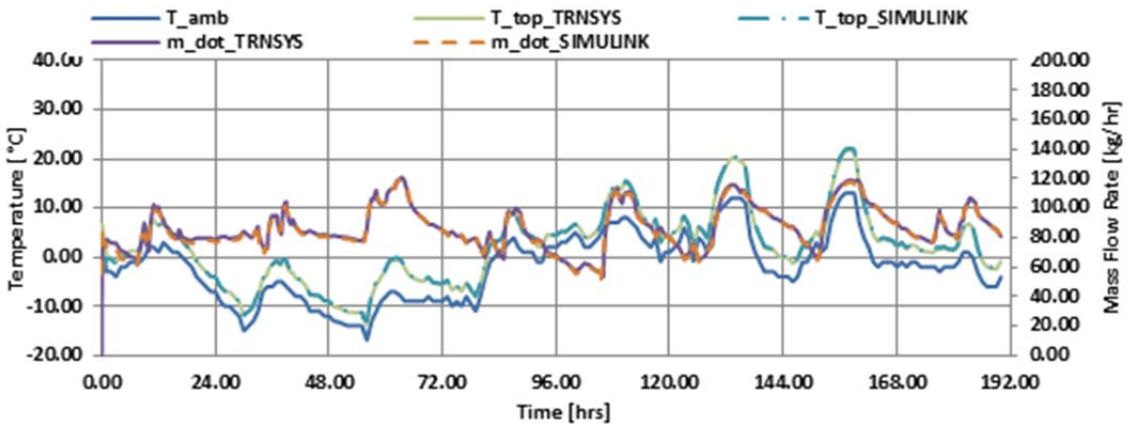

b) Leaving air temperature at the top vent and mass flow rate

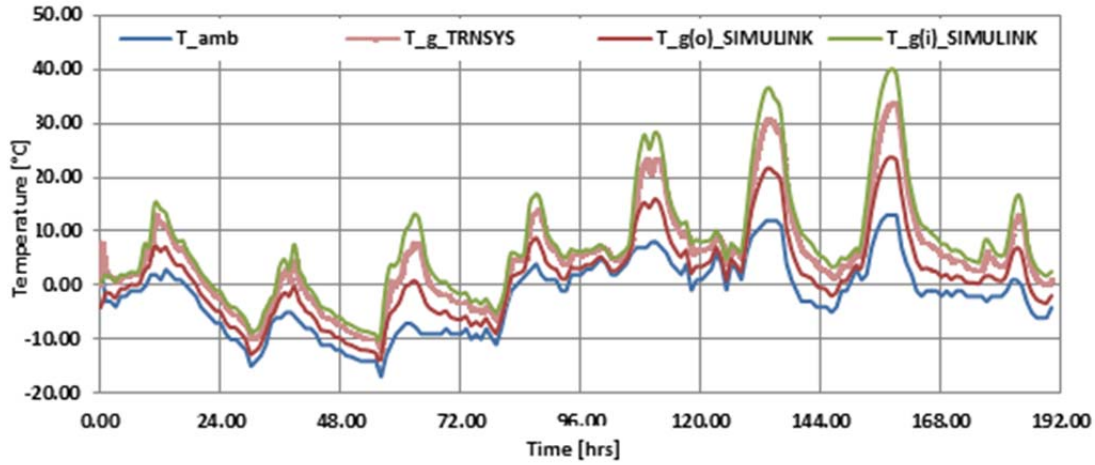

c) Glazing surface Temperatures

Figure 4.14 Verification of ventilated cavity wall against TRNSYS results

4.4 Summary

A list of modules for simulating advanced wall designs has been developed in MATLAB/SIMULINK environment. Different modules including: weather reader, solar processor, wall, glazing and ventilated cavity modules are generated using standard SIMULINK blocks and MATLAB function files. Using these modules, a variety of advanced façade systems can be easily modeled. Examples include a multi-layers wall, ventilated cavity with single wall, ventilated cavity with double walls, multi-cavities with double wall etc. These wall modules can be simulated with or without PCMs. The utilities functions such as weather file reader and solar modules have been verified against results from EnergyPlus. In addition, two wall designs; multi-layers wall and ventilated cavity wall have been verified against EnergyPlus and TRNSYS. The models have shown good agreement with results from EnergyPlus and TRNSYS. This verifies the reliability of the design tool for modeling advanced façade systems.

CHAPTER 5: SIMULATION OF ADVANCED FAÇADE SYSTEMS USING ADVFACSY TOOLBOX

Latent heat storage using embedded-PCM in building enclosure is a promising technology to reduce the inherited climatic deficiency of lightweight buildings. PCM can be integrated into active or passive building systems. In this chapter, the passive use of PCM is investigated for lightweight envelope in residential buildings. Various PCM locations are considered in different orientations for multilayer wall design. The performance of PCM layer is investigated under fixed indoor environment and varying outdoor environment using TMY weather file. The results from this chapter give insights on the performance of PCM under ideal indoor environment. Furthermore, cavity design with PCM is investigate to further enhance the heating performance of PCM. Design guidelines are developed for using PCM in multilayer walls and ventilated cavity designs. These guidelines can be used as a design tool for new installations or retrofitting efforts in residential building.

5.1 PCM's Containment

PCM can be integrated into envelope systems using different approaches. Recent studies have outlined various containment technologies for PCMs such as: impregnation, micro-encapsulation, shape-stabilized PCMs and macro-encapsulation using containers [13, 24]. Traditionally, building material such as wood or wallboard is soaked into PCMs at liquid state [129, 135, 195]. One disadvantage of the imbibing process is that PCMs tend to leak during the melting process. To retain the structural integrity, the mass of PCMs is limited when using this method. In addition, some PCMs are corrosive but also vaporize due to environmental exposure

when at liquid state. Therefore, containment is perhaps a necessity to overcome the above limitations. One solution to overcome the leakage problem is to encapsulate the PCM into small capsules using "*Microencapsulation*" containment technology. PCMs are enclosed into microscopic polymer shells to form powder which is added to building materials as those illustrated in **Figure 5.1**.

a) PCM powder at room conditions [264]

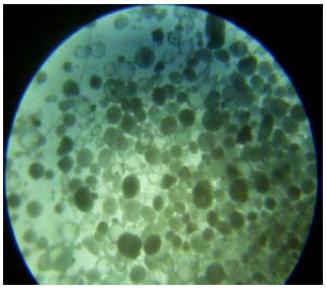

b) A particle of PCM powder under 40X microscope [264]

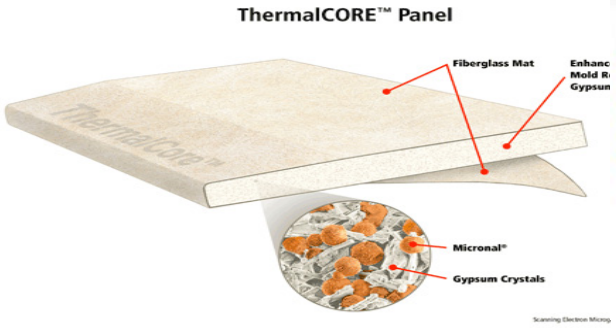

c) ThermalCORE® by Natural Gypsum [265]

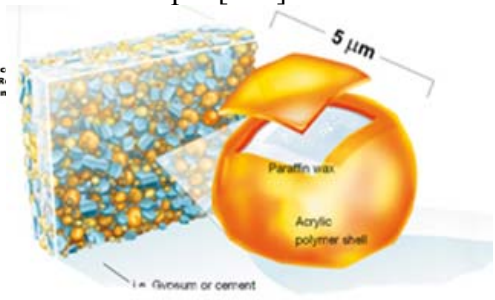

d) Micronal® PCM by BSAF [266]

e) RUBITHERM® GR by RUBITHERM [267]

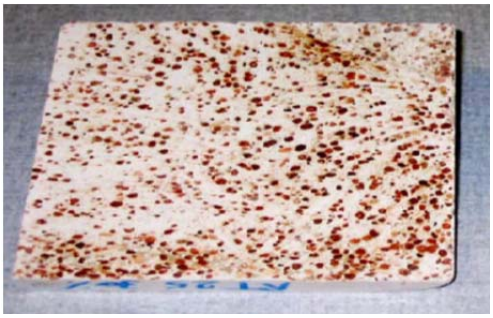

f) Gypsum-granulate sample [149]

Figure 5.1 Examples of microencapsulation of PCMs in powder format

It is likely that microencapsulated PCM changes its shape during the phase change process. Therefore, PCMs can be mixed with supporting materials such as high density polyethylene [268], thermoplastic elastomer poly(styrene–butadiene–styrene) [269] or others [9] to form a composite material in a process referred to a *"Shape Stabilization"* as shown in **Figure 5.2**. This method protects the shape of PCM capsule when it undergoes phase change due to the additional structural strength offered by the composite material. In addition, more latent storage mass can be incorporated into supporting materials and hence more thermal storage. The supporting materials complement the PCMs performance by increasing its cycling stability and improve the heat transfer if graphite or carbon fiber materials are added [9, 25].

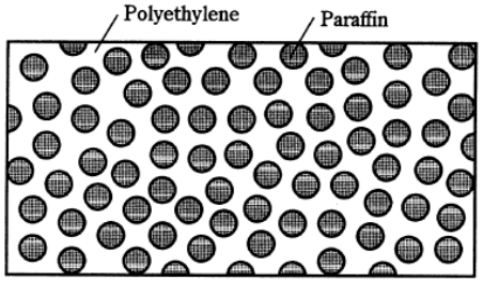

a) Concept of shaped-stabilized paraffin mixed with Polyethylene [268]

b) Shape-stabilized PCM plate developed by[9]

Figure 5.2 Example of shaped-stabilized PCM with supporting materials

Another viable method for PCM containment is when they are enclosed into containers. This containment technology is referred to as *"Macroencapsulation"*. Macroencapsulation using containers such as PVC panels [174], plastic rigid containers [270], aluminum foils [271], tubes [199], steel containers [120], sandwiched between laminated layers [131], or enclosed by plastic sheets [160] are common methods to hold PCMs in place. This method offers extreme

flexibility since pure PCMs can be incorporated. One example of the macroencapsulation technology of pure PCMs is illustrated in **Figure 5.3**.

a) BioPCM® Matt by Phase Change Energy Solutions [272]

b) BioPCM integrated into wall systems [272]

Figure 5.3 Example of macroencapsulated PCM using plastic sheet

5.2 Input parameters for modeling PCMs

Previous section provides a wide variation of containment technology for integrating PCM into building envelope. It is however important to elucidate on how to interpret the input parameters that are necessary for PCM modeling. Manufacturers of PCMs normally provide minimal design data using different testing protocols such as differential scanning calorimetry (DSC) [273] and T-history method [274]. The data determined from the lab tests are then used to derive important thermal characteristics such as melting temperature, melting temperature range, latent heat, as well as the basic thermal properties such as thermal conductivity, density and

specific heat capacity [275]. Some PCMs thermal properties are illustrated in the enthalpy-temperature (h-T) performance curve as shown in **Figure 5.4**.

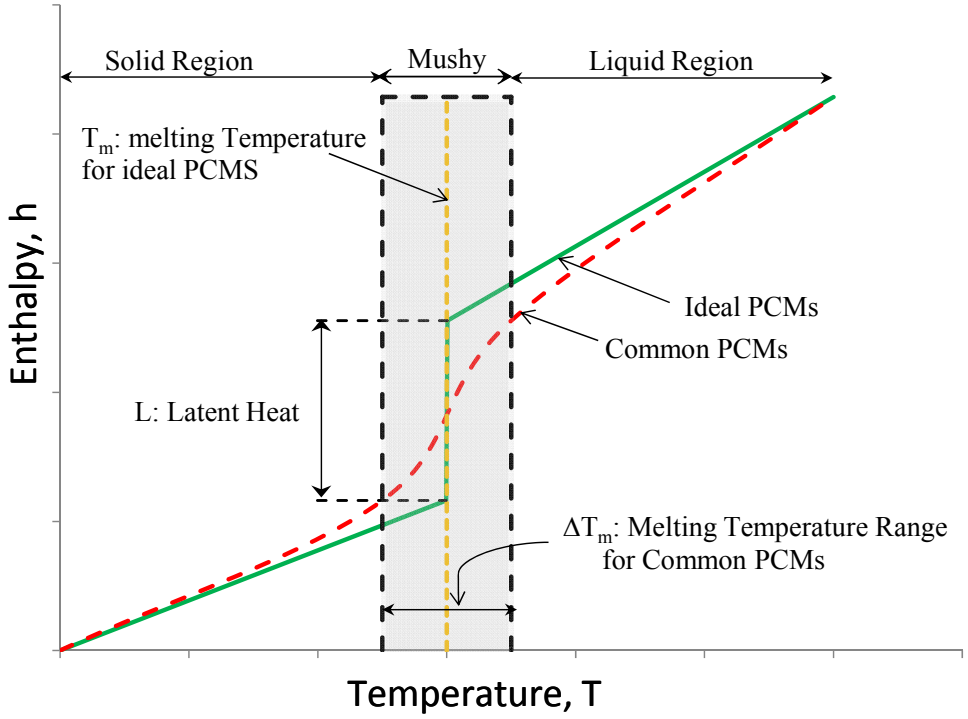

Figure 5.4 PCMs thermal properties necessary for modeling input

When raw PCM's powder capsules are mixed with building materials such as cellulose insulation or other similar materials, then it is perhaps difficult to conduct lab tests to derive the necessary thermal properties. The thermal data for the raw PCM capsules have to be supplied by the manufactures though. Under this situations, the thermal characteristics of the blended materials can be derived for PCM modeling using the methodology described by [206]. Based on this approach, the effective properties are determined using the materials thermal properties. The PCM capsules are distributed in the insulation and therefore the mass of PCM per unit surface area of the wall is used to quantify the PCM amount, m''_{PCM}. The mass quantity and the

insulation's thickness are then used to determine the equivalent PCM density, ρ''_{PCM}, using the following equation:

$$\rho''_{PCM} = \frac{m''_{PCM}}{thickness} \quad \text{Equation 5-1}$$

The effective thermal properties (i.e., density, specific heat capacity and latent heat) of the mixture can then be calculated as follows:

$$\rho_{mix} = \rho_{main\ material} + \rho''_{PCM} \quad \text{Equation 5-2}$$

$$c_{p,mix} = \frac{c_{p,main\ material} * \rho_{main\ material} + c_{p,PCM} * \rho''_{PCM}}{\rho_{mix}} \quad \text{Equation 5-3}$$

$$L_{mix} = \frac{L_{PCM} * \rho''_{PCM}}{\rho_{mix}} \quad \text{Equation 5-4}$$

To be conservative, the thermal conductivity of the mixture is assumed to be the same as that of the main primary material, cellulose insulation for example. This assumption is experimentally shown to be reasonable when small amount of PCM is added [276].

5.3 Methodology for the parametric study of multilayer PCM-enhanced Walls

5.3.1 Simulation Parameters

The intermediate model in SIMULINK can be used to study the performance of a standalone exterior envelope assuming a predefined indoor air temperature representing interior boundary conditions. It is assumed that the heating season is from January to end of April and again from October to end of December. During this period the indoor air temperature is unchanged at 22°C. Similarly for cooling season, it is assumed to be from May to end of September where the cooling setpoint is constant at 24°C. The exterior boundary conditions are provided using the weather reader and solar model developed under this work. The inside and

outside convective heat transfer coefficients are important factors that may influence the efficiency of the PCM-enhanced walls. For this study, the internal convective heat transfer coefficient is assumed to be 4.43 $W/m^2.K$ based on experimental results from Liu and Awbi for PCM wallboards under natural convection [277]. The outside convective heat transfer coefficient is based on ASHRAE winter design conditions [278]. **Table 5-1** provides assumptions of boundary conditions used in the simulations.

Table 5-1 Parameters assumed for modeling PCM-enhanced multilayer wall

Parameter	**Values**	**Units**
Indoor Temperature		
Winter season: Jan-April & Oct-Dec	22	°C
Summer season: May-Sept	24	°C
External Convective Heat transfer Coefficient	29.30	$W/m^2.K$
Internal Convective Heat transfer Coefficient	4.43	$W/m^2.K$
Solar absorption	0.6	[-]
Weather file	EPW for Golden, Co.	
Simulation Time	Yearly Simulation at sub-hourly time step of 5 minutes	

Although they might be significant in thermal performance of PCMs, the loads from windows (through conduction and solar radiation), air infiltration, and internal heat gains are not considered in this investigation. The main objective of this parametric analysis is to study the general behavior and identify the overall trend of PCM's thermal performance under typical meteorological weather data.

Four performance indicators have been selected to investigate the impact of PCM: peak heating load, annual heating load, peak cooling load and annual cooling load. The peak heating load is the maximum instantaneous heat flux from indoor environment to the wall surface. The

peak heating load is used for sizing heating systems. The annual heating load is the summation of heat flux from the indoor to the wall's surface over time step for one year. When the annual heating load is divided by the heating equipment's efficiency, the annual heating energy is determined. The peak cooling load, on the other hand, is the maximum instantaneous heat flux from interior wall's surface to the indoor. The peak cooling load is used for sizing cooling systems. The annual cooling load is the summation of the heat flux from the wall's surface to the indoor environment over time step calculated for one year. When the heat flux from the wall to the indoor air is divided by the cooling system efficiency (coefficient of performance (COP) for air conditioners) and integrated over time step, the annual cooling energy is determined.

For all cases, the PCMs are assumed to be concentrated as a separate layer. Such systems have been proved to offer higher potential for heating and cooling application when compared to the randomly distributed mixed system [130]. Lightweight wall system for residential building is selected. The reference wall is developed for Golden, CO. climate based on the Building America House Simulation Protocols [279, 280]. This analysis can be used for new design or for retrofitting existing buildings. The thermal properties are listed in **Table 5-2**.

Table 5-2 Thermal properties of base case of a wall assembly for Golden, CO.

Sketch	Material	Thickness [mm]	Thermal Conductivity [W/(m.K)]	Density [kg/m^3]	Heat Capacity [J/(kg.K)]
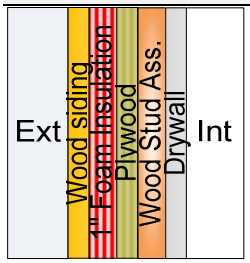	Wood Siding (Exterior)	12.5	0.1400	530	900
	XPS Insulation	25	0.0278	40	800
	OSB (plywood)	12.5	0.1400	650	1200
	Wood Stud Assembly	137.5	0.0600	120	1036
	Gypsum (Interior)	12.5	0.2100	700	1000

5.3.2 Environmental Conditions and Simulation Results for the base case

Figure 5.5 shows the outdoor air temperature (Toutdoor) and the solar air temperature (Tsol_air) for extreme winter and summer weeks. Solar air temperature is an effective outdoor air temperature that combines the effect of convection and radiation. Therefore, it is different from orientation to another due to solar radiation effect.

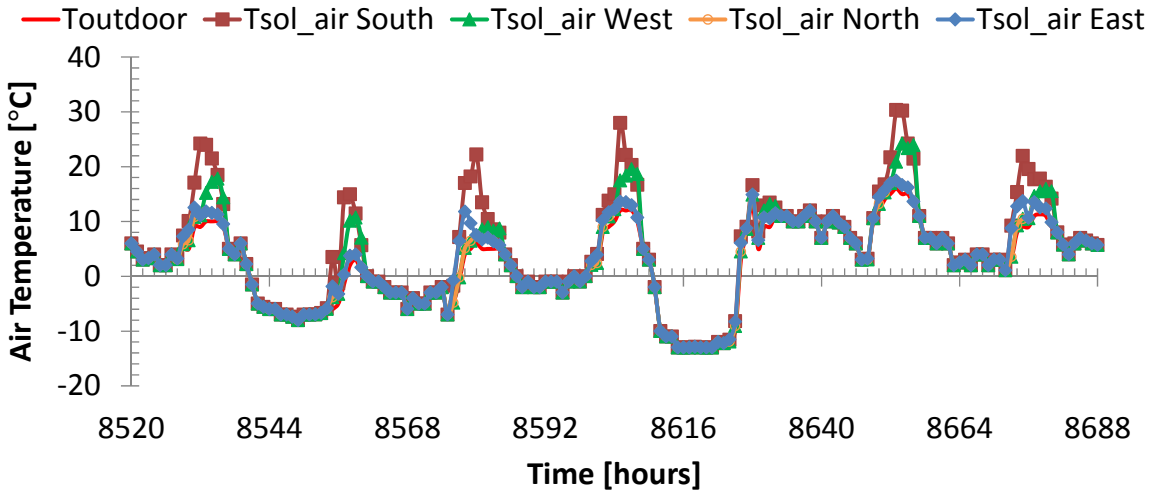

a) Extreme winter week (Dec 15:Dec 21)

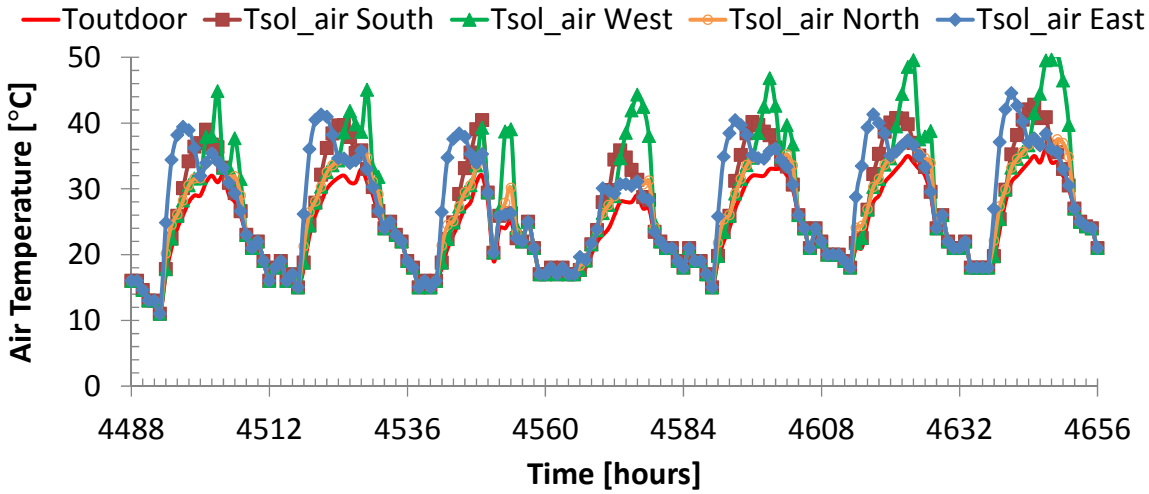

b) Extreme summer week (Jul 6:Jul 12)

Figure 5.5 Environmental conditions of extreme winter and summer week for Golden, CO.

The base case wall design is run for different orientations. The results of different performance indicators are shown in **Table 5-3**. The peak heating loads for all orientation is the same as expected since no solar radiation is available at the peak heating time. West wall has the maximum peak cooling load followed by south, east and finally north. North wall has the highest annual heating load. This is logic since minimal solar radiation is received on north and therefore more heating load is expected. East wall has the highest annual cooling load followed by west, south and finally north.

Table 5-3 Thermal performance indicators for Base case Wall in Golden, CO

Orientation	Annual Cooling Load [kWh]	Annual Heating Load [kWh]	Peak Cooling Load [kW]	Peak Heating Load [kW]
South	937.6	22803.8	3.04	11.83
West	982.5	24291.3	4.06	11.84
North	594.5	25404.2	2.67	11.84
East	1050.7	24230.7	2.99	11.84

5.3.3 Thermal properties of PCMs

The thermal behavior of PCMs is highly dynamic when exposed to dynamic environmental conditions. Outside the phase change regime, PCMs behave in a similar fashion to other sensible materials. The design determinants are based on many factors such as PCMs location in the wall, wall orientation, solar radiation, internal gains, color of the surface, ventilation rate, latent heat, melting temperature, melting range [281]. For this study the parameters vary include the;

1. location of the PCM in the wall,
2. latent heat of fusion,
3. melting temperature,

4. melting temperature range and
5. wall orientations

Three PCM locations are considered relative to the wood stud assembly (i.e., the assembly is mainly insulation); PCM to the interior side (iPCM), PCM in the middle (midPCM), and PCM to the exterior side (ePCM). The PCM thermal properties are varied relative to the reference wall as illustrated in **Table 5-4**.

Table 5-4 Parameters considered for the parametric study for PCM-enhanced Walls

Wall Design Sketch	Latent Heat [kJ/kg]	T_m [°C]	ΔT_m [°C]	Orientation	Simulation/ orientation	Total Simulations
Interior PCM: iPCM 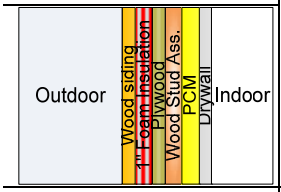	50-400 (50 increment)	18-28 (1 increment)	0.1,0.2, 1,2,4, 8,12	South , West, North, East	616	2464
Middle PCM: midPCM 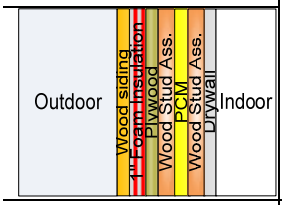	50-400 (50 increment)	15-35 (5 increment)	0.1,0.2,1,2, 4,8,12	South , West, North, East	280	1120
Exterior PCM: ePCM 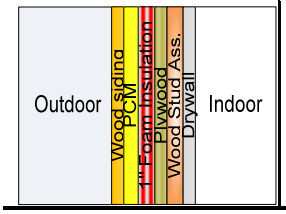	50-400 (50 increment)	10-40 (5 increment)	0.1,1, 2,4,8, 12	South , West, North, East	336	1344

Since the technology is immature yet, many PCMs are partially developed or under development. **Figure 5.6** shows samples of commercially available PCMs as reported recently by [282-284]. For this study, a wide variation of PCM properties such as melting temperature and latent heat are considered for each three PCM-enhanced walls (i.e., iPCM, midPCM, ePCM)

as depicted in **Figure 5.6**. The selection domain of PCMs thermal properties lay within the building's external and internal environmental conditions.

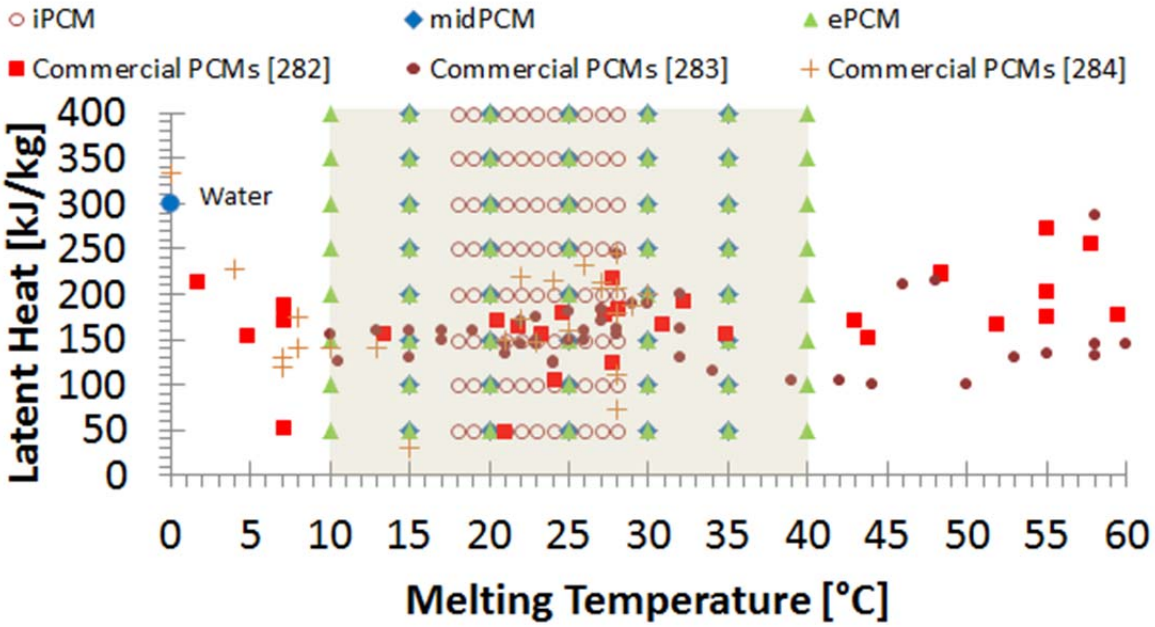

Figure 5.6 PCMs thermal properties considered for the parametric study with samples of commercial products

5.4 Simulation of Multilayer PCM wall

Using the above assumptions and the design parameters, a series of simulation runs are carried out. For making the analysis simpler, the melting range can be categorized into: narrow meting range (0.1-1°C) and wide melting range (2-12°C). In addition, the latent heat can be categorized into; light latent heat (50-100 kJ/kg), medium latent heat (150-250 kJ/kg) and high latent heat (300-400 kJ/kg).

5.4.1 PCM to the interior of the wall

5.4.1.1 South Wall

In this case, the PCM is located to the interior side of the wall exposed to typical boundary conditions experienced in buildings as explained earlier. The reductions in annual cooling and heating loads for a south wall are shown in **Figure 5.7**. The figure summarizes the impact of the latent heat of fusion, melting temperature and the melting temperature range. Interesting insights can be drawn from **Figure 5.7** (a). First, the optimal melting temperature for maximum savings in annual cooling load is close to the cooling setpoint (i.e., 24°C) for PCMs with melting range from 0.1-2°C. This PCM group tends to reach significant savings in annual cooling load at a latent heat of 100kJ/kg with marginal savings afterwards. For this melting range, the savings are clearly sensitive to the cooling set-point especially for those at very narrow melting range (0.1-1°C). The degree of sensitivity tends to decrease as the melting temperature becomes wider. In particular, for PCMs with very wide melting range (8-12°C), the reduction in annual cooling load is constant across the melting temperatures with a gradual increase in savings as the latent heat increases. Overall, the PCMs with narrow melting range (0.1-1°C) show significant savings in annual cooling loads; 63-95% , 81-99.97% and 90-100% for low, medium and high latent heat respectively relative to the base case (i.e., no PCM). With annual cooling load's savings of 100%, an adiabatic wall is possible for high latent heat cases. PCMs with wide melting range (2-12°C) show annual cooling load's savings from 16-63%, 33-78%, 49-85% for low, medium and high latent heat respectively compared to the base case.

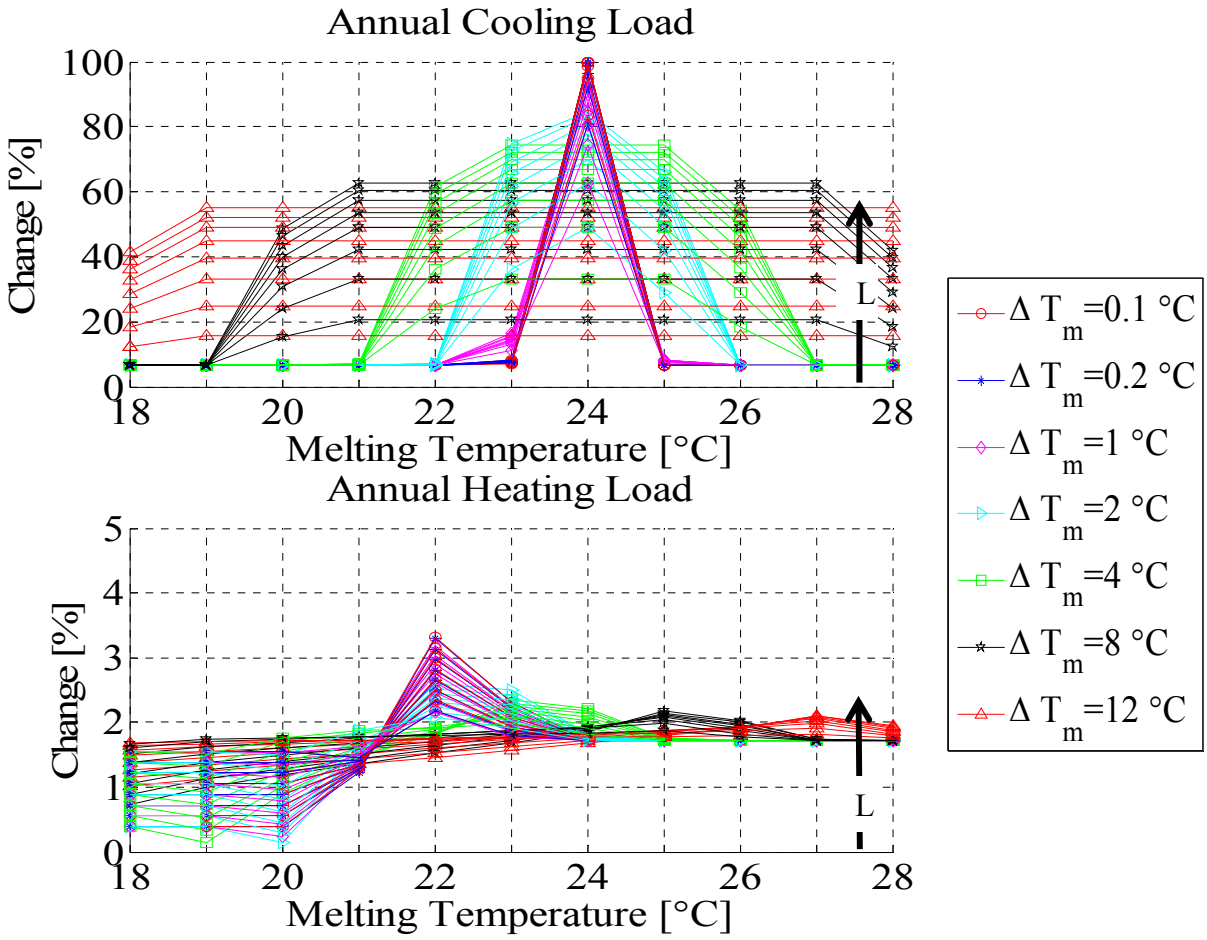

a) Percentage reductions in annual cooling and heating loads across all parameters

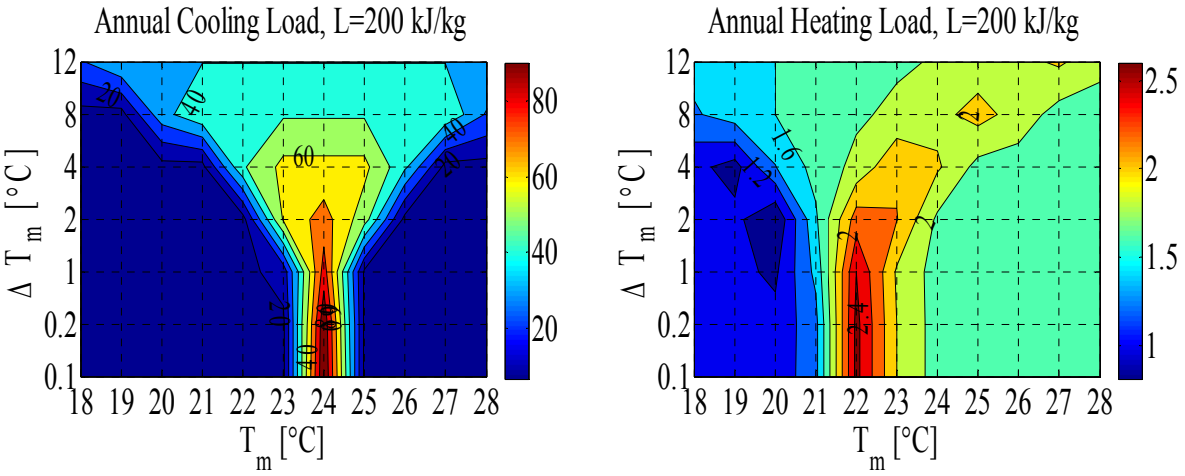

b) A contour plot for the case of 200 kg/kJ showing reduction in annual cooling and heating loads

Figure 5.7 Percentage reductions in annual cooling and heating loads for the south wall

The reduction in annual heating loads is low when compared to the cooling as illustrated in **Figure 5.7** (a). The savings achieved in annual heating load ranges between 1.5% and 3% across all parameters. The heat stored in the PCM layer is perhaps low due to large temperature gradient between the inside and outside surface temperatures. The greatest savings in annual heating load occurs at the heating set-point (i.e., 22°C) for PCMs with narrow melting temperatures (0.1-1°C) but less significant for PCMs with wide melting temperature. It is also observed that as the melting range increases, the optimal melting temperature moves to the right. For example, when the melting range is 2°C, the optimal melting temperature is 23°C and when melting range is 12C°, the optimal temperature is 27°C. A contour slice showing the reduction in annual cooling and heating loads across one case of latent heat is shown in **Figure 5.7** (b).

Other interesting performance indicators for the effectiveness of PCM walls are the peak cooling and heating loads. **Figure 5.8** illustrates the reductions in these two indicators. Similar to the annual cooling load, the maximum reductions in peak cooling load happens at cooling set-point temperature. It is interesting to note that PCMs with wide melting range temperatures maintain a similar load reduction regardless of the melting temperature.

On the other hand, the maximum reduction in peak heating load occurs at 19°C (3°C below the heating set-point temperature). The maximum reduction in peak heating load is close to 20% for high latent heat compared to nearly 3 % for low latent heat. Generally speaking, the PCMs with narrow melting range is superior to wide melting range in achieving maximum reductions but best works at tight indoor environmental conditions (as assumed in this case). PCMs with wide melting range are conservative option and are less sensitive to the indoor environmental conditions since flat savings can be achieved across the melting temperature and range. It can be inferred that this category with wide melting range is a conservative option since

it is not sensitive to the typical indoor air temperature. This is especially useful in applications when the operation conditions are uncertain.

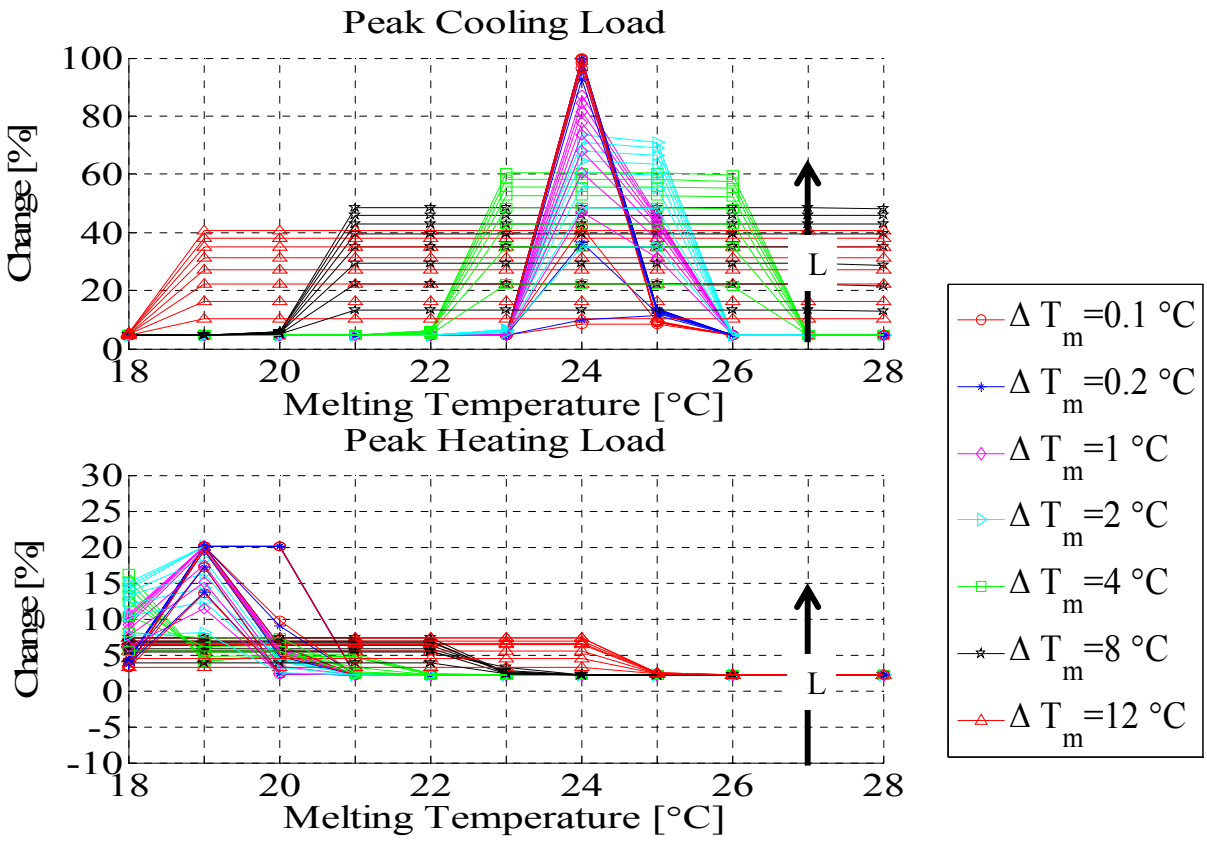

a) Percentage reductions in peak cooling and heating loads across all parameters

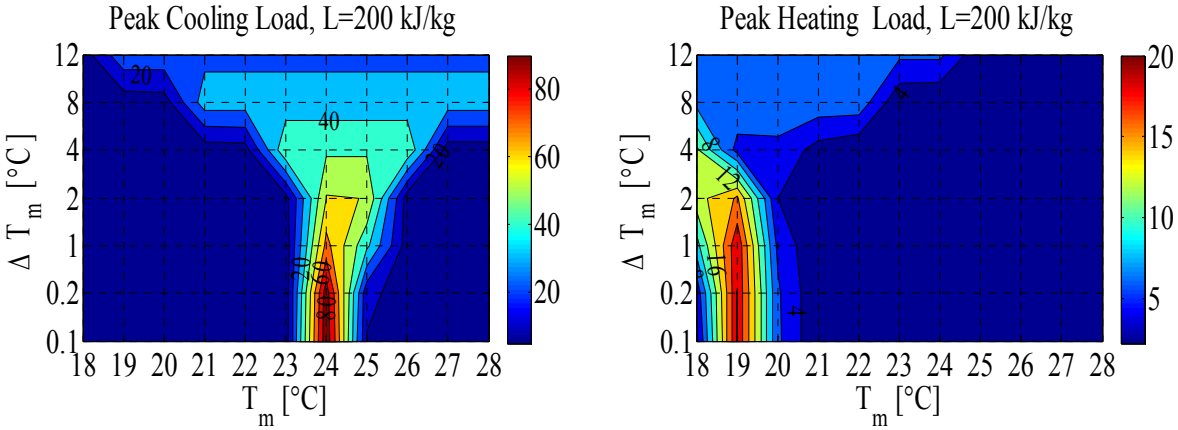

b) A contour plot for the case of 200 kg/kJ showing reduction in peak cooling and heating loads

Figure 5.8 Percentage reductions in peak cooling and heating loads for south wall when PCM to the interior

One of the most important benefits of using PCM is to shift the loads to times when energy cost is cheap. Since the reduction in peak cooling loads is significant, the time shift for this indicator is considered. **Figure 5.9** shows the peak cooling load shift for PCM-enhanced wall under various thermal properties. The figure shows that the peak cooling load is shifted as the latent heat increases. Although, the desirable load shift would be few hours relative to the peak of the base case (presumably at low energy cost), it is remarkable to note that peak cooling load is entirely eliminated for latent heat cases greater than 300 kJ/kg (i.e., adiabatic cases). It is also observed that the maximum shift occurs at the cooling set point temperature (i.e., 24°C). In addition, the greatest shift happens close to a melting range of 1°C for a latent heat less than 100 kJ/kg. However, the maximum shift moves to the lower limit of narrow melting range (0.1°C) when the latent heat is greater than 100 kJ/kg.

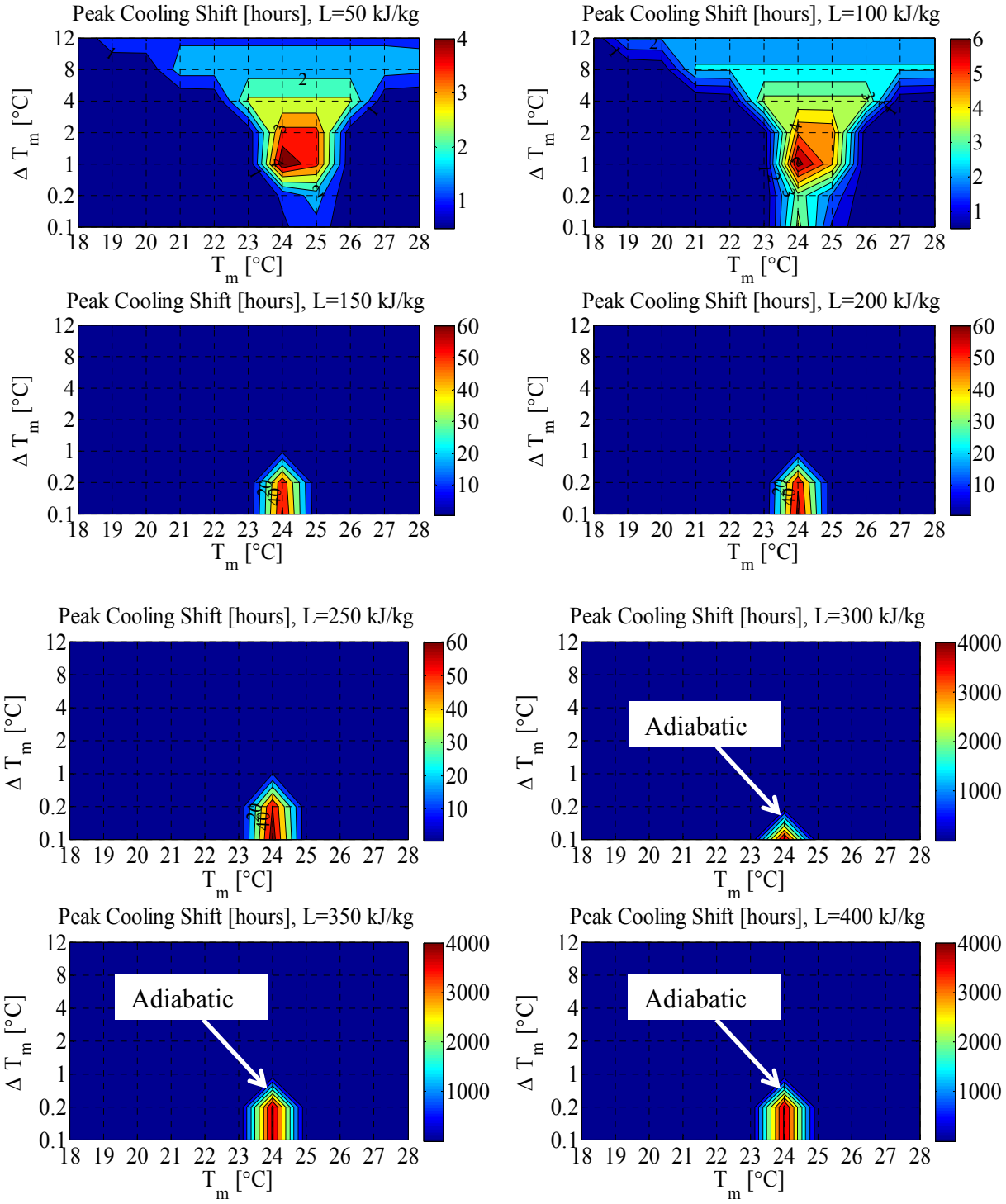

Figure 5.9 Peak cooling shifts in hours compared to the base case

5.4.1.2 Impact of wall orientations

The orientation is of a particular interest when envelopes are studied. This is mainly due to the variations of solar radiation received on different orientations. Similar analysis to the South wall is also performed for other orientations; West, North and East. Since the overall trend is similar to the South wall, the results for all orientations are summarized and compared in **Table 5-5**. The contour plots are provided in **Appendix A**. West wall performs in a similar fashion to the south wall. North wall performs slightly better than all other orientations in terms of annual cooling load. This is perhaps due to the low cooling load that this orientation experiences when compared to others. The east wall performs the lowest than all other orientations. For all orientations, the reduction in annual heating load is low as it ranges from 1.2-3.3% across all PCM thermal properties.

Table 5-5 Rough reductions in cooling and heating loads for PCM-enhanced Walls in Golden, CO when PCM to the interior side

Orientation		Reduction in Annual Cooling Load [%]		Reduction in Annual Heating Load [%]		Reduction in Peak Cooling Load [%]		Reduction in Peak Heating Load [%]		Peak Cooling Shift [hours]	
South	ΔT_m [°C] / L [kJ/kg]	0.1-1	2-12	0.1-1	2-12	0.1-1	2-12	0.1-1	2-12	0.1-1	2-12
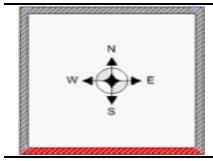	50-100	63-95	16-63	2.2-2.3	1.7-2.2	8-61	10-49	11.5-13.6	3.3-8.2	1-6	1-5
	150-250	81-99.97	33-78	2.5-2.8	1.7-2.4	68-99.6	22-65	17.6-20	4.8-18.2	7-66	3-7
	300-400	90-100*	49-85	2.9-3.3	1.5-2.6	82-100*	35-74	20	4.1-20	10-AD*	4-8
West	ΔT_m [°C] / L [kJ/kg]	0.1-1	2-12	0.1-1	2-12	0.1-1	2-12	0.1-1	2-12	0.1-1	2-12
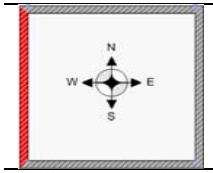	50-100	63-93	16-63	2.-2.18	1.7-2	28-49	13-52	10.4-16.3	2.9-11	2.7-3.3	1-4
	150-250	80-99.77	33-78	2.3-2.6	1.6-2.2	70-99	25-67	16.5-20.5	4.8-17.1	6.3-61	1.9-5.8
	300-400	90-100	33-85	2.7-3	1.4-2.4	82-100	38-75	20.04	4.2-20.5	8.7-AD*	2.8-7.2
North	ΔT_m [°C] / L [kJ/kg]	0.1-1	2-12	0.1-1	2-12	0.1-1	2-12	0.1-1	2-12	0.1-1	2-12
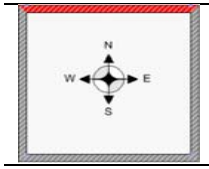	50-100	68-98	16-68	1.8-2	1.5-1.8	7-95	9-48	9.9-16.1	2.9-10.6	0.6-56	1-4
	150-250	87-100*	35-85	2.1-2.4	1.36-2	67-100*	21-65	16.3-20.2	4.8-16.9	6-AD*	2-6
	300-400	95-100*	52-91	2.5-2.8	1.2-2.2	84-100*	34-75	20.2	4.1-20.2	9-AD*	3-7
East	ΔT_m [°C] / L [kJ/kg]	0.1-1	2-12	0.1-1	2-12	0.1-1	2-12	0.1-1	2-12	0.1-1	2-12
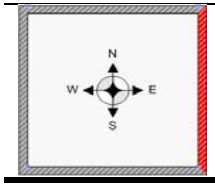	50-100	53-87	13-53	1.9-2	1.6-1.9	7-35	7-39	10.5-16.5	3.4-11.2	1.4-4.8	1.3-4.6
	150-250	71-99	27-68	2.2-2.4	1.4-2.1	23-97	16-55	16.7-20.1	5.1-17.3	2.7-67	2.4-6.4
	300-400	83-99.94	40-76	2.6-3	2.6-3	72-99	27-64	20.14	4.3-20.1	9.3-79	3.5-7.8

Notes: * AD: adiabatic

5.4.2 PCM in the middle of the wall

5.4.2.1 South Wall

For this design, the PCM is located in the middle of the wood-insulation assembly as shown in **Table 5-2** (refer to midPCM case). The reductions in annual cooling and heating loads for a south wall are shown in **Figure 5.10**. For annual cooling load (**Figure 5.10** (a)), the minimum annual cooling loads savings from PCM is around 19%. It is interesting to note that the PCMs with wide melting range (2-12°C) perform better than those at narrow melting range (0.1-1°C). Since the PCM layer is not in direct contact with indoor environment, the maximum reduction in annual cooling load occurs at 1°C above the cooling set point. The best melting temperature ranges are 4°C, 2°C, 8°C and 12°C, respectively when the melting temperature is 24°C. The reduction in annual cooling load is gradually increasing from around 55% for the latent heat case of 50kJ/kg to almost 90% for the latent heat case of 400kJ/kg when the melting temperature range is 4°C (~13% for every 100kJ/kg). Similar observation with lower saving is observed for 2°C melting range. The other two cases of the wide melting range; 8 and 12°C show a higher potential over a temperature range of 20-25°C with great savings around 20°C making them conservative options. The narrow melting range (0.1-1°C) show low savings in annual cooling load. For this group, the reductions in annual cooling load ranges from 36% for the latent heat of 50kJ/kg to 54% for the latent heat case of 400kJ/kg (~5% for every 100 kJ/kg). The reduction in annual heating loads is low when compared to the annual cooling load. The savings ranges from a minimum of 1.5 to a maximum of 3%. The greatest savings in annual heating load occurs at 2°C below the heating set-point (i.e., 22°C) for melting range of 0.1-4°C. At this optimal melting temperature, the savings increases from 2% to 3% for 50kJ/kg and

400kJ/kg respectively. The savings trend is similar to the case when PCM is located to the interior side of the wall in direct contact with the indoor environment. This is perhaps an indication that the PCM layer is storing the heat that otherwise will be lost from indoor to outdoor. Therefore, the PCM location has a minor effect in heating savings since a similar heat loss is expected. A contour plot showing the reduction in annual cooling and heating loads across one case of latent heat is shown in **Figure 5.10** (b).

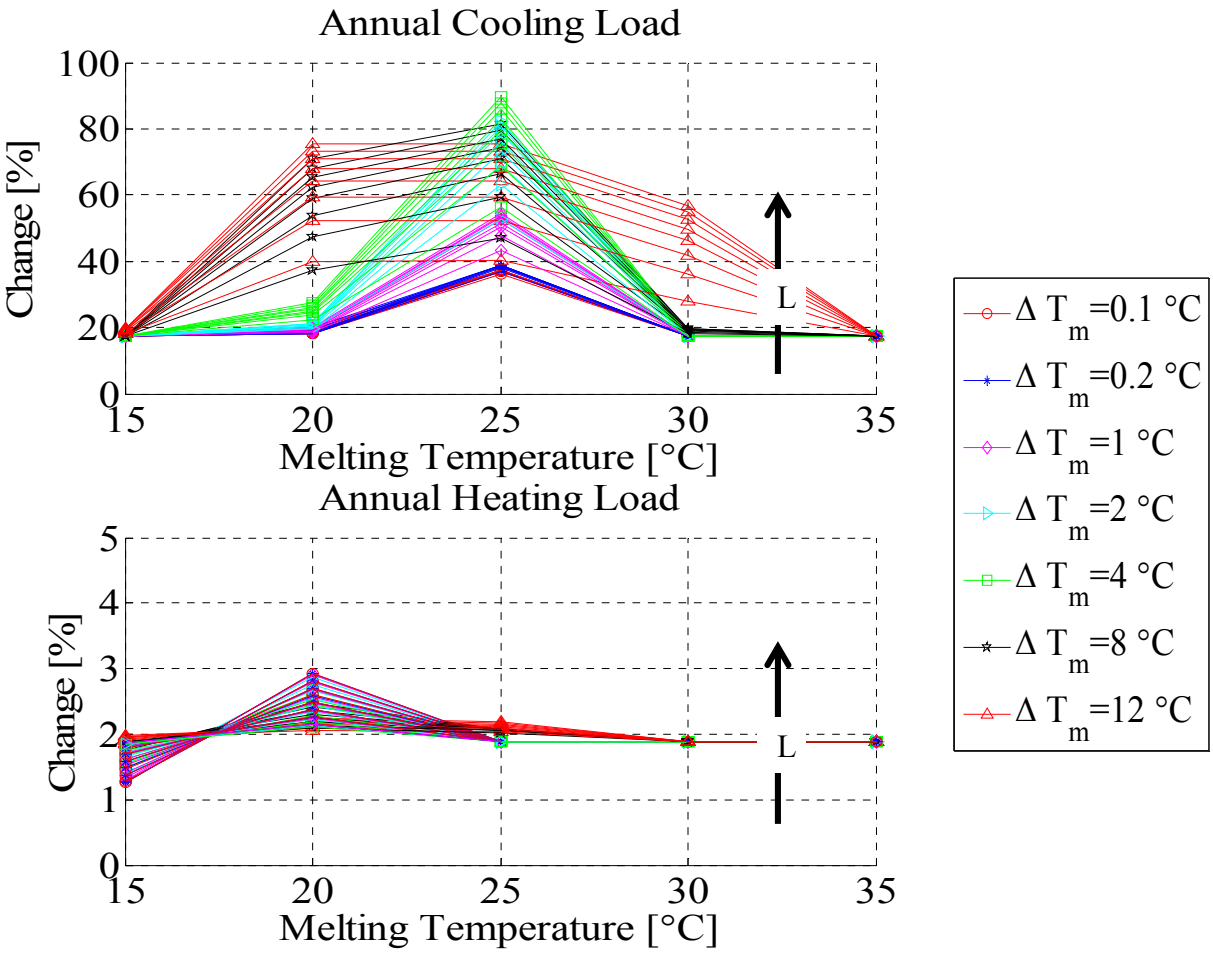

a) Percentage reductions in annual cooling and heating loads across all parameters

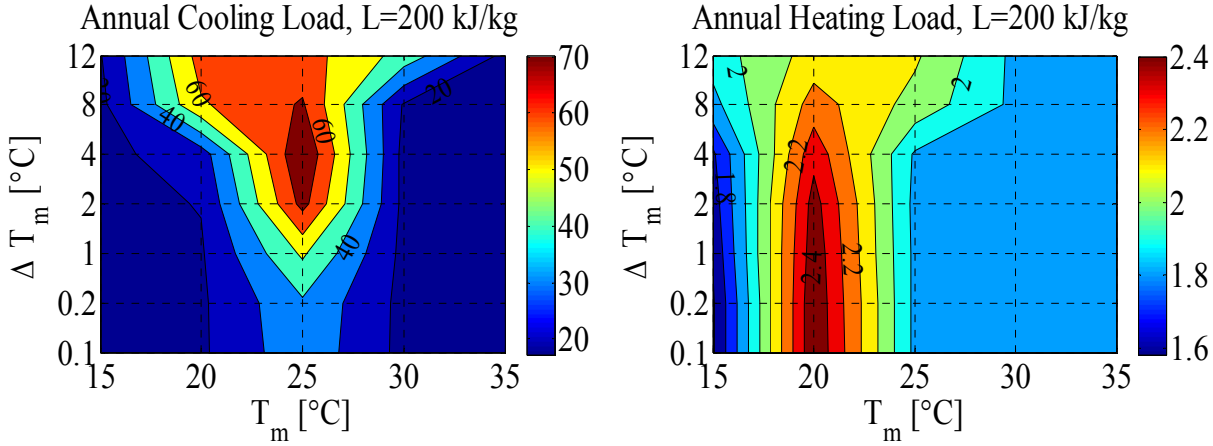

b) A contour plot for the case of 200 kg/kJ showing reduction in annual cooling and heating loads

Figure 5.10 Percentage reductions in annual cooling and heating loads for the south wall when PCM layer in the middle

Peak cooling and heating load for this design is illustrated in **Figure 5.11**(a). On the contrary to the annual cooling load, the interesting point to note here is that PCM with a narrow melting range (0.1-1°C) show significant reduction in peak cooling load. This is particularly happening when the PCM is with latent heat below 250kJ/kg. Thereafter, as the latent heat increases, the performance of PCM with 2°C melting range exceeds the PCM with narrow melting ranges (0.1-1°C). The next best performance PCM is the one with 1°C melting range. **Figure 5.11** (b) and (c) show the contours plots across 200 and 400kJ/kg latent heat cases to illustrate this shift in performance. It is expected that the saving in peak load favors PCM with narrow melting range since it happens at a particular time with a corresponding design value. However for the high latent cases (>250 kJ/kg) and the two melting range cases of 1 and 2°C, their performance is slightly above the other wide and narrow melting range cases. At optimal melting temperature of 25°C, the peak cooling load is overall reduced by 53% to 84% for the narrow melting range (0.1-1°C) and from 27-87% for the wide melting range cases (2-12°C) when compared to the base noPCM case.

A similar trend is also observed with reduction in peak heating load. The wide melting range PCMs tends to be superior to those at narrow melting temperature at high latent heat (>250 kJ/kg). The reduction in peak heating load ranges from 3.5% at low latent heat to a maximum of 7.5% for high latent heat. It is clear from the figure that the maximum savings in peak heating load tend to be at temperature lower than 15°C which is the minimum value considered under this parametric case.

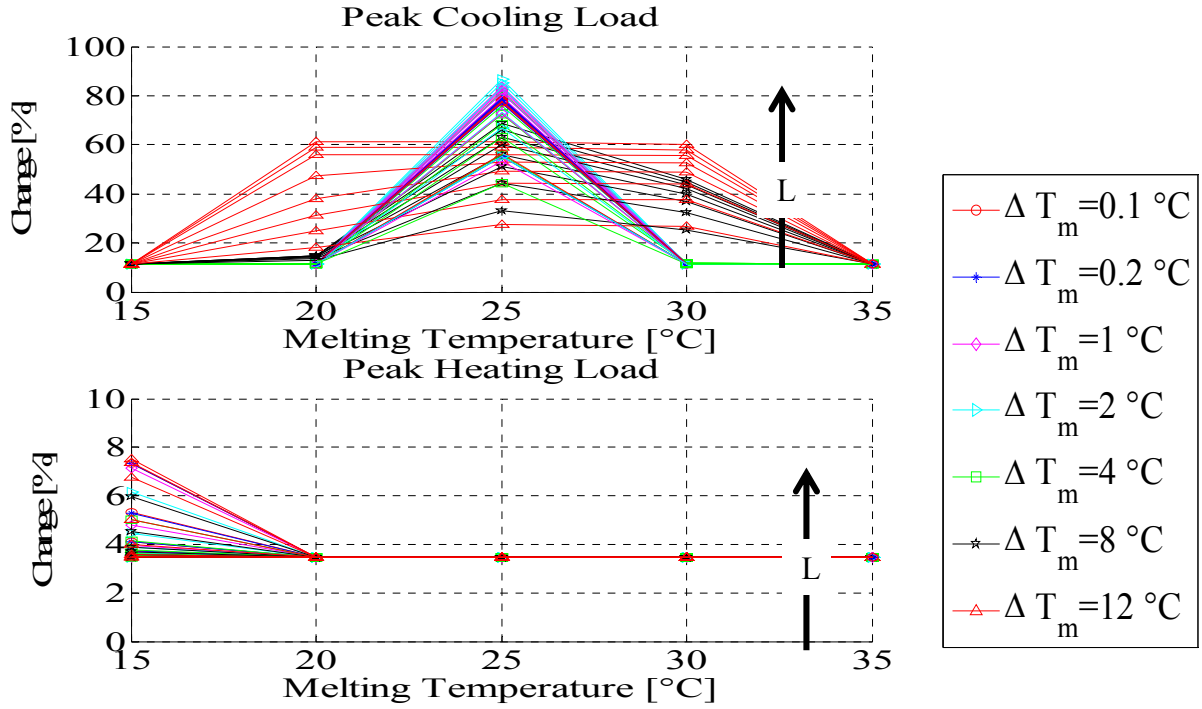

a) Percentage reductions in peak cooling and heating loads across all parameters

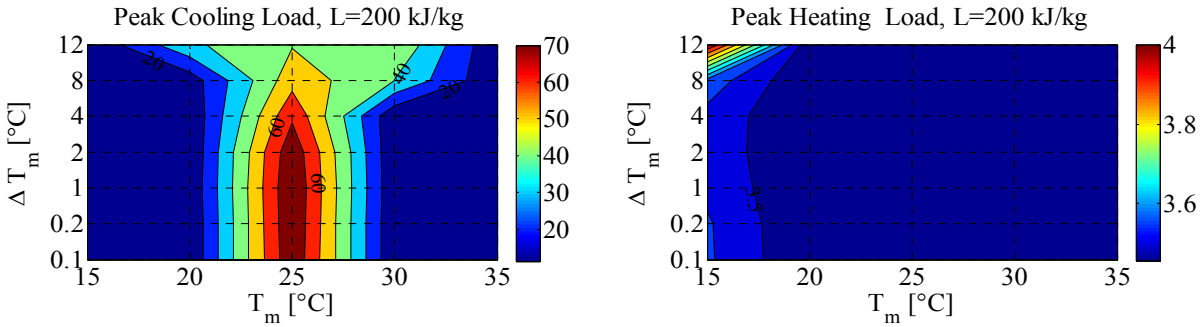

b) A contour plot for the case of 200 kg/kJ showing reduction in peak cooling and heating loads

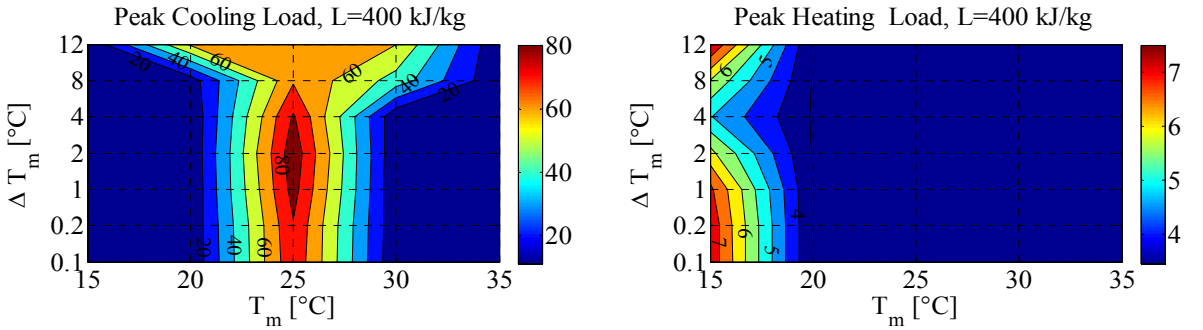

c) A contour plot for the case of 400 kg/kJ showing reduction in peak cooling and heating loads

Figure 5.11 Percentage reductions in peak cooling and heating loads for south wall

Figure 5.12 shows that the peak cooling load is shifted as the latent heat increases. The shift occurs at 1°C above the cooling setpoint. At this optimal melting temperature (i.e., 25°C), the peak cooling is shifted by 3.5 hours to a maximum of 18 hours when latent heat increase from 50kJ/kg to 400 kJ/kg. Narrow melting temperature range attains the maximum peak cooling shift.

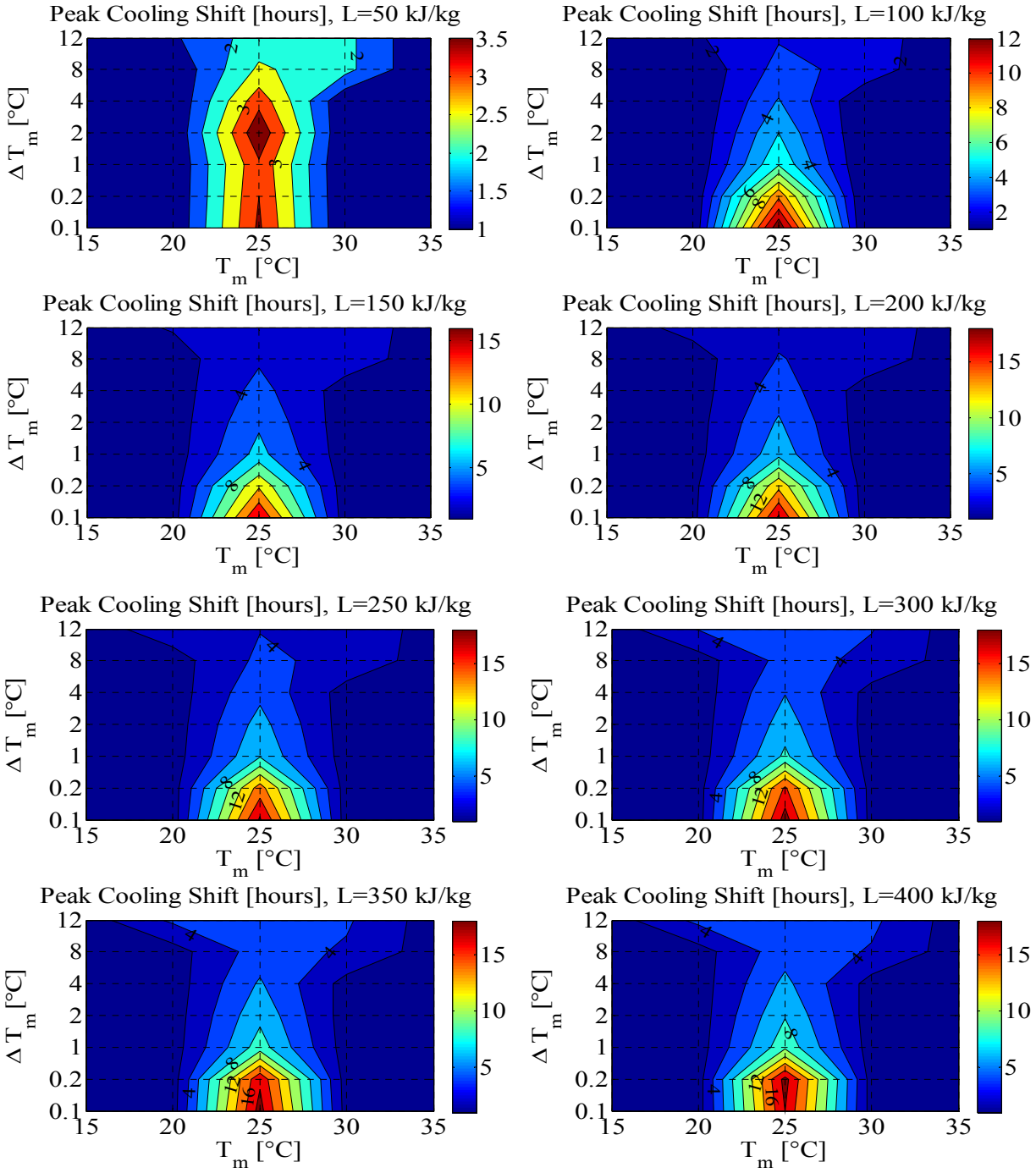

Figure 5.12 Peak cooling shifts in hours compared to the base case

5.4.2.2 Impact of wall orientations

Simulations of PCMs for other orientations; West, North and East are also performed. **Table 5-6** summarizes the results for these cases. Detailed contour plots are provided in **Appendix A**. For annual cooling load, West wall performs marginally better than other walls for PCMs with narrow melting range (0.1-1°C). When compared to south wall, west wall performs 1-2% more. East wall has less reduction in annual cooling load. North wall performs 2-5% better than South and West but 10-20% better than East wall. This is likely due to the small cooling loading from North and therefore more relative savings are achieved. A similar trend is observed when peak cooling load is considered. For all orientations and across all PCM thermal properties, the reduction in annual heating load ranges from 1.7-2.9%. As expected, the reduction in peak heating load is within the same range for all orientations.

Table 5-6 Rough reductions in cooling and heating loads for PCM-enhanced Walls in Golden, CO, PCM in the middle

Orientation		Reduction in Annual Cooling Load [%]		Reduction in Annual Heating Load [%]		Reduction in Peak Cooling Load [%]		Reduction in Peak Heating Load [%]		Peak Cooling Shift [hours]	
South	ΔT_m [°C] / L [kJ/kg]	0.1-1	2-12	0.1-1	2-12	0.1-1	2-12	0.1-1	2-12	0.1-1	2-12
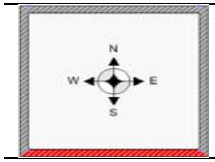	50-100	36-48	40-69	2.1-2.3	2.1-2.2	53-77	27-67	3.5	3.5	3.4-12.8	2.3-5
	150-250	37-53	59-83	2.4-2.6	2.1-2.6	77-81	44-81	3.7	5	6.7-18.3	3.3-6.8
	300-400	37-54	71-90	2.7-2.9	2.2-2.9	79-84	56-87	7.4	7.5	8.4-19	4.1-7.8
West	ΔT_m [°C] / L [kJ/kg]	0.1-1	2-12	0.1-1	2-12	0.1-1	2-12	0.1-1	2-12	0.1-1	2-12
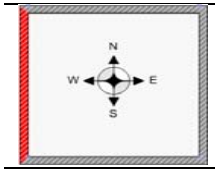	50-100	37-49	40-69	2-2.1	1.9-2.1	33-83	29-70	3.2	3.2	1.3-9.8	1.5-4
	150-250	39-54	60-83	2.2-2.4	2-2.3	80-84	47-82	3.2	3.2-4	5.8-35	2.4-5.6
	300-400	39-56	71-90	2.5-2.7	2.1-2.6	84-87	59-87	3.4-3.7	3.3-6.7	7.6-36.9	3.2-6.8
North	ΔT_m [°C] / L [kJ/kg]	0.1-1	2-12	0.1-1	2-12	0.1-1	2-12	0.1-1	2-12	0.1-1	2-12
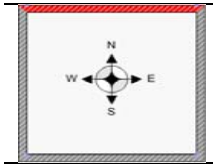	50-100	32-46	42-75	1.8-1.9	1.7-1.8	64-75	26-67	3.2	3.2	3.9-11.7	1.5-4.1
	150-250	33-50	64-89	1.9-2.1	1.8-2	75-80	44-81	3.2	3.2-3.9	5.6-14.3	2.4-5.7
	300-400	33-51	77-95	2.1-2.4	1.8-2.2	75-83	56-87	3.3-3.4	3.3-6.3	7.3-15.2	3.3-6.7
East	ΔT_m [°C] / L [kJ/kg]	0.1-1	2-12	0.1-1	2-12	0.1-1	2-12	0.1-1	2-12	0.1-1	2-12
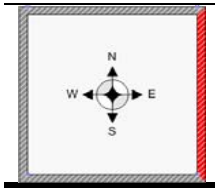	50-100	32-43	33-55	1.9-2	1.8-1.9	9-76	21-59	3.5	3.5	1.8-8.3	2.2-5
	150-250	34-51	50-74	2.1-2.3	1.8-2.2	73-78	36-74	3.5-3.6	3.5-4.6	7.7-38.8	3.3-6.6
	300-400	34-51	61-82	2.4-2.6	1.9-2.4	78-81	47-81	3.7-4.3	3.7-6.6	8.58-53.5	4-51.9

5.4.3 PCM to the exterior of the wall

5.4.3.1 South Wall

The PCM for this design is located to the exterior side; exposed to outside environmental conditions. The PCM layer is covered with wood siding layer. The reductions in annual cooling and heating loads for a south wall with PCM to the exterior are shown in **Figure 5.13**. The saving in annual cooling load starts at a base of around 7% to a maximum of 48%. At a first glance, one may see that the optimal melting temperature is 25°C for maximum savings in annual cooling loads. This is perhaps true for cases when latent heat is greater than 200kJ/kg. A careful look indicates that another optimal melting point is at 20°C for latent heat cases less than 150 kJ/kg. This observation is clear from the contour plots for cases of 150 and 200 kJ/kg. The PCMs with narrow melting temperature (0.1-1°C) show the maximum savings for high latent heat cases at 25°C melting temperature. Those with wide melting range show their maximum savings at 20°C. This might be related to outside environmental conditions. On average and during the summer time, the outside sol air temperature fluctuates between 18°C to 38°C with an average close to mid-twenties. Therefore, the maximum savings in annual cooling load occurs around this average. For PCMs with wide melting range, the optimal melting temperature is less than the average. This group of PCMs can easily cover wide range of outside conditions. The saving in annual heating loads is not significant as it ranges between 1.8% and 2.1% regardless of the variations in thermal parameters.

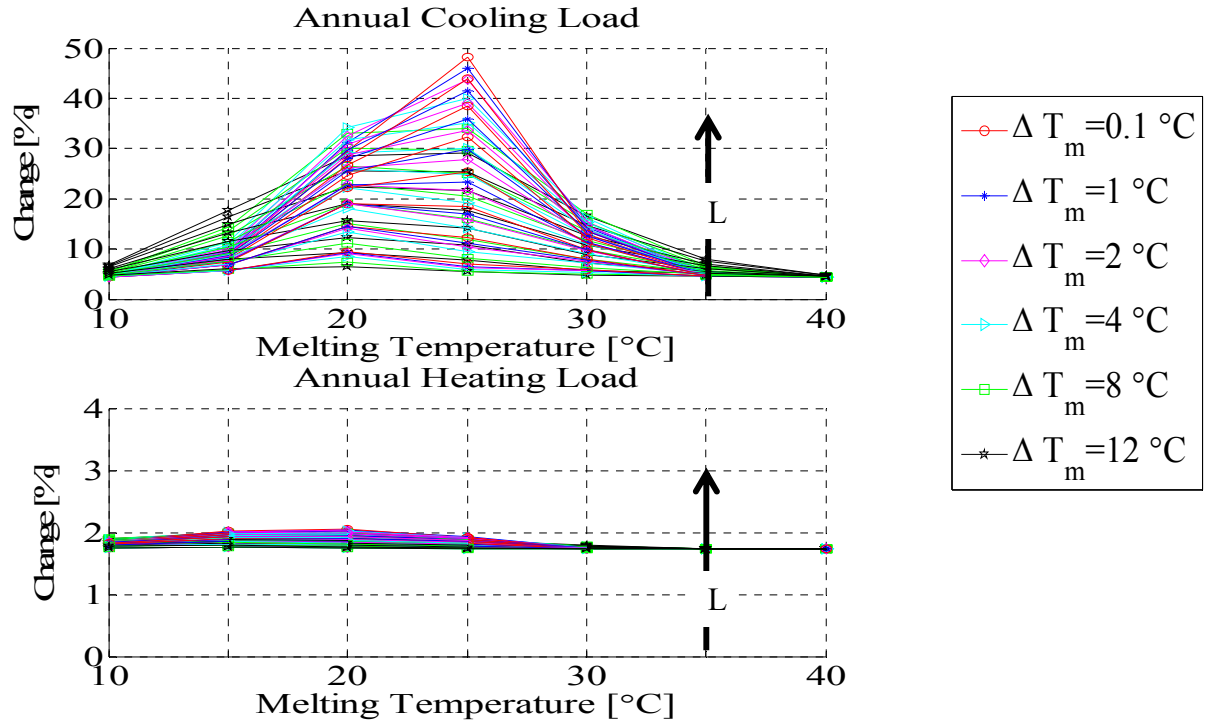

a) Percentage reductions in annual cooling and heating loads across all parameters

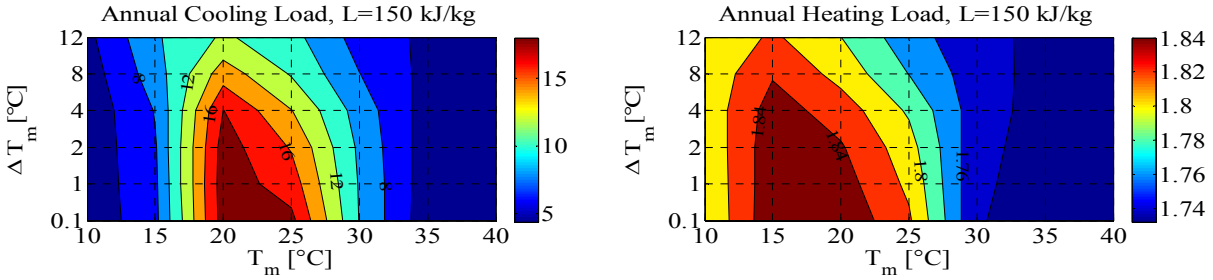

b) A contour plot for the case of 150 kg/kJ showing reduction in annual cooling and heating loads

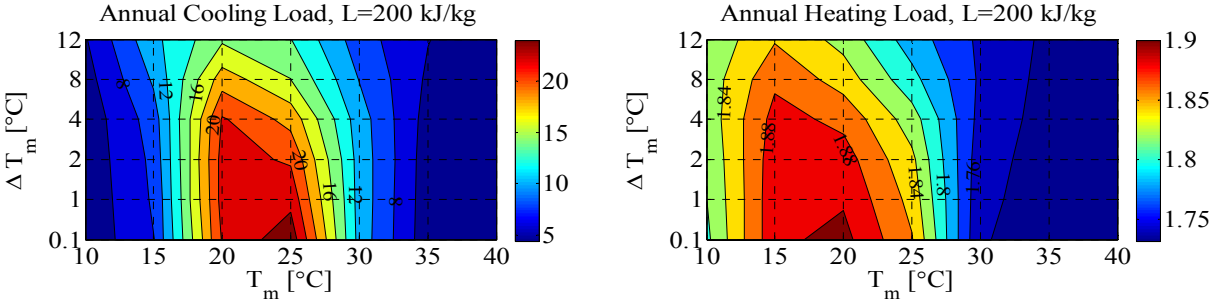

c) A contour plot for the case of 200 kg/kJ showing reduction in annual cooling and heating loads

Figure 5.13 Percentage reductions in annual cooling and heating loads for the south wall

The peak cooling and heating loads are shown in **Figure 5.14**. The reductions in peak cooling load ranges from a minimum of 5% to a maximum of 37%. As shown earlier in **Figure 5.5**, the sol air temperature for south wall fluctuates between 18°C and 38°C. One may expect that the optimal melting temperature for maximum reductions in peak cooling load should also happen close to the peak temperature. However, the maximum reduction in peak cooling load occurs at 30°C which is 8°C below the peak sol air temperature. This optimal melting temperature corresponds to a sol air temperature at 3 hours earlier than the time of the peak. Hence, for a peak cooling load design purpose, one may select a PCM with a melting temperature below the peak sol-air temperature. This will not allow the PCM to reduce the cooling energy but also to shift the peak cooling load to other times. It is worth to mentioned that the wall also exchange heat with the sky, air and ground through long wave radiation. This might drop the surface temperature below that of the sol-air temperature. On the other hand, the reduction in peak heating load is flat at 2% regardless of the variations in PCM properties.

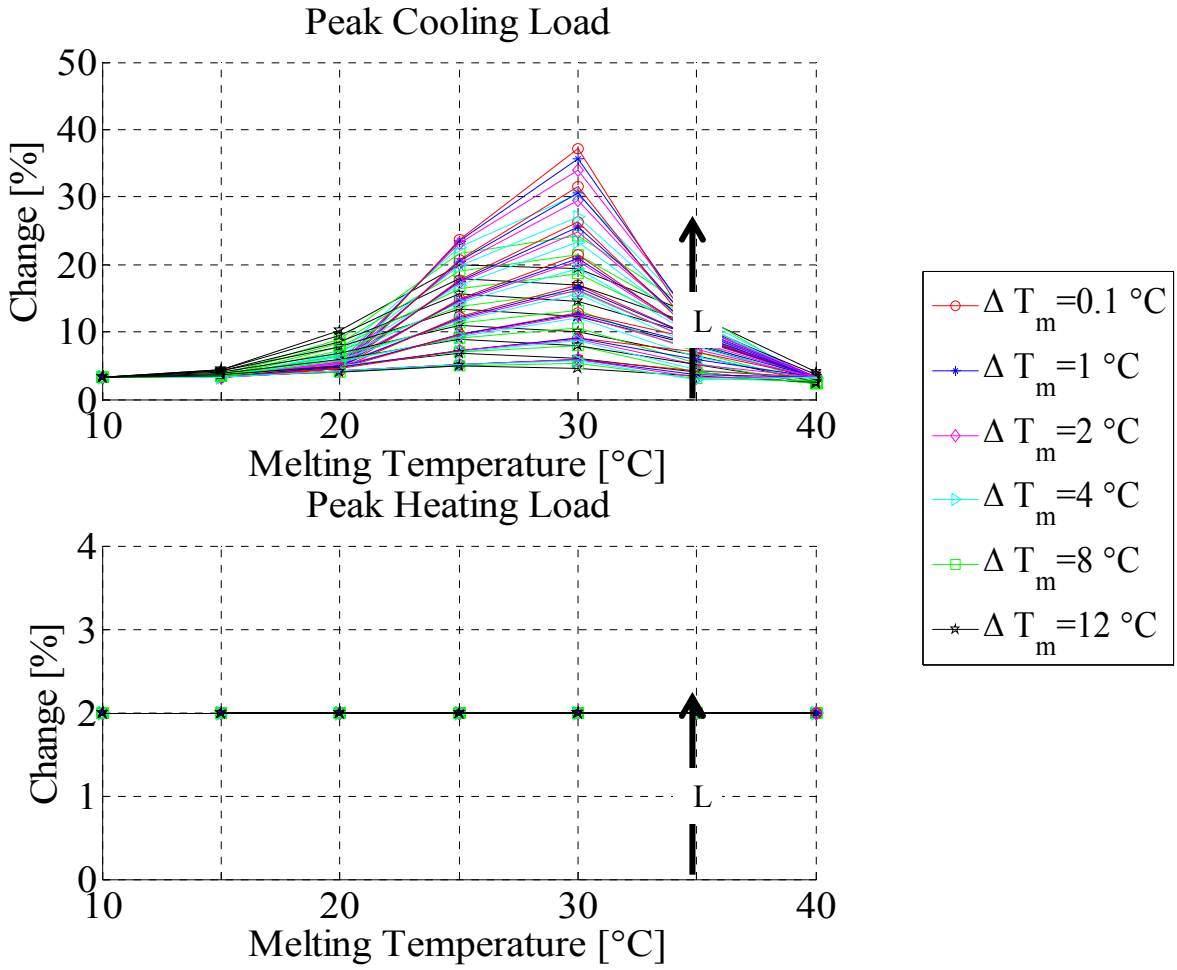

a) Percentage reductions in peak cooling and heating loads across all parameters

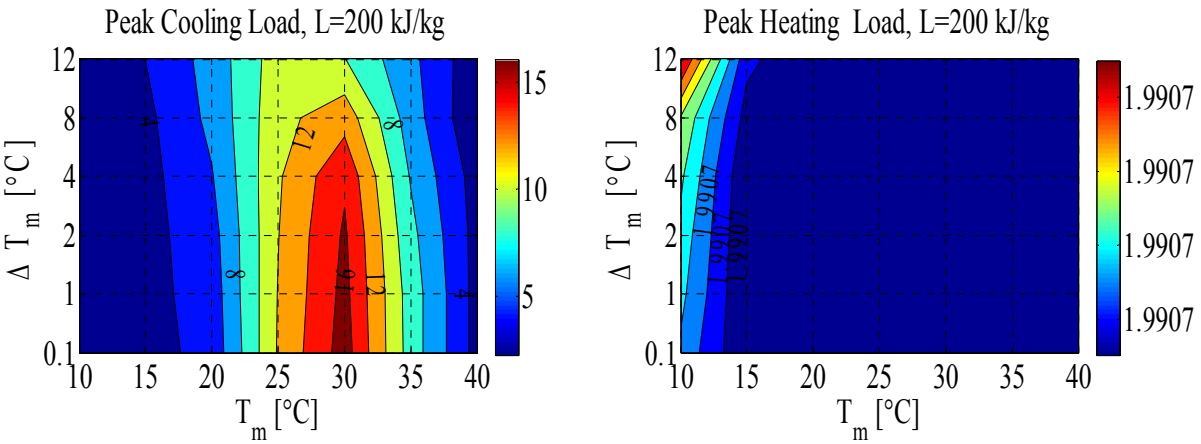

b) A contour plot for the case of 200 kg/kJ showing reduction in peak cooling and heating loads

Figure 5.14 Percentage reductions in peak cooling and heating loads for south wall

Figure 5.15 shows the peak cooling load shift for PCM-enhanced wall under various thermal properties. The figure shows that the peak cooling load is shifted as the latent heat increases. Peak cooling shift ranges from a minimum of 40 minutes to 4 hours. This is insignificant when compared to the previous two designs (PCM to interior and PCM in the middle). In all the cases, the peak cooling load shift occurs close to 35°C. However, the difference between 35C and other temperatures is not significant too.

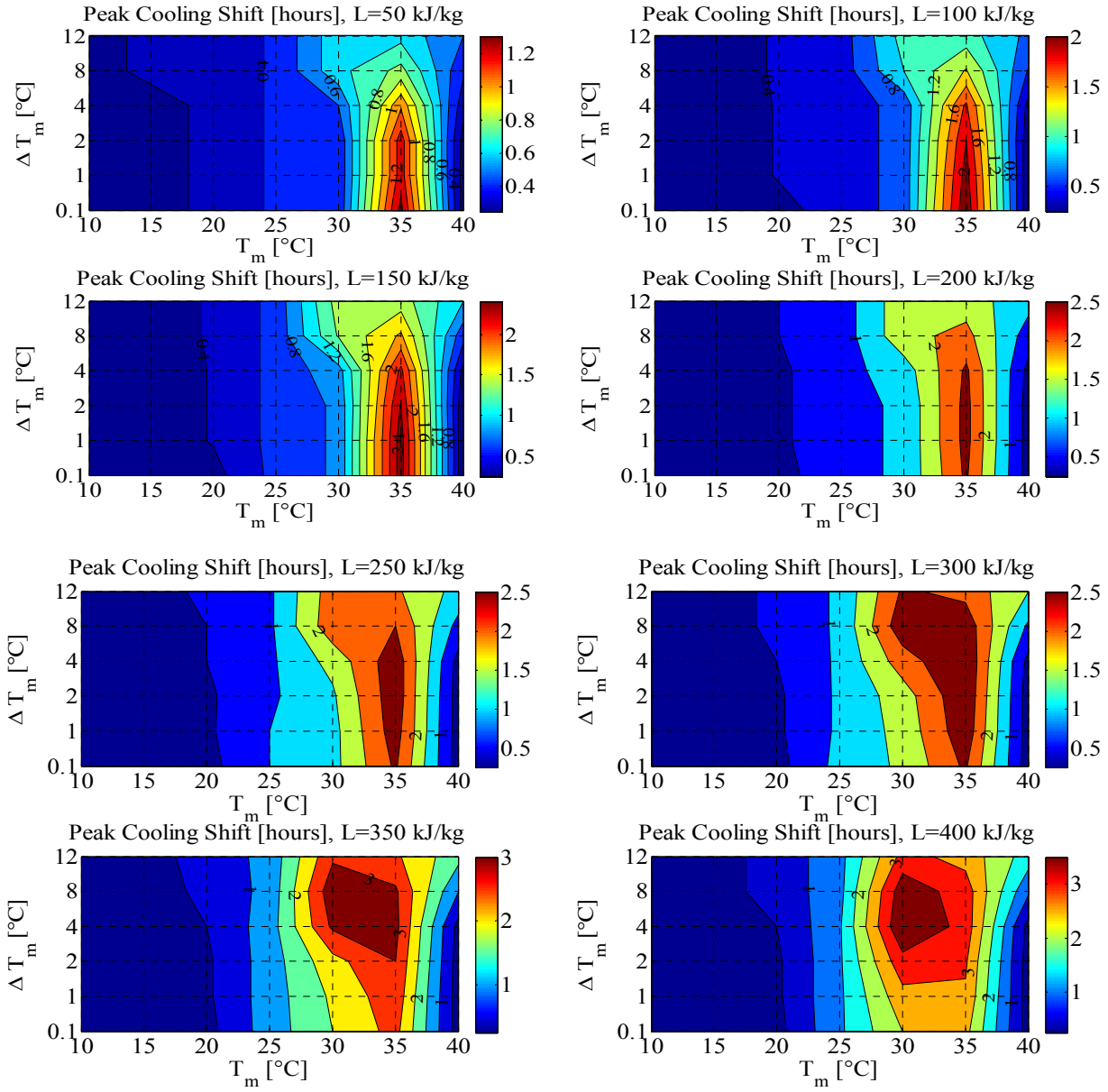

Figure 5.15 Peak cooling shifts in hours compared to the base case

5.4.3.2 Impact of wall orientations

Table 5-7 summarizes the reduction in cooling and heating load both annual and peak for all wall orientations when PCM is located at the exterior side. Detailed contour plots are provided in **Appendix A**. South and West walls show a similar saving potential in annual

cooling load; 7-48% for south and 6-49% for west. The reduction in annual cooling load on North wall ranges from 6-55%. The East wall saves from 6-39% in annual cooling load. For all cases the narrow melting range is superior to the wide melting range. For all orientations and across all PCM thermal properties, the reduction in annual heating load ranges from 1.7-2.1%. With this small savings range in annual heating load, the walls can be ranked from highest to lowest as follow; South, West, East and, finally North. A similar trend is also observed with peak cooling and heating load.

Table 5-7 Rough reductions in cooling and heating loads for PCM-enhanced Walls in Golden, CO, PCM to the exterior

Orientation		Reduction in Annual Cooling Load [%]		Reduction in Annual Heating Load [%]		Reduction in Peak Cooling Load [%]		Reduction in Peak Heating Load [%]		Peak Cooling Shift [hours]	
South	ΔT_m [°C] / L [kJ/kg]	0.1-1	2-12	0.1-1	2-12	0.1-1	2-12	0.1-1	2-12	0.1-1	2-12
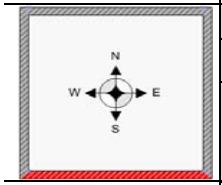	50-100	9-15	7-14	1.8	1.8	6-9	5-9	2	2	1.3-2.2	0.7-2
	150-250	19-32	12-28	1.9-2	1.8-1.9	13-21	8-21	2	2	2.5-2.8	1.5-2.8
	300-400	36-48	22-44	2-2.1	1.9-2	26-37	15-34	2	2	2.6-2.8	2.3-4
West	ΔT_m [°C] / L [kJ/kg]	0.1-1	2-12	0.1-1	2-12	0.1-1	2-12	0.1-1	2-12	0.1-1	2-12
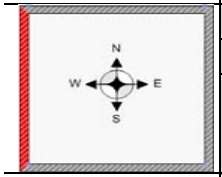	50-100	8-13	6-13	1.7-1.8	1.7-1.8	5-10	5-9	2	2	0.7-1	0.6-1
	150-250	18-32	11-28	1.8-1.9	1.8-1.9	13-22	9-20	2	2	1-2.6	1-2.5
	300-400	36-49	21-45	1.9	1.8-1.9	25-29	16-28	2	2	3.3-3.8	2-3.8
North	ΔT_m [°C] / L [kJ/kg]	0.1-1	2-12	0.1-1	2-12	0.1-1	2-12	0.1-1	2-12	0.1-1	2-12
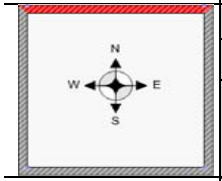	50-100	10-15	6-15	1.7	1.7	5-9	4-8.5	2	2	0.4-0.7	0.5-1.1
	150-250	22-41	12-35	1.7	1.7	13-25	7-22	2	2	0.8-1.8	1-2.3
	300-400	44-55	25-52	1.7	1.7	29-39	14-35	2	2	2.4-6.2	2-5
East	ΔT_m [°C] / L [kJ/kg]	0.1-1	2-12	0.1-1	2-12	0.1-1	2-12	0.1-1	2-12	0.1-1	2-12
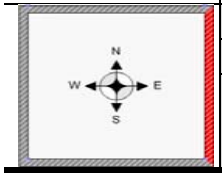	50-100	8-12	6-12	1.7	1.7	4-6	4-6	2	2	1.4-2.4	0.6-2
	150-250	15-26	11-23	1.8	1.7-1.8	9-14	5-13	2	2	2.5-2.8	1.3-2.8
	300-400	29-39	18-35	1.8	1.8	17-25	10-23	2	2	2.7-3	2.1-3.3

5.4.4 Conclusions on Multilayer PCM-enhanced Wall

Generally speaking for the environmental conditions analyzed, the PCM performance in reducing the cooling loads is significant compared to the heating loads. It is however identified that the best location for PCMs is when placed in direct contact with indoor environment. For this design, a narrow melting range (<1°C) coupled with optimal melting temperature close to the heating and cooling setpoints achieve maximum savings in annual heating and cooling loads. However, the PCM performs superior in reducing the cooling loads. For heavy latent heat cases (> 350 kJ/kg), the cooling loads has been entirely eliminated when PCM placed to the interior.

The next best performance is when PCM is located at the middle of the wall. This design concept has indicated that wide melting range (>2°C) is superior. The optimal melting temperature for maximum savings in cooling loads is 1°C higher than the cooling setpoint since it is located further away from the indoor environment. For maximum savings in annual heating loads, the optimal melting temperature is 2°C below the heating setpoint. Since the reduction in heating loads is not significant, the melting range is not sensitive across the variables.

When PCM is placed to exterior side of the wall, the savings in heating and cooling loads is lower than the previous two cases. Similar to middle PCM, the optimal melting temperature for maximum savings in annual cooling load is 1°C higher than the cooling setpoint. For maximum savings in peak cooling load is however around 35°C. The melting range is even less sensitive than the middle case.

5.4.5 Design guidelines for PCM-enhanced multilayer Wall

The previous sections provide details about performance of PCM considering location relative to the main wall elements, PCM thermal properties (i.e., melting temperature, melting range and latent heat), and orientations. Using these set of simulations, design correlations are developed for using PCM as shown in **Figure 5.16**. The followings are the assumptions and conditions for using these guidelines:

1) The correlations are developed using a residential wall design for Golden, CO described in Building America Benchmark [279, 280].
2) The PCM layer is placed in direct contact with the indoor environment and therefore to the interior side of the wall.
3) The correlations are developed based on the following PCM properties:
    a) Optimal melting Temperature of 24°C and 22°C for maximum savings in annual cooling and heating loads, respectively.
    b) Optimal melting range of less than 0.2°C (with exception of a case for the south wall when latent heat=400 kJ/kg, refer to **Table 5-8** for further details).
    c) The latent heat of PCM ranges from 50-400 kJ/kg.

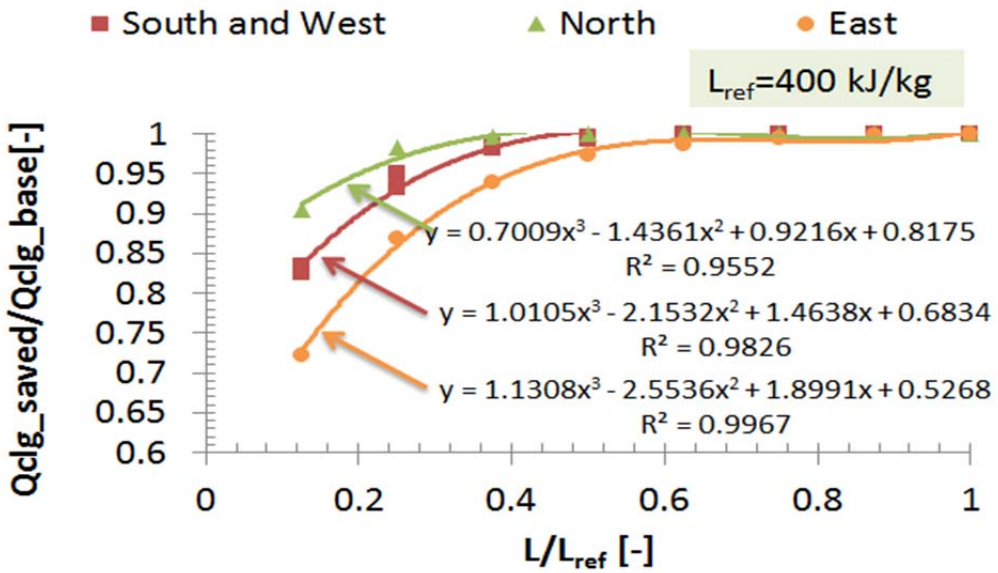

a) Design correlation for maximum savings in annual cooling load for various orientations

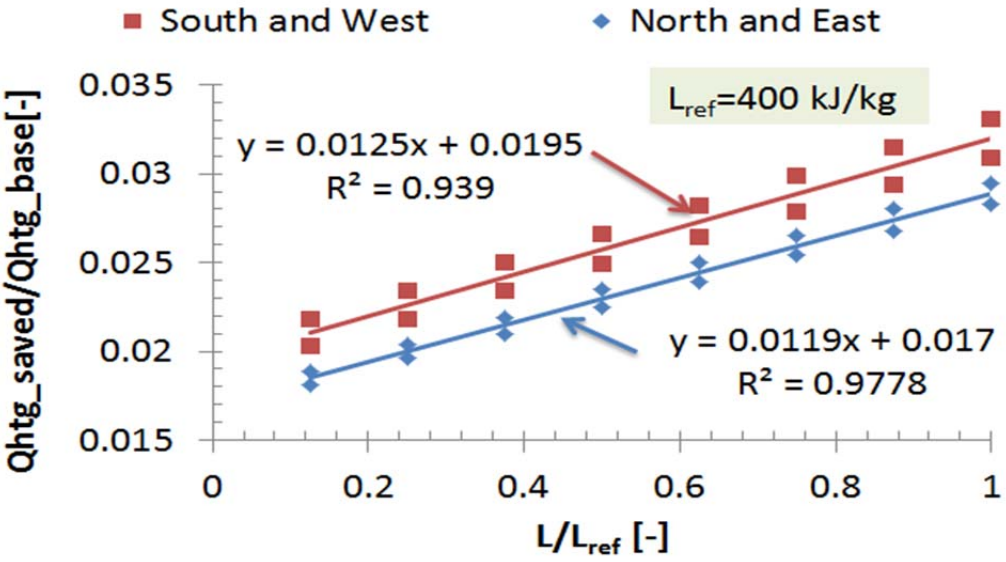

b) Design correlation for maximum savings in annual heating load for various orientations

Figure 5.16 Design correlations for maximum savings in annual loads for all orientations when PCM placed to the interior side of the wall

Table 5-8 Optimal thermal properties for PCM when placed to the interior of a multilayer wall

<table>
<tr><th colspan="9">South Wall</th></tr>
<tr><th></th><th colspan="2">Annual Cooling Load</th><th colspan="2">Annual Heating Load</th><th colspan="2">Peak Cooling Load</th><th colspan="2">Peak Heating Load</th></tr>
<tr><td>L [kJ/kg]</td><td>Tm [°C]</td><td>ΔTm [°C]</td><td>Tm [°C]</td><td>ΔTm [°C]</td><td>Tm [°C]</td><td>ΔTm [°C]</td><td>Tm [°C]</td><td>ΔTm [°C]</td></tr>
<tr><td>50</td><td rowspan="7">24</td><td rowspan="5">0.1</td><td rowspan="7">22</td><td rowspan="7">0.1-0.2</td><td rowspan="7">24</td><td>1</td><td rowspan="7">19</td><td rowspan="2">0.1</td></tr>
<tr><td>100</td><td rowspan="5">0.1</td></tr>
<tr><td>150</td><td rowspan="4">0.1</td></tr>
<tr><td>200</td><td>0.1-0.2</td></tr>
<tr><td>250</td><td rowspan="3">0.1-0.2</td><td>0.1-1</td></tr>
<tr><td>300</td><td rowspan="2">0.1-2</td></tr>
<tr><td>350</td><td rowspan="2">0.1-0.2</td></tr>
<tr><td>400</td><td>0.1-0.2</td><td>0.1-4</td></tr>
<tr><td></td><td colspan="8">West Wall</td></tr>
<tr><td></td><td colspan="2">Annual Cooling Load</td><td colspan="2">Annual Heating Load</td><td colspan="2">Peak Cooling Load</td><td colspan="2">Peak Heating Load</td></tr>
<tr><td>L [kJ/kg]</td><td>Tm [°C]</td><td>ΔTm [°C]</td><td>Tm [°C]</td><td>ΔTm [°C]</td><td>Tm [°C]</td><td>ΔTm [°C]</td><td>Tm [°C]</td><td>ΔTm [°C]</td></tr>
<tr><td>50</td><td rowspan="8">24</td><td rowspan="7">0.1</td><td rowspan="8">22</td><td rowspan="8">0.1-0.2</td><td rowspan="2">25</td><td>1</td><td rowspan="8">19</td><td rowspan="3">0.1</td></tr>
<tr><td>100</td><td>2</td></tr>
<tr><td>150</td><td rowspan="6">24</td><td rowspan="6">0.1</td></tr>
<tr><td>200</td></tr>
<tr><td>250</td><td>0.1-0.2</td></tr>
<tr><td>300</td><td>0.1-1</td></tr>
<tr><td>350</td><td rowspan="2">0.1-2</td></tr>
<tr><td>400</td><td>0.1-0.2</td></tr>
<tr><td></td><td colspan="8">North Wall</td></tr>
<tr><td></td><td colspan="2">Annual Cooling Load</td><td colspan="2">Annual Heating Load</td><td colspan="2">Peak Cooling Load</td><td colspan="2">Peak Heating Load</td></tr>
<tr><td>L [kJ/kg]</td><td>Tm [°C]</td><td>ΔTm [°C]</td><td>Tm [°C]</td><td>ΔTm [°C]</td><td>Tm [°C]</td><td>ΔTm [°C]</td><td>Tm [°C]</td><td>ΔTm [°C]</td></tr>
<tr><td>50</td><td rowspan="7">24</td><td rowspan="3">0.1</td><td rowspan="7">22</td><td>0.1-1</td><td rowspan="7">24</td><td>1</td><td rowspan="7">19</td><td rowspan="2">0.1</td></tr>
<tr><td>100</td><td rowspan="5">0.1-0.2</td><td rowspan="3">0.1</td></tr>
<tr><td>150</td><td rowspan="2">0.1-2</td></tr>
<tr><td>200</td><td>0.1-0.2</td></tr>
<tr><td>250</td><td rowspan="3">0.1-0.2</td><td>0.1-1</td></tr>
<tr><td>300</td><td rowspan="2">0.1-2</td></tr>
<tr><td>350</td><td rowspan="2">0.1-0.2</td></tr>
<tr><td>400</td><td></td></tr>
<tr><td></td><td colspan="8">East Wall</td></tr>
</table>

<table>
<tr><th></th><th colspan="2">Annual Cooling Load</th><th colspan="2">Annual Heating Load</th><th colspan="2">Peak Cooling Load</th><th colspan="2">Peak Heating Load</th></tr>
<tr><td>L [kJ/kg]</td><td>Tm [°C]</td><td>ΔTm [°C]</td><td>Tm [°C]</td><td>ΔTm [°C]</td><td>Tm [°C]</td><td>ΔTm [°C]</td><td>Tm [°C]</td><td>ΔTm [°C]</td></tr>
<tr><td>50</td><td rowspan="8">24</td><td rowspan="8">0.1</td><td rowspan="8">22</td><td rowspan="8">0.1-0.2</td><td rowspan="2">25</td><td>1</td><td rowspan="8">19</td><td rowspan="2">0.1</td></tr>
<tr><td>100</td><td>2</td></tr>
<tr><td>150</td><td rowspan="6">24</td><td>1</td><td rowspan="2">0.1-0.2</td></tr>
<tr><td>200</td><td rowspan="5">0.1</td></tr>
<tr><td>250</td><td rowspan="2">0.1-1</td></tr>
<tr><td>300</td></tr>
<tr><td>350</td><td rowspan="2">0.1-2</td></tr>
<tr><td>400</td></tr>
</table>

5.5 Ventilated PCM-enhanced cavity Wall

The performance of PCM layer in the multilayer wall is superior when savings in annual cooling load is considered. However, the savings in annual heating load reaches a maximum of 3.3% at best. This is an expected result since the winter solar radiation is the only source of heat storage. Due to the insulation level and the cold outside environment, a small amount of this heat can propagate to the PCM layer for storage. In order to enhance the heating performance of PCM layer, a cavity with glazing placed on the exterior side can harvest the solar radiation and increase the storage efficiency of PCM layer. This section investigates this design concept.

5.5.1 Development of a ventilated cavity case

The ventilated cavity wall design consists of several components: the main multilayer wall, a cavity and a glazing. The main multilayer wall investigated in the previous section can be used as the base wall design. The cavity and glazing are two design's considerations that need careful attention.

5.5.1.1 Sensitivity on the cavity parameters

For the cavity, different parameters such as vent area (air inlets at bottom and top of the cavity), gap width, and flow mechanism are required. The air flow can be under natural convection due to buoyancy from either indoor or outdoor, using fixed mass flow rate if fan is used, or no flow is allowed. Therefore, these different design considerations have been investigated with a single glazing on south base case no-PCM wall. For this design, the cavity depth is varied from 0.05 to 0.45m and vent to wall ratio (VWR) is varied from 1-9%. The air flow mechanism is assumed to be under natural convection where the air is either induced from outdoor or indoor environment as show in **Figure 5.17**. **Table 5-9** lists the parameters and assumptions for this simulation case.

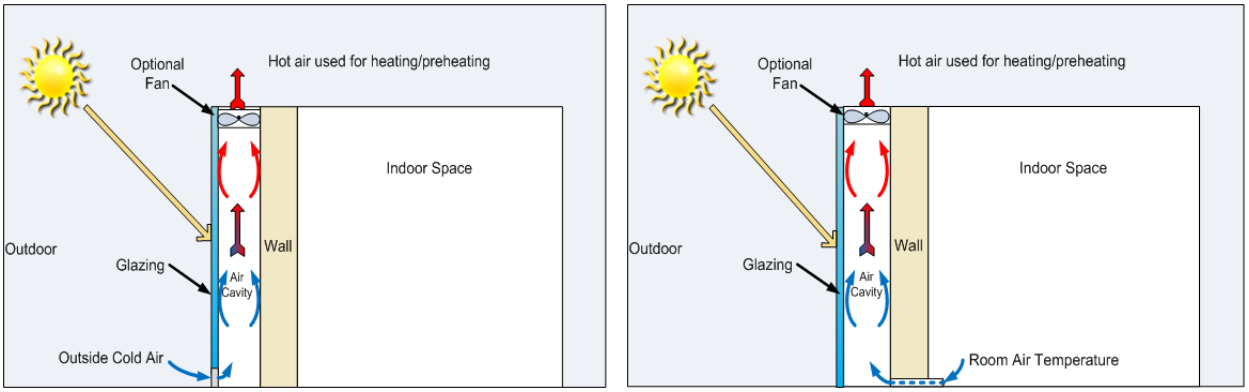

a. Heating Scenario 1 where cold air induced from outdoor

b. Heating Scenario 2 where air in induced from indoor space

Figure 5.17 Air flow mechanism for two heating scenarios under natural convection

Table 5-9 Parameters used for a south ventilated cavity no-PCM wall

Test Parameter	Values	Units
Wall thermal characteristics	Refer to **Table 5-2**	m
Wall height	3	m
Wall width	7	m
Mesh Grid Points	10 per layer	
Indoor Temperature	24 in summer (May-October) 22 in winter season	°C
External Convective Heat transfer Coefficient	29.3	$W/m^2.K$
Internal Convective Heat transfer Coefficient	4.43	$W/m^2.K$
Solar absorption	0.9	
Emissivity of the massive wall	0.9	
Cavity		
Depth, (b)	varies from 0.05 to 0.45	m
Vent Area, (A_v)	vent to wall ratio (VWR) is varied from 1-9%	m^2
Vertical distance between two vents, (Ho)	2.5	m
Flow characteristic	Natural Convection	
Air induced	From outside, inside or no flow	
Glazing		
Number of glazing	1	
Ug	5.91	$W/m^2.K$
Emissivity of the glazing	0.9	
Transmissivity of the glazing, τ	0.81	
Simulation Parameters		
Time Step	5	minutes
Weather file	EPW for Golden, Colorado	

Using the AdvFacSy toolbox, different cases were simulated. **Figure 5.18** shows the results across all the parameters. It is noticed that the annual and peak loads are not sensitive to the cavity parameters when indoor air induced. Slight changes can be observed when the outdoor air induced. Since it harvests solar radiation, the cavity installation has a negative impact on annual and peak cooling loads. Therefore, solar protection should be provided during summer.

The impact of this strategy is not considered because the main goal is to enhance the heating loads.

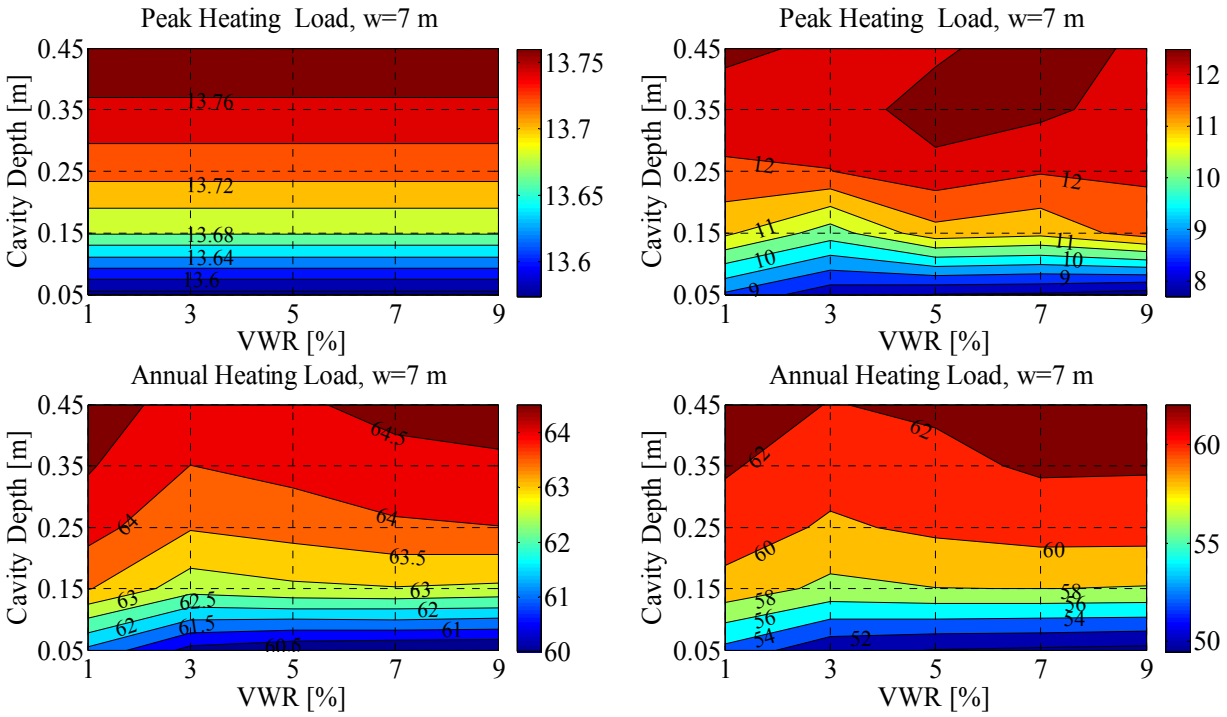

a) Annual and peak heating loads for a cavity under natural convection when indoor air is induced to the cavity

b) Annual and peak heating loads for a cavity under natural convection when outdoor air is induced to the cavity

Figure 5.18 Annual and peak heating loads under various cavity designs for south base wall (no-PCM case)

From the above figure, a cavity width of 0.15 m and a medium vent area (VWR of 5%) for the two designs are further compared with the no flow case. The results of these three designs are shown in **Figure 5.19**. The figure shows that the no flow case is marginally better than the other two cases when the savings in annual heating load is considered, 2.5% more than when the air is induced from indoor and 7.3% more than when air is induced from outdoor. In addition, the reduction in peak heating load is close to the case of the indoor air case and 2% more than outdoor case respectively. However when PCM layer is used, it is expected that that abundant

heat will be available. Therefore, a ventilated cavity with air induced from the indoor is selected for further evaluation. This design gives a flexibility to manipulate the extra heat to meet the heating demand in the zone by introducing the pre-heated air from the top vent or transported to other storage medium elsewhere.

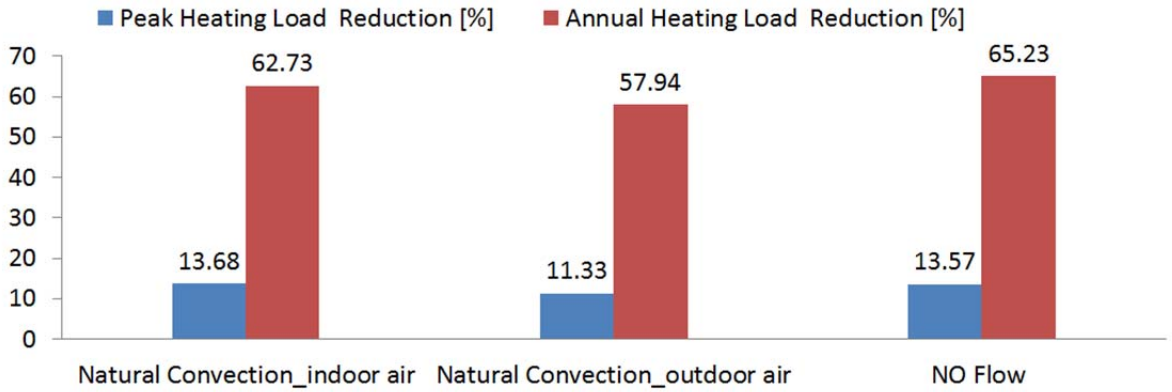

Figure 5.19 Annual and peak heating loads under three flow mechanisms for a south no-PCM cavity case with depth =0.15m and VWR=5%

5.5.1.2 Sensitivity on the glazing type

The glazing system is an important design element in the cavity design. The use of poor glazing may increase the heat loss from the cavity. Therefore, three glazing types have been tested when indoor air is induced. The thermal properties are based on ASHRAE handbook and listed in **Table 5-10**[285].

Table 5-10 Glazing characteristics for the cavity design

Glazing Type*	U value [W/m^2.K]	Solar Transmittance [-]
Single Glazing	5.91	0.81
Double Glazing (6.4 mm air gap)	3.12	0.76
Triple Glazing (6.4 mm air gap)	2.16	0.68

*Glazing thickness is 3.2 mm

Figure 5.20 shows the performance of the three glazing types. The heat loss from the cavity is reduced when more than one glazing is utilized. While the difference in performance is

not significant between the double and triple glazing, the double glazing is selected for the cavity design.

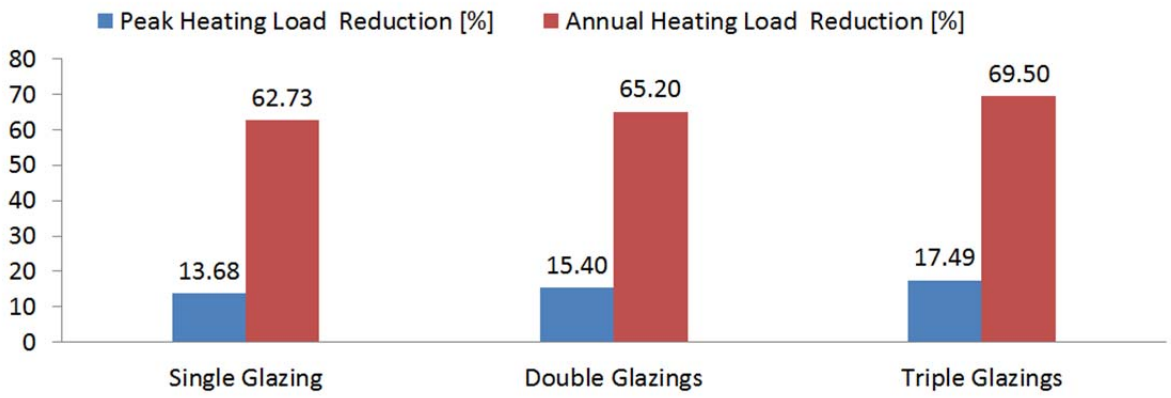

Figure 5.20 Annual and peak loads under three glazing types for a south no-PCM cavity case with depth =0.15m and VWR=5% under natural convection when indoor air induced

5.5.1.3 Simulation results of the no PCM cavity design case

Based on the results of the sensitivity above, the final cavity design is selected. In addition to the assumptions as per **Table 5-9**, the cavity depth of 0.15 m and vent area of 1.05 m^2 (i.e., VWR of 5%) is selected. A double glazing with thermal characteristics explained earlier in **Table 5-10** is also selected. When this case is simulated and compared to the base case of multilayer wall, the results are shown in **Table 5-11**. Although no PCM is used, the cavity alone has improved the savings in annual and peak heating loads when compared to the base case design. This cavity improvement is due to the solar harvesting which consequently conducted through wall to indoor. When the hot air from the cavity is allowed to circulate and utilized to compensate for heat loss, the annual heat load is further reduced and hence is adjusted for this component. This adjustment is a cavity contribution due to convection. This heat recovery is at minimum for North (i.e., 1.42%) and maximum for South wall (i.e., 7.2%). These values will be used later when PCM is evaluated.

Table 5-11 Thermal performance indicators for the no PCM cavity case wall in Golden, CO

Orientation	Reduction in Annual Heating Load [%]*	Reduction in Peak Heating Load [%]	Reduction in Annual Heating Load_Adj [%]	Cavity Contributions due to convection [%]
South	65.20	15.40	72.38	7.20
West	56.20	13.85	60.02	3.82
North	41.87	13.78	43.29	1.42
East	55.98	14.63	63.10	7.10

*cavity contributions due to conduction

5.5.2 PCM to the interior side of the wall

For this case, the PCM is placed to the interior side of the wall in direct exposure to the indoor environment. Using the final design of the cavity and glazing explained in the previous section, a series of simulations are run for latent heat between 50-300 kJ/kg at an increment of 50, melting temperature 20-25°C at an increment of 1°C and melting range of 0.1,1,2,4 and 6°C. The overall goal is to enhance the performance of PCM in winter. Hence, only heating loads are considered for discussion. The contour plots for all the cases are provided in **Appendix B**.

Figure 5.21 shows the results of all orientations across all PCM parameters. The dotted line below all curves represents the contribution of the cavity when PCM is used. It is apparent that the performance of PCM has been improved by introducing the cavity. There is clear distinction in PCM performance as the melting temperature varies. When no cavity is used, the maximum savings in annual heating load is around 3% (refer to **Table 5-5**). When a cavity is introduced in the south wall, the maximum savings in annual heating loads reaches above 95% as shown in **Figure 5.21** (a). Cavity contributes 65% of savings in annual heating loads (refer to **Table 5-11**) and the rest (i.e., of more than 30%) is due to PCM layer.

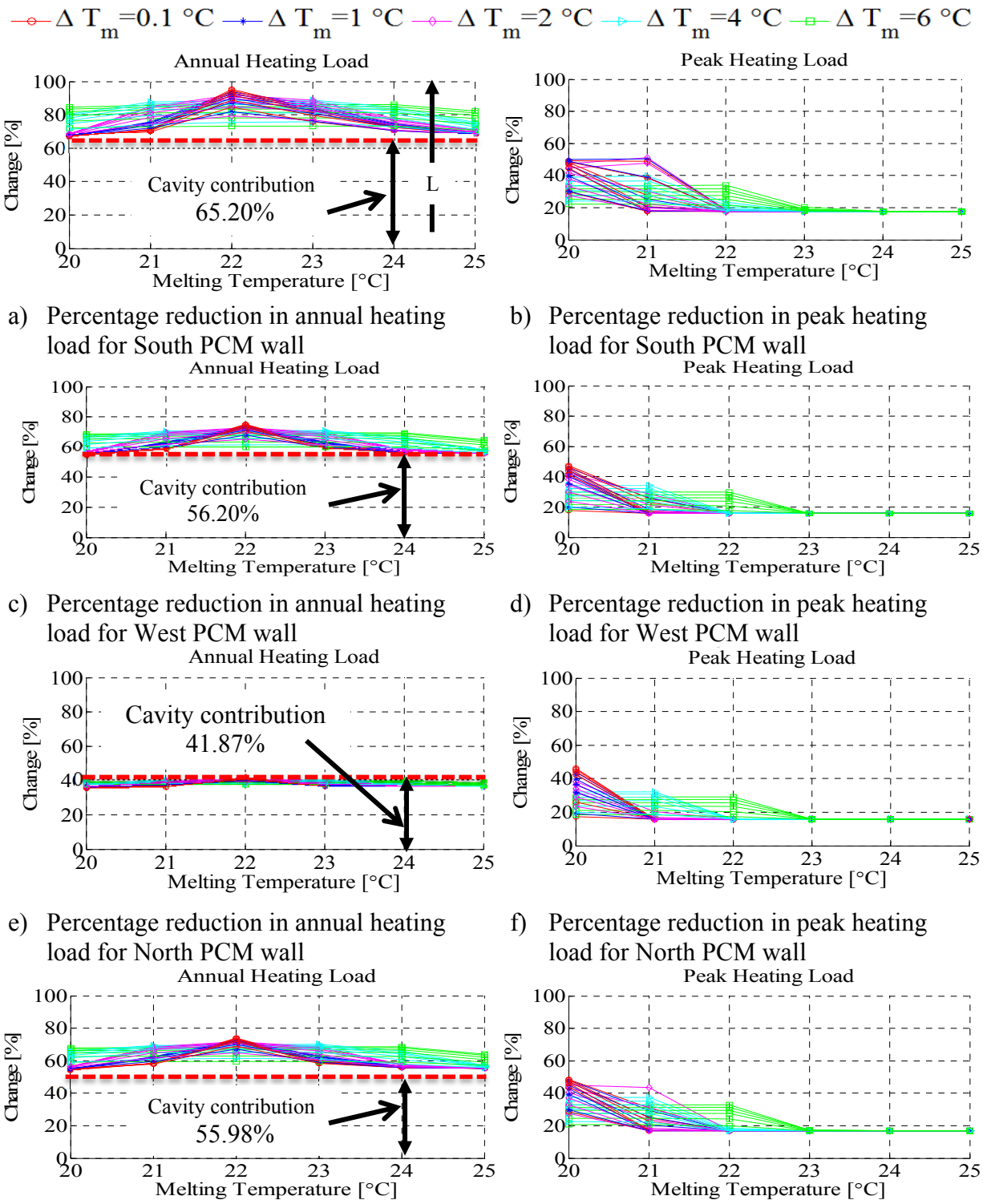

a) Percentage reduction in annual heating load for South PCM wall

b) Percentage reduction in peak heating load for South PCM wall

c) Percentage reduction in annual heating load for West PCM wall

d) Percentage reduction in peak heating load for West PCM wall

e) Percentage reduction in annual heating load for North PCM wall

f) Percentage reduction in peak heating load for North PCM wall

g) Percentage reduction in annual heating load for East PCM wall

h) Percentage reduction in peak heating load for East PCM wall

Figure 5.21 Annual and peak heating loads across PCM parameters for the four orientations, PCM to the interior side

The PCM contributions in west and east are lower than the south wall as shown in **Figure 5.21** (c) and (g). The savings in annual heating loads due to PCM is around 20%, if cavity contribution due to conduction is subtracted (refer to **Table 5-11**). The cavity in North wall is not effective in improving the performance of PCM as shown in **Figure 5.21** (e). When PCM is used, the savings in annual heating loads is less than the case when no PCM is used. This is likely due to the storage of PCM which are not utilized internally to reduce heating load. In all cases, the optimal melting temperature is close to the heating setpoint of 22°C with a narrow melting range of 0.1°C. However, the performance of this group tends to decrease as the melting range moves from the peak. At melting temperature away from the heating setpoint, the PCMs with wide melting range give more savings.

The savings in peak heating load has improved when the cavity design is compared to non-cavity design. For all orientations, the savings in peak heating loads are similar as shown in **Figure 5.21** (b), (d), (f) and (h). For south multilayer PCM wall, a maximum savings in peak load achieved with non-cavity case is 20%. For the cavity design, the maximum savings in peak heating load is around 50%. When cavity contributions are ignored (15.40% as per **Table 5-11**), 34.5% savings in peak heating load is due to the PCM layer only. This is a 14.5% improvement over the non-cavity design. The savings in other orientations are also similar to the south wall. In all cases, the optimal melting temperature is below 20°C with a narrow melting range of 0.1°C. Although temperature below 20°C was not simulated for this simulation run, it is likely the case that the optimal temperature is around 19°C; similar to the multilayer PCM walls (no cavity case).

5.5.3 PCM to the exterior of the wall

For this design, the PCM is placed to the exterior side of the wall; in the cavity side. A number of simulations are performed for latent heat between 50-300kJ/kg at an increment of 50, melting temperature 10-40°C at an increment of 5°C and melting range of 0.1,1,2,4,8 and 12°C. Similar to the previous design case, only heating loads are considered with detailed contour plots provided for all the cases in **Appendix B**.

Figure 5.22 shows the results of all orientations across all PCM parameters. For this design, the savings in annual heating loads ranges between 69-78% for the south wall compared to only 2% when no cavity is used. If the cavity contributions of 65% are removed (refer to **Table 5-11**) then PCM layer contributes 4-13% of the savings in annual heating load. For west and east wall, a similar savings range is achieved; between 59-68% compared to only 1.9% for the no-cavity case. The PCM layer contribution is 3-12% if it is the cavity contribution of 56% is subtracted. The savings in annual heating loads from north cavity is small; 43.5-47%. When cavity contribution (41.87%) is subtracted, the PCM contribution is between 1.7% and 5% compared to 1.7% for no-cavity case. Therefore, placing the cavity on north is not effective to enhance the PCM performance. It is also observed that the variation in melting range has minor impact on PCM performance. In other words, there is no significant distinction between PCMs as their thermal properties vary.

The reduction in peak heating load is similar across all orientations, around 19%. When the cavity contribution is removed, an improvement ranges from 3.5 to 5% is determined compared to a maximum savings of 2% when no cavity is used. Therefore, peak heating load is not improved by the cavity when PCM placed to the exterior side.

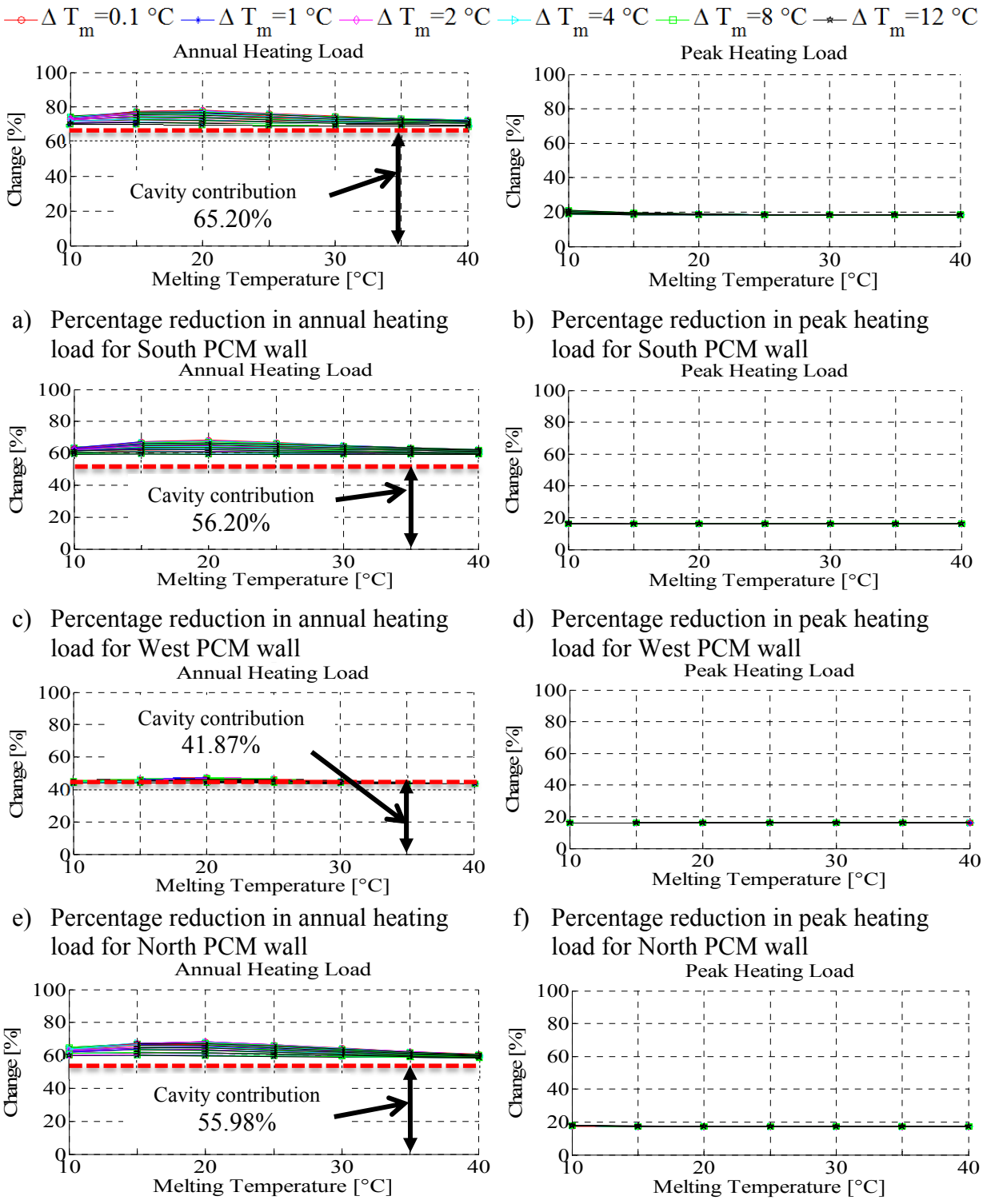

a) Percentage reduction in annual heating load for South PCM wall

b) Percentage reduction in peak heating load for South PCM wall

c) Percentage reduction in annual heating load for West PCM wall

d) Percentage reduction in peak heating load for West PCM wall

e) Percentage reduction in annual heating load for North PCM wall

f) Percentage reduction in peak heating load for North PCM wall

g) Percentage reduction in annual heating load for East PCM wall

h) Percentage reduction in peak heating load for East PCM wall

Figure 5.22 Annual and peak heating loads across PCM parameters for the four orientations, PCM to the exterior side

5.5.4 Conclusions on ventilated PCM-enhanced cavity wall

A clear distinction between PCMs with different melting range is observed. Those with narrow melting range achieve its maximum savings in annual heating loads at melting temperature close to the heating setpoint, following a triangle shape. This group then tends to give low savings as the melting temperature moves away from the setpoint. The savings of the wide melting range is flat and therefore are less sensitive to the heating setpoint. This group can be considered conservative. When the cavity contributions are subtracted, the cavity enhances the performance of interior PCM from 3% with no cavity to 30% for south and 20% for east and west. The cavity on north didn't improve the performance of PCM.

When PCM was placed to interior, the variations in performance between PCMs were clear. However, the variation in performance when PCM placed to the exterior is minimal. The savings in annual heating loads follows a smooth parabolic shape with a noticeable peak at 20°C compared to a triangular shape when PCM placed to interior. When the cavity contributions are subtracted, the cavity has improved the performance of exterior PCM from 2% with no cavity to a maximum of 13% for south, 12% for east and west, and 5% for north.

The triangular shape of PCM performance when placed to the interior side achieves maximum savings in annual heating loads at heating setpoint. However, the smooth parabolic shape of the savings in annual heating loads makes the design of exterior PCM more attractive at melting temperature away from the heating setpoint.

5.5.5 **Design guidelines for PCM-enhanced cavity wall**

Based on the conclusions of the ventilated cavity, the design of PCM when placed to the interior is attractive for achieving maximum savings in annual heating loads. Design correlations have been developed for this particular design under the four orientations as shown in **Figure 5.23**. The followings are the assumptions and conditions for using these guidelines:

1) The correlations are developed using a residential wall design for Golden, CO described in Building America Benchmark [279, 280].
2) The air is induced from indoor environment; an approximate adjustment of +0.025 (i.e., +2.5%) is applied when no flow is considered.
3) A double clear glazing in the cavity is used, an approximate adjustment of -0.03 (i.e., -3%) and +0.04 (i.e., +4%) should be applied for a single and triple glazing respectively.
4) The PCM layer is placed in direct contact with the indoor environment and therefore to the interior side of the wall.
5) The correlations are developed based on an optimal melting Temperature of 22°C, optimal melting range of 0.1°C and latent heat of PCM ranges from 50-300 kJ/kg (refer to **Table 5-12** for further details).

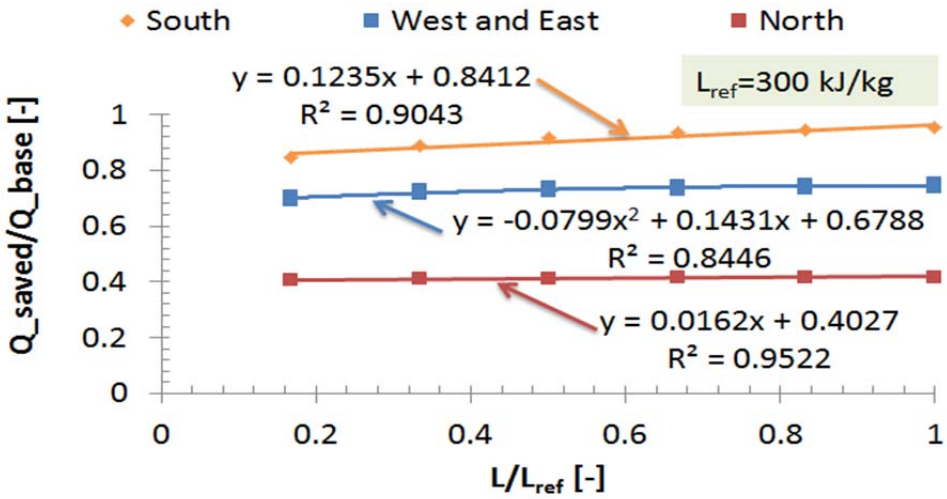

Figure 5.23 Design correlations for maximum savings in annual heating loads for all orientations when PCM placed to the interior side of the cavity wall

Table 5-12 Optimal thermal properties for PCM when placed to the interior of a ventilated cavity

	South			
	Annual Heating Load		**Peak Heating Load**	
L [kJ/kg]	Tm [°C]	ΔTm [°C]	Tm [°C]	ΔTm [°C]
50	22	0.1	20	1
100-200				0.1
250-300				1
	West			
	Annual Heating Load		**Peak Heating Load**	
L [kJ/kg]	Tm [°C]	ΔTm [°C]	Tm [°C]	ΔTm [°C]
50	22	0.1	20	2
100-300				0.1
	North			
	Annual Heating Load		**Peak Heating Load**	
L [kJ/kg]	Tm [°C]	ΔTm [°C]	Tm [°C]	ΔTm [°C]
50	22	0.1	20	2
100				1
150-300				0.1
	East			
	Annual Heating Load		**Peak Heating Load**	
L [kJ/kg]	Tm [°C]	ΔTm [°C]	Tm [°C]	ΔTm [°C]
50-300	22	0.1	20	0.1

These design curves are applicable when the conduction only from the cavity is considered. However, the cavity can provide extra heat through ventilation at the top vent to compensate for heat loss. The cavity contributions due to convection for different orientations have been determined to quantify their significance. When no PCM is used, the cavity contributions are determined earlier in **Table 5-11**. Therefore, the cavity contributions due to convection when using PCM are calculated. **Figure 5.24** illustrates the cavity contributions to balance the heat loss from the wall. As it is clear from the figure, the contributions from cavity are worth considering.

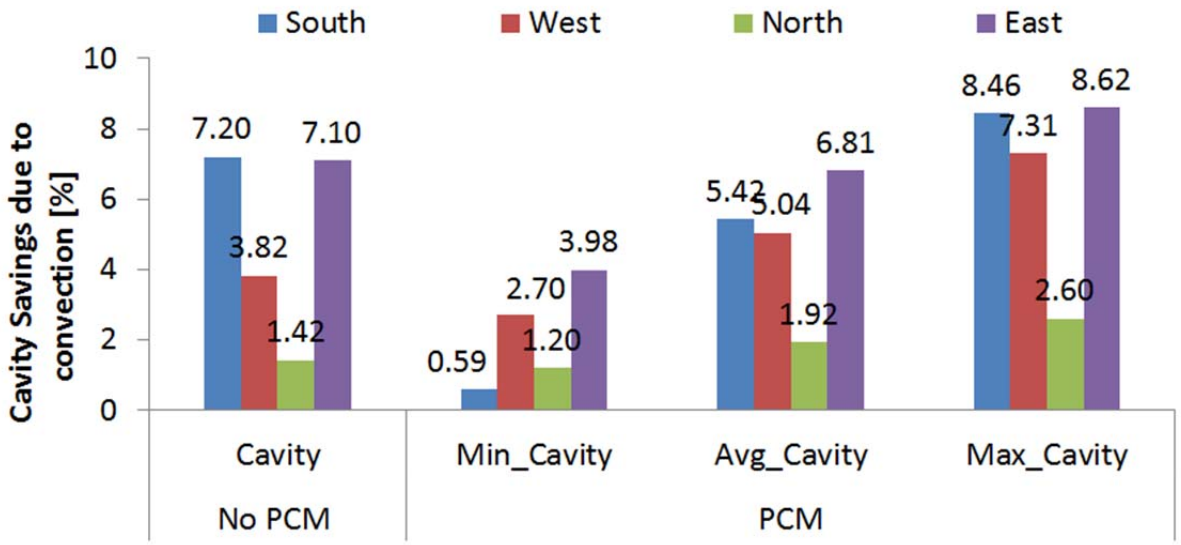

Figure 5.24 Cavity contributions due to convection form top vent balancing the heat loss

The convection contributions should also be accounted for. Therefore, another set of curves has been developed to account for this component as shown in **Figure 5.25**. Once the savings in annual heating loads are determined using **Figure 5.23** for different orientations, one may correct or adjust the savings in annual heating loads for cavity contributions using correlations of **Figure 5.25**.

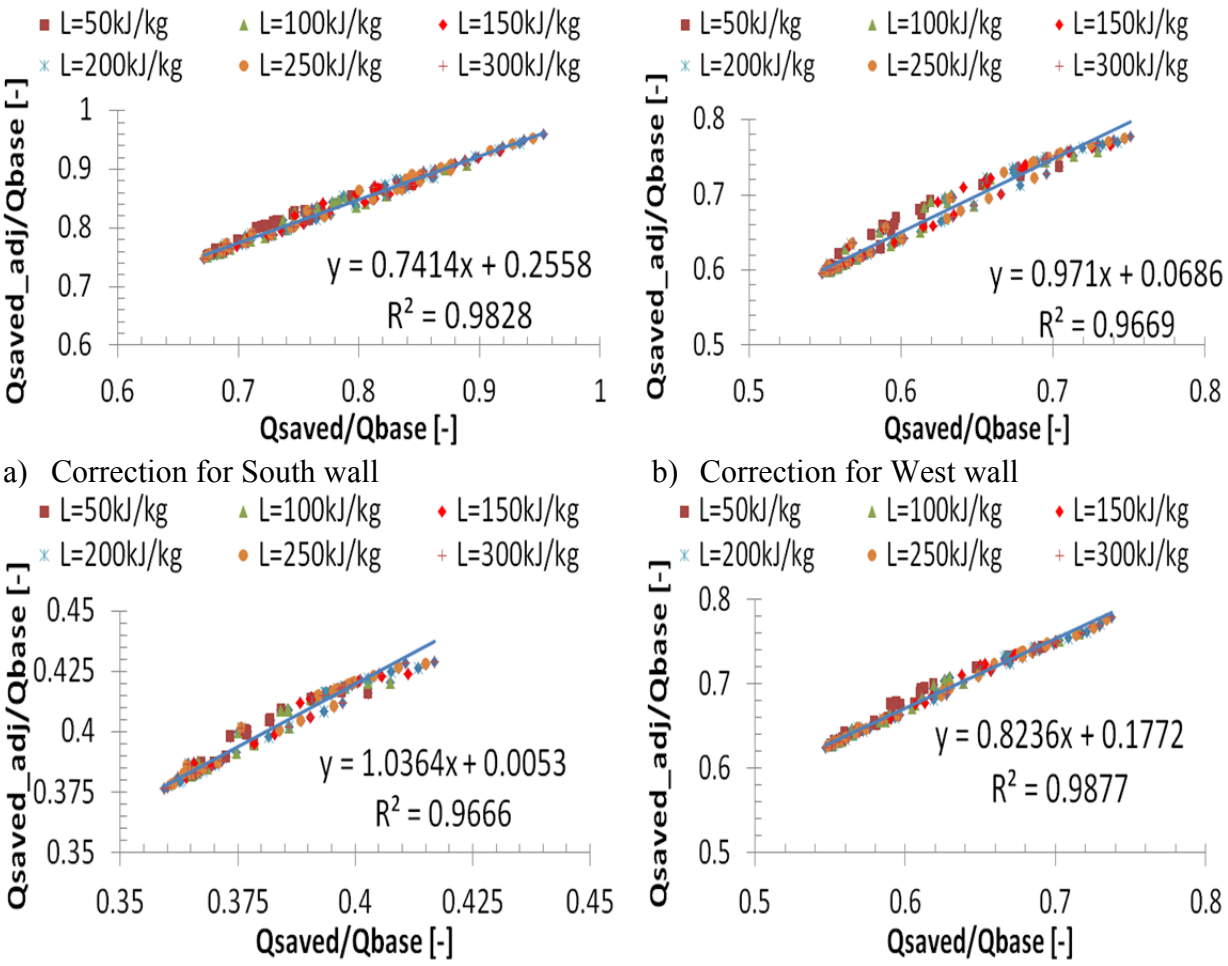

a) Correction for South wall

b) Correction for West wall

c) Correction for North wall

d) Correction for East wall

Figure 5.25 Correlations to correct for cavity contribution due to convection

5.6 Conclusions

A base case multilayer wall is simulated when PCM is placed at different locations; 1) to the interior side, 2) at middle of the wood assembly, sandwiched between insulation, and 3) to the exterior side. The design variations have been evaluated for four orientations; South, West, North and East under the climatic conditions of Golden CO when indoor air temperature is fixed

at cooling and heating setpoints. The thermal properties of PCM; melting temperature, melting range and latent heat are varied across a wide range of variables. It is concluded that best location for PCM is when it is directly exposed to indoor environment. The maximum savings in annual cooling and heating loads are achieved when the melting temperature is close to the cooling and heating setpoints, respectively. The PCM performs superior in reducing the cooling loads. For heavy latent heat cases (> 350 kJ/kg), the cooling loads has been entirely eliminated. Since indoor air temperature is fixed for these cases, fictitious diurnal cycles are naturally created due to changes in outside environmental conditions. However, PCM poorly performs for reducing the heating loads, a maximum reduction of 3%. This is due to the low intensity of available heat source that can be utilized for storage.

In order to enhance the PCM performance during winter, a ventilated cavity is implemented. The PCM location is evaluated for two locations; 1) when placed to the interior side, 2) when placed to the exterior in the cavity side. Similar to multilayer wall, the best location for PCM in cavity design is when placed to the interior side. For PCM to the interior, introducing the cavity has increased the heating performance of PCM during winter from 3% when no cavity to 20-30% for east, west and south orientations. The cavity at north wall has almost no impact in improving the PCM performance.

New design guidelines are developed for two design configurations; 1) multilayer wall, 2) ventilated cavity wall. Optimal thermal properties for PCM are also identified. Furthermore, cavity correlations are proposed to account for convection contributions from the ventilated cavity. These design guidelines are important for first order approximations for the benefit of PCM in new design as well as in retrofits. The methodology can easily be extended to different climates.

CHAPTER 6: MODELS INTEGRATION INTO WHOLE-BUILDING SIMULATION TOOL

Building consists of many complex systems including envelope, mechanical and electrical systems and control devices. Therefore, it is apparent that the standalone toolbox is limited in this regards. However, it is feasible to couple this toolbox with an existing dynamic simulation tool to extend the capability. Since the developed models are based on MATLAB-SIMULINK environment, co-simulation approach is implemented between this package and an energy simulation program. Different coupling approaches have been investigated in this chapter. Generic façade systems are selected for integration into TRNSYS, a whole-building simulation tool. Furthermore, a standard TRNSYS module, Type285, is specifically developed for multilayer wall with and without PCM. The developed models have been verified and some conclusions have been drawn.

6.1 Program Selection for Energy Performance Evaluation

Despite the availability of many energy simulation programs nowadays; many challenges are encountered when detailed simulation methods are sought. At first trial, users may select a program that might meet their objective and soon after find it not suitable to carry out their analysis. It is perhaps difficult to set an explicit procedure for selecting a simulation program that suits every one. Many factors such as accuracy, sensitivity, speed and cost, reproducibility, usability, input complexity, output quality, weather data availability are generally considered during the selection process [286]. In addition to the above factors, flexibility to co-simulation with two or more programs is emerging as new practice of simulating complex building systems.

While these factors are related to the energy simulation programs, other factors related to the users should also be considered. A study has identified three factors that users need to consider: matching the need, the budget (to purchase, training, use, and maintain the software), and the availability of existing computer facilities[152]. In order to utilize the developed toolbox, a co-simulation mechanism is considered for this research. Co-simulation approaches between energy simulation programs and other programs have been studied in literature [287-290]. The most two programs that are well respected in North America's research community are: EnergyPlus [158] and TRNSYS[178]. These two specific programs are highly flexible, well suited for research purposes.

It is possible to couple the developed Toolbox with EnergyPlus using Building Controls Virtual Test Bed (BCVTB), a co-simulation environment developed by Lawrence Berkeley National Laboratory [290]. In addition and based on BCVTB environment, a MATLAB-SIMULINK toolbox *"MLE+"* is available [291]. For both environments, however, the coupling is static where the information exchanges between EnergyPlus and SIMULINK occurs with one time step delay. This approach is acceptable for modeling cases where information is needed after the fact but may not be suitable for PCMs modeling since the interaction is needed simultaneously and iteratively. TRNSYS on the other hand offers an extreme flexibility when co-simulation comes into play. Many features have been introduced in TRNSYS16, including a graphical user interface "Simulation studio" and the possibility to call external programs such as MATLAB, FLUENT and many others [168]. Therefore, TRNSYS simulation package offers more flexibility that suits the objectives of this research.

6.2 Co-simulation of MATLAB/SIMULINK and TRNSYS using TYPE-155

There exists a module "TYPE 155" that couples the MATLAB-SIMULINK environment with TRNSYS simulation package. The co-simulation is simultaneous and information exchanges in an iterative manner between MATLAB and TRNSYS. **Figure 6.1** illustrates the concept of this co-simulation mechanism. A template MATLAB file is provided with TRNSYS package for users to use and modify. The script file acknowledges the TRNSYS structure protocol.

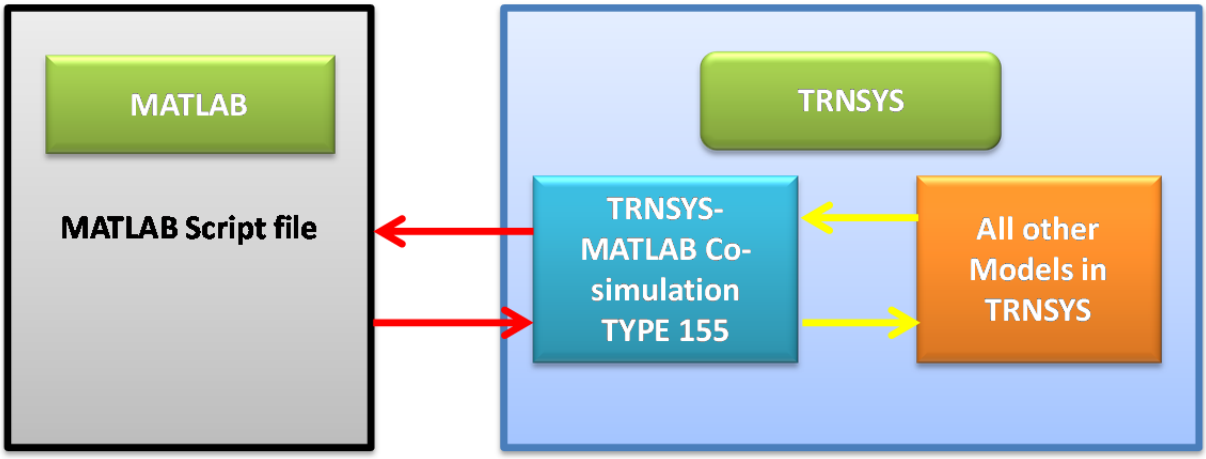

a) TRNSYS-MATLAB co-simulation mechanism using TYPE155

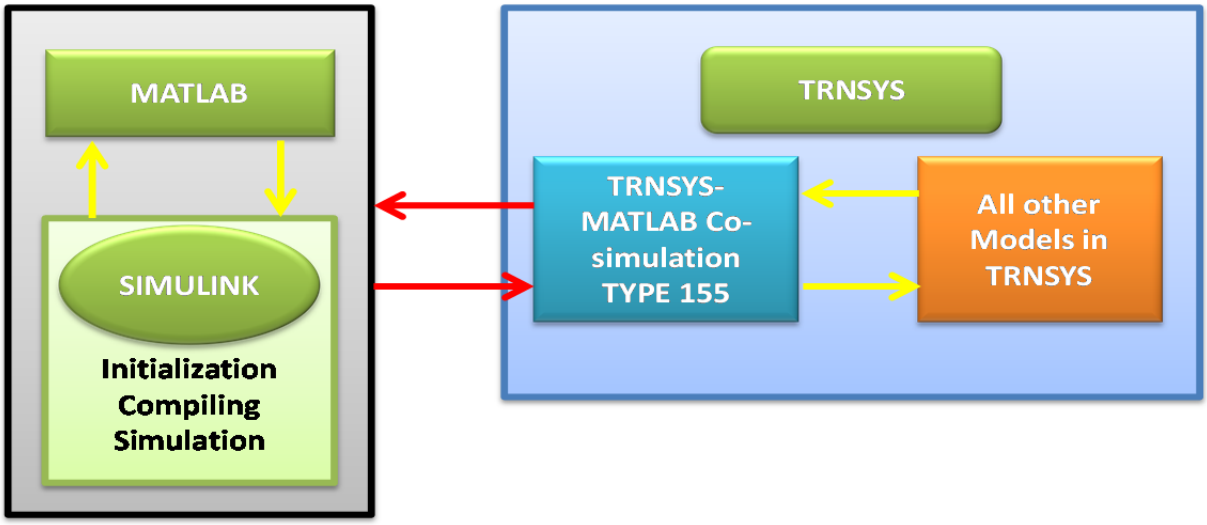

b) TRNSYS-SIMULINK co-simulation mechanism using TYPE155 through MATLAB

Figure 6.1 TRNSYS and MATLAB coupling mechanism using TYPE155

The first approach (**Figure 6.1** (a)) was initially considered to couple a MATLAB script file developed specifically for multilayer PCM-enhanced wall. This MATLAB code is based on numerical solutions described in Chapter 3. Since SIMULINK is an add-on to MATLAB, the same script file with modification can be used. In this case, the SIMULINK project is called inside MATLAB workspace. After implementing and verifying both approaches at early stages of this work, the followings are inferred:

1) Both approaches give reasonable results when compared to the conduction transfer function used in TRNSYS Type56.
2) Although provided with file error coding, MATLAB script was difficult to troubleshoot since MATLAB is run in a hidden form where no access is possible.
3) While many programs are recently installed with 64 bits, MATLAB 32 bits version is the only compatible version to use with TYPE 155.
4) If new version of MATLAB is upgraded, the Type 155 has to be recompiled since new updated libraries have to be used. This creates another challenge since the user has to re-compile the source code.
5) Using approach one, the simulation time for 1 hour time step was significant for a normal machine. Implementing small time steps imposes extra simulation time.
6) Approach two requires more simulation time since SIMULINK has to be called, initialized, and compiled (for the case of embedded MATLB functions) from MATLAB.
7) The SIMULINK call imposes another challenge of keeping the workspace variables for next time step. This could be a hidden source of error.
8) High level of technical expertise in MATLAB is needed with both approaches.

While some of the above limitations are typical, the simulation speed was the major reason to abandon both approaches. The iterative nature of the developed PCM model is perhaps the major reason for the slow simulation. Hence, none of these two approaches meet the requirement.

6.3 Indirect coupling between SIMULINK and TRNSYS

SIMULINK is primarily used for modeling complex dynamic systems. The package has many built-in functions and capabilities. One interesting capability is to convert the SIMULINK project into executable, C++ or even Dynamic-link library (DLL) files using the real time workshop (later known as SIMULINK Coder). Based on this capability and due to the modularity of TRNSYS simulation package, a novel methodology was proposed to export SIMULINK projects to TRNSYS and vice versa [292]. The development team has modified an existing target language compiler (TLC) file complemented with a wrapper to acknowledge the formal TRNSYS type structure. Using this file, any SIMULINK project can be converted into C++ list of codes and subsequently be compiled in Microsoft Visual Studio. Once the C++ files are compiled, one DLL file is generated and automatically copied inside the TRNSYS main folder. This DLL can be used inside TRNSYS simulation studio without installing the MATLAB package. However, a MATLAB Compiler Runtime (MCR) has to be installed in the machine. The MCR is a standalone set of shared libraries and is freely provided by Mathworks for download and use [293]. The MATLAB version used to generate the C++ files has to be considered when installing the MCR. **Figure 6.2** illustrates the converting process of SIMULINK project into a compatible TRNSYS file and the interaction mechanism between the two packages.

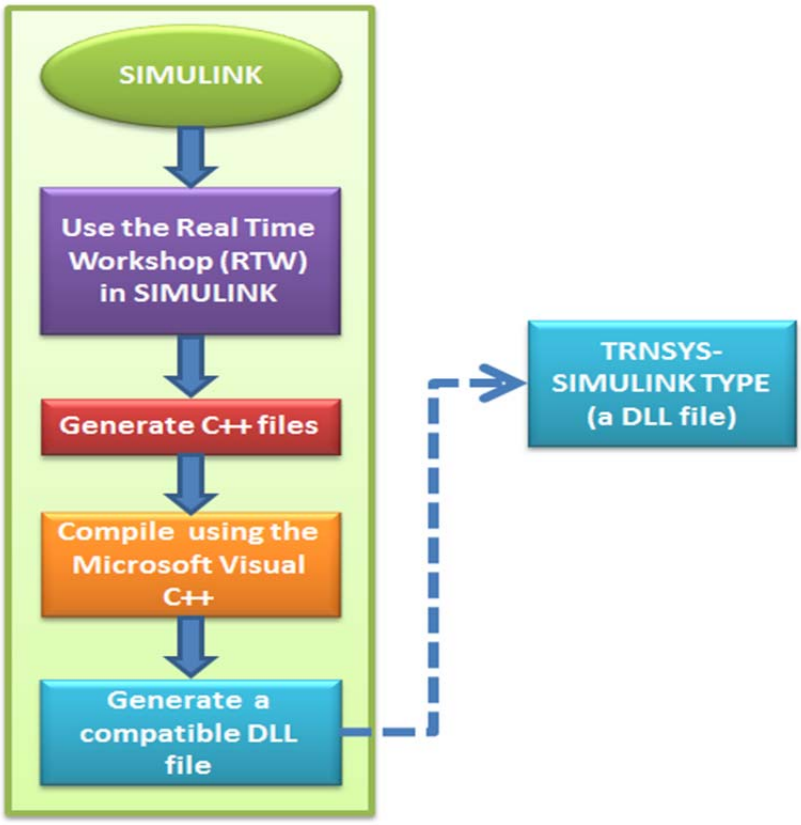

a) Conceptual process of converting SIMULINK project into a compatible TRNSYS DLL file

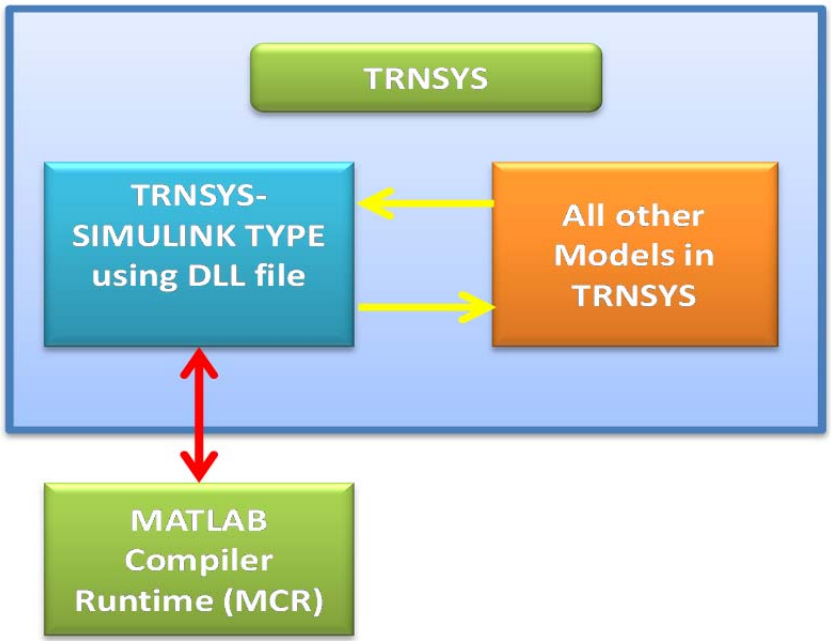

b) Interaction mechanism between TRNSYS_SIMULINK DLL type and the rest of TRNSYS types

Figure 6.2 The indirect coupling mechanism between SIMULINK and TRNSYS software package

In order to use the indirect coupling approach, the SIMULINK project must be prepared in a specific manner. The typical TRNSYS type consists of list of inputs, parameters and outputs. On contrary to standard TRNSYS types, the type generated using the SIMULINK environment needs to be with inputs and outputs. Although not changing from one time step to another, all parameters should be set up as inputs in SIMULINK project. **Figure 6.3** illustrates the configuration of SIMULINK project before the conversion process. In a SIMULINK language, all blocks within the project must be contained within one sub-system block that has inputs and outputs. In addition, static memory has to be allocated before generating the C++ codes. Since SIMULINK uses the time step to numerically solve the blocks, time step should be provided as an input to the block. A detailed and illustrative procedure for compiling the SIMULINK modules for TRNSYS is included in **Appendix C**.

Figure 6.3 Configuration of SIMULINK project before converting into compatible TRNSYS Type

6.4 Coupling mechanism between external Wall Type and Multi-zone Type 56

Generally speaking, any Type in TRNSYS can be represented as a black box model as illustrated in **Figure 6.4**. The type requires inputs, parameters and outputs. Inputs are necessary variables during the simulation and can be outputs from other types within TRNSYS Simulation studio. Example includes solar radiation, temperatures, convective heat transfer coefficients etc. Although the inputs tend to change from one time step to another, they can be constant.

Parameters are data that are unchanged over the simulation time such as wall area for example. They can directly be provided at the component level or via external text files. Outputs are the results generated inside the black box. Outputs can directly be plotted during the simulation using online plotter in Simulation studio or saved to external text files for post processing.

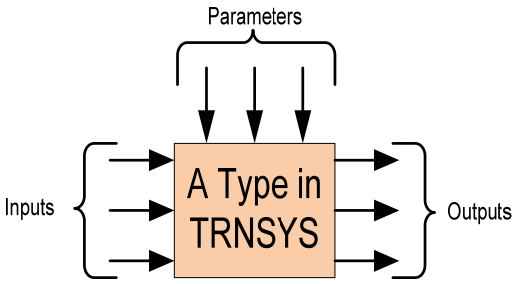

Figure 6.4 Black box representation of a Type in TRNSYS

The multi-zone Type 56 in TRNSYS uses transfer function method to model the heat transfer across the walls. It also provides flexibility to integrate special designed walls using the concept of boundary temperature. Using this capability, one can externally model a wall and provide the surface temperature as a boundary value to Type 56 for indoor air heat balance calculations. **Figure 6.5** illustrates the concept of boundary temperature between any generic wall type and Type 56. Both types exchange intermediate values in iterative process until the convergence is achieved during a time step. In order to have a complete coupling, the external wall type should use a dummy massless layer. Since it is considered a dummy layer, the massless layer should have a very small resistance and thickness. To ensure a perfect contact, the convective heat transfer coefficient should be set below 0.001 at the back side of the massless layer.

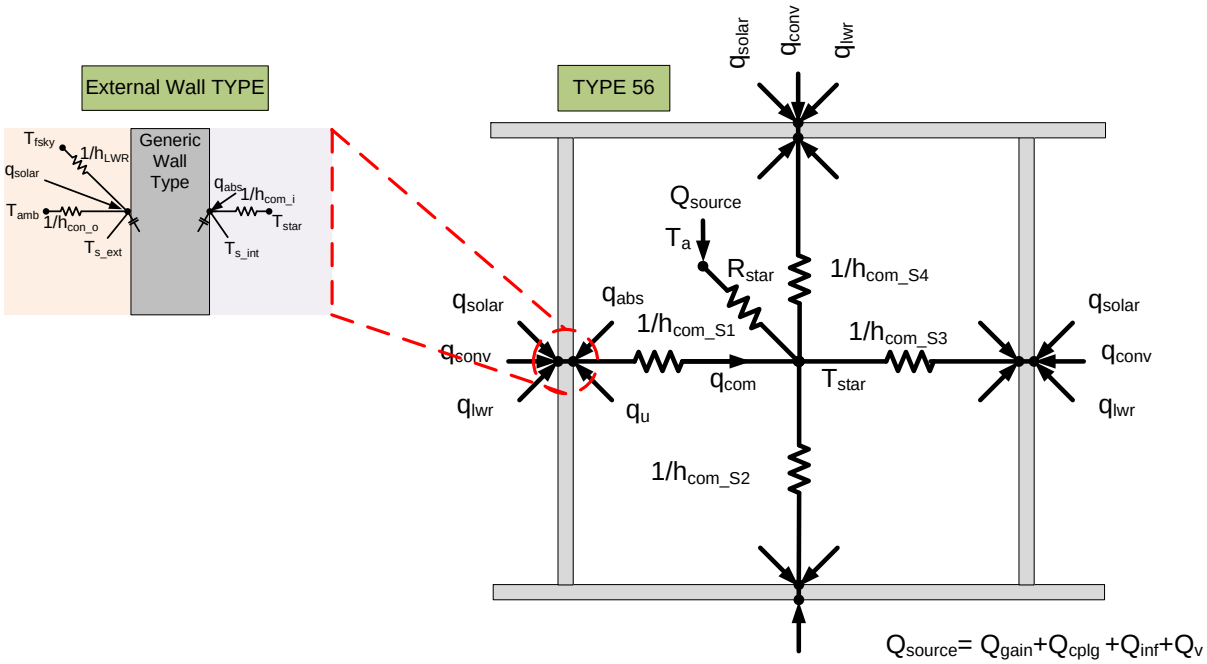

Figure 6.5 Coupling mechanism of external wall types and multi-zones Type 56 in TRNSYS

6.5 Development and verifications of TRNSYS_SIMULINK Types

The SIMULINK "AdvFacSy" toolbox developed under this research has the capability to model different advanced façade systems. **Figure 6.6** shows a list of generic façade designs that are selected for integration with TRNSYS. The wall block can model six layers and four layers for single and double walls respectively. The inputs of thermo-physical properties must be provided in TRNSYS simulation studio for each single layer. These generic designs can be used to model walls with or without PCMs and in any order. The mathematical and numerical backgrounds for all these designs have been discussed in Chapter 3 and Chapter 4.

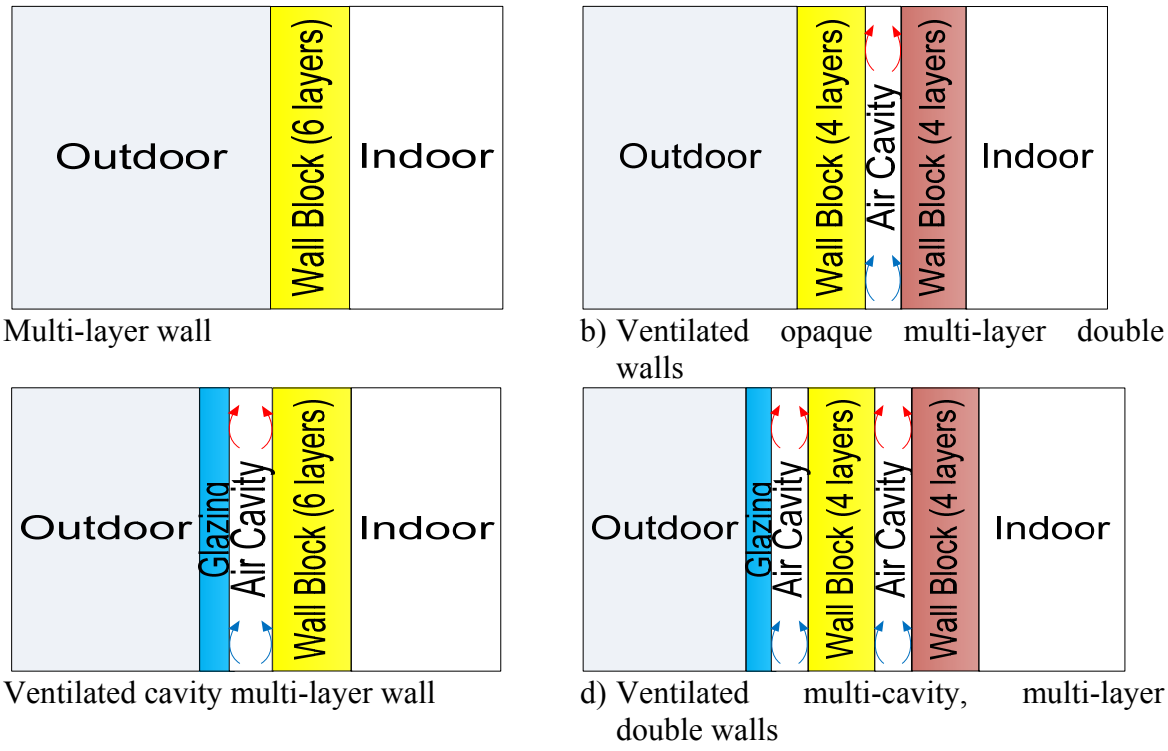

a) Multi-layer wall

b) Ventilated opaque multi-layer double walls

c) Ventilated cavity multi-layer wall

d) Ventilated multi-cavity, multi-layer double walls

Figure 6.6 Generic wall designs developed in SIMULINK, compiled and integrated into TRNSYS

6.5.1 Multi-layer Wall System: Type 816

Following the previous guidelines and methodology, a multilayer wall SIMULINK project has been developed. **Figure 6.7** provides the SIMULINK blocks representation of the multilayer wall. As stated early, all low level blocks should be contained within one subsystem. In TRNSYS simulation studio, Type 816 is linked with other types in TRNSYS as shown in **Figure 6.8**. Other types provide inputs and parameters for simulation. In this case, the parameters are considered as inputs since the current integration mechanism in SIMULINK accepts inputs only.

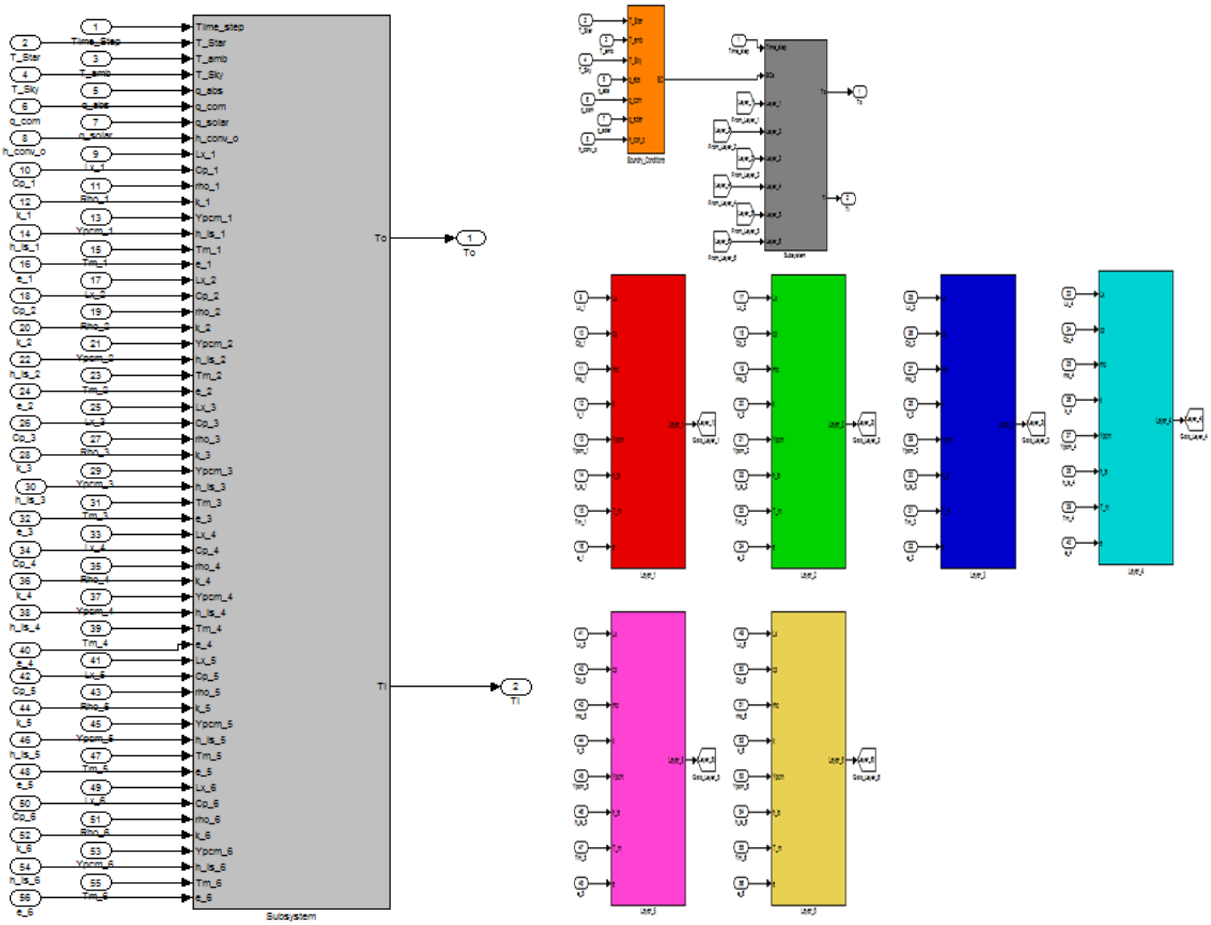

a) High level SIMULINK block representing the Multi-layer wall contained in one sub-system block

b) Collection of inputs: parameters for each layer and boundary conditions

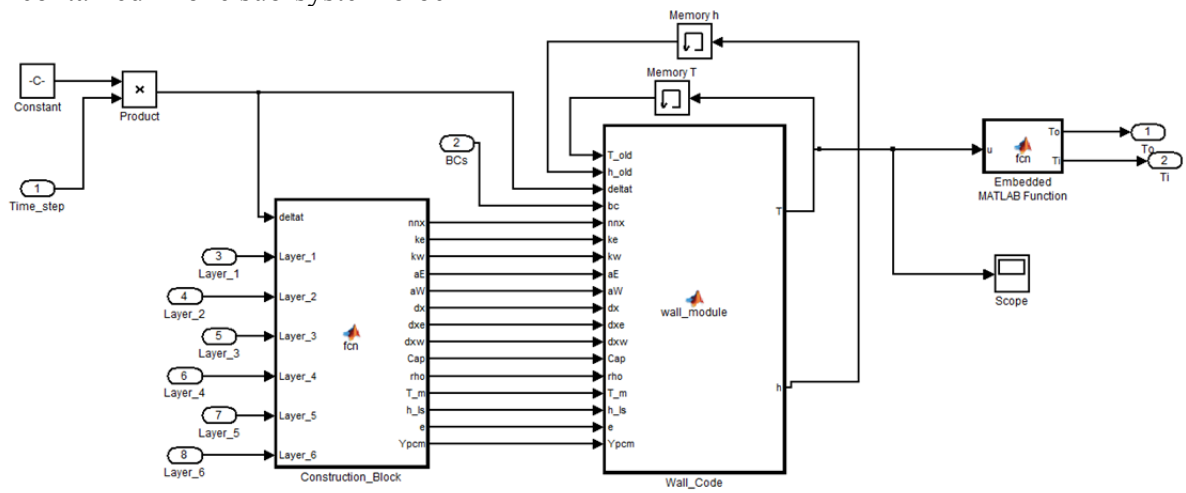

c) Low level SIMULINK blocks showing the main code structure

Figure 6.7 Multi-layer wall Type 816 representation in SIMULINK project for compiling process

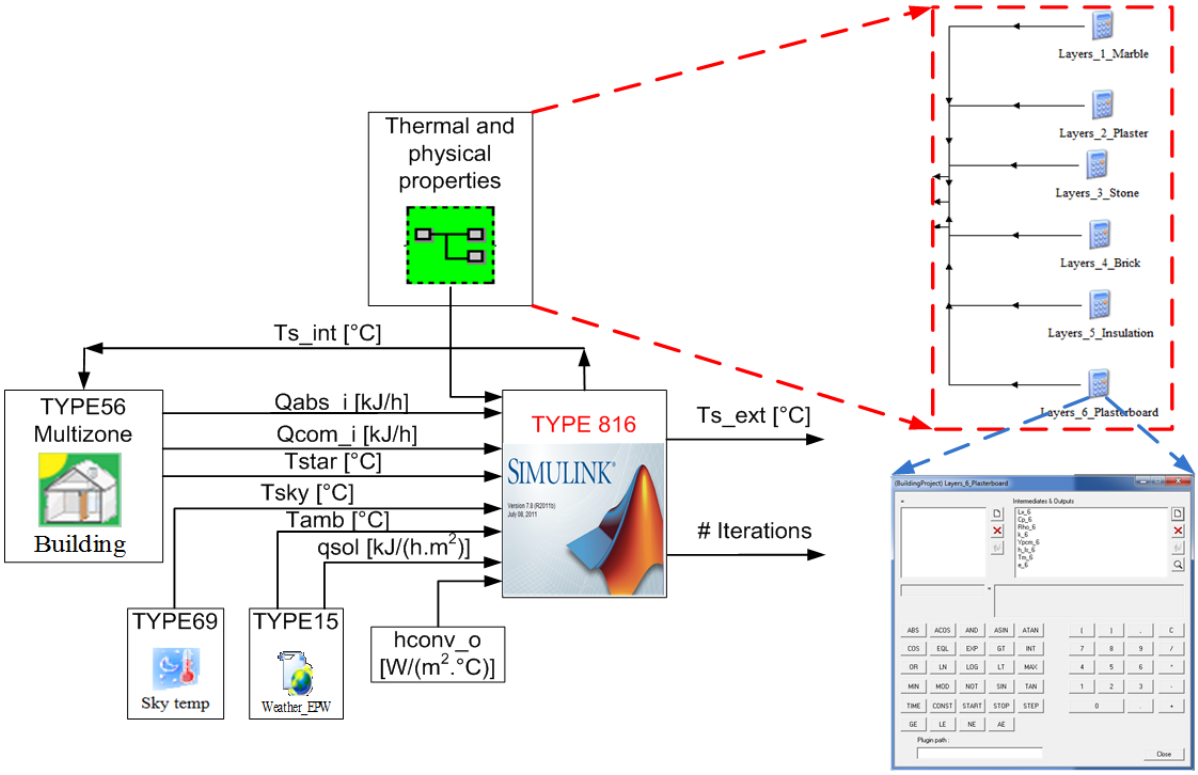

Figure 6.8 Configuration and integration of Type 816 with other types in TRNSYS

The multi-zone Type 56 uses the transfer function method to model the heat transfer across the wall. Therefore, Type 816 has been verified against the results from the condition transfer function (CTF) of TRNSYS Type56. The BESTEST case 600 free floating is assumed for this verification but without window on the south [294]. Only south wall was changed to test different wall constructions and compared to a similar wall using Type 56. Interior and exterior surface temperatures of the three different south walls are compared as shown in **Figure 6.9**.

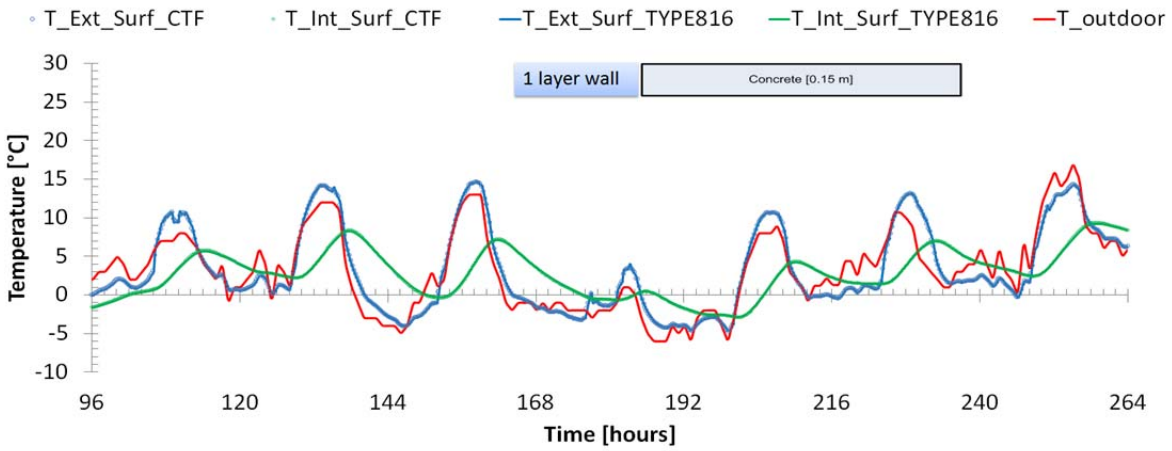

a) One layer massive concrete wall

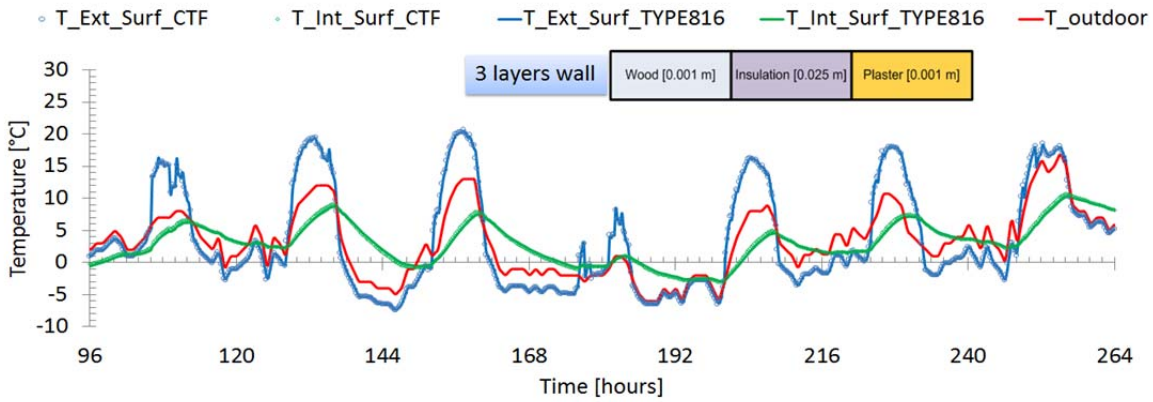

b) Three layers light weight wall

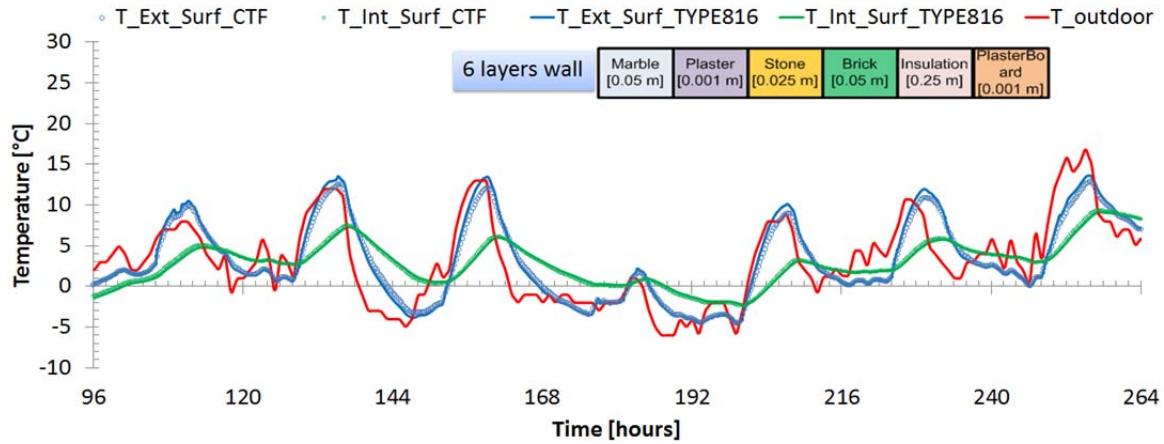

c) Six layers heavily insulated wall

Figure 6.9 Verification of Type816 against results from condition transfer function (CTF) of TRNSYS at 15 minutes time step

The results show that Type816 developed using SIMULINK predicts results close to the results from the TRNSYS CTF method in Type56. However, the results of exterior surface temperature of case-3 (the six layers highly insulated wall, refer to **Figure 6.9** (c)) deviate slightly from the TRNSYS results. This has however been discussed in the literature [295-297]. These studies have highlighted that CTF algorithm likely fail for cases of highly insulated or thermally massive envelopes.

6.5.2 Ventilated opaque multi-layer double walls: Type 930

This generic wall type consists of two blocks of wall systems: exterior and interior wall leaf. A ventilated cavity is placed between the two wall blocks. The air can be circulated using a predetermined constant air flow representing a forced convection case using a fan, natural convection due to thermal buoyancy only, or unvented air case (i.e., no air circulation). When air is circulated, it can be induced from either indoor or outdoor environment via air inlets at the bottom of the cavity. The air can be supplied to the indoor or transported elsewhere via air inlets at the top of the cavity. The high level SIMULINK blocks are shown in **Figure 6.10** and the low level blocks are shown in **Figure 6.11**. At high level subsystem SIMULINK block, eighty three inputs are required and eleven outputs are extracted. A similar concept of multilayer wall Type 816 (refer to **Figure 6.8**) is also applied when coupling this type with multi-zone Type 56 in TRNSYS.

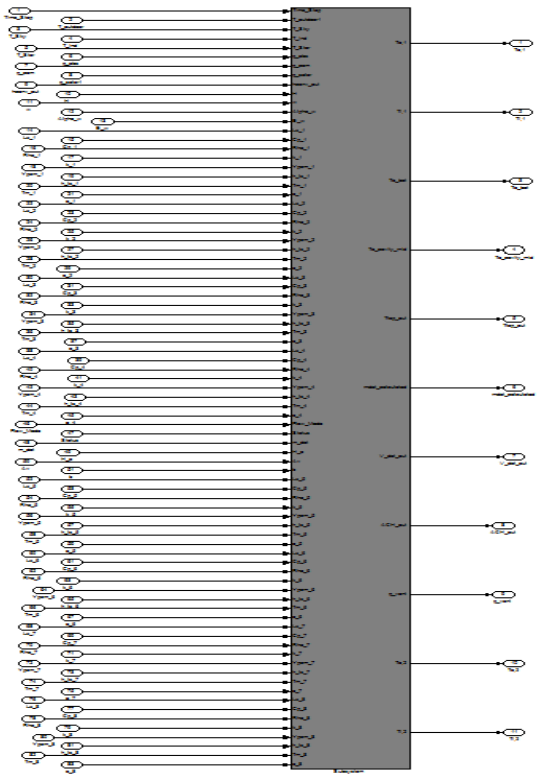

a) High level SIMULINK block representing the Ventilated opaque multi-layer double walls contained in one sub-system block

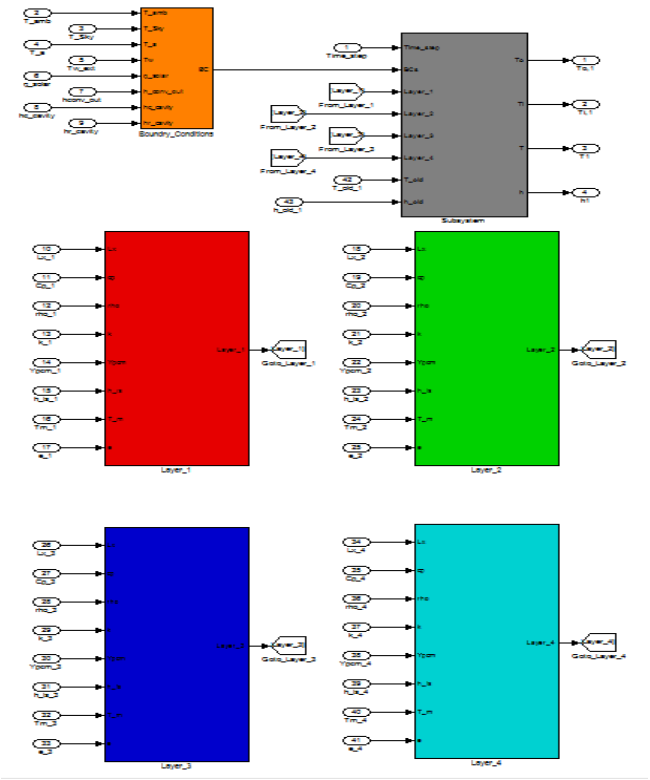

b) Collection of inputs at Wall block level

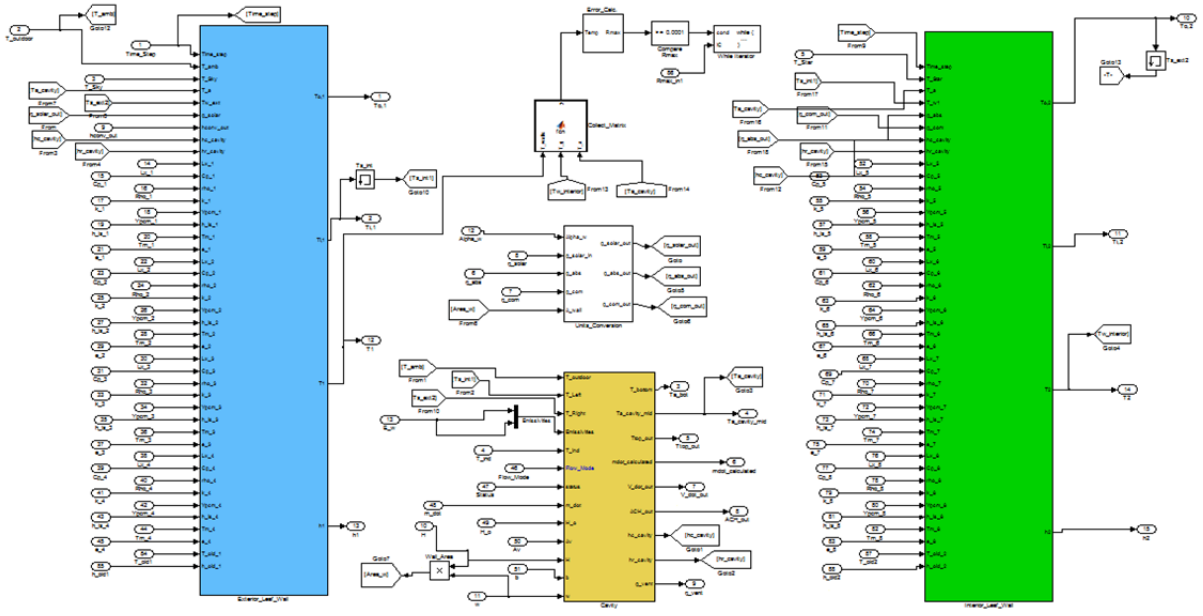

c) Low level multilayer double walls (two walls and one cavity)

Figure 6.10 High level SIMULINK blocks representing TYPE 930; the multi-layer double walls for compiling process

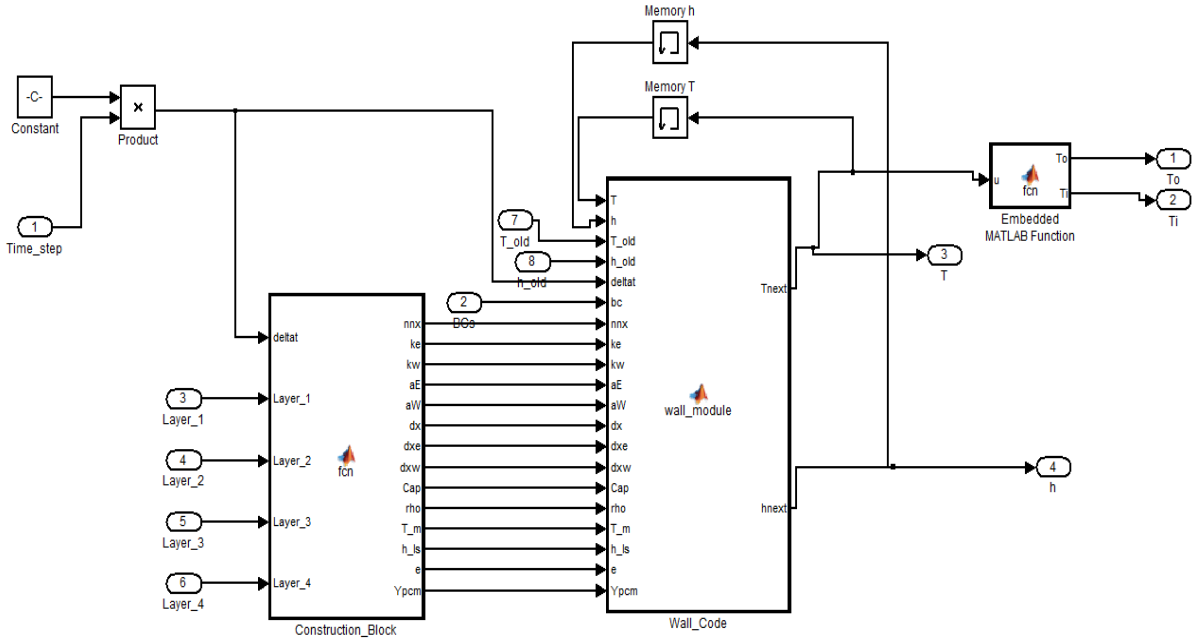

a) Low level SIMULINK blocks showing the main code structure for one wall block

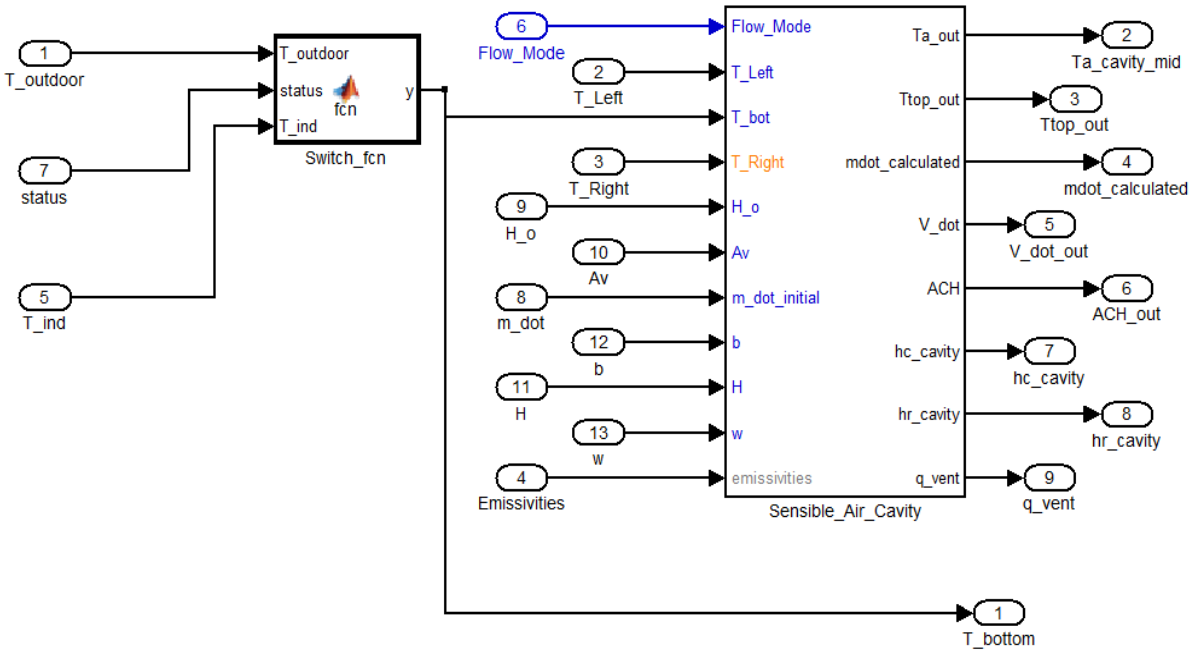

b) Low level SIMULINK blocks showing the main code structure of the air cavity

Figure 6.11 Low level SIMULINK blocks representing TYPE 930; the multi-layer double walls for compiling process

6.5.3 **Ventilated cavity multi-layer wall: Type 921**

This design consists of a six layers wall block with a ventilated cavity including glazing module on exterior side. The ventilated cavity in this design works in a similar fashion as Type 930. The high level SIMULINK blocks are structurally similar to the previous Types. The low level SIMULINK for this type is shown in **Figure 6.12**. At high level subsystem SIMULINK block, sixty three inputs are required and eleven outputs are extracted.

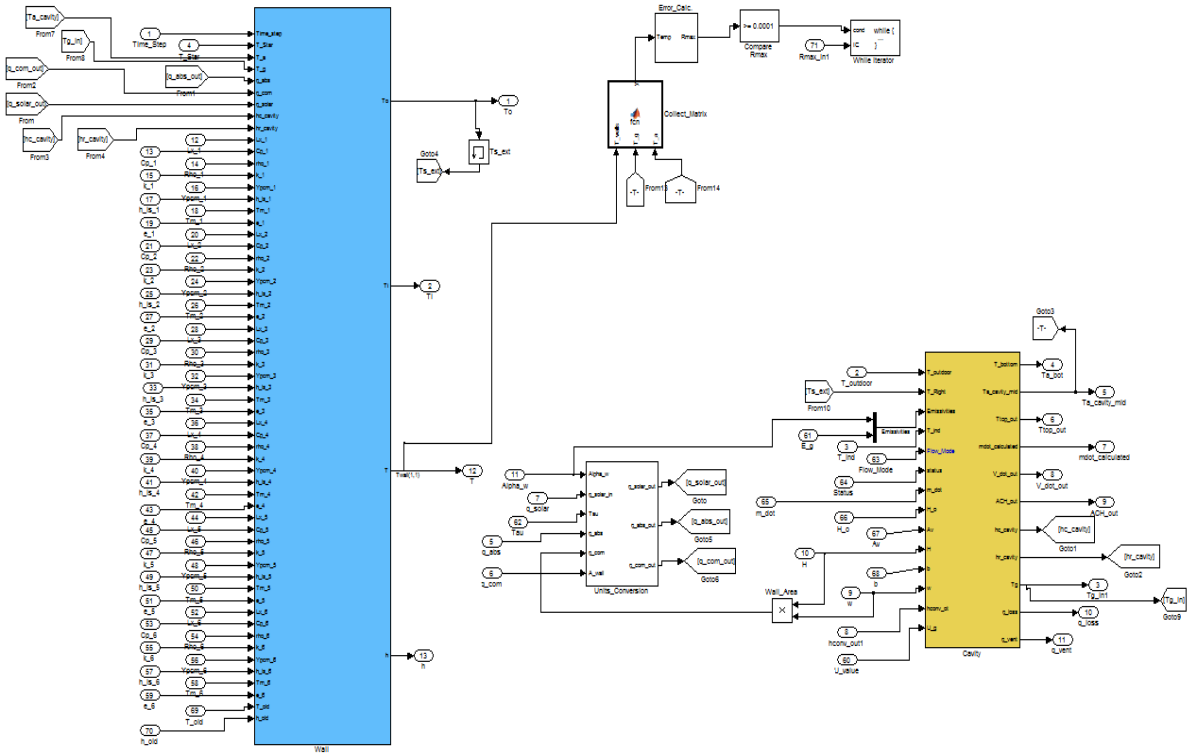

Figure 6.12 Low level SIMULINK blocks representing TYPE 921; the ventilated cavity multi-layer wall for compiling process

The ventilated cavity wall is sometimes referred as “TROMBE” wall when a thermally massive layer is utilized for collecting solar energy for heating the apace. TROMBE wall concept was originally described by Edward Morse on a patent in 1881 [298]. This design was not popular until early 70s when a French engineer Felix Trombe tested the concept.

For verification purposes, a thermal storage wall Type36 in TRNSYS is used. Type 36 can only model a single massive layer, similar to TROMBE wall concept. The layer is divided into small volumes and is internally solved in TRNSYS. For some situations (i.e., large time steps), Typ36 doesn't numerically converge and the program terminates. The time step must be reduced to small values to overcome the numerical instability. The simulation parameters and thermo-physical properties of the ventilated cavity are listed in **Table 6-1**. Two verification cases are presented as shown schematically in **Figure 6.13**.

Table 6-1 Parameters used for a south ventilated cavity "TROMBE" Wall

Test Parameter	Layer: Concrete	Units
Wall height	3	m
Wall width	2	m
Thermal Conductivity	2.922	W/m.K
Density	1900	kg/m^3
Specific Heat Capacity	949	J/kg.K
Thickness	0.15	m
Mesh Grid Points	10	
Indoor Temperature	20	°C
External Convective Heat transfer Coefficient	29.3	$W/m^2.K$
Internal Convective Heat transfer Coefficient	8.29	$W/m^2.K$
Solar absorption	0.9	
Emissivity of the massive wall	0.9	
Cavity		
Depth, (b)	0.2	m
Vent Area, (A_v)	0.09	m^2
Vertical distance between two vents, (Ho)	2.5	m
Flow characteristic	Natural Convection	
Air induced	From outside or inside	
Glazing		
Number of glazing	1	
Emissivity of the glazing	0.9	
Transmissivity of the glazing, τ	0.81	
Simulation Parameters		
Time Step	5	minutes
Weather file	EPW for Golden, Colorado	

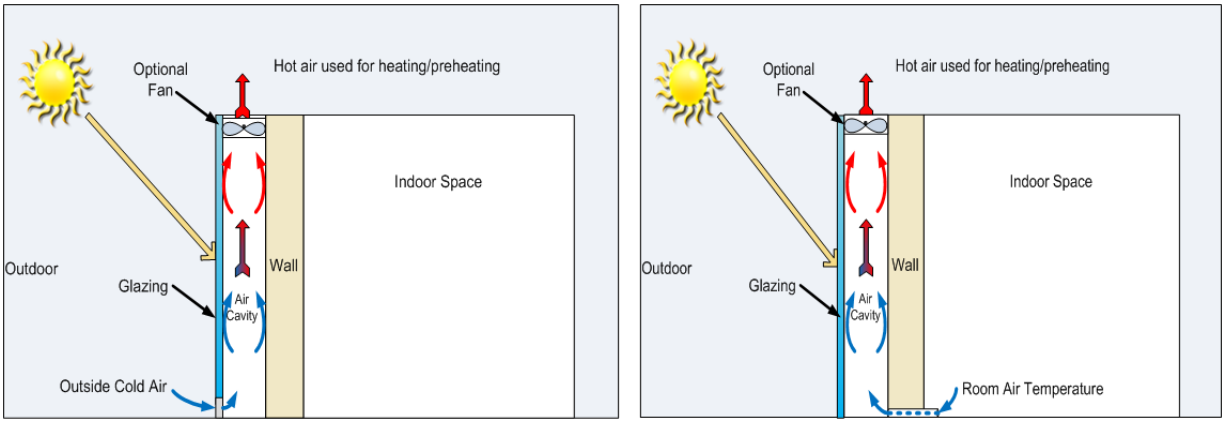

a. Heating Scenario 1 where cold air induced from outdoor

b. Heating Scenario 2 where air in induced from indoor space

Figure 6.13 Verification cases for ventilated cavity wall Type 921 under two heating scenarios under natural convection

The first verification case is when outside air is allowed to enter the cavity. **Figure 6.14** shows the results from both the TRNSYS Type36 and the compiled SIMULINK Type921. The results of many performance indicators from Type 921 are in good agreement with Type 36.

The second tested case is when the air is induced from the indoor environment. The results for this case are shown in **Figure 6.15**. Similar to the previous verification case, the results from the developed type is in good agreement with Type36. The results also show that when the indoor air temperature is higher than the cavity temperature, no buoyancy occurs and therefore no air flow is circulated.

A similar comparison was also done under the no flow case and forced convection case under different scenarios. For all these scenarios, the compiled SIMULINK code was working in a similar fashion to Type 36. Therefore, it can be concluded that the compiled SIMULINK Type921 can be used with high confidence when compared to TRNSYS Type36. The advantageous of this type over Type36 is the ability to model multilayer with and without PCMs.

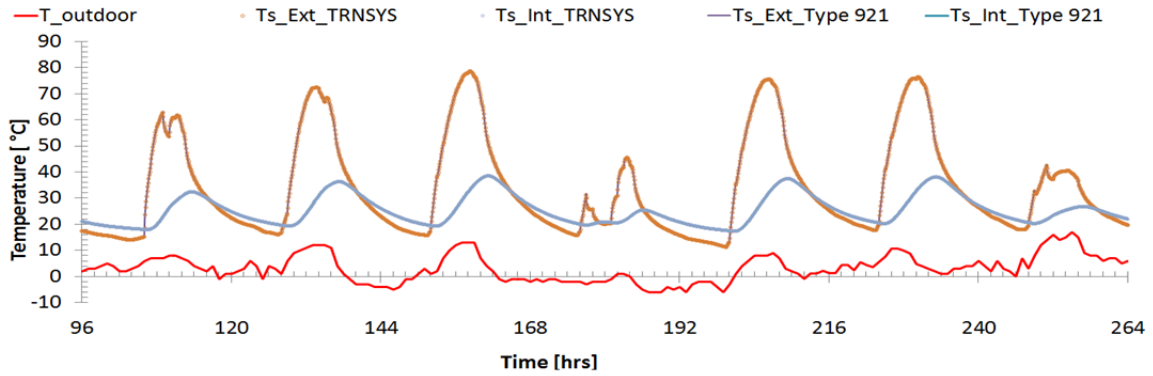

a) Exterior and interior surface temperatures of the wall

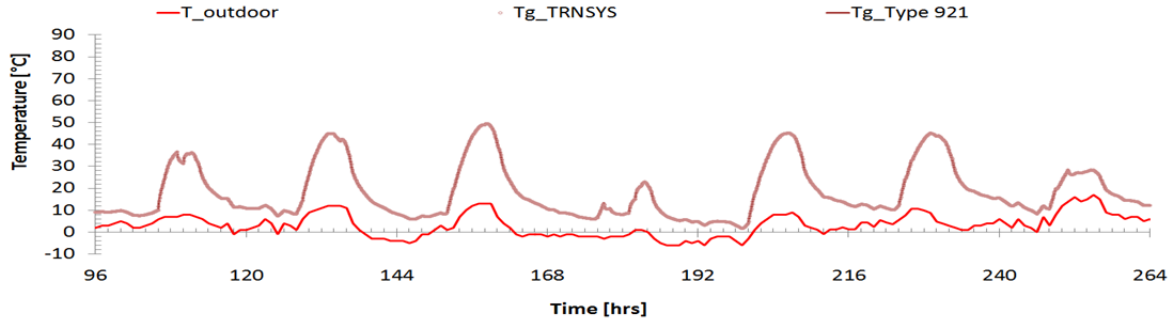

b) Glazing surface temperature

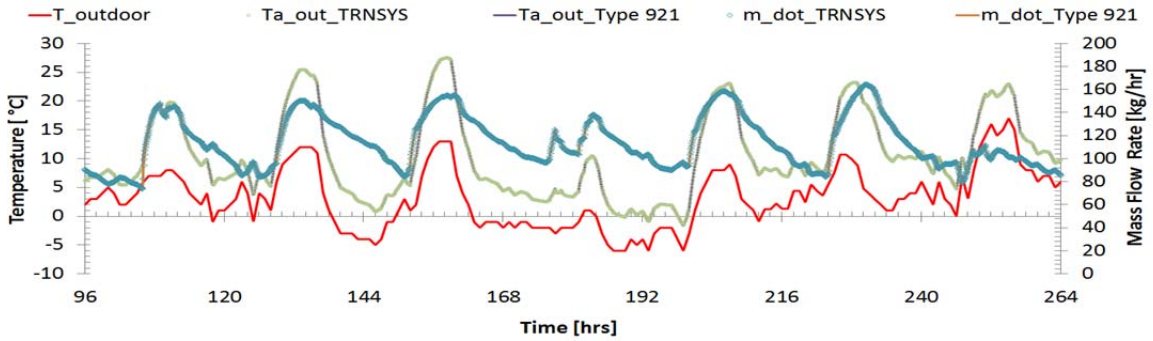

c) Air outlet Temperature and mass flow rate from the cavity

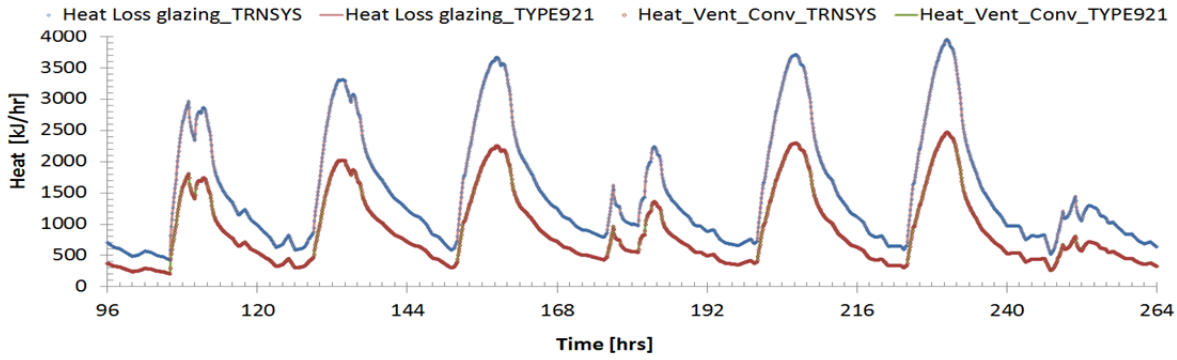

d) Heat loss from glazing to outside environment and heat recovered from the cavity

Figure 6.14 Comparison between TRNSYS Type 36 and TRNSYS_SIMULINK Type 921 for natural convection case, outdoor air induced in the cavity

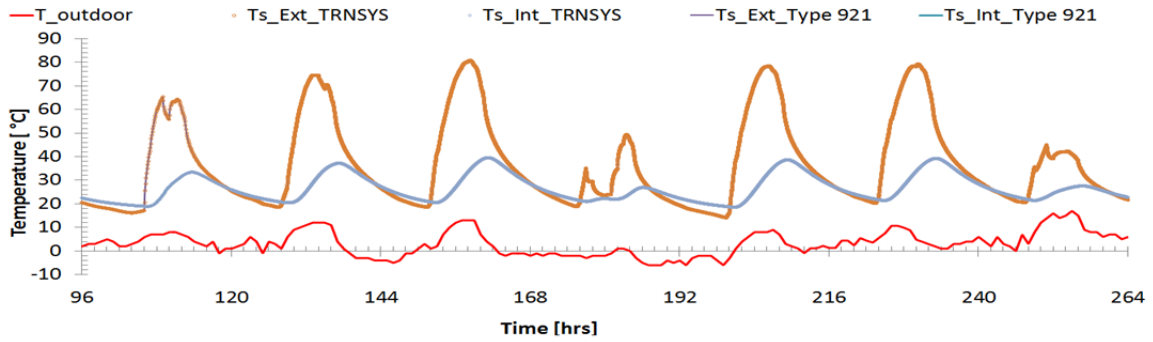

a) Exterior and interior surface temperature of the wall

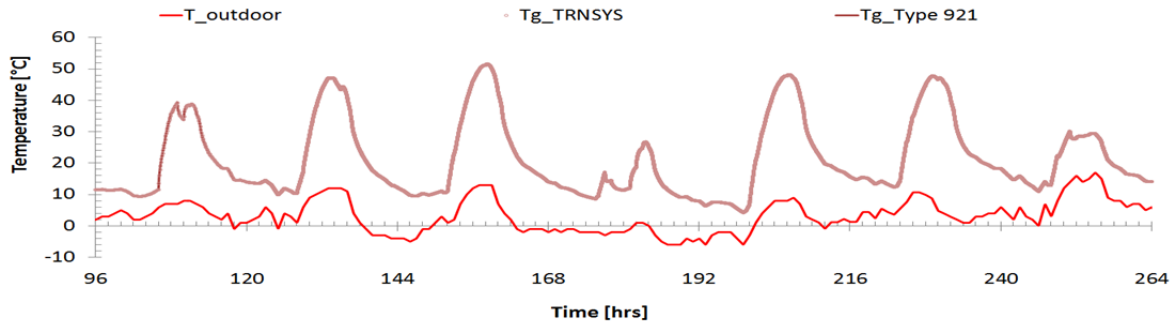

b) Glazing temperatures

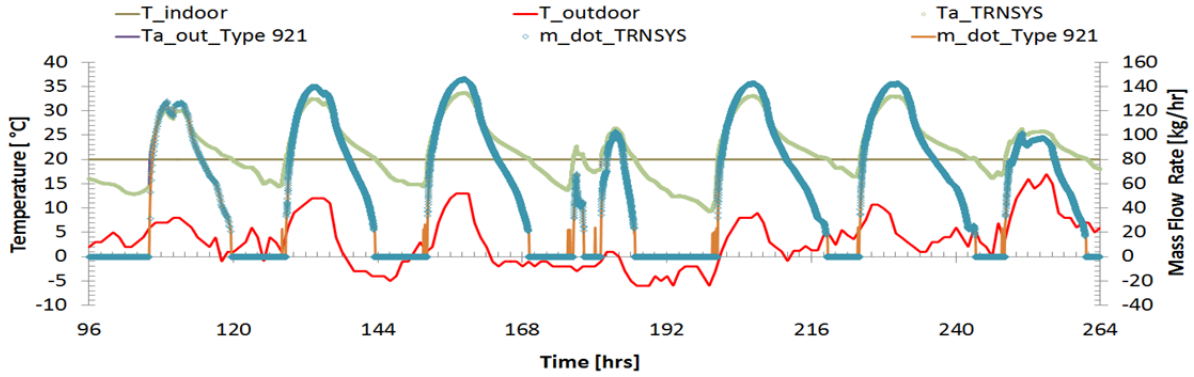

c) Air outlet Temperature and mass flow rate from the cavity

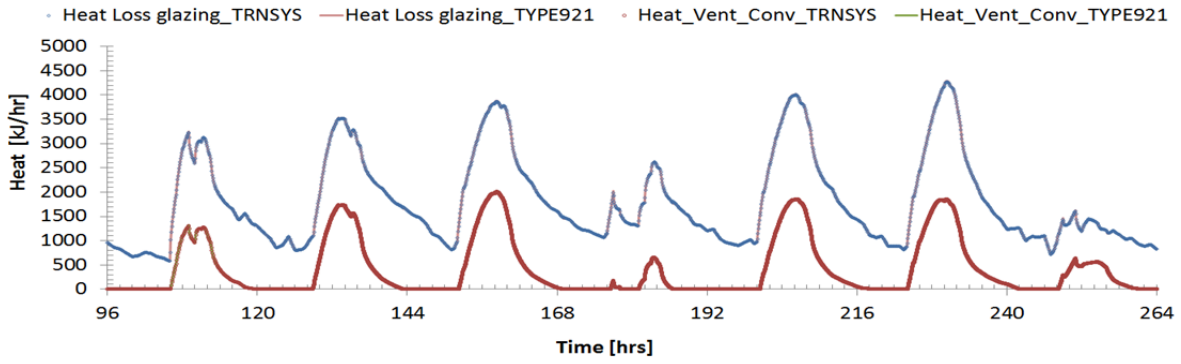

d) Heat loss from glazing to outside environment and heat recovered from the cavity

Figure 6.15 Comparison between TRNSYS Type 36 and TRNSYS_SIMULINK Type 921 for natural convection case, indoor air induced in the cavity

6.5.4 Ventilated multi-cavity, multi-layer double walls: Type 940

Trombe with Jacques Michel has modified the classical TROMBE wall design and filed a patent for what is known now as a TROMBE-MICHEL wall [299]. This improved design has been generated in SIMULINK and consequently compiled for TRNSYS. The compiled Type offers the ability to model multilayer double walls with two cavities; one external and the second is sandwiched between the two wall blocks. Each wall block can model a maximum of four layers. The low level SIMULINK blocks are shown in **Figure 6.16**. Other low level SIMULINK blocks are similar to Type 921. At high level subsystem SIMULINK block, ninety three inputs are required and twenty outputs are extracted. The coupling mechanism between this type and Type 56 is performed in a similar way to that of Type 816 (refer to **Figure 6.8**).

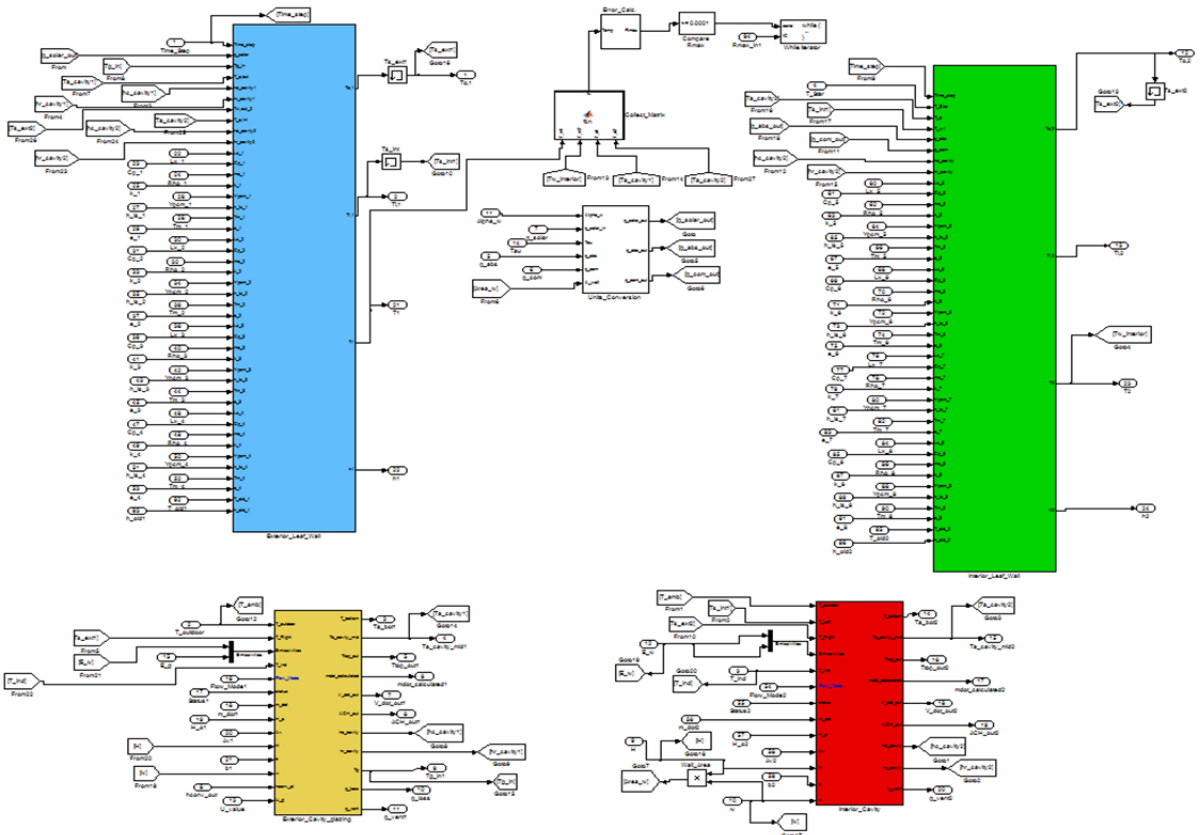

Figure 6.16 Low level SIMULINK blocks representing TYPE 940; the multi-cavity and multi-layer double walls for compiling process

6.6 Drawbacks of indirect coupling between SIMULINK and TNRSYS

Despite the simplicity in using SIMULINK for setting different advanced wall designs and subsequently compiling for TRNSYS, there exist several drawbacks of this approach. TRNSYS is well known for its numerical instability since types are solved numerically in sequential order where one type's inputs depend on the other type's outputs. Since the communication between the compiled SIMULINK types and TRNSYS happens via the MATLAB Compiler Runtime (MCR), the interaction between these two packages is still unknown. Therefore, adding new types that uses another simulation package may add to the already sensitive structure of TRNSYS.

One advantage of using the traditional TRNSYS type is the utilization of one single type several times in the simulation studio (i.e., called units in TRNSYS). This is not possible using the compiled SIMULINK since the copied version overwrites the original one. Therefore, new type with different number has to be compiled through SIMULINK for each new component used. This adds to the computation overhead since TRNSYS has to call many DLL at the same time compared to only one DLL when using the standard TRNSYS type.

In order to compile the code, a static or predefined memory is required before generating C++ files in SIMULINK. In addition, the current coupling requires that parameters should be provided as inputs to SIMULINK. Therefore, the number of inputs to SIMULINK project becomes high. Since all these inputs have to be provided in TRNSYS simulation studio, it becomes unpractical for some complex system.

6.7 Development of Multi-layer Wall in TRNSYS: Type 285

For decades, Types in TRNSYS have been developed using FORTRAN programming language. In order to overcome the above drawbacks, a multi-layer wall type "Type 285" was developed. This step was taken to reduce the number of wall Types that otherwise have to be generated using SIMULINK approach. Type 285 has inputs, real-time outputs and other outputs saved to external files, defined parameters and a text file for thermo-physical properties for wall layers as shown in **Figure 6.17**. Detailed inputs, parameters and outputs for this type are provided in **Appendix D.**

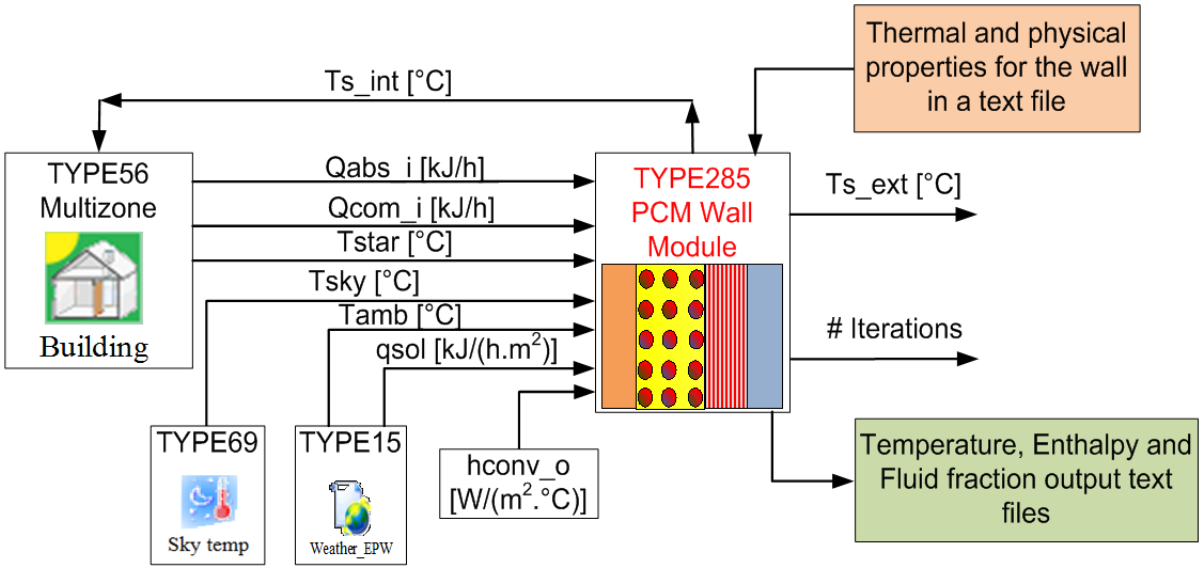

Figure 6.17 Configuration and integration of Type 285 with other types in TRNSYS

6.7.1 Integration mechanism between Wall Type 285 and Multi-zone Type 56

Similar to other types described above, Type 285 is coupled with Type 56 using the concept of boundary temperature as shown in **Figure 6.18**. Both types exchange intermediate values in iterative process until the convergence is achieved during a time step.

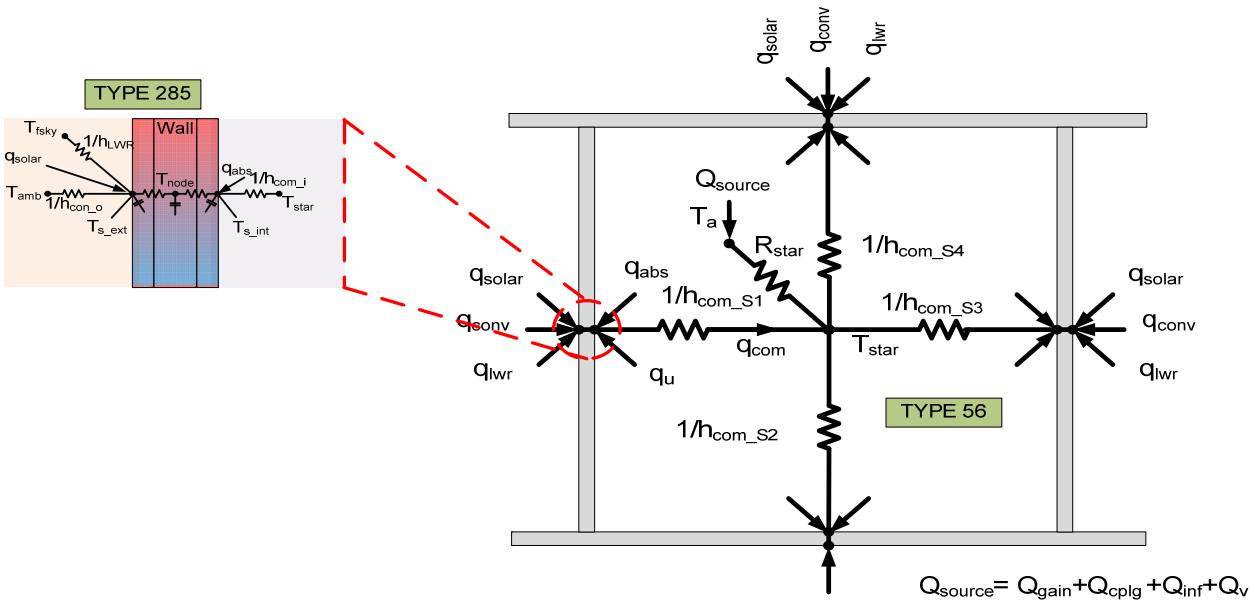

Figure 6.18 Coupling mechanism of Type 285 with multi-zone Type 56

Inside Type 56, Type 285 uses a dummy massless layer with very small resistance and thickness as illustrated in **Figure 6.19**.

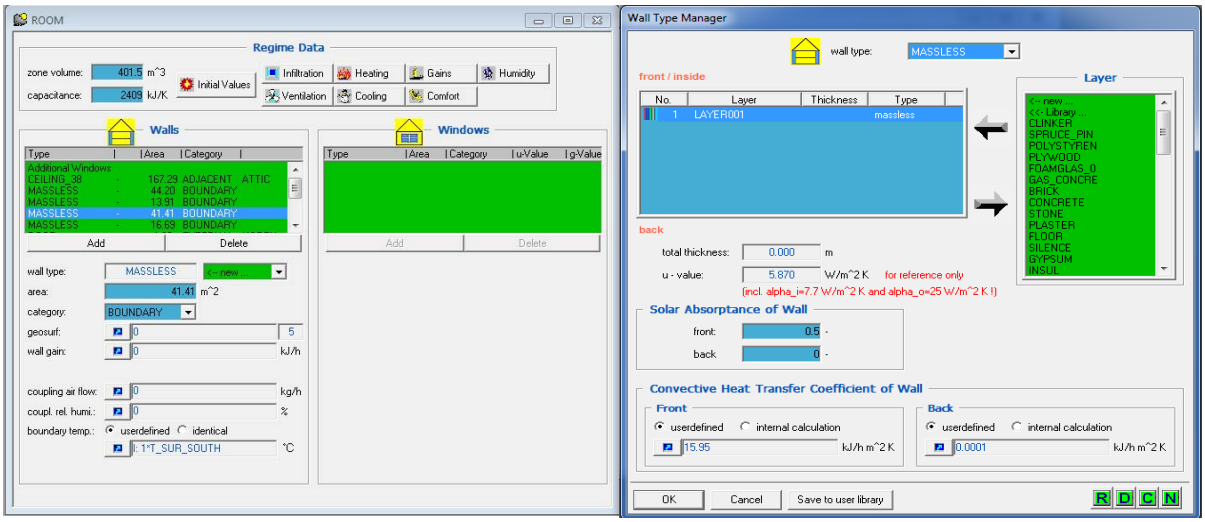

Figure 6.19 Defining the walls inside multi-zone Type 56 when using Type 285

6.7.2 Necessary external files

Type 285 requires one important external file. The file contains necessary thermal and physical properties of wall's layers. An example of a wall that has 4 layers; external layer with

PCM is provided in **Appendix D**. The information must be provided in the order shown in the text file. The layers are organized from exterior to interior side; where exterior layer is first and interior layer is last. In addition, the number of layers in the text file must match the one in Type285 parameter input menu (refer to parameter #1 in **Table D-3** in **Appendix D**). This is required as a quality assurance step. The mismatch between these two values generates a fatal error and subsequently a termination occurs. One text file is necessary for each wall design. The same text file can be used multiple times by various walls in one project. However, two text files are necessary if two different wall designs are considered.

6.7.3 Verification cases for TYPE 285

Four different cases are used to verify the predictions of Type285; lightweight, medium weight, thermally massive wall and finally a wall with PCM. The thermo-physical properties of these four cases are listed in **Table 6-2**. Since the purpose is to verify the numerical predictions, some of material's thermal properties are hypothetical. The prediction of exterior and interior surface temperatures of south wall from Type285 is compared to TRNSYS CTF method implemented in Type56, and the compiled SIMULINK Type 816 as shown in **Figure 6.20**. All types are implemented for the free floating BESTEST case where high windows to wall ratio (55%) is on south. The results show that all the types are in good agreement with each other when the interior surface temperatures are considered. However, the predictions of exterior surface temperatures for the highly insulated wall (Wall case#3) from Type285 and Type816 deviate from those of TRNSYS CTF.

Table 6-2 Thermo-physical properties of wall designs used for verifying Type 285

Sketch	Material	Thickness [mm]	Thermal Conductivity [W/(m.K)]	Density [kg/m^3]	Heat Capacity [J/(kg.K)]	Latent Heat [kJ/kg]	Melting Temp. [°C]	Melting Range [°C]
Wall case#1								
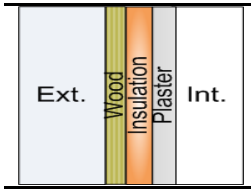	Wood siding	9	1.8	530	900			
	Insulation	66	0.04	12	840			
	Plaster (Interior)	12	0.16	950	840			
Wall case#2								
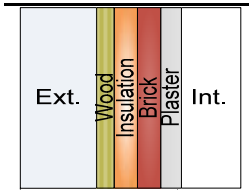	Wood siding	9	1.8	530	900			
	Insulation	66	0.04	12	840			
	Brick	25	0.89	1800	1000			
	Plaster (Interior)	12	0.16	950	840			
Wall case#3								
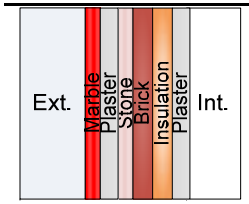	Marble	25	2.94	2550	840			
	Plaster	1	1.39	2000	1000			
	Stone	25	1.39	2000	1000			
	Brick	50	0.89	1800	1000			
	Insulation	25	0.037	16	1030			
	Plaster	1	0.16	950	840			
Wall case#4								
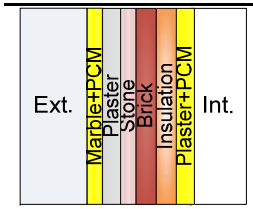	Marble+ PCM	25	2.94	2550	840	200	10	0.1
	Plaster	1	1.39	2000	1000			
	Stone	25	1.39	2000	1000			
	Brick	50	0.89	1800	1000			
	Insulation	25	0.037	16	1030			
	Plaster+ PCM	1	0.16	950	840	208	25	0.1

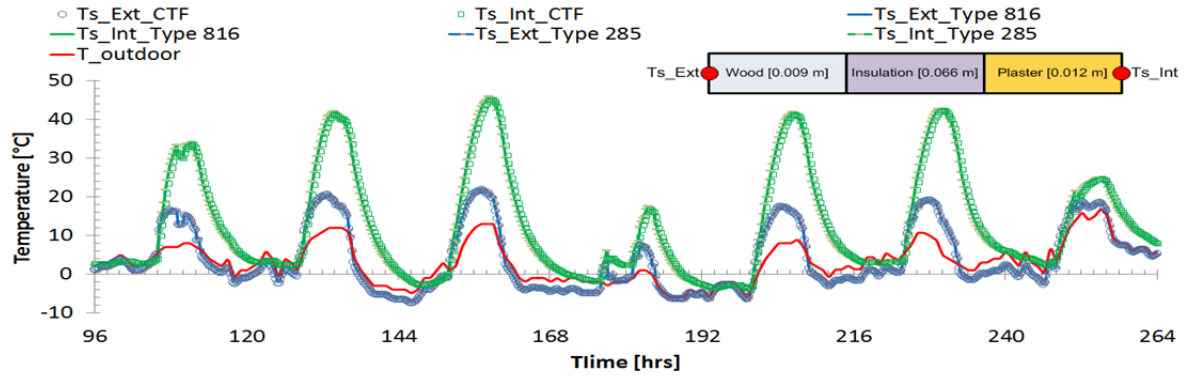

a) Wall case#1 (15 minutes Time step)

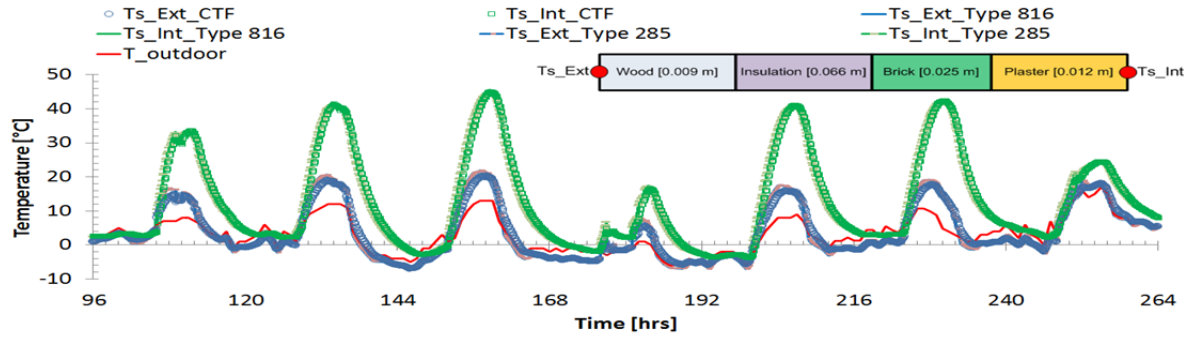

b) Wall case#2 (5 minutes Time step)

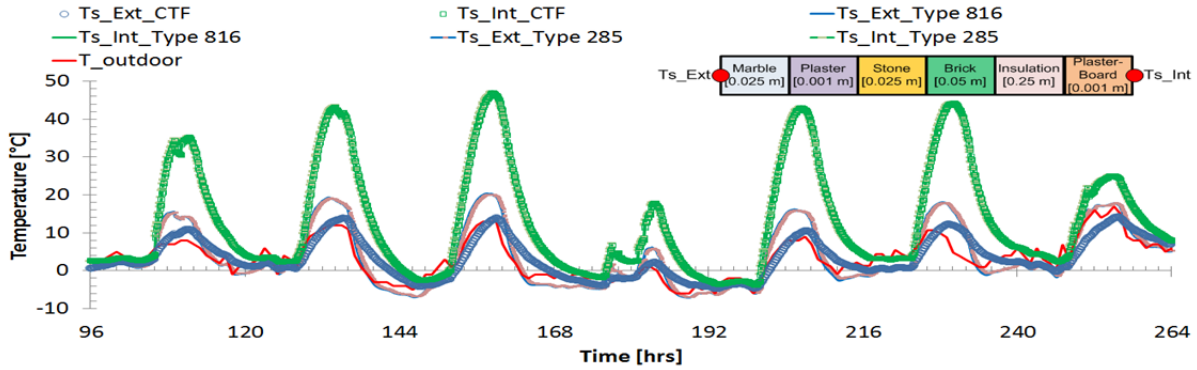

c) Wall case#3 (5 minutes Time step)

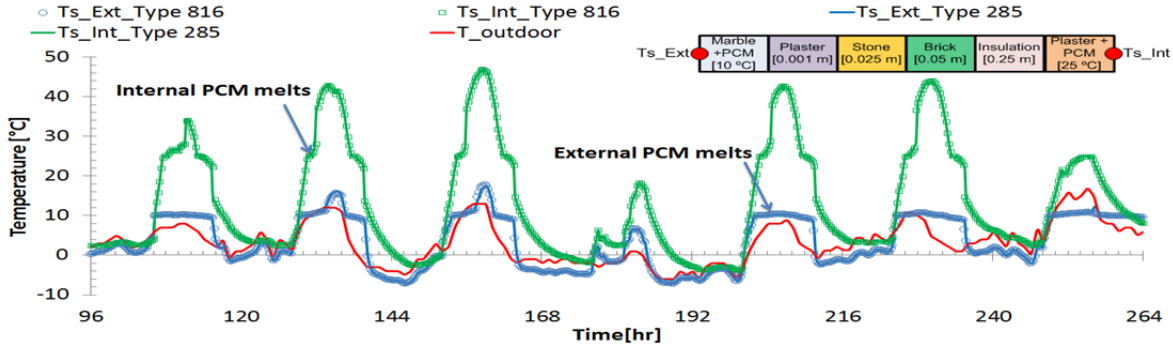

d) PCM Wall case#4 (15 minutes Time step)

Figure 6.20 South wall surface temperatures comparison between TRNSYS CTF, Type 816 and Type 285

6.8 Summary

The AdvFacSy toolbox provides flexibility to setup different complex façade systems. It became necessary to utilize the flexibility and the capability of this toolbox. This chapter described various ways of coupling the toolbox's modules into TRNSYS. The TRNSYS Type-155 provides the fundamental coupling between TRNSYS and MATLAB simulation package. This approach was tested at the initial stage of this research. The simulation speed was found unpractical due to the iterative nature of the developed codes.

Another promising methodology was explored where C++ codes are generated from the SIMULINK project. This approach is not widely common but provides tremendous flexibility. For any SIMULINK project, C++ codes are generated and subsequently compiled into single DLL file. This compiled version can be used directly in TRNSYS like any other conventional DLL without the need to install MATLAB/SIMULINK software package. Four generic façade systems; a multilayer wall design, and three versions of ventilated cavity designs were selected for integration into TRNSYS using this approach. However, the approach was not free of limitations. The major challenge found was the generation of different compiled DLL file for every component that needs to be modeled. For modeling a simple single zone, four DLL files with different TRNSYS numbering are needed. Therefore, a generic wall type is developed using FORTRAN for modeling multilayer walls with and without PCM. This type provides extreme flexibility in modeling many layers with different thermal and physical properties.

Majority of the developed models have been verified against TRNSYS modules using simplified cases. Using the test cases, the developed models show good agreement with results from TRSNSY modules. It is observed, however, that the prediction of exterior surface temperatures of the developed models deviate from those of TRNSYS especially for multilayer

and heavily insulated envelops. This has not significant impact on indoor surface temperatures and therefore no major worries when energy performance is evaluated.

CHAPTER 7: MODELING RESIDENTIAL BUILDING WITH PCM-ENHANCED WALLS IN TRNSYS

This chapter evaluates the performance of phase change materials (PCMs) in a typical residential building utilizing "TRNSYS", a whole building simulation tool. In particular, parameters that enhance or hinder the performance of PCMs are evaluated. Optimal thermal properties of PCMs such as melting temperature and melting range are identified for four US representative climates. In addition to the technical feasibility of PCMs, a simplified economic analysis using a payback period approach is also conducted for different climates. Using the set of simulation runs, design correlations have been developed. Furthermore, few demonstration cases have been explored to identify conditions and situations at which PCM performance is improved.

7.1 Modeling of the base case residential building

Skin-load dominated buildings such as residential types are greatly influenced by the surrounding climatic conditions. Selecting proper envelope design can significantly reduce the heating and cooling loads, consequently reducing the energy consumption. Therefore, this building typology has been selected to evaluate the thermal performance of PCM under dynamic environmental conditions using weather file. Many resources can be used for setting up a base case residential building for energy evaluation. For this work, Building America House Simulation Protocols published by NREL was the main source used [280]. However, other reports have also been utilized to set other assumptions [300, 301]. The literature published in this regard uses 2009 IECC as a compliance tool with other standards such as ASHARE 90.2 as

complementary references. The following sections describe the general assumptions used for the modeling of the base case residential building.

7.1.1 Architectural characteristics

The building is modeled assuming a single story, detached house. As a simplification, the house is modeled with two thermal zones: main conditioned zone and unconditioned but vented attic zone. The two zones are separated by a highly insulated ceiling assembly. The roof slope is assumed to be 4:12 with no overhang, no internal or external shading is assumed. No garage is included in the base case. According to U.S. Census' Survey of Construction database, Kneifel [300] has presented the results of the house floor areas as shown in **Figure 7.1**. Based on the highest frequency, a total floor area of 1800 ft^2 is considered for this study. The basic characteristics for this house are listed in **Table 7-1**. The envelope thermo-physical characteristics are described in **Table 7-2**.

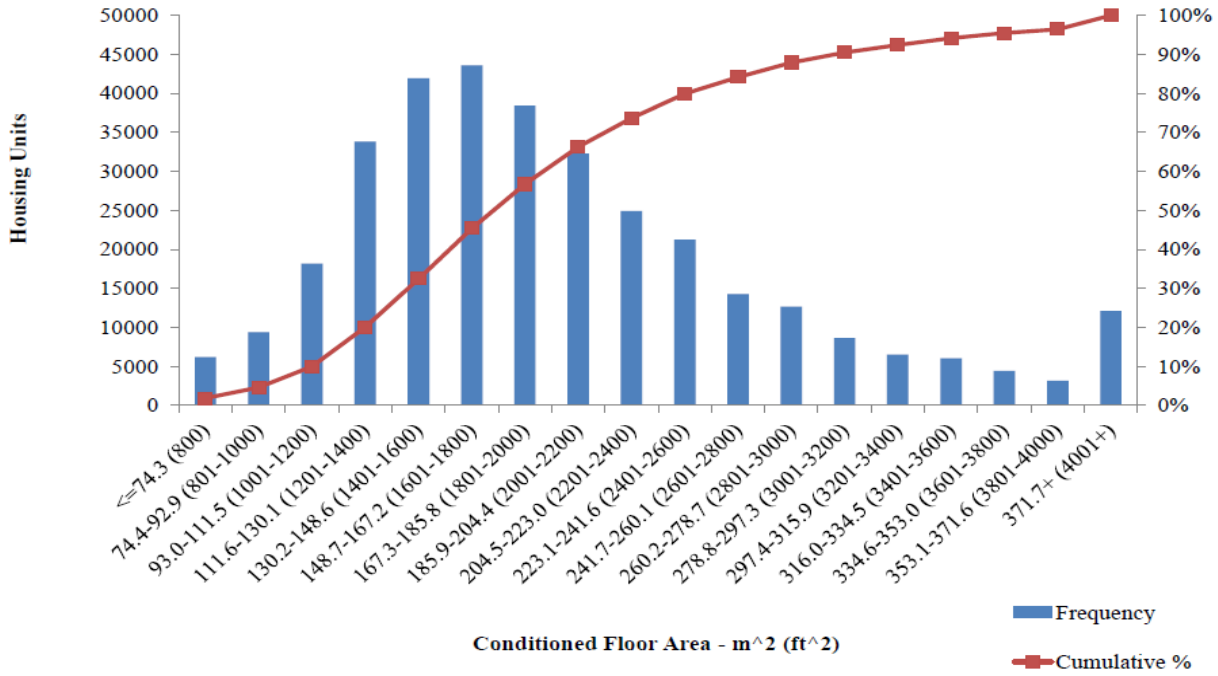

Figure 7.1 Conditioned floor area of new one story single-family housing [300]

Table 7-1 Characteristics of the base case of Residential Building for Golden, CO

Parameter	Description	Remarks
Shape/ Dimensions	One story (3 bedrooms, 3 baths) Front of house faces north Aspect ratio: 1:1 Roof slope: 4:12 Conditioned Floor Area = 167.29 m^2 (1800 ft^2) Walls width= 12.93m (42.42 ft) Floor to Ceiling height=2.4m (8ft)	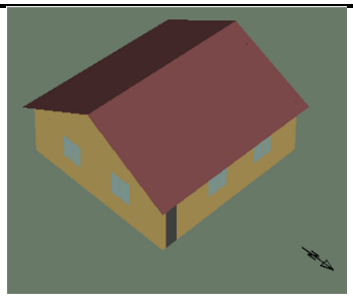
Modeling Zones	Two thermal zones: main zone and attic zone	vented attic
Foundation	Refer to **Table 7-2**	As per Building America benchmark [280]
Exterior Walls	Refer to **Table 7-2**	
Ceiling R-Value	Refer to **Table 7-2**	
Solar absorptivity	Roof=0.9, Wall=0.6	
Window Area/Distribution	15% of exterior wall area, uniformly distributed in all orientations	
Window Type	Double glazing: U = 1.98 $W/m^2.K$ SHGC = 0.35	TRNSYS doesn't use SHGC but an equivalent window is selected [301]
Infiltration Model	Room zone: ASHRAE K1,K2, K3 model	
	Attic Zone: 10 * infiltration $_{\text{Room zone}}$	As per [301]
Internal Loads (refer to section on Internal heat gain)		
Max lighting power	553.6 W radiative power = 0.4 convective power =0.6	As per Building America benchmark [280] Refer to **Figure 7.2** for internal load schedule
Max equipment power	Sensible= 733.3 W Latent =89.3 W	
Max Occupancy load (3 People)	Sensible= 225 W Latent =225 W	
Operation setpoints	Cooling setpoint= 24°C Heating setpoint= 22°C	
Weather file	TMY3 for Golden-NREL, CO. TRNSYS simulation is run with 5 minutes time step	

Table 7-2 Envelope's thermal characteristics of the base case for Golden, CO climate zone

Sketch	Material	Thickness [mm]	Thermal Conductivity [W/(m.K)]	Density [kg/m^3]	Heat Capacity [J/(kg.K)]
Wall					
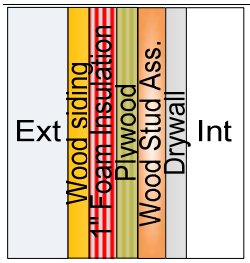	Wood Siding (Exterior)	12.5	0.1400	530	900
	XPS Insulation	25	0.0278	40	800
	OSB (plywood)	12.5	0.1500	650	1200
	Wood Stud Assembly	137.5	0.0653	120	1036
	Gypsum (Interior)	12.5	0.2100	700	1000
		Total R-value [m^2.K/W]= 3.43 (R19)			
Ceiling					
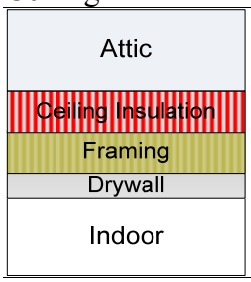	Ceiling Insulation (attic side)	136	0.0411	1380	37
	Framing	140	0.0514	1405	93
	Drywall (interior)	13	0.1600	1088	802
		Total R-value [m^2.K/W]= 6.11(R35)			
Slab on grade					
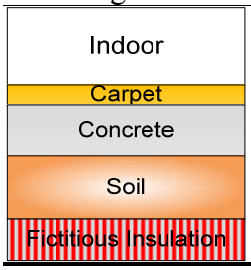	Carpet (interior)	25	0.0693	1255	32
	Concrete	102	1.31	837	2247
	Soil	305	0.8763	837	1600
	Resistive Insulation	R-value [m^2.K/W] = 1.76 (R10)			

7.1.2 **HVAC system**

TRNSYS can be used to model HVAC systems in a building at two modeling levels: energy rate control and temperature level control. The first modeling level assumes an ideal control of the thermal zone. This simplified approach assumes that the HVAC system operates at an ideal efficiency. The energy is added or extracted to the zone level to meet the heating or cooling load as needed to control the indoor air temperature within the desirable setpoints.

Therefore, the thermostat dynamics are not captured. This method is quick, simple and more appropriate for studies that are aimed at zone level evaluation. The second modeling level, however, considers the modeling details of the HVAC systems. At this detailed level, the HVAC system and its associated control systems must be defined in TRNSYS simulation studio. This way the effect of system efficiency can be modeled and evaluated. In this work, the first modeling approach (i.e., energy rate control) is adopted to evaluate the impact of phase change materials (PCMs) on the heating and cooling loads at zone level. They are calculated based on 22°C heating set-point and 24°C cooling set-point as per Building America House Simulation Protocols [280]. Therefore, the results hereafter should be interpreted without the HAVC system's efficiency.

7.1.3 **Internal heat gain**

Internal heat gain emitted by people, lighting and appliances has a significant impact on total zone load and consequently energy consumption. To simplify the inputs in TRNSYS, the schedule and the maximum wattage are determined from the peak consumption load profile and the total electricity consumption estimate provided by the Building America House Simulation Protocols [280]. For the conditioned space and a three bedrooms house, the equipment load is calculated as shown in **Table 7-3**. The load is then lumped so that the sensible load per day is 11.6 kWh and for latent is 1.41 kWh. Using the same reference, the daily lightings load is also determined to be 4.325 kWh. The maximum load can be calculated by multiplying these daily loads by the corresponding normalized load profile. For this house, a three people are assumed to occupy the house. It is assumed that each occupant produce 75 W sensible and 75 W latent heat. When the normalization is removed, the lighting, equipment and occupants load profiles used in

the TRNSYS are shown in **Figure 7.2**. To simplify the inputs further, no monthly adjustments as suggested by [280] are performed for the schedules.

Table 7-3 Daily equipment load for a 1800 ft^2 conditioned area, 3 bedroom house

Equipment Type	Sensible load [kWh/day]	Latent load [kWh/day]
Clothes Washer	0.170	0.000
Dish-Washer	0.288	0.072
Combined DHW	1.247	0.000
Bath	0.109	0.000
Shower	0.434	0.413
Sinks	0.181	0.082
Fridge	1.189	0.000
Clothes Dryer	0.548	0.157
Range	0.757	0.505
Misc. Elec. Loads	6.676	0.182
Total equipment load	11.599	1.410

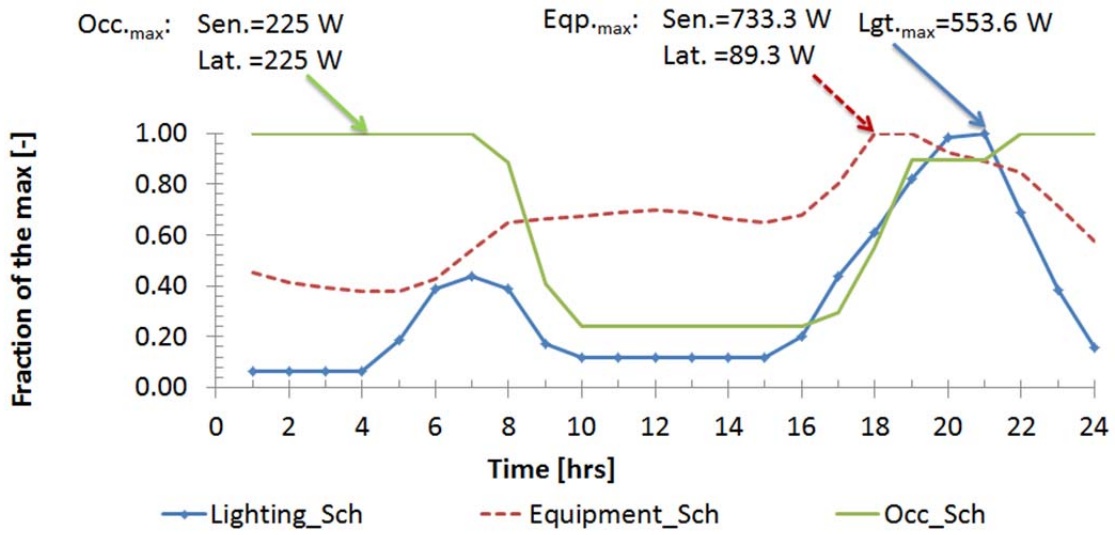

Figure 7.2 Internal load schedule for the base case residential building

7.1.4 **Other assumptions related to the thermal zone**

In TRNSYS, the convective heat transfer coefficient can be assumed a constant or varies if empirical equations are used. In addition, the interior convective heat transfer coefficient can be internally calculated using embedded algorithm. For this study case, the internal convective heat transfer coefficient is assumed to be constant at 4.43 $W/m^2.K$ based on experimental results from Liu and Awbi for PCM wallboards under natural convection [277]. The outside convective heat transfer coefficient is assumed to be constant at 18 $W/m^2.K$ as per the TRNSYS default value, presumably for cold climates[301].

The thermal mass of furniture, contents and internal structural walls should be accounted for when modeling thermal zones. ASHRAE 90.2 specifies the requirements for the thermal mass [302]. According to the standard, a value of 3.6 kg of 5 cm wood per square foot of conditioned space should be assumed for the furniture. For the structural mass, a value of 2.3 kg of 1.3 cm gypsum wall board per square foot of conditioned space. Using the guidelines, an area of 162 m^2 of wood and 414 m^2 of gypsum board are specified in TRNSYS as calculated in **Table 7-4**.

Table 7-4 Internal thermal mass assumed for the modeling the thermal zone

Material for thermal mass	ASHRAE_90.2 [kg/ft^2 of conditioned space]	Required Mass [kg]	Density [kg/m^3]	Mass per area [kg/m^2]	Area [m^2]	Specific Capacity [J/kg.K]
5 cm of Wood	3.6	6480	800	40	162	2000
1.3 cm of Gypsum board	2.3	4140	803	10	414	1088

The thermal capacitance of air node is another important factor that should be considered when TRNSYS is used as a modeling tool. The thermal capacitance of the air node should be multiplied several times the default value in TRNSYS. This is a practice used to stabilize the

prediction of indoor air temperature. Although not published, energy modelers use a multiplier between 5-20 times the default values in TRNSYS. One study has specified a value of 20 when using TRNSYS [301]. For this study, the thermal capacitance of the air node is increased by a factor of 5.

7.2 Wall Designs and PCM Parameters Selection

The external wall in the base case is modified by placing the PCM to the interior side (iPCM), in the middle of the wood assembly (midPCM), and to the exterior side of the wall (ePCM). **Table 7-5** provides the different designs and the parameters considered for the parametric study.

Table 7-5 Parameters considered for the parametric study for PCM-enhanced Walls

Wall Design Sketch	Latent Heat [kJ/kg]	T_m [°C]	ΔT_m [°C]	Orientation	Total Runs
Interior PCM: iPCM 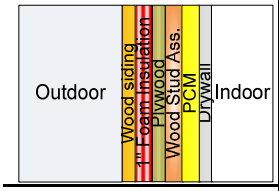	50-300 (50 increment)	21-27 (1 increment)	0.1, 1, 2,4, 6, 8	All orientations	252
Middle PCM: midPCM 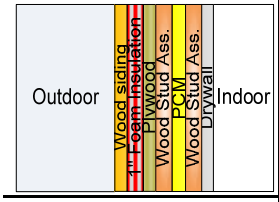	50-300 (50 increment)	10-35 (5 increment)	0.1, 1, 2, 4, 8, 12	All orientations	216
Exterior PCM: ePCM 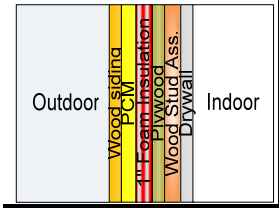	50-200 (50 increment)	10-40 (5 increment)	0.1, 1, 2, 4, 8, 12	All orientations	168

Chapter 5 has given insights on the range of effective parameters and therefore is considered here. It was found previously that when PCM is located to the exterior, it has very low impact on the thermal performance of the envelope. **Figure 7.3** illustrates the range of parameters considered for this case.

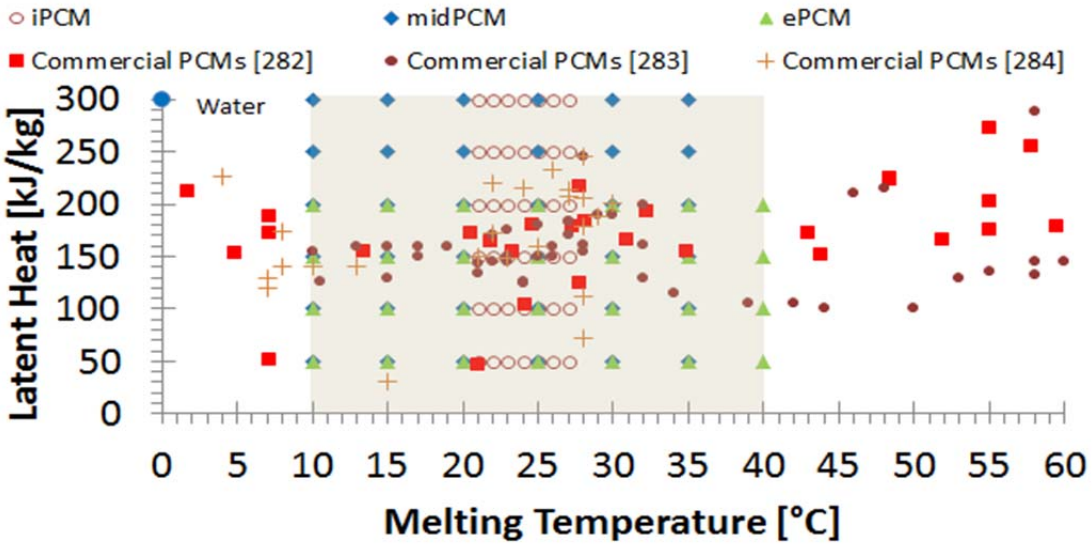

Figure 7.3 PCMs thermal properties considered for the whole house parametric study

7.3 Modeling of PCM-enhanced multilayer wall

The main objective of this task is to determine the optimal thermal properties of PCMs for reducing the annual heating, and cooling loads. The simulations are performed for all parameters. Since the trend is similar, selected results are presented in this section. **Figure 7.4** shows the impact of locating the PCM on the annual loads for the latent heat case of 200 kJ/kg. When PCM is located to the interior side, maximum cooling savings of 6% occurs 1°C below the cooling setpoint with 1°C melting temperature range being the best. The savings in annual heating loads is 2.4% and occurs at the heating setpoint with a 2°C melting temperature range. As the PCM location moves away from the indoor environment, the savings becomes less. The lowest savings are observed when the PCM is located on the exterior. For the PCM to the

middle, the savings in cooling load drops by almost half and optimal properties moves to the wide melting range side of 4°C. The maximum savings in annual heating load is in the range of 1.8% which is not significantly different than the iPCM case but the melting range covers wider melting range region (2-8°C) as depicted in **Figure 7.4** (b). The optimal temperature for maximum savings in cooling and heating is 20°C. The lowest savings are observed when the PCM is located to the exterior side with optimal thermal properties on the cold side.

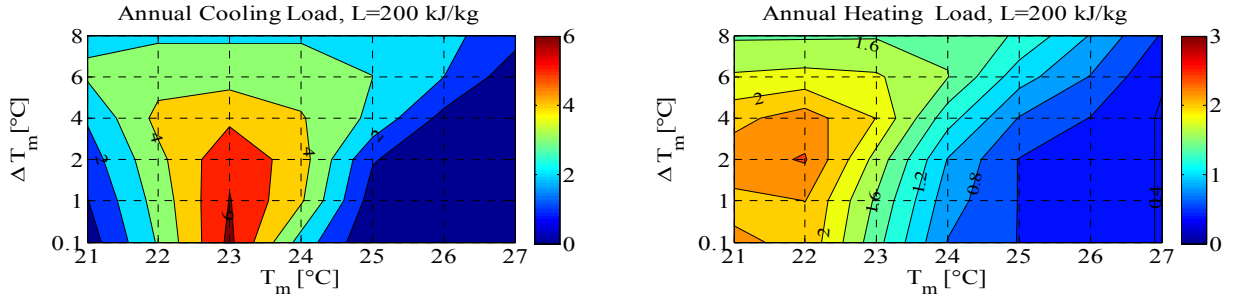

a) Percentage savings in annual cooling and heating loads when PCM is located to the interior side (iPCM case)

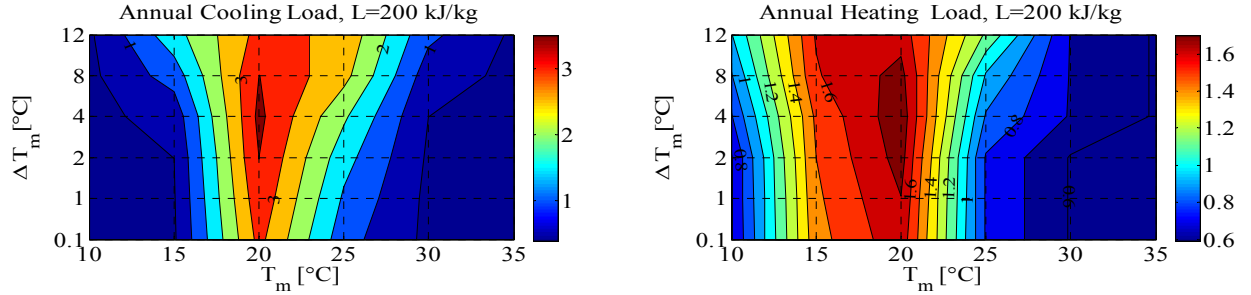

b) Percentage savings in annual cooling and heating loads when PCM is located in the middle (midPCM case)

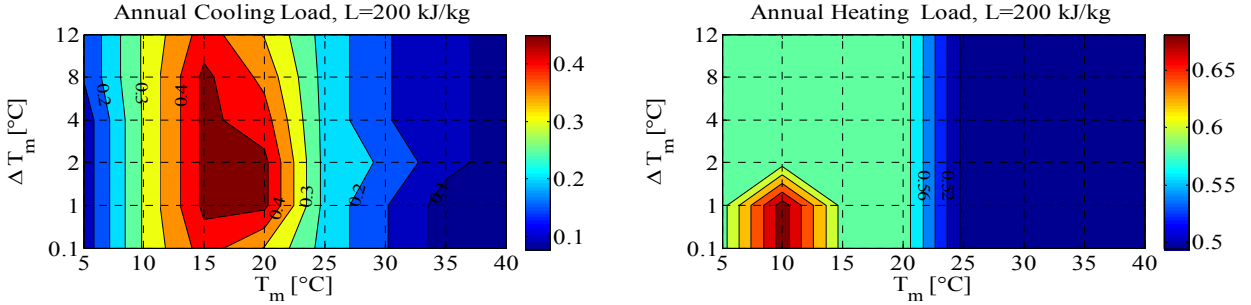

c) Percentage savings in annual cooling and heating loads when PCM is located to the exterior side (ePCM case)

Figure 7.4 Percentage savings in annual loads for the case of 200 kJ/kg for different PCM's locations

From the above results, it is clear that maximum savings in annual heating and cooling loads are achieved when PCM is located to the interior. The optimal melting temperatures are close to the setpoints; cooling and heating setpoints. For maximum savings in cooling load, the optimal melting temperature is a degree below the setpoint with a melting range of less than or equal to 1°C. For maximum savings in heating load, the optimal melting temperature is at the heating setpoint with a melting range of 2°C. Therefore, selecting a PCM with properties close to these optimal values could reduce both the heating and cooling loads at the same time. Other designs (i.e., when PCM is far from the indoor environment) clearly show that optimal thermal properties are few degrees below the heating or cooling setpoints for the cold climate of Colorado. The thermal performance of this category is low when compared to the PCM that is located into direct contact with the indoor environment.

7.4 Impact of orientation when the PCM is placed to interior side

The previous section considers the use of different PCM configurations in all orientations. The best PCM location was found to the interior side of the wall. Therefore, the iPCM case (i.e., PCM to the interior side) is selected to study the impact PCM on individual orientation on annual loads. In order to simplify the analysis, the medium latent heat case of 200kJ/kg is selected. In addition, the optimal melting temperature and melting range that achieve maximum savings in cooling and heating loads from previous section are considered.

The results for every orientation are shown in **Table 7-6**. In addition to cooling and heating load, the annual load is also included. The shaded cells in the table show the optimal melting temperature, melting range and the corresponding savings for every orientation. Regardless of the orientations, the optimal melting temperature for maximum savings in cooling

load is 23°C with melting range of 1°C. Similarly for a maximum savings in heating loads, the optimal melting temperature is 22°C with a melting range of 2°C. Although the savings are insignificant, the table shows that the maximum is achieved by south, west, east, and north, respectively. When the total annual load is considered, the optimal temperature is 23°C with a melting range of 2°C. Regardless of the orientation, this is perhaps a conservative design choice.

Table 7-6 Impact of internal PCM on annual loads when placed at different orientations

Orientation	T_m [°C]	ΔT_m [°C]	Heating reduction [%]	Cooling reduction [%]	Total reduction [%]
East Wall 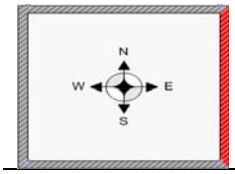	22	1	0.62	1.03	0.72
	22	2	0.65	1.14	0.77
	23	1	0.50	1.80	0.82
	23	2	0.52	1.77	0.83
South Wall 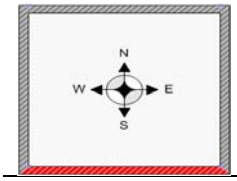	22	1	0.68	0.96	0.75
	22	2	0.74	1.07	0.82
	23	1	0.55	1.84	0.86
	23	2	0.59	1.69	0.86
West Wall 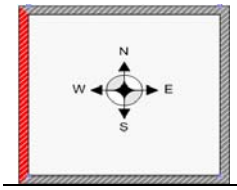	22	1	0.67	0.99	0.75
	22	2	0.74	1.07	0.82
	23	1	0.53	1.69	0.82
	23	2	0.58	1.58	0.83
North Wall 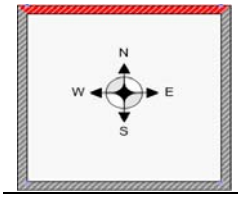	22	1	0.62	0.99	0.71
	22	2	0.67	1.10	0.77
	23	1	0.48	1.66	0.76
	23	2	0.52	1.55	0.77
All Walls 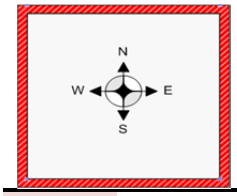	22	1	2.20	3.43	2.45
	22	2	2.42	3.74	2.56
	23	1	1.57	6.05	2.48
	23	2	1.73	5.82	2.69

Maximum savings in annual heating loads
Maximum savings in annual cooling loads
Maximum savings in annual total loads

7.5 Hybrid PCM layers when placed to the interior side

According to **Table 7-6**, the maximum savings in annual cooling and heating loads occur at different PCM thermal properties. Therefore, it is necessary to test hybrid PCM layers with different thermal properties; one dedicated for reducing cooling load and another for reducing heating load. The design configurations and thermal properties are listed in **Table 7-7**.

For a single PCM layer, the latent heat of 200kJ/kg is used as a reference design. For wall designs with multiple PCM layers (wall design#2(WD#2) and WD#3), the reference latent heat of 200kJ/kg is divided into two halves: one for reducing cooling load and another for heating. This latent heat distribution is suggested to compare with single PCM layer case. The difference between WD#2 and WD#3 is the arrangement of PCM layers. PCM-1 layer (i.e., dedicated for cooling load) is located close to the interior for WD#2 and PCM-2 (i.e., dedicated for heating load) is swapped the location with PCM-1 for WD#3. This is considered to evaluate the sensitivity of PCM order on both heating and cooling loads. Since the heating is dominant in Colorado climate, WD#4 is designed with more latent heat on PCM-2 layer to reduce the heating load. The order of PCM layers is similar to WD#2. This test case is considered to evaluate the impact of latent heat distribution on heating and cooling loads.

The results for these four cases are shown in **Figure 7.5**. The hybrid PCM layers design performs slightly better than a single PCM layer (i.e., 1% better) when savings in annual heating load is considered. The savings in cooling load doesn't improve when compared to the single PCM layer case. In addition, the order of PCM layers is not important when hybrid PCM layers are considered as a design option. Manipulating the distribution of latent heat beyond a 50-50% share doesn't improve the overall thermal performance of PCM.

Table 7-7 Design configurations for single and hybrid PCM layers

Wall Design Sketch*	PCM layer	Latent Heat [kJ/kg]	T_m [°C]	ΔT_m [°C]
WD#1: One PCM layer				
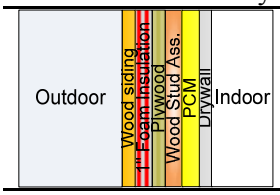	PCM	200	23	2
WD#2: Two PCM layers (Latent heat distribution: 50%clg_50%htg)**				
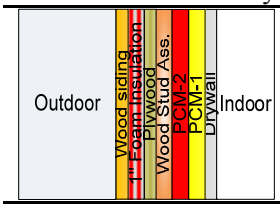	PCM-1(for Cooling)	100	23	1
	PCM-2 (for Heating)	100	22	2
WD#3: Two PCM layers (Latent heat distribution: 50% htg_50%clg)**				
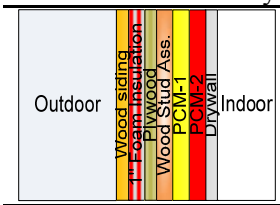	PCM-1(for Cooling)	100	23	1
	PCM-2 (for Heating)	100	22	2
WD#4: Two PCM layers (Latent heat distribution: 25%clg_75%htg)***				
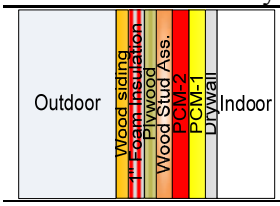	PCM-1(for Cooling)	50	23	1
	PCM-2 (for Heating)	150	22	2

Notes: * properties of other layers are as per **Table 7-2**
** latent heat of 200kJ/kg is equally distrbuted for heating and cooling
*** 75% of 200kJ/kg latent heat is for heating and 25% for cooling

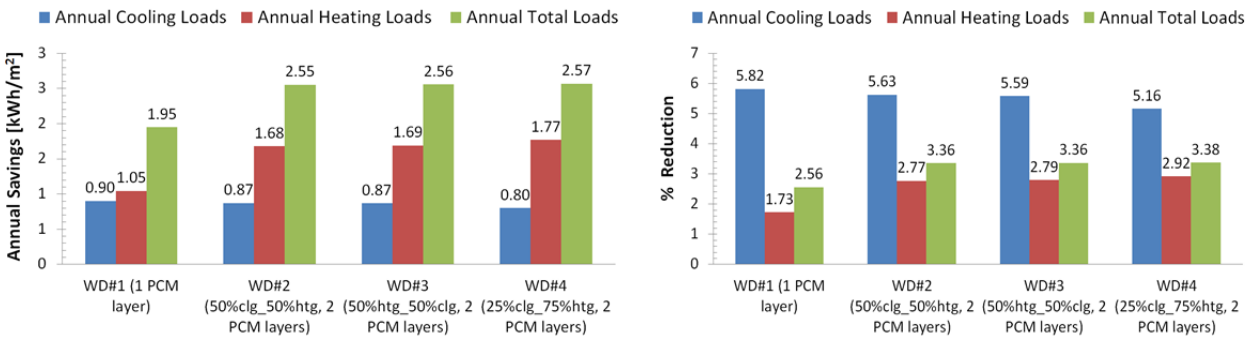

a) Savings in annual loads per floor area b) Percentage reductions in annual loads

Figure 7.5 Impact of hybrid PCM layers on annual loads when PCM placed to the interior side

7.6 Seasonal Performance of PCM when placed to the interior side

Since it offers more insights on ideal conditions of PCM's performance, it is important to know the seasonal response of PCM. Therefore, a PCM design case placed to the interior side of the wall is simulated in all exterior walls. A medium latent heat of 200kJ/kg with a melting temperature of 23°C and melting range of 2°C is selected for this seasonal analysis. **Figure 7.6** illustrates the results of this design case. For the climate of Colorado, PCM performs the best in the transition months. In particular, the savings in heating loads start to increase in March (1%) and reach a maximum savings of 10% in May. The maximum savings in cooling loads occur in May too at almost 23% and reduce significantly during the summer months.

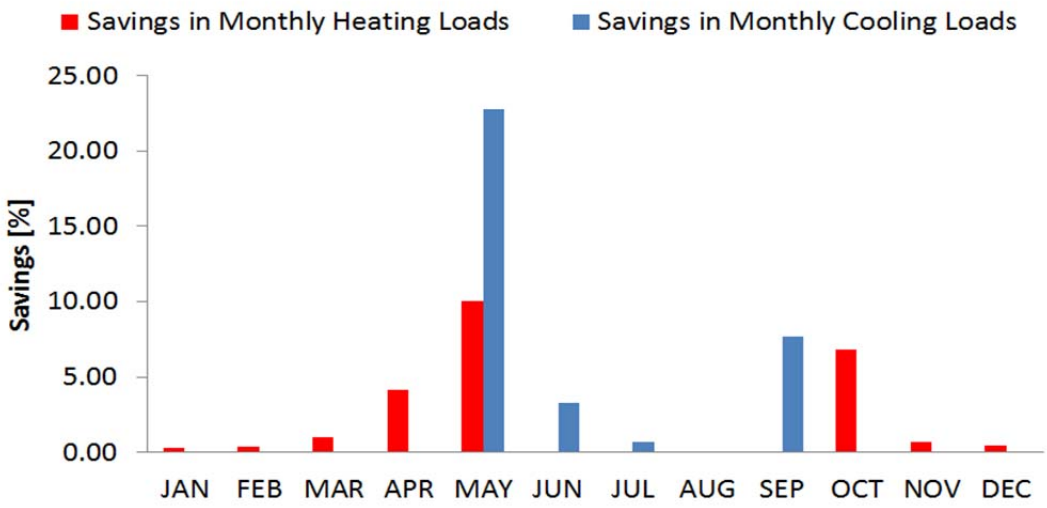

Figure 7.6 Seasonal performance of PCM wall when placed to the interior in all orientations

It is clear that during the extreme months, PCM performs less than expected. Therefore, a closer look into PCM layer level is necessary to gain more insights. A PCM layer in the south wall only is simulated to evaluate the dynamics during May where PCM performs the best among all months. **Figure 7.7** provides more insights on the performance of the PCM during the month of May. The PCM case is also compared with the base case (i.e., no-PCM case). Since

PCM layer behaves similarly in all days of May, only three days are selected. **Figure 7.7** (a) illustrates the performance of PCM layer with three subplots. The first subplot indicates the charging process (i.e., storing heat) and discharging process (i.e., releasing heat) of PCM during the time step of 5 minutes. The second subplot shows the cumulative heat that is absorbed and released in the layer over the simulation time. The third subplot depicts the interior and exterior surface temperature of south wall with the zone indoor air temperature. According to these three subplots, it is clear that the heat is released during the night and stored during the day based on the exterior and interior surface temperatures. A maximum exterior surface temperature of 32°C and a minimum interior surface temperature of 4°C (amplitude of 28°C and an average of 14°C) can be observed from the figure for these three days. The south wall is responding to the outside climatic conditions due to this diurnal cycle as the exterior surface temperature goes above and below the indoor air temperature during a day. This diurnal change makes the PCM layer to go through a full cycle of charging and discharging during a day. In all these three days, the PCM layer never reaches its maximum capacity but full discharge occurs in the last day.

This dynamic behavior has resulted in reduction of cooling and heating demand when compared to the no-PCM case as shown in **Figure 7.7** (b). Fluctuation of the demand during the time period is due to the addition and subtraction of heat from the zone level to maintain the air temperature at the desirable setpoints. The same fluctuation is also observed with PCM layer as a response to the zone demand.

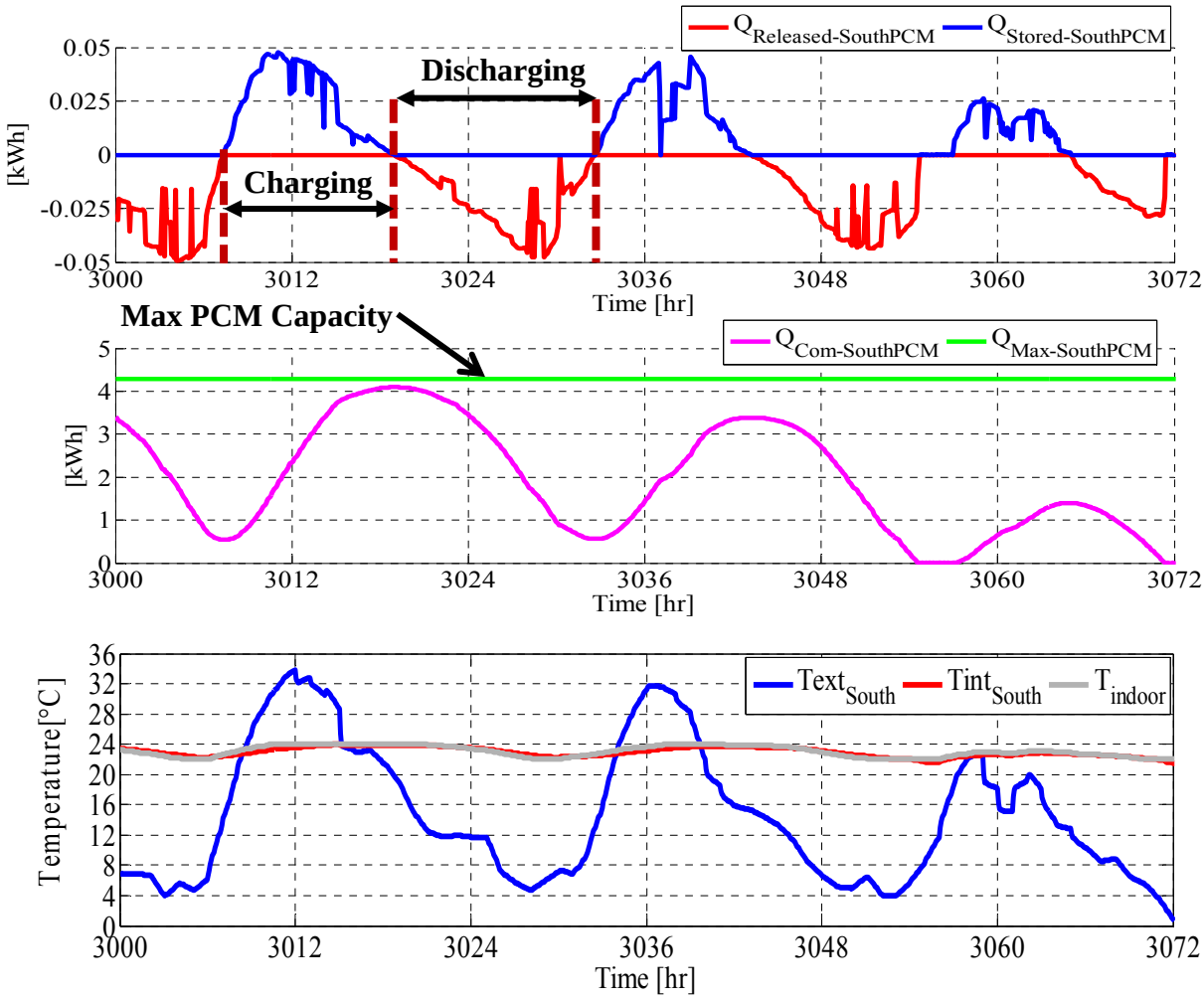

a) PCM's layer performance at south wall

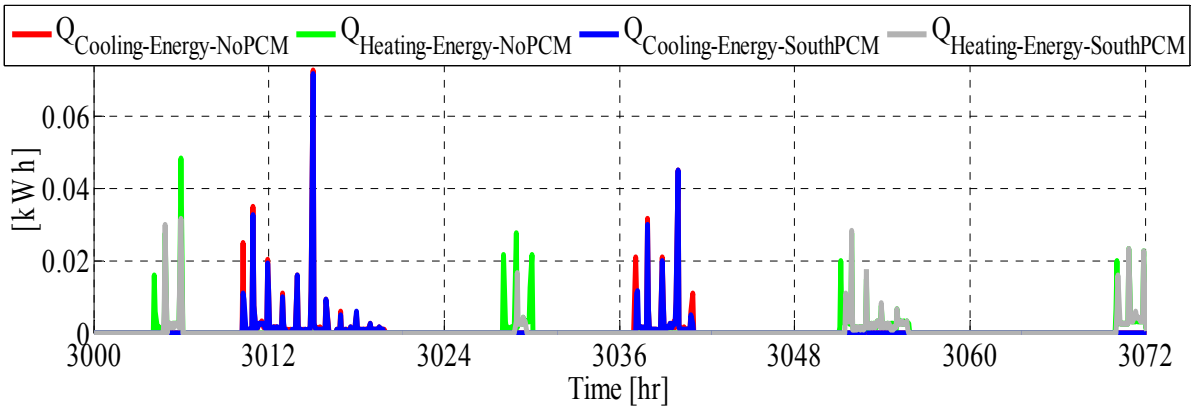

b) Zone demand response during the time period of 5 minutes

Figure 7.7 PCM's charging and discharging process and its impact on Zone demand from 6th - 9th May

In cooling dominated months, the PCM reaches its maximum heat storage capacity where the phase state is at liquid most of the time. **Figure 7.8** clearly shows this phenomenon. PCM absorbs the heat from outside due to the heat gain and from inside due the internal heat gain. Although PCM releases the stored heat during the night due to heat loss to the outside environment, it is not enough to fully discharge the stored heat as clear from the figure. The discharging process is slow due to the high level of insulation. Most of the time PCM operates at its maximum capacity with limited option to fully discharge the heat for the next day cycle. Hence, the cooling demand of the wall with PCM during August is similar to the case with no PCM. In order to enhance the PCM's performance, the outside cooled air can be utilized to flush the stored heat.

A reverse phenomenon occurs during the heating dominated months. The PCM is at solid state since all zonal heat is either consumed instantaneously to meet the heating demand or lost to outside due to large temperature difference between inside and outside. Therefore, there is no extra heat that can be stored by PCM for later use. To enhance the PCM performance during winter, heat source such as solar energy is necessary.

The yearly fluid fraction of PCM is shown in **Figure 7.9**. As expected from previous analysis, PCM state is either at solid or liquid state in most of the yearly time. Less than 20% of the time, PCM is going through the mushy region which indicates a marginal phase change process.

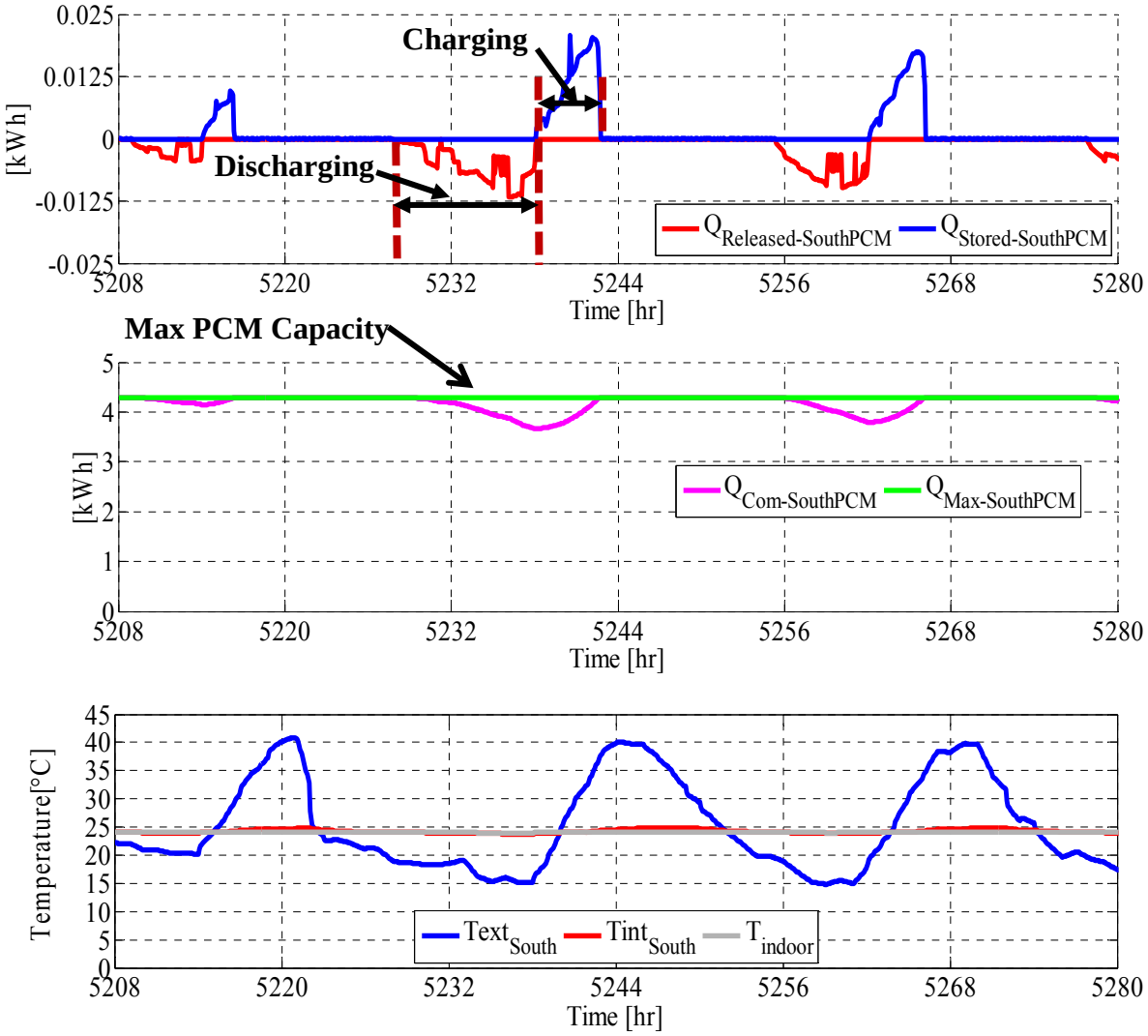

c) PCM's layer performance at south wall

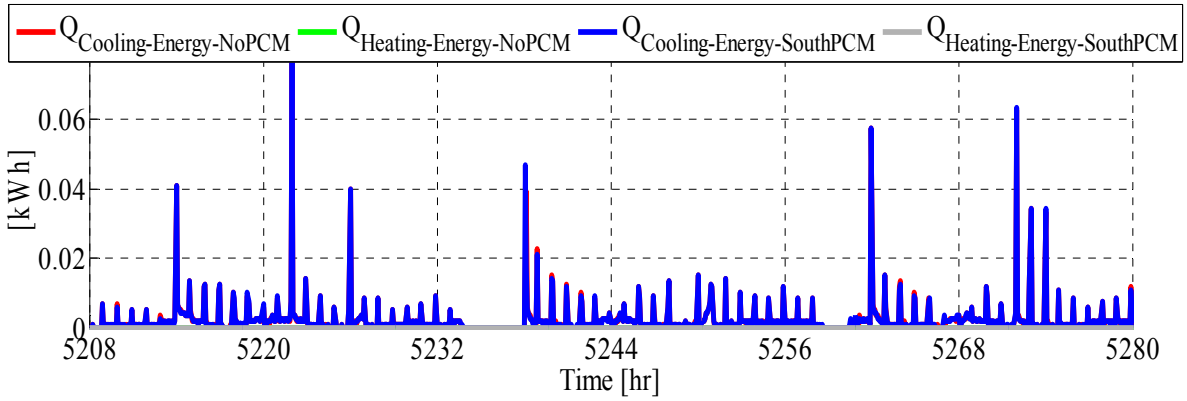

d) Zone demand response during the time period of 5 minutes

Figure 7.8 PCM's charging and discharging process and its impact on Zone demand from 6th - 9th August

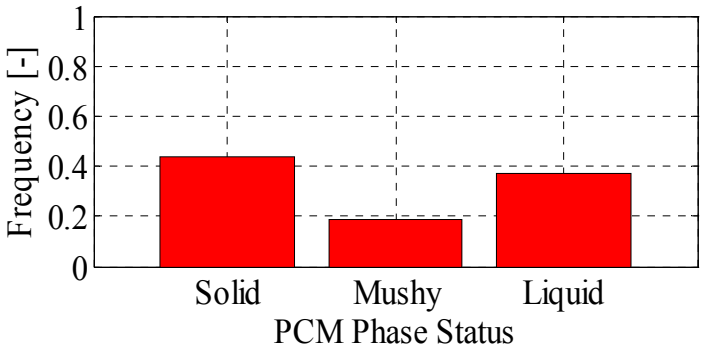

Figure 7.9 Yearly fluid fraction of PCM for the south wall

A performance indicator is necessary when evaluating the PCM effectiveness. The number of full charging and discharging cycles can be used for this purpose. It has been observed that PCM undergoes a partial charging and discharging cycle when it is under fully passive conditions. Under ideal conditions, PCM can achieve one full charging and discharging cycle per day, 365 cycles in a year. This is a fair assumption since environmental condition follows a near sinusoidal form on a daily bases. Therefore, the yearly PCM efficiency can be defined as follows:

$$\eta_{PCM} = \frac{actual\ cycles}{ideal\ cycles} = \frac{Total\ \#\ of\ charging\ or\ discharging\ cycles}{365} \qquad \text{Equation 7-1}$$

A full charging cycle or a discharging cycle is equivalent to the maximum capacity of the PCM layer, a latent heat of fusion. For the PCM layer in south wall for the above case, the number of charging or discharging cycles for the whole year is found to be 98.6 cycles. This number is found when the total absorbed heat of PCM layer [in kWh] in a year (or total released heat) is divided by the maximum latent heat capacity of PCM layer [in kWh]. Then using the above relationship, the PCM efficiency is 27%.

7.7 Sensitivity analysis

Utilizing the results from the previous section, only south wall is designed with PCM. The PCM is placed to the interior side of the wall. This design case will be referred as a "south-PCM" case with a medium latent heat of 200kJ/kg. The optimal melting temperature is assumed to be 23°C with a melting range of 2°C. A series of sensitivity tests are performed to evaluate the thermal performance of PCM.

7.7.1 Impact of PCM area to the total wall area

In case of expensive PCMs, it is natural to utilize a portion of the wall. This section examines the impact of PCM area relative to the total wall area. As stated early, the PCM is placed to the interior side of the south wall. The area of PCM is varied with respect to the total south wall area. **Figure 7.10** shows the impact of PCM areas variations on annual heating, cooling and total load. It is clearly shown that the savings are linearly related to the wall area. The cooling load is more sensitive to the variations in PCM's area than the heating load.

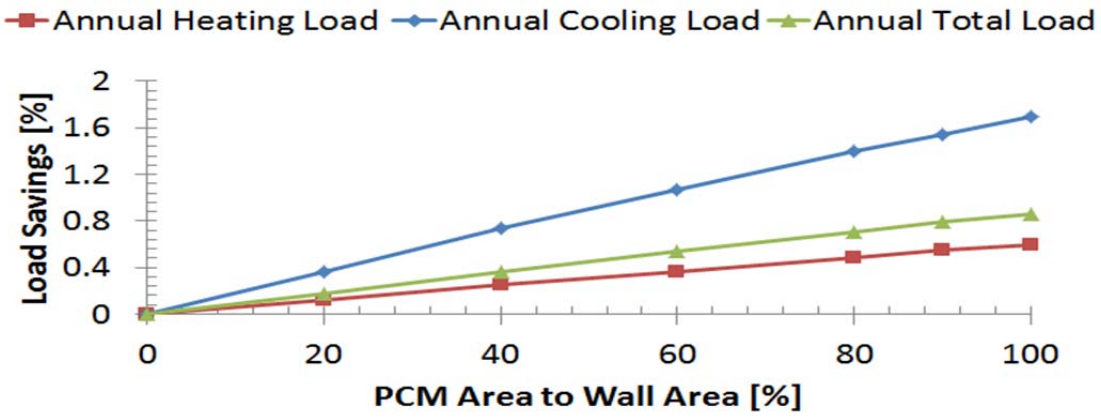

Figure 7.10 Impact of PCM area with respect to total south wall area when PCM to the interior

7.7.2 The amount of direct solar radiation on the wall

When PCM is located to the interior side, savings are based on concurrence of charging/discharging process and heating/cooling demand. During the heating season, the stored heat will be released when environmental condition suits the PCM operating condition, reducing the heating load. However during the cooling season, this heat might have an undesirable impact since it has to be charged back to the space at a later time period. Since it is not used for heating purposes, the stored heat would be removed by the mechanical systems as a cooling demand. Therefore, this section will examine the sensitivity of PCM to solar radiation as a source of heat that has to be manipulated.

7.7.2.1 Focusing the solar radiation on the PCM-enhanced south wall

By default, Type 56 in TRNSYS16 uses factors for distributing the total entering direct solar radiation as well as the diffusive radiation by absorptance weighted area ratios [303]. According to the manual, explicit distribution factors for direct solar radiation can also defined. Using this factor, the direct solar radiation to the internal surface of the south wall was varied from 0.025 to 1, where the 0.025 is the base case factor calculated for south-PCM wall by TRNSYS. According to the new factor for the south wall, the distribution factors to other surfaces should be adjusted. For this case, the factors are externally recalculated and redistributed based on absorptance weighted area ratios. The factors are provided to Type 56 as inputs. When the factor for south-PCM wall is 1 for example, it is assumed that all other surfaces in the zone received zero direct solar radiation. In all these cases, the diffusive radiations are unchanged, since it is calculated and distributed internally by TRNSYS.

Figure 7.11 shows the impact of varying the factor on the annual heating, cooling and total loads. As expected, more radiation on the PCM-enhanced wall has undesirable effect on the cooling load. More radiation is stored and later released to the space for the mechanical system to remove, resulting in lower savings in annual cooling load as the factor increases. However, this is favorable when heating is considered as more heat can be used for reducing the heat demand. For PCM to be more effective, it should be exposed to direct solar radiation during the heating season to store the heat for heating purposes. Similarly during the cooling season, the heat must be flushed by other means before it is converted into a cooling load. Therefore, charging and discharging mechanism play an important factor in PCM effectiveness.

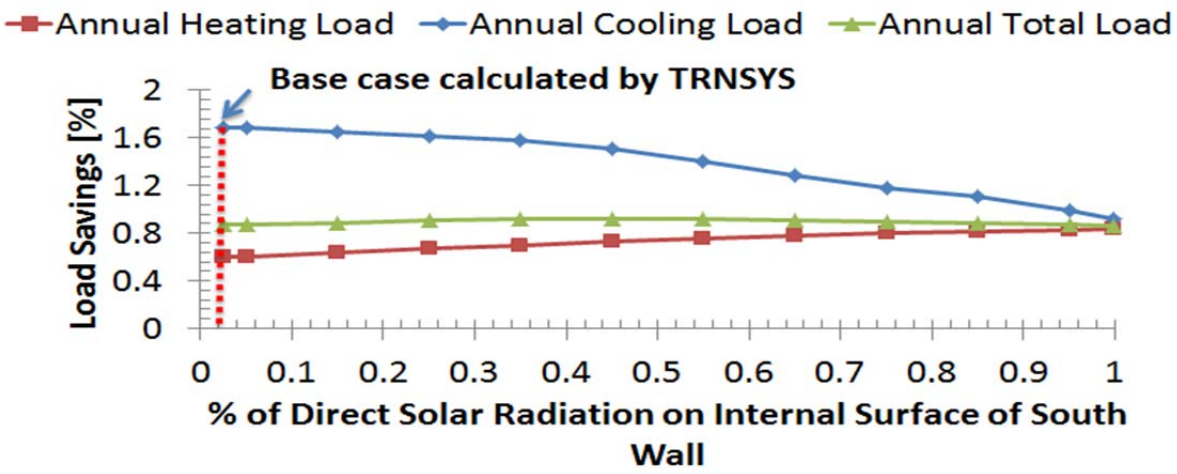

Figure 7.11 Impact of direct solar radiation on the annual loads

7.7.2.2 Reducing the solar radiation by adjusting the external shading factor

The amount of solar radiation received may influence the zone loads. This section examines the performance of the PCM when solar radiation received on internal surfaces is reduced to minimum. In this case and apart from the radiation power of lighting, the convective heat transfer will be a dominant mechanism as solar radiation received in the zone decreases.

In the original base case, no external or internal shading is added. Therefore, external shading factor is applied equally to all orientations for both the base case and the case of a south-PCM wall. For a fair comparison, the shading factor is increased for both the base case and the south-PCM wall case. **Figure 7.12** shows the results of the increasing the shading factor for both the base case and the PCM-south wall case. As solar radiation received on internal surfaces reduces, the benefit from the PCM reduces too. The saving in annual loads reduces as the shading factor increases. The savings becomes unchanged after 60% shading factor. According to **Figure 7.12** (b), it might look decisive when comparing the percentage reduction rather than the absolute values. The percentage reduction shows an increase in annual cooling savings after 60% reduction in solar radiation.

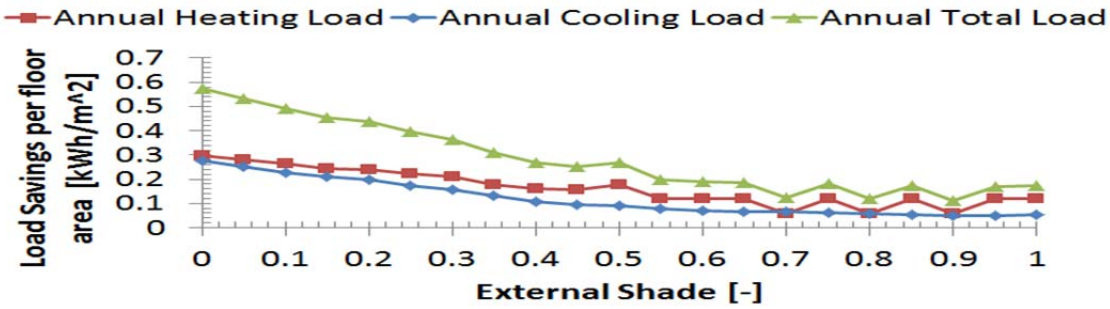

a) Savings in annual cooling, heating and total loads with increases in external shading factor

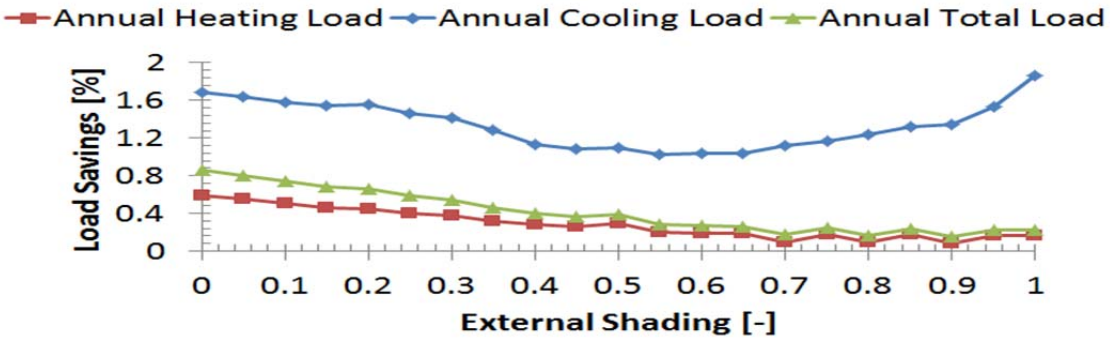

b) Percentage savings in annual cooling, heating and total loads with increases in external shading factor

Figure 7.12 Impact of increasing external shading on the annual loads

7.7.2.3 Increasing the solar radiation through variation in WWR

It is apparent from previous sections that increasing the solar radiation can reduce the annual heating loads. In order to quantify the benefits of this climatic parameter, the windows to wall ratio (WWR) is increased for both the base case (no PCM at all) and the south-PCM wall case. The comparison is performed between these two cases when the WWR is increased from 15% to 60% on south wall only. As seen from **Figure 7.13**, the savings in both cooling and heating loads increases as the WWR increases. Although the savings are insignificant, the maximum is achieved at approximately 35% WWR. The south-PCM wall area becomes smaller as the WWR is increased. This explains the reason behind the low savings in the annual loads after the value of 35% WWR. It is interesting to note that the PCM performance at 60% WWR is still better than that at 15%. This is related to the high solar radiation received, absorbed and subsequently released when favorable environmental condition occurs.

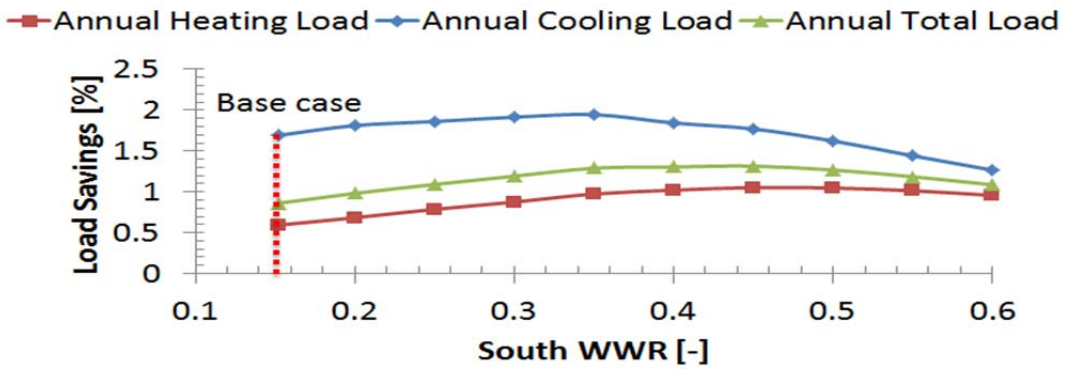

Figure 7.13 Impact of varying the WWR on annual loads

7.7.3 Impact of the internal convective heat transfer coefficient

Convective heat transfer coefficient is of a primary importance. It is a factor that determined the amount of heat transferred from the wall surfaces to the indoor environment and vice versa. The base case assumes a constant value of 4.43 $W/m^2.K$ based on experimental

results from Liu and Awbi for PCM wallboards under natural convection [277]. However, there might be uncertainty associated with this value. Therefore, the interior convective heat transfer coefficient is varied. The variation represents a value in a very slow natural convection, 1 $W/m^2.K$, to a value as high as 19 $W/m^2.K$ representing an air movement under forced convection. The variations are performed for both the base case and the south-PCM case. The comparison is done between these two cases at each new value. As seen from **Figure 7.14**, as the convective heat transfer coefficient increases the savings decreases. It is also interesting to note that heating demand increases with high convective coefficient. This is likely due to the flushing mechanism that is associated with high convective heat transfer coefficient.

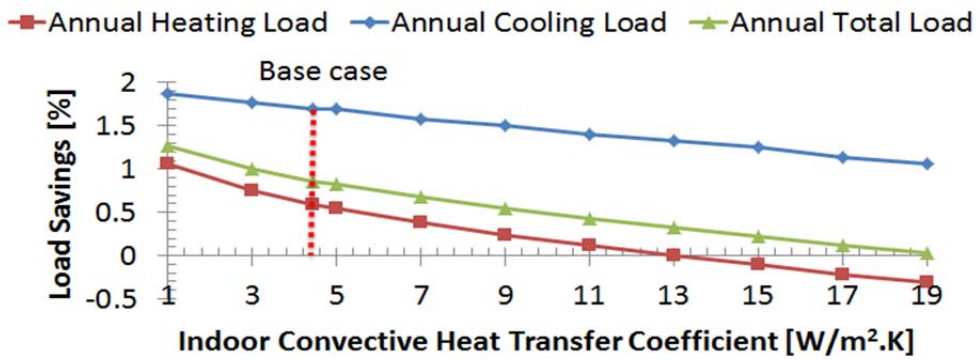

Figure 7.14 Impact of varying the interior convective heat transfer coefficient on annual loads

7.7.4 Impact of the PCM conductivity

Thermal conductivity of PCMs is another important factor that enhances the heat storage, charging and discharging process. For this case, the thermal conductivity has been varied to evaluate the impact on annual loads as shown in **Figure 7.15**. Reducing the conductivity increases the savings in heating load. Under passive heating, PCMs with low conductivity will absorb the heat slowly but also releases the heat back slowly. The slow mechanism provides the stored heat for longer period. On the other hand, savings in cooling load reduces as the

conductivity decreases. Similarly, the slow mechanism provides the stored heat for longer period which has to be partly removed by the mechanical systems. However at a conductivity value of more than 0.10 W/m.K, no major improvement or deterioration in savings is observed for both cooling and heat loads.

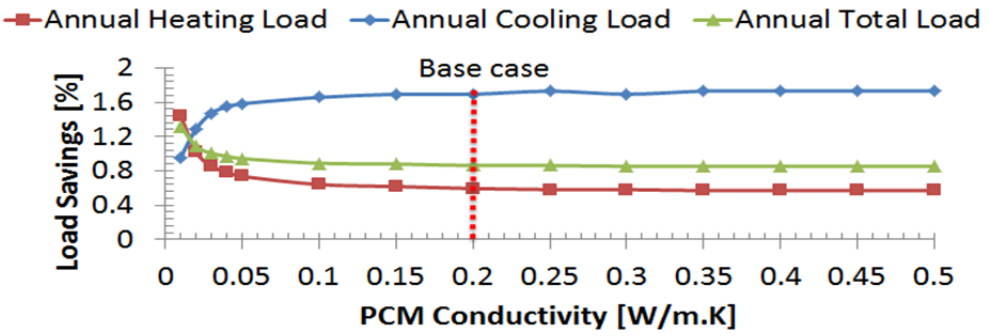

Figure 7.15 Impact of varying the PCM conductivity on annual loads

7.7.5 Impact of the PCM thickness

Besides the latent heat of fusion, the PCM thickness is likely to influence the cooling or heating demand. The PCM thickness of the base case is 12.5 mm. The thickness is increased on increment of 12.5 mm for 10 cases. The results are shown in **Figure 7.16**. A PCM thickness of more than 37.5 mm doesn't improve the savings in annual cooling load. The annual heating load increases linearly with the increases in PCM's thickness. However, a maximum improvement of 1% in savings of annual heating loads is not significant for a 10 times increases in the thickness.

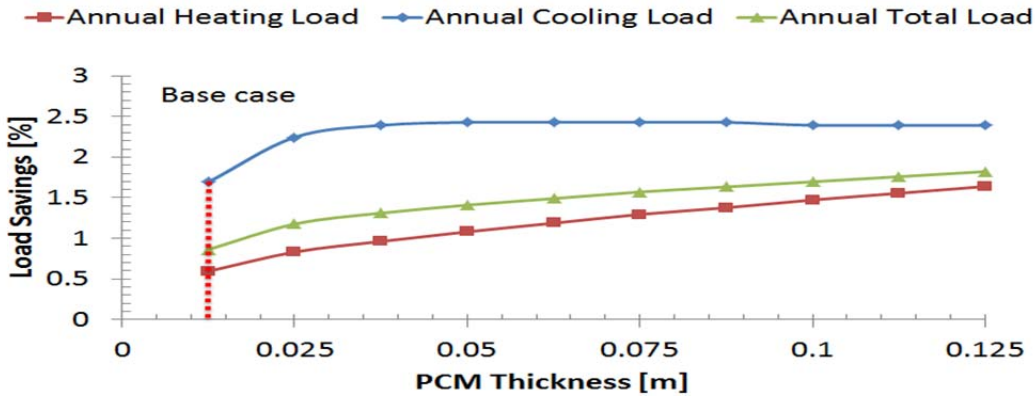

Figure 7.16 Impact of varying the PCM thickness on annual loads

7.7.6 Impact of zone's setpoint on the optimal PCM properties

Defining the optimal PCM properties are as good as defining the environmental control conditions. It is likely possible that the optimal PCM thermal properties developed for one environmental setting may not be optimal when condition changes. The base cooling and heating setpoints are 24°C and 22°C respectively. For comparison, the setting points are changed for both the base case design and the south-PCM case. The PCM's optimal thermal properties selected from previous sections are kept constant, L=200 kJ/kg, T_m=23°C, ΔT_m=2°C. **Figure 7.17** illustrates the impact of varying the cooling and heating setpoints on annual loads. First, the cooling setpoint was varied from 22-24°C while the heating setpoint is kept constant at 22°C. Then, the heating setpoint was varied at 18-24°C while the cooling setpoint is unchanged at 24°C.

It is clearly shown that the PCM is sensitive to both cooling and heating setpoints. It is interesting to note that the maximum savings in annual total load from PCM are achieved when the cooling setpoint is decreased by 1°C (new setpoint is 23°C) or heating setpoint is increased by 1°C (the new heating setpoint is 23°C). Increasing or decreasing the setpoints beyond this limit makes the PCM less effective. No savings in annual cooling loads, if the cooling setpoint

changed to 26°C or above. This means that the optimal thermal properties for PCM derived for the base case will also change with changes in the cooling and heating setpoints.

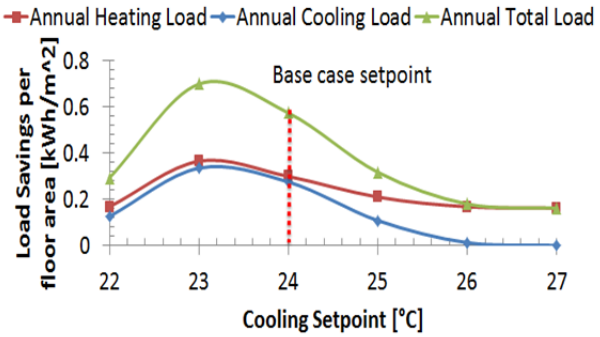

a) Savings in annual loads with variations in cooling setpoint

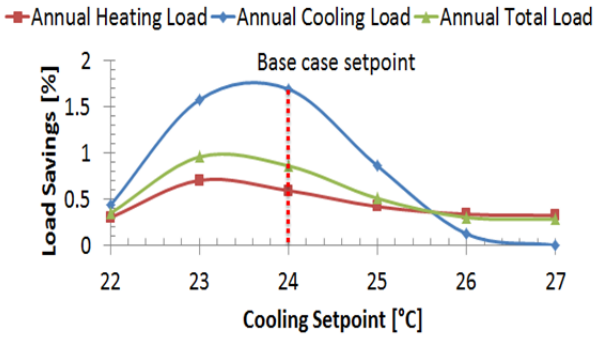

b) Percentage savings in annual loads with variations in cooling setpoint

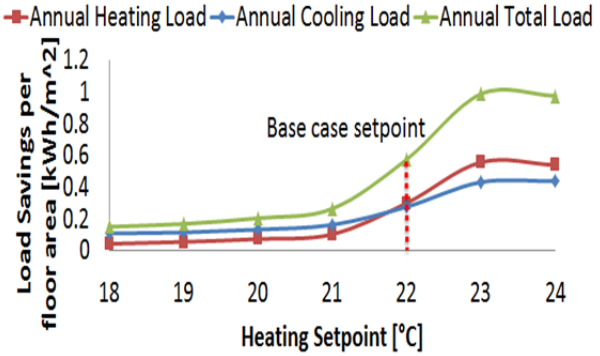

c) Savings in annual loads with variations in heating setpoint

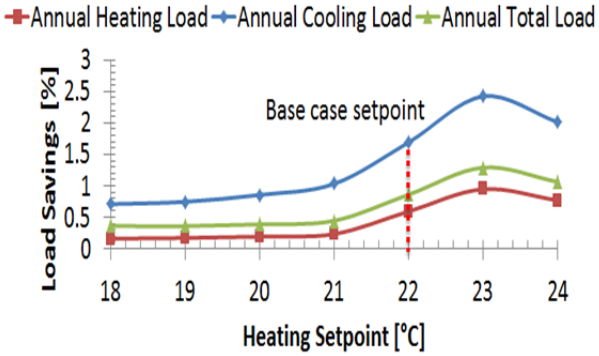

d) Percentage savings in annual loads with variations in heating setpoint

Figure 7.17 Impact of varying the zone cooling and heating setpoints on annual loads

7.8 Optimal PCM thermal properties for different zone setpoints

This section further explores the impact of setpoints on the PCM's thermal properties for maximum savings in annual loads.

7.8.1 A medium latent heat case of 200kJ/kg

When the cooling setpoint is varied from 24°C to 27°C, the heating setpoint is kept unchanged at 22°C. **Figure 7.18** shows the impact of varying the cooling setpoint on annual

loads for the medium latent heat of 200kJ/kg under varying melting temperature and melting range. According to the figure, the maximum savings in both annual cooling and heating load occurs at the small dead-band (tight environmental condition), refer to **Figure 7.18** (a). As the cooling setpoint increases, the saving in both heating and cooling loads reduces. This is likely due to the distribution of latent heat storage over larger temperature dead-band. For a dead band of 2°C, the savings is 6% for cooling loads and 3% for heating loads. As the dead-band increases to 4°C, the savings in cooling load is 3% and savings in heating load is only 1.6%. A loss of 25% savings in annual loads (cooling and heating load) is observed with a 1°C increase in cooling setpoint.

Apart from savings, the figure also shows that the optimal melting temperature changes with changes in cooling setpoint. The change in the melting temperature is consistent across all the cases, with every 1°C increase in cooling setpoint there is a degree increase in the optimal melting temperature. Across all the cases, the optimal melting temperature is always 1°C below the cooling setpoint. The melting range is not significantly changed; 1°C melting range is near optimal. Since the heating setpoints are unchanged, no changes in the optimal melting temperature or melting range are observed for maximum savings in annual heating load. Across the cases, the optimal melting temperature is around the heating setpoint of 22°C with a melting range of 2°C.

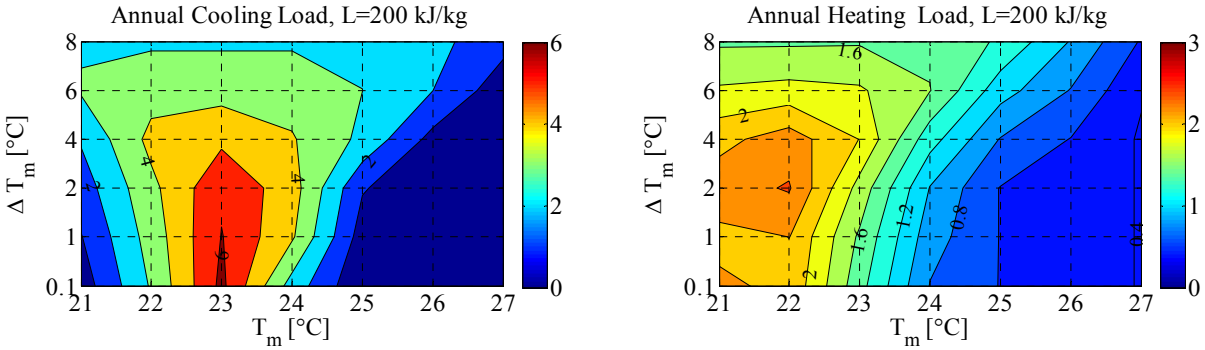

a) Percentage savings in annual loads for cooling setpoint of 24°C and heating setpoint of 22°C (Base case settings)

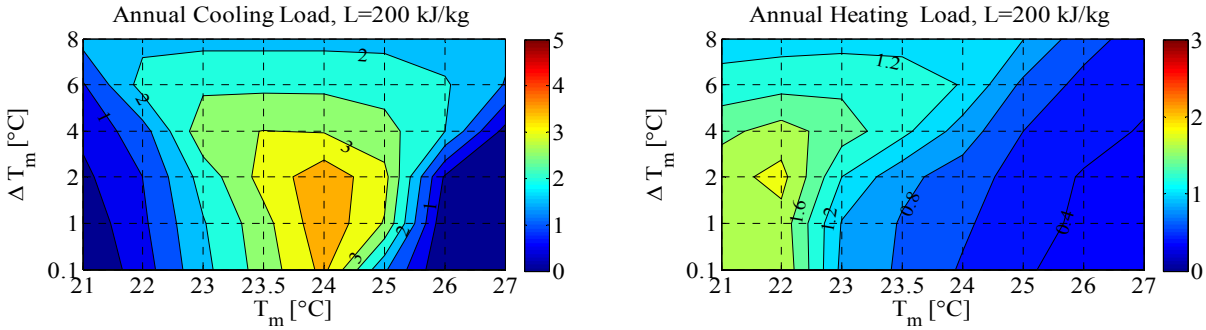

b) Percentage savings in annual loads for cooling setpoint of 25°C and heating setpoint of 22°C

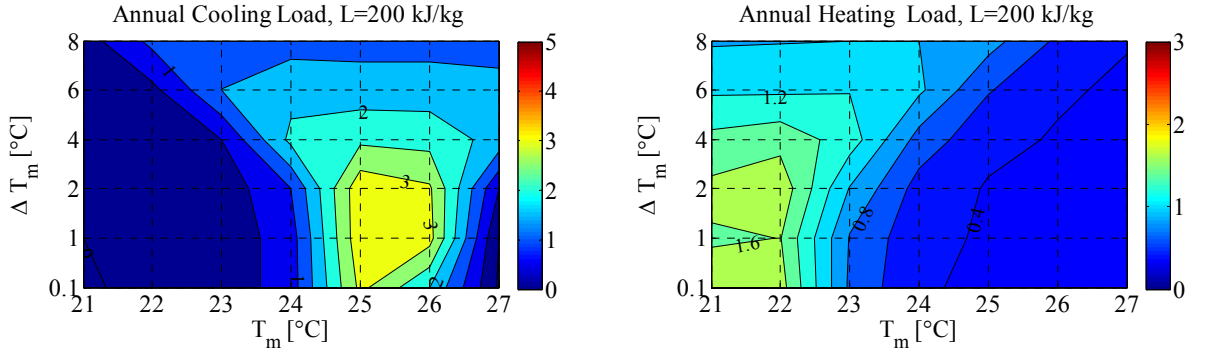

c) Percentage savings in annual loads for cooling setpoint of 26°C and heating setpoint of 22°C

Figure 7.18 Percentage savings in annual loads when varying the cooling setpoint for latent heat case of 200 kJ/kg with constant heating setpoint

A similar exercise is conducted when heating setpoint is varied from 20°C to 22°C while the cooling setpoint is maintained at 24°C. The results are shown in **Figure 7.19**. The maximum savings in heating loads occurs at 22°C (a heating setpoint) and maximum savings in cooling

load occurs at 23°C (a degree below the cooling setpoint). At 4°C dead-band, the savings are 2.5% and 2.4% for both cooling and heating loads compared to 6% and 3% at 2°C dead band.

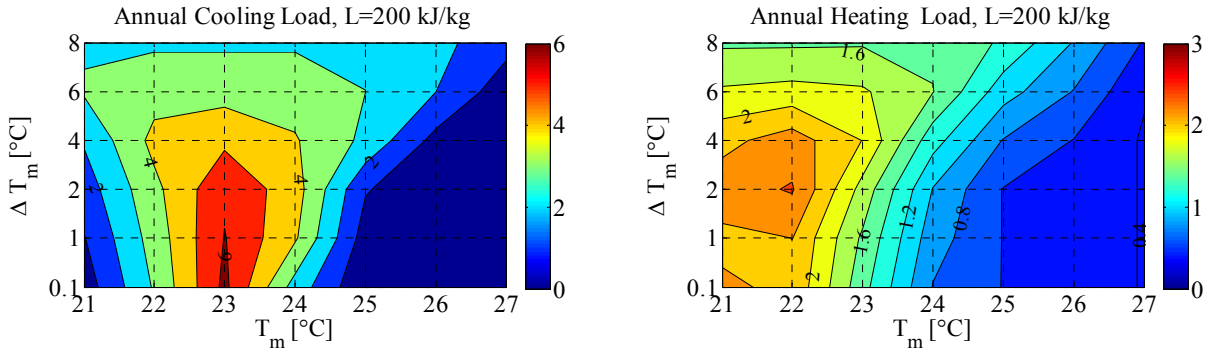

a) Percentage savings in annual loads for cooling setpoint of 24°C and heating setpoint of 22°C

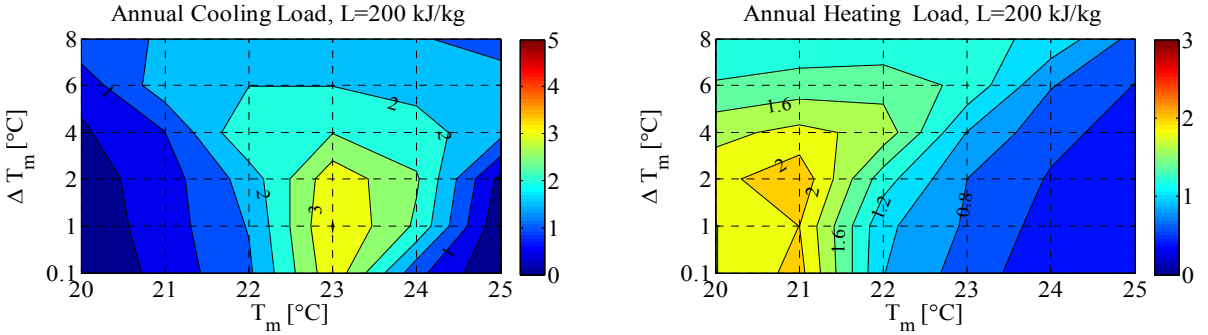

b) Percentage savings in annual loads for cooling setpoint of 24°C and heating setpoint of 21°C

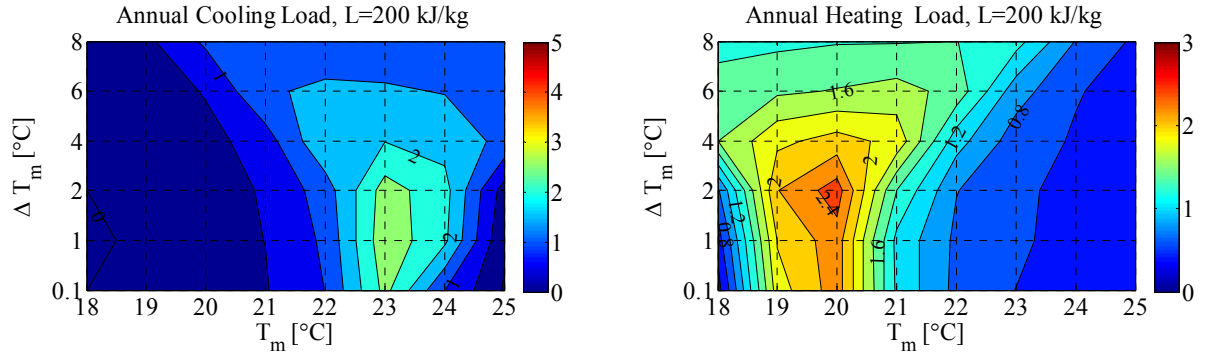

c) Percentage savings in annual loads for cooling setpoint of 24°C and heating setpoint of 20°C

Figure 7.19 Percentage savings in annual loads when varying the heating setpoint and cooling setpoint is constant for latent heat case of 200 kJ/kg

Since the cooling setpoint is constant for all the cases, the optimal thermal properties of PCM (i.e., melting temperature and melting range) for maximum savings in annual cooling load

are constant too. The optimal thermal properties of PCMs for maximum savings in annual heating loads move with changes in heating setpoint. In all cases, the optimal melting temperature is at the heating setpoint while the near-optimal melting range is close to 2°C.

7.8.2 Optimal thermal properties of PCM for the reference building case conditions

A pattern in optimal thermal properties of PCM can clearly be drawn from the medium case of 200kJ/kg. Therefore, the same has been carried out for the other PCM thermal properties. The latent heat is varied from 50-300kJ/kg, the melting temperature varied from 21-27°C, and melting range are 0.1,1,2,4,6 and 8°C. The indoor environmental conditions are kept unchanged as per the base case house model. The main goal is to draw design guidelines of optimal thermal properties mainly the melting temperature and melting range of PCMs. **Table 7-8** lists the optimal thermal properties of PCM for the base case. The optimal PCM thermal properties are based on maximum savings achieved in annual heating and cooling loads.

Table 7-8 Optimal melting temperature and melting range across the latent heat under the reference building case

Maximum savings in annual heating loads				Maximum savings in annual cooling loads			
L [kJ/kg]	Tm [°C]	ΔTm [°C]	% Savings	L [kJ/kg]	Tm [°C]	ΔTm [°C]	% Savings
50	22	1	1.28	50	23	2	1.54
100	22	2	1.78	100	23	0.1	3.78
150	22	2	2.15	150	23	0.1	5.43
200	22	2	2.42	200	23	2	5.82
250	22	2	2.62	250	23	1	6.78
300	22	4	2.80	300	23	1	7.32

L: latent heat, Tm: melting temperature, ΔTm: melting range

The results from this case indicated that the optimal thermal properties for maximum savings in annual heating and cooling loads are different. However, a pattern can clearly be identified from the table especially for the melting temperature. For maximum savings in annual heating loads, an optimal melting temperate of 22°C is found across all the latent heat cases. For maximum savings in annual cooling load, an optimal temperature of 23°C is found, a 1°C below the cooling setpoint. Determining the optimal melting range is perhaps difficult since no clear pattern can be found. Many PCM cases show a melting range of 2°C for maximum savings in annual heating loads. This conclusion can be summarized in **Figure 7.20**.

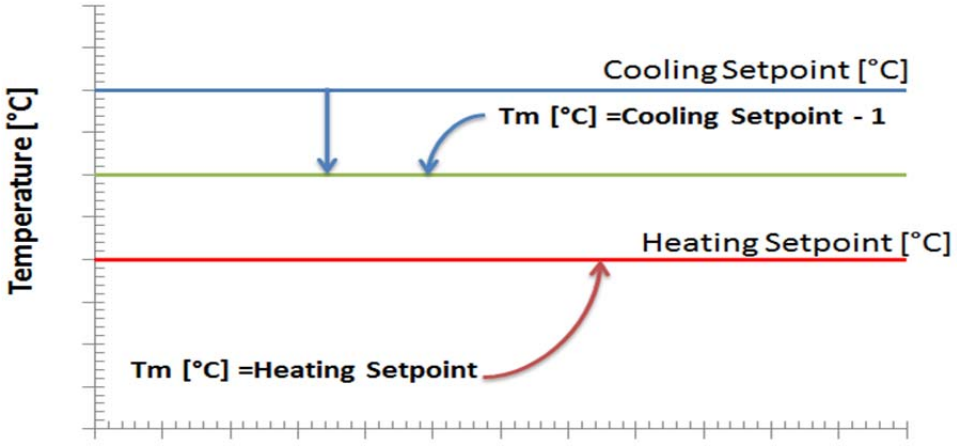

Figure 7.20 Optimal melting temperature of PCM for maximum savings in cooling and heating loads

7.8.3 Optimal PCM thermal properties under various setpoints

A pattern in optimal thermal properties of PCM was drawn for the base case under the environmental conditions specified by Building America benchmark. Therefore, another set of simulations were carried out to draw more general guidelines on optimal thermal properties of PCM (melting temperature and melting range) under different cooling and heating setpoints.

Table 7-9 lists the optimal PCM thermal properties across all the cases. The table shows that a pattern can be identified but no rigorous rule can be extracted for all setpoints.

Table 7-9 Optimal melting temperature and melting range across the latent heat under various heating and cooling setpoints

Optimal PCM thermal properties for maximum savings in annual heating loads

Heating: 22°C Cooling: 25°C

L [kJ/kg]	Tm [°C]	ΔTm [°C]	% Savings
50	21	0.1	1.06
100	21	0.1	1.42
150	21	0.1	1.61
200	22	2	1.87
250	22	2	2.05
300	22	2	2.21

Heating: 22°C Cooling: 26°C

L [kJ/kg]	Tm [°C]	ΔTm [°C]	% Savings
50	21	0.1	1.05
100	21	0.1	1.05
150	21	0.1	1.61
200	22	2	1.73
250	22	2	1.92
300	22	2	2.05

Heating: 21°C Cooling: 24°C

L [kJ/kg]	Tm [°C]	ΔTm [°C]	% Savings
50	20	0.1	1.17
100	21	1	1.56
150	21	0.1	1.86
200	21	2	2.15
250	21	2	2.37
300	21	2	2.54

Heating: 20°C Cooling: 24°C

L [kJ/kg]	Tm [°C]	ΔTm [°C]	% Savings
50	19	0.1	1.29
100	20	1	1.81
150	20	2	2.19
200	20	1	2.31
250	20	2	2.73
300	20	2	2.94

Optimal PCM thermal properties for maximum savings in annual cooling loads

Heating: 22°C Cooling: 25°C

L [kJ/kg]	Tm [°C]	ΔTm [°C]	% Savings
50	24	1	1.43
100	24	0.1	2.63
150	24	0.1	3.30
200	24	1	3.87
250	24	1	4.35
300	24	2	4.68

Heating: 22°C Cooling: 26°C

L [kJ/kg]	Tm [°C]	ΔTm [°C]	% Savings
50	26	0.1	1.44
100	26	1	2.19
150	26	1	2.82
200	25	1	3.38
250	25	2	3.94
300	25	2	4.38

Heating: 21°C Cooling: 24°C

L [kJ/kg]	Tm [°C]	ΔTm [°C]	% Savings
50	23	2.0	1.07
100	23	0.1	2.18
150	23	1	2.98
200	23	1	3.52
250	23	1	3.90
300	23	1	4.20

Heating: 20°C Cooling: 24°C

L [kJ/kg]	Tm [°C]	ΔTm [°C]	% Savings
50	24	0.1	0.89
100	23	0.1	1.79
150	23	1	2.37
200	23	1	2.84
250	23	1	3.15
300	23	1	3.42

L: latent heat, Tm: melting temperature, ΔTm: melting range

For maximum savings in annual heating loads and when the cooling setpoint is varied between 25 and 26°C (heating setpoint is fixed at 22°C), the optimal melting temperature is at the heating setpoint for the latent heat cases greater than 200kJ/kg. For the same cooling setpoints range above, an optimal melting temperature of 1°C below the heating setpoint is found for the latent heat cases lower than 200kJ/kg.

When the heating setpoint is varied between 20 and 21°C (cooling setpoint is fixed at 24°C), the optimal melting temperature is at heating setpoint for the latent heat cases greater than 100kJ/kg. For the same heating setpoints range, an optimal melting temperature of 1°C below the heating setpoint is found for latent heat case of 50kJ/kg.

For maximum savings in annual cooling loads and when the cooling setpoint is increased or the heating setpoint is decreased by 1°C, the optimal melting temperature is always 1°C below the cooling setpoint. When the cooling setpoint is increased by 2°C, the optimal melting temperature is at the cooling setpoint for latent heat cases of lower than 150 kJ/kg and 1°C below the cooling setpoint for latent heat cases greater than 200kJ/kg. The optimal melting temperature is 1°C below the setpoint for all the cases except the case of 50kJ/kg when the heating setpoint is lowered to 20°C (2°C below the heating setpoint).

In all considered cases, the melting range is different for each case. Although some pattern is obvious, it is concluded that no rigorous and universal rules can be deducted for optimal thermal properties when the heating and cooling setpoints are varied outside the base case conditions. This means that a case by case should be considered when the setpoitns differ from those in the reference building.

7.9 Thermal performance of PCM under four US representative climates

This section provides insights on the thermal performance of PCM under various US climates. For this analysis and based on the US climatic zone shown in **Figure 7.21**, three additional cities representing other climatic zones are selected; Phoenix (Climate Zone-2), Atlanta (Climate Zone-3), and Seattle (Climate Zone-4) as shown in **Table 7-10**.

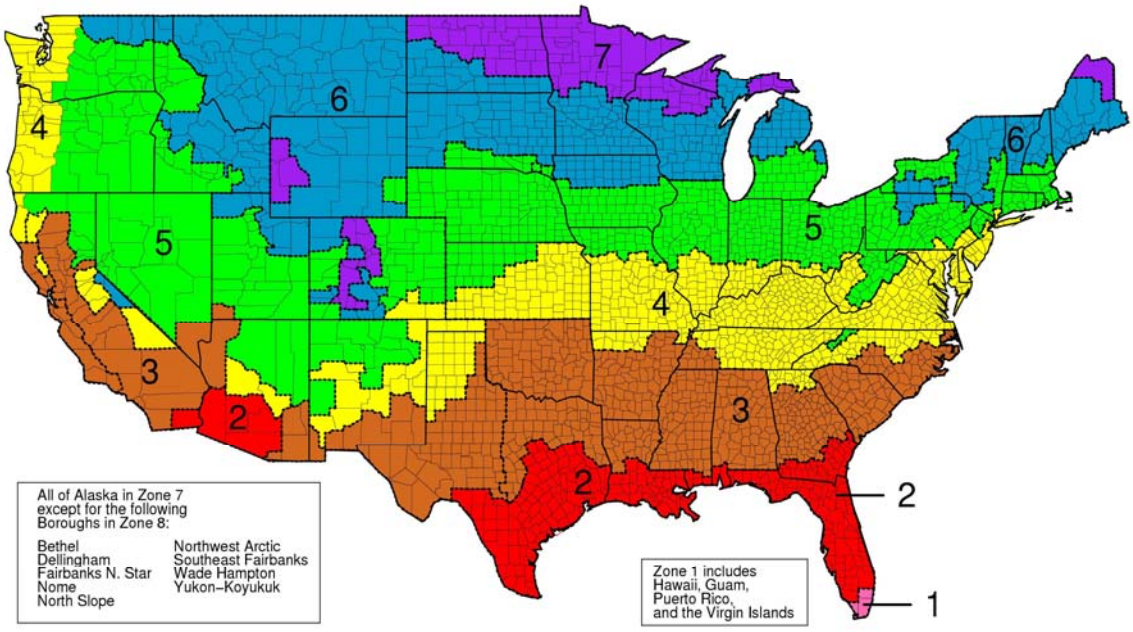

Figure 7.21 USA Climate Zones in ASHRAE Standard 90.1-2004 [304]

The number of cooling degree-days (CDD) on the base of 65°F (18.3°C) is three times different between Phoenix, Atlanta, Golden and Seattle. For heating degree-days (HDD), the difference is 1.5 times between Golden, Seattle and Atlanta. The heating is not dominant in Phoenix. The results of the base case under the four climates are shown in **Table 7-11**.

Table 7-10 House base case according to Building America benchmark 2010 for different climates

	Climate Zone-2		Climate Zone-3		Climate Zone-4		Climate Zone-5	
	Phoenix, AZ		Atlanta, GA		Seattle, WA		Golden, CO	
	HDD65F	CDD65F	HDD65F	CDD65F	HDD65F	CDD65F	HDD65F	CDD65F
	977.4	4789.8	2714.4	1830.6	4224.6	181.8	6008.4	595.8
Parameter								
Wall insulation R-value								
Wood assembly	13		13		13		13	
Insulating sheathing							5	
Ceiling Insulation R-value	30		30		38		38	
Slab on grade R-value	0		0		10		10	
Solar absorptivity								
Roof	0.9		0.9		0.9		0.9	
Wall	0.6		0.6		0.6		0.6	
Window								
WWR [%]	15		15		15		15	
U-value [Btu/hr-F-ft²]	0.4		0.4		0.35		0.35	
SHGC [-]	0.3		0.3		0.35		0.35	

Table 7-11 Annual loads for the base case house for the four US climates

City	Annual Cooling Load [kWh]	Annual Heating Load [kWh]	Peak Cooling Load [kW]*	Peak Heating Load [kW]*
Phoenix, AZ	25170	143	8.14	1.71
Atlanta, GA	5341	6468	4.59	7.37
Seattle, WA	1044	8329	3.16	4.59
Golden, CO	2595	10130	3.50	8.49

Notes: * Peak loads are based on TMY3 weather file

7.9.1 **Simulation of a medium latent heat case of 200kJ/kg**

All walls in the base case house are placed with PCM to the interior side. Many researches including this one found that the best PCM location is when it is placed into direct contact with indoor environment [305-309].

Figure 7.22 shows the results of the medium case of 200kJ/kg with different melting temperatures and melting range under the four representative US climates. The first observation from the figure is that all the cases have a similar trend of optimal melting temperatures and its melting range. For maximum savings in annual cooling loads, the optimal melting temperature is a degree below the cooling setpoint of 24°C. For maximum savings in heating loads, the optimal melting temperature is at the heating setpoint of 22°C. The PCM layer performs better when the melting range is between 0.1-1°C for maximum savings in annual cooling loads. For maximum savings in heating loads, a wide melting range of 2°C should be selected.

For this latent heat case, the maximum savings percentage in cooling loads are achieved in Seattle (12%), Golden (6%), Atlanta (2.5%) and finally Phoenix (0.6%). Since the annual cooling load of the base case of some cities such as Seattle is low, the savings is high. The cities with high cooling load such as Phoenix achieve small relative savings in annual cooling load. The same applies for the relative savings in annual heating loads. Cities with low heating loads achieve maximum savings. The percentage savings in annual heating loads for the three cities; Golden, Atlanta and Seattle ranges from 2.5% to 3.5%. Since it is relative to the base load, the percentage savings is sometimes misleading. This will be further analyzed for extreme two cases in the sections below.

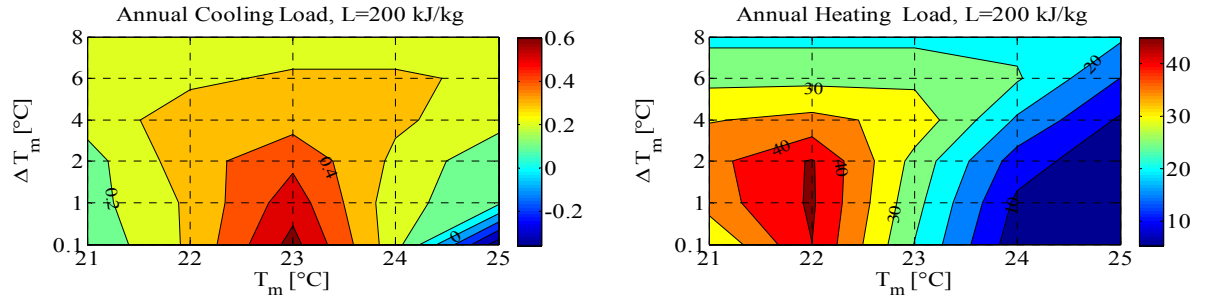

a) Percentage savings in annual loads for Phoenix, AZ

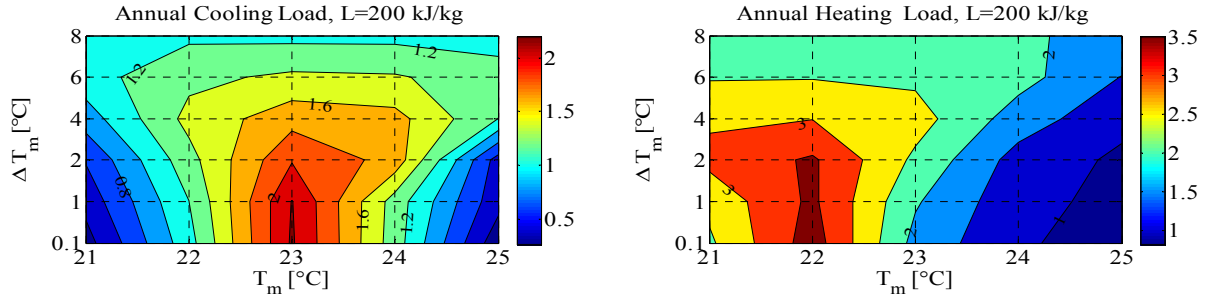

b) Percentage savings in annual loads for Atlanta, GA

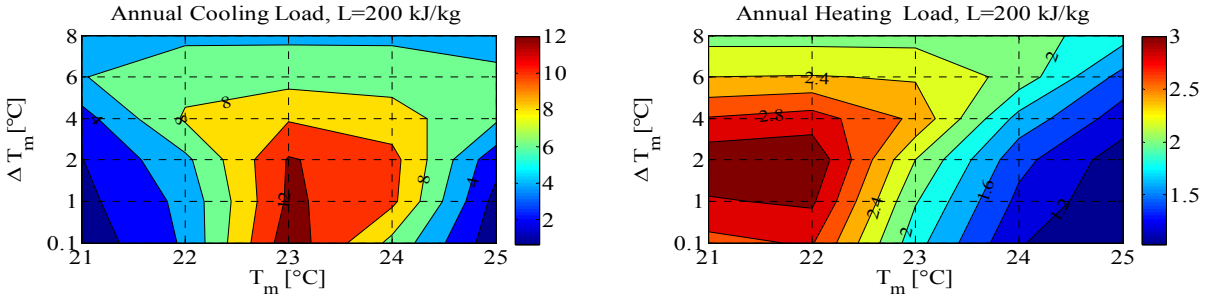

c) Percentage savings in annual loads for Seattle, WA

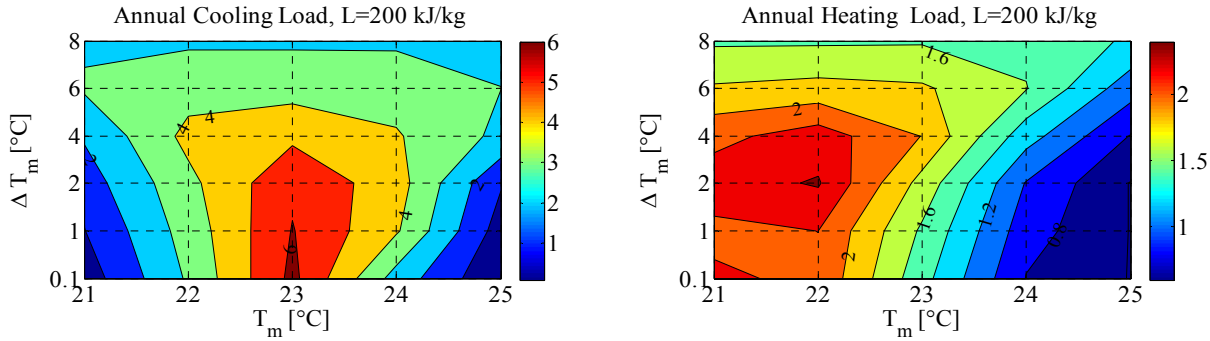

d) Percentage savings in annual loads for Golden, CO

Figure 7.22 Percentage reductions in annual loads due to PCM of various properties under four US climates

7.9.2 Simulation of latent heat cases of 50-300kJ/kg

Other cases of latent heat are also simulated to achieve two objectives; 1) to identify the optimal melting temperature and melting range across the different latent heat cases for different climates, 2) to develop design correlations. Based on simulation of the medium case, other latent heat cases of 50-300kJ/kg with melting temperature between 18-27°C and a melting range between 0.1-8°C are simulated for different climates. For Phoenix climate, the melting temperature was varied from 19-28°C to capture the effect of hot climate. The relative savings in annual and peak loads are used for this analysis. Contour plots showing the reductions in annual and peak loads for the four climates across the PCM thermal properties are provided in **Appendix E**.

Generally speaking, the optimal melting temperature for maximum savings in annual heating loads is at the heating setpoint of 22°C as shown in **Figure 7.23**. There are cases where the optimal melting temperature is 1°C below the heating setpoint especially in Phoenix (a case of 50 kJ/kg) and in Seattle (cases of 50 and 100 kJ/kg). Across the four climates, the maximum savings in annual cooling loads occur at an optimal melting temperature of 23°C (1°C below the cooling setpoint of 24°C). It is observed that finding an optimal melting range is also challenging. For many climates to achieve maximum savings in heating loads, a wide melting range temperature of 2°C is necessary. Atlanta is an exception where the maximum savings in annual heating loads occur with melting range of 0.1°C. Together with proper melting temperature, a tight melting range of 0.1°C will achieve maximum savings in annual cooling load. However, Golden climate favors a melting range between 1-2°C depending on the latent heat.

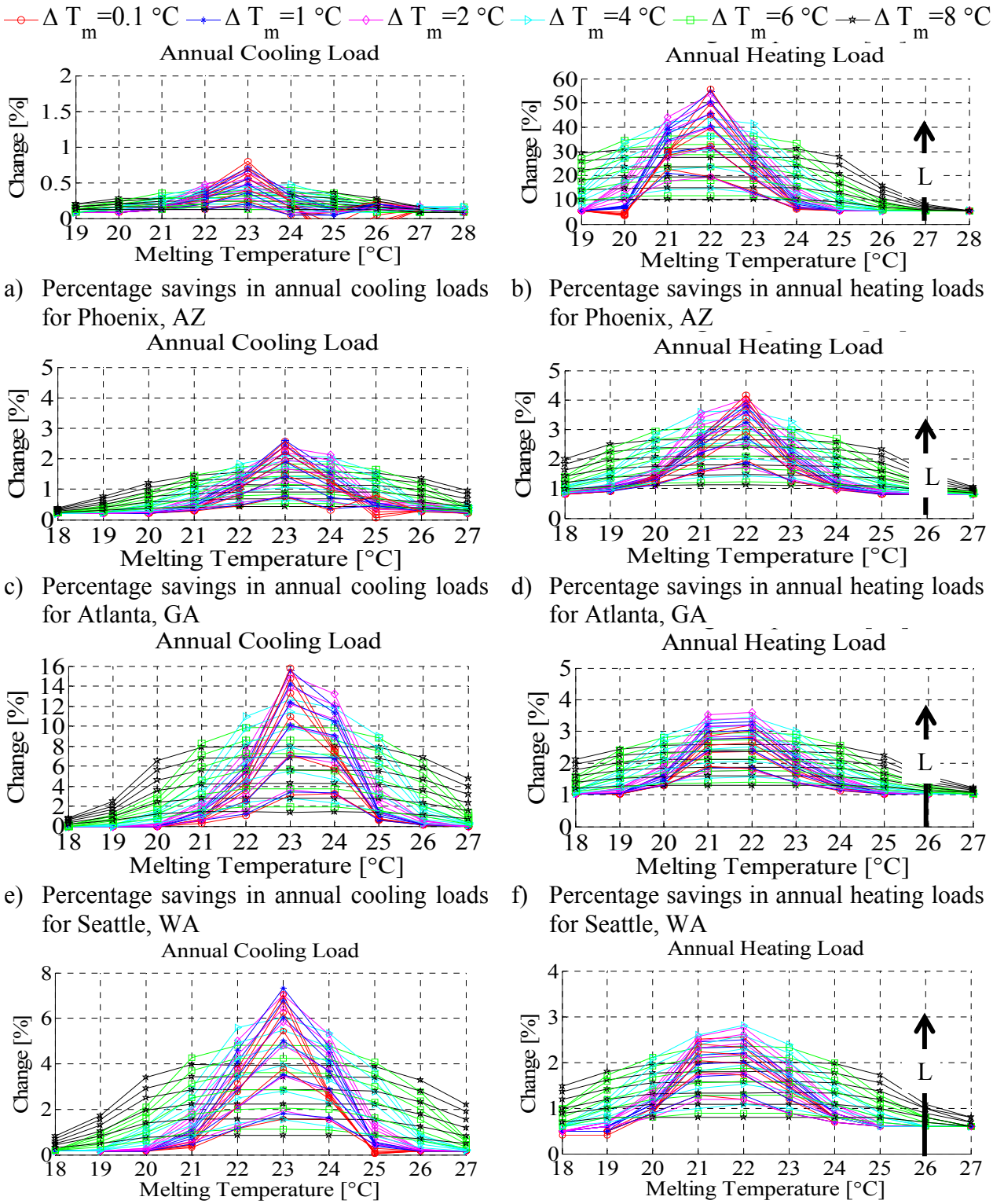

a) Percentage savings in annual cooling loads for Phoenix, AZ

b) Percentage savings in annual heating loads for Phoenix, AZ

c) Percentage savings in annual cooling loads for Atlanta, GA

d) Percentage savings in annual heating loads for Atlanta, GA

e) Percentage savings in annual cooling loads for Seattle, WA

f) Percentage savings in annual heating loads for Seattle, WA

g) Percentage savings in annual cooling loads for Golden, CO

h) Percentage savings in annual heating loads for Golden, CO

Figure 7.23 Percentage savings in annual loads across all parameters for the four US cities

From the simulation results, the optimal PCM thermal properties are summarized for maximum savings in annual heating and cooling loads as listed in **Table 7-12**. The maximum reductions in annual cooling load at the high latent heat case of 300kJ/kg are 0.8%, 2.6%, 7.3%, and 15.8% for Phoenix, Atlanta, Golden, and Seattle, respectively. For the low latent heat case of 50kJ/kg, the maximum reductions are 0.24%, 0.8%, 1.54%, and 3.6% for Phoenix, Atlanta, Golden and Seattle, respectively. On the other hand, the maximum reductions in annual heating load at the high latent heat case of 300kJ/kg are 55.8%, 4.2%, 3.6%, and 2.8% for Phoenix, Atlanta, Seattle, and Golden, respectively. The maximum reductions in annual heating load for the low latent heat case of 50kJ/kg are 22.6%, 2%, 1.9%, and 1.3% for Phoenix, Atlanta, Seattle, and Golden, respectively.

In addition to annual load, peak load is another performance indicator that is of a particular interest when thermal storage is utilized in buildings. **Figure 7.24** shows the percentage reductions in both peak cooling and heating loads for the four US cities. The optimal melting temperature for maximum reductions in peak cooling load occurs at a degree higher than the cooling setpoint of 24°C for the climates of Atlanta, Golden and Seattle, but a two degree above the cooling setpoint is observed for the hot climate of Phoenix as shown in **Figure 7.24** (a), (c), (e), and (g). However, there are some exceptional extreme cases that show different optimal melting temperature than the generalized trend. For example, the case of 300kJ/kg under Seattle climate shows an optimal temperature of 24°C and the case of 50kJ/kg shows an optimal temperature of 26°C and 27°C for Atlanta and Phoenix respectively.

Table 7-12 Optimal melting temperature and melting range across the latent heat for maximum annual loads for the four US climates under the base setpoints

Optimal PCM thermal properties for maximum savings in annual heating loads

Phoenix, AZ

L [kJ/kg]	Tm [°C]	ΔTm [°C]	% Savings
50	21	0.1	22.59
100	22	0.1	32.09
150	22	1	40.25
200	22	1	45.73
250	22	1	50.21
300	22	0.1	55.82

Atlanta, GA

L [kJ/kg]	Tm [°C]	ΔTm [°C]	% Savings
50	22	0.1	1.95
100	22	0.1	2.92
150	22	0.1	3.40
200	22	0.1	3.76
250	22	0.1	4.02
300	22	0.1	4.17

Seattle, WA

L [kJ/kg]	Tm [°C]	ΔTm [°C]	% Savings
50	21	0.1	1.88
100	21	1	2.41
150	22	2	2.85
200	22	2	3.17
250	22	2	3.41
300	22	2	3.59

Golden, CO

L [kJ/kg]	Tm [°C]	ΔTm [°C]	% Savings
50	22	1	1.28
100	22	2	1.78
150	22	2	2.15
200	22	2	2.42
250	22	2	2.62
300	22	4	2.80

Optimal PCM thermal properties for maximum savings in annual cooling loads

Phoenix, AZ

L [kJ/kg]	Tm [°C]	ΔTm [°C]	% Savings
50	23	0.1	0.24
100	23	0.1	0.36
150	23	0.1	0.56
200	23	0.1	0.64
250	23	0.1	0.72
300	23	0.1	0.79

Atlanta, GA

L [kJ/kg]	Tm [°C]	ΔTm [°C]	% Savings
50	23	1	0.79
100	23	0.1	1.46
150	23	0.1	1.93
200	23	0.1	2.23
250	23	0.1	2.43
300	23	1	2.60

Seattle, WA

L [kJ/kg]	Tm [°C]	ΔTm [°C]	% Savings
50	23	2	3.64
100	23	0.1	7.14
150	23	0.1	10.94
200	23	0.1	13.29
250	23	0.1	14.76
300	23	0.1	15.80

Golden, CO

L [kJ/kg]	Tm [°C]	ΔTm [°C]	% Savings
50	23	2	1.54
100	23	0.1	3.78
150	23	0.1	5.43
200	23	2	5.82
250	23	1	6.78
300	23	1	7.32

L: latent heat, Tm: melting temperature, ΔTm: melting range

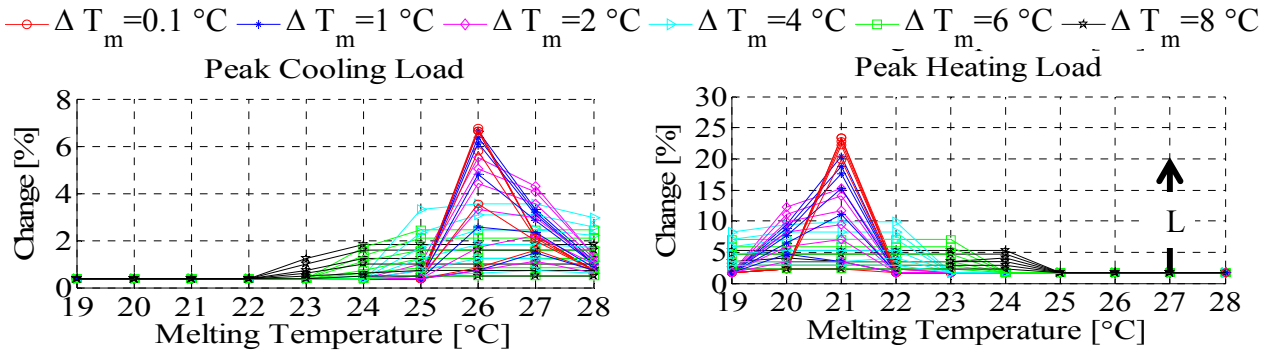

a) Percentage savings in peak cooling loads for Phoenix, AZ

b) Percentage savings in peak heating loads for Phoenix, AZ

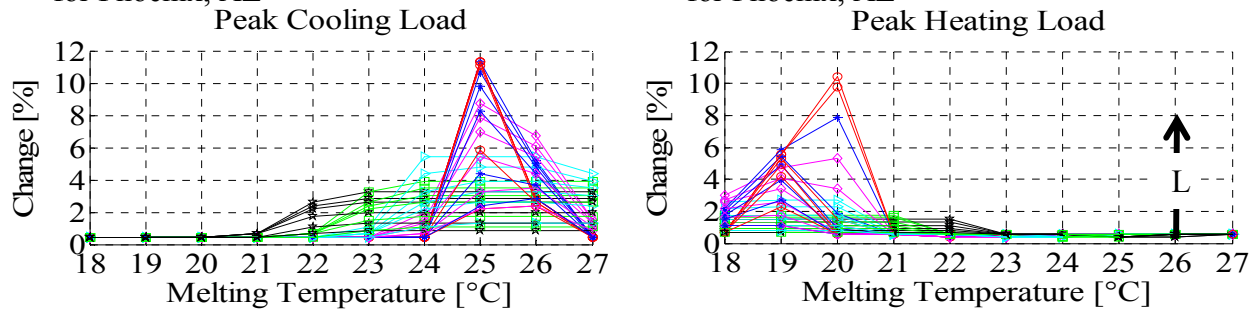

c) Percentage savings in peak cooling loads for Atlanta, GA

d) Percentage savings in peak heating loads for Atlanta, GA

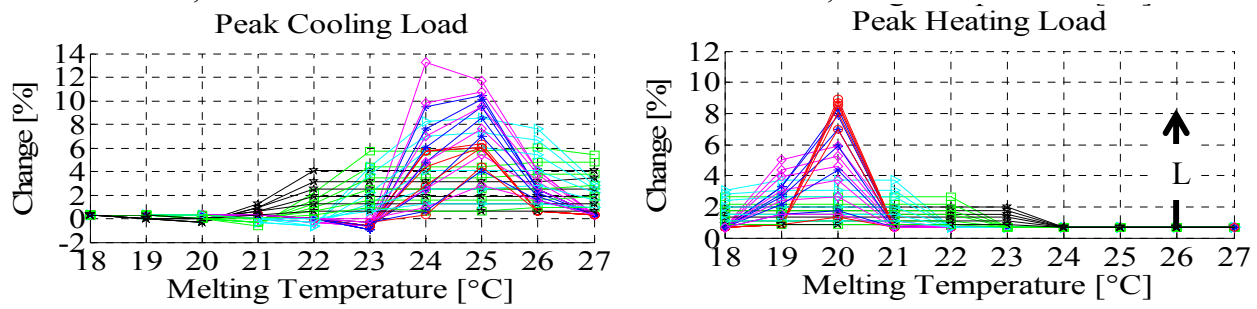

e) Percentage savings in peak cooling loads for Seattle, WA

f) Percentage savings in peak heating loads for Seattle, WA

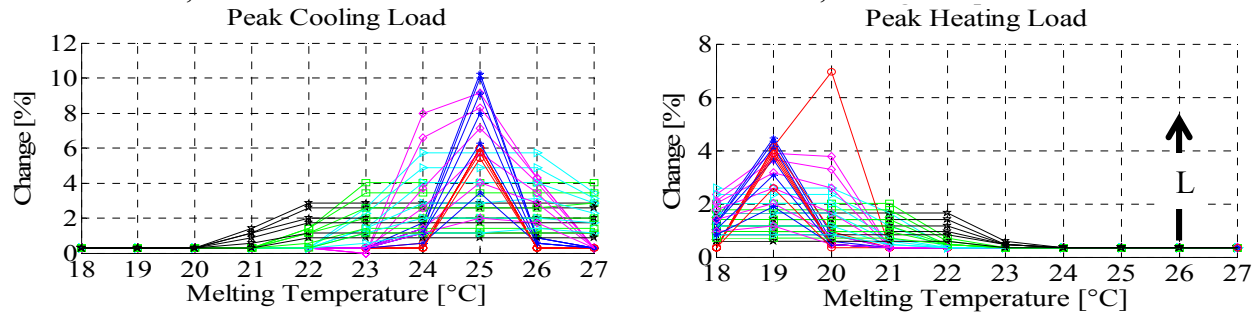

g) Percentage savings in peak cooling loads for Golden, CO

h) Percentage savings in peak heating loads for Golden, CO

Figure 7.24 Percentage savings in peak loads across all parameters for the four US cities

For Atlanta and Phoenix, a melting range of 0.1-1°C is preferable compared to a melting range of 0.1-2°C for Golden and Seattle climates. The maximum reductions in peak cooling load at the high latent heat case of 300kJ/kg are 6.8%, 10.3%, 11.3%, and 13.3% for Phoenix, Golden, Atlanta, and Seattle respectively. The maximum reductions in peak cooling load at the low latent heat case of 50kJ/kg are 1.6%, 2.8%, 4.4%, and 5.4% for Phoenix, Atlanta, Seattle and Golden respectively. Both cases represent the extreme high and low savings for latent heat cases at optimal melting temperature and melting range as summarized in **Table 7-13**.

On the other hand, the optimal melting temperature for maximum reductions in peak heating load occurs at 20-21°C for Phoenix as depicted in **Figure 7.24** (b). The other three climates favor a degree lower melting temperature than Phoenix (i.e., 19-20°C) as clear from **Figure 7.24** (d), (f), and (h). The maximum reductions in peak heating load at the high latent heat case of 300kJ/kg are 7%, 9%, 10.5%, and 23% for Golden, Seattle, Atlanta and Phoenix respectively. The maximum reductions in peak heating load at the low latent heat case of 50kJ/kg are 1.7%, 2.3%, 2.6%, and 4.7% for Seattle, Atlanta, Golden, and Phoenix respectively. The results are summarized in **Table 7-13**.

For all climates, there is no additional benefit of installing PCM with latent heat greater than 150 kJ/kg. Beyond this value, there are no significant reductions in both peak heating and cooling loads.

Table 7-13 Optimal melting temperature and melting range for maximum savings in peak loads across the latent heat for the four US climates under the base setpoints

Optimal PCM thermal properties for maximum savings in peak heating loads

Phoenix, AZ

L [kJ/kg]	Tm [°C]	ΔTm [°C]	% Savings
50	20	1	4.68
100	21	0.1	19.88
150	21	0.1	22.22
200	21	0.1	22.81
250	21	0.1	23.39
300	21	0.1	23.39

Atlanta, GA

L [kJ/kg]	Tm [°C]	ΔTm [°C]	% Savings
50	19	0.1	2.31
100	19	0.1	4.21
150	19	0.1	4.88
200	19	0.1	5.29
250	20	0.1	9.77
300	20	0.1	10.45

Seattle, WA

L [kJ/kg]	Tm [°C]	ΔTm [°C]	% Savings
50	20	1	1.74
100	20	0.1	6.97
150	20	0.1	8.06
200	20	0.1	8.50
250	20	0.1	8.71
300	20	0.1	8.93

Golden, CO

L [kJ/kg]	Tm [°C]	ΔTm [°C]	% Savings
50	19	0.1	2.59
100	19	0.1	3.77
150	19	0.1	3.89
200	19	1	4.12
250	19	1	4.36
300	20	0.1	6.95

Optimal PCM thermal properties for maximum savings in peak cooling loads

Phoenix, AZ

L [kJ/kg]	Tm [°C]	ΔTm [°C]	% Savings
50	27	0.1	1.60
100	26	0.1	3.56
150	26	0.1	5.77
200	26	0.1-1	6.63
250	26	0.1-1	6.63
300	26	0.1-1	6.76

Atlanta, GA

L [kJ/kg]	Tm [°C]	ΔTm [°C]	% Savings
50	26	1	2.83
100	25	0.1	5.88
150	25	0.1	11.11
200	25	0.1	11.33
250	25	0.1	11.33
300	25	0.1-1	11.33

Seattle, WA

L [kJ/kg]	Tm [°C]	ΔTm [°C]	% Savings
50	25	0.1	4.43
100	25	1	6.96
150	25	1	8.54
200	25	1-2.	9.49
250	25	2	10.76
300	24	2	13.29

Golden, CO

L [kJ/kg]	Tm [°C]	ΔTm [°C]	% Savings
50	25	0.1	5.43
100	25	1	6.29
150	25	1	8.00
200	25	1	9.14
250	25	1	10.00
300	25	1	10.29

L: latent heat, Tm: melting temperature, ΔTm: melting range

7.9.3 **Analysis of extreme PCM cases**

This section provides technical and economic insights on two extreme PCM cases; 1) a latent heat case of 300kJ/kg which provides maximum savings in annual heating and cooling load and 2) the case of 50kJ/kg which provides minimum savings in annual heating and cooling load. All other PCM intermediate cases perform between these two extremes. The results are based on the optimal PCM properties for each case as presented earlier in **Table 7-12**. **Table 7-14** lists the results of the base no-PCM case and the two extreme optimized cases.

Table 7-14 Annual loads for the two extreme cases in four US cities

	Base Case (no PCM)	PCM Case of 50 kJ/kg	PCM Case of 300 kJ/kg	Savings for PCM Case of 50 kJ/kg*	Savings for PCM Case of 300 kJ/kg**
Annual Heating Loads [kWh]					
Phoenix	143.4	111	63.35	32.4	80.05
Atlanta	6468	6342	6198	126	270
Seattle	8329	8172	8030	157	299
Golden	10130	10000	9846	130	284
Annual Cooling Loads [kWh]					
Phoenix	25170	25110	24970	60	200
Atlanta	5341	5299	5202	42	139
Seattle	1044	1006	879.1	38	164.9
Golden	2595	2545	2405	50	190

Notes:
*: minimum savings case, **: maximum savings case

According to **Table 7-14**, the results can be manipulated using different measures. Percentage of savings, a normalized savings per floor area and energy cost are three measures that can provide more information on the thermal performance of PCM. The energy cost is determined using a nominal fixed COP of 3.28 for the air conditioning system (~ EER=11.2) and a furnace efficiency of 0.78 based on Building America benchmark [280]. Therefore, the savings in annual heating and cooling loads are divided by these values to get the total electrical and gas

energy consumption. The electrical and gas cost are assumed to be fixed and based on US Energy Information Administration (EIA) database [310, 311].

Table 7-15 Energy cost for the four US cities

City	Electricity cost [$/kWh]*	Gas cost [$/ft^3]**	Gas cost [$/kWh]
Phoenix, AZ	0.1184	0.01575	0.05431
Atlanta, GA	0.1142	0.01623	0.055966
Seattle, WA	0.0867	0.01187	0.040931
Golden, CO	0.1193	0.00831	0.028655

Notes: * EIA database for electrical cost [310], ** EIA database for gas cost [311]

Figure 7.25 illustrates the three indicators for evaluating the PCM thermal performance in the four cities. This figure clearly shows that the percentage savings may be a decisive indicator for climates that have small or large cooling or heating loads. The absolute savings and energy cost can be complementary indicators and give more insights. For example in Phoenix, the percentage savings in annual heating load varies from 23-56% but the corresponding absolute values are 0.19 kWh/m^2 and 0.48kWh/m^2. In Seattle, the absolute savings ranges from 0.94-1.79 kWh/m^2 which only represents 1.9 to 3.6% savings. The reverse happens when cooling load is evaluated for these particular two cities. It is also observed that PCM performs better in Seattle than in Golden despite the high heating degree days in Golden. According to the IECC code (refer to **Table 7-10**), Colorado climate should have an extra insulation level at exterior side which is not mandated for Seattle climate.

In order to evaluate the significant of the savings, energy cost is a necessary indicator. **Figure 7.25** (e) and (f) shows the energy cost of heating and cooling. The annual total energy cost savings for Phoenix ranges between 4.5-$13, Atlanta between 11-$24, Seattle 9-$20 and Golden 6.5-$17. This saving is not significant when compared to the current cost of PCM.

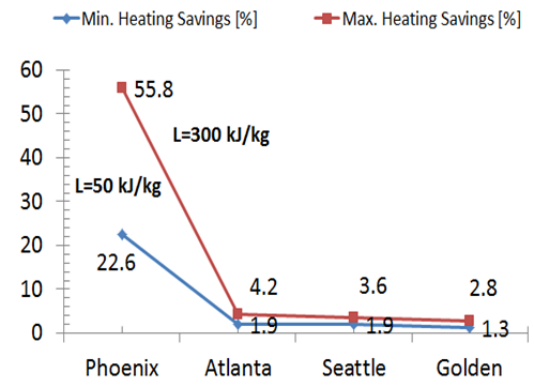

a) Percentage savings in annual heating load

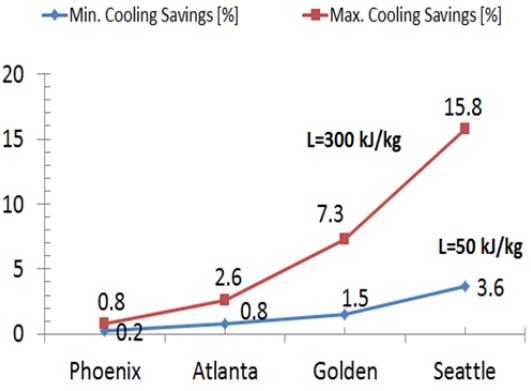

b) Percentage savings in annual cooling load

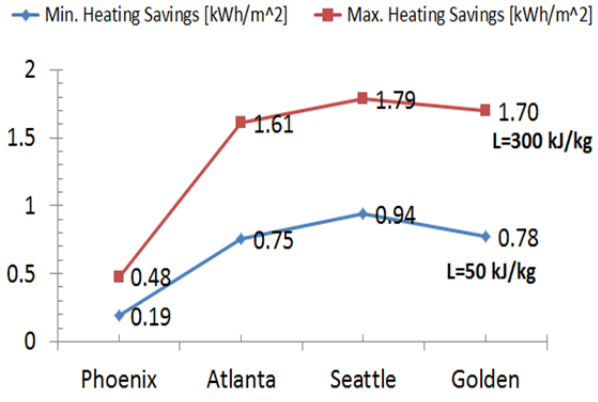

c) Normalized savings in annual heating load per floor area

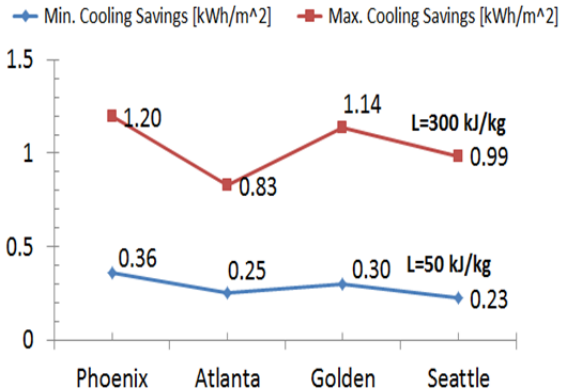

d) Normalized savings in annual cooling load per floor area

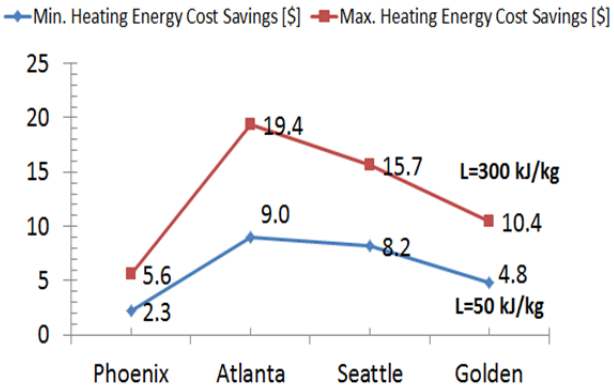

e) Heating energy cost savings

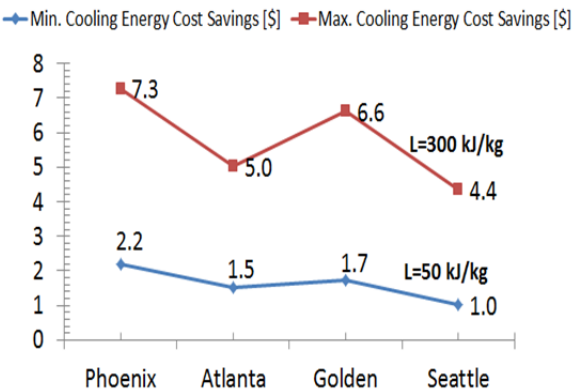

f) Cooling energy cost savings

Figure 7.25 Performance measures for PCM under four US climates for the extreme optimized cases

7.9.4 Simple payback period for the extreme PCM cases

It is apparent that the energy cost savings from PCM is not significant. However, a simplified payback period can be used to further quantify the economic feasibility of PCM in different climates. The PCM market in USA is still immature and therefore getting a price for PCM is challenging. One manufacturer provides the retail price of one of its product line [272, 312]. The information is used to approximate the price of the extreme two cases as illustrated in **Table 7-16**.

Table 7-16 Capital cost of PCM [272, 312]

	Mass per area [kg/m^2]	Thickness [m]	Latent heat [kJ/kg]	Retail price of PCM [$/ft^2]	Normalized Cost [$/ft^2/kJ/kg]	Total cost for the house [$]**
50 kJ/kg Case	2.734	0.0125	50	1.25	0.02503	1418
23QFGM51*	2.734	0.0125	200	4.86	0.02503	
300 kJ/kg Case	2.734	0.0125	300	7.50	0.02503	8505

*used as a base to determine the cost of other cases
**Wall areas=105.216 m^2

The payback period is simply calculated by dividing the total cost of PCM product by the total annual energy cost savings. **Figure 7.26** shows the simple payback period for the four climates and the two extreme optimized cases. It is clear enough that none of the optimized cases is economically feasible when simple payback period is used.

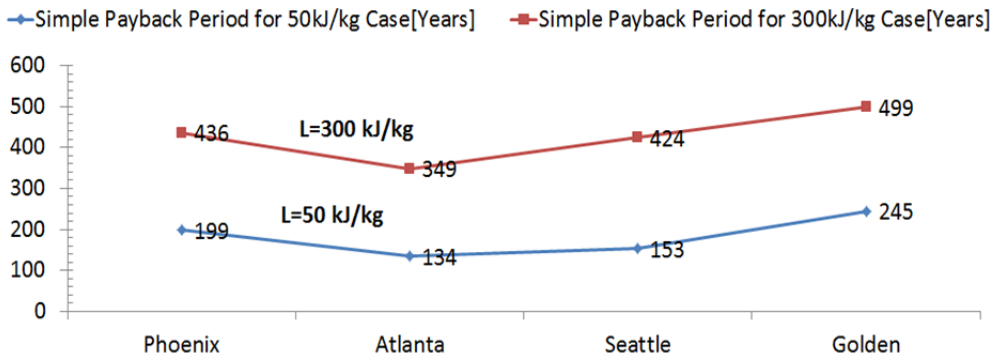

Figure 7.26 Simple payback period for using PCM under different climates

It is perhaps important to determine the desirable PCM capital cost to make it feasible. If a 5 years payback period is selected, then the capital PCM cost should be reduced or even eliminated as illustrated in **Figure 7.27**. Under passive natural means, PCM is not economically attractive. However, PCM should be complemented with other passive strategies to charge and discharge the heat. This will probably enhance the PCM performance and subsequently feasible for use.

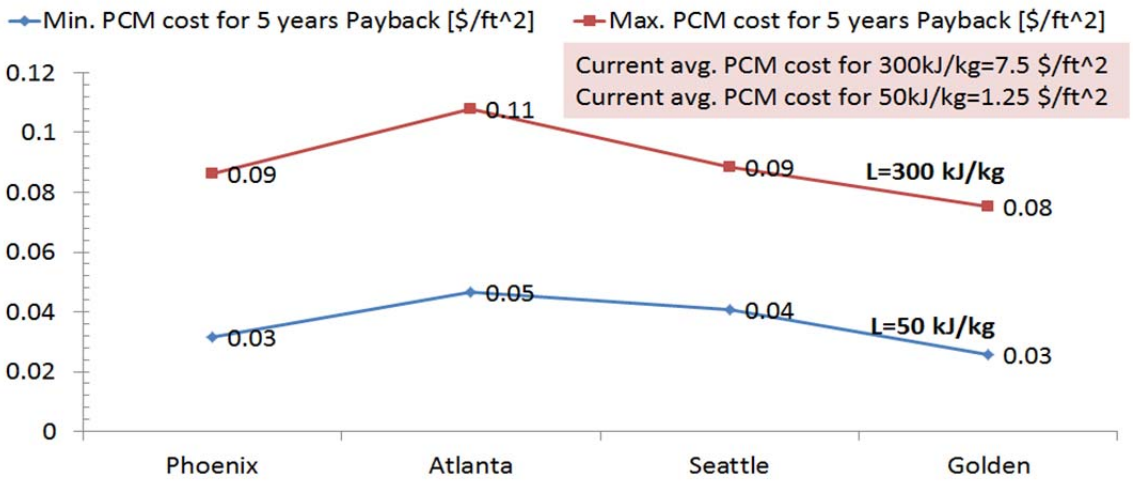

Figure 7.27 Desirable PCM's cost for a simple payback period of 5 years

7.10 Development of design guidelines for PCM-enhanced walls

Using the results from the set of simulations, design correlations have been developed for the residential building under the four representative US climates as depicted in **Figure 7.28**. Maximum savings in annual heating and cooling loads occur at different optimal PCM thermal properties. Therefore, two regression curves have been developed, one for maximum savings in annual heating loads and another for maximum savings in annual cooling loads. The correlations

are initially tested with linear relationship. If R^2 is low, then a polynomial of a second order is tried. The followings are the assumptions and conditions for using these guidelines:

1) The correlations are developed using a residential house described in Building America Benchmark [279, 280].
2) The PCM layer is placed in direct contact with the indoor environment and therefore to the interior side of the wall and in all orientations equally.
3) The correlations are based on the following PCM thermal properties:
    a) Optimal melting Temperature between 21-22°C and optimal melting range between 0.1-2°C for maximum savings in annual heating loads (with the exception of one extreme case of 300kJ/kg for Golden climate which has an optimal melting range of 4°C, refer to **Table 7-12** for further details).
    b) Optimal melting Temperature of 23°C and optimal melting range between 0.1-2°C for maximum savings in annual cooling loads.
    c) The latent heat of PCM ranges from 50-300 kJ/kg.

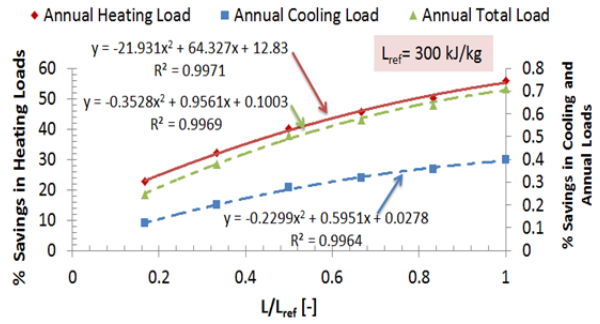

a) Correlations for maximum savings in annual heating loads, Phoenix

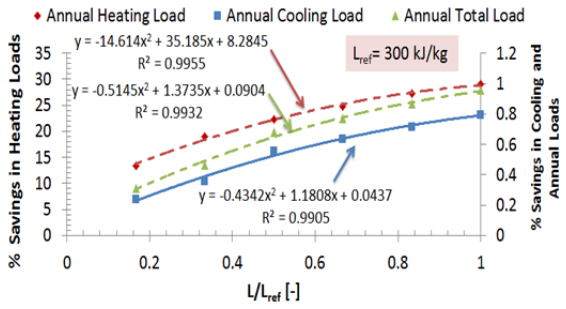

b) Correlations for maximum savings in annual cooling loads, Phoenix

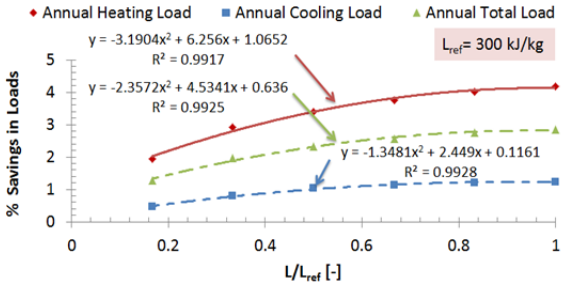

c) Correlations for maximum savings in annual heating loads, Atlanta

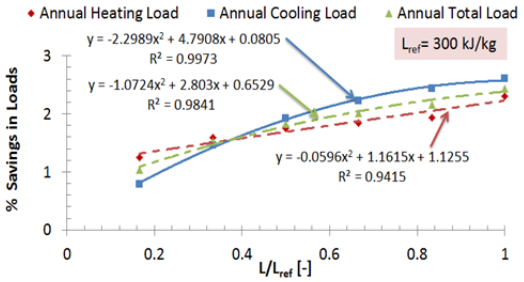

d) Correlations for maximum savings in annual cooling loads, Atlanta

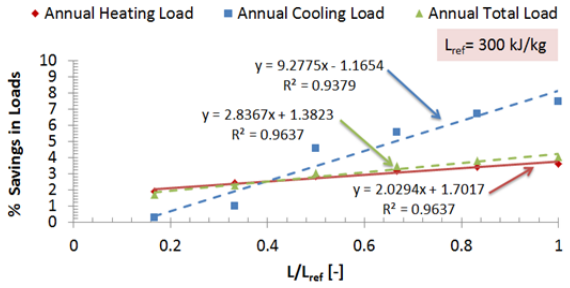

e) Correlations for maximum savings in annual heating loads, Seattle

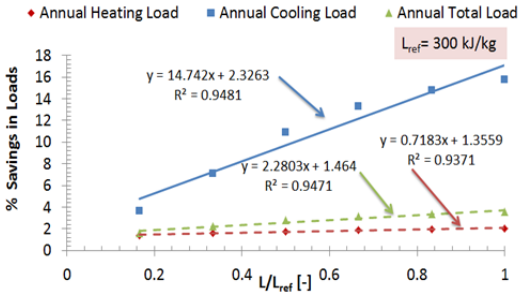

f) Correlations for maximum savings in annual cooling loads, Seattle

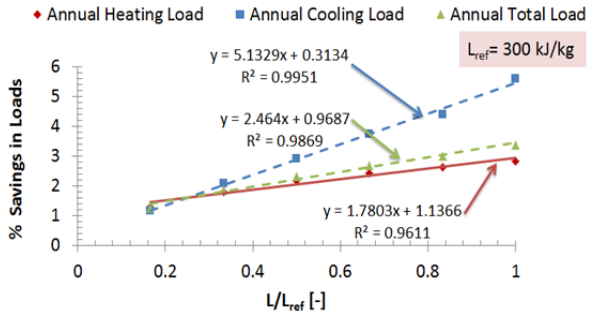

g) Correlations for maximum savings in annual heating loads, Golden

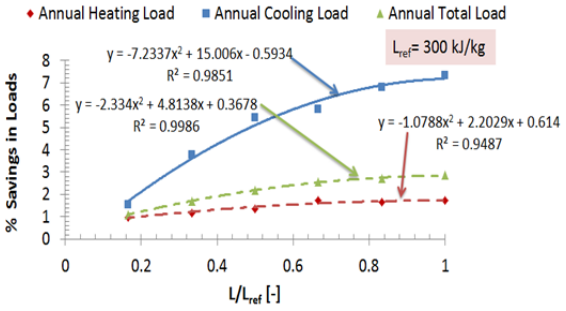

h) Correlations for maximum savings in annual cooling loads, Golden

Figure 7.28 Design correlations for the reference case under optimal PCM thermal properties for four US climates

7.11 Generic Solutions for improved PCM performance

Phase change materials can be integrated into either passive or active building's systems. Passive systems perform their intended function using explicit inherited properties with no or negligible external aid. On the other hand, active systems are those associated with using mechanical, electrical and electronic equipment to perform their intended function.

One of the simplest and easiest solutions is when PCM incorporated into drop ceiling of a zone. A Bio-based PCM panels have been proposed for installation in a drop ceiling of a new naturally ventilated office space at the University of Washington, Molecular Engineering and Sciences building, in Seattle as shown in **Figure 7.29** [313]. Hybrid (automatically or manually) controlled windows are installed to discharge the PCM when outside air is favorable.

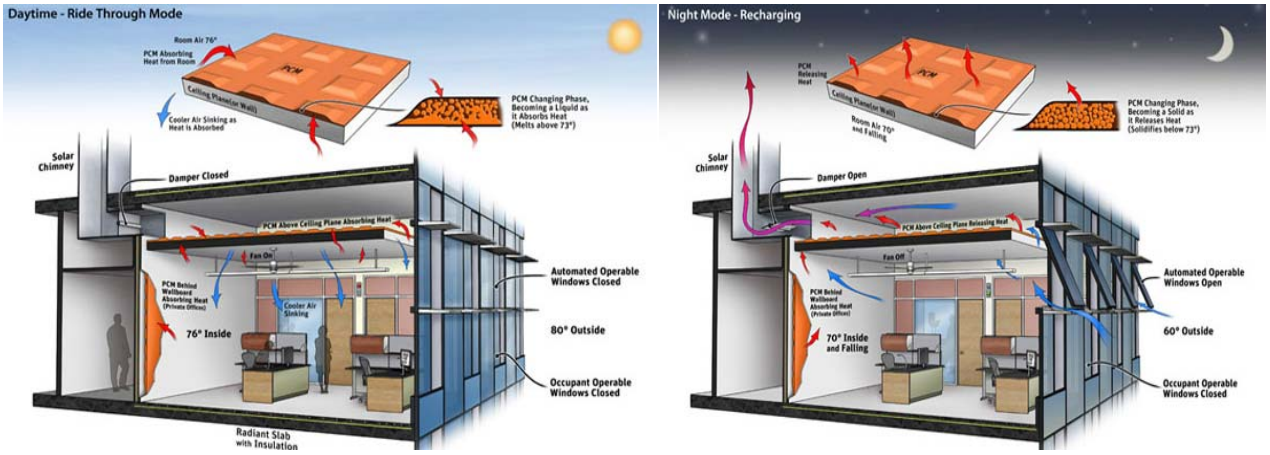

a) Charging PCM by zonal load in a summer day

b) Discharging PCM using outside cooled air in a summer night

Figure 7.29 Thermal activation of PCM-enhanced using passive strategies [313]

An example of a PCM ceiling design integrated with active system is shown in **Figure 7.30** [314]. This design concept is mainly useful for peak shavings. During the day, return hot air is circulated into the drop ceiling during its journey back to air handling unit, allowing the PCM

to charge. When energy is cheap, the PCM ceiling boards are discharged using mechanical air conditioning.

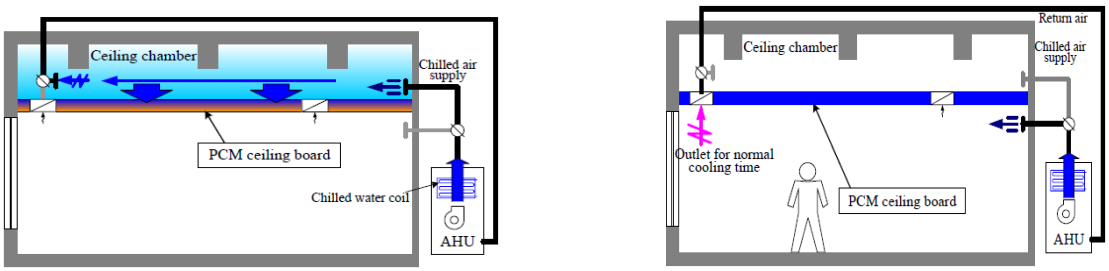

a) Discharging the PCM using mechanical AC b) Normal cooling time

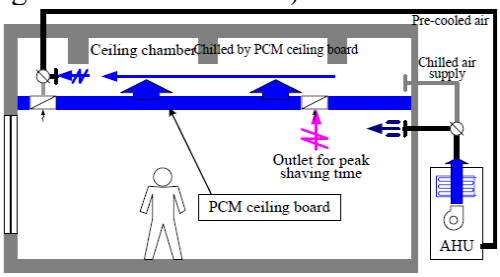

c) Charging the PCM with returned hot air through drop ceiling

Figure 7.30 Thermal activation of PCM-enhanced ceiling using active system [314]

PCM can be embedded into floor systems as shown in **Figure 7.31** [315]. The PCM-enhanced concrete floor is charged by the direct exposure to the solar radiation during the day. During the night, the PCM is then naturally discharged to meet the heating demand.

a) Charging the PCM-enhanced floor during the day using passive solar

b) Discharging the PCM during the nigh times

c) PCM-enhanced hollow core floor

Figure 7.31 Activation of PCM-enhanced hollow core floor using passive strategies [315]

The most common integration approaches for PCM in buildings is when installed in wall systems. In addition to PCM-enhanced multilayer wall, PCM can be integrated into ventilated cavity walls as shown in **Figure 7.32**. PCM can be utilized in south wall for solar collection and consequently discharged when heat demand is required. Different designs, operational strategies and controlled mechanism can be used to passively or actively charge and discharge the PCM. Air is commonly used as a heat transfer medium but embedded pipes can be integrated into the PCM-enhanced wall. Using the embedded pipes, water can be utilized to quickly charge and discharge the PCM.

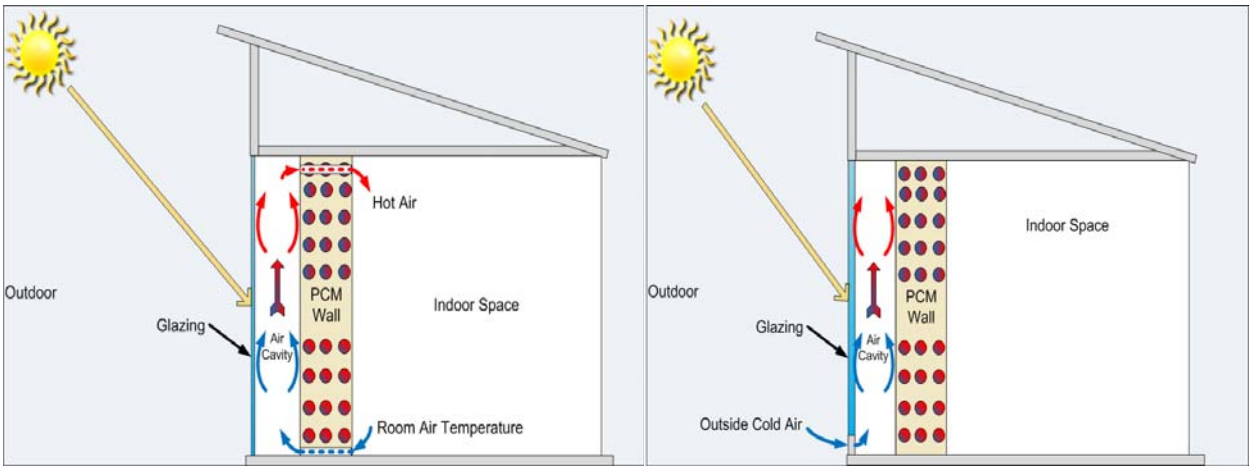

a) PCM-enhanced ventilated cavity wall: indoor air induction

b) PCM-enhanced ventilated cavity wall: outdoor air induction

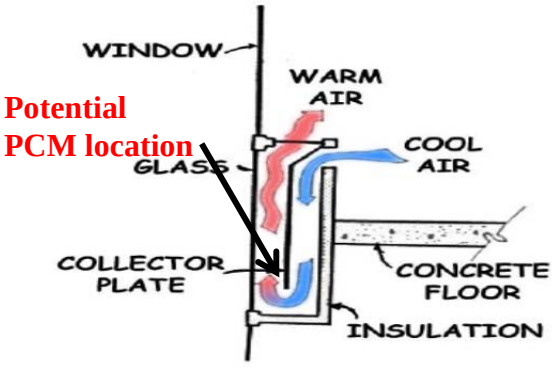

c) Actual installation of a wall solar collector in Odeillo, France [316]

d) Wall collector in a modern office space

Figure 7.32 Design and operational concept of PCM-enhanced ventilated cavity wall

In summary, PCM can be integrated into different building enclosures; ceiling, floor, or walls. The PCM can be thermally activated (i.e., charged or discharged) using passive strategies such as solar radiation from the sun, internal heat gain, or using outside cooled air via natural ventilation. Active systems can also be used to thermally activate the PCM especially when the energy is available at low cost. To be fully exploited, PCM should go through a charging and discharging cycle at least one time a day. Multiple cycles can be achieved through active systems which demand tuned control algorithms for optimizing the charging and discharging process to meet the zone demand. The following section will evaluate some of these design concepts to improve the PCM's thermal performance.

7.12 Conditions and strategies where PCM's performance is improved

The thermal performance of PCM under the base case residential building and environmental boundary conditions is found to be under expectations. This section further explores the performance of PCM under slightly different boundary conditions and non-traditional design strategies. The section is aimed to provide more insights into conditions and design strategies where PCM exhibits an improved thermal performance.

7.12.1 Thermal performance of PCM under ideal boundary conditions

One of the main advantages of PCM is its ability to store significant thermal energy within a small volume compared to a sensible thermal storage such as concrete for example. This feature has not been fully realized under the natural outdoor environmental conditions. The objective of this section is to evaluate the potential of outdoor environmental conditions to

improve the charging and discharging of PCM when hypothetical boundary conditions are imposed on the house model.

For this analysis and for a reasonable comparison, two designs are considered: 1) a 12.5 mm thin PCM layer and 2) a 150 mm thick concrete layer. For both designs, the layers are placed to the interior side and integrated into the base case wall described in **Table 7-2**. For the PCM-enhanced wall design, a medium latent heat of 200kJ/kg with melting temperature of 23°C and a melting range of 2°C is assumed in all walls. For the concrete layer, a heat capacity of 800J/kg-K, density of 2315 kg/m^3 and conductivity of 0.733 W/m-K are assumed.

Among other months in the year, the PCM performance was found superior during May. **Figure 7.33** shows the outdoor environmental conditions during this month in Golden, CO. The outdoor air temperature is generally following a sinusoidal form with diurnal cycles occurring between the day and night. Consequently, PCM charging and discharging cycle process was naturally enhanced.

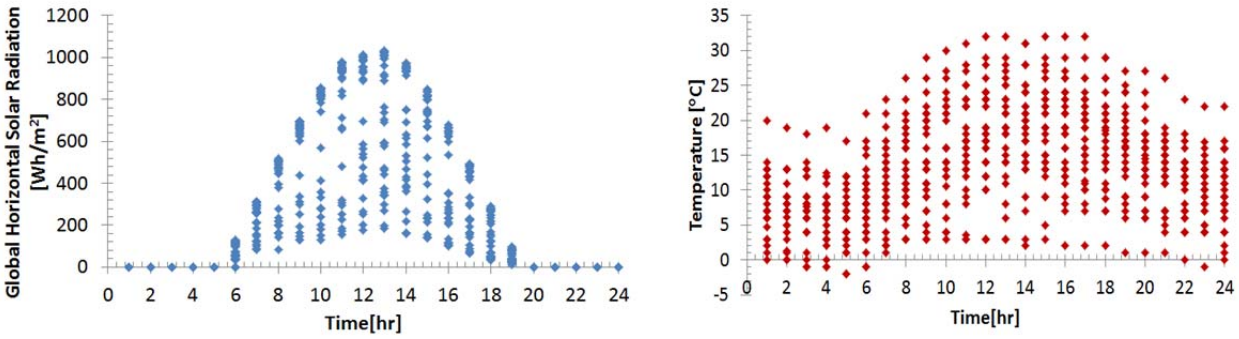

a) Hourly global solar radiation for the month of May

b) Hourly outdoor air temperature for the month of May

Figure 7.33 Weather data for the month of May in Golden, CO.

In order to exploit this further, the outdoor air temperature in TRNSYS is altered using the following simplified sinusoidal equation:

$$T_{out}(t) = T_{amp} * \sin(Freq * t + Phase) + T_{bias}$$ Equation 7-2

Where: Freq [rad/sec]= $\frac{2*\pi}{24*3600}$, Phase [rad]= $\frac{-90*\pi}{180}$, T_{bias} [°C]: meduim temperature , T_{amp} [°C]: amplitude temperature

Using Equation 7-2, the outdoor air temperature is varied using different values of T_{bias} and T_{amp}. Two cases are tested: 1) case-1 where T_{bias} is assumed constant and T_{amp} is varied, 2) case-2 where T_{bias} is varied and T_{amp} is kept constant.

For case-1, the T_{bias} is assumed to be constant at 23°C, close to both the PCM melting temperature and the average of thermostat setpoints (T_{clg}=24°C, T_{htg}=22°C). The amplitude temperature, T_{amp}, is varied between 1 and 40°C. The resultant outdoor air temperature profiles from this variation are shown in **Figure 7.34**. In TRNSYS, the residential building model is exposed to every outdoor air temperature profile shown in the figure during the month of May for the three design cases: 1) the base case wall design, 2) the PCM-enhanced wall design case and 3) the concrete wall design case. The solar radiation is kept unchanged as per the TMY3 weather file.

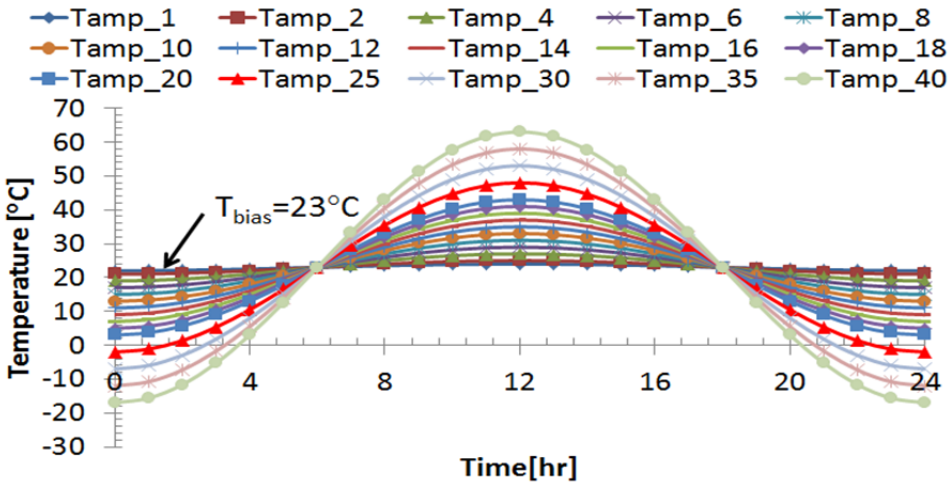

Figure 7.34 Case-1 ideal outdoor air temperature profile for the month of May

Using the above ideal boundary conditions, the results are shown in **Figure 7.35**. It is interesting to note that the thin PCM layer can deliver comparable saving's trend to the thick and massive concrete layer when exposed to similar boundary conditions. The maximum savings in the monthly cooling and heat loads are achieved when amplitude is 25°C (i.e., ΔT=50°C, T_{max}=48°C, T_{min}=-2°C). The maximum savings in heating loads is 81% and 87% for PCM and concrete layer respectively. The maximum savings in cooling loads is 13% and 18% for PCM and concrete layer, respectively. After amplitude of 29°C, no absolute savings are achieved from PCM layer.

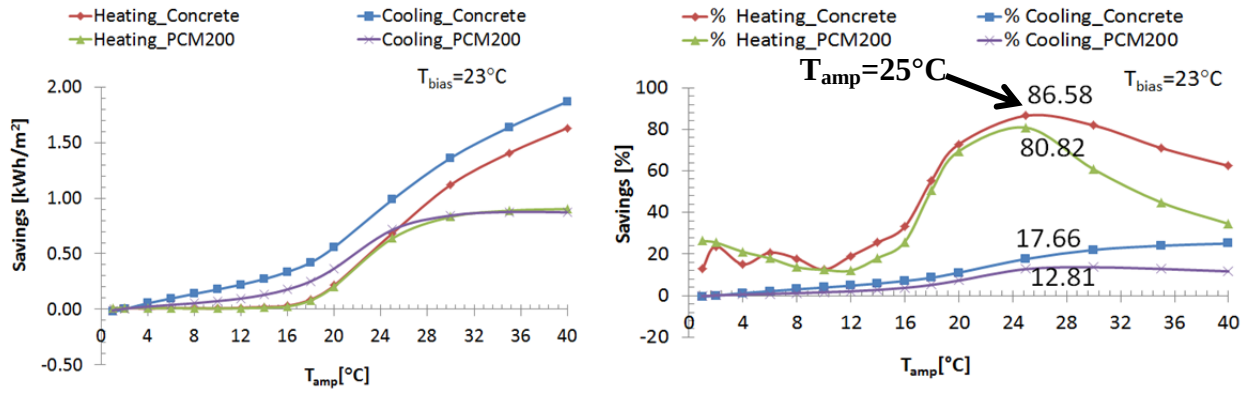

a) Savings in loads per floor area during the month of May

b) Percentage savings in loads during the month of May

Figure 7.35 Savings in loads under case-1 ideal boundary conditions for the month of May in Golden, CO.

For case-2, the amplitude is fixed at 25°C and the T_{bias} is varied from 1°C to 29°C. The resultant outdoor air temperature profiles are shown in **Figure 7.36**.

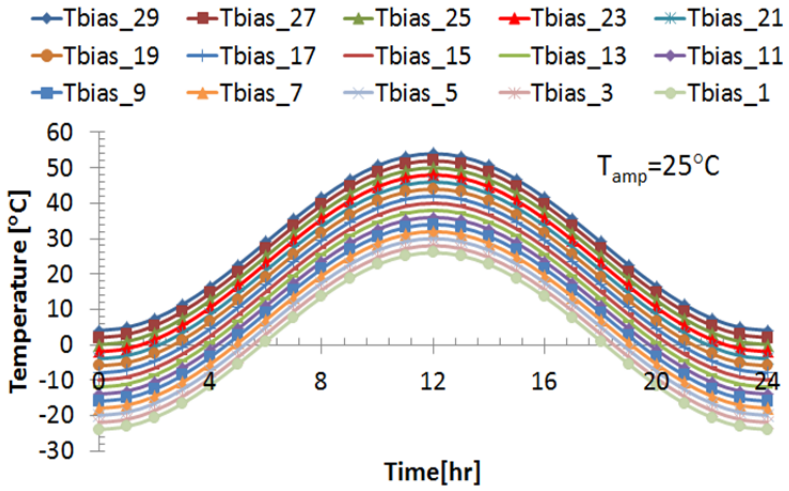

Figure 7.36 Case-2 ideal outdoor air temperature profile for the month of May

Similar simulation tests are carried out using the above ideal outdoor air temperature profiles. The results are shown in **Figure 7.37**. According **Figure 7.37** (a), the maximum absolute savings in both heating and cooling loads for both PCM and concrete designs are achieved when the T_{bias} is 15°C. As clear from **Figure 7.37** (b), the maximum percentage savings in cooling loads occurs at T_{bias} of 3-6°C and the maximum savings in heating loads occurs at T_{bias} of 23°C.

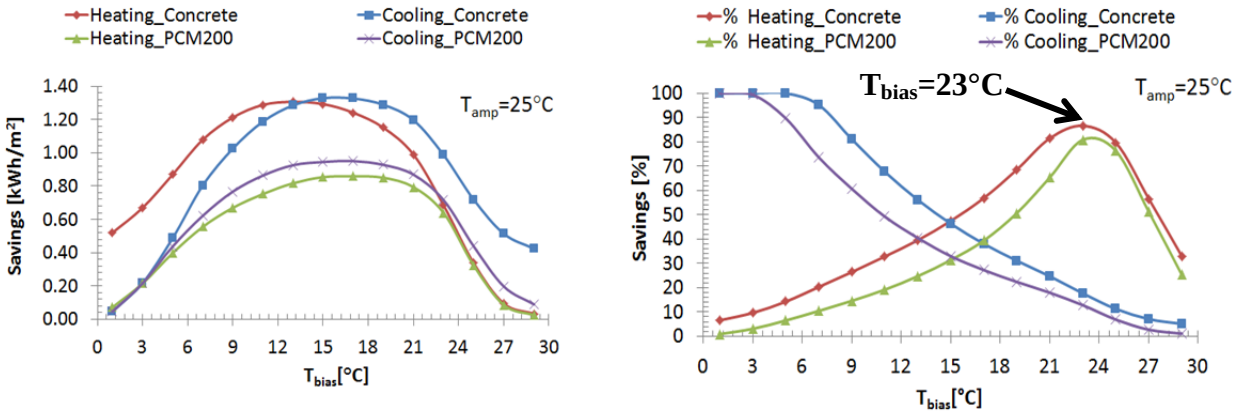

a) Savings in loads per floor area during the month of May

b) Percentage savings in loads during the month of May

Figure 7.37 Savings in loads under case-2 ideal boundary conditions for the month of May in Golden, CO.

The data results from case-1 and case-2 ideal boundary conditions show that the PCM performance has been enhanced. The thin PCM layer has approximately a comparable performance trend as a thick and massive concrete layer if appropriate boundary conditions are available. For maximum PCM performance under the building America house benchmark, the difference between the maximum daily and minimum night temperatures (T_{max}=48°C, T_{min}=-2°C) should be 50°C with an average air temperature around the PCM melting temperature. It is unfortunate that these ideal boundary conditions would not be experienced in every month of the year under natural climatic conditions. However, it is an interesting demonstration case that shows the potential of PCM under favorable boundary conditions. This favorable condition has also been cited by Kosny et. al. to achieve high PCM thermal performance [317].

7.12.2 Thermal performance of PCM-enhanced heavy massive walls

The study in this Chapter mainly focuses on the application of PCM when integrated into lightweight structure in a typical residential building. One may argue that PCM's performance can be enhanced when integrated into sensible heat storage materials such as concrete. Therefore, this section evaluates this particular design concept. **Table 7-17** provides the thermo-physical properties for the design options considered to evaluate the PCM performance. For a fair comparison to the lightweight wall design considered previously for residential building, the base case wall is designed with a similar thermal resistance (i.e., R-18) but with a thermally massive material; a concrete block instead of wood assembly. Two designs are considered: 1) PCM is located to the interior side, and 2) PCM is concentrated in the middle of concrete block. The PCM latent heat is fixed at 200 kJ/kg but the melting temperatures and melting range are varied as listed in **Table 7-17**.

Table 7-17 Thermo-physical properties of thermally insulated massive wall designs enhanced with PCM layer

Sketch	Material	Thickness [mm]	Thermal Conductivity [W/(m.K)]	Density [kg/m^3]	Heat Capacity [J/(kg.K)]	Latent Heat [kJ/kg]	Melting Temp. [°C]	Melting Range [°C]
Base Case Wall Design (thermally insulated massive wall)*								
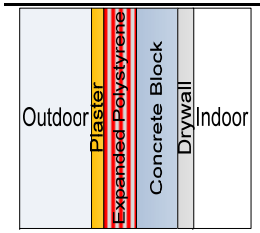	Plaster	12.5	0.72	840	1860			
	Expanded Polystyrene	100	0.034	24	1250			
	Concrete Block	200	1.02	2020	920			
	Gypsum	12.5	0.21	1200	1000			
Wall Design#1 (PCM to interior)								
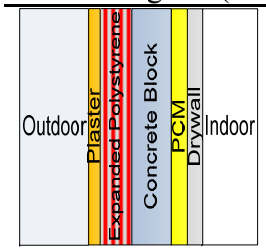	Plaster	12.5	0.72	840	1860			
	Expanded Polystyrene	100	0.034	24	1250			
	Concrete Blk	200	1.02	2020	920			
	PCM	12.5	0.2	235	1970	200	(18-27)	(0.1,1,2, 4,6,8)
	Gypsum	12.5	0.21	1200	1000			
Wall Design#2 (PCM in the middle)								
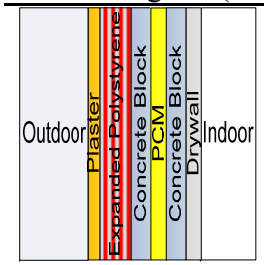	Plaster	12.5	0.72	840	1860			
	Expanded Polystyrene	100	0.034	24	1250			
	Concrete Blk	100	1.02	2020	920			
	PCM	12.5	0.2	235	1970	200	(10-35)	(0.1,1,2, 4,8,12)
	Concrete Blk	100	1.02	2020	920			
	Gypsum	12.5	0.21	1200	1000			

Notes: *this design has a similar R-value (R-18) as the lightweight wall used in residential building case

The percentage reductions in annual heating and cooling loads for both designs are shown in **Figure 7.38**. When the figure is compared to the lightweight wall results presented early in **Figure 7.4**, it is clear that PCM performs better when integrated into lightweight wall rather than with heavy massive wall. The optimal PCM thermal properties are not significantly different for both designs except for the maximum savings in heating loads. For maximum savings in heating loads, the heavy massive structure favors tight melting range compared to lightweight structures regardless of PCM location. Since sensible storage can absorb the heat energy at wide operational regime compared to PCM which only work at narrow operational conditions, PCM's energy storage becomes weak and secondary. Additionally, the high level of insulation may also contribute to the low performance of PCM, hindering its discharging process especially in summer for reducing the cooling loads.

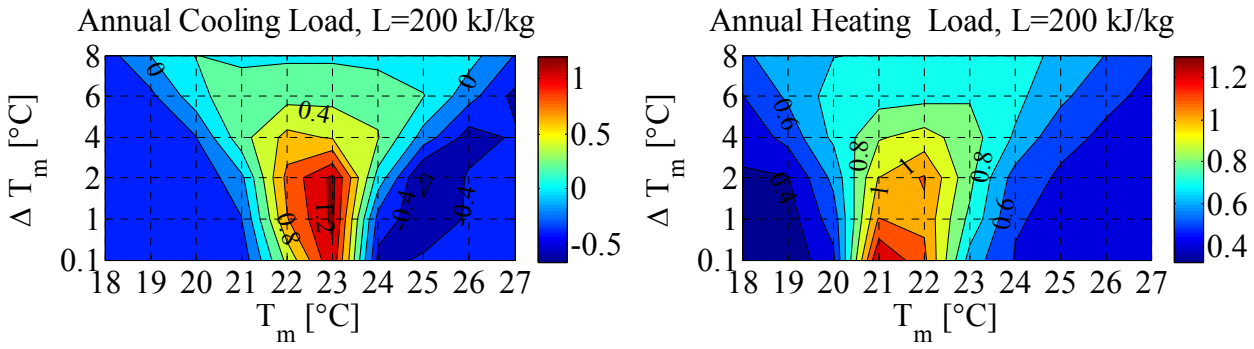

a) Percentage savings in annual cooling and heating loads when PCM is located to the interior

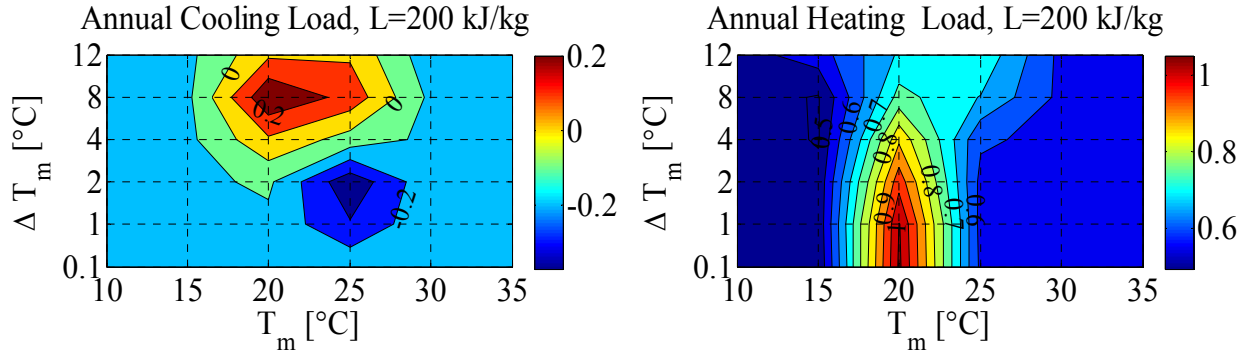

b) Percentage savings in annual cooling and heating loads when PCM is located to the middle

Figure 7.38 Percentage savings in annual loads for the case of 200 kJ/kg for thermally massive insulated PCM-enhanced walls with different PCM's locations

The performance of thermally massive and insulated PCM-enhanced walls is not better than the lightweight PCM-enhanced walls due to many reasons including the high level of insulation. Therefore, the insulation layer is eliminated from all thermally massive wall designs. This design concept might not comply with the local or national code but rather to evaluate the PCM performance when insulation is eliminated. Two PCM locations are considered: 1) one to the interior side and 2) another in the middle as previously tested. **Figure 7.39** shows the results for these two designs when the insulation layer is removed. It is clearly shown that the performance of non-insulated massive wall has been enhanced compared to the insulated wall design when PCM is utilized.

When PCM is placed to the interior side, the savings in annual cooling loads is at least 4% more than when it is placed in the middle. The optimal melting temperature is 1°C below the cooling setpoint (i.e., 23°C) at melting range of 0.1°C. When PCM is placed to the middle, the optimal melting temperature is 1°C above the cooling setpoint (i.e., 25°C) at a wider melting range of 4°C. The savings in annual heating loads is similar for both PCM designs. Both PCM locations favor wide melting range of 8°C for maximum savings in annual heating loads. The melting temperature is 15°C for middle PCM compared to 18°C for interior PCM.

In summary, the PCM performance is enhanced when used with non-insulated thermally massive wall designs than when used with insulated designs. In summer, the charging and discharging process is improved since daily diurnal cycles are naturally provided by the local climate. In winter and when insulation is not used, heat losses are increased. However and through its journey to the sink (i.e., the outside environment), PCM stores the lost heat and utilizes the stored energy for heating purposes when necessary. It can be concluded that the

mechanism of charging and discharging process of PCM has been enhanced by the absent of thermal insulation.

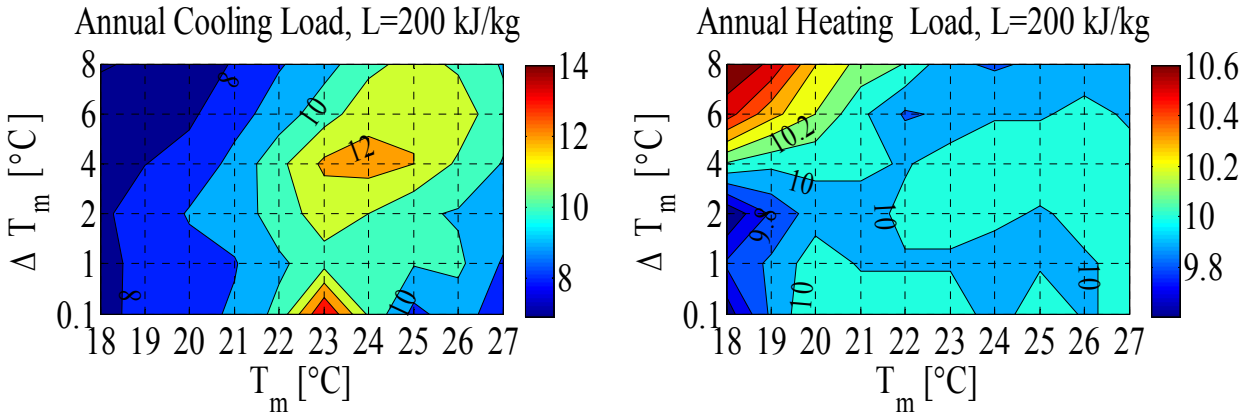

a) Percentage savings in annual cooling and heating loads when PCM is located to the interior

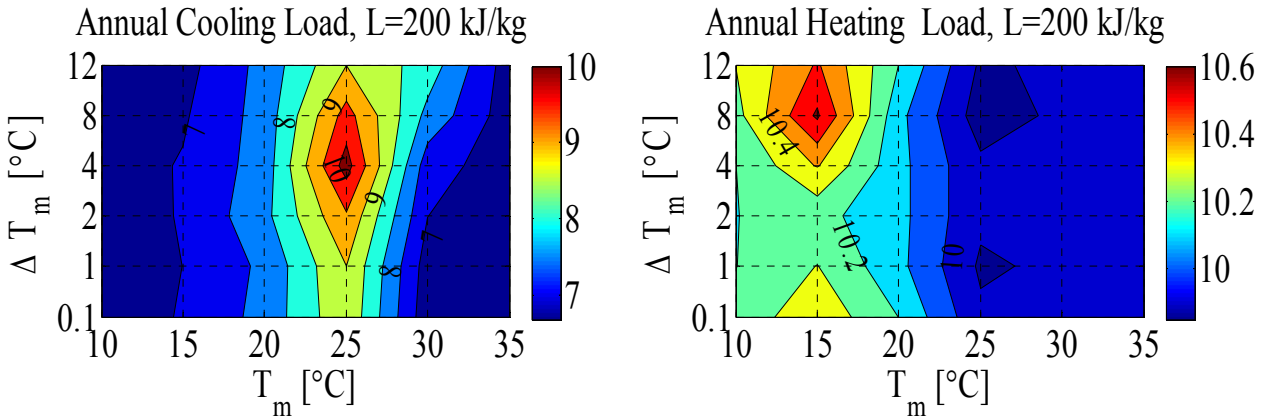

b) Percentage savings in annual cooling and heating loads when PCM is located in the middle

Figure 7.39 Percentage savings in annual loads for the case of 200 kJ/kg for thermally massive non-insulated PCM-enhanced walls with different PCM's locations

7.12.3 **Design demonstrations of improved PCM performance**

Under prescribed base case residential house assumptions and typical boundary conditions, the PCM layer is scarcely exploited resulting in unexpected thermal performance. This is likely due the lack of a heat source in winter (i.e., poor PCM charging) and the availability of abundant heat in summer season coupled with poor PCM discharging mechanism.

During these particular seasons, the PCM is either at solid or liquid state hindering its intended potential. Solar radiation can be a good source of heat during winter. Therefore, allowing more solar radiation to enter the zone would improve the storage efficiency of PCM. In summer, the cold outside air through natural ventilation can be introduced to flush the stored heat and subsequently improve the discharging process. The following sections provide two demonstrated designs where thermal performance of PCM is improved. These two designs are not optimized or fine-tuned for maximum potential but provide demonstration examples.

7.12.3.1 Design Case-1: High WWR and Summer Natural Ventilation

This design is intended to evaluate the PCM performance under design conditions different than the base case proposed by Building America benchmark. Therefore, it is a demonstration case rather than optimal design strategies. Combinations of design and operation strategies are implemented. Window to wall ratio (WWR) is increased to allow more solar radiation to enter the space. A 2" insulation is installed on windows to control heat loss in winter during the night and heat gain in summer during the day. In order to flush the stored heat in PCM, natural ventilation is also implemented. No optimization efforts are conducted for the operation strategies rather than allowing outside cold air to enter during summer nighttime. The PCM layer is placed to the interior side of the wall and in all orientations. The latent heat is 200kJ/kg with melting temperature of 23°C and melting range of 2°C.

Figure 7.40 shows the results as the design strategies are added. Case-1 represents the unmodified cases (the base case and the PCM case). The WWR is increased from 0.15 to 0.35 for all orientations with a 2" insulation on the glazing. Then, the natural outside cool air is introduced to the space at 2 ACH using a simple natural ventilation rule. In summer (beginning

of May to end of September), the outside air is introduced to the space during the night only when the outside air temperature between 12°C and 24°C. Case-2 shows that once the WWR is increased, the heating and cooling loads increase. When outside cooled air is allowed to enter the space, the cooling load decreases. The savings in loads increases from 1.7% to 4.8% for heating loads and from 5.8% to 16% for cooling. This case illustrates that PCM can achieve more savings when complemented with other design strategies.

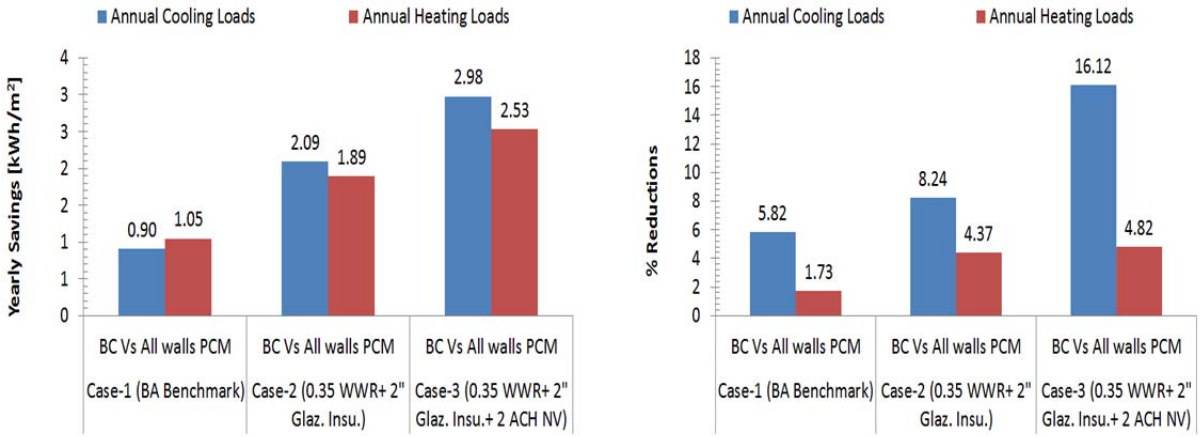

a) Savings in annual heating and cooling loads per floor area

b) Percentage savings in annual heating and cooling loads

Figure 7.40 Demonstration case of improved PCM performance

7.12.3.2 Design Case-2: Cavity south Wall

This design case is an implementation of a cavity façade system. The main objective is to examine the benefit of a cavity as a source of heat for PCM layer. The cavity parameters assumed for this design is listed in **Table 7-18**. A non-vented cavity and a double glazing are added to the base case south wall keeping other walls without modification. The properties of the base wall are described in **Table 7-2**. One case is run without the PCM layer and other is with

PCM on the interior side of the wall. The PCM layer is assumed to be with a medium latent heat of 200kJ/kg with melting temperature of 23°C and melting range of 1°C. Using the cavity design, there is a risk of increasing the cooling demand due to the large amount of heat absorption during summer. Therefore, a shading schedule is implemented to control the glazing's transmisivity during the summer season only (May to October).

Table 7-18 Parameters used for a south cavity PCM-enhanced wall

Test Parameter	Values	Units
Wall height	2.4	m
Wall width	15.68	m
External Convective Heat transfer Coefficient	17.78	$W/m^2.K$
Internal Convective Heat transfer Coefficient	4.43	$W/m^2.K$
Solar absorption	0.9	
Emissivity of the massive wall	0.9	
Cavity		
Depth, (b)	0.15	m
Vent Area, (A_v)	0.09	m^2
Vertical distance between two vents, (Ho)	2.2	m
Flow characteristic	No flow	
Glazing		
Number of glazing	2	
Emissivity of the glazing	0.9	
Transmissivity of the glazing, τ	0.79	
Ug	3.21	$W/m^2.K$
Simulation Parameters		
Time Step	1	minute
Weather file	EPW for Golden, Colorado	

Figure 7.41 shows the results for the two cases: a) case 1: the base case against a south wall with PCM, b) case 2: the base case with south cavity wall against a case with south cavity wall with PCM. The figure demonstrates that the cavity can improve the performance of PCM since more heat is provided during the heating season. The reduction in annual heating loads for a south wall with PCM is only 0.59% compared to 7.2% when a cavity is used.

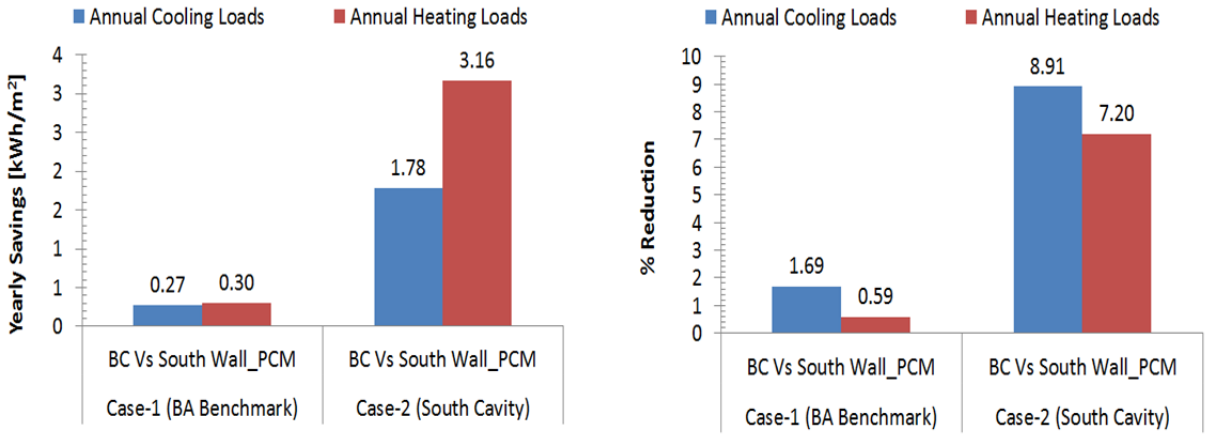

a) Savings in annual heating and cooling loads per floor area

b) Percentage savings in annual heating and cooling loads

Figure 7.41 Cavity south wall case for demonstration of improved PCM performance

7.13 Summary

Performance of phase change materials are highly influenced by the surrounding environmental conditions. Therefore, different parameters have been studied to gain detailed insights of PCM thermal performance. Full parametric analysis is performed for the climate of Golden, Colorado. The first design question is where to place the PCM relative to the insulation. Three different locations are studied; 1) to the interior side, 2) sandwiched between the insulation in wood assembly, and 3) to the exterior side exposed to outside environment. The best location for PCM is found to be on interior side; in direct contact with the indoor environment. Since different orientation receives unequal amount of solar radiation, the orientation is also examined. When this was evaluated, the PCM layer is placed to the interior side. The impact of orientation is marginal on the performance of PCM performance. The exterior solar radiation has minor impact since the same level of thermal insulation is installed in all orientations. However, the

orientations for best PCM performance can be listed in the following order; south, west and east and finally north. The results also show that the maximum savings in annual heating and cooling loads occur at different PCM thermal properties. Therefore, hybrid PCM designs (two PCM layers; one for dealing with cooling and another for heating) were evaluated. A slightly improved performance (~1% more savings in annual heating load) is observed; with a 50-50 latent heat distribution being a reasonable assumption.

The seasonal performance is of a particular importance. It is found that PCM performs relatively better during transition months, especially in May and less during summer and winter months. During the month of May, high diurnal cycle is observed promoting the charging and discharging process. The heat absorbed in the day is released back to the environment at night. Unfortunately, this ideal condition is not always available in other months. The lack of large diurnal changes keeps the PCM at liquid state during summer and at solid state during the winter hindering its high thermal potential. It is also worth mentioning that in summer of Colorado there is a temperature difference between the day and night temperatures. However, the discharging process is slow and subsequently not enough to fully discharge the stored heat. The slow discharging process is likely due to the high level of insulation that reduces the heat loss to the outside. Introducing the cooled outside air through natural ventilation can potentially enhance the discharging process of PCM in summer months.

Sensitivity analysis was also performed to study the impact of different parameters on the thermal performance of PCM. Among the important parameters are the solar radiation and zone setpoints. In winter, the PCM performance has improved as the solar radiation increases. The PCM performance is found to be sensitive to zone setpoints. The optimum thermal properties tuned for one setpoint is found to under-performed under different setpoints. Generally speaking,

the optimal melting temperature of PCM for maximum savings in cooling loads is 1°C below the cooling setpoint and at heating setpoint for maximum savings in heating loads.

In addition to the Golden Co. climate (cold climate), three other representative US climates are selected; Phoenix, AZ. (hot dry climate), Atlanta, GA. (temperate climate) and Seattle, WA. (marine climate). For all climates, the PCM is placed to the interior side. The performance of PCM is found to behave in a similar fashion across the climates. **Table 7-19** provides the summary results of savings in annual and peak loads for the two extreme latent heat cases (50 and 300 kJ/kg) with corresponding optimal PCM thermal properties and potential savings for the four US cities.

Table 7-19 Summary of results for the four US cities

Latent heat case [kJ/kg]	Cities	Annual Heating Loads*			Annual Cooling Loads*		
		Tm [°C]	ΔTm [°C]	Savings [%]	Tm [°C]	ΔTm [°C]	Savings [%]
50	Phoenix, AZ.	21	0.1	22.59	23	0.1	0.24
	Atlanta, GA.	22		1.95		1	0.79
	Seattle, WA.	21		1.88		2	3.64
	Golden, CO.	22	1	1.28			1.54
300	Phoenix, AZ.	22	0.1	55.82		0.1	0.79
	Atlanta, GA.			4.17		1	2.60
	Seattle, WA.		2	3.59		0.1	15.80
	Golden, CO.		4	2.80		1	7.32
Latent heat case [kJ/kg]	Cities	Peak Heating Loads			Peak Cooling Loads		
		Tm [°C]	ΔTm [°C]	Savings [%]	Tm [°C]	ΔTm [°C]	Savings [%]
50	Phoenix, AZ.	20	1	4.68	27	0.1	1.60
	Atlanta, GA.	19	0.1	2.31	26	1	2.83
	Seattle, WA.	20	1	1.74	25	0.1	4.43
	Golden, CO.	19	0.1	2.59			5.43
300	Phoenix, AZ.	21	0.1	23.39	26	0.1-1	6.76
	Atlanta, GA.	20		10.45	25		11.33
	Seattle, WA.			8.93	24	2	13.29
	Golden, CO.			6.95	25	1	10.29

Notes: * Heating setpoint is 22°C and cooling setpoint is 24°C

For benchmark comparison, the results in this table can be compared to those summarized in **Table 2-4**. Medina and co-workers reported an average reduction of 9-11% in space cooling and a reduction of 5.7-15% in peak heating load in Lawrence, Kansas [14, 199-201]. Based on simulation under Dayton climate, Kissock found that the peak and annual cooling loads were reduced by 19% and 13%, respectively [195]. Using EnergyPlus, Tabares reported a peak cooling reduction of 4% in the peak month of July in Phoenix [35]. The results from the literature are in agreement to the results obtained from this study as clear in **Table 7-19**.

In all climates, the optimal melting temperature for maximum savings in cooling load is 1°C below the cooling setpoint and at the heating setpoint for maximum savings in heating loads, with some exceptions for extreme cases. For a heavy latent heat case of 300kJ/kg, the maximum percentage savings in annual cooling load range from 0.8-15.8% with low in Phoenix and high in Seattle. The maximum percentage savings in annual heating load range from 2.8-55.8% with low in Golden and high in Phoenix. In terms of absolute values, maximum savings in cooling loads ranges from 0.83-1.2 kWh/m^2 with low in Atlanta and high achieved in Phoenix. The maximum absolute savings in annual heating loads range from 0.49-1.79 kWh/m^2, low in Phoenix and high in Seattle. Despite the high heating degree day of Golden when compared to Seattle, PCM achieves marginal savings in annual heating load. The enhanced performance in Seattle is found due to the different insulation level requirements for both climates; an extra R5 is mandated for Colorado climate. When a simple payback period analysis is performance for all climates, PCM is found economically unfeasible with the current market price. This finding assumes that PCM charge and discharges its heat under natural means. Using the set of simulation runs from this study, design correlations were developed for all climates.

Across the latent heat parameters (50-300 kJ/kg), the reduction in peak heating loads is 3-7%, 2-9%, 2-10% and 5-23% for Golden, Seattle, Atlanta and Phoenix respectively. The reduction in peak cooling loads is 5-10%, 4-13%, 3-11%, 2-7% in Golden, Seattle, Atlanta and Phoenix respectively.

Several cases have been explored to gain insights about conditions and strategies beyond the Building America benchmark case at which PCM shows improved performance. Boundary conditions were hypothetically altered in TRNSYS for the month of May to determine the favorable diurnal cycle (i.e., day and night outdoor air temperature). For a 12.5 mm thin PCM layer with a latent heat of 200kJ/kg to achieve a reduction of 81% in monthly heating loads and 13% in monthly cooling load, an average air temperature of 23°C with a diurnal temperature of 50°C (i.e., T_{max}=48°C and T_{min}=-2°C) should be facilitated throughout the month. This is an ideal boundary condition that is impossible to have in all days of the month.

Integrating PCM with insulated and heavy massive concrete wall didn't help to enhance the PCM's thermal performance. However when insulation is entirely eliminated from the base case and the PCM-enhanced heavy massive wall, PCM's performance has been enhanced due to improvement in charging during winter and discharging during summer.

In addition, other demo designs were simulated to enhance the performance of PCM; one using high WWR and natural ventilation in summer and another using cavity in the south wall with shading during summer. Although not fully optimized or fine-tuned, both designs enhanced the performance of PCM. For the design case-1, the savings in annual cooling loads increases from 6% to 16% when shading during the day is used and cooled outside air is introduced during summer night. The savings in annual heating savings increases from 1.7% to 5% with increasing the WWR complemented with glazing's insulating during the night. In design case-2, none

vented cavity is installed in south with and without PCM. In order to reduce the cooling load due to the cavity, shading is implemented on glazing during the summer day. The savings in annual cooling loads improved from 1.7% for none cavity PCM design to 9% for cavity PCM design on south wall only. The savings in annual heating loads improved from 0.6% to 7%. Both demo designs show that PCM performance can be enhanced if complemented with other passive strategies.

CHAPTER 8: CONCLUSIVE SUMMARY AND FUTURE WORK

8.1 Conclusions

The research performed in this Dissertation has been mainly motivated by the desire to develop generic, quick and yet accurate numerical model for simulating the heat transfer process associated with phase change for building applications; in particular for PCM-enhanced façade systems. The model has been developed and selected to be a base for a newly developed toolbox in SIMULINK for modeling Advanced Façade System; entitled 'AdvFacSy". A selective advanced set of façade systems has been fully integrated into TRNSYS, a whole-building simulation tool. The integration has extended the capability and flexibility of utilizing the AdvFacSy modules in whole-building systems context. The following sections summarize the results and concluding remarks from this research work.

8.1.1 Numerical modeling of phase change materials

The literature in Chapter 2 has indicated that PCMs can be modeled using four generic methods; enthalpy, heat capacity, temperature-transforming and heat source methods. Every method offers advantages and imposes limitations. The task has been focused to explore the capabilities and limitations of three common methods; enthalpy, heat capacity and heat source methods. Using these three generic methods and two numerical solvers; Tri-diagonal matrix algorithm (TDMA or Thomas algorithm) and Gauss–Seidel iterative algorithm (G-S), eight computational models as shown in **Table 8-1** have been developed in MATLAB/SIMULINK environment, verified using comparative results from EnergyPlus and validated using

experimental results from the literature. The hybrid correction scheme (EM_HCS_TDMA) is proposed and validated under this research work. All models agree well with both the experimental and comparative results except the non-iterative correction scheme (i.e., EM_NIC_TDMA).

Table 8-1 Summary of the eight computational models for modeling PCMs

Method	Solver	Scheme Identification	Correction Step
Enthalpy Method (EM)	G-S	Generic (EM_Generic_GS)	No
	TDMA	Iterative Correction Scheme (EM_ICS_TDMA)	Yes
	TDMA	Hybrid Correction Scheme* (EM_HCS_TDMA)	Yes
	TDMA	Non-Iterative Correction Scheme (EM_NIC_TDMA)	Yes
Heat Capacity Method (HCM)	TDMA	HCM_TDMA	No
	G-S	HCM_GS	No
Heat Source Method (HSM)	TDMA	HSM_TDMA	Yes
	G-S	HSM_GS	Yes

G-S: Gauss-Seidel, TDMA: Tri-Diagonal Matrix Algorithm
* proposed and validated under this research work

The models were then thoroughly tested for their sensitivity to PCM properties; latent heat and melting range at different time steps. The sensitivity study is performed to evaluate the computational efficiency and the prediction accuracy under different PCM properties. The results have given more insights on how the models perform and can be summarized as follows:

1) Models that use correction schemes are less sensitive to the latent heat and melting temperature range variations with the exception of the non-iterative scheme (EM_NIC_TDMA) which is found inaccurate for all cases. The maximum time step could be 15 minutes yet within the NRMSE limit of 1% but using a 5 minute time step would not add a considerable CPU time.
2) For a simplified PCM-enhanced wall model, the proposed improvement implemented in the hybrid correction scheme (EM_HCS_TDMA) has resulted in CPU time savings of 20% and

4% at 1 and 5 minute time step respectively when compared to the fastest and most conservative method; the iterative correction scheme (EM_ICS_TDMA). This improvement is significant when a PCM model is sought for implementation into whole building simulation tool that runs on yearly simulation at sub-hourly time step.

3) Direct solver (TDMA) is not recommended for the heat capacity method when PCM exhibits a narrow melting range (< 1°C).
4) Generally, the heat capacity method is found to be sensitive to the melting range and its predictions get more accurate as the melting range increases above 1°C. Since this method uses numerical approximation for predicting heat capacity term, the approximation becomes smoother with wide melting range. Therefore, it is recommended to use this method for PCMs that has a wide melting range; >1 °C. A time step of less than 5 minutes is necessary to achieve accurate results.
5) Heat source method, the TDMA and G-S versions, shows good results when compared to others but is slower than the linearized enthalpy methods; which are the fastest schemes at small time steps. Although the heat source method uses a correction scheme too, the method utilizes an under-relaxation factor that hindered its speed.
6) The general enthalpy method is computationally intensive and doesn't offer an advantage for potential implementation into building simulation tools.

It is concluded that only two schemes out of eight developed can be considered as potential candidates for integrating into whole building simulation tool; the linearized enthalpy method with the iterative correction scheme (EM_ICSS_TDMA) and the hybrid correction scheme (EM_HCS_TDMA). These two schemes offer many advantages over others:

1) Flexibility to use with large time steps (a maximum of 15 minutes) and still within 1% NRMSE.
2) Computational efficiency as they are 3-10 times faster than others based on the time step used.
3) Less sensitive to the variation of PCM properties; latent heat and melting range and hence stable in their numerical predictions.

8.1.2 Modeling and simulation of advanced façade systems

Based on the conclusion from the previous phase, a library of modules for modeling advanced façade systems, entitled 'AdvFacSy", has been developed using the GUI interface of SIMULINK. With this toolbox, many advanced facade systems with and without PCM can be easily modeled with minimal parameters input. Different designs have been verified using well established programs such EnergyPlus and TRNSYS. This tool offers flexibility and opportunity to evaluate innovative façade designs that is not possible to do with current state of the art simulation tools without workarounds. Two advanced façade systems were modeled using the AdvFacSy toolbox; multilayer PCM-enhanced wall and ventilated cavity PCM-enhanced wall. Using the results from these simulations, new design guidelines were developed. However, the overall goal was to answer fundamental design questions:

1) Where do we place PCM layer?

In order to answer this question, three PCM locations were tested with a typical multilayer wall in a residential building; a) in direct contact with the indoor environment (to the interior side of the wall), b) sandwiched in the wood stud assembly (middle PCM case), c) to the exterior side of the wall. The simulations were run for all four orientations; south, west, north

and east and for a wide range of PCM thermal properties. For all orientations, the best performance for PCM was found to be to the interior side of the wall; in direct contact with indoor environment. The second best location is when the PCM is in the middle and finally to exterior side. The indoor environmental conditions for these cases are fixed and the outside vary following a TMY weather file. Due to diurnal changes between the day and night of outside environmental conditions, the savings in annual cooling loads are significant. In some cases, the cooling loads were entirely eliminated. However, the savings in annual heating loads were around 3% at maximum. During winter, no extra heat is stored in PCM and therefore the potential is low. Therefore, a ventilated cavity is added to harvest more solar radiation to enhance the storage performance of PCM in winter.

2) Can a ventilated cavity enhance the performance of PCM layer for heating?

Installing a cavity might impose a significant cooling load. This design should be implemented with a solar protection during summer time. Since the overall goal in this design is to evaluate the potential of a cavity in enhancing the PCM performance for reducing the annual heating load, the impact on cooling load is not discussed.

The ventilated cavity might impose different boundary conditions. Hence, two PCM locations relative to the insulation are also studied; 1) to the interior and 2) exterior side and for all four wall orientations. Similar to the multilayer wall, it is concluded that the interior side PCM performs the best in all orientations. Less savings in annual heating loads are observed when PCM is placed in the cavity side; the exterior side of the wall.

For reducing the heating loads, the PCM performance has indeed been enhanced when the cavity design is used. For interior PCM case, the savings in annual heating load increases from only 3% for no-cavity case to 30% when cavity is installed for the south wall case; after

subtracting the cavity contributions. A similar enhancement but less magnitude has been observed for west and east; ~20% savings in annual heating loads. Although cavity has contributed in savings of annual heating load on north wall due to the diffusive solar radiation, the PCM performance was not improved. Therefore, it is concluded that if a cavity is used, then it should be installed on south, east and west. No cavity for north is recommended since no improvement in PCM performance is observed.

3) What are the optimal thermal properties of PCM layer?

For the case of best PCM location (i.e., interior side), the optimal melting temperature for maximum savings in annual cooling loads was found to follow the cooling setpoint of 24°C. Similarly for the maximum savings in annual heating loads, the optimal melting temperature is at heating setpoint of 22°C. Narrow melting range of less than 0.2°C was found to enhance the PCM layer for both cooling and heating savings. Similar to multilayer walls, the optimal melting temperature for the cavity design is following the heating setpoint for maximum savings in annual heating load. A similar melting range is also applicable for the cavity case.

8.1.3 Integration of the toolbox into TRNSYS

Various coupling approaches have been tested between the AdvFacSy toolbox and TRNSYS; a whole-building simulation tool. The first approach was using the already available TRNSYS Type-155 which directly couples the MATLAB environment with TRNSYS. This approach was computationally inefficient especially with the iterative nature of the numerical model for PCM-enhanced façade system. A novel methodology proposed by Riederer et. al.[292] to export the SIMULINK projects to TRNSYS and vice versa is then evaluated. Using this approach, it was possible to indirectly couple the toolbox with TRNSYS without the need of

MATLAB/SIMULINK. A list of C++ codes are generated and consequently compiled for direct use in TRNSYS. One minor limitation of this approach is the need to compile the façade design for multiple uses. Therefore, a TRNSYS Type-285 was specifically developed for multilayer wall with and without PCM using FORTRAN. Once compiled, the developed type gives more flexibility as multiple walls can be used. Majority of the integrated models have been verified against TRNSYS modules using simplified cases. Using the test cases, the developed models show good agreement with results from TRSNSY modules. This integration effort has extended the use of the toolbox to evaluate advanced façade systems at building system level.

8.1.4 Simulation of PCM-enhanced façade systems in TRNSYS

The integrated toolbox models in TRNSYS have been used to evaluate the thermal performance of PCM in a typical residential building. Similar to the standalone simulations, different PCM locations are tested in a whole building setup. The PCM to the interior is found to be the best. For this design, the orientation has insignificant impact on the performance of PCM. However, the difference can be observed with best being south, west and east, and finally north. Since optimal PCM's thermal properties are different for heating and cooling loads, hybrid PCM layers have also been simulated. The results show a marginal improvement when compared to a single PCM layer.

Seasonally, the PCM performs the best in transition months especially during the month of May. The study indicated that high diurnal cycles occur in this month. The PCM is charged and discharged within a 24 hours period for many days during this month. Although diurnal cycles are observed in summer month of August, the charging and discharging process is slow; the PCM is at liquid state most of the time. The insulation hindered the charging and discharging

process. Similarly in winter, the PCM is at liquid state since internal heat load is directly used to meet the heating demand and no access is absorbed for storage.

A comprehensive sensitivity study is performed for different design parameters pertained to PCM under the climatic conditions of Golden, Colorado. Among the important parameters are the solar radiation and zone setpoints. The following can be concluded:

1) In winter, the PCM performance has improved as the solar radiation increases. Focusing the direct solar radiation to PCM has increased the savings since more heat can be directed to PCM instead of other surfaces. Reducing the solar radiation has improved the savings in annual cooling load but has reduced the savings in annual heating loads. Increasing the WWR is a good option for increasing the solar radiation and subsequently enhancing the PCM performance for maximum savings in annual heating loads.
2) The PCM performance is found to be sensitive to zonal setpoint. The optimal PCM thermal properties tuned for a setpoint (heating and cooling) is found to under-perform under different setpoints. A loss of 25% in savings is observed with a 1°C increase in cooling setpoint or a 1°C decrease in heating setpoint. This reveals that PCM is sensitive to setpoint and a case by case should be considered for optimization. Generally speaking, the optimal melting temperature of PCM for maximum savings in cooling loads is 1°C below the cooling setpoint and at a heating setpoint for maximum savings in heating loads. The melting range is difficult to determine for each case which demand careful attention.

Other three US representative climates; Phoenix, AZ (hot dry climate), Atlanta, GA (temperate climate) and Seattle, WA (marine climate) has been selected to gain more insights on the thermal performance of PCM. After considering the system efficiency, the savings from PCM for all cases are insignificant when converted to dollar's value; Phoenix ranges between

4.5-$13, Atlanta between 11-$24, Seattle 9-$20 and Golden 6.5-$17. Simple payback period showed that the PCM is not economically attractive at the current market price. It is concluded that under natural means, PCM can't be fully utilized to its maximum potential. Using the results, new design guidelines are developed for these four climates.

Despite the PCM's performance in reducing both the annual heating and cooling loads, the reductions in peak heating and cooling loads are appealing. Across the latent heat parameters (50-300 kJ/kg), the reduction in peak heating loads is 3-7%, 2-9%, 2-10% and 5-23% for Golden, Seattle, Atlanta and Phoenix respectively. The reduction in peak cooling loads is 5-10%, 4-13%, 3-11%, 2-7% in Golden, Seattle, Atlanta and Phoenix respectively.

From the sensitivity analysis, other complementary conditions and design strategies could enhance the PCM performance during winter and summer. Therefore, several cases were explored to gain more insights about conditions and strategies at which PCM shows improved performance. For the medium latent heat case of 200kJ/kg, a diurnal temperature cycle of T_{max}=48°C and T_{min}=-2°C was found to achieve a reduction of 81% in monthly heating loads and 13% in monthly cooling load. This finding shows that PCM needs aggressive boundary conditions to achieve high performance. The favorable boundary conditions would be less aggressive with less insulation level.

Integrating PCM with insulated and heavy massive concrete wall has not improved the PCM thermal performance. However when insulation is entirely eliminated from the base case and the PCM-enhanced heavy massive wall, PCM's performance has been enhanced due to improvement in charging during winter and discharging during summer. Therefore, managing the charging and discharging process is a key in improving the PCM performance.

Additionally, two design demos are implemented to improve the PCM performance; 1) high WWR in all walls coupled with glass insulation in winter night and natural ventilation during summer day, 2) using none vented cavity in the south wall for harvesting solar radiation and shading during the summer time. Although not fully optimized or fine-tuned, both designs enhanced the performance of PCM. For the design case-1, the saving in annual heating loads increases from 1.7% to 5%. The savings in annual cooling loads increase from 6% to 16% when shading is used during the day and cooled outside air is introduced during summer night. For design case-2, the savings have improved from 0.6% to 7% and from 1.7% to 9% in annual heating loads and cooling loads respectively. Both demo designs show that PCM performance can be enhanced if complemented with other passive strategies.

8.2 Future work

The areas for further research can be explored the following directions.

8.2.1 Modeling of phase change materials

The numerical module for simulating PCM developed in this research work is not free of limitations. Although not important for PCM types in building application at this current state, the model does not include the hysteresis or subcooling phenomena. Improving the model could provide more insights into the PCM performance when these two phenomena are inherited in some PCM types.

8.2.2 Improving the AdvFacSy toolbox in SIMULINK

Currently, AdvFacSy toolbox can be used to model standalone façade systems with fixed indoor environmental conditions and outside varying climatic conditions using TMY weather file. Although it has been slightly explored, the SIMULINK capability to model the dynamic system can be fully utilized to model whole building zones. This will add to the already flexibility of the tool where the whole building can be simulated utilizing the many other toolboxes in SIMULINK.

8.2.3 Enhancing the charging and discharging process of PCM

This research work has highlighted the ideal environmental conditions for PCM performance in achieving maximum savings in cooling and heating loads. When standalone designs are evaluated for example, maximum savings in annual cooling load are achieved when high diurnal change occurs; under fixed indoor and varying outdoor environmental conditions. For maximum savings in heating loads, a source of heat is necessary to enhance PCM performance. When whole building is simulated, the ideal conditions have occasionally occurred during transition months such as May for example. In other months, PCM has low performance under natural means since it is either at solid or liquid state; outside its performance range. The demonstration designs have supported the concept of complementing the PCM with other design strategies to enhance the thermal performance. Therefore, exploring the thermal activation using passive or active means would result in significant enhancement of PCM thermal performance. For example, a thermal activation using embedded pipes in PCM layer via hot water in winter from solar water heating and cold water in summer night could significantly improve the charging and discharging process of PCM.

REFERENCES

[1] U.S. Department of Energy (DOE). 2011 Buildings Energy Data Book. 2012.

[2] Said SAM, Abdelrahman MA. Energy efficiency of a building in the eastern province of Saudi Arabia: parametric analysis with DOE2.1A. Anglais. 1989;95 147-52

[3] Ahmed A, Elhadidy MA. Energy Conservation Measures for a Typical Detached Single Family House in Dhahran. The first Symposium on Energy Conservation and Management in Buildings Conference. Saudi Arabia2002. p. 31-42.

[4] Fazio, Athienitis A, Marsh C, Rao. Environmental Chamber for Investigation of Building Envelope Performance. Journal of Architectural Engineering. 1997;3:97-102.

[5] Givoni B. Man, climate and architecture: Van Nostrand Reinhold; 1981.

[6] Telkes M. Thermal energy storage in salt hydrates. Solar Energy Materials. 1980;2:381-93.

[7] Koschenz M, Lehmann B. Development of a thermally activated ceiling panel with PCM for application in lightweight and retrofitted buildings. Energy and Buildings. 2004;36:567-78.

[8] Zalba B, Marín JM, Cabeza LF, Mehling H. Free-cooling of buildings with phase change materials. International Journal of Refrigeration. 2004;27:839-49.

[9] Zhang YP, Lin KP, Yang R, Di HF, Jiang Y. Preparation, thermal performance and application of shape-stabilized PCM in energy efficient buildings. Energy and Buildings. 2006;38:1262-9.

[10] Arkar C, Vidrih B, Medved S. Efficiency of free cooling using latent heat storage integrated into the ventilation system of a low energy building. International Journal of Refrigeration. 2007;30:134-43.

[11] Cabeza LF, Castellón C, Nogués M, Medrano M, Leppers R, Zubillaga O. Use of microencapsulated PCM in concrete walls for energy savings. Energy and Buildings. 2007;39:113-9.

[12] Castell A, Martorell I, Medrano M, Pérez G, Cabeza LF. Experimental study of using PCM in brick constructive solutions for passive cooling. Energy and Buildings. 2010;42:534-40.

[13] Zhou D, Zhao CY, Tian Y. Review on thermal energy storage with phase change materials (PCMs) in building applications. Applied Energy. 2012;92:593-605.

[14] Fang Y, Medina MA. Proposed Modifications for Models of Heat Transfer Problems Involving Partially Melted Phase Change Processes. Journal of ASTM International. 2009;6.

[15] Hawes DW. Latent Heat Storage in Concrete. Montreal: Concordia University; 1991.

[16] Kubiszewski I. Telkes, Maria. In: Saundry P, editor. The Encyclopedia of Earth: http://wwweoearthorg/article/Telkes,_Maria ,2006 [Accessed: October/29/2012].

[17] Harland A. Just a Phase? Assessment of the Potential for Phase Change Materials in New Zealand Buildings: Victoria University of Wellington; 2010.

[18] Baetens R, Jelle BP, Gustavsen A. Phase change materials for building applications: A state-of-the-art review. Energy and Buildings. 2010;42:1361-8.

[19] Khudhair AM, Farid MM. A review on energy conservation in building applications with thermal storage by latent heat using phase change materials. Energy Conversion and Management. 2004;45:263-75.

[20] Zhang Y, Zhou G, Lin K, Zhang Q, Di H. Application of latent heat thermal energy storage in buildings: State-of-the-art and outlook. Building and Environment. 2007;42:2197-209.

[21] Tyagi VV, Buddhi D. PCM thermal storage in buildings: A state of art. Renewable and Sustainable Energy Reviews. 2007;11:1146-66.

[22] Pasupathy A, Velraj R, Seeniraj RV. Phase change material-based building architecture for thermal management in residential and commercial establishments. Renewable and Sustainable Energy Reviews. 2008;12:39-64.

[23] Zhu N, Ma Z, Wang S. Dynamic characteristics and energy performance of buildings using phase change materials: A review. Energy Conversion and Management. 2009;50:3169-81.

[24] Kuznik F, David D, Johannes K, Roux J-J. A review on phase change materials integrated in building walls. Renewable and Sustainable Energy Reviews. 2011;15:379-91.

[25] Cabeza LF, Castell A, Barreneche C, de Gracia A, Fernández AI. Materials used as PCM in thermal energy storage in buildings: A review. Renewable and Sustainable Energy Reviews. 2011;15:1675-95.

[26] Osterman E, Tyagi VV, Butala V, Rahim NA, Stritih U. Review of PCM based cooling technologies for buildings. Energy and Buildings. 2012;49:37-49.

[27] Knaack U. Façades: Principles of Construction: Birkhäuser; 2007.

[28] Quesada G, Rousse D, Dutil Y, Badache M, Hallé S. A comprehensive review of solar facades. Opaque solar facades. Renewable and Sustainable Energy Reviews. 2012;16:2820-32.

[29] Saadatian O, Sopian K, Lim CH, Asim N, Sulaiman MY. Trombe walls: A review of opportunities and challenges in research and development. Renewable and Sustainable Energy Reviews. 2012;16:6340-51.

[30] Sadineni SB, Madala S, Boehm RF. Passive building energy savings: A review of building envelope components. Renewable and Sustainable Energy Reviews. 2011;15:3617-31.

[31] Psarompas AM. Solarwall Energy Performance Assessment: University of Strathclyde; 2001.

[32] Anderson B, Total Environmental Action inc, Los Alamos Scientific Laboratory, Los Alamos National Laboratory. Passive solar design handbook: Van Nostrand Reinhold Co.; 1984.

[33] Loonen RCGM. Climate Adaptive Building Shells: What can we simulate? : Eindhoven University of Technology; 2010.

[34] Zhai Z, Maute K, Qi HJ, Ding Y, Andreas F. EFRI-SEED #1038305: Living Wall Materials and Systems for Automatic Building Thermo-Regulation. 2010.

[35] Tabares-Velasco PC, Christensen C, Bianchi M. Verification and validation of EnergyPlus phase change material model for opaque wall assemblies. Building and Environment. 2012;54:186-96.

[36] Bontemps A, Ahmad M, Johannès K, Sallée H. Experimental and modelling study of twin cells with latent heat storage walls. Energy and Buildings. 2011;43:2456-61.

[37] Sadasivam S, Almeida F, Zhang D, Fung AS. An Iterative Enthalpy Method to Overcome the Limitations in ESP-r's PCM Solution Algorithm. Anglais. 2011;117:100-7.

[38] Dutil Y, Rousse D, Lassue S, Zalewski L, Joulin A, Virgone J, et al. Modeling phase change materials behavior in building applications: Comments on material characterization and model validation. Renewable Energy. 2014;61:132-5.

[39] Perino M. IEA-ECBCS Annex 44: Integrating Environmentally Responsive Elements in Buildings, "State-of-the-art Review Vol.2A. Responsive Building Elements" International Energy Agency; 2008.

[40] Voller VR. An Overview of Numerical Methods for Solving Phase Change Problems. In: Minkowycz WJ, Sparrow EM, editors. Advances in numerical heat transfer: Taylor & Francis; 1997. p. 341-80.

[41] Crank J. Free and moving boundary problems: Clarendon Press; 1984.

[42] Alexiades V, Solomon AD. Mathematical modeling of melting and freezing processes: Hemisphere Pub. Corp.; 1993.

[43] Özışık N. Heat Conduction: Wiley; 1993.

[44] Voller VR, Swenson JB, Kim W, Paola C. An enthalpy method for moving boundary problems on the earth's surface. International Journal of Numerical Methods for Heat & Fluid Flow. 2006;16:641 - 54.

[45] Idelsohn S, Storti M, Crivelli L. Numerical methods in phase-change problems. Archives of Computational Methods in Engineering. 1994;1:49-74.

[46] Basu B, Date A. Numerical modelling of melting and solidification problems—A review. Sadhana. 1988;13:169-213.

[47] Hu H, Argyropoulos SA. Mathematical modelling of solidification and melting: a review Modelling and Simulation in Materials Science and Engineering. 1996;4:371-96.

[48] Voller VR, Swaminathan CR, Thomas BG. Fixed grid techniques for phase change problems: A review. International Journal for Numerical Methods in Engineering. 1990;30:875-98.

[49] Furzeland RM. A Comparative Study of Numerical Methods for Moving Boundary Problems. IMA Journal of Applied Mathematics. 1980;26:411-29.

[50] Clavier L, Arquis E, Caltagirone JP, Gobin D. A fixed grid method for the numerical solution of phase change problems. International Journal for Numerical Methods in Engineering. 1994;37:4247-61.

[51] Rolph WD, Bathe K-J. An efficient algorithm for analysis of nonlinear heat transfer with phase changes. International Journal for Numerical Methods in Engineering. 1982;18:119-34.

[52] Shamsundar N, Sparrow EM. Analysis of Multidimensional Conduction Phase Change Via the Enthalpy Model. Journal of Heat Transfer. 1975;97:333-40.

[53] Swaminathan CR, Voller VR. On the enthalpy method. Int J Num Meth Heat Fluid Flow. 1993;3:233-44.

[54] Albasiny EL. The solution of non-linear heat-conduction problems on the Pilot Ace. Proceedings of the IEE - Part B: Radio and Electronic Engineering. 1956;103:158-62.

[55] White RE. An Enthalpy Formulation of the Stefan Problem. SIAM Journal on Numerical Analysis. 1982;19:1129-57.

[56] Eyres NR, Hartree DR, Ingham J, Jackson R, Sarjant RJ, Wagstaff JB. The Calculation of Variable Heat Flow in Solids. Philosophical Transactions of the Royal Society of London Series A, Mathematical and Physical Sciences. 1946;240:1-57.

[57] Bonacina C, Comini G, Fasano A, Primicerio M. Numerical solution of phase-change problems. International Journal of Heat and Mass Transfer. 1973;16:1825-32.

[58] Morgan K. A numerical analysis of freezing and melting with convection. Computer Methods in Applied Mechanics and Engineering. 1981;28:275-84.

[59] Hsiao JS, Chung BTF. An Efficient Algorithm for Finite Element Solution to Two-Dimensional Heat Transfer With Melting and Freezing. Journal of Heat Transfer. 1986;108:462-4.

[60] Pham QT. A fast, unconditionally stable finite-difference scheme for heat conduction with phase change. International Journal of Heat and Mass Transfer. 1985;28:2079-84.

[61] Faghri A, Zhang Y. Transport phenomena in multiphase systems: Elsevier Academic Press; 2006.

[62] Zeng X, Faghri A. Temperature-Transforming Model for Binary Solid-Liquid Phase-Change Problems Part I: Mathematical Modeling and Numerical Methodology Numerical Heat Transfer, Part B: Fundamentals. 1994;25:467-80.

[63] Zeng X, Faghri A. Temperature-Transforming Model for Binary Solid-Liquid Phase-Change Problems Part II: Numerical Simulation. Numerical Heat Transfer, Part B: Fundamentals. 1994;25:481-500.

[64] Cao Y, Faghri A, Soon CW. A numerical analysis of Stefan problems for generalized multi-dimensional phase-change structures using the enthalpy transforming model. International Journal of Heat and Mass Transfer. 1989;32:1289-98.

[65] Voller VR. Implicit Finite—difference Solutions of the Enthalpy Formulation of Stefan Problems. IMA Journal of Numerical Analysis. 1985;5:201-14.

[66] Voller VR. Fast Implicit Finite-Difference Method for the Analysis of Phase Change Problems. Numerical Heat Transfer, Part B: Fundamentals. 1990;17:155-69.

[67] Swaminathan CR, Voller VR. Towards a general numerical scheme for solidification systems. International Journal of Heat and Mass Transfer. 1997;40:2859-68.

[68] Costa M, Buddhi D, Oliva A. Numerical simulation of a latent heat thermal energy storage system with enhanced heat conduction. Energy Conversion and Management. 1998;39:319-30.

[69] Salcudean M, Abdullah Z. On the numerical modelling of heat transfer during solidification processes. International Journal for Numerical Methods in Engineering. 1988;25:445-73.

[70] McAdie RL, Cross JT, Lewis RW, Gethin DT. A finite element enthalpy technique for solving coupled nonlinear heat conduction/mass diffusion problems with phase change. International Journal of Numerical Methods for Heat & Fluid Flow. 1995;5:907-21.

[71] Kelley CT. Iterative methods for linear and nonlinear equations: Society for Industrial and Applied Mathematics; 1995.

[72] Williams MA, Wilson DG. Iterative solution of a nonlinear system arising in phase-change problems. SIAM J Sci Stat Comput. 1990;11:1087-101.

[73] Knoll DA, Keyes DE. Jacobian-free Newton-Krylov methods: a survey of approaches and applications. J Comput Phys. 2004;193:357-97.

[74] Kelley CT. Solving nonlinear equations with Newton's method: Society for Industrial and Applied Mathematics; 2003.

[75] Patankar SV. Numerical heat transfer and fluid flow: Hemisphere Pub. Corp.; 1980.

[76] Shamsundar N, Rooz E. Numerical methods for moving boundary problems. In: Minkowyex WJ, Sparrow EM, Schneider GE, Pletcher RH, editors. Handbook of Numerical Heat Transfer. New York: Wiley-Interscience; 1988.

[77] Pham QT. Modelling heat and mass transfer in frozen foods: a review. International Journal of Refrigeration. 2006;29:876-88.

[78] Poirier D, Salcudean M. On numerical methods used in mathematical modeling of phase change in liquid metals. Journal of Heat Transfer. 1988;110:562-70.

[79] Heim D. Isothermal storage of solar energy in building construction. Renewable Energy. 2010;35:788-96.

[80] Poirier DJ. On numerical methods used in mathematical modelling of phase change in liquid metals: University of Ottawa (Canada). ; 1986.

[81] Hashemi HT, Sliepcevich CM. A numerical method for solving two-dimensional problems of heat conduction with change of phase. Chemical Engineering ProgSympseries. 1967;63:34-41.

[82] Virgone J, Noël J, Reisdorf R, Lyon U. Numerical study of the influence of the thickness and melting point on the effectiveness of phase change materials: application to the renovation of a low inertia school Building Simulation 2009: 11th International IBPSA Conference. Glasgow, Scotland,2009.

[83] Egolf PW, Manz H. Theory and modeling of phase change materials with and without mushy regions. International Journal of Heat and Mass Transfer. 1994;37:2917-24.

[84] Feustel HE. Simplified Numerical Description of Latent Storage Characteristics for Phase Change Wallboard. Lawrence Berkeley Laboratory Report, LBL-36933 University of California, Berkeley; 1995.

[85] Fachinotti VD, Cardona A, Huespe AE. A fast convergent and accurate temperature model for phase-change heat conduction. International Journal for Numerical Methods in Engineering. 1999;44:1863-84.

[86] Comini G, Del Guidice S, Lewis RW, Zienkiewicz OC. Finite element solution of non-linear heat conduction problems with special reference to phase change. International Journal for Numerical Methods in Engineering. 1974;8:613-24.

[87] Morgan K, Lewis RW, Zienkiewicz OC. An improved algrorithm for heat conduction problems with phase change. International Journal for Numerical Methods in Engineering. 1978;12:1191-5.

[88] Del Giudice S, Comini G, Lewis RW. Finite element simulation of freezing processes in soils. International Journal for Numerical and Analytical Methods in Geomechanics. 1978;2:223-35.

[89] Lemmon E. Multidimensional integral phase change approximations for finite element conduction codes. In: Lewis RW, Morgan K, Zienkiewicz OC, editors. Numerical Methods in Heat Transfer. New York Wiley; 1981. p. 201–13.

[90] Pham QT. The use of lumped capacitance in the finite-element solution of heat conduction problems with phase change. International Journal of Heat and Mass Transfer. 1986;29:285-91.

[91] Comini G, Giudice SD, Saro O. A conservative algorithm for multidimensional conduction phase change. International Journal for Numerical Methods in Engineering. 1990;30:697-709.

[92] Pham QT. Comparison of general-purpose finite-element methods for the Stefan problem. Numerical Heat Transfer, Part B: Fundamentals. 1995;27:417-35.

[93] Yao M, Chait A. An alternative formulation of the apparent heat capacity method for phase-change problems. Numerical Heat Transfer, Part B: Fundamentals. 1993;24:279-300.

[94] Gong Z-X, Mujumdar AS. Non-convergence versus non-conservation in effective heat capacity methods for phase change problems. International Journal of Numerical Methods for Heat & Fluid Flow. 1997;7:565-79.

[95] Storti M, Crivelli LA, Idelsohn SR. An efficient tangent scheme for solving phase-change problems. Computer Methods in Applied Mechanics and Engineering. 1988;66:65-86.

[96] Cao Y, Faghri A. A Numerical Analysis of Phase-Change Problems Including Natural Convection. Journal of Heat Transfer. 1990;112:812-6.

[97] Wang S, Faghri A, Bergman TL. A comprehensive numerical model for melting with natural convection. International Journal of Heat and Mass Transfer. 2010;53:1986-2000.

[98] Zhanhua M, Yuwen Z. Solid velocity correction schemes for a temperature transforming model for convection phase change. International Journal of Numerical Methods for Heat & Fluid Flow. 2006;16:204 - 25.

[99] Verma P, Varun, Singal SK. Review of mathematical modeling on latent heat thermal energy storage systems using phase-change material. Renewable and Sustainable Energy Reviews. 2008;12:999-1031.

[100] Regin AF, Solanki SC, Saini JS. Heat transfer characteristics of thermal energy storage system using PCM capsules: A review. Renewable and Sustainable Energy Reviews. 2008;12:2438-58.

[101] Zalba B, Marín JM, Cabeza LF, Mehling H. Review on thermal energy storage with phase change: materials, heat transfer analysis and applications. Applied Thermal Engineering. 2003;23:251-83.

[102] Dutil Y, Rousse DR, Salah NB, Lassue S, Zalewski L. A review on phase-change materials: Mathematical modeling and simulations. Renewable and Sustainable Energy Reviews. 2011;15:112-30.

[103] Agyenim F, Hewitt N, Eames P, Smyth M. A review of materials, heat transfer and phase change problem formulation for latent heat thermal energy storage systems (LHTESS). Renewable and Sustainable Energy Reviews. 2010;14:615-28.

[104] Caldwell J, Kwan YY. Numerical methods for one-dimensional Stefan problems. Communications in Numerical Methods in Engineering. 2004;20:535-45.

[105] Kaushik SC, Sodha MS, Bhardwaj SC, Kaushik ND. Periodic heat transfer and load levelling of heat flux through a PCCM thermal storage wall/roof in an air-conditioned building. Building and Environment. 1981;16:99-107.

[106] Chandra S, Kumar R, Kaushik S, Kaul S. Thermal performance of a non-air-conditioned building with PCCM thermal storage wall. Energy Conversion and Management. 1985;25:15-20.

[107] Voelker C, Kornadt O, Ostry M. Temperature reduction due to the application of phase change materials. Energy and Buildings. 2008;40:937-44.

[108] Zhu N, Wang S, Xu X, Ma Z. A simplified dynamic model of building structures integrated with shaped-stabilized phase change materials. International Journal of Thermal Sciences. 2010;49:1722-31.

[109] Zhu N, Wang S, Ma Z, Sun Y. Energy performance and optimal control of air-conditioned buildings with envelopes enhanced by phase change materials. Energy Conversion and Management. 2011;52:3197-205.

[110] Drake JB. A study of the optimal transition temperature of PCM (phase change material) wallboard for solar energy storage. 1987.

[111] Huang MJ, Eames PC, Norton B. Thermal regulation of building-integrated photovoltaics using phase change materials. International Journal of Heat and Mass Transfer. 2004;47:2715-33.

[112] Huang MJ. The effect of using two PCMs on the thermal regulation performance of BIPV systems. Solar Energy Materials and Solar Cells. 2011;95:957-63.

[113] Huang MJ, Eames PC, Hewitt NJ. The application of a validated numerical model to predict the energy conservation potential of using phase change materials in the fabric of a building. Solar Energy Materials and Solar Cells. 2006;90:1951-60.

[114] Huang MJ, Eames PC, Norton B. Comparison of Predictions Made Using a New 3D Phase Change Material Thermal Control Model with Experimental Measurements and Predictions Made Using a Validated 2D Model. Heat Transfer Engineering. 2007;28:31-7.

[115] Sá AV, Azenha M, de Sousa H, Samagaio A. Thermal enhancement of plastering mortars with Phase Change Materials: Experimental and numerical approach. Energy and Buildings. 2012;49:16-27.

[116] Almeida F, Zhang D, Fung AS, Leong WH. Comparison of Corrective Phase Change Material Algorithm With ESP-r Simulation. Proceedings of Building Simulation 2011: 12th Conference of International Building Performance Simulation Association. Sydney,2011.

[117] Chen C, Guo H, Liu Y, Yue H, Wang C. A new kind of phase change material (PCM) for energy-storing wallboard. Energy and Buildings. 2008;40:882-90.

[118] Pasupathy A, Velraj R. Mathematical Modeling and Experimental Study on Building Ceiling System Incorporating Phase Change Material (PCM) for Energy Conservation. ASME Conference Proceedings. 2006:59-68.

[119] Pasupathy A, Velraj R. Effect of double layer phase change material in building roof for year round thermal management. Energy and Buildings. 2008;40:193-203.

[120] Pasupathy A, Athanasius L, Velraj R, Seeniraj RV. Experimental investigation and numerical simulation analysis on the thermal performance of a building roof incorporating phase change material (PCM) for thermal management. Applied Thermal Engineering. 2008;28:556-65.

[121] Lin K, Zhang Y, Xu X, Di H, Yang R, Qin P. Modeling and simulation of under-floor electric heating system with shape-stabilized PCM plates. Building and Environment. 2004;39:1427-34.

[122] Xu X, Zhang Y, Lin K, Di H, Yang R. Modeling and simulation on the thermal performance of shape-stabilized phase change material floor used in passive solar buildings. Energy and Buildings. 2005;37:1084-91.

[123] Zhou G, Zhang Y, Wang X, Lin K, Xiao W. An assessment of mixed type PCM-gypsum and shape-stabilized PCM plates in a building for passive solar heating. Solar Energy. 2007;81:1351-60.

[124] Mazo J, Delgado M, Marin JM, Zalba B. Modeling a radiant floor system with Phase Change Material (PCM) integrated into a building simulation tool: Analysis of a case study of a floor heating system coupled to a heat pump. Energy and Buildings. 2012;47:458-66.

[125] Jin X, Zhang X. Thermal analysis of a double layer phase change material floor. Applied Thermal Engineering. 2011;31:1576-81.

[126] Ansuini R, Larghetti R, Giretti A, Lemma M. Radiant floors integrated with PCM for indoor temperature control. Energy and Buildings. 2011;43:3019-26.

[127] Weinläder H, Pottler K, Beck A, Fricke J. Angular-dependent measurements of the thermal radiation of the sky. High Temperatures–High Pressures. 2002;34:185–92.

[128] Weinläder H, Beck A, Fricke J. PCM-facade-panel for daylighting and room heating. Solar Energy. 2005;78:177-86.

[129] Kedl RJ. Conventional Wallboard With Latent Heat Storage For Passive Solar Applications. Energy Conversion Engineering Conference, 1990 IECEC-90 Proceedings of the 25th Intersociety1990. p. 222-5.

[130] Kim JS, Darkwa K. Simulation of an integrated PCM–wallboard system. International Journal of Energy Research. 2003;27:215-23.

[131] Kim JS, Darkwa J. Enhanced performance of laminated PCM wallboard for thermal energy storage in buildings. Energy Conversion Engineering Conference,2002. p. 647-51.

[132] Darkwa K, Kim JS. Dynamics of energy storage in phase change drywall systems. International Journal of Energy Research. 2005;29:335-43.

[133] Darkwa K, O'Callaghan PW. Simulation of phase change drywalls in a passive solar building. Applied Thermal Engineering. 2006;26:853-8.

[134] Kuznik F, Virgone J, Noel J. Optimization of a phase change material wallboard for building use. Applied Thermal Engineering. 2008;28:1291-8.

[135] Athienitis AK, Liu C, Hawes D, Banu D, Feldman D. Investigation of the thermal performance of a passive solar test-room with wall latent heat storage. Building and Environment. 1997;32:405-10.

[136] Ait Hammou Z, Lacroix M. A new PCM storage system for managing simultaneously solar and electric energy. Energy and Buildings. 2006;38:258-65.

[137] Arnault A, Mathieu-Potvin F, Gosselin L. Internal surfaces including phase change materials for passive optimal shift of solar heat gain. International Journal of Thermal Sciences. 2010;49:2148-56.

[138] Joulin A, Younsi Z, Zalewski L, Rousse DR, Lassue S. A numerical study of the melting of phase change material heated from a vertical wall of a rectangular enclosure. International Journal of Computational Fluid Dynamics. 2009;23:553-66.

[139] Joulin A, Younsi Z, Zalewski L, Lassue S, Rousse DR, Cavrot J-P. Experimental and numerical investigation of a phase change material: Thermal-energy storage and release. Applied Energy. 2011;88:2454-62.

[140] COMSOL Inc. URL: http://www.comsol.com/ [Accessed: October/23/2012].

[141] ANSYS Inc. - FLUENT. URL: http://www.ansys.com/. [Accessed: October/23/2012].

[142] The Radiation Safety Information Computational Center (RSICC) - HEATING. URL: http://www-rsicc.ornl.gov/codes/psr/psr1/psr-199.html. [Accessed: October/23/2012].

[143] Lamberg P, Lehtiniemi R, Henell A-M. Numerical and experimental investigation of melting and freezing processes in phase change material storage. International Journal of Thermal Sciences. 2004;43:277-87.

[144] Baghban MH, Hovde PJ, Gustavsen A. Numerical Simulation of a Building Envelope with High Performance Materials. COMSOL Conference. Paris,2010.

[145] Hasse C, Grenet M, Bontemps A, Dendievel R, Sallée H. Realization, test and modelling of honeycomb wallboards containing a Phase Change Material. Energy and Buildings. 2011;43:232-8.

[146] Gowreesunker BL, Tassou SA, Kolokotroni M. Improved simulation of phase change processes in applications where conduction is the dominant heat transfer mode. Energy and Buildings. 2012;47:353-9.

[147] Izquierdo-Barrientos MA, Belmonte JF, Rodríguez-Sánchez D, Molina AE, Almendros-Ibáñez JA. A numerical study of external building walls containing phase change materials (PCM). Applied Thermal Engineering. 2012;47:73-85.

[148] American Society of Heating Refrigerating Air-conditioning Engineers, Enermodal Engineering Limited, Oak Ridge National Laboratory, Polish Academy of Sciences. Modeling two-and three-dimensional heat transfer through composite wall and roof assemblies in transient energy simulation programs (1145 - TRP): Part I : final report: American Society of Heating, Refrigerating and Air-Conditioning Engineers; 2001.

[149] Ahmad M, Bontemps A, Sallée H, Quenard D. Experimental investigation and computer simulation of thermal behaviour of wallboards containing a phase change material. Energy and Buildings. 2006;38:357-66.

[150] Kosny J, Stovall TK, Shrestha SS, Yarbrough DW. Theoretical and Experimental Thermal Performance Analysis of Complex Thermal Storage Membrane Containing Bio-Based Phase Change Material (PCM). Thermal Performance of the Exterior Envelopes of Whole Buildings XI International Conference. Clearwater Beach, FL,2010.

[151] Tabares-Velasco PC, Christensen C, Bianchi MVA. Validation Methodology to Allow Simulated Peak Reduction and Energy Performance Analysis of Residential Building Envelope with Phase Change Materials. 2012 ASHRAE Annual Conference. San Antonio, Texas,2012.

[152] Hong T, Chou SK, Bong TY. Building simulation: an overview of developments and information sources. Building and Environment. 2000;35:347-61.

[153] U.S.A. Department of Energy Building Energy Software Tools Directory. URL: http://apps1.eere.energy.gov/buildings/tools_directory/. [Accessed: October/23/2012].

[154] Crawley DB, Hand JW, Kummert M, Griffith BT. Contrasting the capabilities of building energy performance simulation programs. Building and Environment. 2008;43:661-73.

[155] Barbour JP, Hittle DC. Modeling Phase Change Materials With Conduction Transfer Functions for Passive Solar Applications. Journal of Solar Energy Engineering. 2006;128:58-68.

[156] U.S.A. Department of Energy New Features in Version 2.0.0. URL: http://apps1.eere.energy.gov/buildings/energyplus/energyplus_archives.cfm#v4. [Accessed: October/23/2012].

[157] Pedersen CO. Advance Zone Simulation in ENERGYPLUS: Incorporation of Variable Properties and Phase Change Material (PCM) Capability Building Simulation 2007,. China,2007.

[158] U.S.A. Department of Energy - EnergyPlus Engineering Reference. URL: http://apps1.eere.energy.gov/buildings/energyplus/pdfs/engineeringreference.pdf. [Accessed: October/23/2012].

[159] Castell A, Medrano M, Castellón C, Cabeza LF. Analysis of the simulation models for the use of PCM in buildings. Effstock 2009 Thermal Energy Storage for Efficiency and Sustainability. Stockholm (Sweden),2009.

[160] Muruganantham K. Application of Phase Change Material in Buildings: Field Data vs. EnergyPlus Simulation: Arizona State University; 2010.

[161] Tardieu A, Behzadi S, Chen JJ, Farid MM. Computer Simulation and Experimental Measurements for an Experimental PCM-Impregnated Office Building Proceedings of Building Simulation 2011: 12th Conference of International Building Performance Simulation Association. Sydney,2011.

[162] Zhuang C, Deng A, Chen Y, Li S, Zhang H, Fan G. Validation of Veracity on Simulating the Indoor Temperature in PCM Light Weight Building by EnergyPlus. In: Li K, Fei M, Jia L, Irwin G, editors. Life System Modeling and Intelligent Computing: Springer Berlin / Heidelberg; 2010. p. 486-96.

[163] Campbell KR. Phase Change Material as a Thermal Storage Device for Passive Houses: Portland State University; 2011.

[164] Chan ALS. Energy and environmental performance of building façades integrated with phase change material in subtropical Hong Kong. Energy and Buildings. 2011;43:2947-55.

[165] Kuznik F, Virgone J, Roux J-J. Energetic efficiency of room wall containing PCM wallboard: A full-scale experimental investigation. Energy and Buildings. 2008;40:148-56.

[166] Shrestha S, Miller W, Stovall T, Desjarlais A, Childs K, Porter W, et al. Modeling PCM-Enhanced Insulation System and Benchmarking ENERGYPLUS Against Controlled Field Data. Proceedings of Building Simulation 2011: 12th Conference of International Building Performance Simulation Association. Sydney,2011.

[167] Tabares-Velasco PC, Griffith B. Diagnostic test cases for verifying surface heat transfer algorithms and boundary conditions in building energy simulation programs. Journal of Building Performance Simulation. 2011:1-18.

[168] Bradley D, Kummert M. New Evolutions in TRNSYS-A Selection of Version 16 Features. Proceedings of Building Simulation 2005: 9th Conference of International Building Performance Simulation Association. Montréal, Canada,2005.

[169] Ghoneim AA, Klein SA, Duffie JA. Analysis of collector-storage building walls using phase-change materials. Solar Energy. 1991;47:237-42.

[170] Ghoneim AA. Efficient Collection and Storage of Solar Energy: UNIVERSITY OF ALEXANDRIA; 1989.

[171] Stritih U, Novak P. Solar heat storage wall for building ventilation. Renewable Energy. 1996;8:268-71.

[172] Stritih U. Heat transfer enhancement in latent heat thermal storage system for buildings. Energy and Buildings. 2003;35:1097-104.

[173] Jokisalo J LP, Siren K. Suitability of building construction materials in short-term energy storage-office room simulations. Proceedings of IEA Annex 10-PCMs and Chemical Reactions for Thermal Energy Storage, 3rd Workshop. Finland, 1999. p. 11-8.

[174] Ahmad M, Bontemps A, Sallée H, Quenard D. Thermal testing and numerical simulation of a prototype cell using light wallboards coupling vacuum isolation panels and phase change material. Energy and Buildings. 2006;38:673-81.

[175] Ibáñez M, Lázaro A, Zalba B, Cabeza LF. An approach to the simulation of PCMs in building applications using TRNSYS. Applied Thermal Engineering. 2005;25:1796-807.

[176] Schranzhofer H, Puschnig P, Heinz A, Streicher W. Validation of a TRNSYS simulation model for PCM energy storage and PCM wall construction element. Ecostock Conference,2006.

[177] Kuznik F, Virgone J, Johannes K. Development and validation of a new TRNSYS type for the simulation of external building walls containing PCM. Energy and Buildings. 2010;42:1004-9.

[178] Thermal Energy System Specialists LLC -TESS Libraries - Individual Component Libraries. URL: http://www.trnsys.com/tess-libraries/individual-components.php [Accessed: October/23/2012].

[179] University of Strathclyde - Energy Systems Research Unit - ESP-r. URL: http://www.esru.strath.ac.uk/Programs/ESP-r.htm [Accessed: October/23/2012].

[180] Heim D. Two Solution Methods of Heat Transfer with Phase Change Within Whole Building Dynamic Simulation. Proceedings of Building Simulation 2005: 9th Conference of International Building Performance Simulation Association. Montréal, Canada,2005.

[181] Heim D, Clarke JA. Numerical modelling and thermal simulation of PCM–gypsum composites with ESP-r. Energy and Buildings. 2004;36:795-805.

[182] Schossig P, Henning HM, Gschwander S, Haussmann T. Micro-encapsulated phase-change materials integrated into construction materials. Solar Energy Materials and Solar Cells. 2005;89:297-306.

[183] Fernandes NTA, Costa VAF. Use of Phase-Change Materials as Passive Elements for Climatization Purposes in Summer: The Portuguese Case. International Journal of Green Energy. 2009;6:302-11.

[184] Almeida F, Zhang D, Fung AS, Leong WH. Investigation of Multilayered Phase-Change-Material Modeling in ESP-R. International High Performance Buildings Conference. Purdue,2010.

[185] Sigalas G. Computational Optimization of Passive use of Phase Change Materials in Lightweight Low-Energy Houses. Eindhoven: University of Technology; 2011.

[186] AALBORG University - Danish Building Research Institute. URL: http://www.en.sbi.dk/publications/programs_models/bsim/about-bsim. [Accessed: October/23/2012].

[187] Rose J, Lahme A, Christensen NU, Heiselberg P, Hansen M. Numerical Method for Calculating Latent Heat Storage in Constructions Containing Phase Change Material Building Simulation 2009: 11th International IBPSA Conference. Glasgow, Scotland,2009.

[188] Stetiu C, Feustel HE, Winkelmann FC. Development of a Simulation Tool to Evaluate the Performance of Radiant Cooling Ceilings. Lawrence Berkeley Laboratory Report, LBL-37300: University of California, Berkeley; 1995.

[189] Kissock K. ESim Building Energy Simulation Software. Department of Mechanical and Aerospace Engineering, University of Dayton, Dayton, OH. ; 1997.

[190] Valentin Energy Software - PCMExpress. URL: http://www.valentin.de/en/products/pcm/58/pcm-express. [Accessed: October/23/2012].

[191] Stetiu C. Radiant Cooling in US Office Buildings: Towards Eliminating the Perception of Climate-Imposed Barriers: University of California Berkeley; 1997.

[192] Sowell EF, Haves P. Efficient solution strategies for building energy system simulation. Energy and Buildings. 2001;33:309-17.

[193] Feustel HE, Stetiu C. Thermal Performance of Phase Change Wallboard for Residential Cooling Application. Lawrence Berkeley Laboratory Report, LBL-38320 University of California, Berkeley; 1997.

[194] University of Dayton- Mechanical and Aerospace Engineering-ESim. URL: http://academic.udayton.edu/kissock/http/RESEARCH/EnergySoftware.htm [Accessed: October/23/2012].

[195] Kelly Kissock J, Michael Hannig J, Whitney TI, Drake ML. Testing and simulation of phase change wallboard for thermal storage in buildings. In: Morehouse JM, Hogan RE, editors. International Solar Energy Conference. Albuquerque,: American Society of Mechanical Engineers; 1998.

[196] Gatzka B, Valentin G. PCMexpress – Planning and Simulation Programme for the Use of Phase Change Materials (PCM) in buildings: Demonstrating its use in residential and office buildings in Ireland. International Conference for Sustainable Energy Storage 2011. Belfast, UK,2011.

[197] Colclough S, Griffiths P, Gschwander S. Thermal Energy Storage and the Passive House Standard: How PCM incorporated into wallboard can aid thermal comfort. PLEA2009 - The 26th Conference on Passive and Low Energy Architecture. Quebec City- Canada, 2009.

[198] Kissock K. Thermal Load Reduction from Phase-Change Building Components in Temperature Controlled Buildings. ASME International Solar Energy Conference. Madison, WI, June.2000.

[199] Zhang M, Medina MA, King JB. Development of a thermally enhanced frame wall with phase-change materials for on-peak air conditioning demand reduction and energy savings in residential buildings. International Journal of Energy Research. 2005;29:795-809.

[200] Medina MA, King JB, Zhang M. On the heat transfer rate reduction of structural insulated panels (SIPs) outfitted with phase change materials (PCMs). Energy. 2008;33:667-78.

[201] Evers AC, Medina MA, Fang Y. Evaluation of the thermal performance of frame walls enhanced with paraffin and hydrated salt phase change materials using a dynamic wall simulator. Building and Environment. 2010;45:1762-8.

[202] Lee KO, University of Kansas. Civil E, Engineering A. Using Hydrated Salt Phase Change Materials for Residential Air Conditioning Peak Demand Reduction and Energy Conservation in Coastal and Transitional Climates in the State of California: University of Kansas; 2013.

[203] Biswas K, Childs PW, Atchley JA. Field Testing of Nano-PCM Enhanced Building Envelope Components. 2013. p. Medium: ED.

[204] Affiliated Engineers. Preliminary analysis of PCM strategies, "URL: www.phasechange.com/Research%20Library/OSH_JC_PCM_Analysis.pdf". [Accessed: April/09/2014].

[205] Stetiu C, Feustel HE. Phase change wallboard and mechanical night ventilation in commercial buildings. Lawrence Berkeley Laboratory Report: University of California, Berkeley; 1998.

[206] Childs KW, Stovall TK. Potential Energy Savings Due to Phase Change Material in a Building Wall Assembly: An Examination of Two Climates. 2012. p. Medium: ED.

[207] Seong Y-B, Lim J-H. Energy Saving Potentials of Phase Change Materials Applied to Lightweight Building Envelopes. Energies. 2013;6:5219-30.

[208] Diaconu BM, Cruceru M. Novel concept of composite phase change material wall system for year-round thermal energy savings. Energy and Buildings. 2010;42:1759-72.

[209] Shukla N, Fallahi A, Kosny J. Performance characterization of PCM impregnated gypsum board for building applications. Energy Procedia. 2012;30:370-9.

[210] Ramprasad C, Edwin S. L, Daniel E. F. An Enhanced Simulation Model for Building Envelopes with Phase Change Materials. Anglais. 2013;119.

[211] Swaminathan C, Voller V. A general enthalpy method for modeling solidification processes. Metallurgical and Materials Transactions B. 1992;23:651-64.

[212] Spitler JD, Rees SJ, Xiao D, Mechanical OSUSo, Engineering A, American Society of Heating R, et al. Development of an Analytical Verification Test Suite for Whole Building Energy Simulation Programs: Building Fabric : ASHRAE 1052-RP Final Report: Oklahoma State University, School of Mechanical and Aerospace Engineering; 2001.

[213] Sunliang C. State of the art thermal energy storage solutions for high performance buildings. Finland: University of Jyväskylä; 2010.

[214] Haavi T, Murphy MA, Kuznik F, Gustavsen A. Zero emission building envelopes - numerical simulations of a Well-insulated building with phase change material panels Integrated in the floor. Proceedings of Building Simulation 2011: 12th International IBPSA Conference. Sydney, 14-16 November2011.

[215] Polly B, Kruis N, Roberts D. Assessing and Improving the Accuracy of Energy Analysis for Residential Buildings. 2011:Medium: ED; Size: 41 pp.

[216] Perez GAC. Hybrid Models for Hydrological Forecasting: Integration of Data-Driven and Conceptual Modelling Techniques: CRC Press/Balkema; 2009.

[217] MATLAB File Exchanger. URL: http://www.mathworks.com/matlabcentral/fileexchange/18798-timeit-benchmarking-function. [Accessed: November/20/2013].

[218] Mathworks. URL: http://www.mathworks.com/. [Accessed: November/01/2012].

[219] Cigler J, Tomáško P, Široký J. BuildingLAB: A tool to analyze performance of model predictive controllers for buildings. Energy and Buildings. 2013;57:34-41.

[220] Chen Y, Treado S. Development of a simulation platform based on dynamic models for HVAC control analysis. Energy and Buildings. 2014;68, Part A:376-86.

[221] Kulkarni MR, Hong F. Energy optimal control of a residential space-conditioning system based on sensible heat transfer modeling. Building and Environment. 2004;39:31-8.

[222] Riederer P. Matlab/simulink for building and hvac simulation - state of the art. Proceedings of Building Simulation 2005: 9th Conference of International Building Performance Simulation Association. Montréal, Canada,2005.

[223] Gamberi M, Manzini R, Regattieri A. Simulink© simulator for building hydronic heating systems using the Newton–Raphson algorithm. Energy and Buildings. 2009;41:848-55.

[224] Marsik T, Johnson R. Use of Simulink to evaluate the air-quality and energy performance of HRV-equipped residences in Fairbanks, Alaska. Energy and Buildings. 2008;40:1605-13.

[225] van Schijndel AWM. Integrated Heat Air and Moisture Modeling and Simulation: Technische Universiteit Eindhoven; 2007.

[226] Kalagasidis AS, Weitzmann P, Nielsen TR, Peuhkuri R, Hagentoft C-E, Rode C. The International Building Physics Toolbox in Simulink. Energy and Buildings. 2007;39:665-74.

[227] Qin M, Belarbi R, Aït-Mokhtar A, Allard F. Simulation of coupled heat and moisture transfer in air-conditioned buildings. Automation in Construction. 2009;18:624-31.

[228] Mendes N, Oliveira G H C, Araújo H X, S CL. A MATLAB-based simulation tool for building thermal performance analysis. Proceedings of Building Simulation 2003: Eighth International IBSA Conference. Endhoven,2003.

[229] Ma P, Wang L-S, Guo N. Modeling of TABS-based thermally manageable buildings in Simulink. Applied Energy. 2013;104:791-800.

[230] Yu B, van Paassen AHC. Simulink and bond graph modeling of an air-conditioned room. Simulation Modelling Practice and Theory. 2004;12:61-76.

[231] Wilcox S, Marion W. Users Manual for TMY3 Data Sets (Revised). Related Information: Supercedes April 2008 version2008. p. Medium: ED; Size: 58 pp.

[232] Duffie JA, Beckman WA. Solar Engineering of Thermal Processes: Wiley; 2006.

[233] Klucher TM. Evaluation of models to predict insolation on tilted surfaces. Solar Energy. 1979;23:111-4.

[234] J.E. H, J.A. D. Calculations of the solar radiation incident on an inclined surface. Proc of First Canadian Solar Radiation Data Workshop Canada: Ministry of Supply and Services; 1980.

[235] Reindl DT, Beckman WA, Duffie JA. Diffuse fraction correlations. Solar Energy. 1990;45:1-7.

[236] Muneer T. Solar Radiation and Daylight Models: Taylor & Francis; 2012.

[237] Perez R, Seals R, Ineichen P, Stewart R, Menicucci D. A new simplified version of the perez diffuse irradiance model for tilted surfaces. Solar Energy. 1987;39:221-31.

[238] Perez R, Ineichen P, Seals R, Michalsky J, Stewart R. Modeling daylight availability and irradiance components from direct and global irradiance. Solar Energy. 1990;44:271-89.

[239] Loutzenhiser PG, Manz H, Felsmann C, Strachan PA, Frank T, Maxwell GM. Empirical validation of models to compute solar irradiance on inclined surfaces for building energy simulation. Solar Energy. 2007;81:254-67.

[240] Utzinger DM. Analysis of building components related to direct solar heating of buildings: University of Wisconsin--Madison.; 1979.

[241] Randall KR, Mitchell JW, El-Wakil MM. Natural Convection Heat Transfer Characteristics of Flat Plate Enclosures. Journal of Heat Transfer. 1979;101:120-5.

[242] Mercer WE, Pearce WM, Hitchcock JE. Laminar Forced Convection in the Entrance Region Between Parallel Flat Plates. Journal of Heat Transfer. 1967;89:251-6.

[243] Kays WM, Crawford ME. Convective heat and mass transfer: McGraw-Hill; 1980.

[244] Hollands KGT, Unny TE, Raithby GD, Konicek L. Free Convective Heat Transfer Across Inclined Air Layers. Journal of Heat Transfer. 1976;98:189-93.

[245] Shen J, Lassue S, Zalewski L, Huang D. Numerical study on thermal behavior of classical or composite Trombe solar walls. Energy and Buildings. 2007;39:962-74.

[246] Cane RLD, Hollands KGT, Raithby GD, Unny TE. Free Convection Heat Transfer Across Inclined Honeycomb Panels. Journal of Heat Transfer. 1977;99:86-91.

[247] Athienitis AK, Ramadan H. Numerical model of a building with transparent insulation. Solar Energy. 1999;67:101-9.

[248] ElSherbiny SM, Raithby GD, Hollands KGT. Heat Transfer by Natural Convection Across Vertical and Inclined Air Layers. Journal of Heat Transfer. 1982;104:96-102.

[249] Manz H. Numerical simulation of heat transfer by natural convection in cavities of facade elements. Energy and Buildings. 2003;35:305-11.

[250] Wright JL. A Correlation to Quantify Convective Heat Transfer Between Vertical Window Glazings. Anglais. 1996;102:940-6.

[251] ISO 15099. Thermal performance of windows, doors and shading devices -- Detailed calculations. International Organization for Standardization; 2003.

[252] Fishenden MW, Saunders OA. An Introduction to Heat Transfer, By M. Fishenden and O.A. Saunders1950.

[253] Zalewski L, Chantant M, Lassue S, Duthoit B. Experimental thermal study of a solar wall of composite type. Energy and Buildings. 1997;25:7-18.

[254] Tsuji T, Nagano Y. Characteristics of a turbulent natural convection boundary layer along a vertical flat plate. International Journal of Heat and Mass Transfer. 1988;31:1723-34.

[255] Ji J, Luo C, Sun W, Yu H, He W, Pei G. An improved approach for the application of Trombe wall system to building construction with selective thermo-insulation façades. Chinese Science Bulletin. 2009;54:1949-56.

[256] Smolec W, Thomas A. Theoretical and experimental investigations of heat transfer in a trombe wall. Energy Conversion and Management. 1993;34:385-400.

[257] Pratt RG, Laboratory CSUSEA. Turbulent Free Convection Duct Flows in Trombe Walls: Solar Energy Applications Laboratory, Colorado State University; 1980.

[258] Akbarzadeh A, Charters WWS, Lesslie DA. Thermocirculation characteristics of a Trombe wall passive test cell. Solar Energy. 1982;28:461-8.

[259] Churchill SW, Chu HHS. Correlating equations for laminar and turbulent free convection from a vertical plate. International Journal of Heat and Mass Transfer. 1975;18:1323-9.

[260] Zrikem Z, Bilgen E. Theoretical study of a composite Trombe-Michel wall solar collector system. Solar Energy. 1987;39:409-19.

[261] Churchill SW, Usagi R. A general expression for the correlation of rates of transfer and other phenomena. AIChE Journal. 1972;18:1121-8.

[262] Bar-Cohen A, Rohsenow WM. Thermally Optimum Spacing of Vertical, Natural Convection Cooled, Parallel Plates. Journal of Heat Transfer. 1984;106:116-23.

[263] Seferis P, Strachan P, Dimoudi A, Androutsopoulos A. Investigation of the performance of a ventilated wall. Energy and Buildings. 2011;43:2167-78.

[264] Fang Y, University of Kansas. Civil E, Engineering A. A Comprehensive Study of Phase Change Materials (PCMs) for Building Walls Applications: University of Kansas; 2009.

[265] National Gypsum URL: http://www.thermalcore.info/product-info.htm [Accessed: January/16/2014].

[266] BASF URL: http://www.basf.co.uk/ecp1/UK_Ireland/en/content/Products_Industries/Solutions/basf_house/07_The_Materials/06_Phase_Change_Materials/Phase_Change_Materials. [Accessed: January/16/2014].

[267] RUBITHERM URL: http://www.rubitherm.de/english/index.htm. [Accessed: January/17/2014].

[268] Inaba H, Tu P. Evaluation of thermophysical characteristics on shape-stabilized paraffin as a solid-liquid phase change material. Heat and Mass Transfer. 1997;32:307-12.

[269] Xiao M, Feng B, Gong K. Preparation and performance of shape stabilized phase change thermal storage materials with high thermal conductivity. Energy Conversion and Management. 2002;43:103-8.

[270] Carbonari A, De Grassi M, Di Perna C, Principi P. Numerical and experimental analyses of PCM containing sandwich panels for prefabricated walls. Energy and Buildings. 2006;38:472-83.

[271] Konuklu Y, Paksoy HO. Phase Change Material Sandwich Panels for Managing Solar Gain in Buildings. Journal of Solar Energy Engineering. 2009;131:041012-7.

[272] Phase Change Energy Solutions URL: http://www.phasechange.com/index.php/en/about/biopcm-biopcmat-thermastix. [Accessed: January/16/2014].

[273] Wunderlich B. Thermal Analysis. In: Buschow KHJ, Cahn RW, Flemings MC, Ilschner B, Kramer EJ, Mahajan S, et al., editors. Encyclopedia of Materials: Science and Technology (Second Edition). Oxford: Elsevier; 2001. p. 9134-41.

[274] Zhang Y, Jiang Y. A simple method, the T-history method, of determining the heat of fusion, specific heat and thermal conductivity of phase-change materials. Measurement Science and Technology. 1999;10:201.

[275] Günther E, Hiebler S, Mehling H, Redlich R. Enthalpy of Phase Change Materials as a Function of Temperature: Required Accuracy and Suitable Measurement Methods. International Journal of Thermophysics. 2009;30:1257-69.

[276] Jan Kośny, Yarbrough D, William Miller, Thomas Petrie, Phillip Childs, Azam Mohiuddin Syed. 2006/07 Field Testing of Cellulose Fiber Insulation Enhanced with Phase Change Material ORNL/TM-2007/186. 2008. p. Medium: ED.

[277] Liu H, Awbi HB. Performance of phase change material boards under natural convection. Building and Environment. 2009;44:1788-93.

[278] ANSI/ASHRAE Standard 140-2011. Standard Method of Test for the Evaluation of Building Energy Analysis Computer Programs: Atlanta, GA: ASHRAE.; 2011.

[279] Engebrecht-Metzger C, Wilson E, Horowitz S. Addendum to the Building America House Simulation Protocols. 2012. p. Medium: ED; Size: 36 pp.

[280] Hendron R, Engebrecht C. Building America House Simulation Protocols (Revised). Related Information: Supercedes September 2010 version2010. p. Medium: ED; Size: 88 pp.

[281] Soares N, Costa JJ, Gaspar AR, Santos P. Review of passive PCM latent heat thermal energy storage systems towards buildings' energy efficiency. Energy and Buildings. 2013;59:82-103.

[282] Mehling H, Cabeza LF. Heat and Cold Storage with PCM: An Up to Date Introduction Into Basics and Applications: Springer; 2010.

[283] Tatsidjodoung P, Le Pierrès N, Luo L. A review of potential materials for thermal energy storage in building applications. Renewable and Sustainable Energy Reviews. 2013;18:327-49.

[284] Iten M, Liu S. A work procedure of utilising PCMs as thermal storage systems based on air-TES systems. Energy Conversion and Management. 2014;77:608-27.

[285] American Society of Heating R, Engineers A-C. ASHRAE Handbook: Fundamentals: American Society of Heating, Refrigerating, and Air-Conditioning Engineers; 2005.

[286] American Society of Heating R, Engineers AC, Parsons R. 1997 ASHRAE Handbook: Fundamentals: American Society of heating refrigerating and air aconditioning enginerers; 1997.

[287] Zhai Z, Chen Q, Haves P, Klems JH. On approaches to couple energy simulation and computational fluid dynamics programs. Building and Environment. 2002;37:857-64.

[288] Mirsadeghi M. Co-simulation of building energy simulation and computational fluid dynamics for whole-building heat, air and moisture engineering: Eindhoven University of Technology; 2011.

[289] Trˇcka M. Co-simulation for Performance Prediction of Innovative Integrated Mechanical Energy Systems in Buildings: Eindhoven University of Technology; 2008.

[290] Wetter M. Co-simulation of building energy and control systems with the Building Controls Virtual Test Bed. Journal of Building Performance Simulation. 2010;4:185-203.

[291] Nghiem TX. MLE+ manual URL: http://www.seas.upenn.edu/~nghiem/mleplus.html. [Accessed: November/01/2012].

[292] Riederer P, Keilholz W, Ducreux V. Coupling of TRNSYS with SIMULINK – a method to automatically export and use TRNSYS models within SIMULINK and vice versa. Proceedings of Building Simulation 2009: 11th Conference of International Building Performance Simulation Association. Glasgow, Scotland,2009.

[293] Mathworks. URL: http://www.mathworks.com/products/compiler/mcr/. [Accessed: February/03/2014].

[294] Judkoff R, Neymark J. International Energy Agency building energy simulation test (BESTEST) and diagnostic method. Other Information: Supercedes report DE94000280; PBD: Feb 1995; PBD: 1 Feb 19951995. p. Medium: ED; Size: 296 pages.

[295] Beccali G, Cellura M, Brano VL, Orioli A. Is the transfer function method reliable in a European building context? A theoretical analysis and a case study in the south of Italy. Applied Thermal Engineering. 2005;25:341-57.

[296] Giuliani M, Avesani S, Oberegger UF. Quantitative comparison of massive walls thermal response among commercial software. Proceedings of Building Simulation 2013: 13th Conference of International Building Performance Simulation Association. Chambéry, France,2013.

[297] Delcroix B, Kummert M, Daoud A, Hiller M. Improved conduction transfer function coefficients generation in TRNSYS multizone building model Proceedings of Building Simulation 2013: 13th Conference of International Building Performance Simulation Association. Chambéry, France,2013.

[298] MORSE ES. WARMING AND VENTILATING APARTMENTS BY THE SUN S RAYS. In: Office USP, editor. USA1881.

[299] Trombe F, Michel J. NATURALLY AIR-CONDITIONED DWELLINGS. In: Patent US, editor. France 1972.

[300] Kneifel J. NIST TN - 1765: Prototype Residential Building Designs for Energy and Sustainability Assessment. 2012.

[301] Armin Rudd, Hugh I. Henderson J, Daniel Bergey, Don B. Shirey, ASHRAE. Energy Efficiency and Cost Assessment of Humidity Control Options for Residential Buildings : ASHRAE 1449-RP Final Report: Building Science Corp., CDH Energy Corp., and University of Central Florida / Florida Solar Energy Center,; 2013.

[302] American Society of Heating R, Engineers A-C, Institute ANS. Energy Efficient Design of Low Rise Residential Buildings: American Society of Heating, Refrigerating and Air-Conditioning Engineers; 2004.

[303] TRANSSOLAR Energietechnik GmbH. TRNSYS 16: A TRaNsient SYstem Simulation program, Volume 6: Multizone Building modeling with Type56 and TRNBuild. 2007.

[304] American Society of Heating R, Engineers A-C, America IESoN. Energy standard for buildings except low-rise residential buildings: American Society of Heating, Refrigerating and Air-Conditioning Engineers; 2004.

[305] Stovall TK, Tomlinson JJ. What are the Potential Benefits of Including Latent Storage in Common Wallboard? Journal of Solar Energy Engineering. 1995;117:318-25.

[306] Peippo K, Kauranen P, Lund PD. A multicomponent PCM wall optimized for passive solar heating. Energy and Buildings. 1991;17:259-70.

[307] Neeper DA. Thermal dynamics of wallboard with latent heat storage. Solar Energy. 2000;68:393-403.

[308] Soares N, Gaspar AR, Santos P, Costa JJ. Multi-dimensional optimization of the incorporation of PCM-drywalls in lightweight steel-framed residential buildings in different climates. Energy and Buildings. 2014;70:411-21.

[309] Wang J, Long E, Qin W, Xu L. Ultrathin envelope thermal performance improvement of prefab house by integrating with phase change material. Energy and Buildings. 2013;67:210-6.

[310] Energy Information Administration. Electric Power Monthly URL: http://www.eia.gov/electricity/monthly/epm_table_grapher.cfm?t=epmt_5_6_a. [Accessed: April/13/2014].

[311] Energy Information Administration. Natural Gas Prices URL: http://www.eia.gov/dnav/ng/ng_pri_sum_a_EPG0_PRS_DMcf_a.htm. [Accessed: April/13/2014].

[312] Crossett JD. Cost of BioPCM product. 2013.

[313] Affiliated Engineers. URL: http://www.aeieng.com/services/sustainability/phase_change_materials.php. [Accessed: April/08/2014].

[314] KONDO, #160, Takeshi, IBAMOTO, Tadahiko. Research on thermal storage using rock wool phase-change material ceiling board. New York, NY, ETATS-UNIS: American Society of Heating, Refrigerating and Air-conditioning Engineers; 2006.

[315] Karim L, Barbeon F, Gegout P, Bontemps A, Royon L. New phase-change material components for thermal management of the light weight envelope of buildings. Energy and Buildings. 2014;68, Part B:703-6.

[316] Anderson B, Riordan M. The solar home book: heating, cooling, and designing with the sun: Cheshire Books; 1976.

[317] Kosny J, Kossecka E, Brzezinski A, Tleoubaev A, Yarbrough D. Dynamic thermal performance analysis of fiber insulations containing bio-based phase change materials (PCMs). Energy and Buildings. 2012;52:122-31.

APPENDICES

Appendix A: Contour plots for multilayer PCM-enhanced walls for Golden, CO

Appendix A.1 South Wall

Appendix A.1.1 PCM to the interior

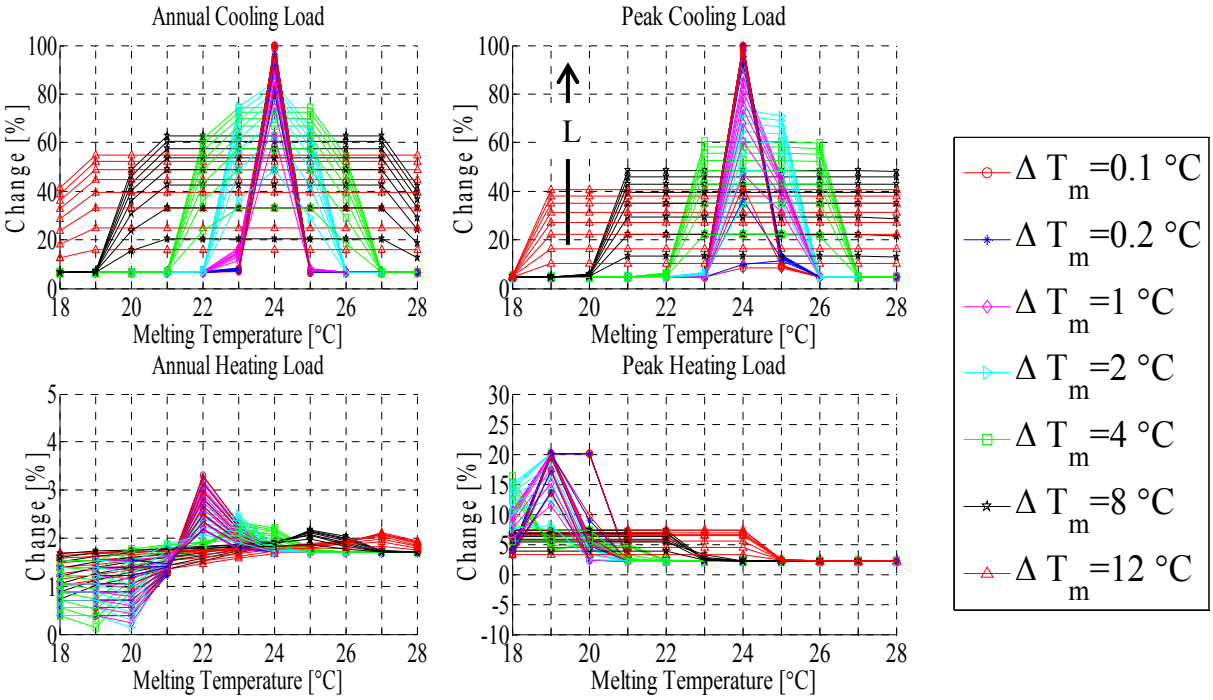

a) Percentage reductions in cooling and heating loads across all parameters

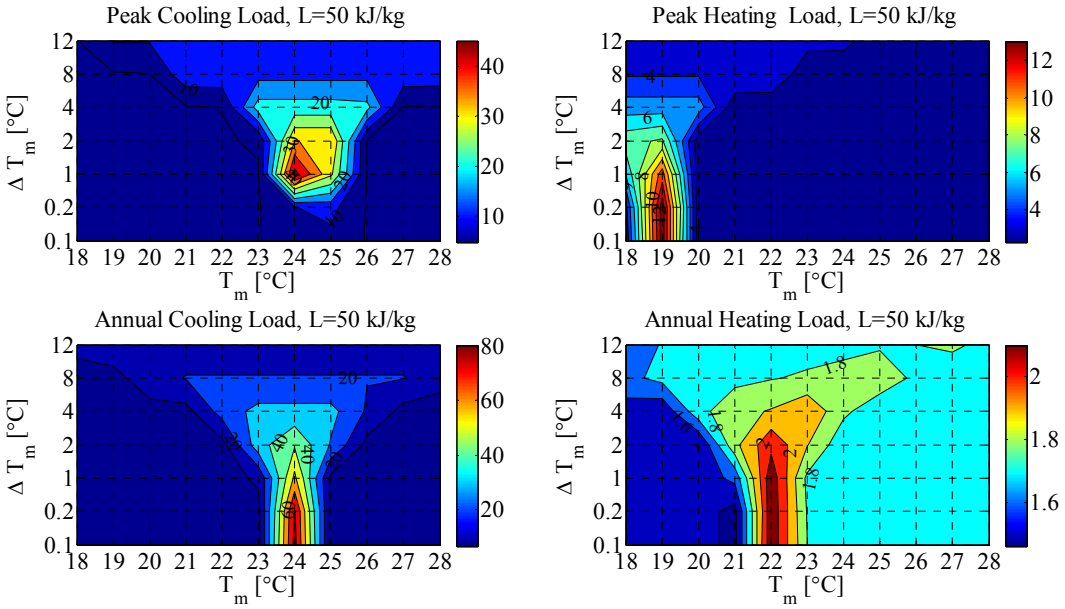

b) A contour plot for the case of 50 kg/kJ showing percentage reduction in cooling and

heating loads

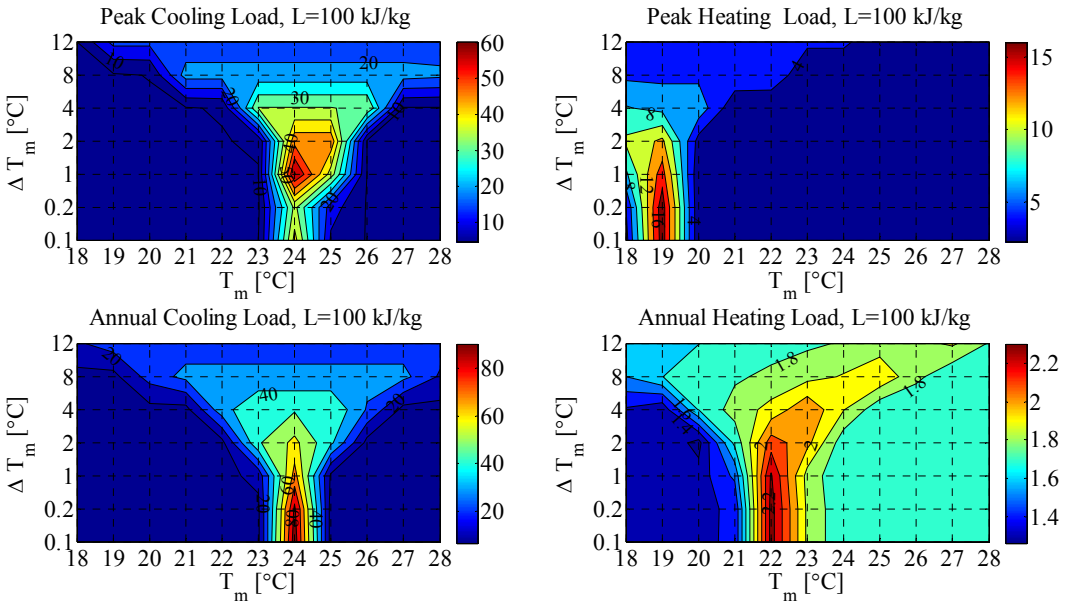

c) A contour plot for the case of 100 kg/kJ showing percentage reduction in cooling and heating loads

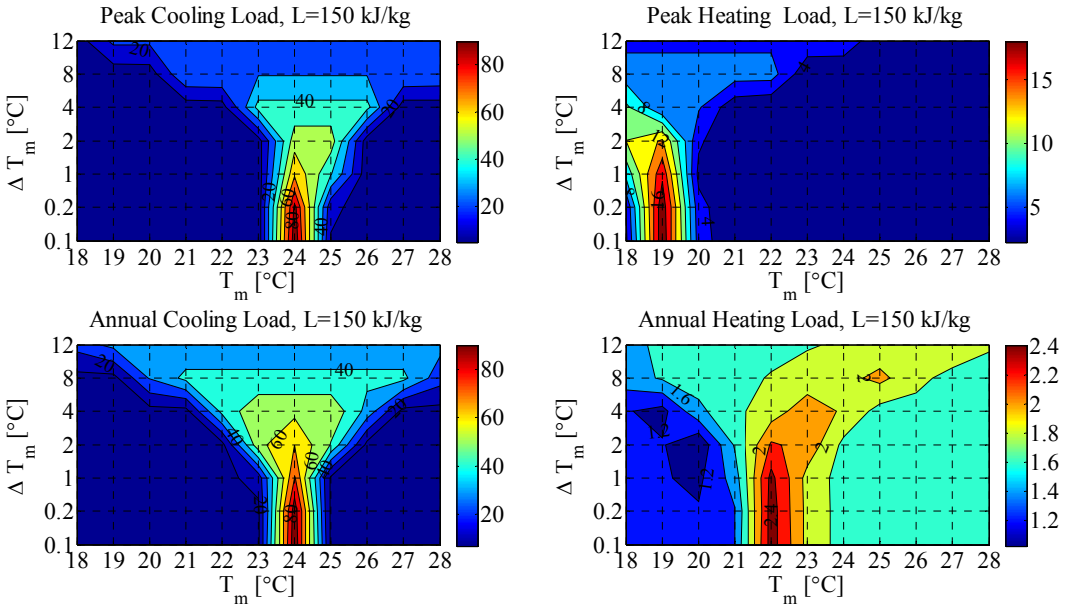

d) A contour plot for the case of 150 kg/kJ showing percentage reduction in cooling and heating loads

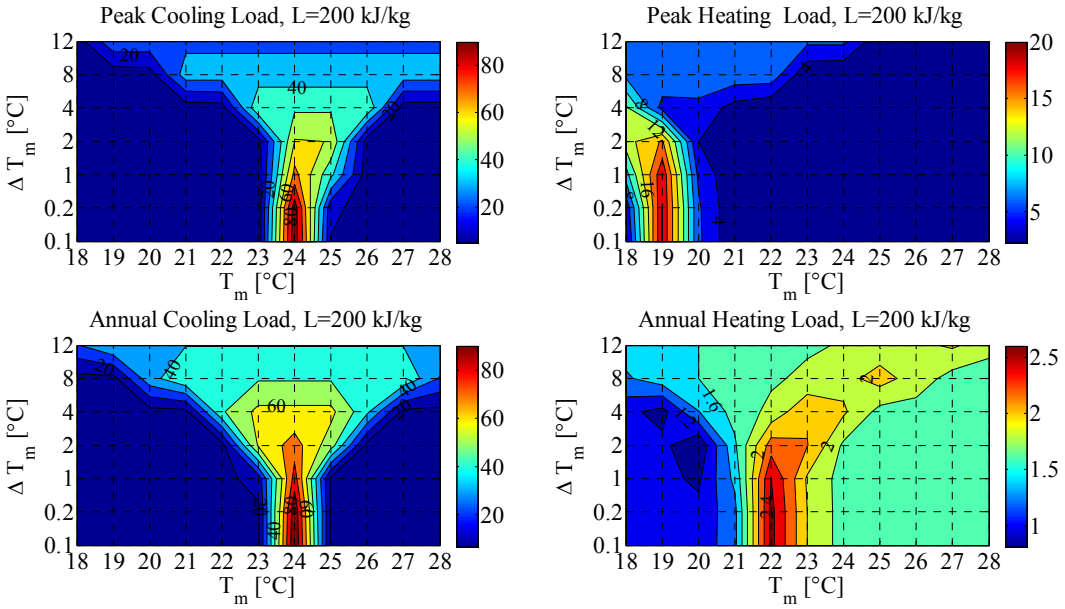

e) A contour plot for the case of 200 kg/kJ showing percentage reduction in cooling and heating loads

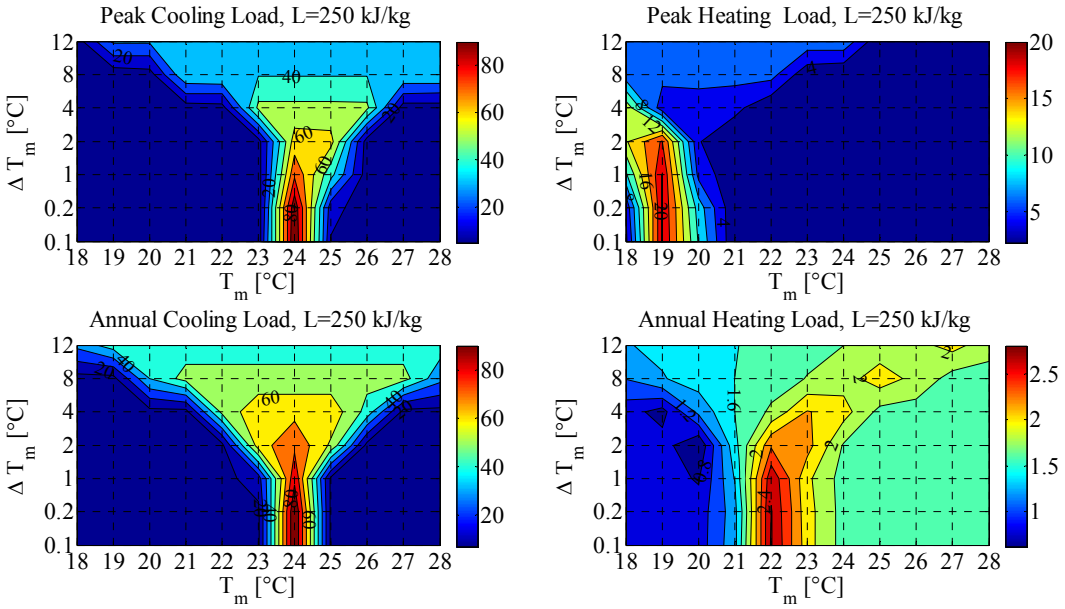

f) A contour plot for the case of 250 kg/kJ showing percentage reduction in cooling and heating loads

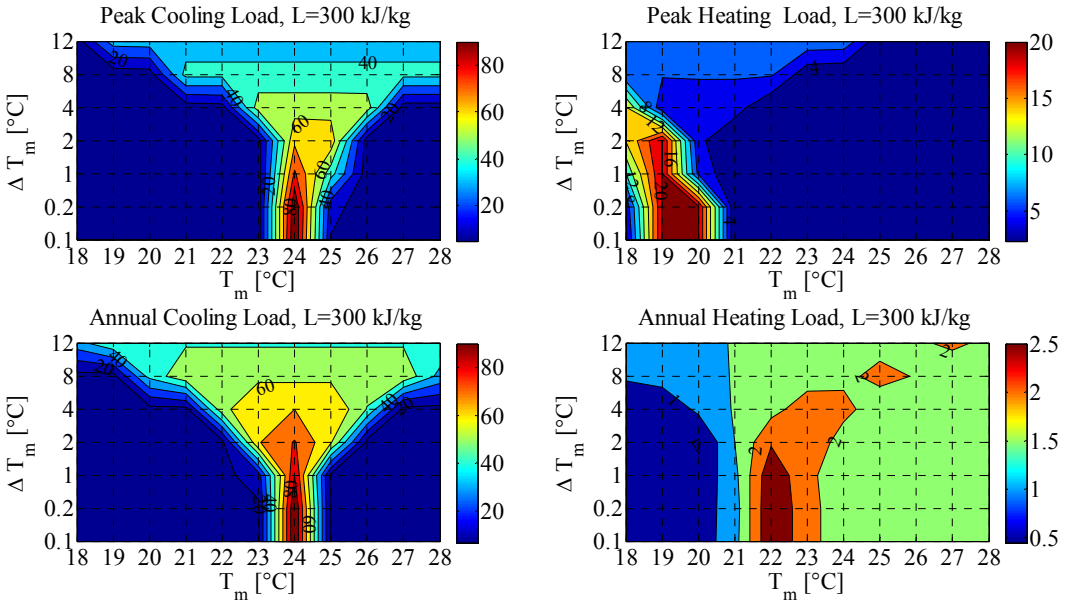

g) A contour plot for the case of 300 kg/kJ showing percentage reduction in cooling and heating loads

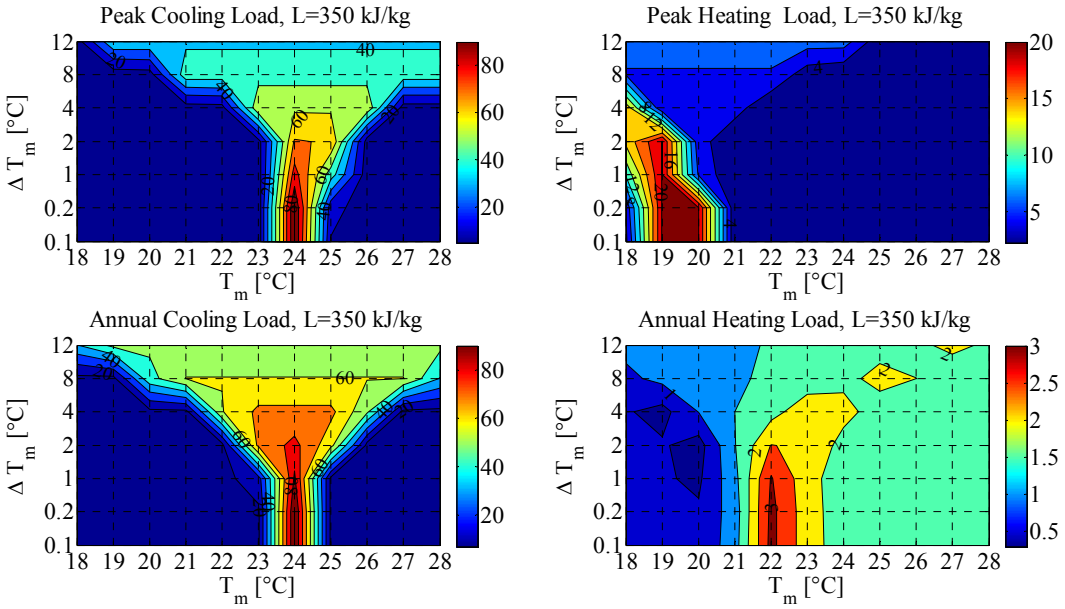

h) A contour plot for the case of 350 kg/kJ showing percentage reduction in cooling and heating loads

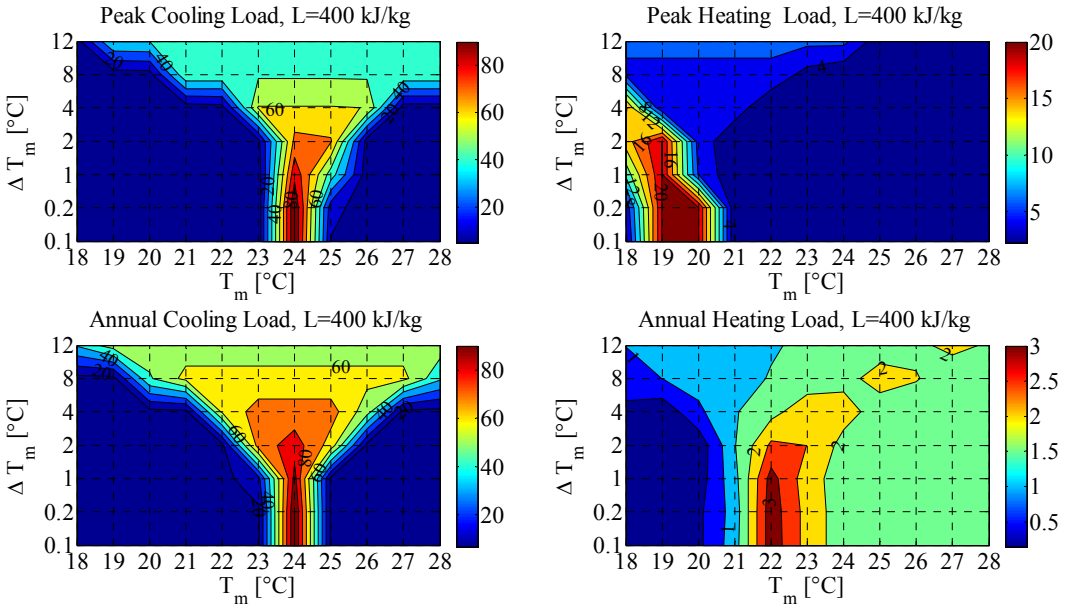

i) A contour plot for the case of 400 kg/kJ showing percentage reduction in cooling and heating loads

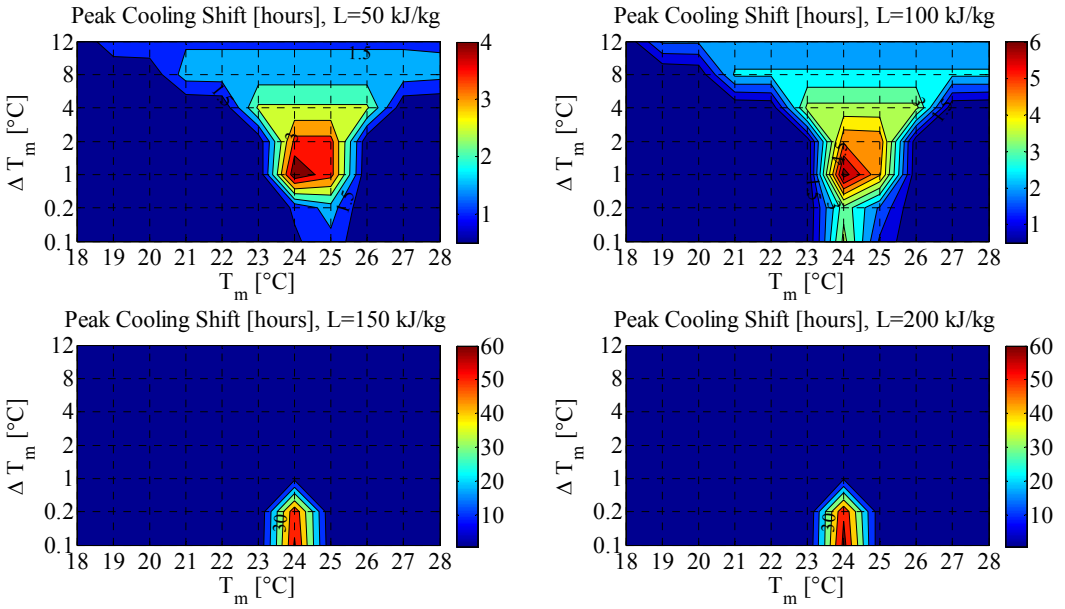

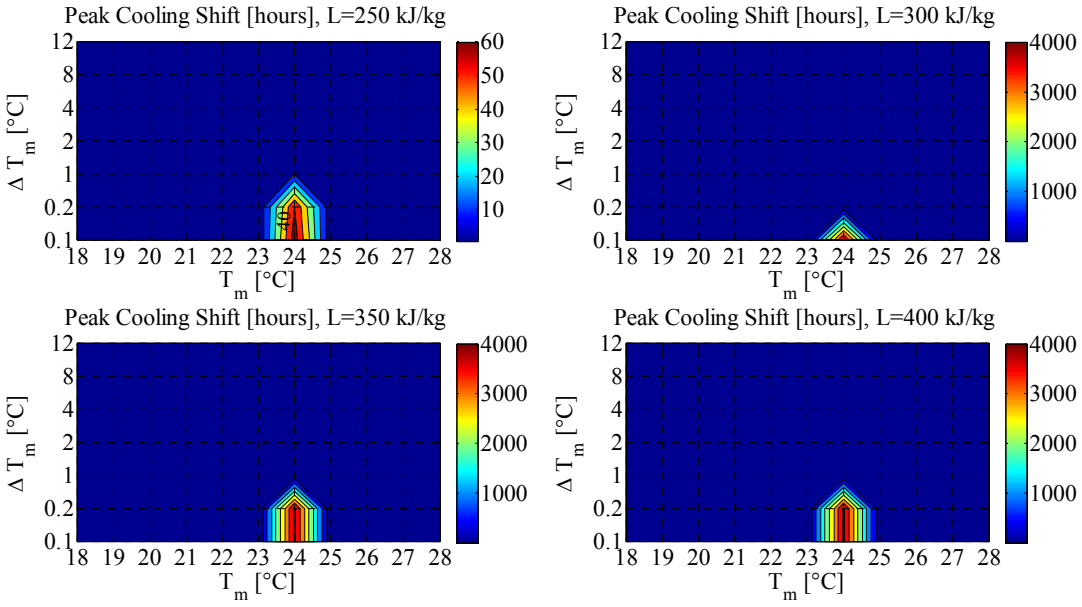

j) A contour plot for the peak cooling shift in hours

Figure A.1 Percentage reductions in cooling and heating loads for south wall when PCM to the interior , Golden, CO

Appendix A.1.2 PCM in the middle

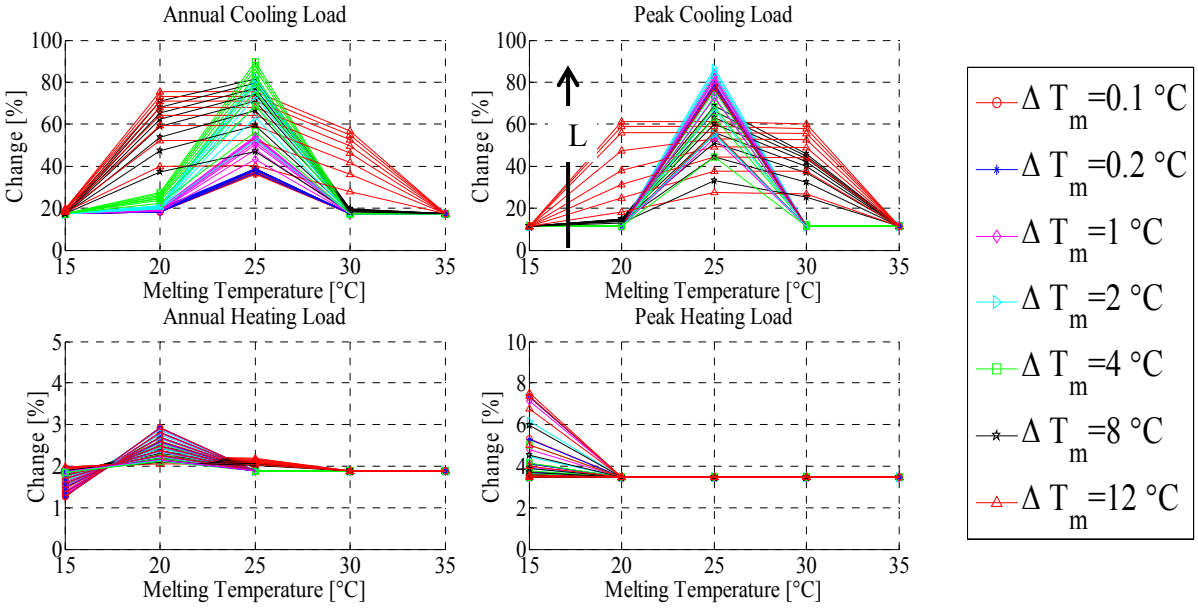

a) Percentage reductions in cooling and heating loads across all parameters

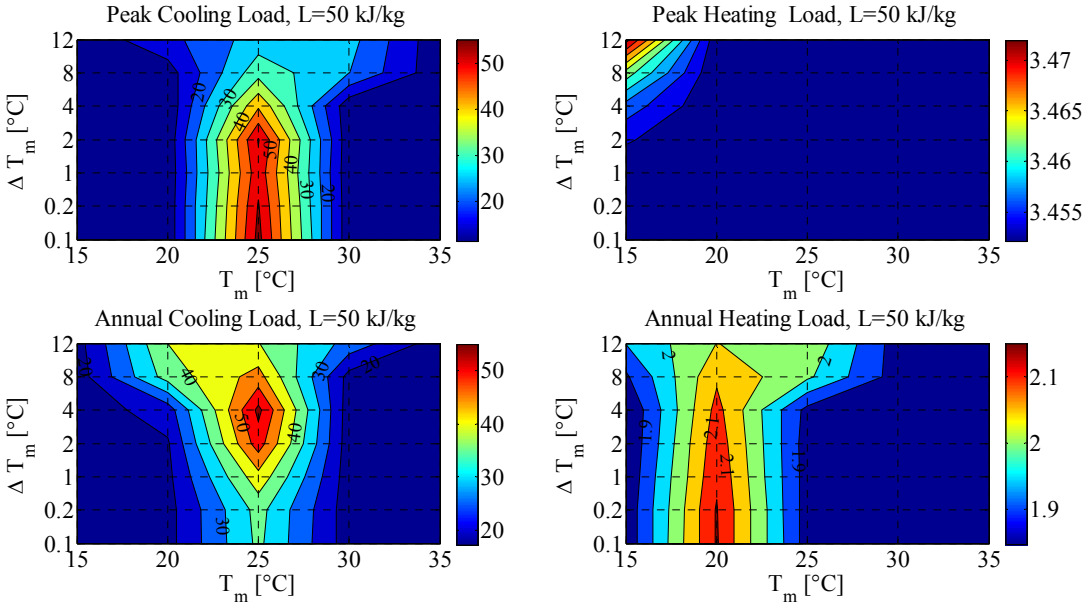

b) A contour plot for the case of 50 kg/kJ showing percentage reduction in cooling and heating loads

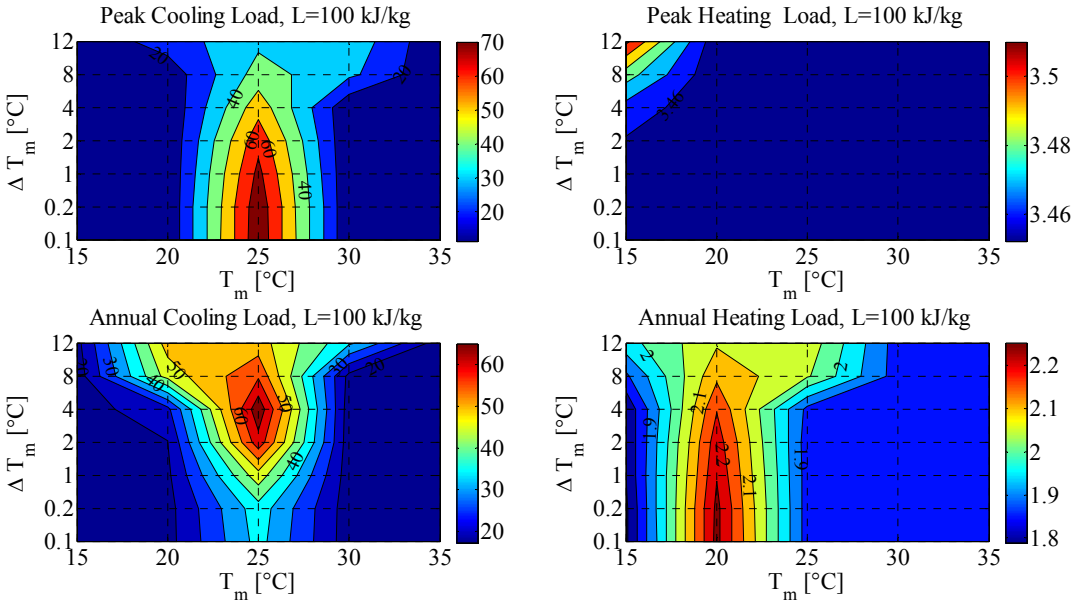

c) A contour plot for the case of 100 kg/kJ showing percentage reduction in cooling and heating loads

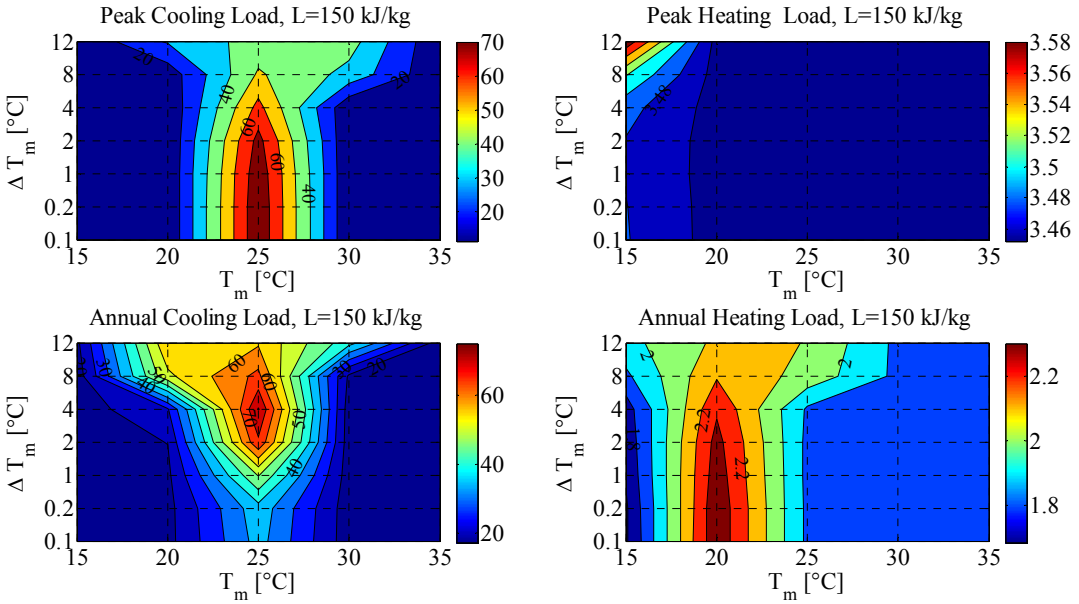

d) A contour plot for the case of 150 kg/kJ showing percentage reduction in cooling and heating loads

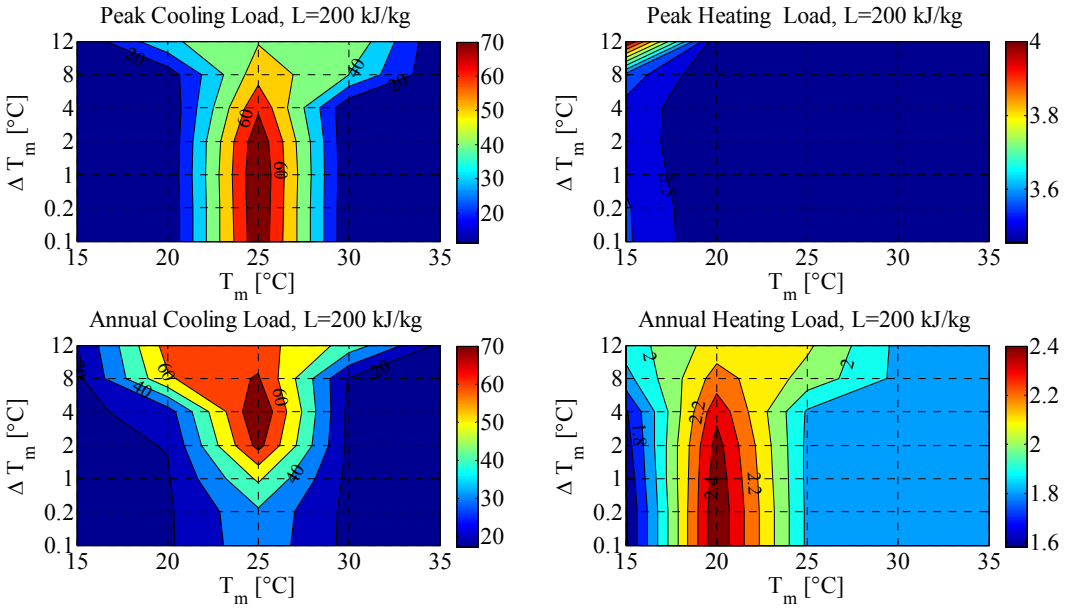

e) A contour plot for the case of 200 kg/kJ showing percentage reduction in cooling and heating loads

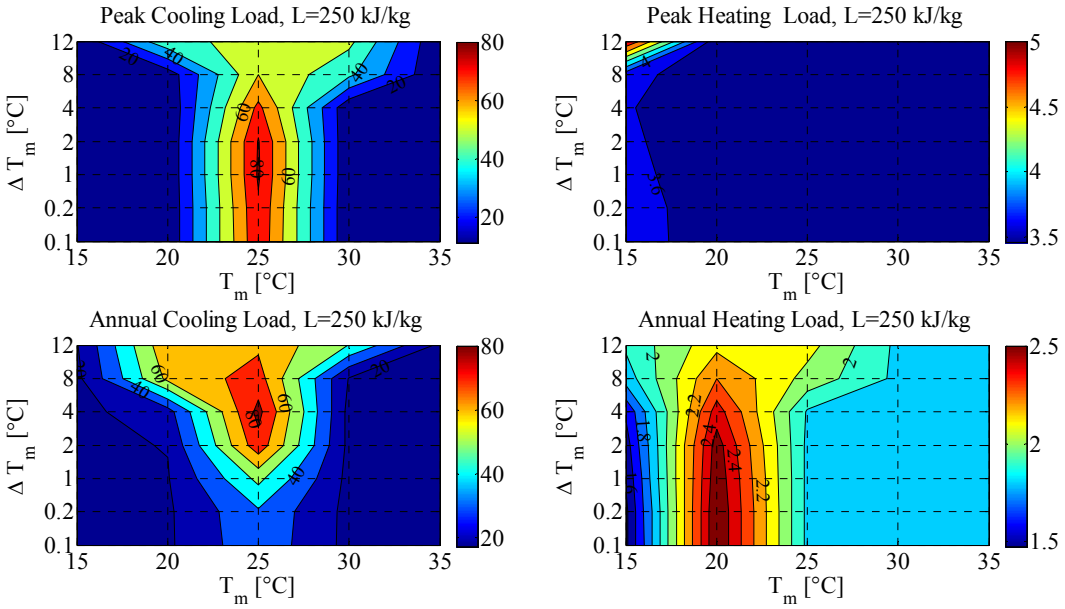

f) A contour plot for the case of 250 kg/kJ showing percentage reduction in cooling and heating loads

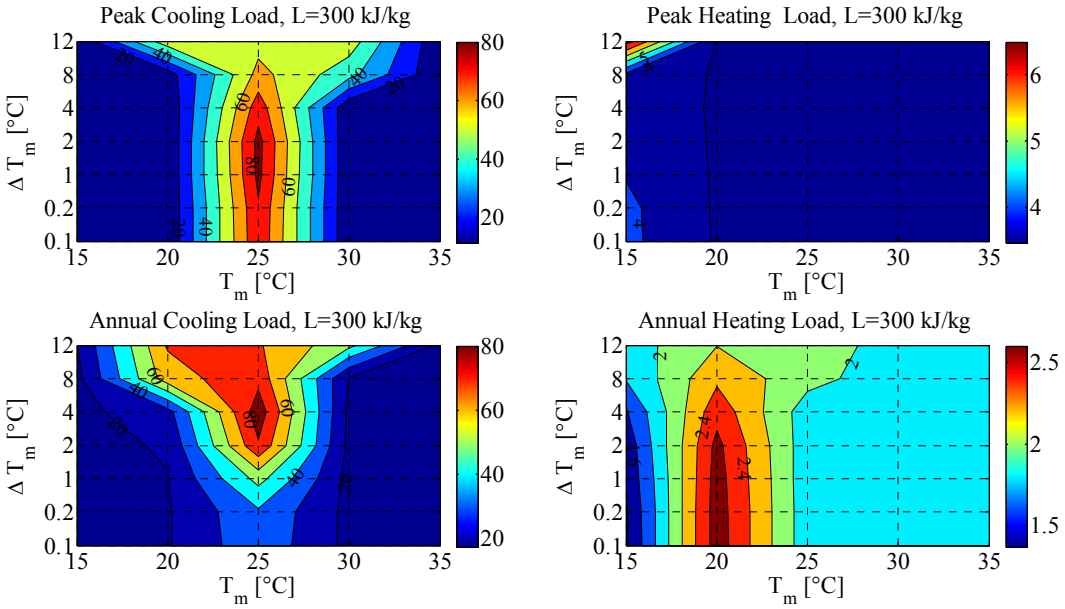

g) A contour plot for the case of 300 kg/kJ showing percentage reduction in cooling and heating loads

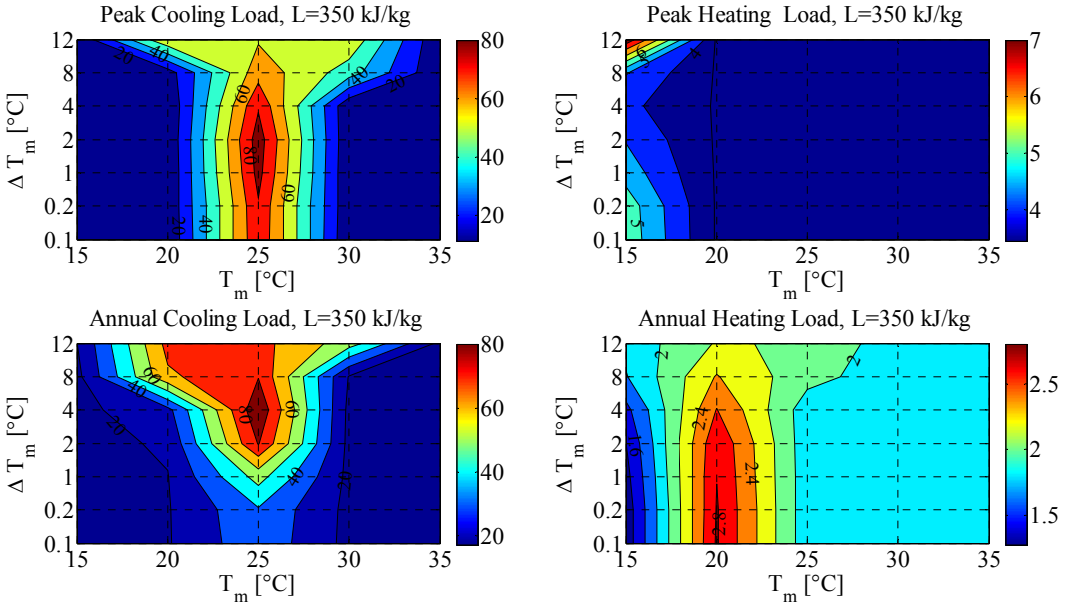

h) A contour plot for the case of 350 kg/kJ showing percentage reduction in cooling and heating loads

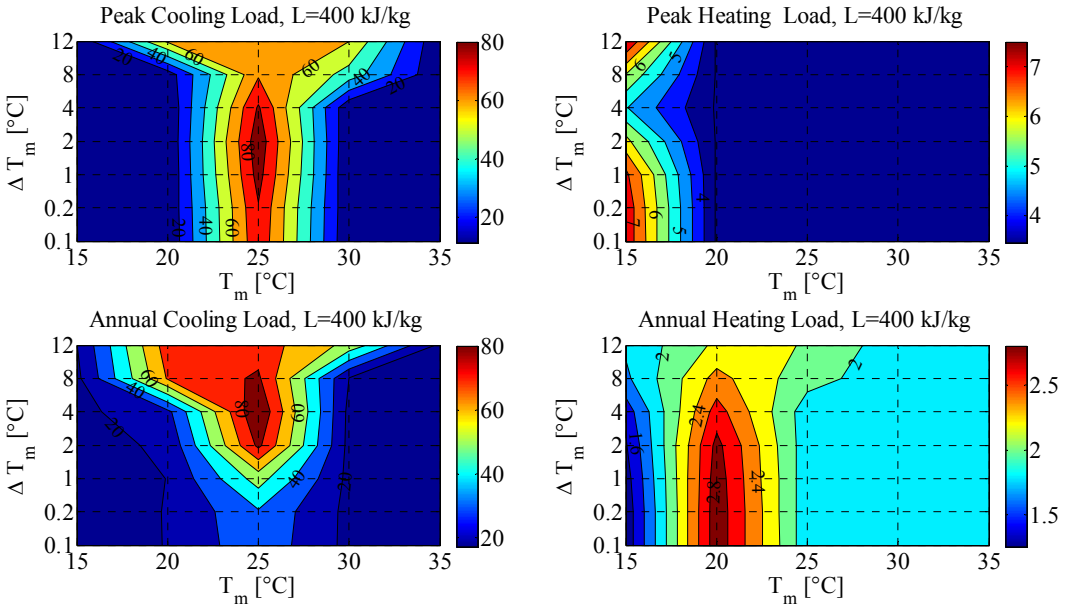

i) A contour plot for the case of 400 kg/kJ showing percentage reduction in cooling and heating loads

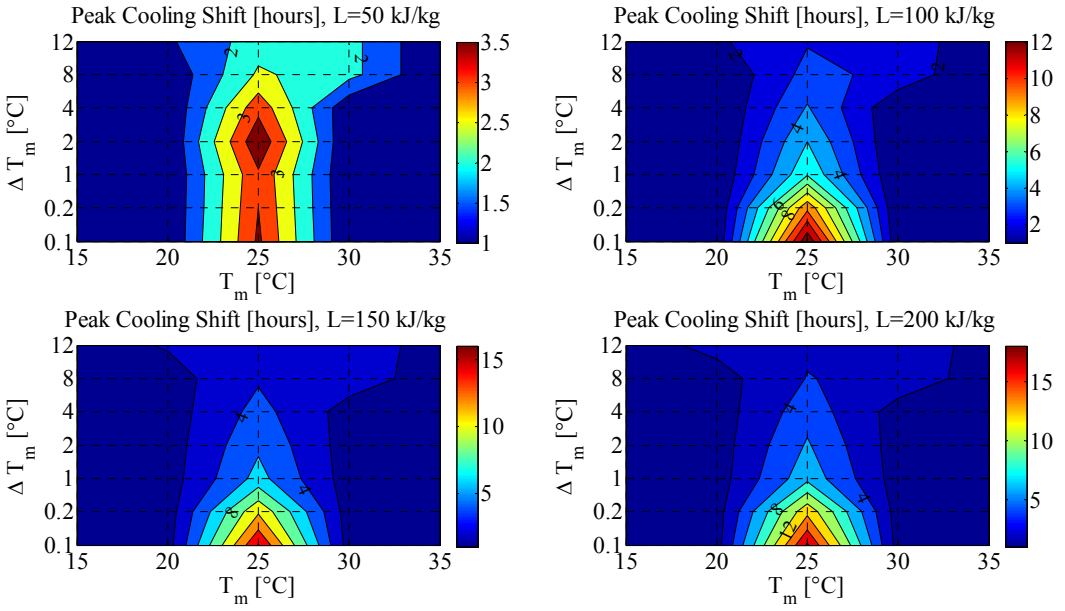

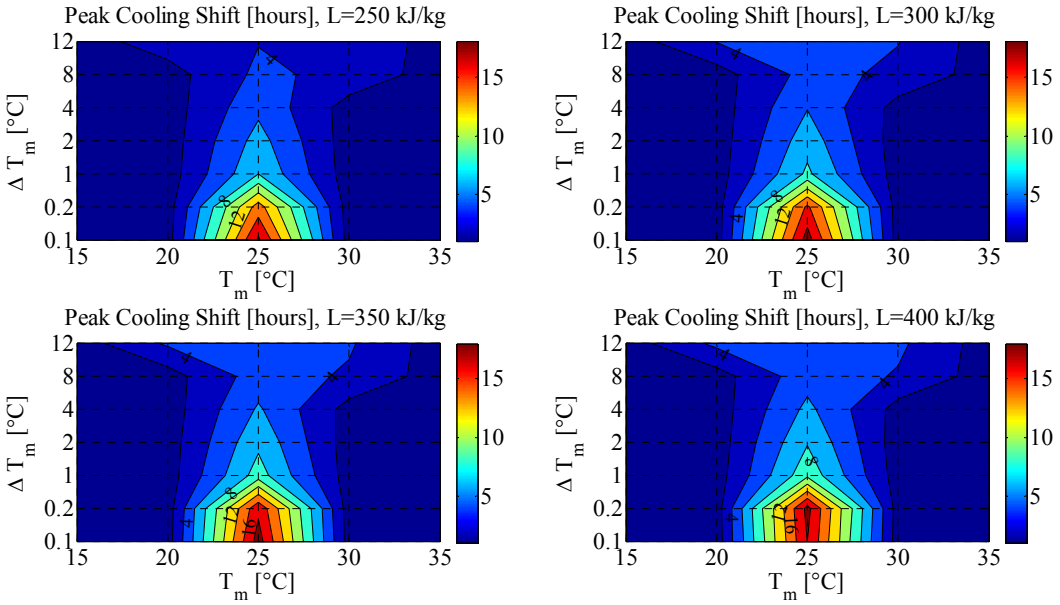

j) A contour plot for the peak cooling shift in hours

Figure A.2 Percentage reductions in cooling and heating loads for south wall when PCM in the middle, Golden, CO

Appendix A.1.3 PCM to the exterior

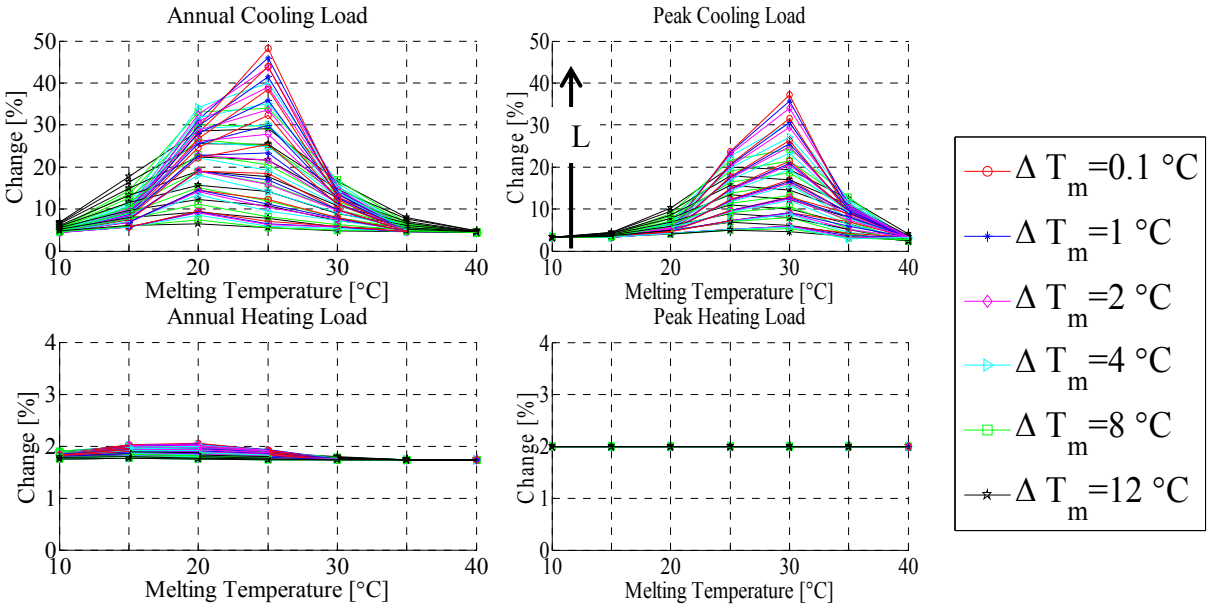

a) Percentage reductions in cooling and heating loads across all parameters

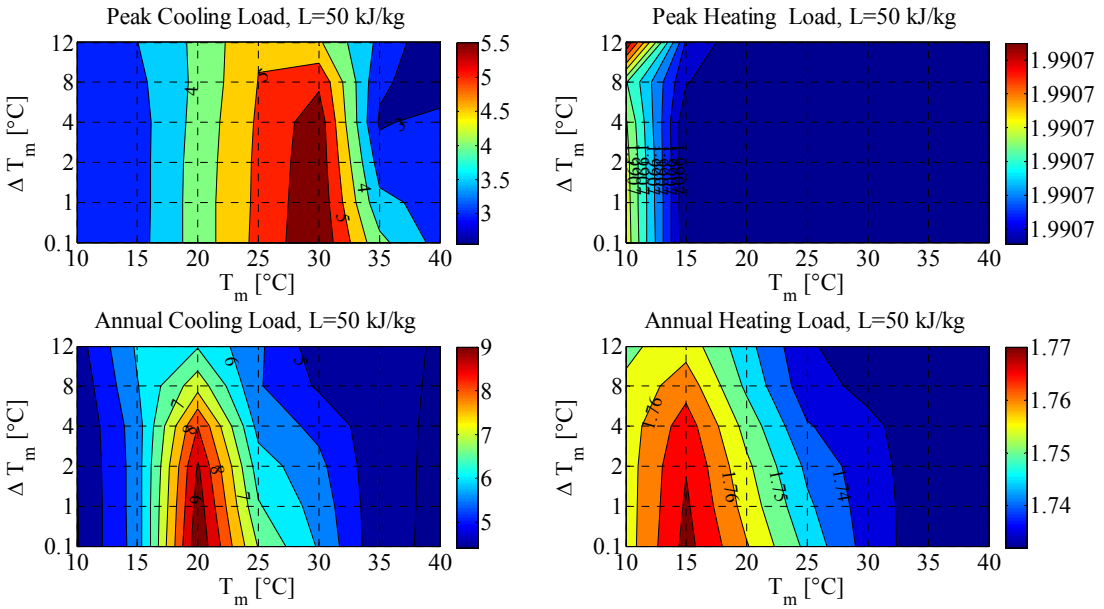

b) A contour plot for the case of 50 kg/kJ showing percentage reduction in cooling and heating loads

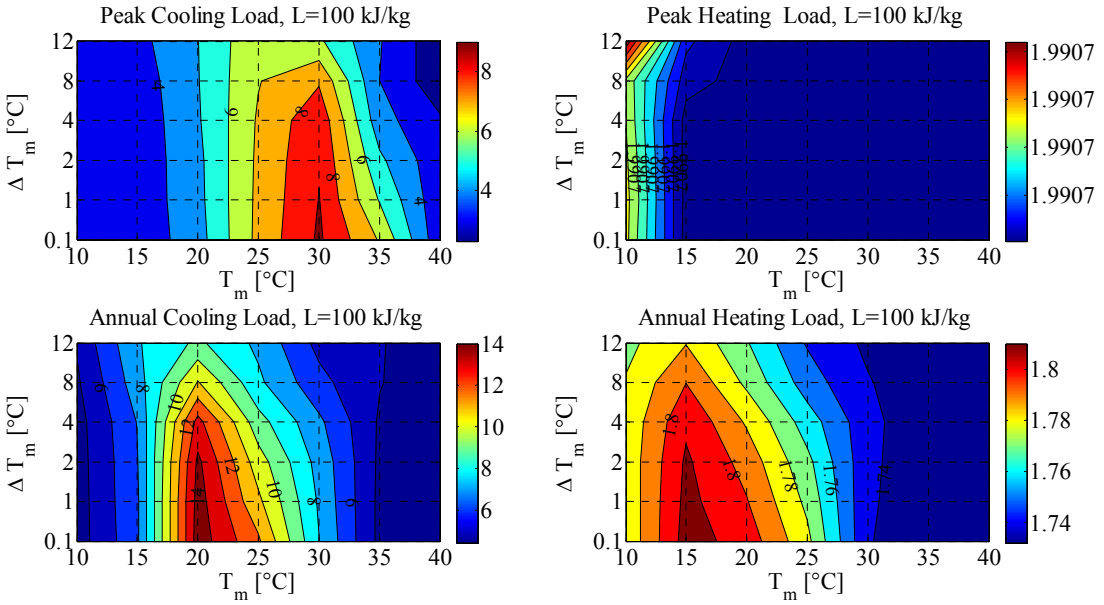

c) A contour plot for the case of 100 kg/kJ showing percentage reduction in cooling and heating loads

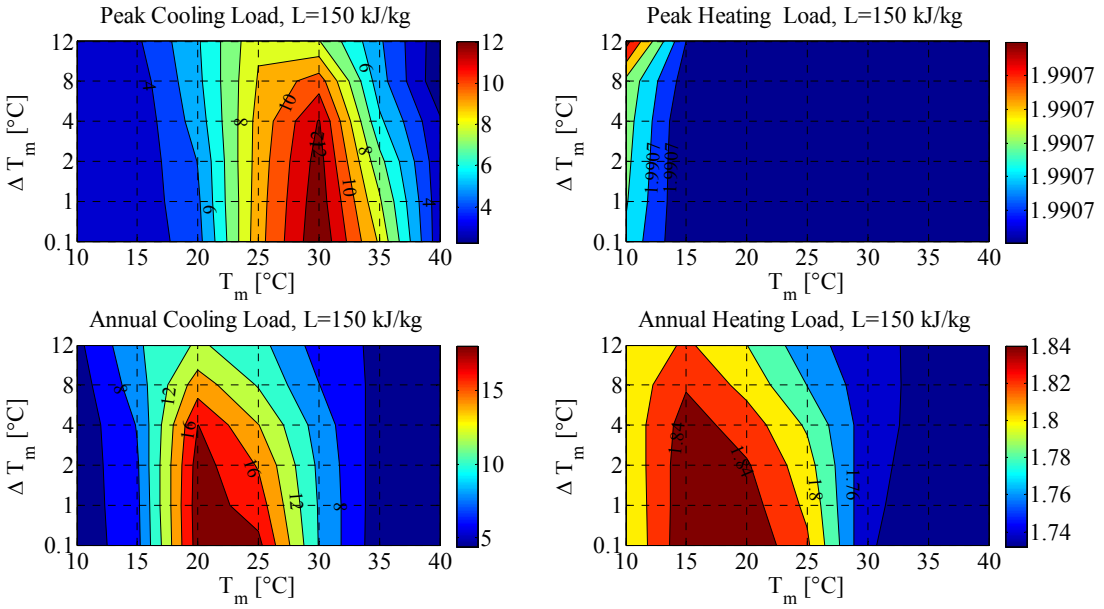

d) A contour plot for the case of 150 kg/kJ showing percentage reduction in cooling and heating loads

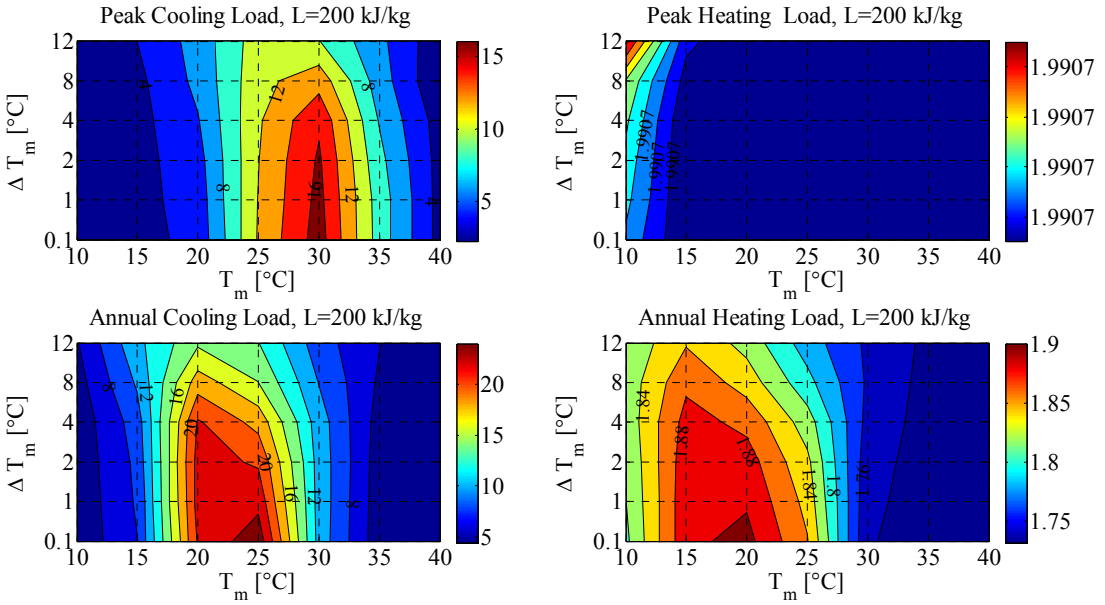

e) A contour plot for the case of 200 kg/kJ showing percentage reduction in cooling and heating loads

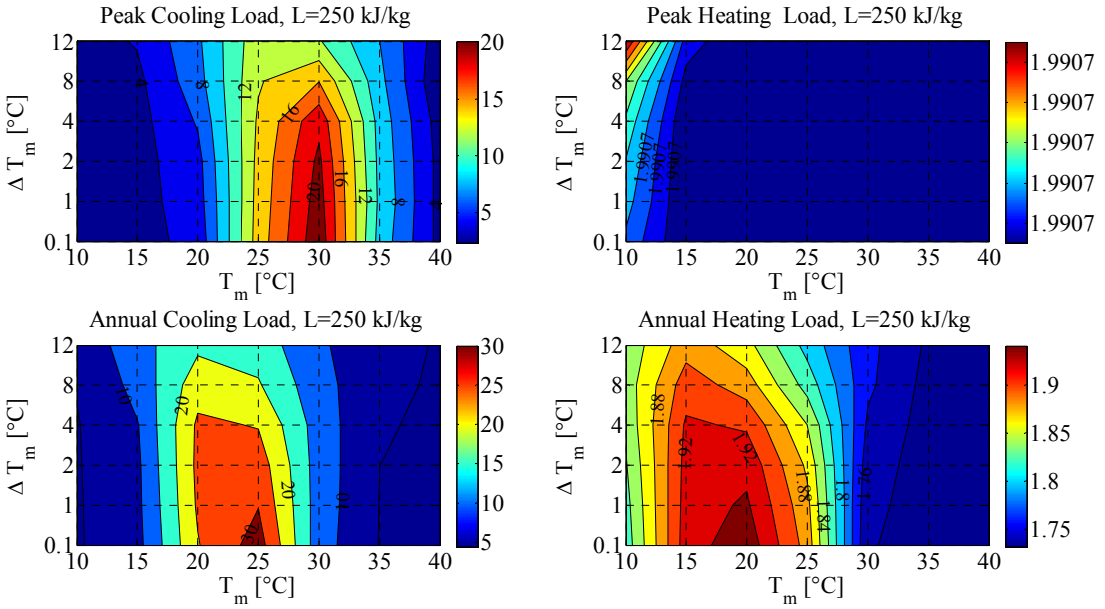

f) A contour plot for the case of 250 kg/kJ showing percentage reduction in cooling and heating loads

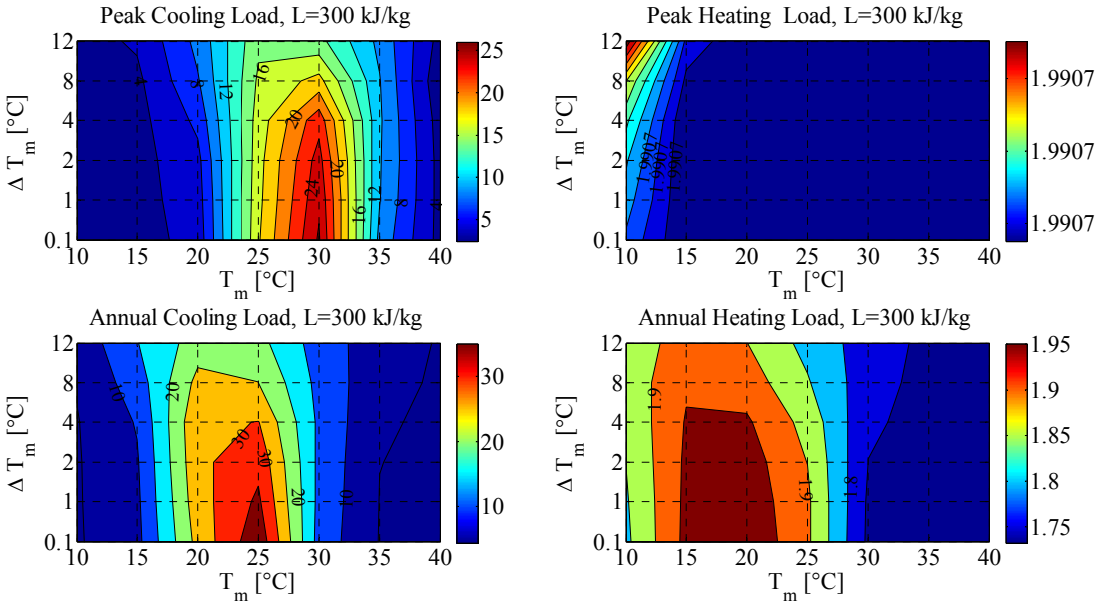

g) A contour plot for the case of 300 kg/kJ showing percentage reduction in cooling and heating loads

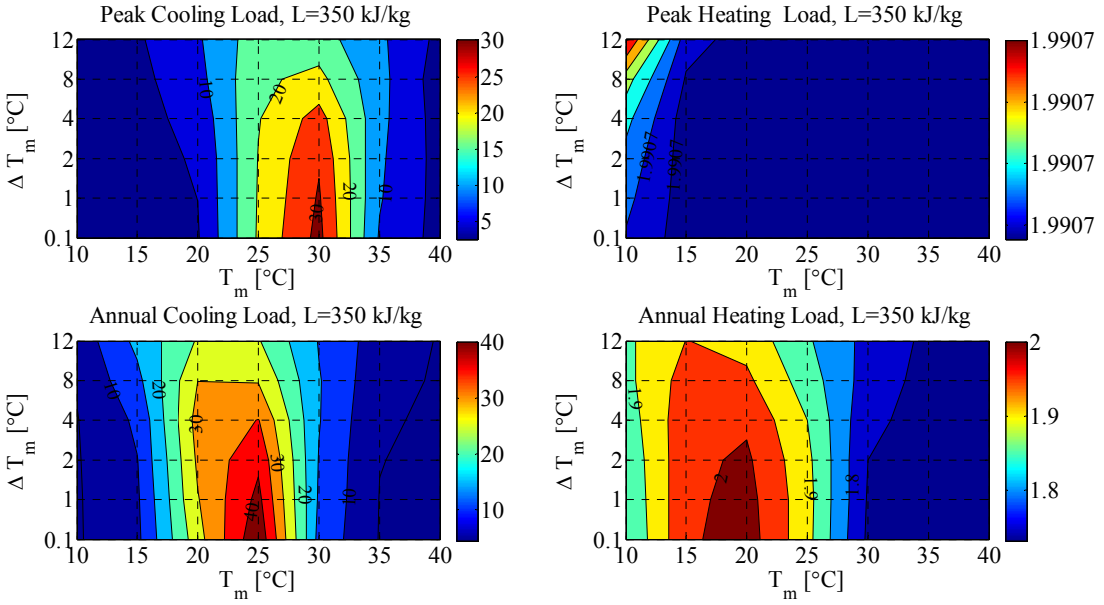

h) A contour plot for the case of 350 kg/kJ showing percentage reduction in cooling and heating loads

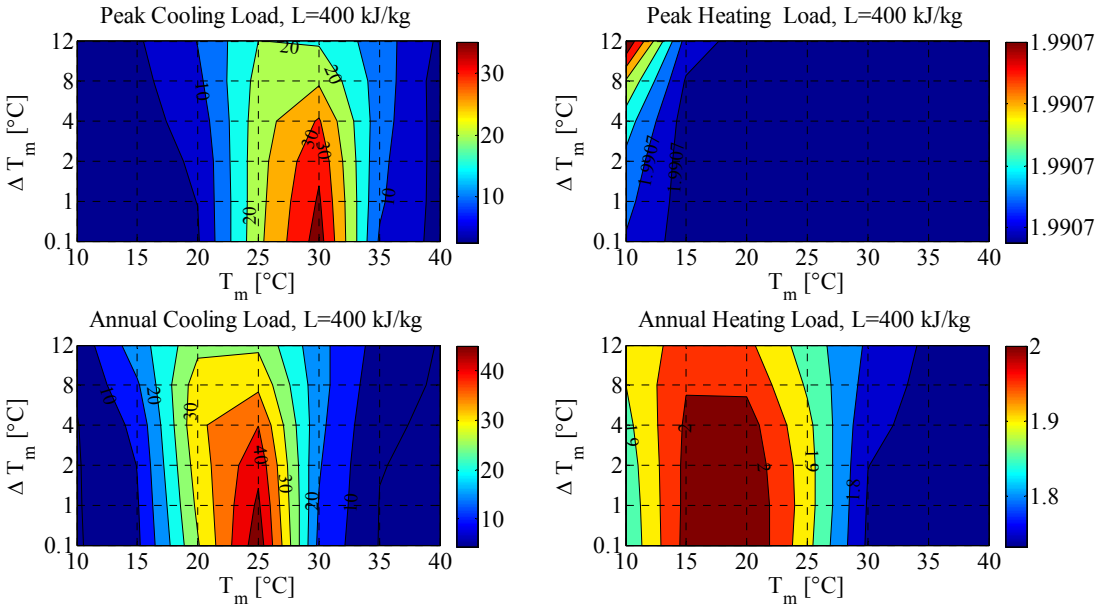

i) A contour plot for the case of 400 kg/kJ showing percentage reduction in cooling and heating loads

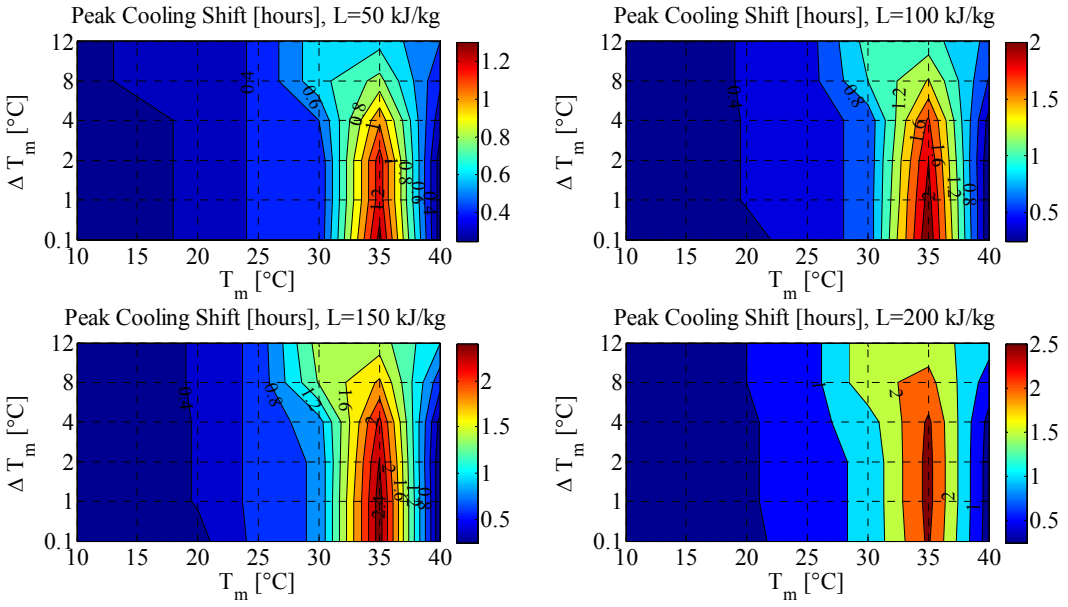

j) A contour plot for the peak cooling shift in hours

Figure A.3 Percentage reductions in cooling and heating loads for south wall when PCM to the exterior, Golden, CO

Appendix A.2 West Wall

Appendix A.2.1 PCM to the interior

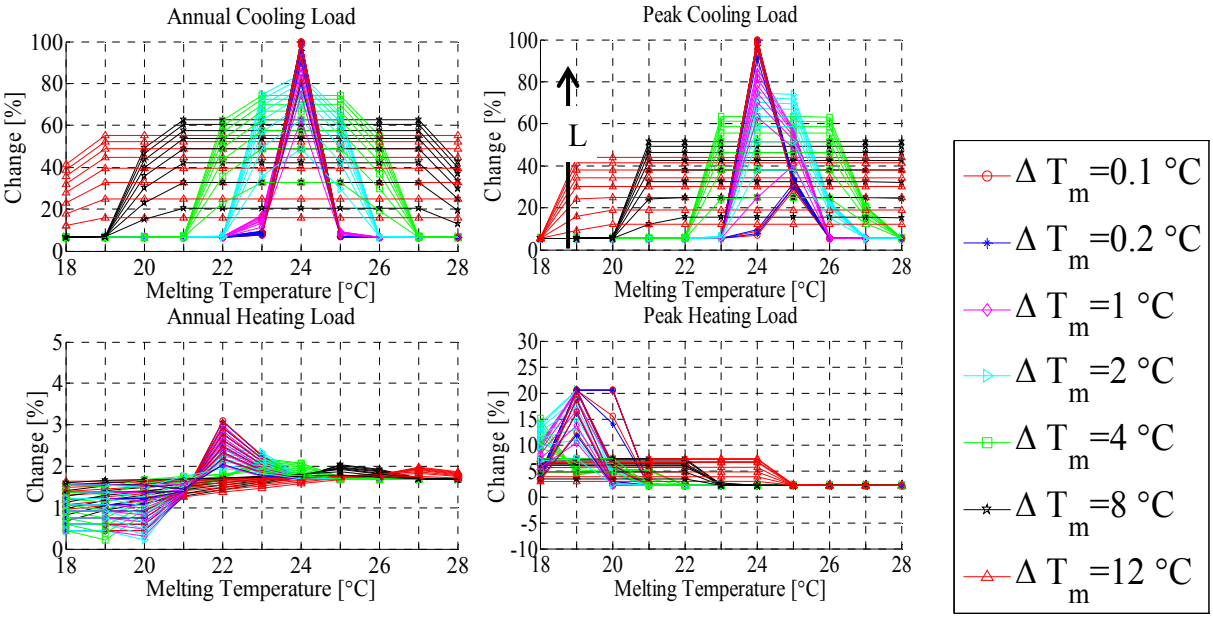

a) Percentage reductions in cooling and heating loads across all parameters

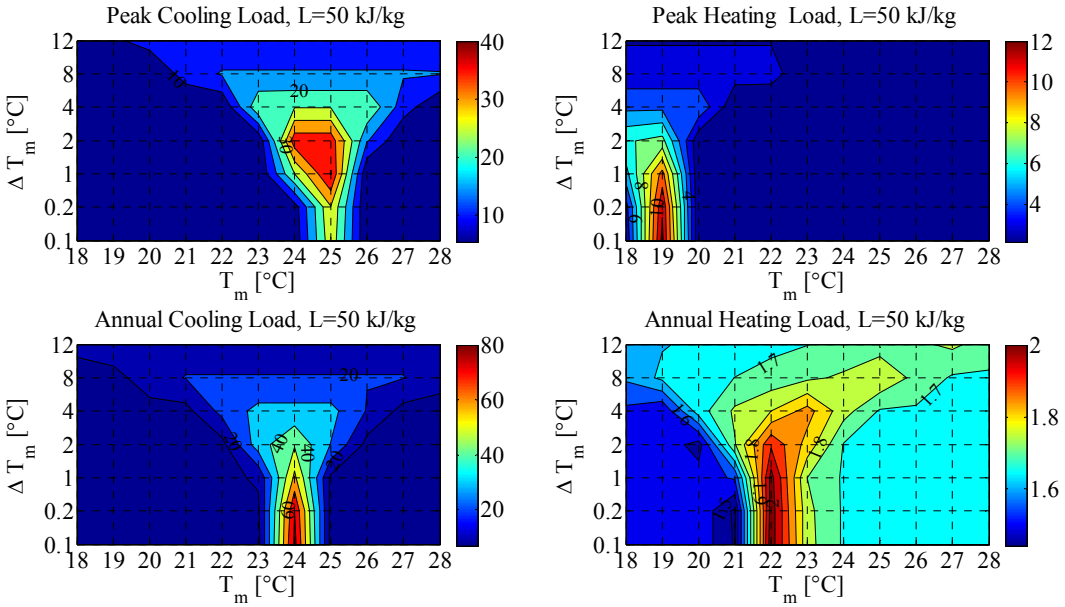

b) A contour plot for the case of 50 kg/kJ showing percentage reduction in cooling and heating loads

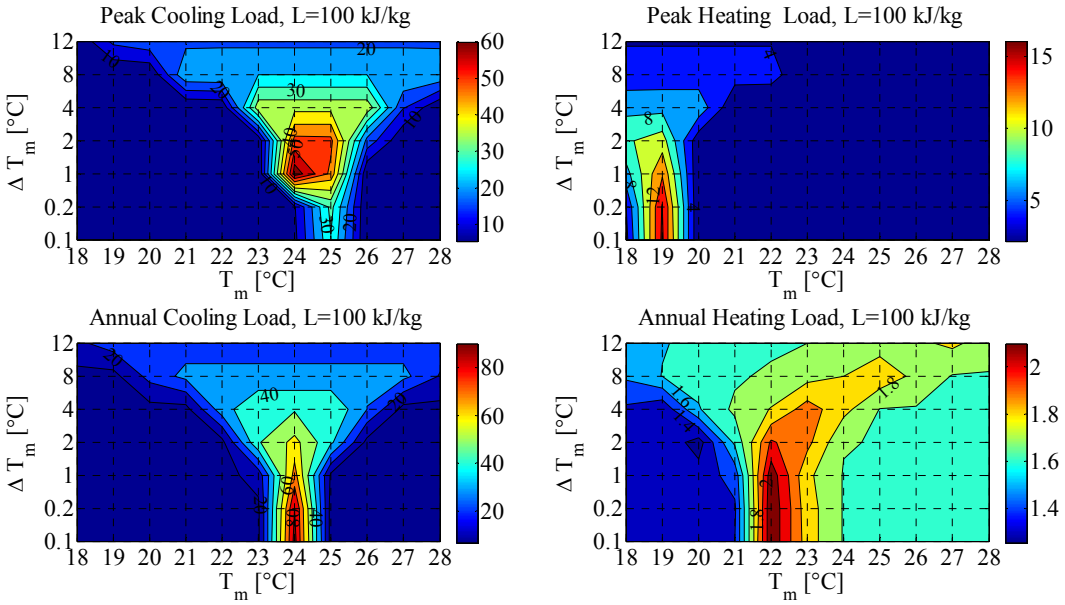

c) A contour plot for the case of 100 kg/kJ showing percentage reduction in cooling and heating loads

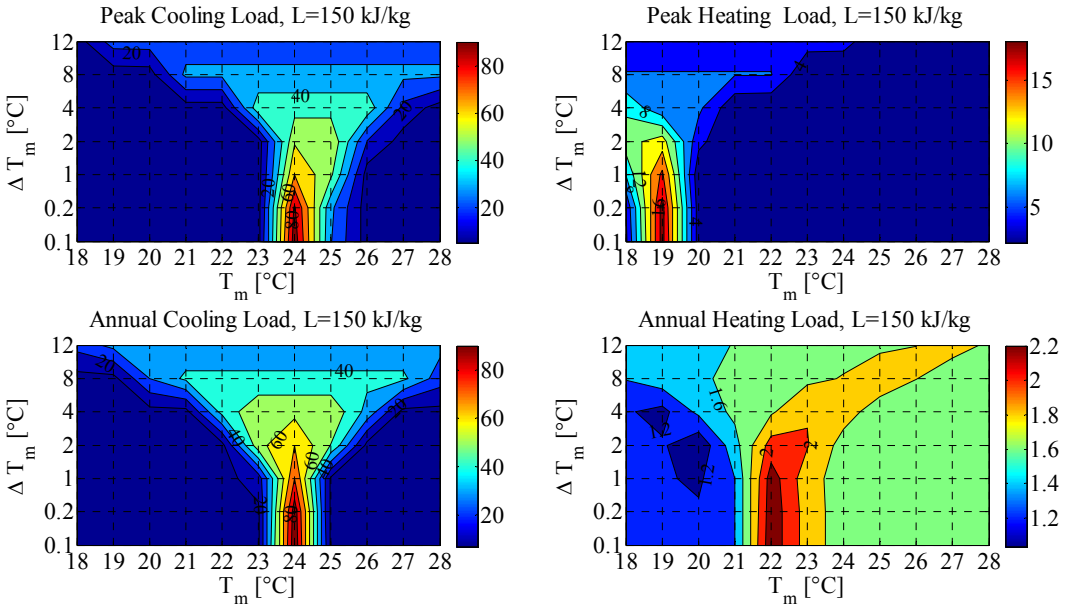

d) A contour plot for the case of 150 kg/kJ showing percentage reduction in cooling and heating loads

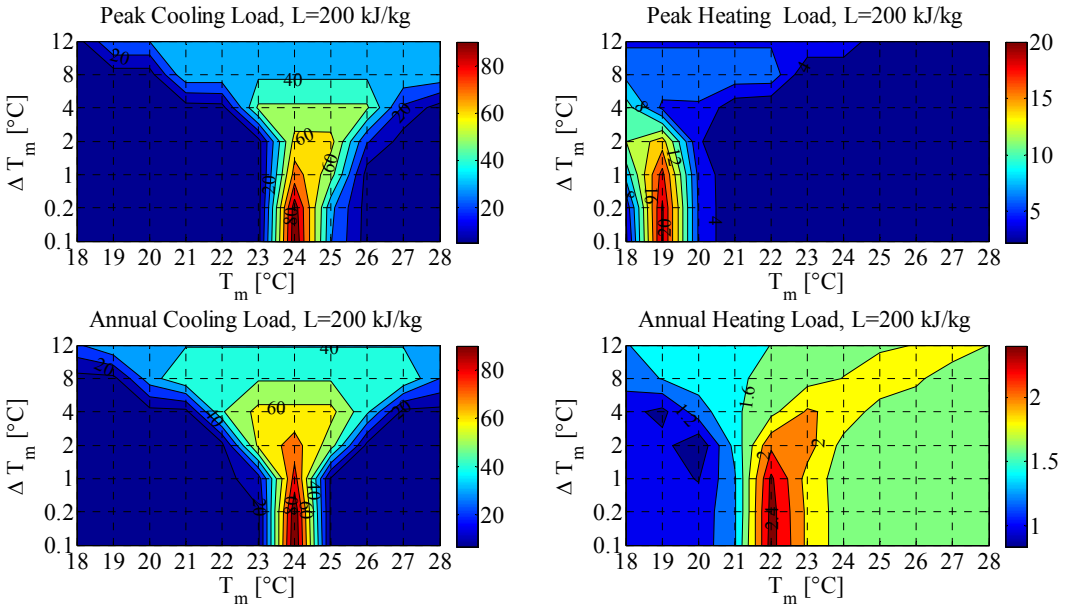

e) A contour plot for the case of 200 kg/kJ showing percentage reduction in cooling and heating loads

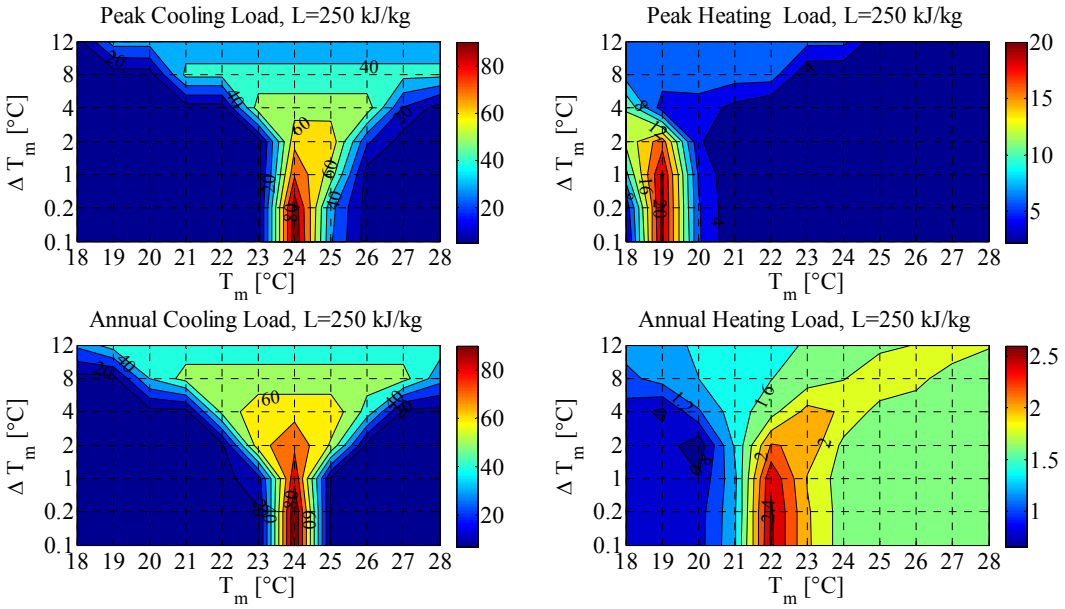

f) A contour plot for the case of 250 kg/kJ showing percentage reduction in cooling and heating loads

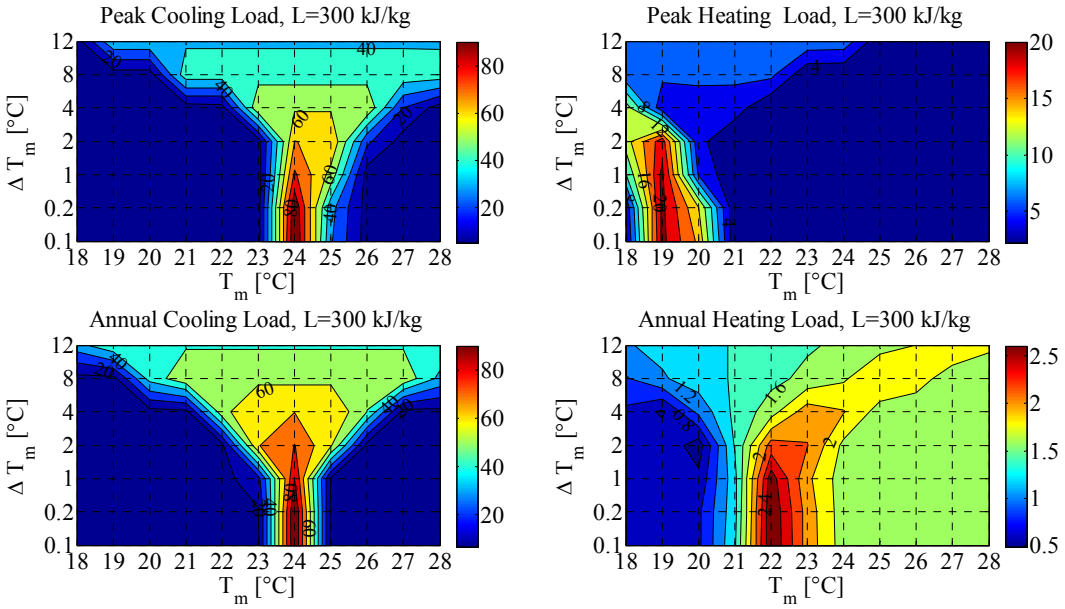

g) A contour plot for the case of 300 kg/kJ showing percentage reduction in cooling and heating loads

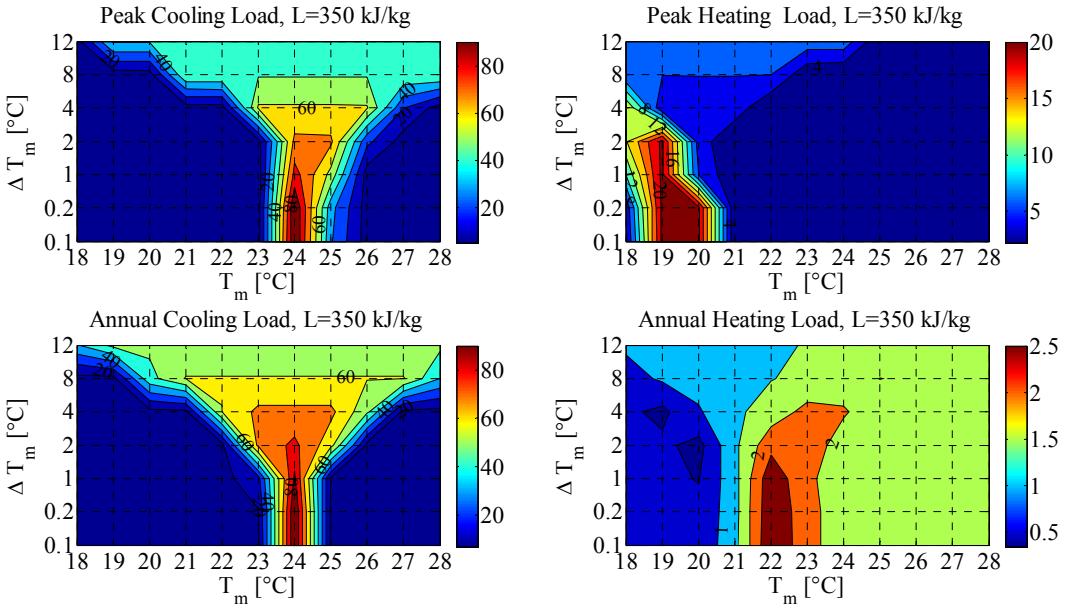

h) A contour plot for the case of 350 kg/kJ showing percentage reduction in cooling and heating loads

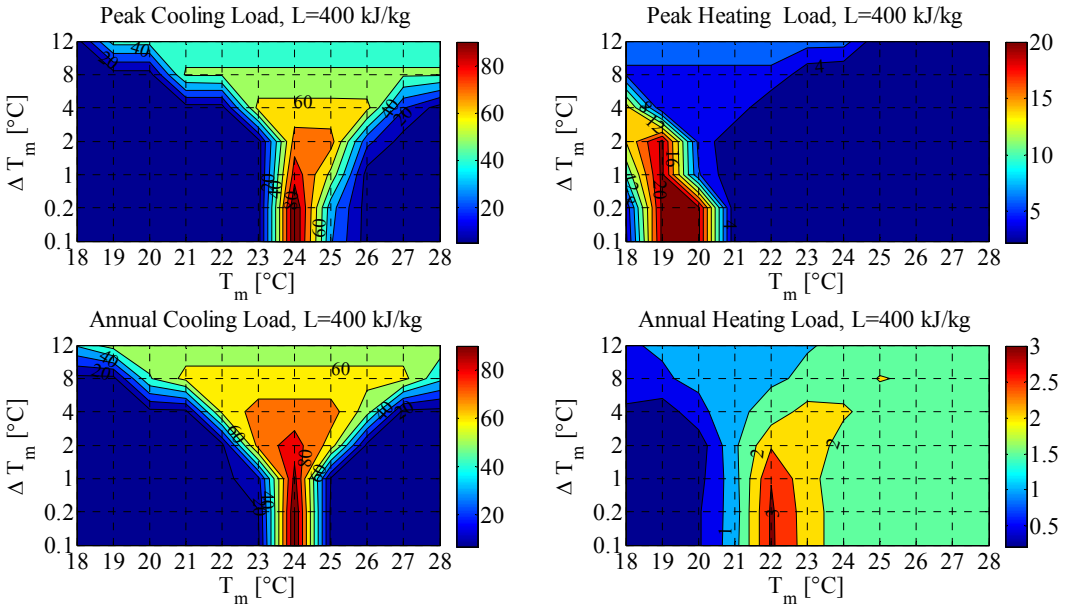

i) A contour plot for the case of 400 kg/kJ showing percentage reduction in cooling and heating loads

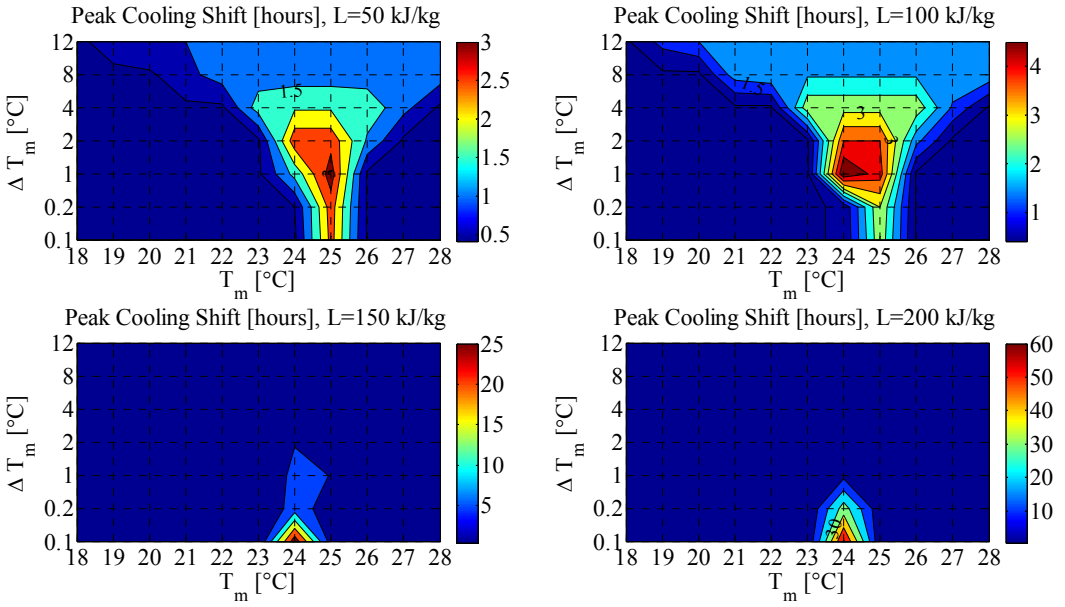

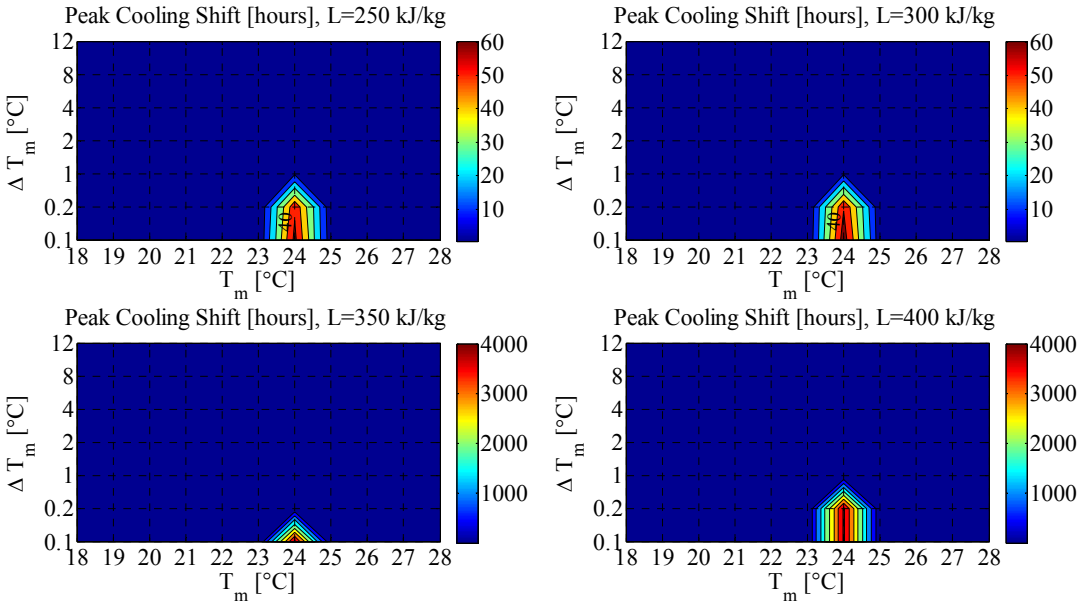

j) A contour plot for the peak cooling shift in hours

Figure A.4 Percentage reductions in cooling and heating loads for West wall when PCM to the interior, Golden, CO

Appendix A.2.2 PCM in the middle

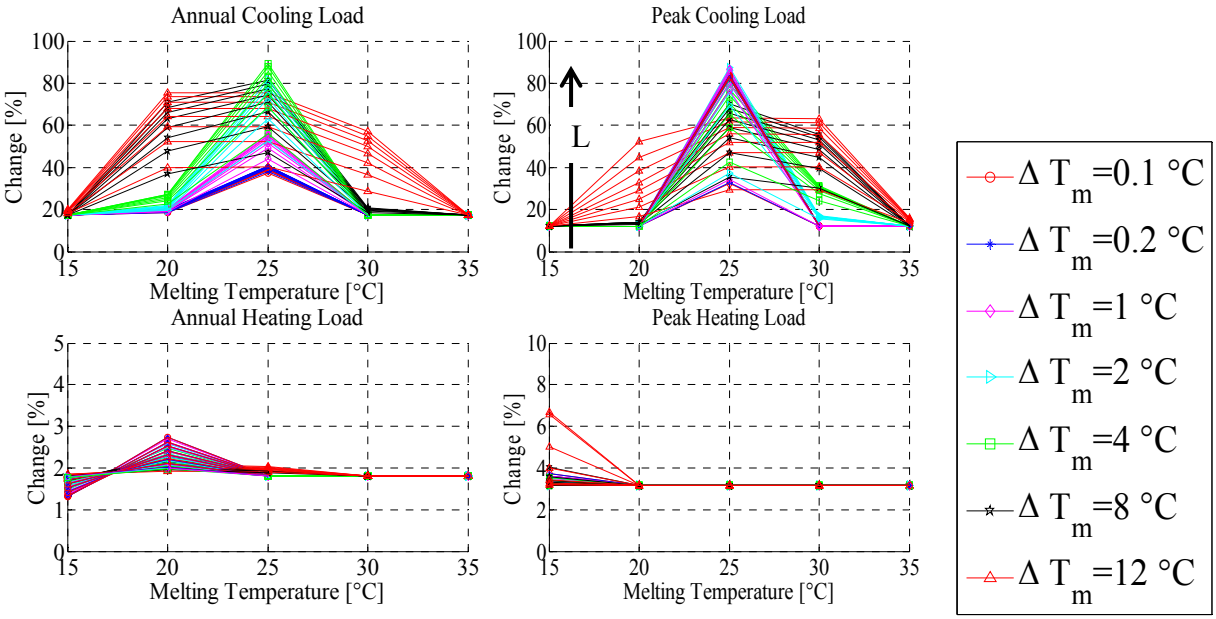

a) Percentage reductions in cooling and heating loads across all parameters

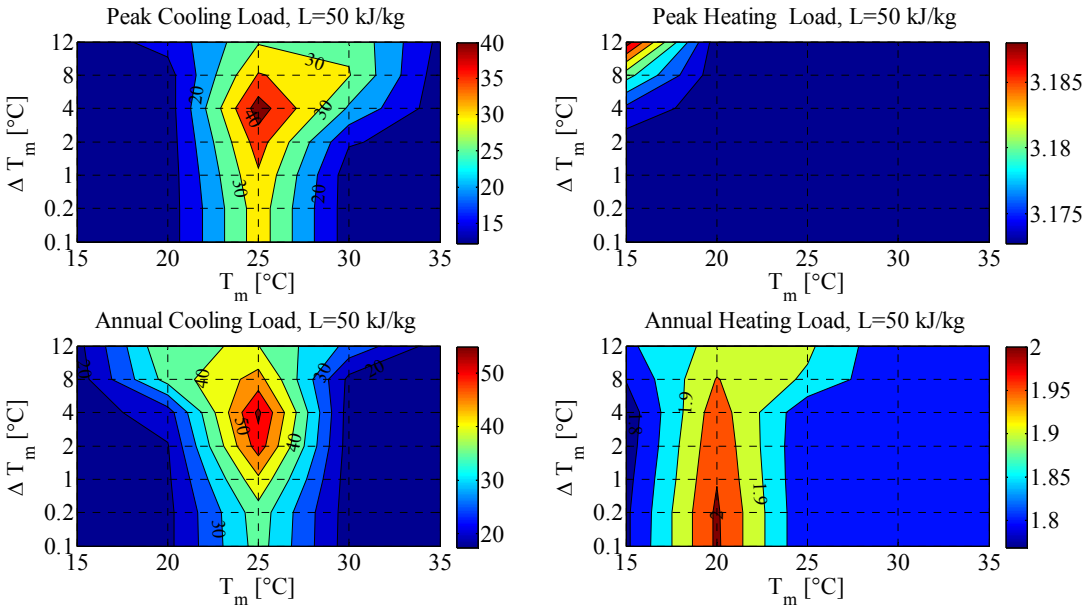

b) A contour plot for the case of 50 kg/kJ showing percentage reduction in cooling and heating loads

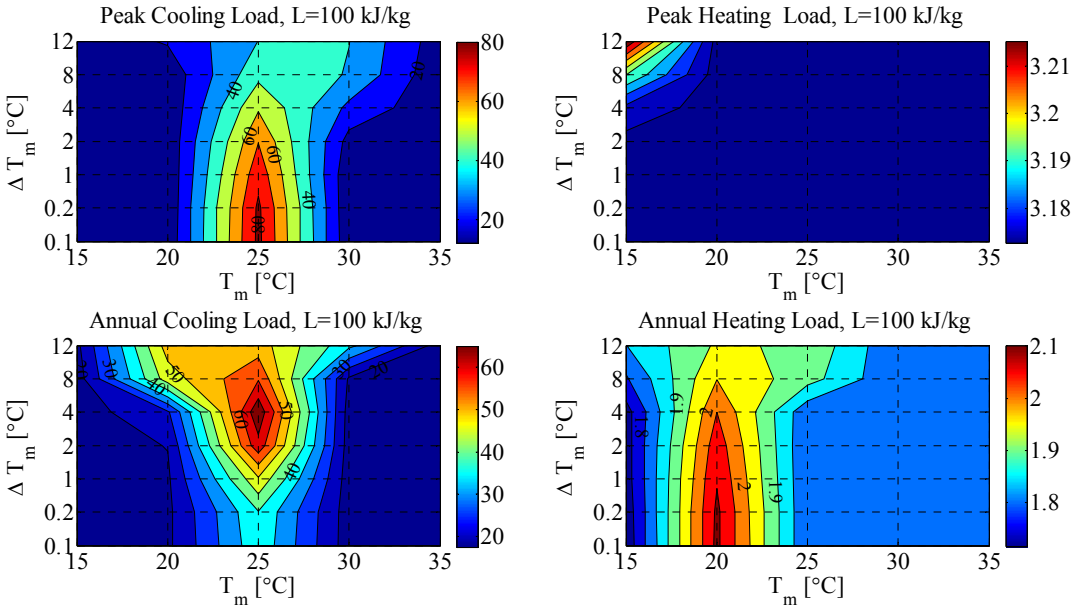

c) A contour plot for the case of 100 kg/kJ showing percentage reduction in cooling and heating loads

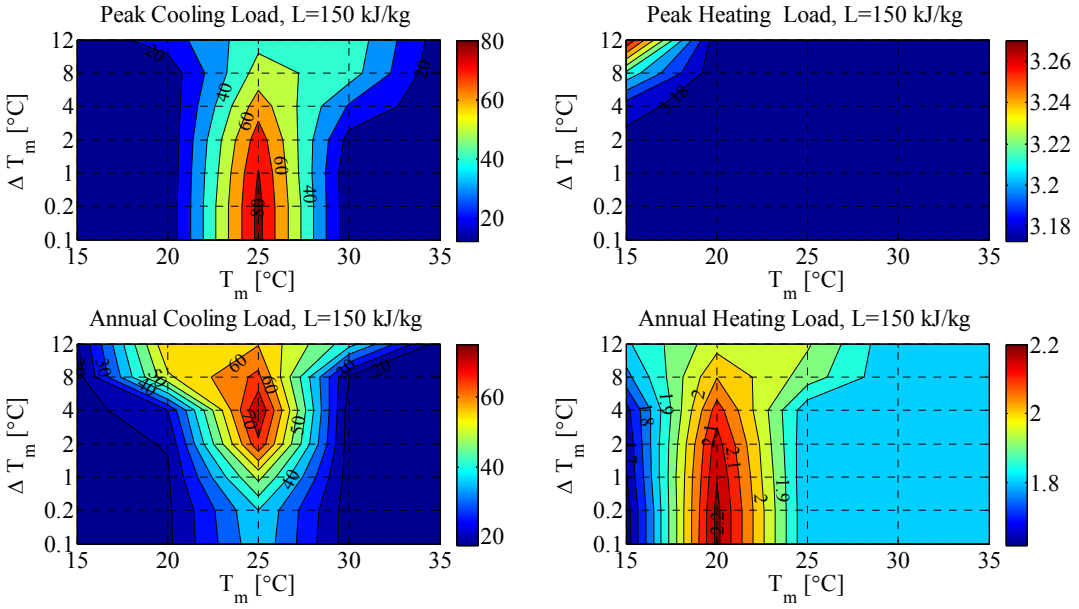

d) A contour plot for the case of 150 kg/kJ showing percentage reduction in cooling and heating loads

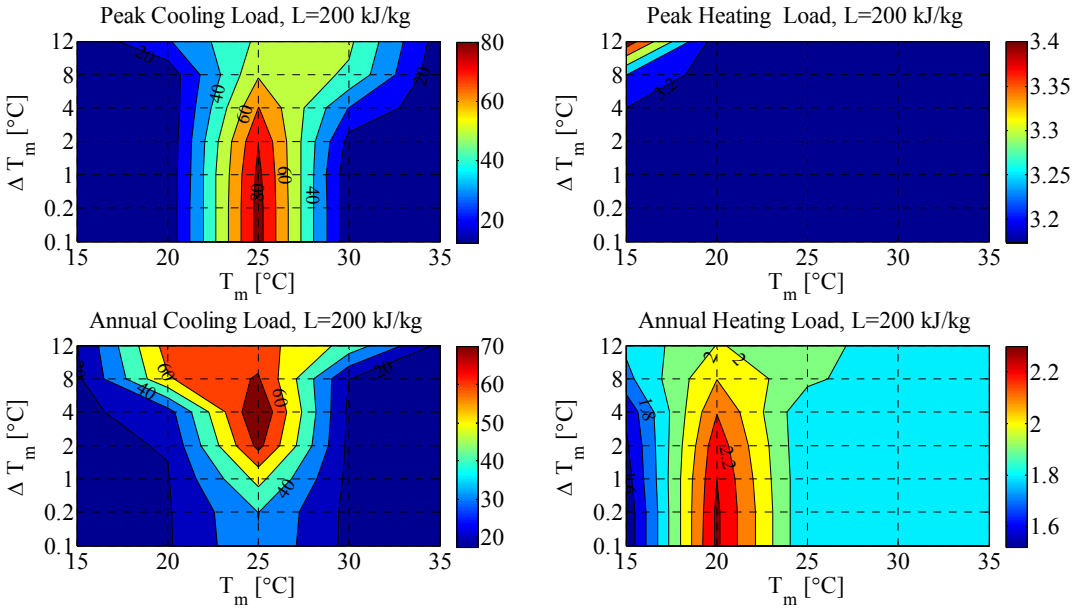

e) A contour plot for the case of 200 kg/kJ showing percentage reduction in cooling and heating loads

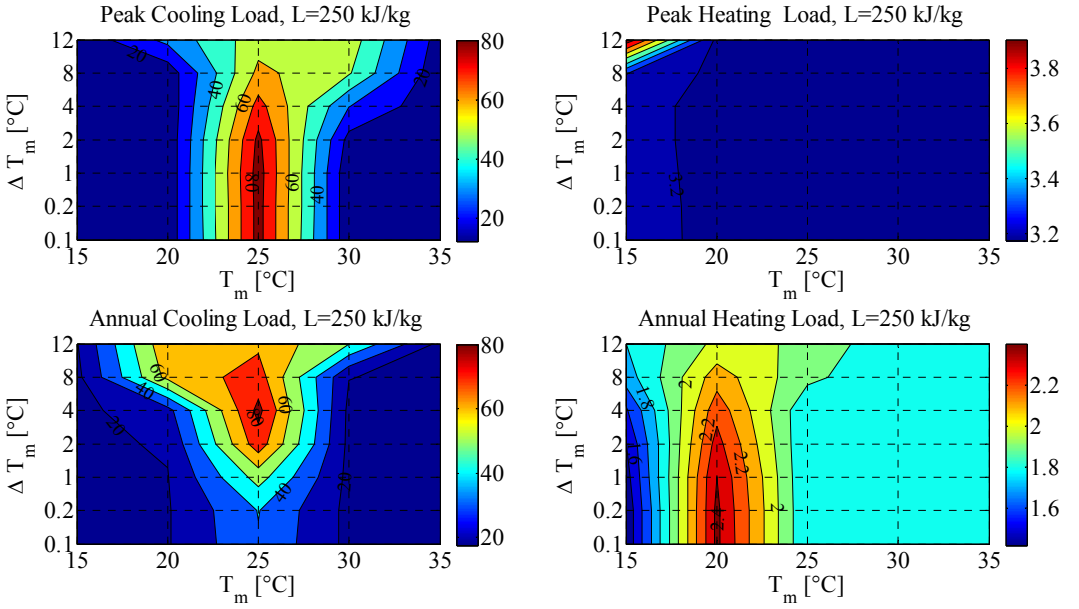

f) A contour plot for the case of 250 kg/kJ showing percentage reduction in cooling and heating loads

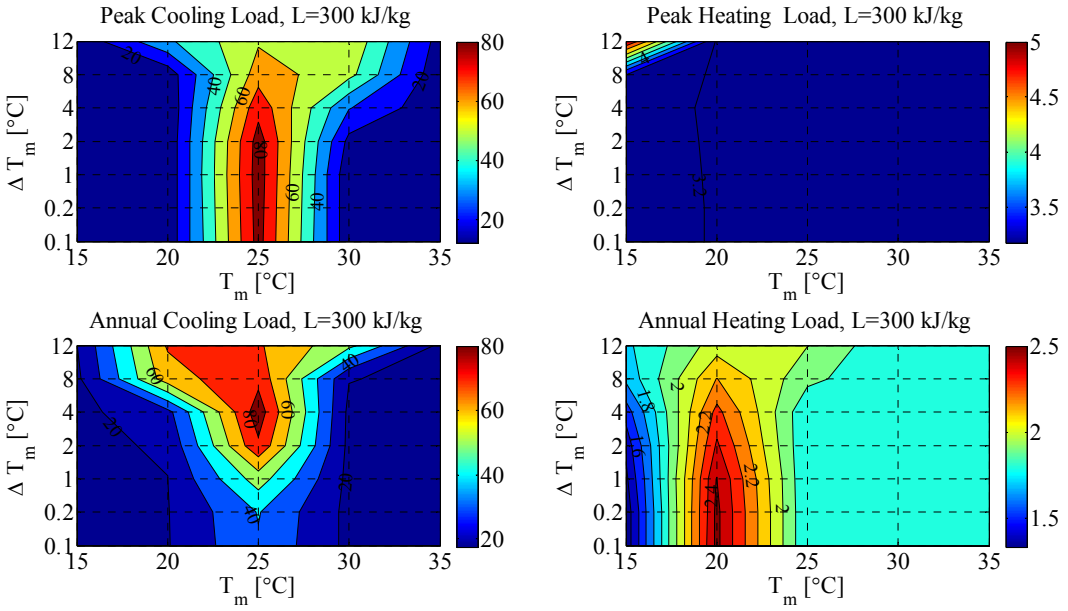

g) A contour plot for the case of 300 kg/kJ showing percentage reduction in cooling and heating loads

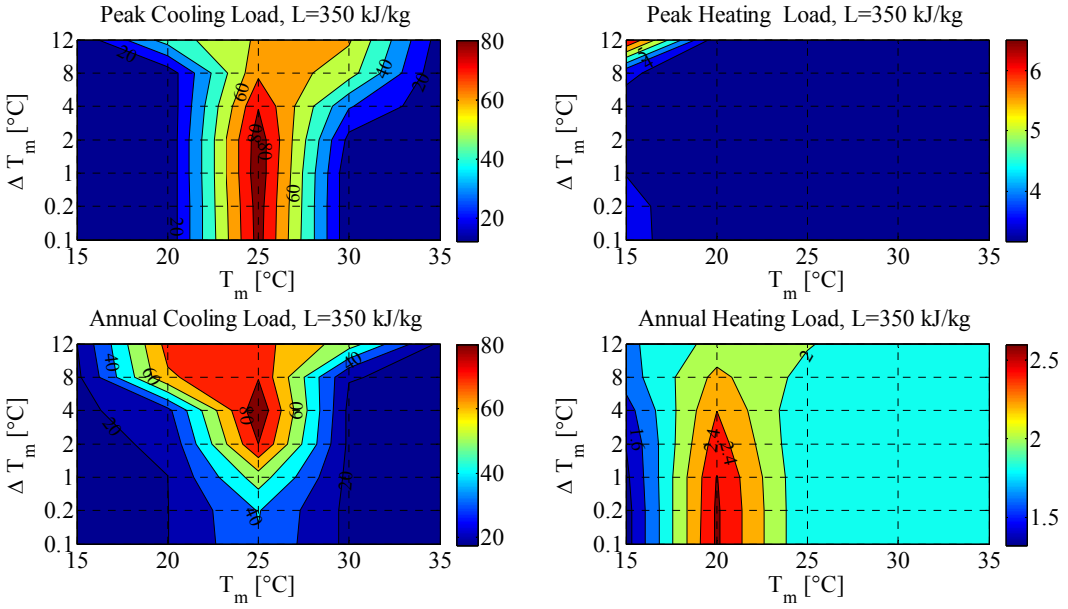

h) A contour plot for the case of 350 kg/kJ showing percentage reduction in cooling and heating loads

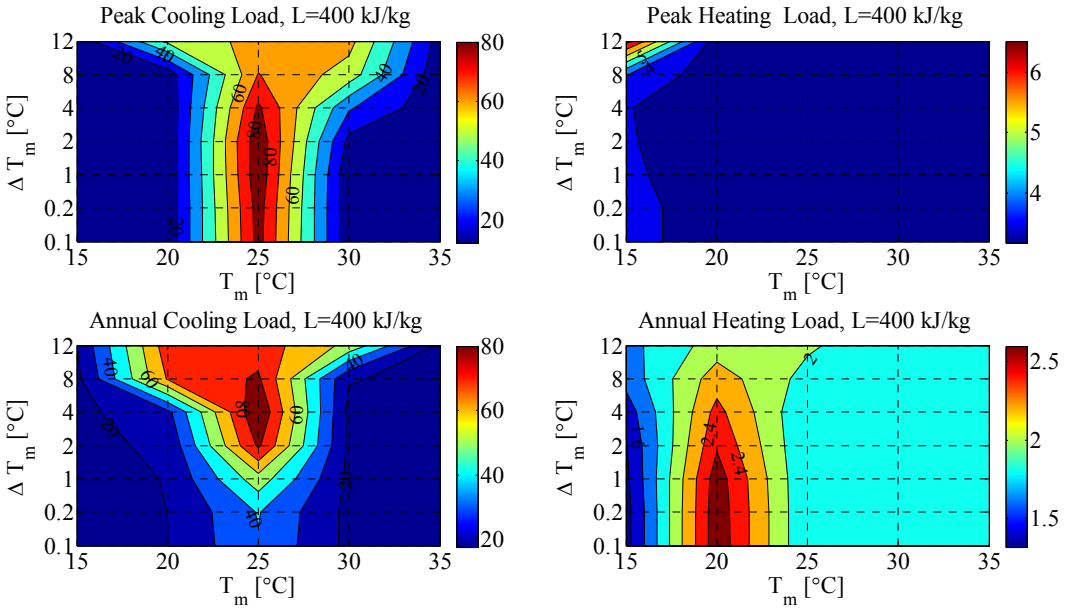

i) A contour plot for the case of 400 kg/kJ showing percentage reduction in cooling and heating loads

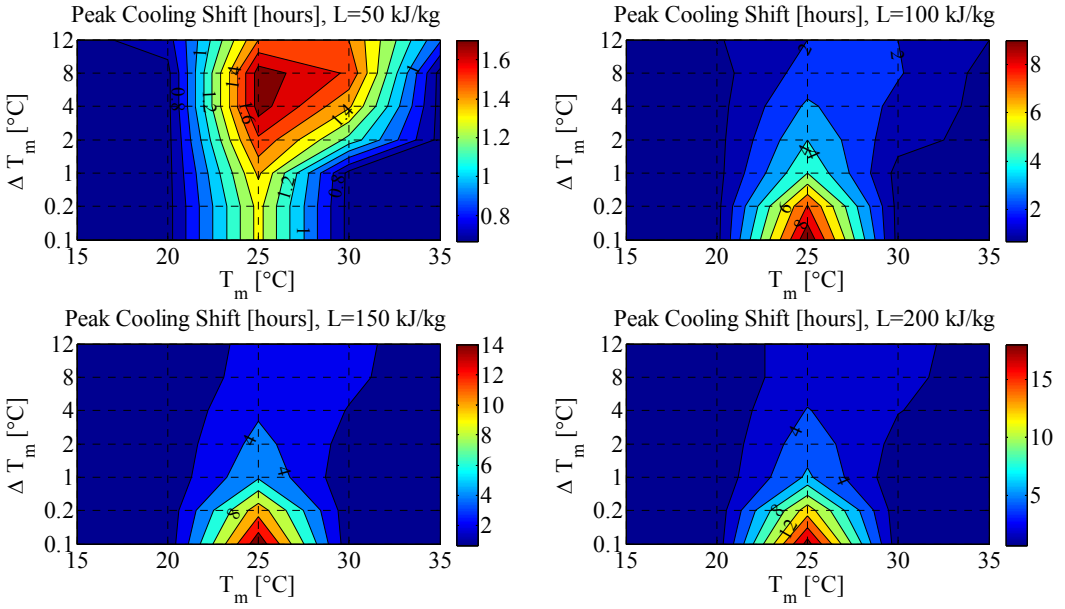

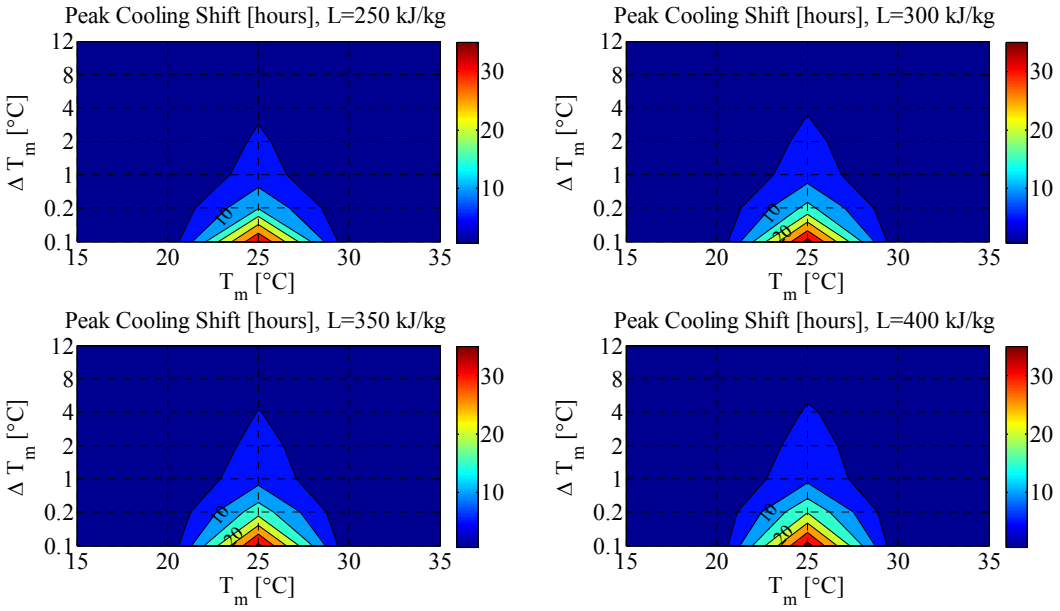

j) A contour plot for the peak cooling shift in hours

Figure A.5 Percentage reductions in cooling and heating loads for West wall when PCM in the middle, Golden, CO

Appendix A.2.3 PCM to the exterior

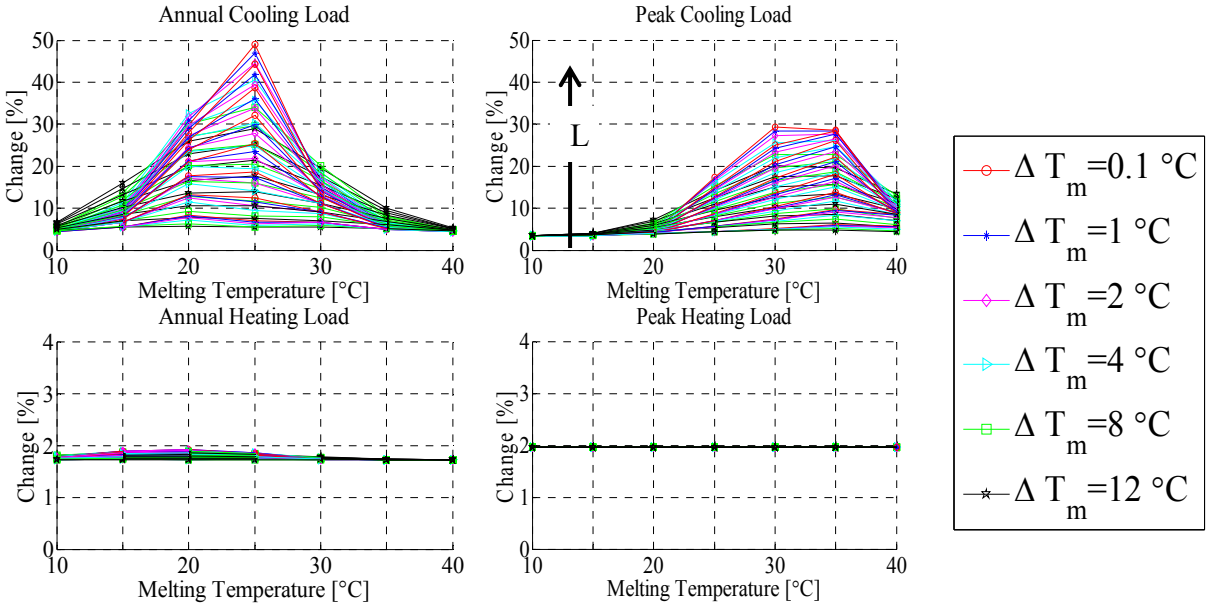

a) Percentage reductions in cooling and heating loads across all parameters

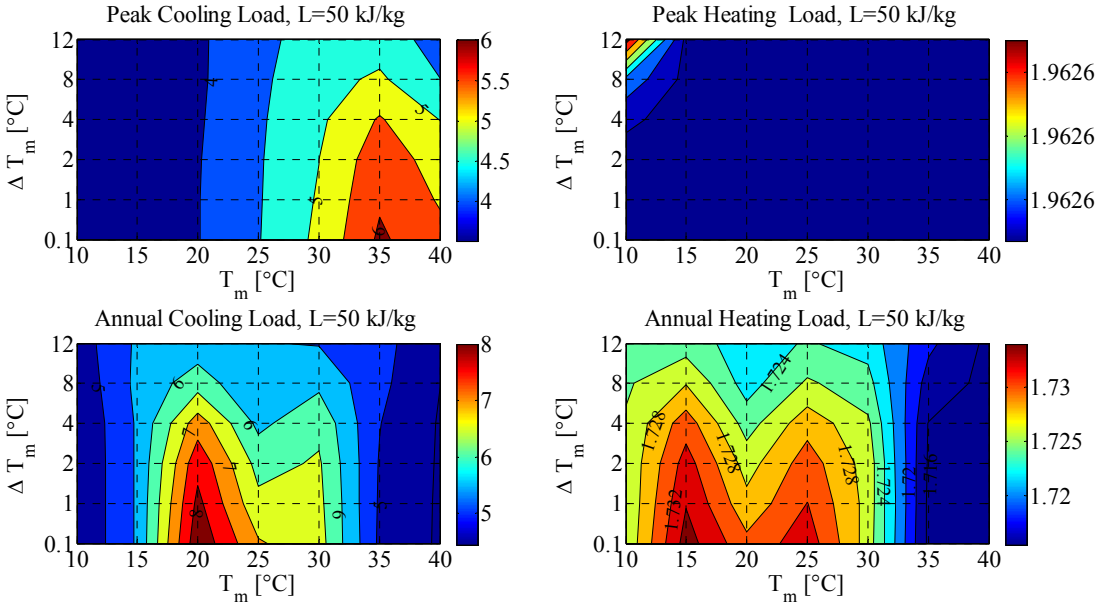

b) A contour plot for the case of 50 kg/kJ showing percentage reduction in cooling and heating loads

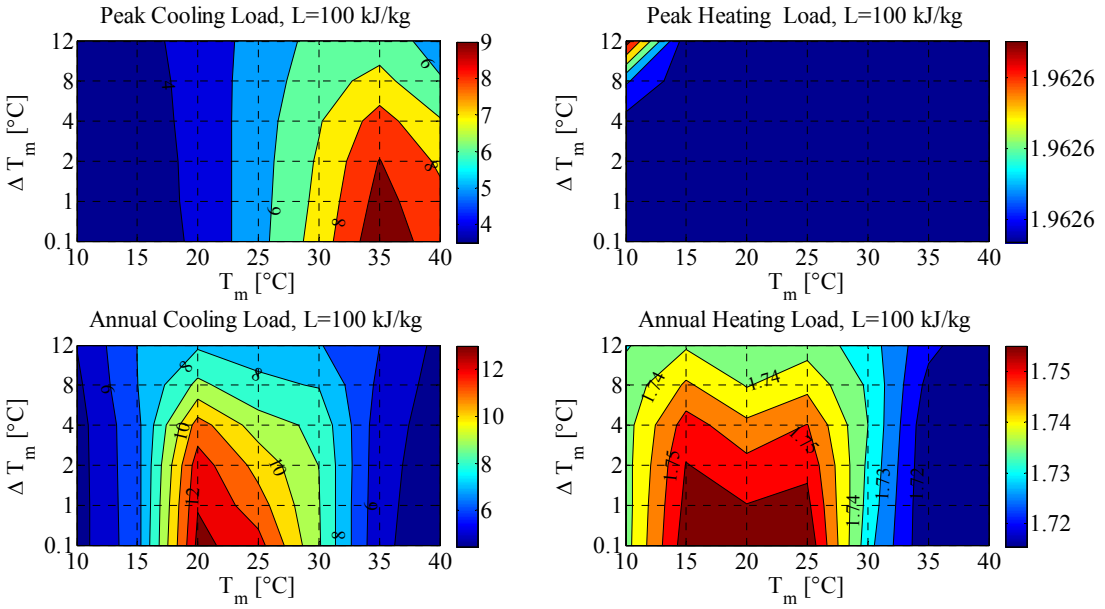

c) A contour plot for the case of 100 kg/kJ showing percentage reduction in cooling and heating loads

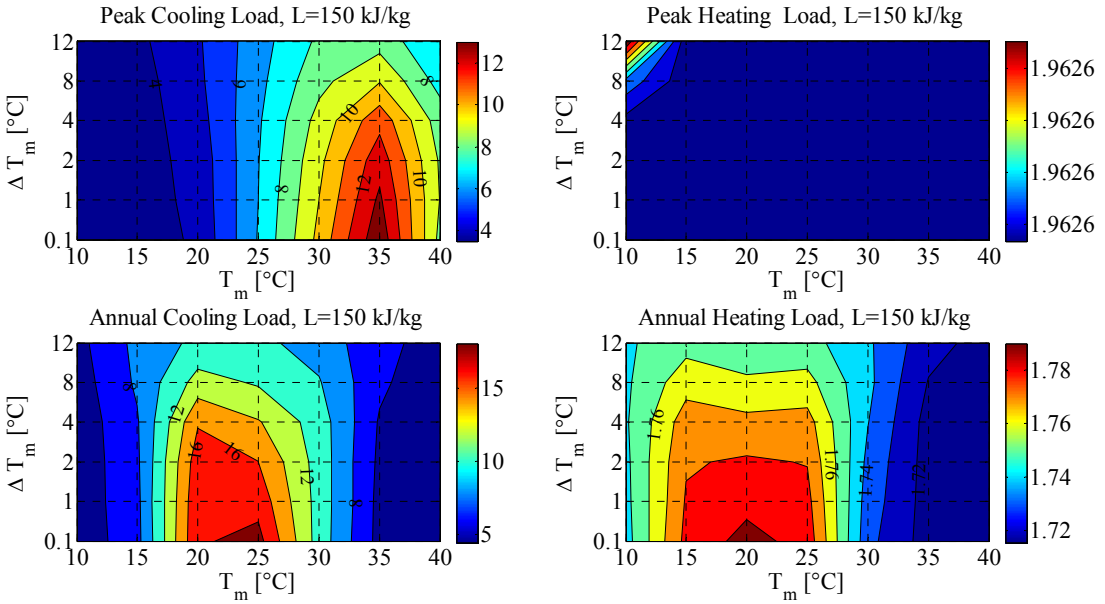

d) A contour plot for the case of 150 kg/kJ showing percentage reduction in cooling and heating loads

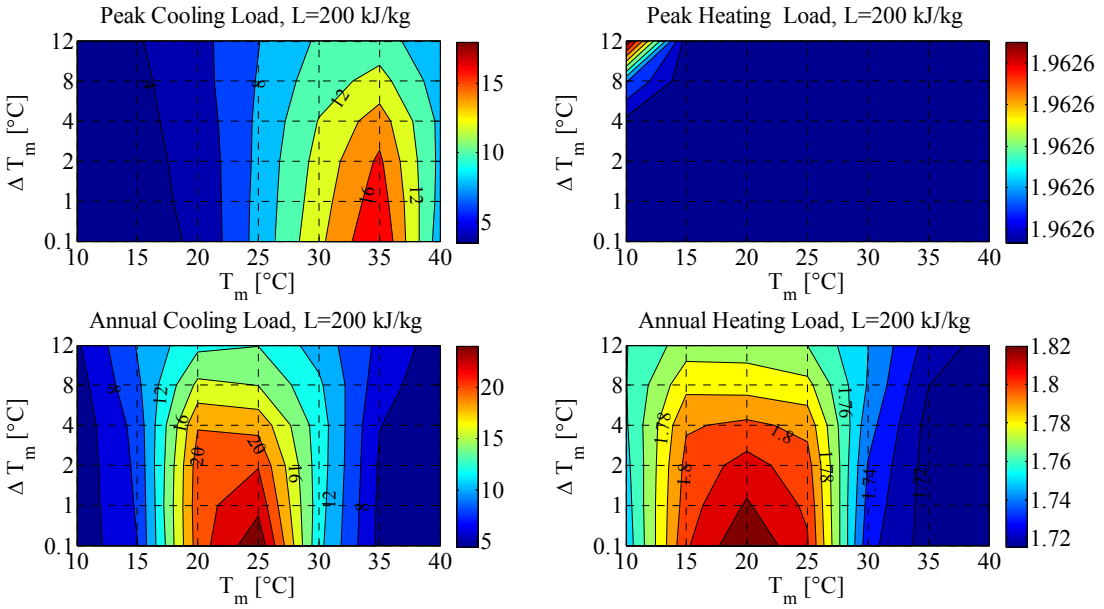

e) A contour plot for the case of 200 kg/kJ showing percentage reduction in cooling and heating loads

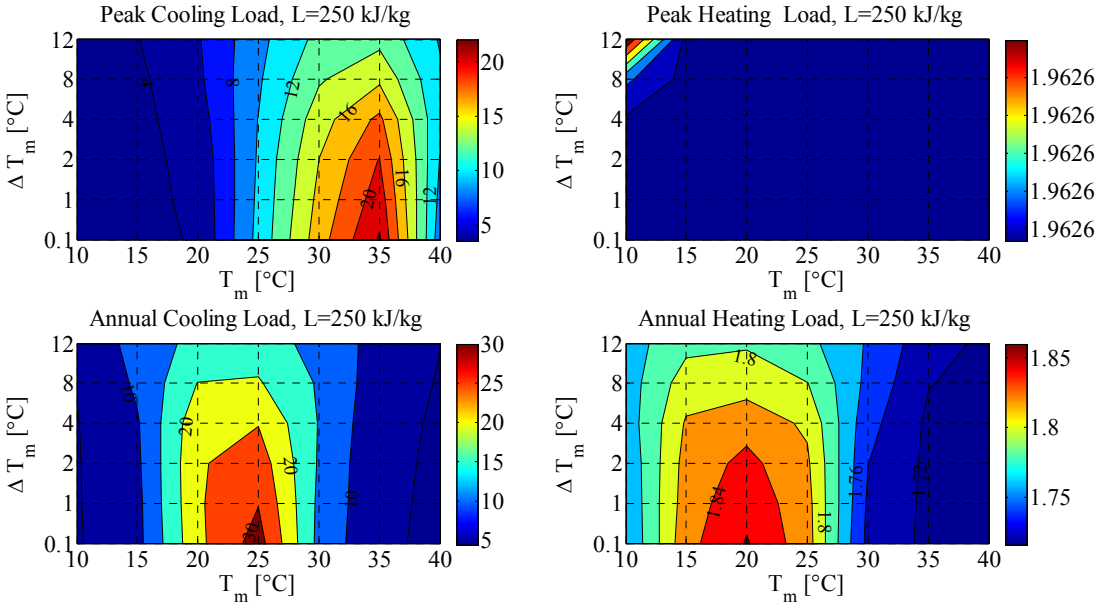

f) A contour plot for the case of 250 kg/kJ showing percentage reduction in cooling and heating loads

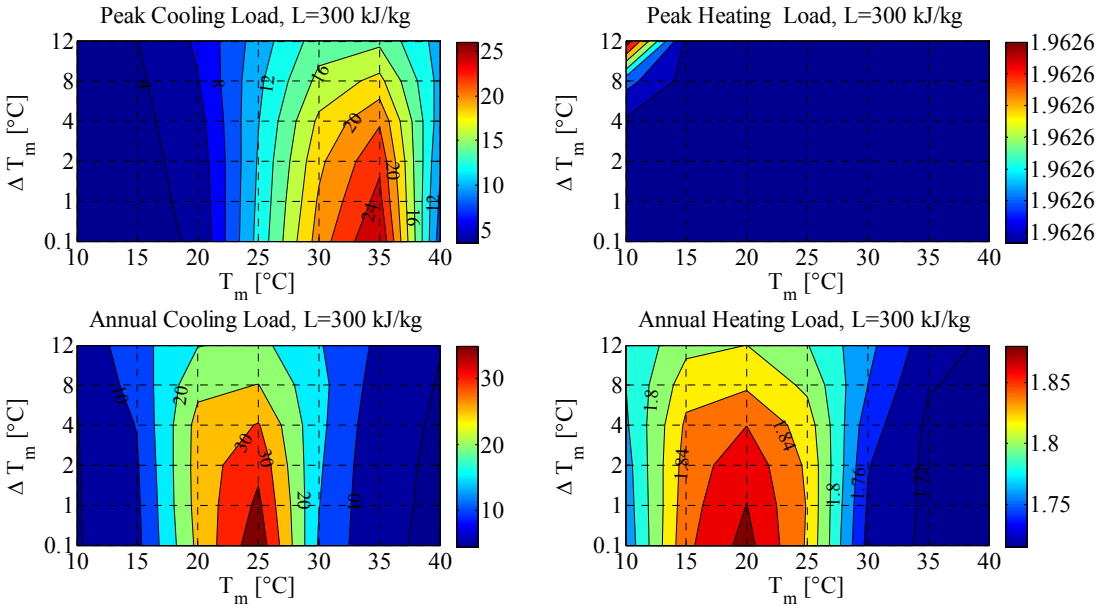

g) A contour plot for the case of 300 kg/kJ showing percentage reduction in cooling and heating loads

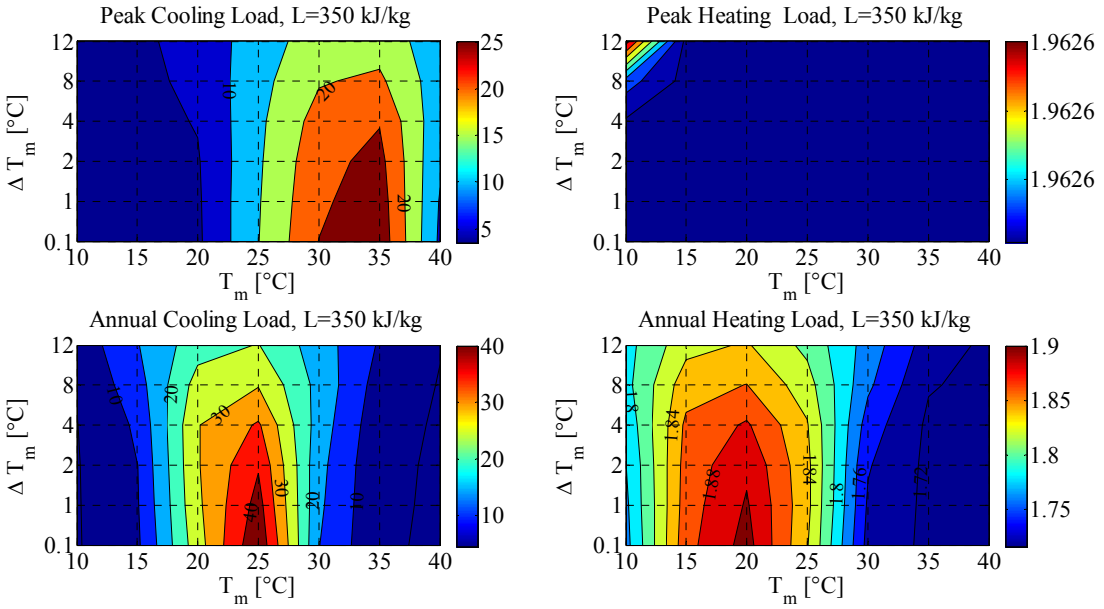

h) A contour plot for the case of 350 kg/kJ showing percentage reduction in cooling and heating loads

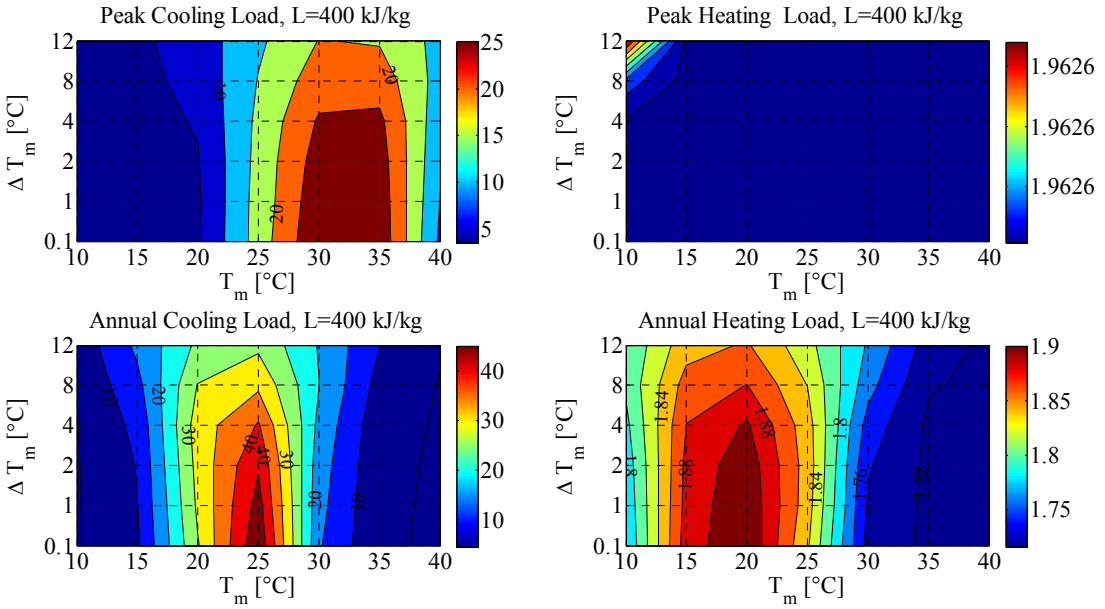

i) A contour plot for the case of 400 kg/kJ showing percentage reduction in cooling and heating loads

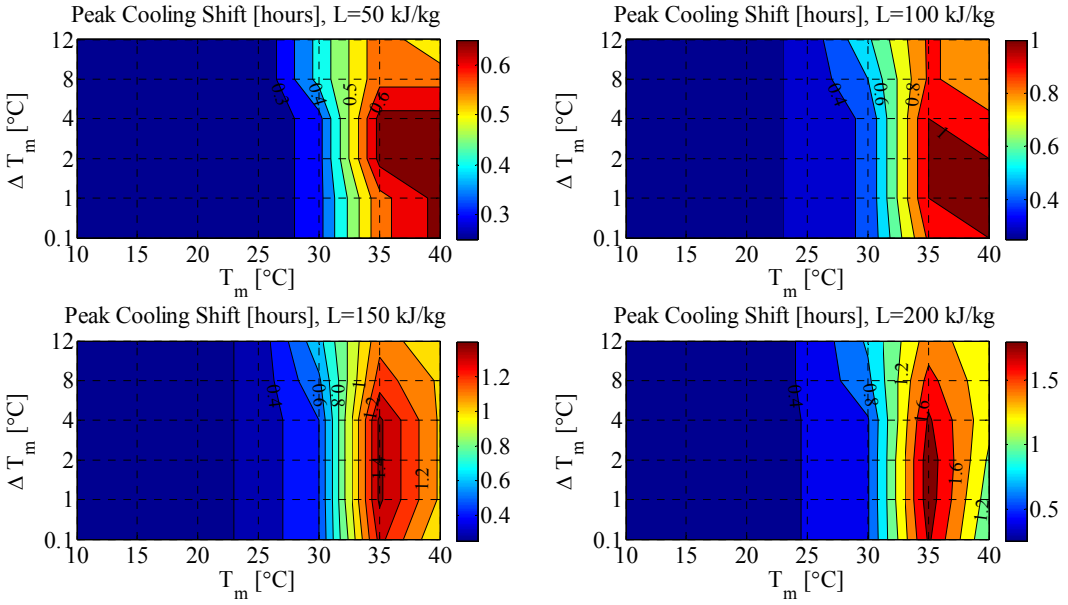

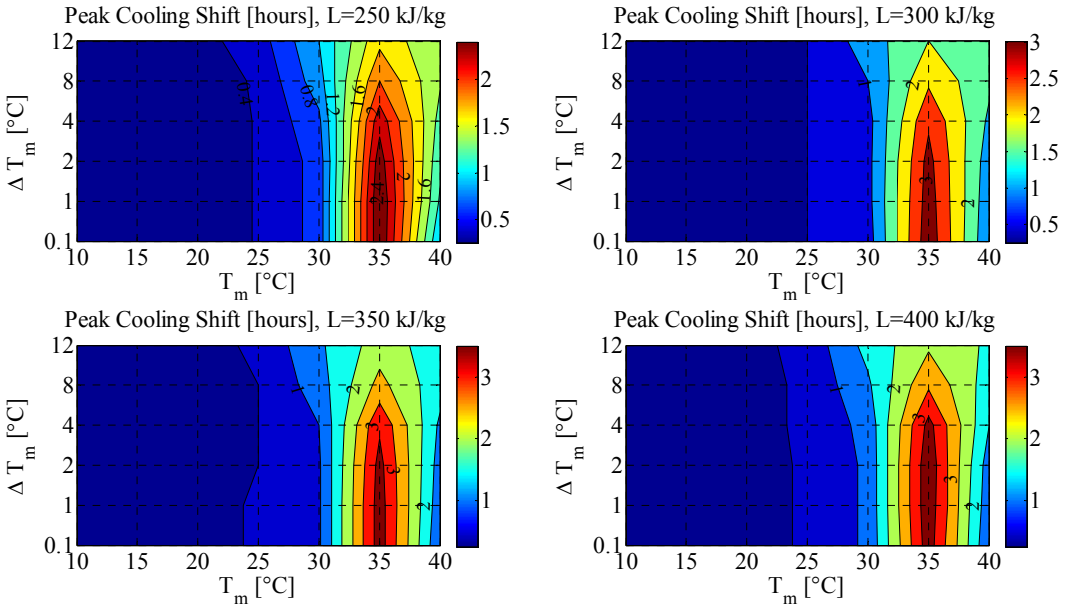

j) A contour plot for the peak cooling shift in hours

Figure A.6 Percentage reductions in cooling and heating loads for West wall when PCM to the exterior, Golden, CO

Appendix A.3 North Wall

Appendix A.3.1 PCM to the interior

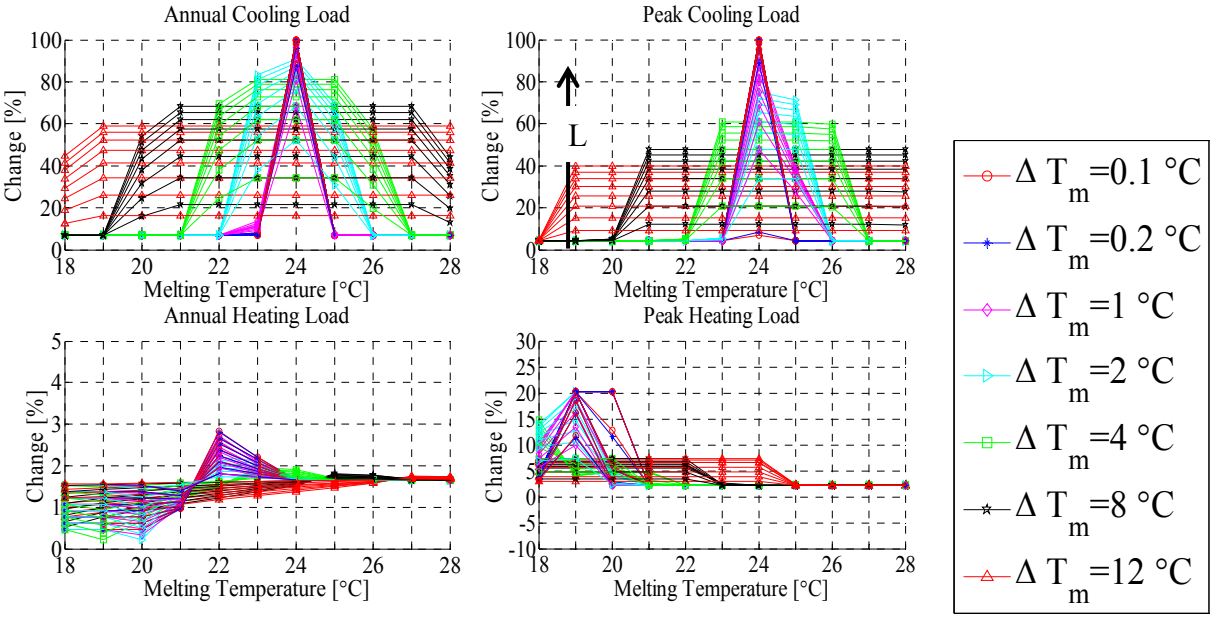

a) Percentage reductions in cooling and heating loads across all parameters

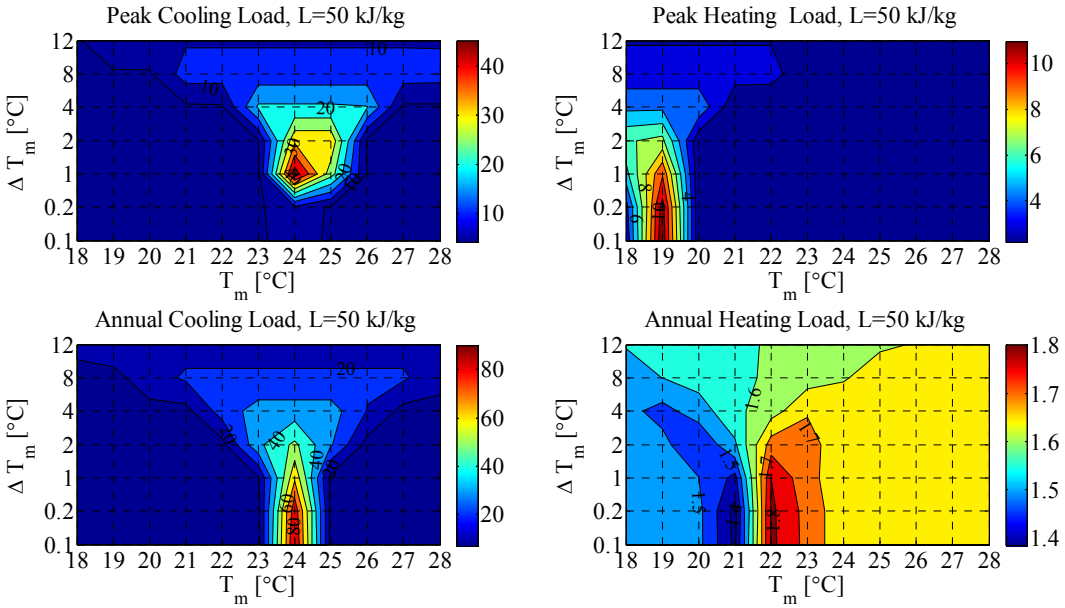

b) A contour plot for the case of 50 kg/kJ showing percentage reduction in cooling and heating loads

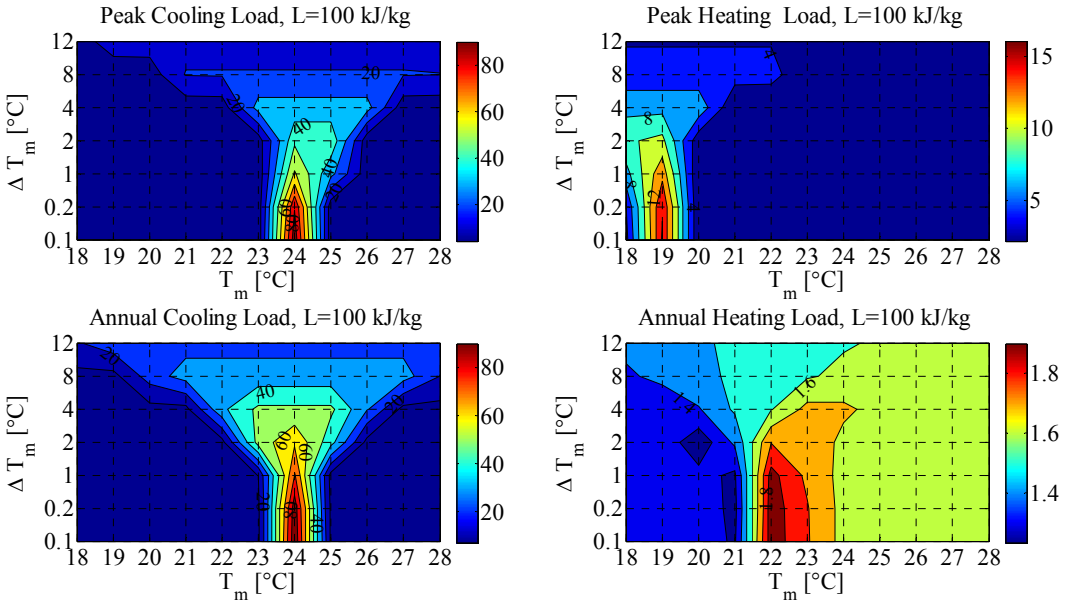

c) A contour plot for the case of 100 kg/kJ showing percentage reduction in cooling and heating loads

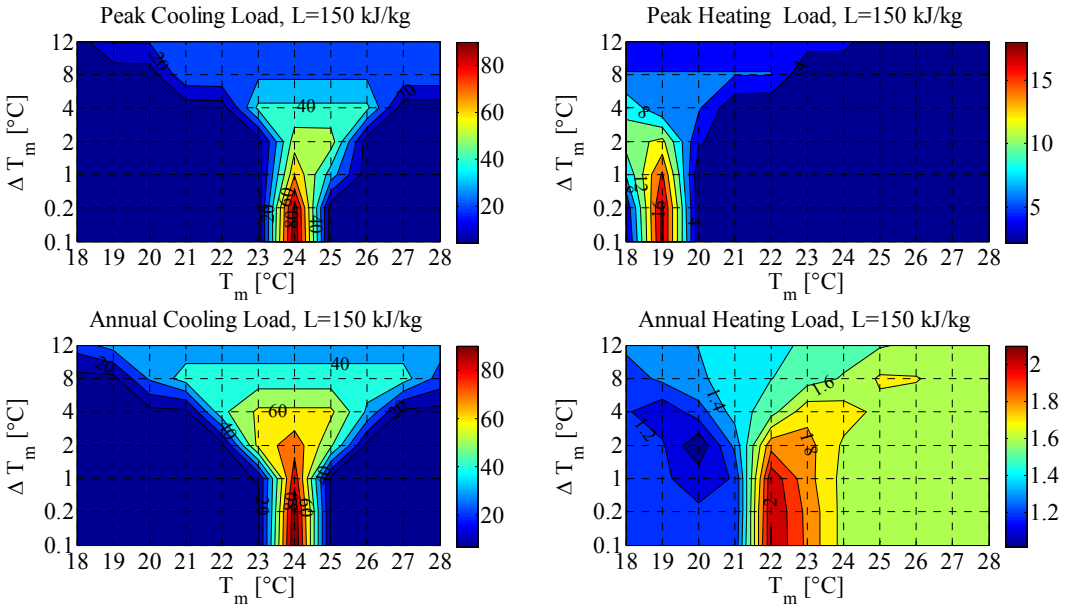

d) A contour plot for the case of 150 kg/kJ showing percentage reduction in cooling and heating loads

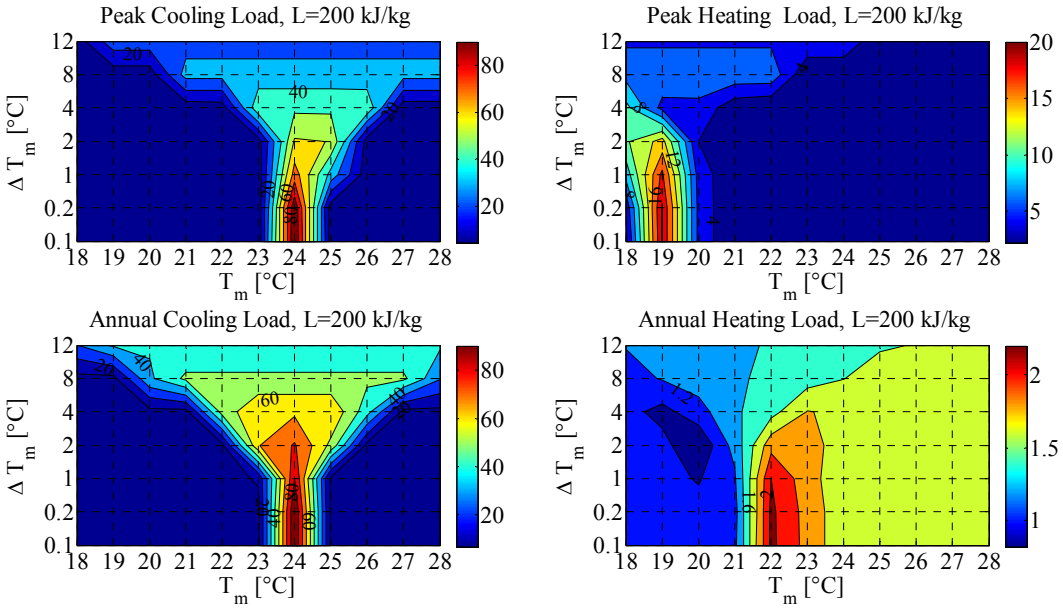

e) A contour plot for the case of 200 kg/kJ showing percentage reduction in cooling and heating loads

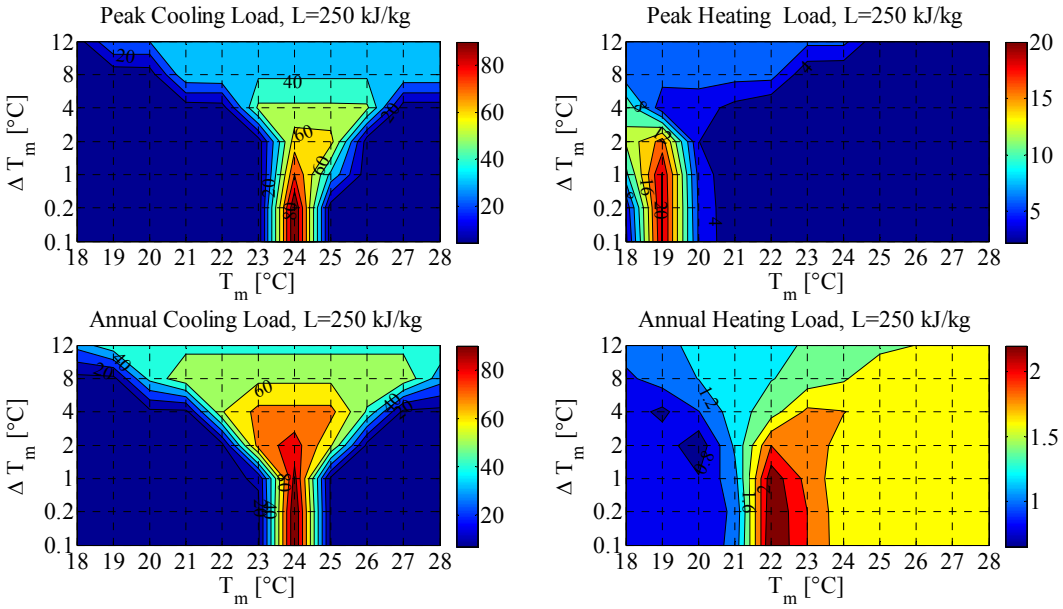

f) A contour plot for the case of 250 kg/kJ showing percentage reduction in cooling and heating loads

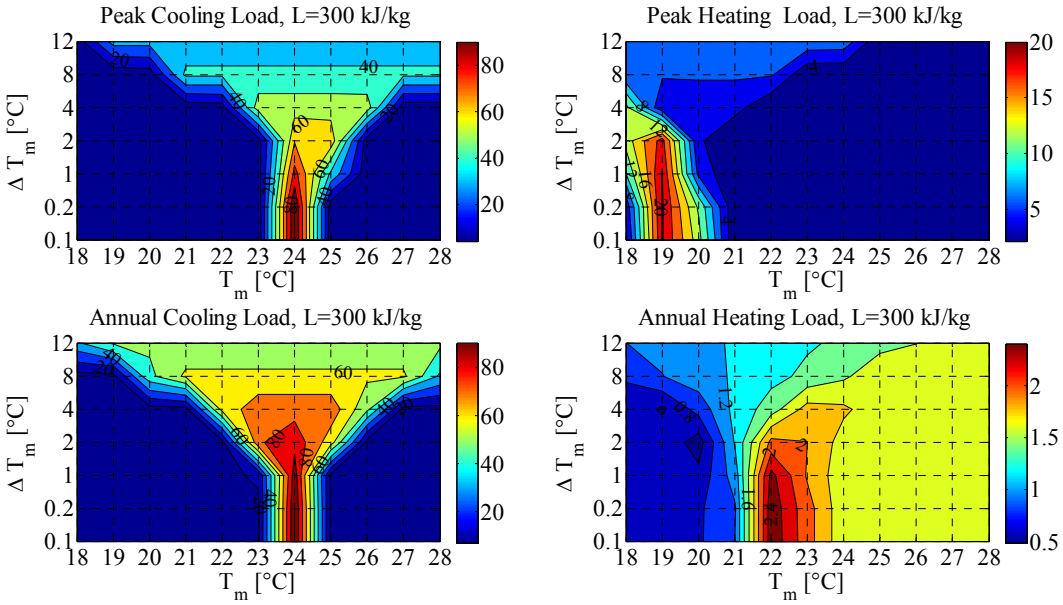

g) A contour plot for the case of 300 kg/kJ showing percentage reduction in cooling and heating loads

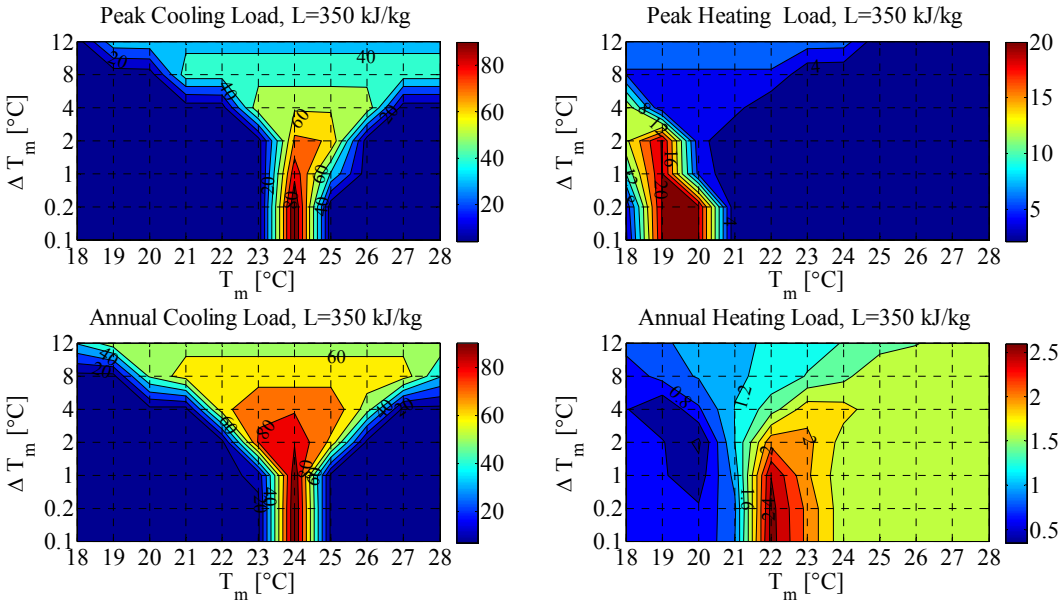

h) A contour plot for the case of 350 kg/kJ showing percentage reduction in cooling and heating loads

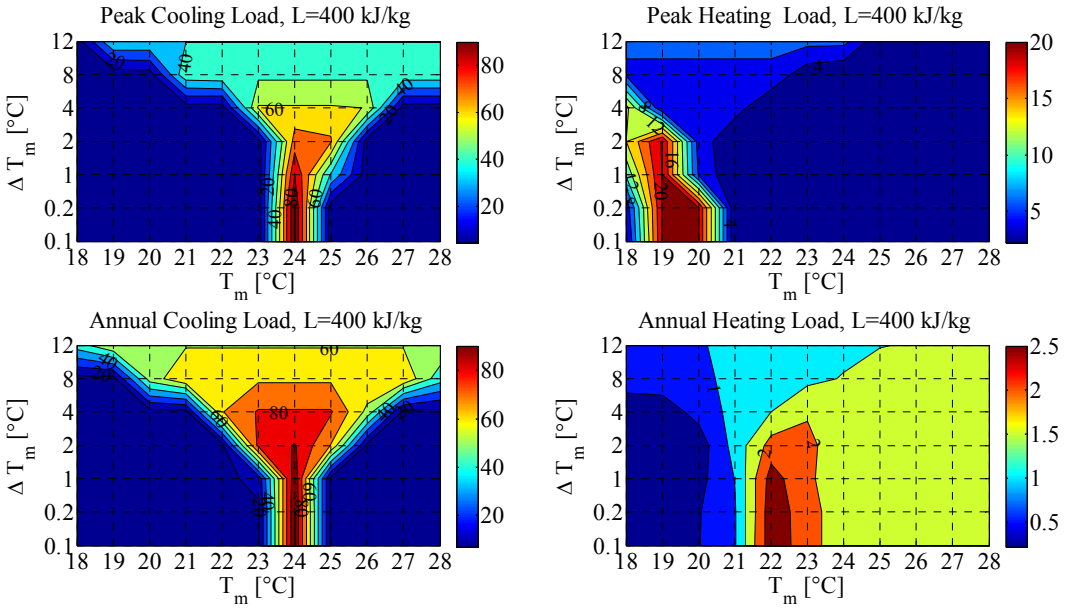

i) A contour plot for the case of 400 kg/kJ showing percentage reduction in cooling and heating loads

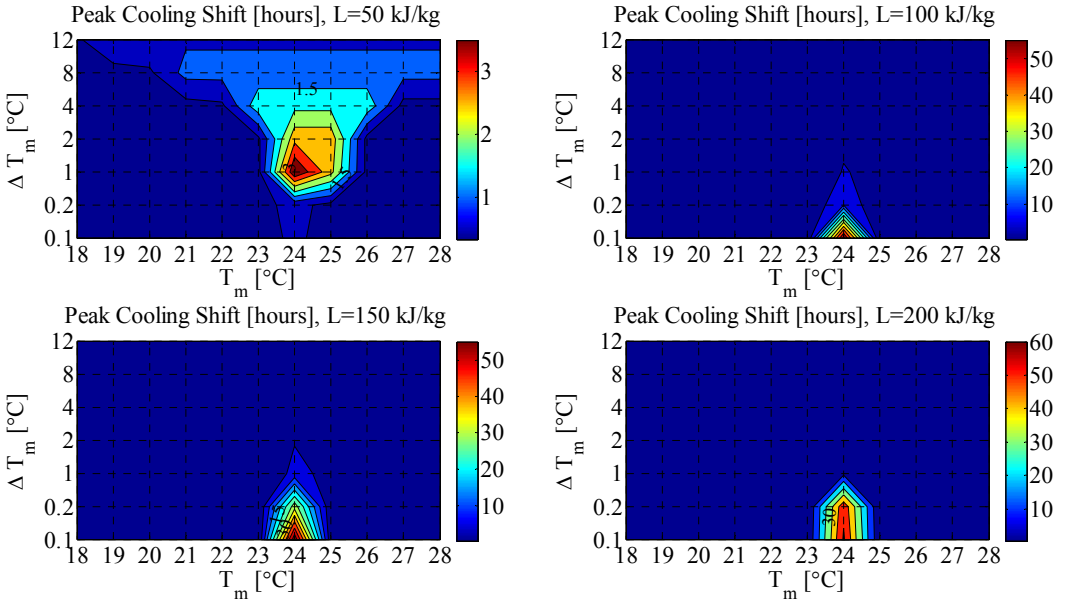

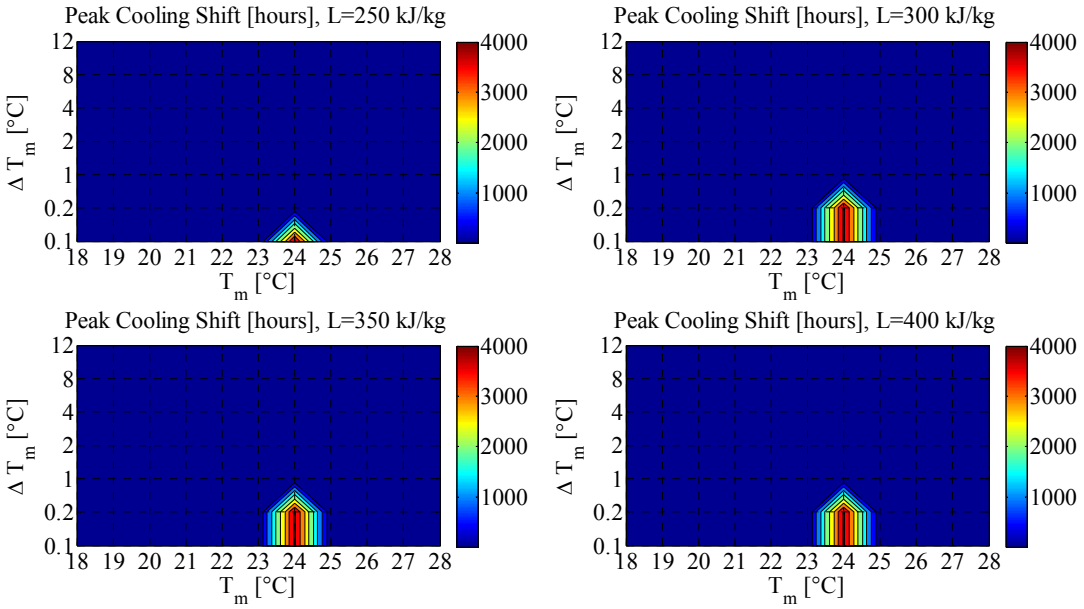

j) A contour plot for the peak cooling shift in hours

Figure A.7 Percentage reductions in cooling and heating loads for North wall when PCM to the interior, Golden, CO

Appendix A.3.2 PCM in the middle

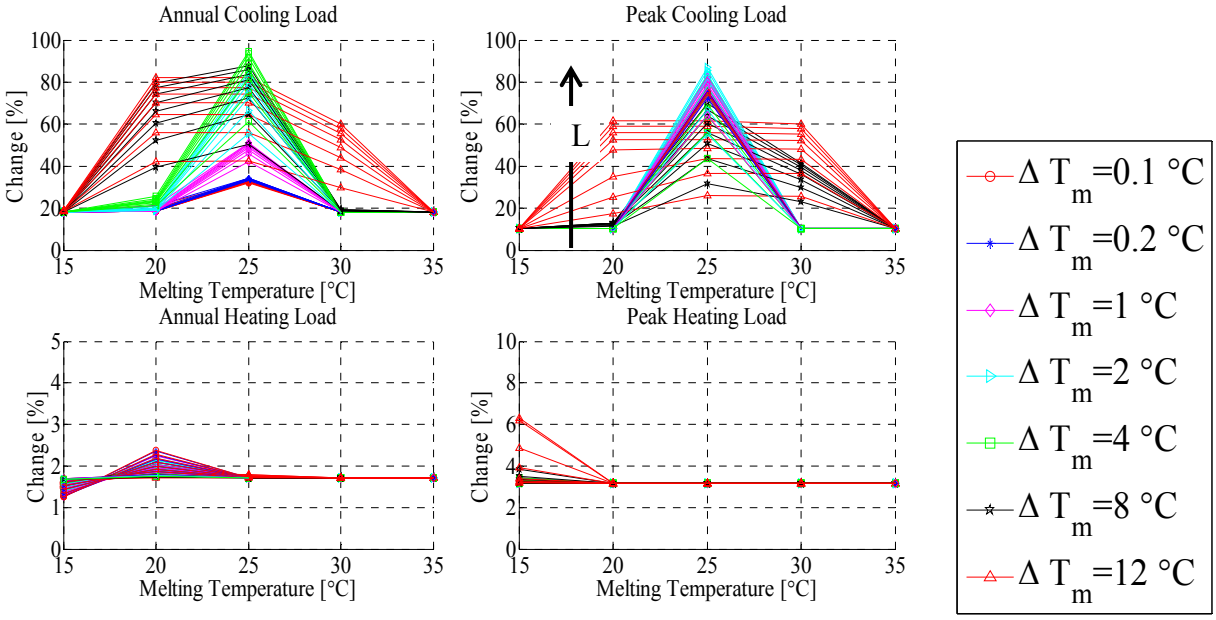

a) Percentage reductions in cooling and heating loads across all parameters

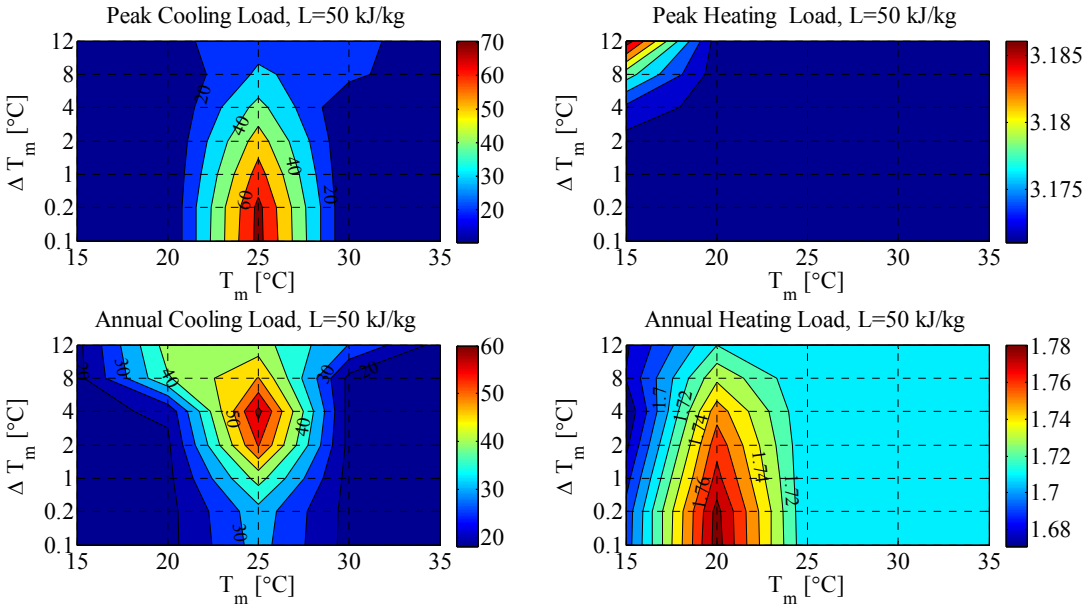

b) A contour plot for the case of 50 kg/kJ showing percentage reduction in cooling and heating loads

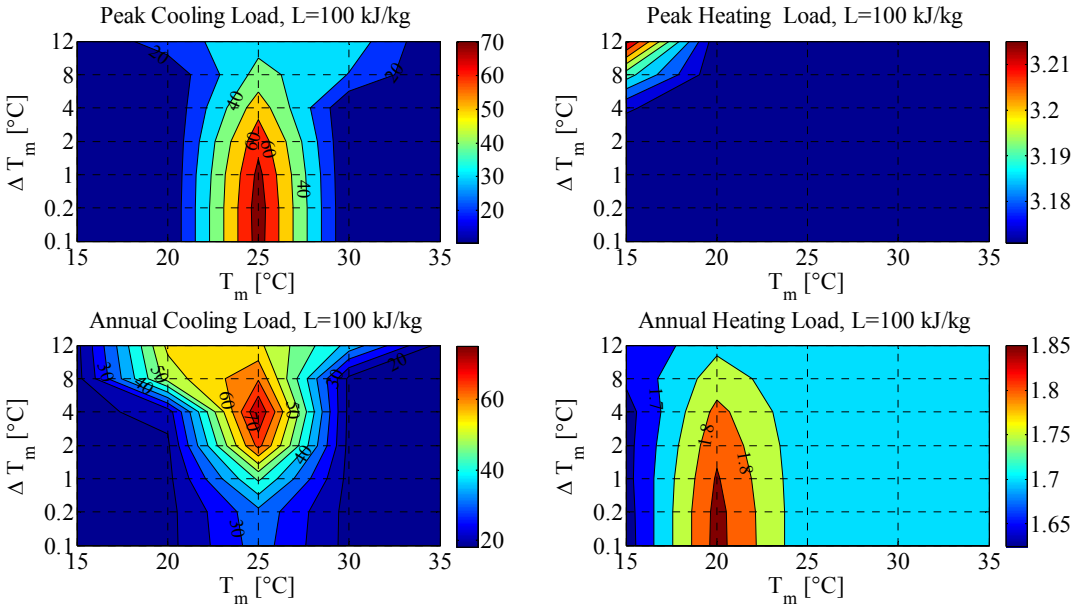

c) A contour plot for the case of 100 kg/kJ showing percentage reduction in cooling and heating loads

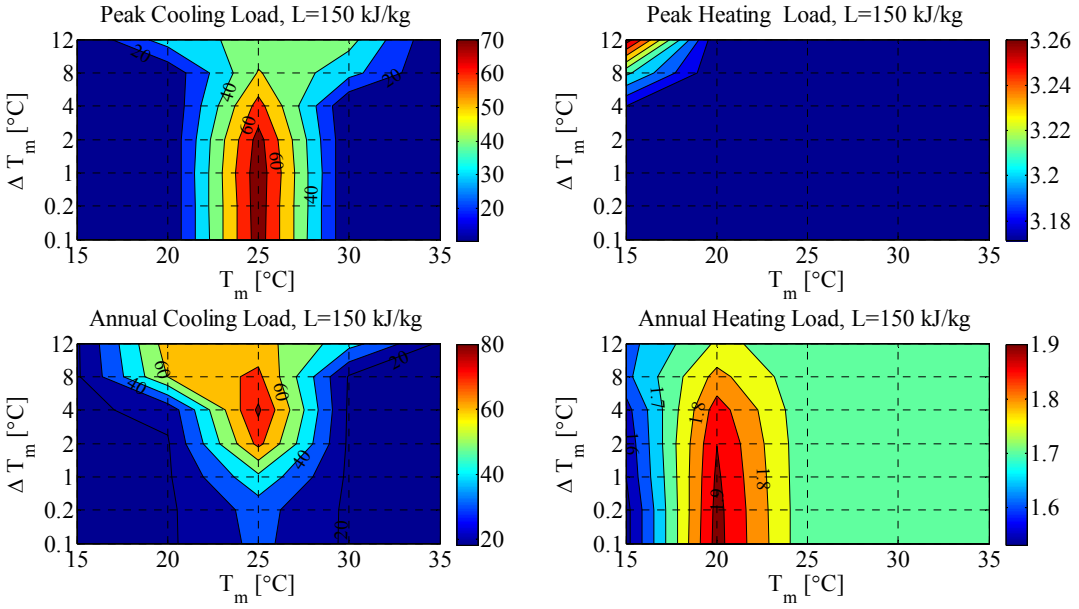

d) A contour plot for the case of 150 kg/kJ showing percentage reduction in cooling and heating loads

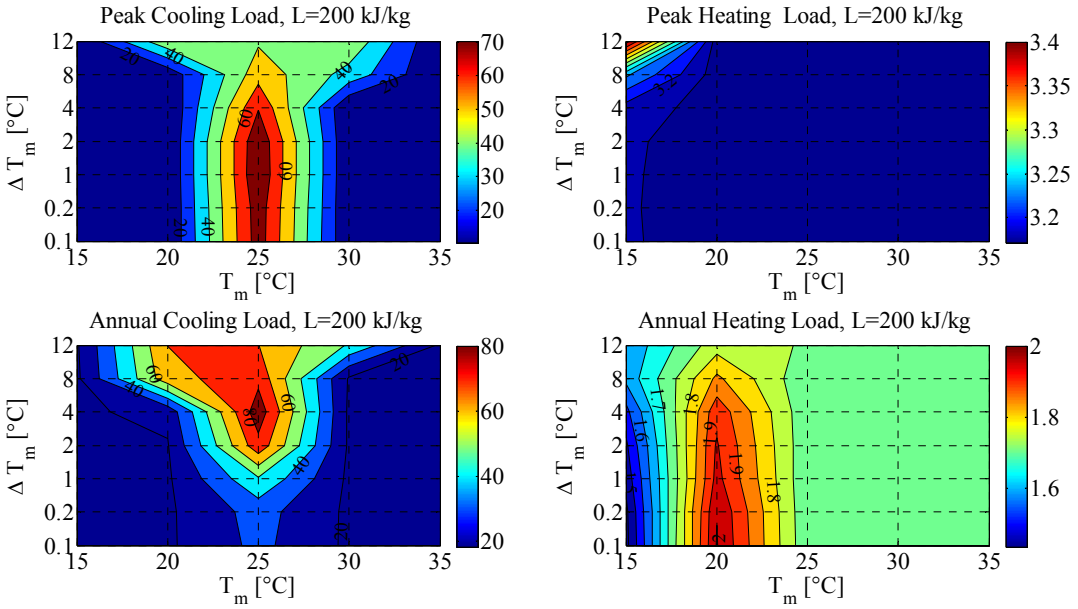

e) A contour plot for the case of 200 kg/kJ showing percentage reduction in cooling and heating loads

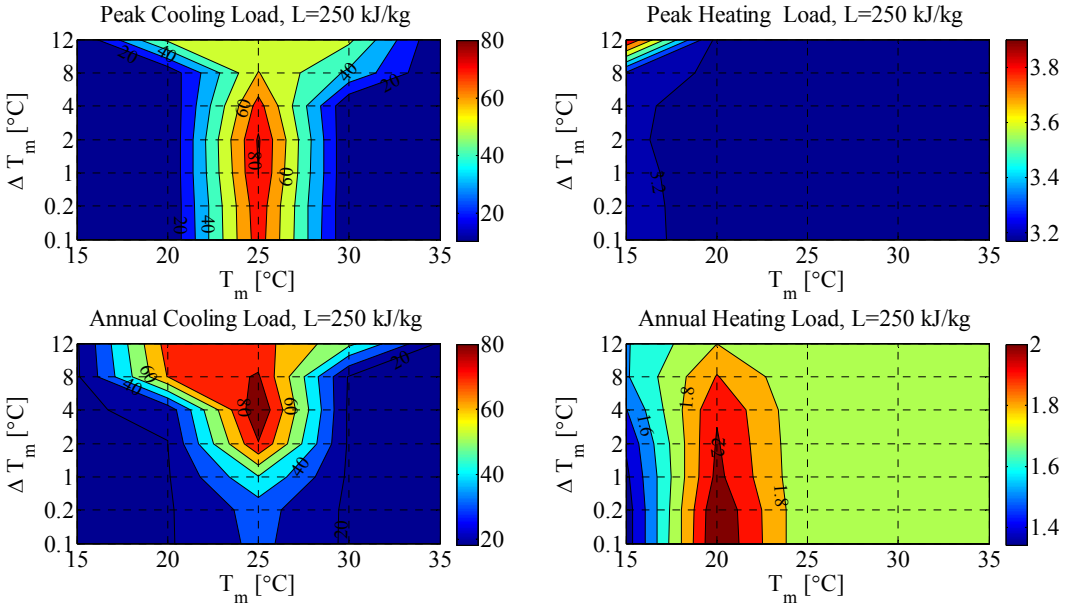

f) A contour plot for the case of 250 kg/kJ showing percentage reduction in cooling and heating loads

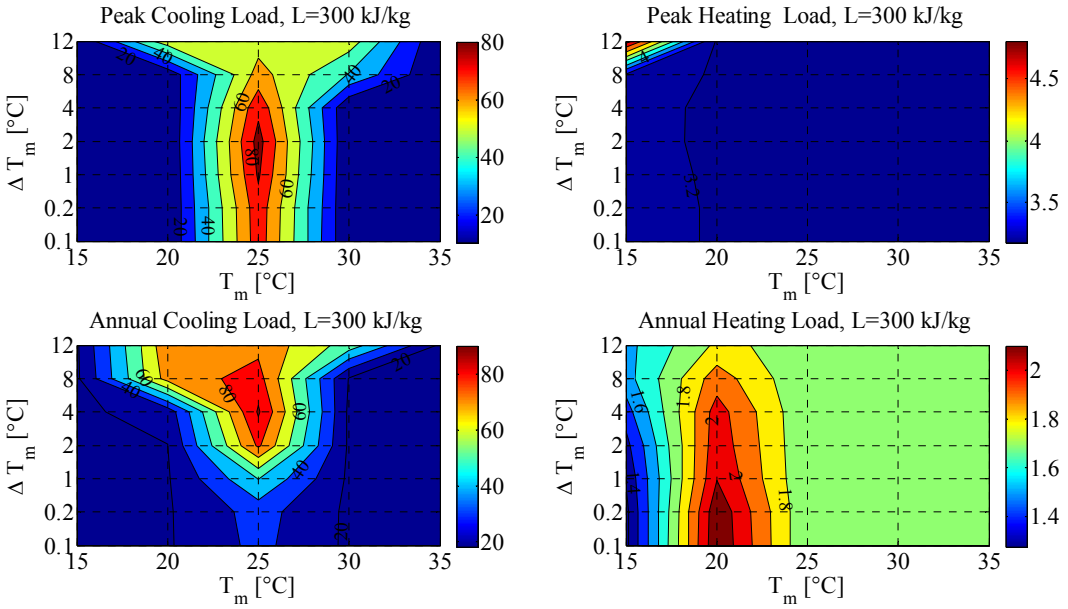

g) A contour plot for the case of 300 kg/kJ showing percentage reduction in cooling and heating loads

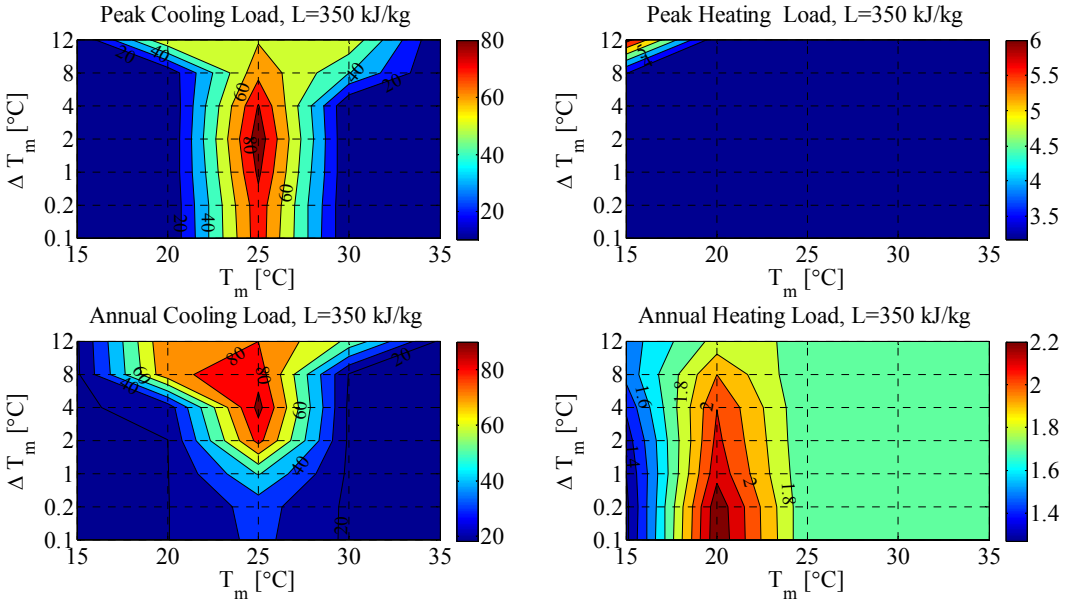

h) A contour plot for the case of 350 kg/kJ showing percentage reduction in cooling and heating loads

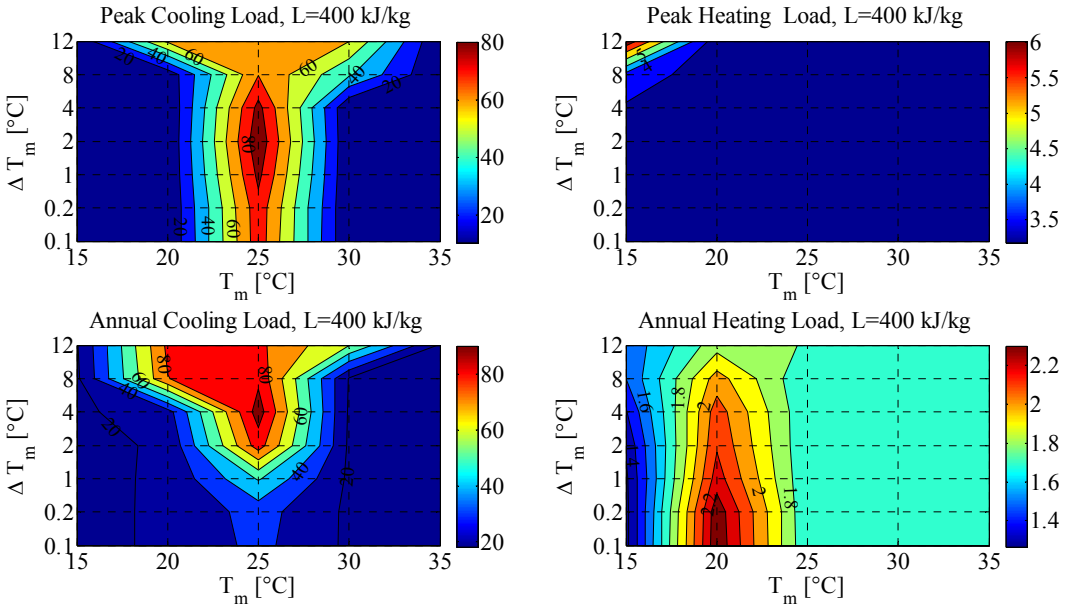

i) A contour plot for the case of 400 kg/kJ showing percentage reduction in cooling and heating loads

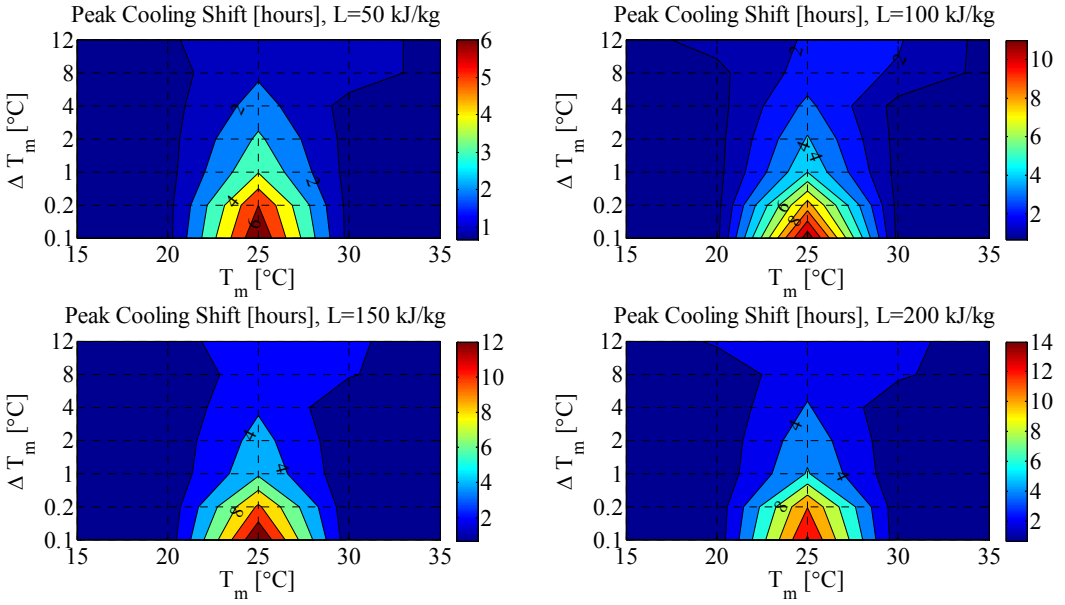

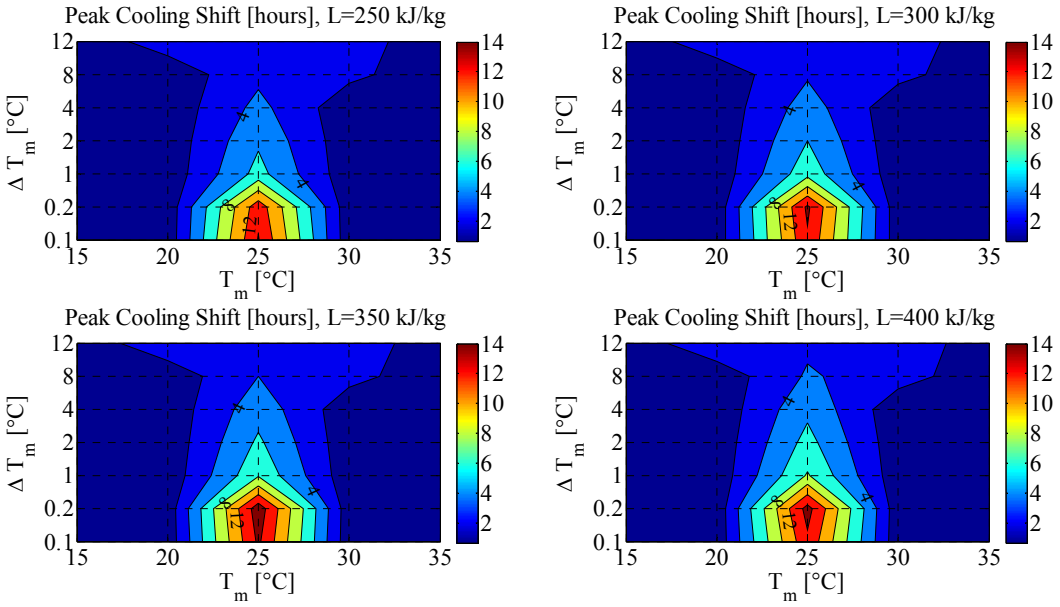

j) A contour plot for the peak cooling shift in hours

Figure A.8 Percentage reductions in cooling and heating loads for North wall when PCM in the middle, Golden, CO

Appendix A.3.3 PCM to the exterior

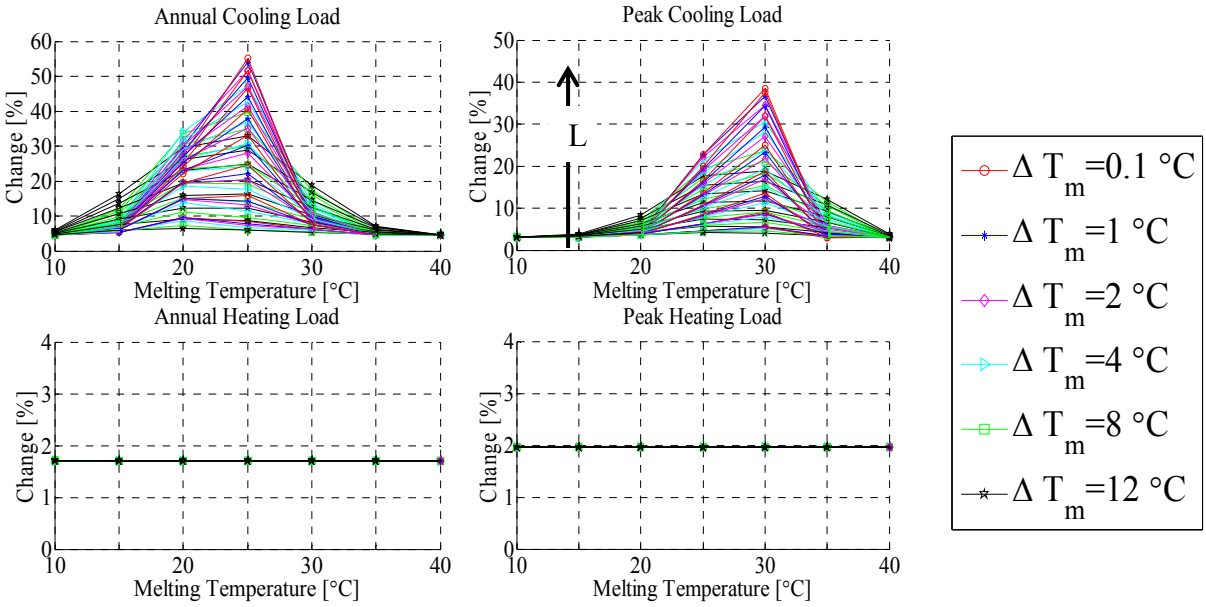

a) Percentage reductions in cooling and heating loads across all parameters

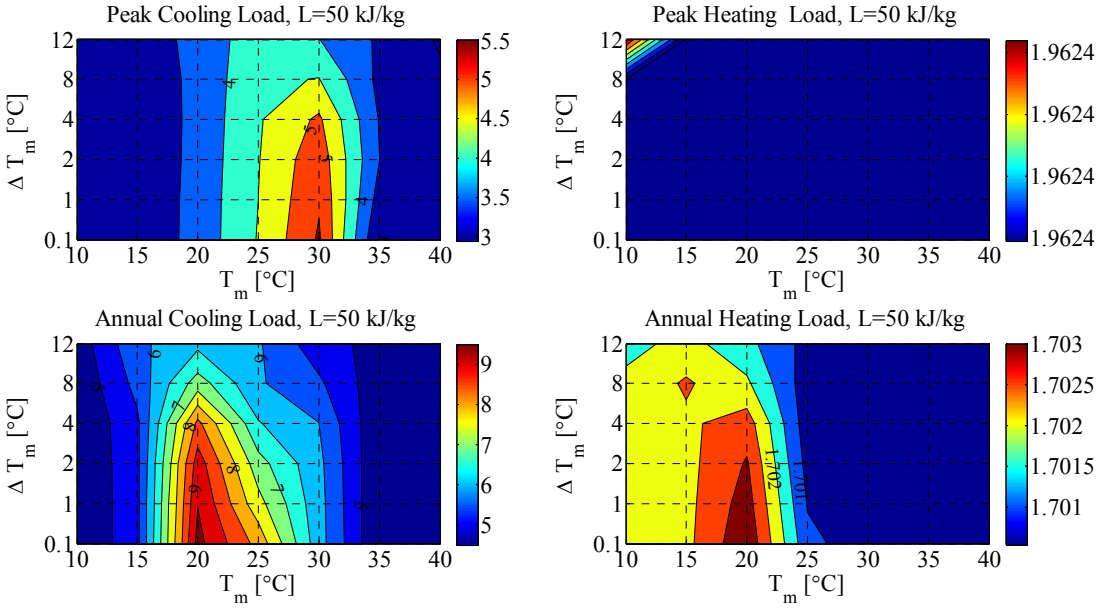

b) A contour plot for the case of 50 kg/kJ showing percentage reduction in cooling and heating loads

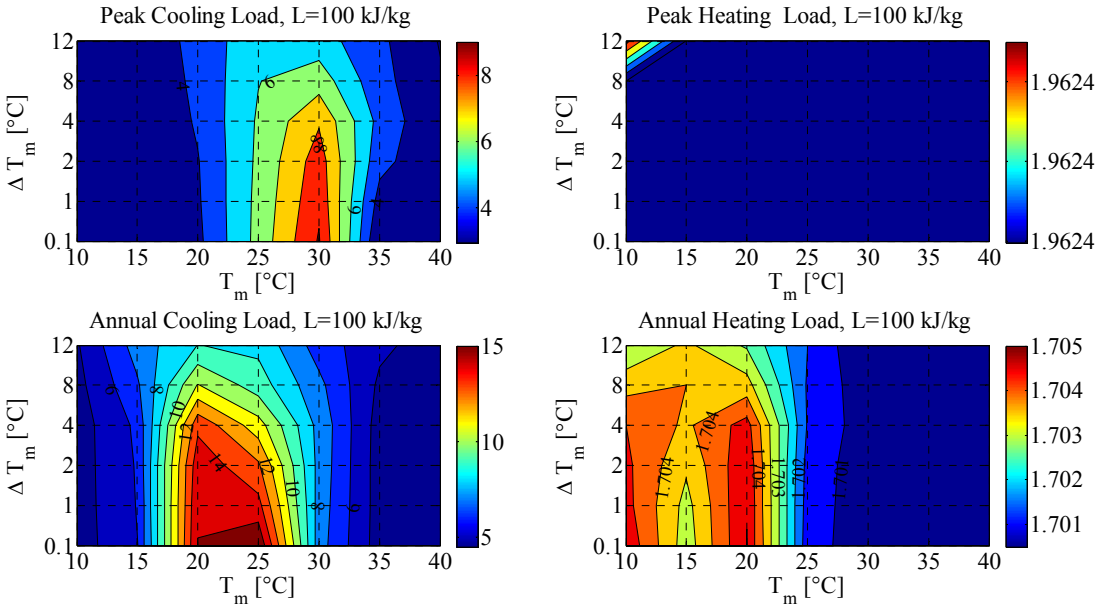

c) A contour plot for the case of 100 kg/kJ showing percentage reduction in cooling and heating loads

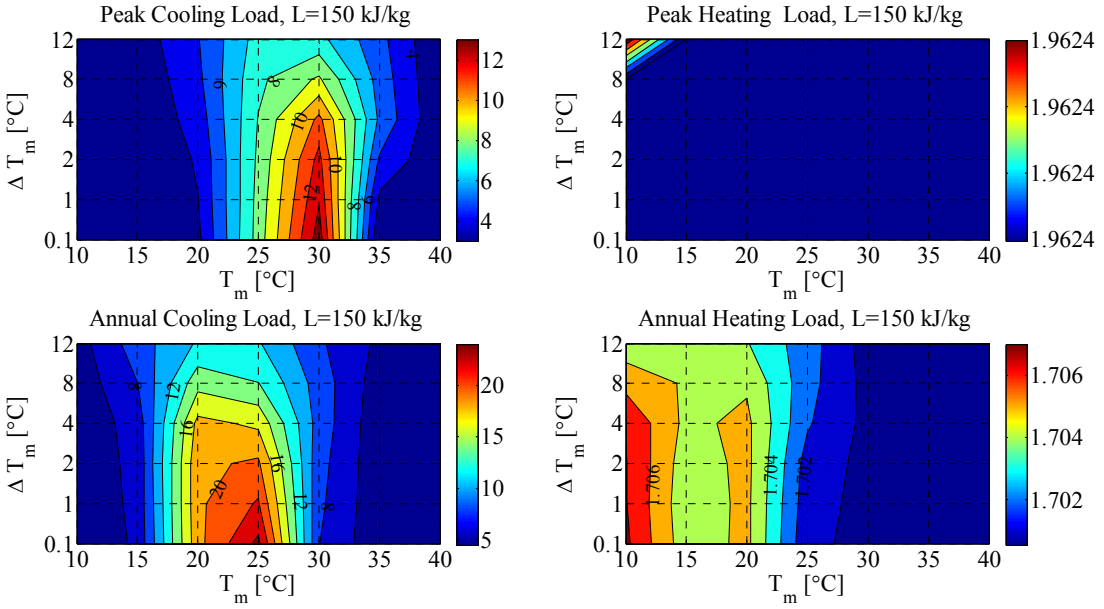

d) A contour plot for the case of 150 kg/kJ showing percentage reduction in cooling and heating loads

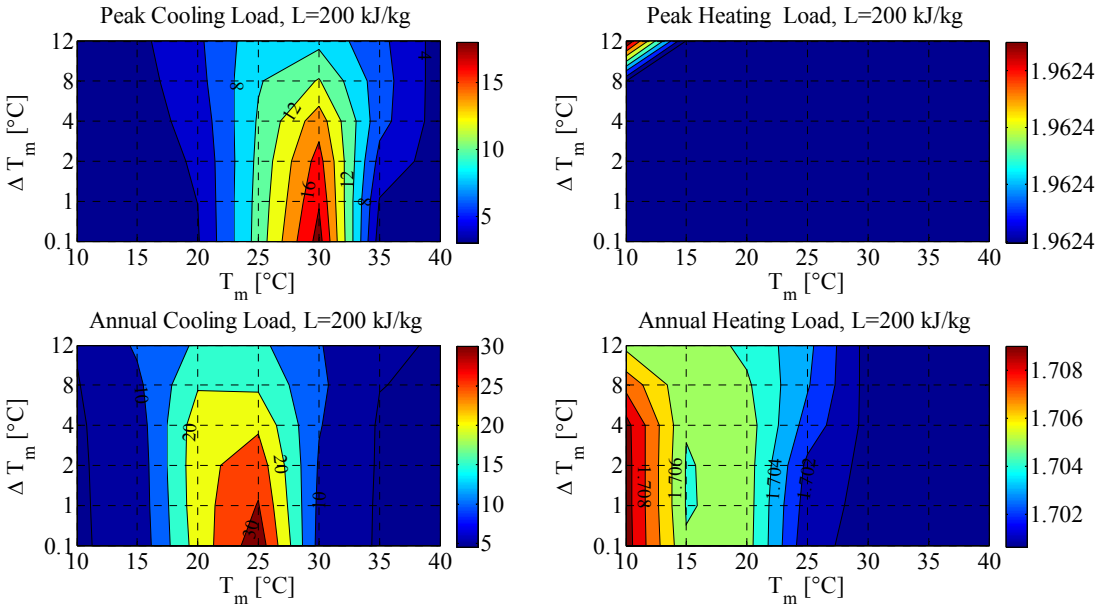

e) A contour plot for the case of 200 kg/kJ showing percentage reduction in cooling and heating loads

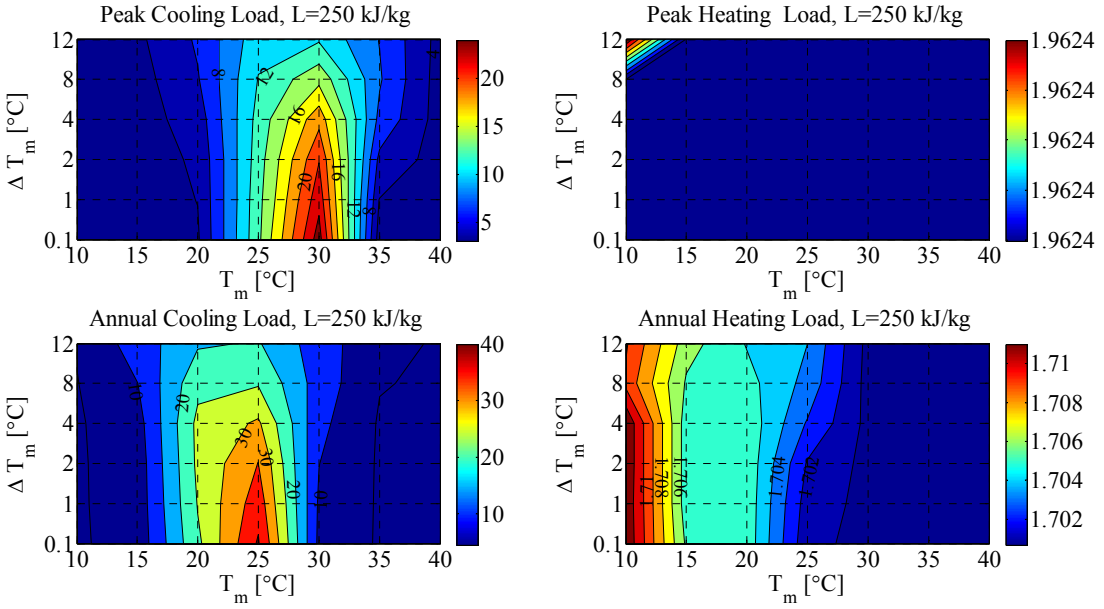

f) A contour plot for the case of 250 kg/kJ showing percentage reduction in cooling and heating loads

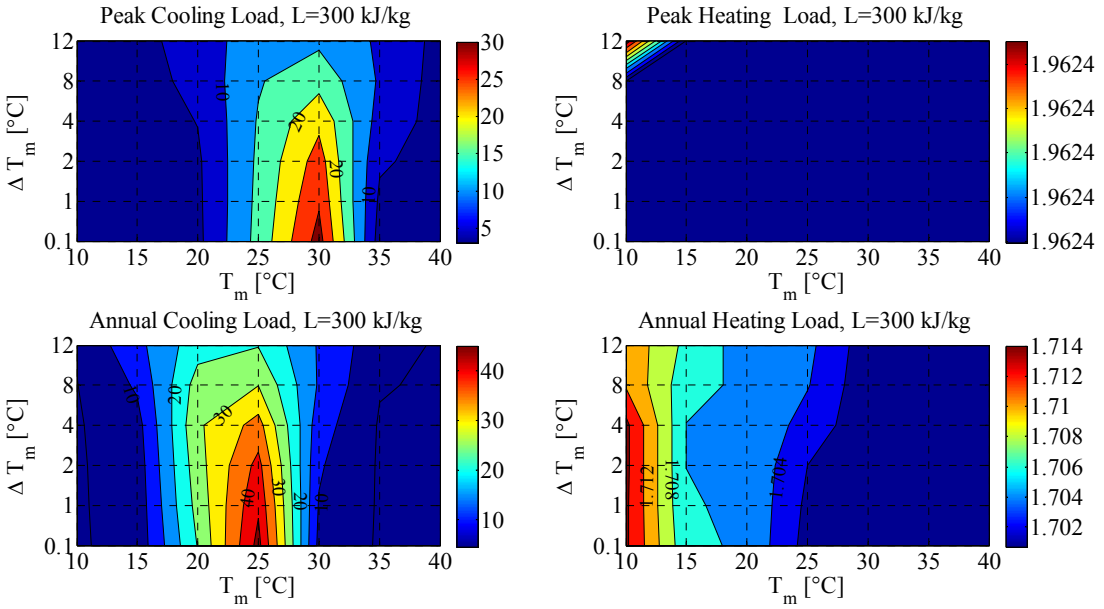

g) A contour plot for the case of 300 kg/kJ showing percentage reduction in cooling and heating loads

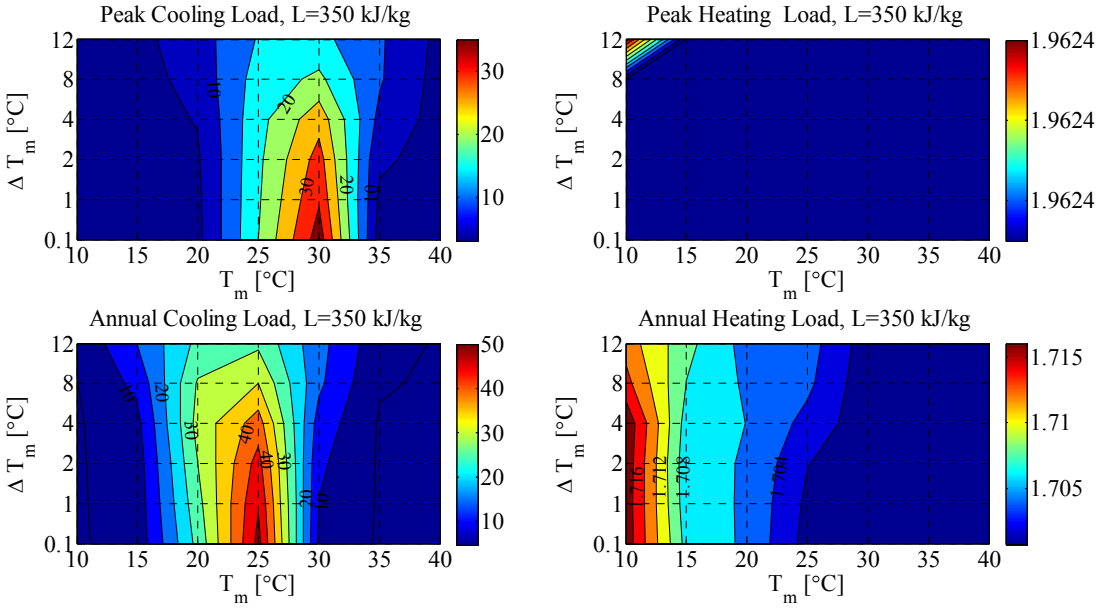

h) A contour plot for the case of 350 kg/kJ showing percentage reduction in cooling and heating loads

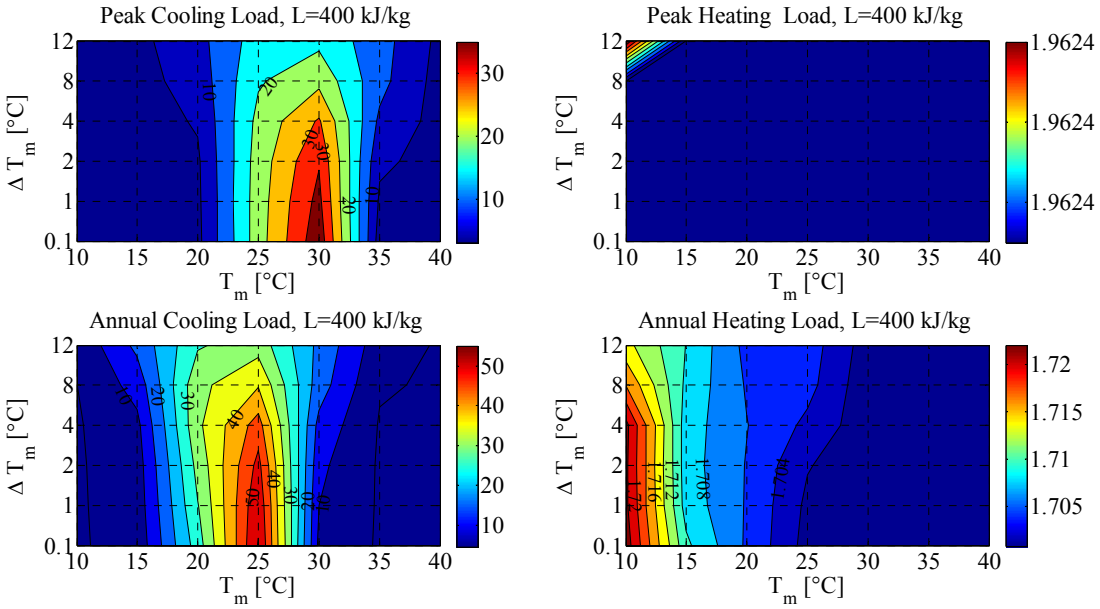

i) A contour plot for the case of 400 kg/kJ showing percentage reduction in cooling and heating loads

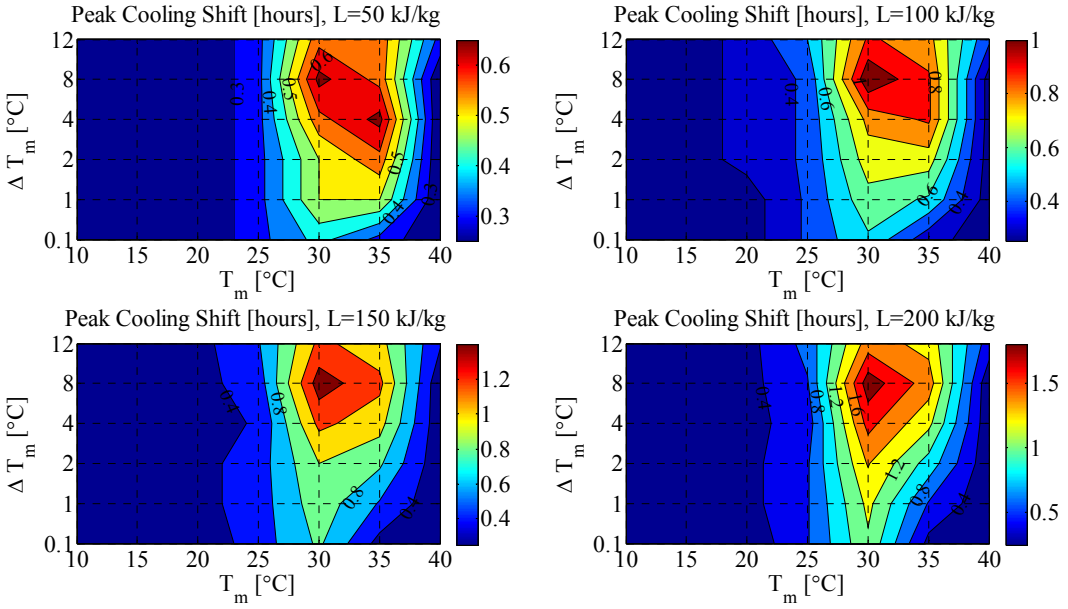

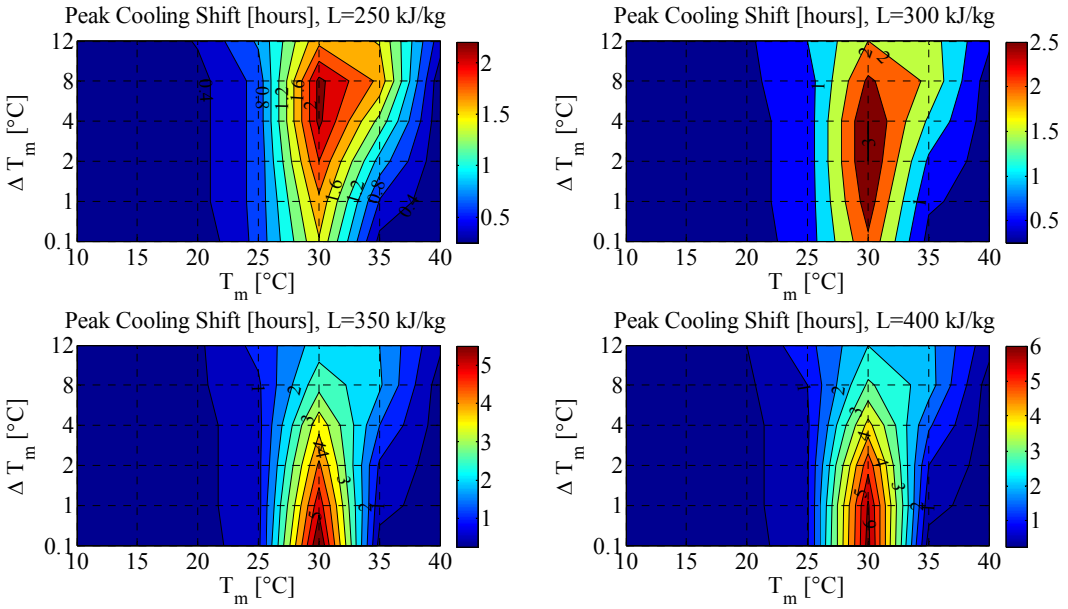

j) A contour plot for the peak cooling shift in hours

Figure A.9 Percentage reductions in cooling and heating loads for North wall when PCM to the exterior, Golden, CO

Appendix A.4 East Wall

Appendix A.4.1 PCM to the interior

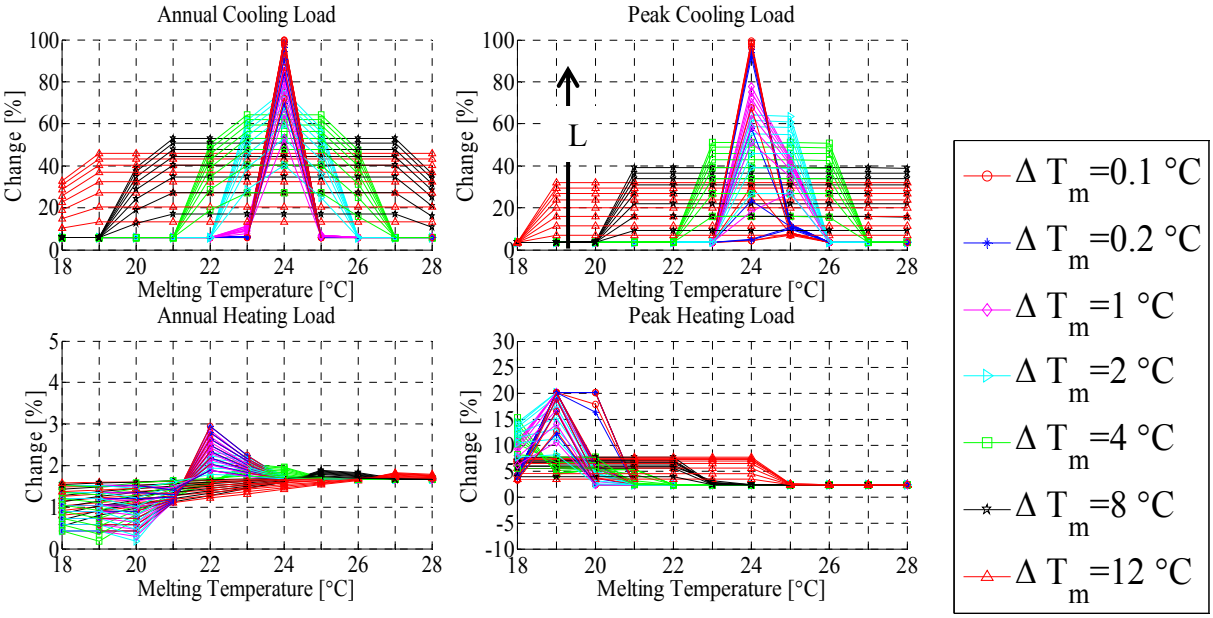

a) Percentage reductions in cooling and heating loads across all parameters

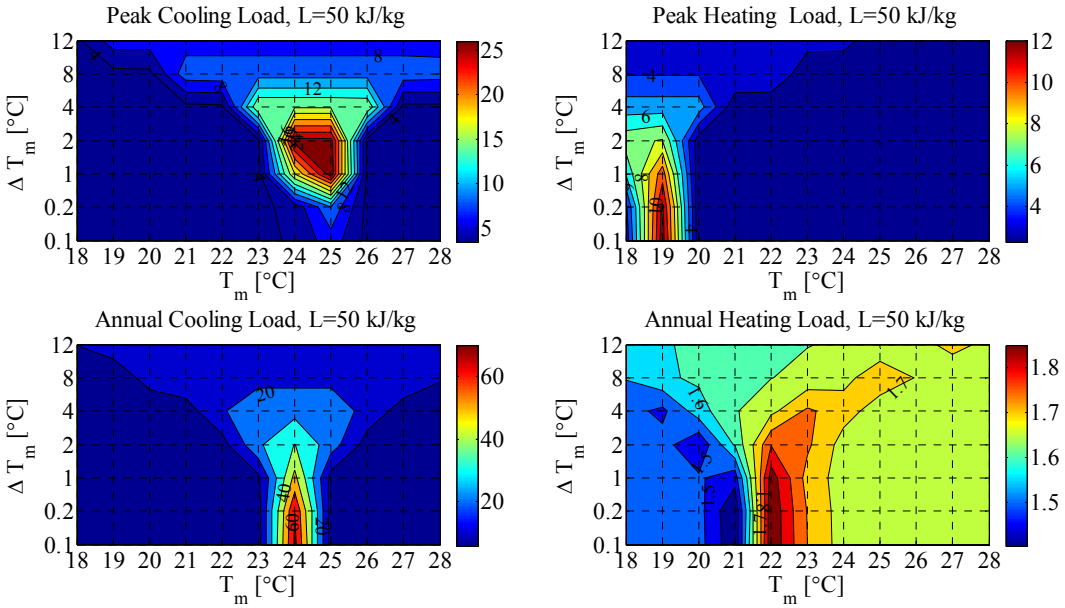

b) A contour plot for the case of 50 kg/kJ showing percentage reduction in cooling and heating loads

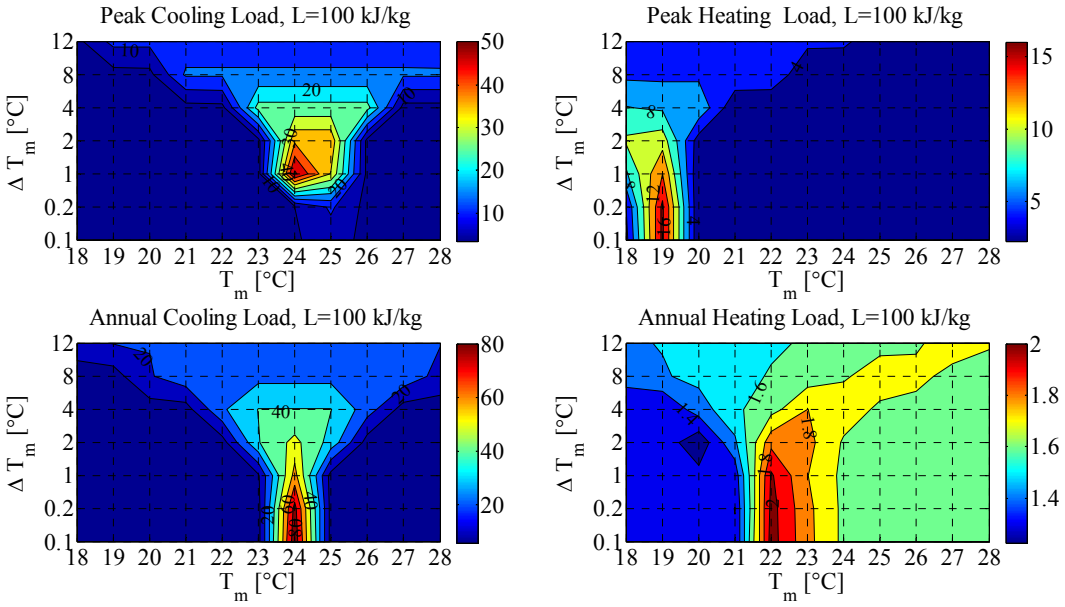

c) A contour plot for the case of 100 kg/kJ showing percentage reduction in cooling and heating loads

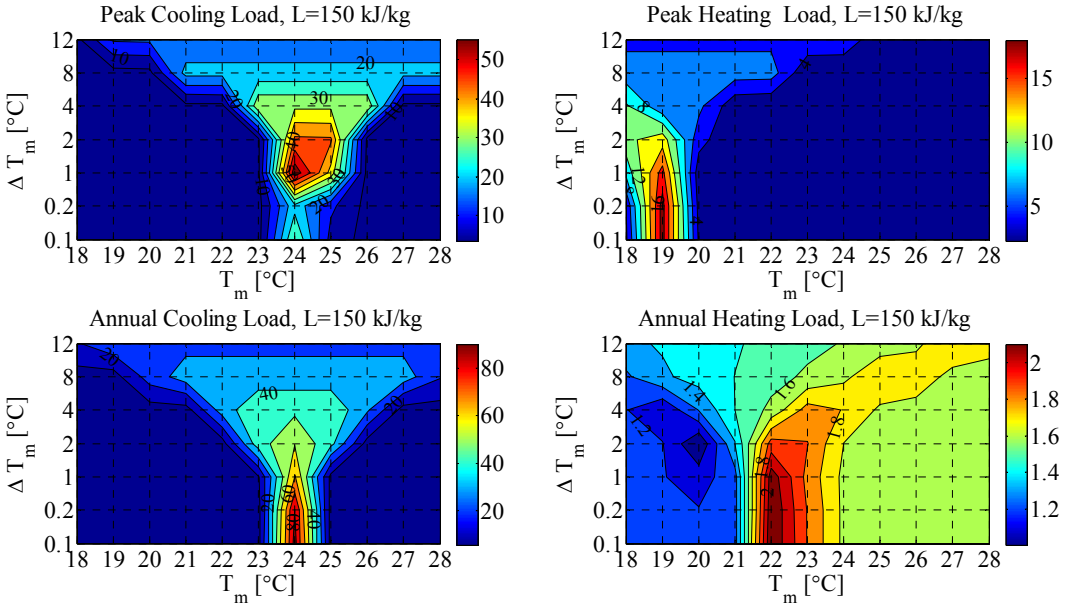

d) A contour plot for the case of 150 kg/kJ showing percentage reduction in cooling and heating loads

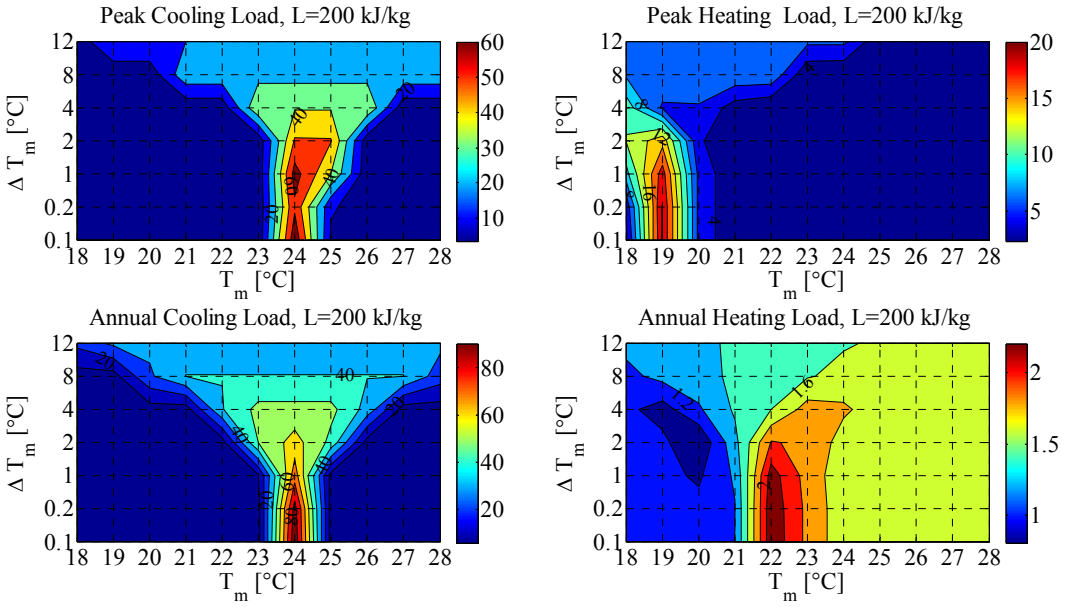

e) A contour plot for the case of 200 kg/kJ showing percentage reduction in cooling and heating loads

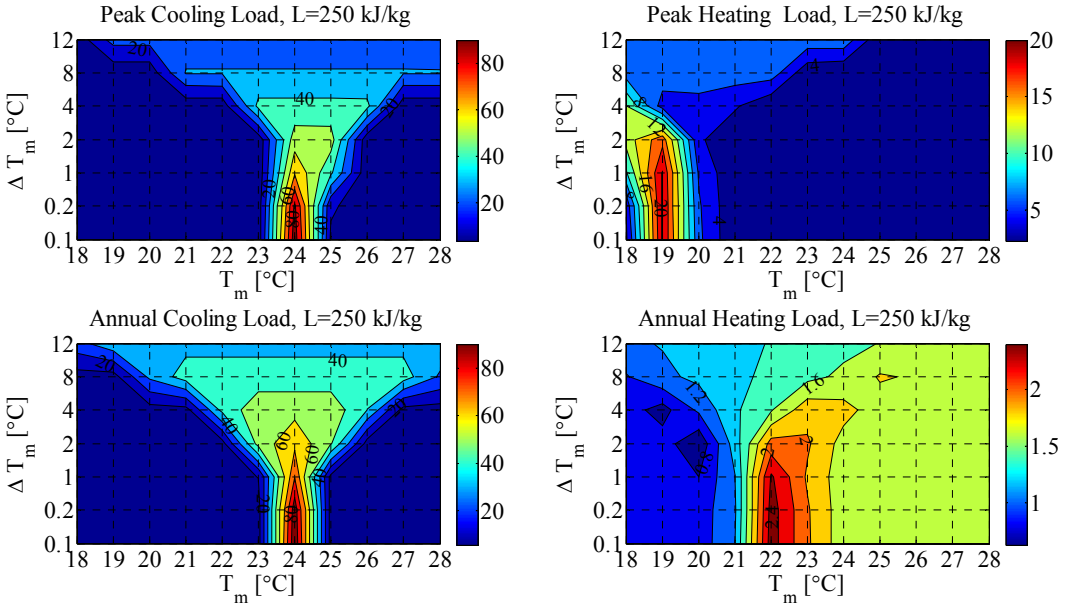

f) A contour plot for the case of 250 kg/kJ showing percentage reduction in cooling and heating loads

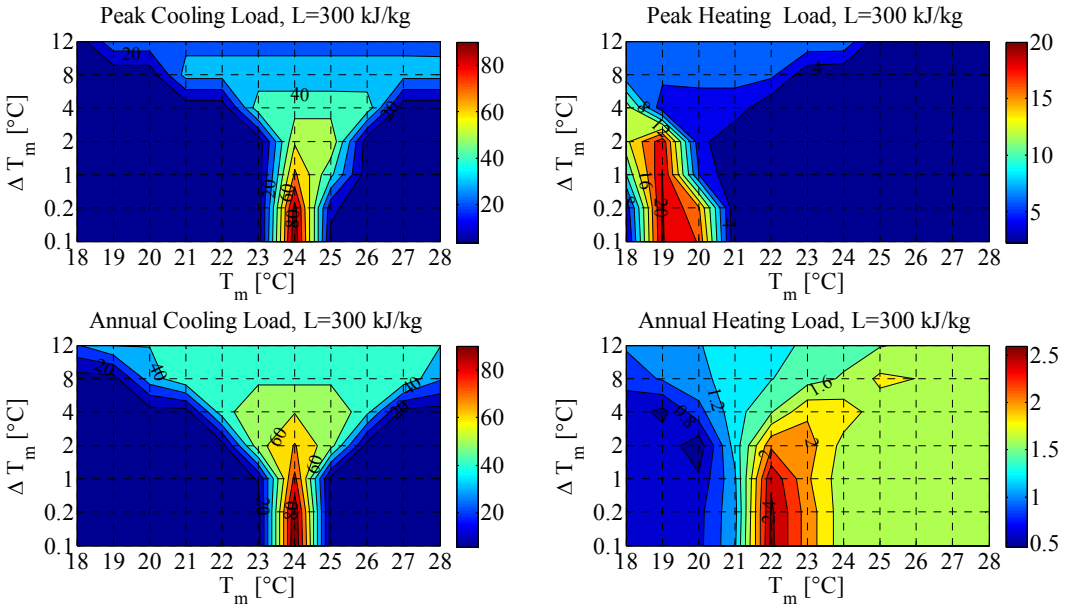

g) A contour plot for the case of 300 kg/kJ showing percentage reduction in cooling and heating loads

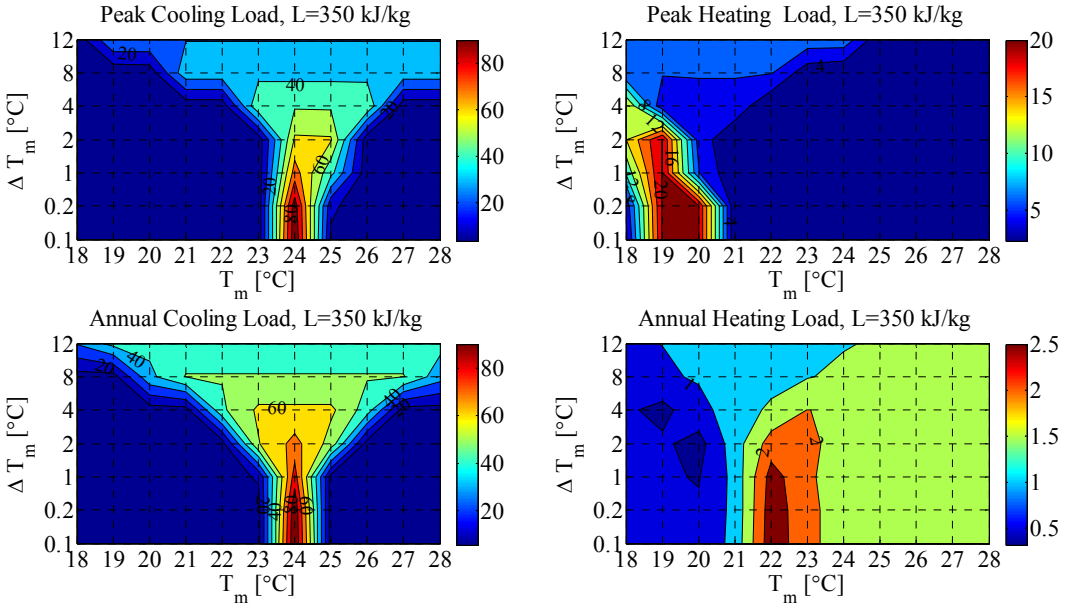

h) A contour plot for the case of 350 kg/kJ showing percentage reduction in cooling and heating loads

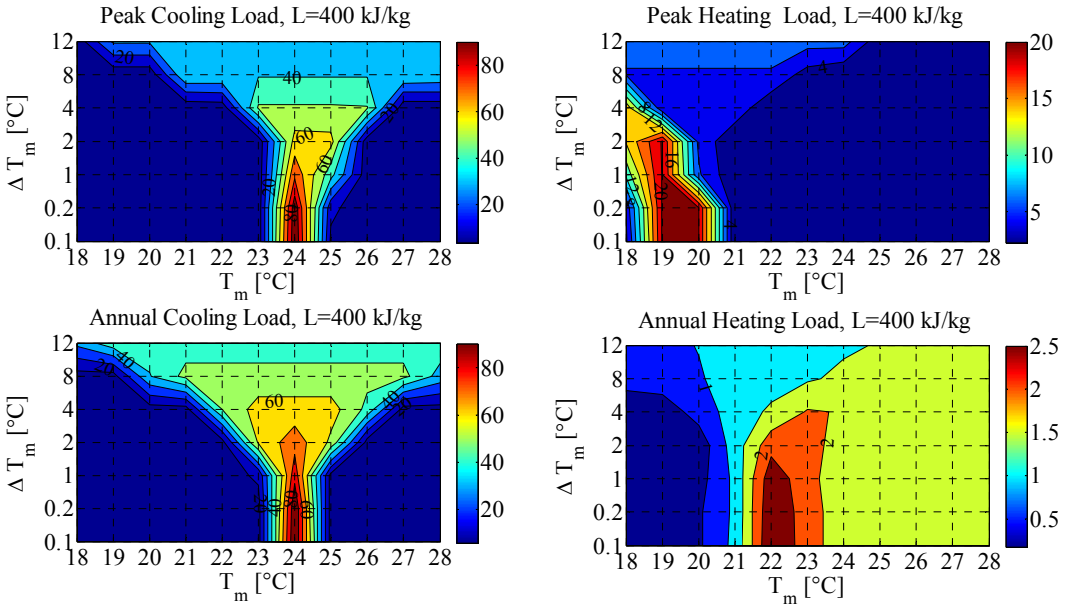

i) A contour plot for the case of 400 kg/kJ showing percentage reduction in cooling and heating loads

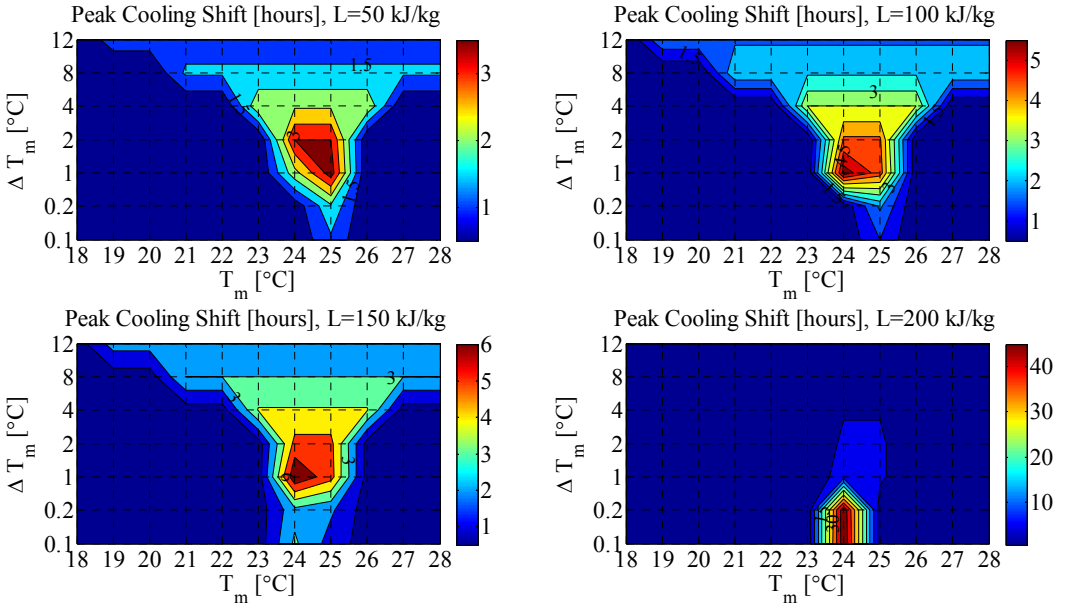

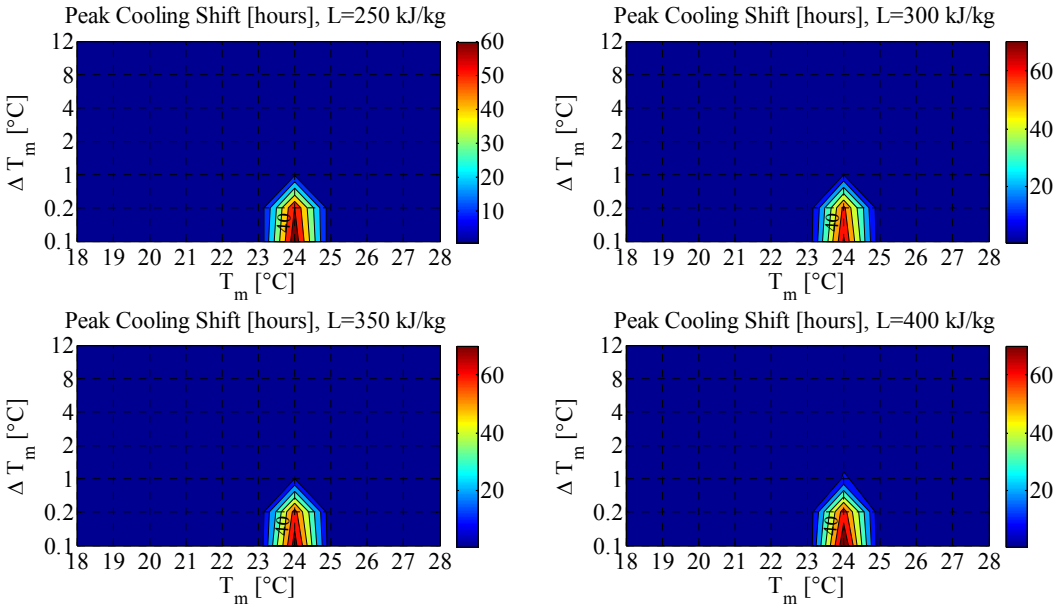

j) A contour plot for the peak cooling shift in hours

Figure A.10 Percentage reductions in cooling and heating loads for East wall when PCM to the interior, Golden, CO

Appendix A.4.2 PCM in the middle

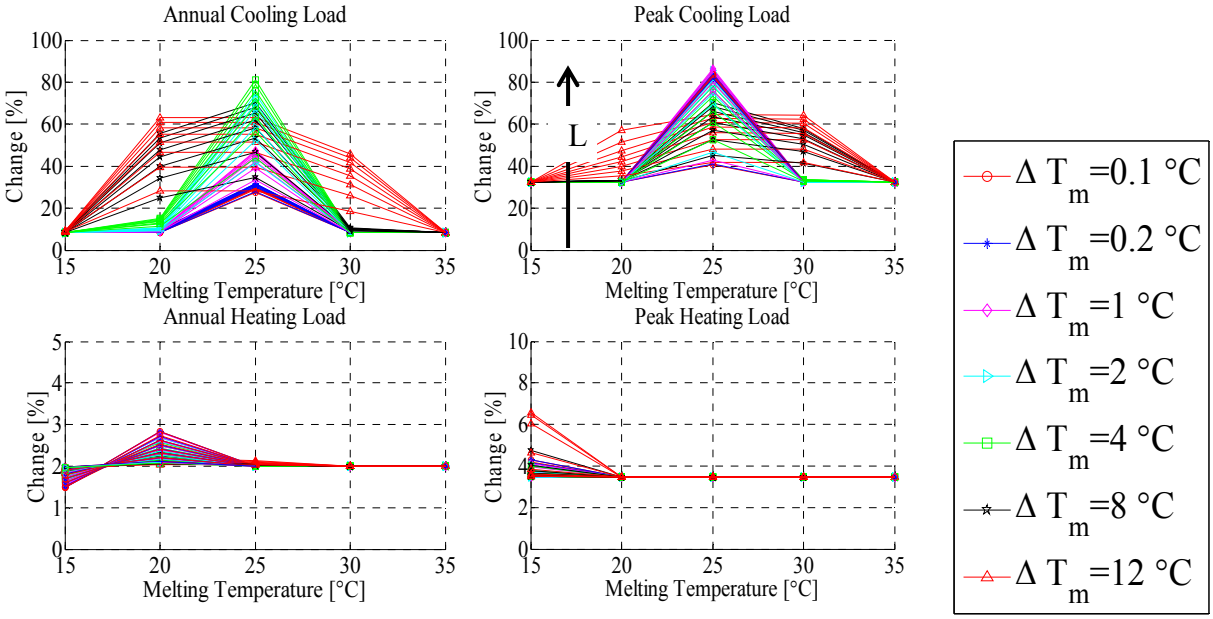

a) Percentage reductions in cooling and heating loads across all parameters

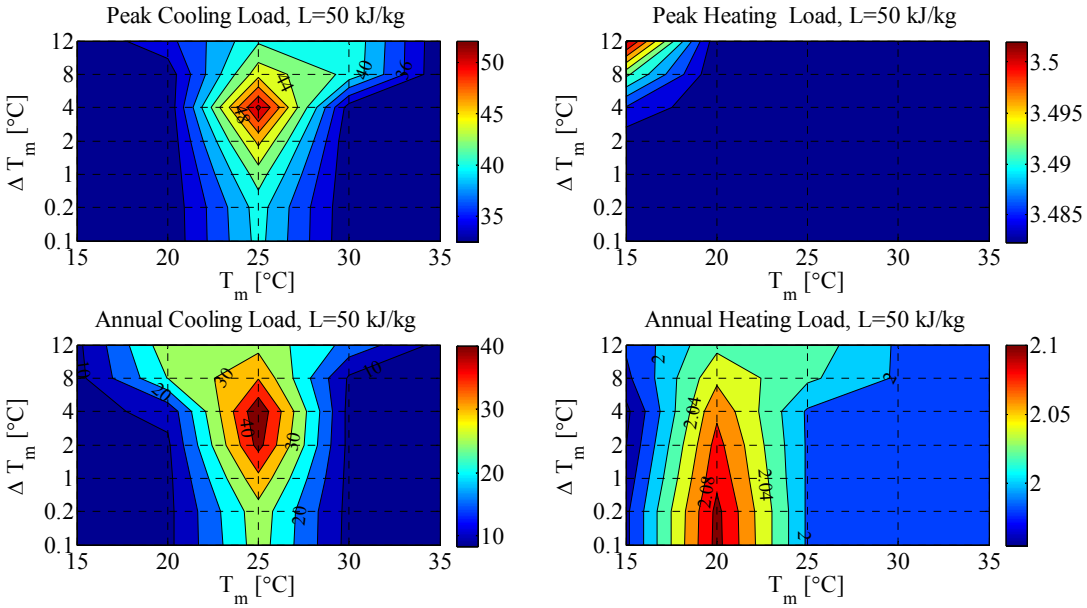

b) A contour plot for the case of 50 kg/kJ showing percentage reduction in cooling and heating loads

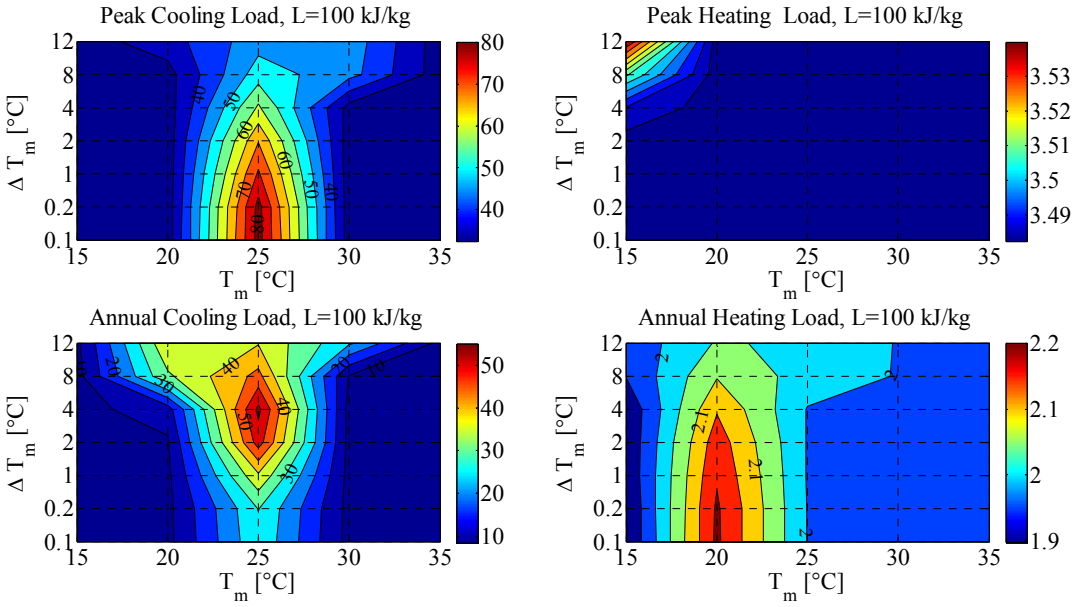

c) A contour plot for the case of 100 kg/kJ showing percentage reduction in cooling and heating loads

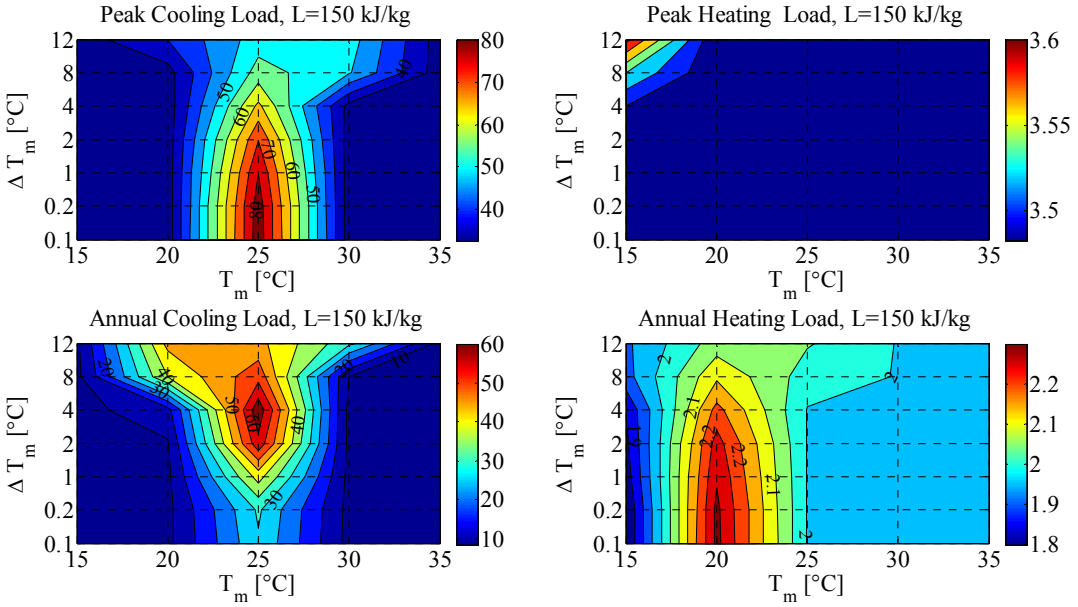

d) A contour plot for the case of 150 kg/kJ showing percentage reduction in cooling and heating loads

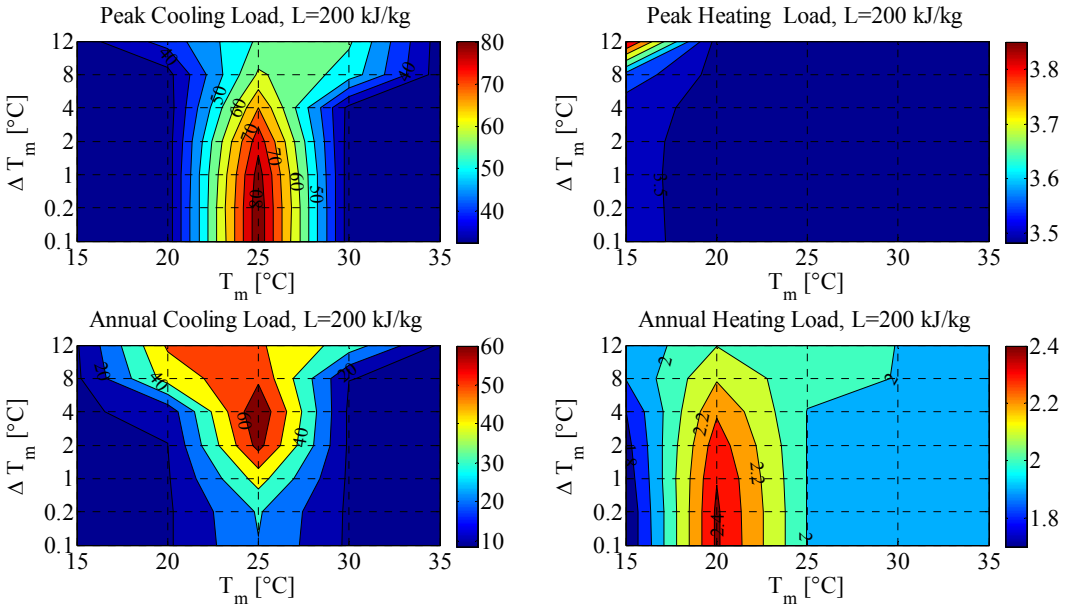

e) A contour plot for the case of 200 kg/kJ showing percentage reduction in cooling and heating loads

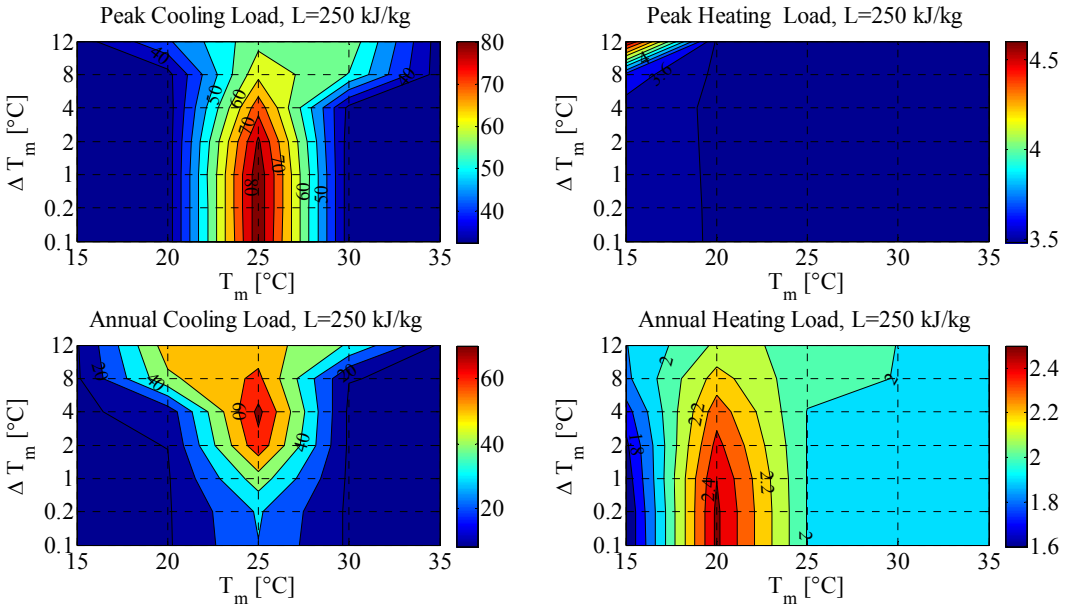

f) A contour plot for the case of 250 kg/kJ showing percentage reduction in cooling and heating loads

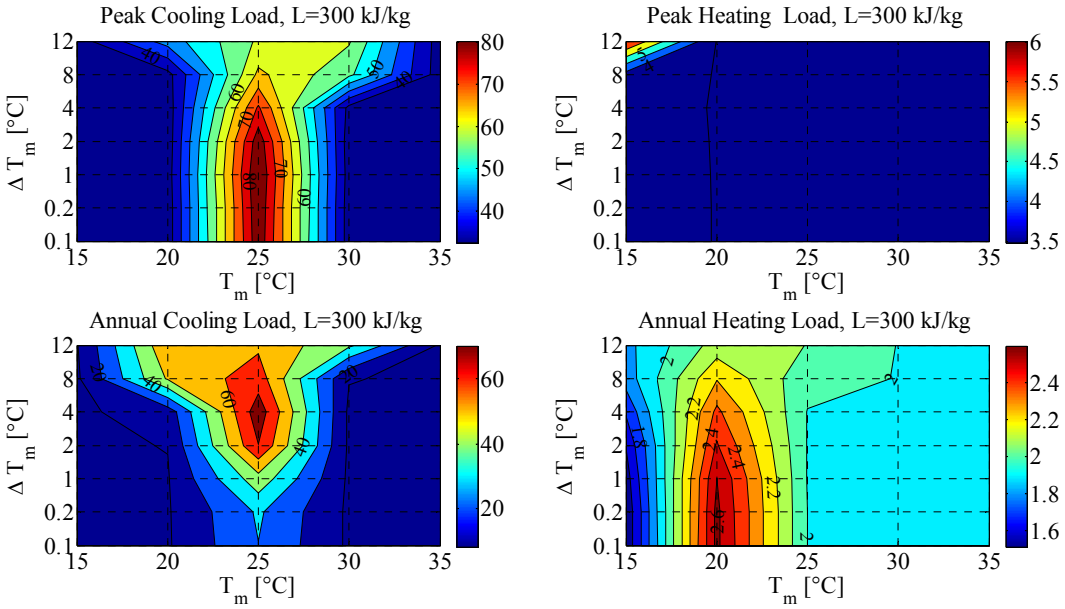

g) A contour plot for the case of 300 kg/kJ showing percentage reduction in cooling and heating loads

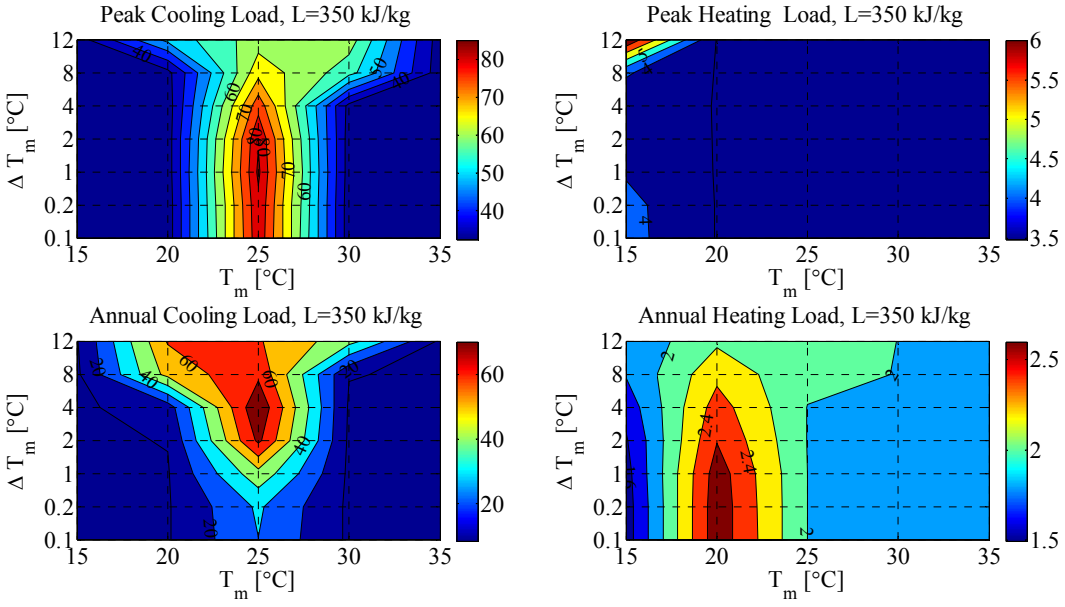

h) A contour plot for the case of 350 kg/kJ showing percentage reduction in cooling and heating loads

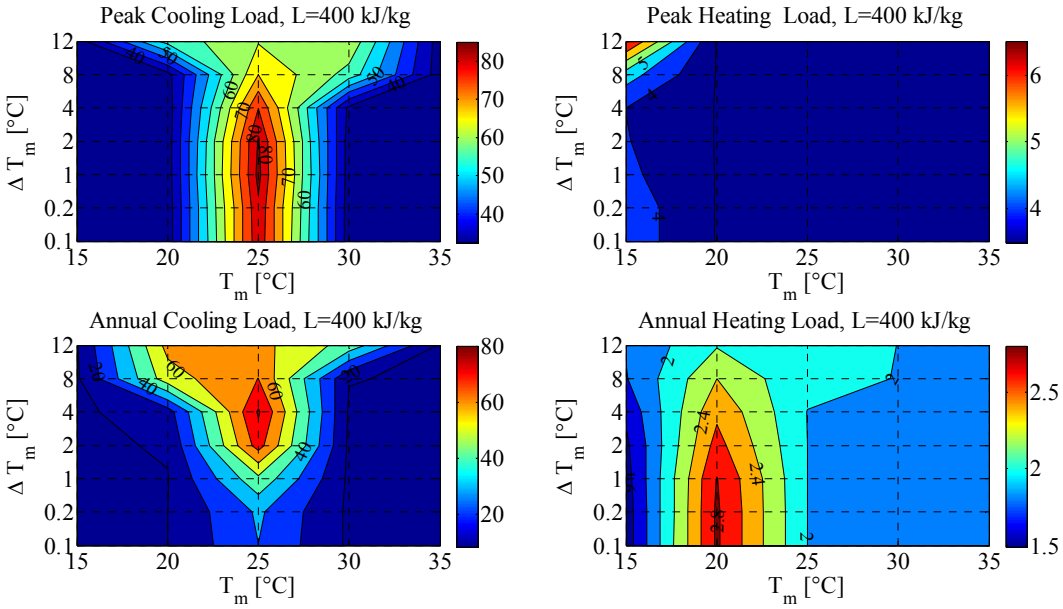

i) A contour plot for the case of 400 kg/kJ showing percentage reduction in cooling and heating loads

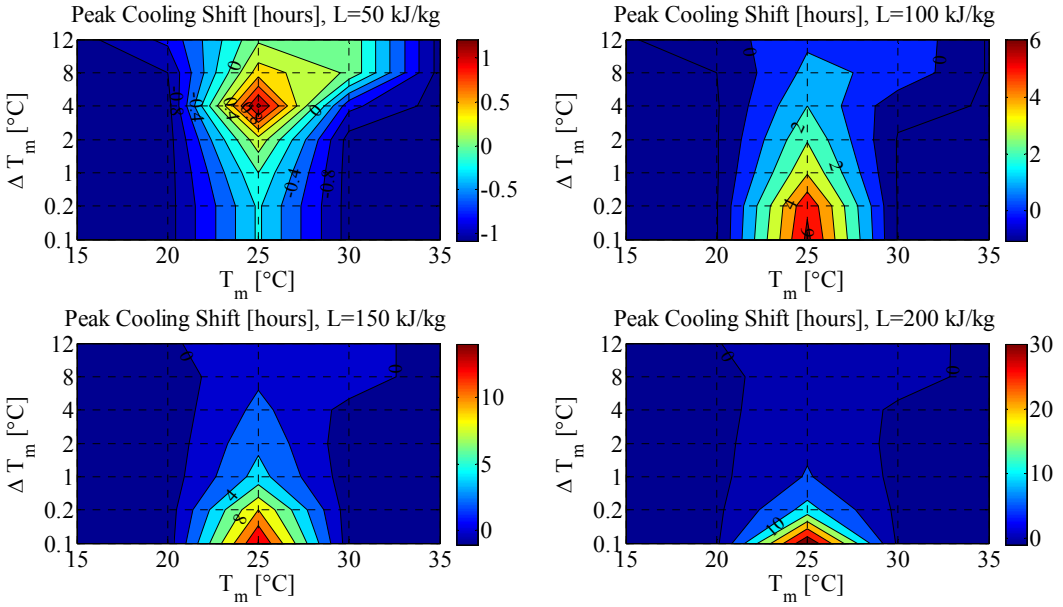

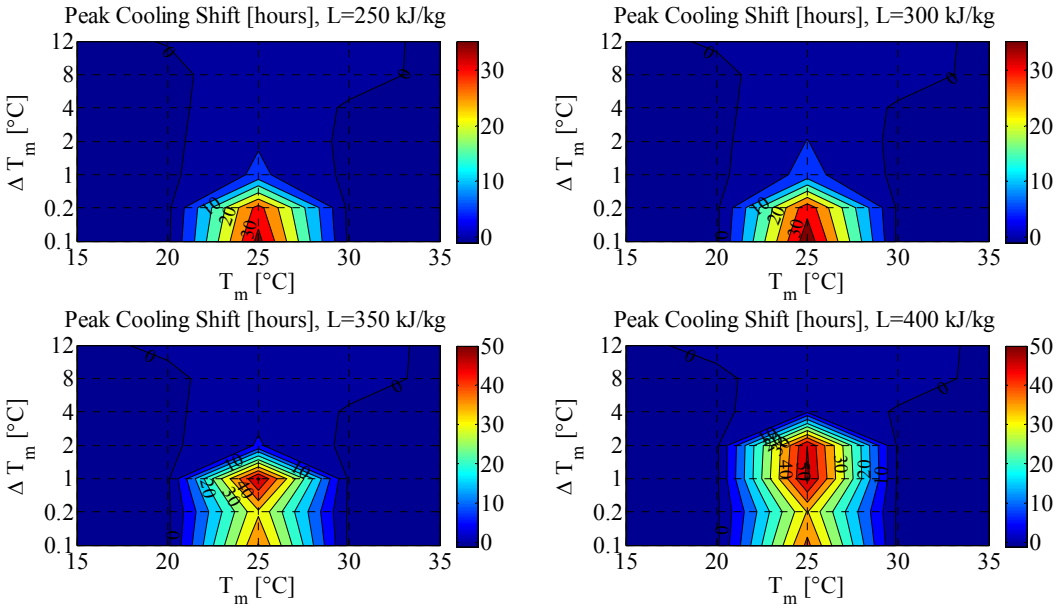

j) A contour plot for the peak cooling shift in hours

Figure A.11 Percentage reductions in cooling and heating loads for East wall when PCM in the middle, Golden, CO

Appendix A.4.3 PCM to the exterior

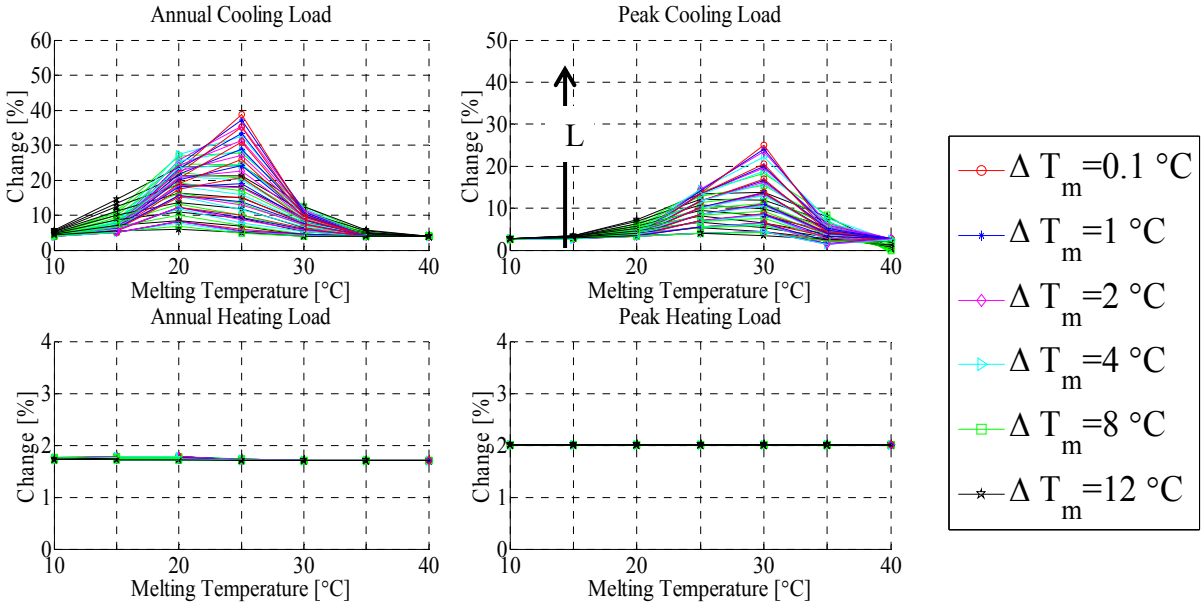

a) Percentage reductions in cooling and heating loads across all parameters

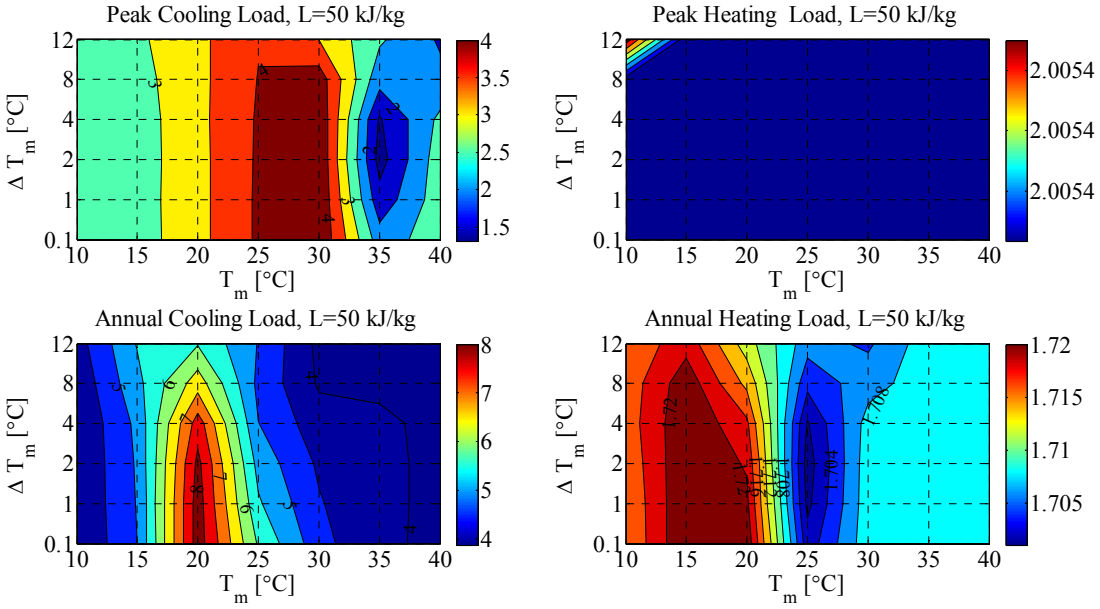

b) A contour plot for the case of 50 kg/kJ showing percentage reduction in cooling and heating loads

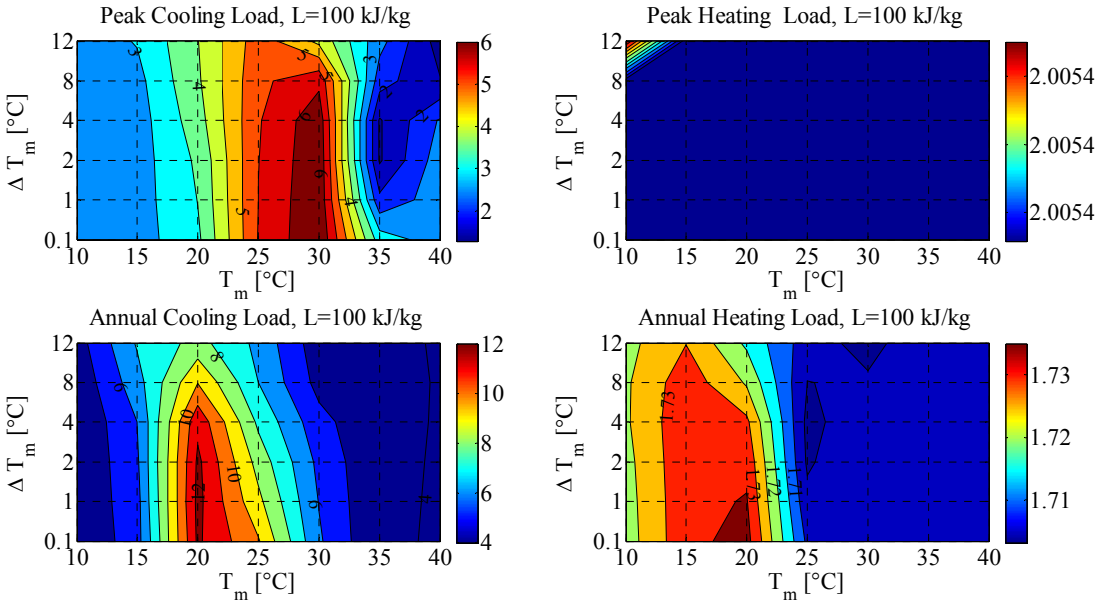

c) A contour plot for the case of 100 kg/kJ showing percentage reduction in cooling and heating loads

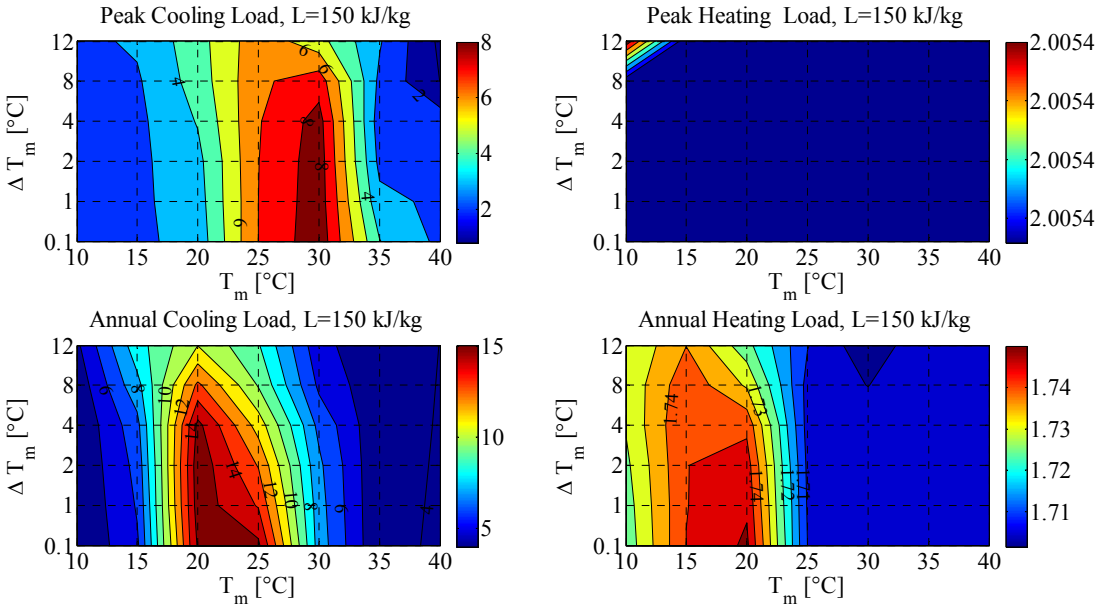

d) A contour plot for the case of 150 kg/kJ showing percentage reduction in cooling and heating loads

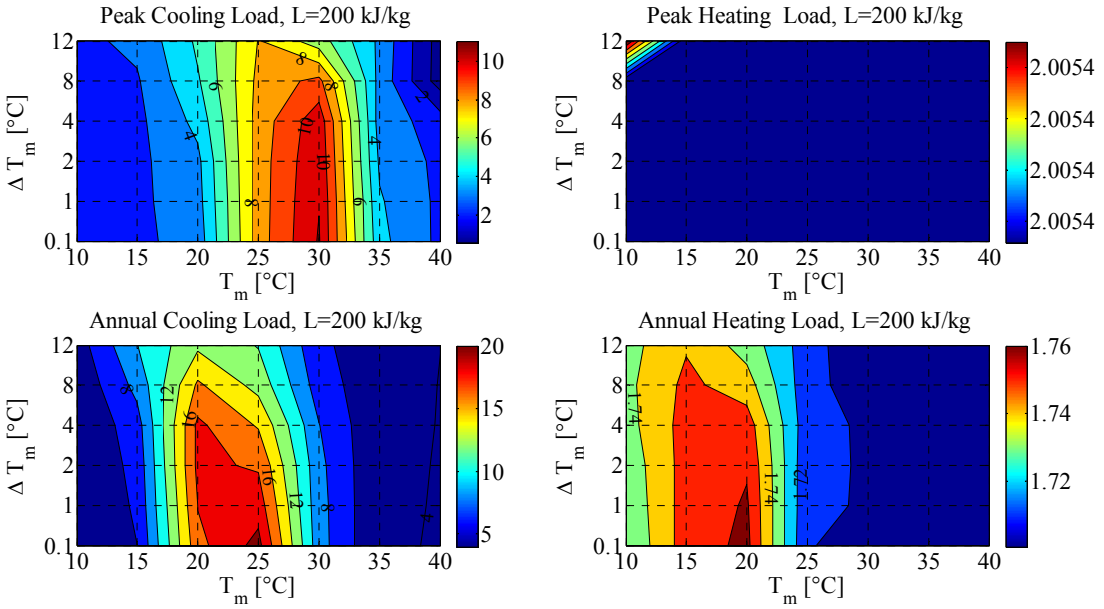

e) A contour plot for the case of 200 kg/kJ showing percentage reduction in cooling and heating loads

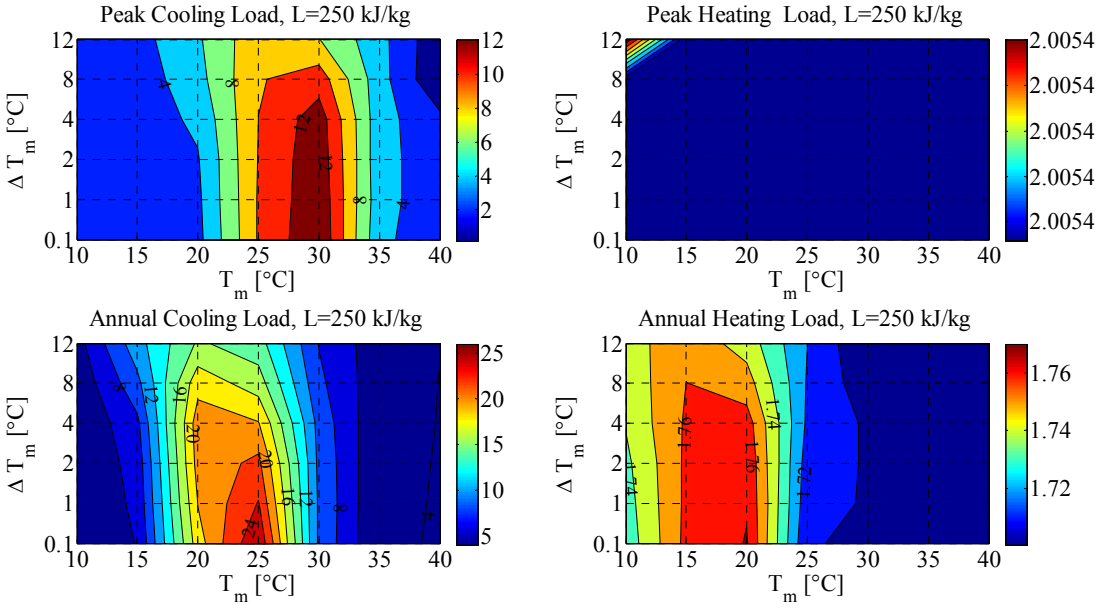

f) A contour plot for the case of 250 kg/kJ showing percentage reduction in cooling and heating loads

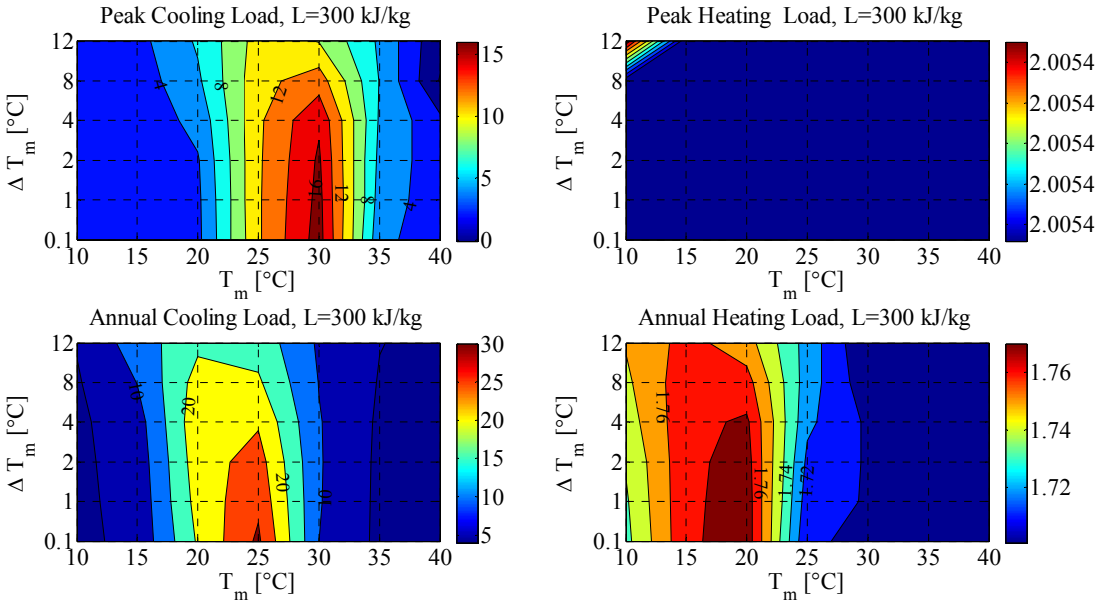

g) A contour plot for the case of 300 kg/kJ showing percentage reduction in cooling and heating loads

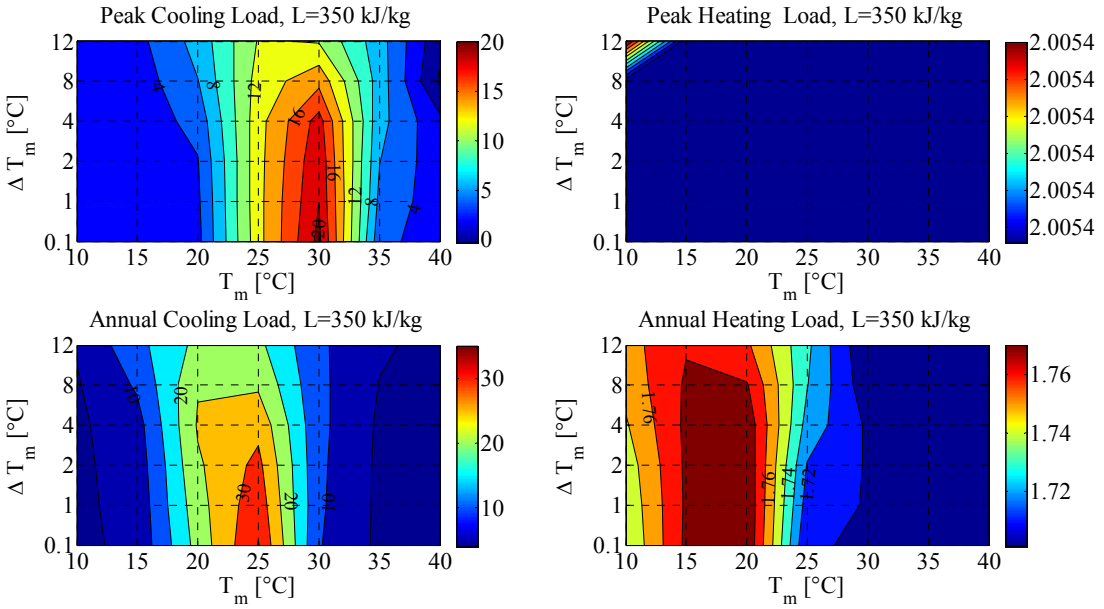

h) A contour plot for the case of 350 kg/kJ showing percentage reduction in cooling and heating loads

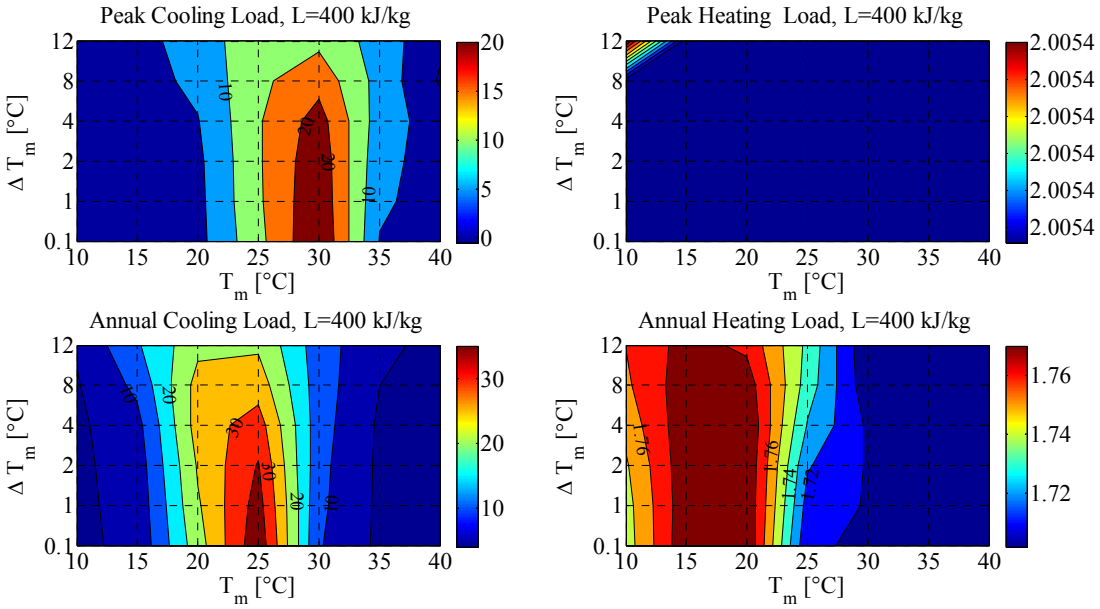

i) A contour plot for the case of 400 kg/kJ showing percentage reduction in cooling and heating loads

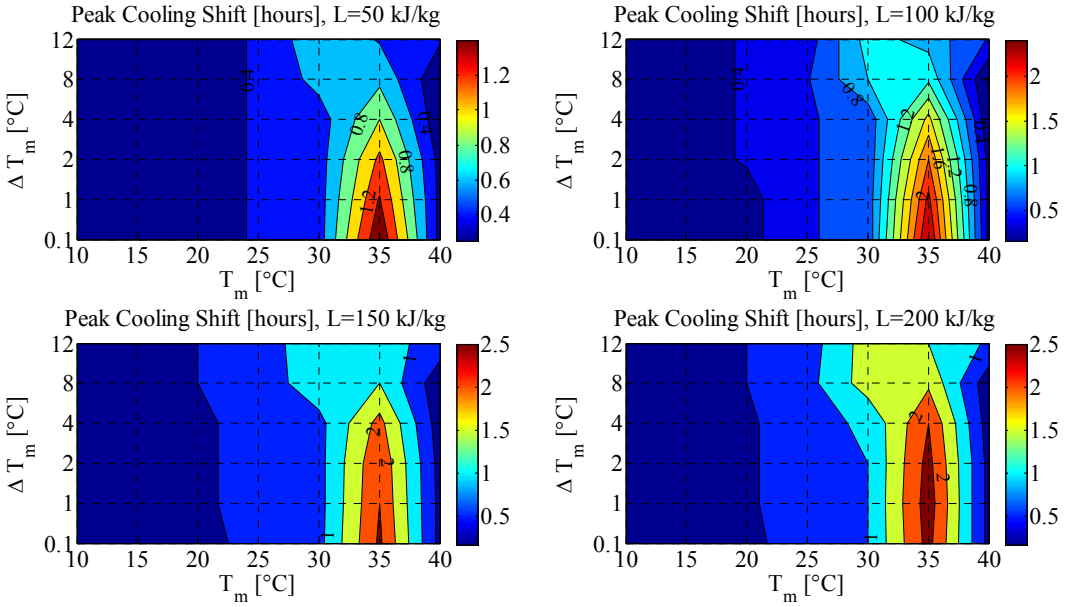

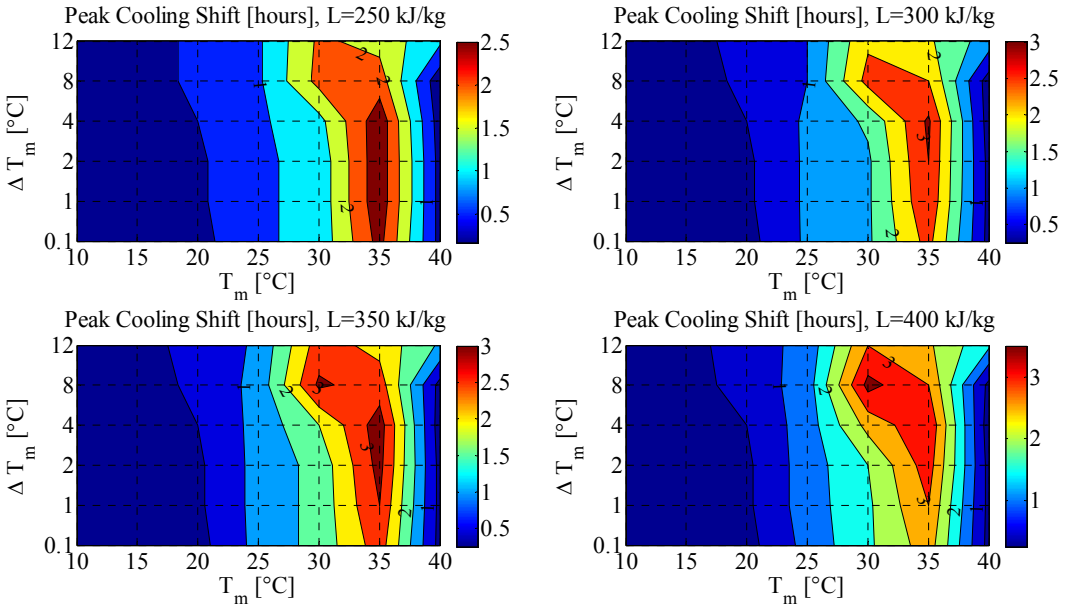

j) A contour plot for the peak cooling shift in hours

Figure A.12 Percentage reductions in cooling and heating loads for East wall when PCM to the exterior , Golden, CO

Appendix B: Contour plots for ventilated PCM-enhanced cavity walls for Golden, CO

Appendix B.1 South Wall

Appendix B.1.1 PCM to the interior

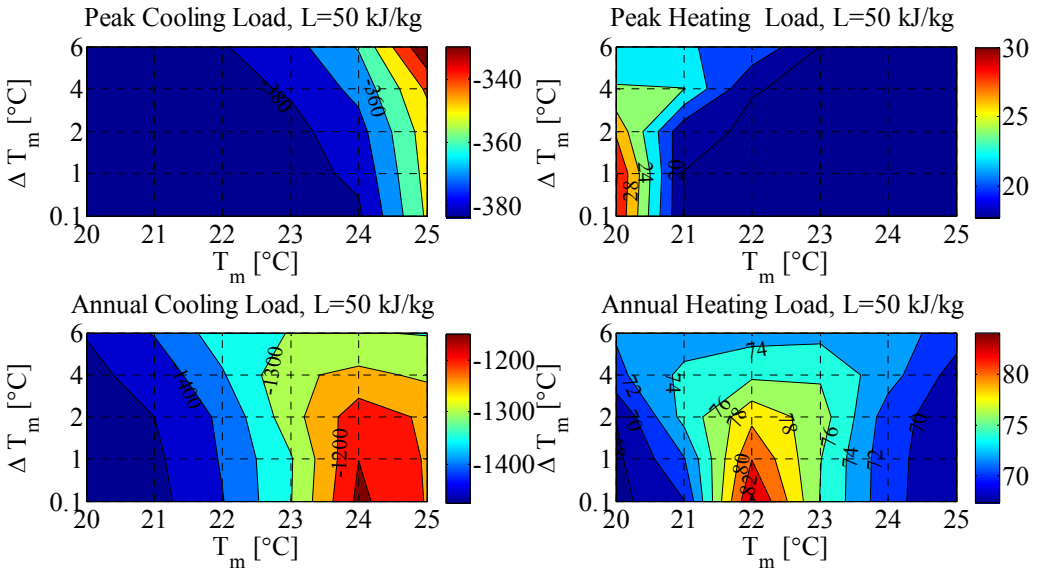

a) A contour plot for the case of 50 kg/kJ showing percentage reduction in cooling and heating loads

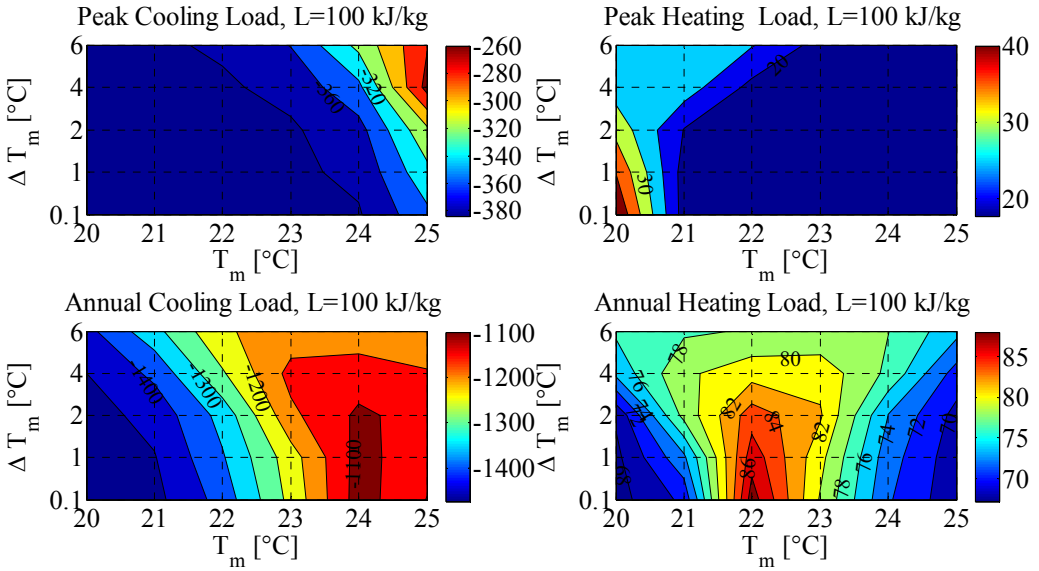

b) A contour plot for the case of 100 kg/kJ showing percentage reduction in cooling and heating loads

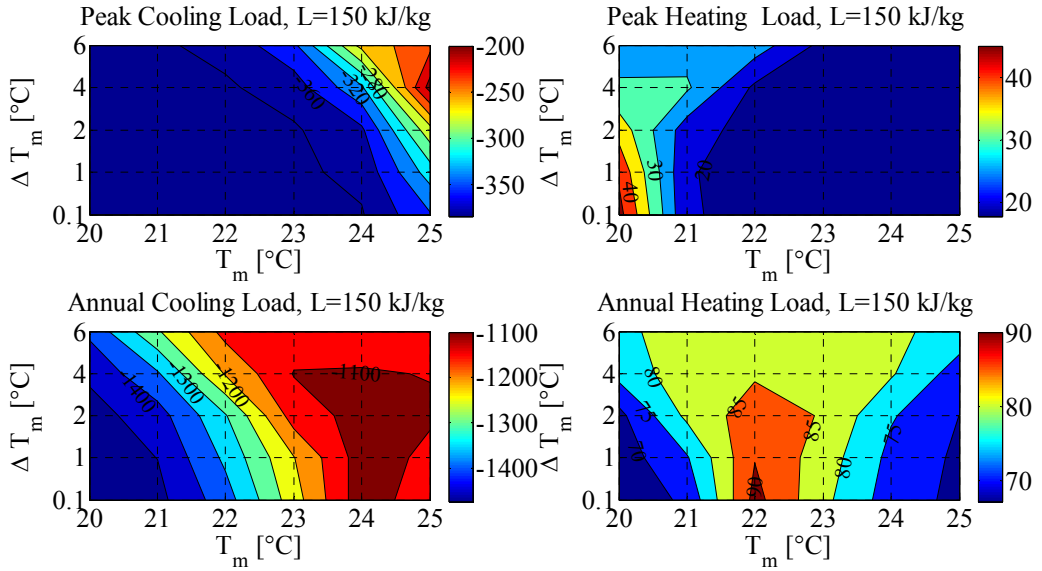

c) A contour plot for the case of 150 kg/kJ showing percentage reduction in cooling and heating loads

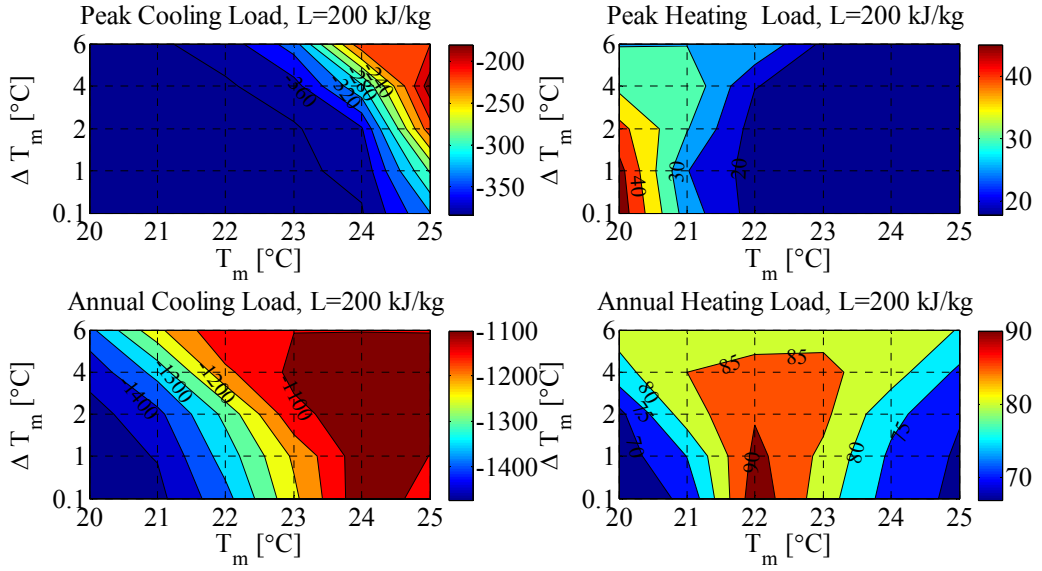

d) A contour plot for the case of 200 kg/kJ showing percentage reduction in cooling and heating loads

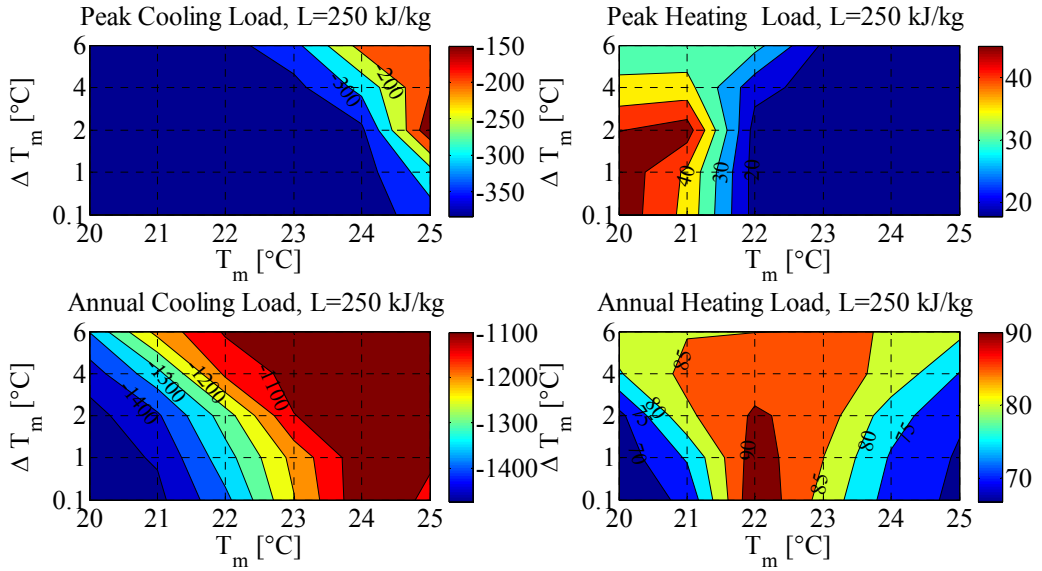

e) A contour plot for the case of 250 kg/kJ showing percentage reduction in cooling and heating loads

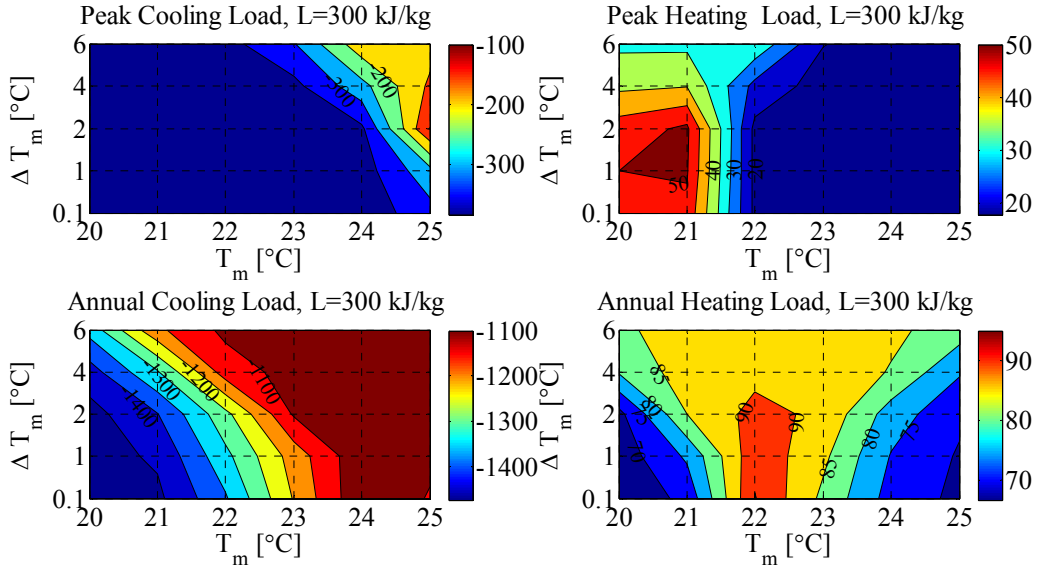

f) A contour plot for the case of 300 kg/kJ showing percentage reduction in cooling and heating loads

Figure B.1 Percentage reductions in cooling and heating loads for south cavity wall when PCM to the interior, Golden, CO

Appendix B.1.2 PCM to the exterior

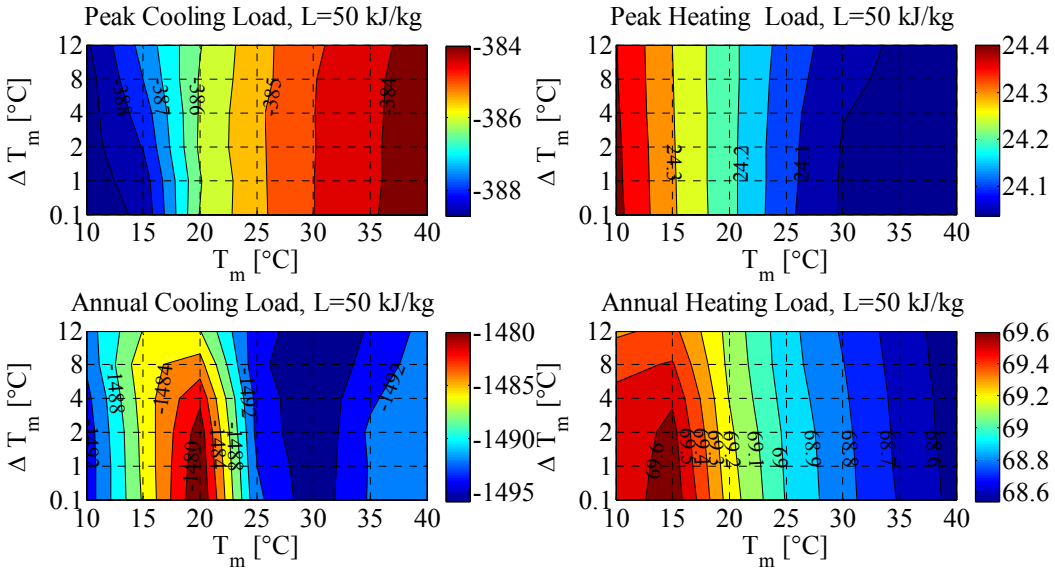

a) A contour plot for the case of 50 kg/kJ showing percentage reduction in cooling and heating loads

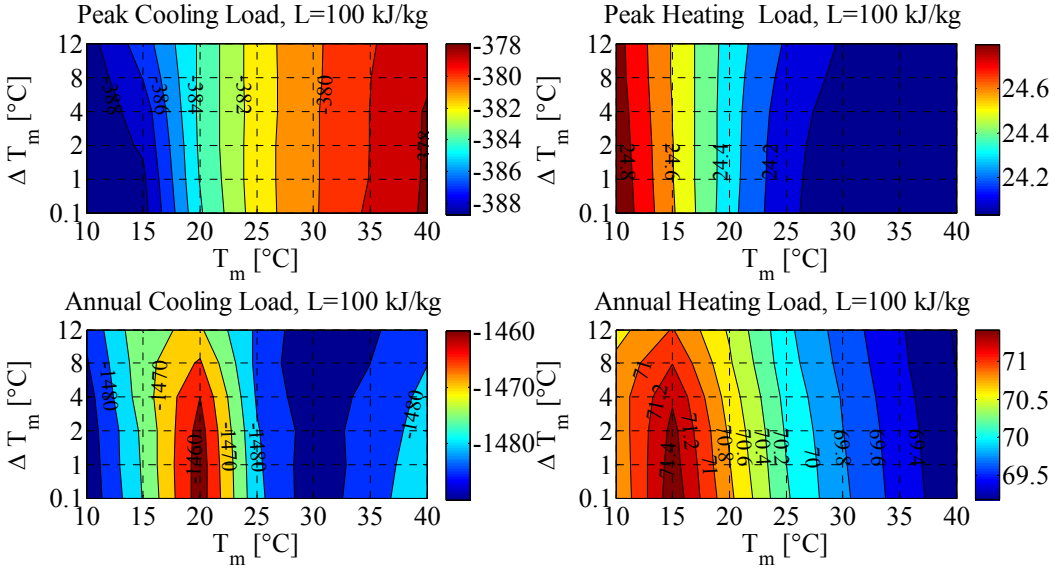

b) A contour plot for the case of 100 kg/kJ showing percentage reduction in cooling and heating loads

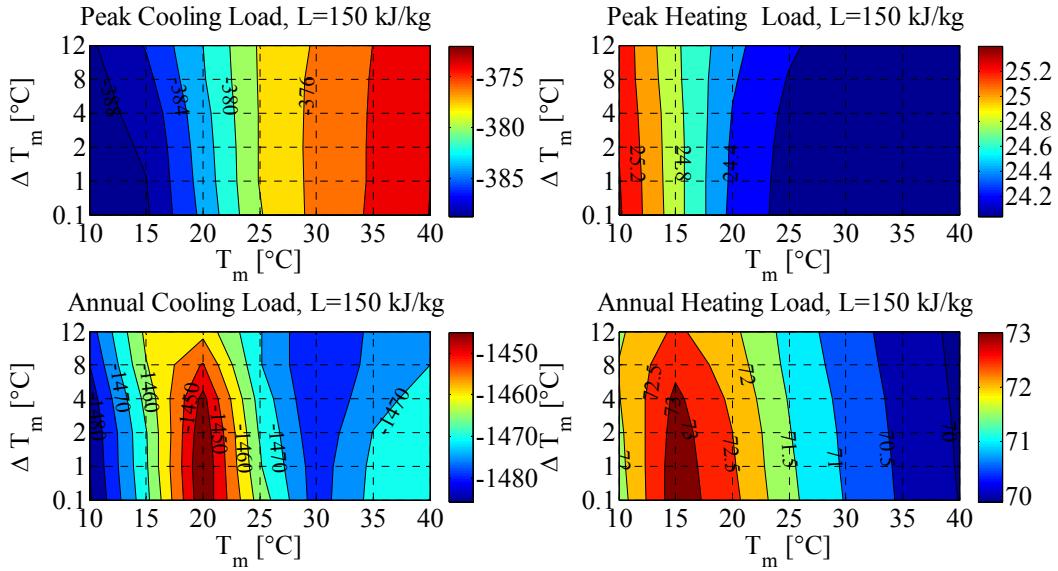

c) A contour plot for the case of 150 kg/kJ showing percentage reduction in cooling and heating loads

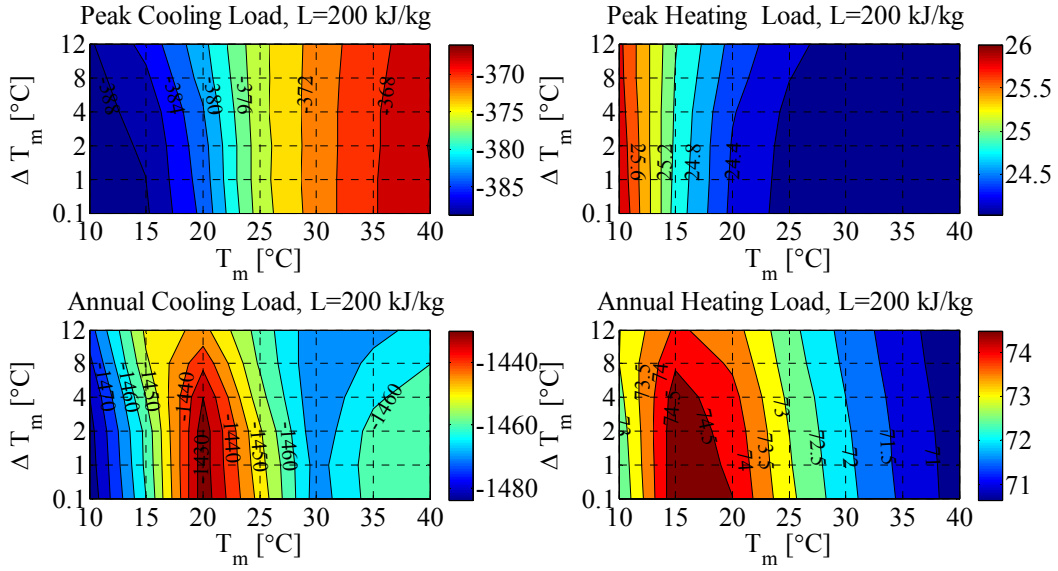

d) A contour plot for the case of 200 kg/kJ showing percentage reduction in cooling and heating loads

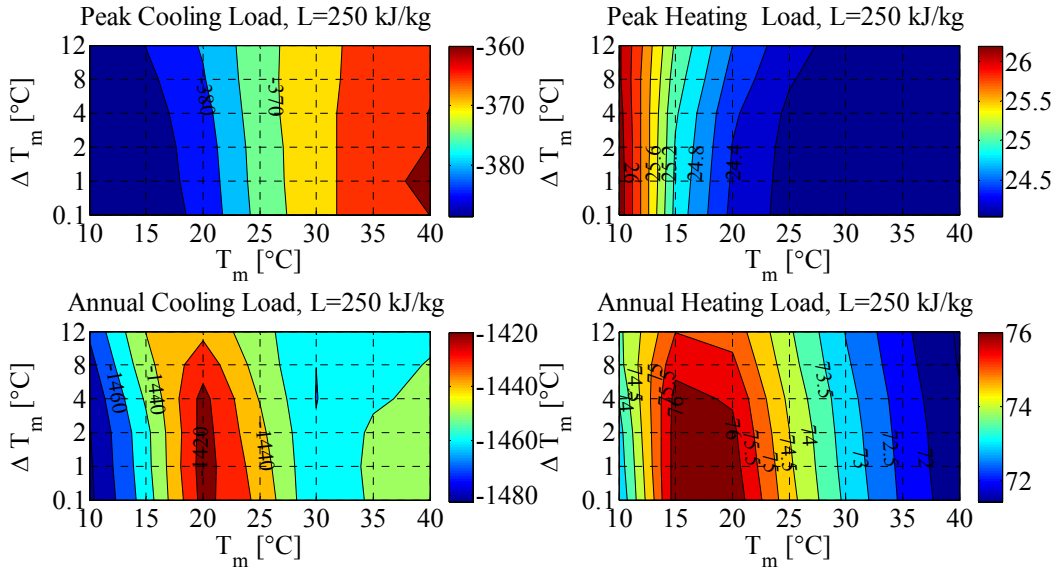

e) A contour plot for the case of 250 kg/kJ showing percentage reduction in cooling and heating loads

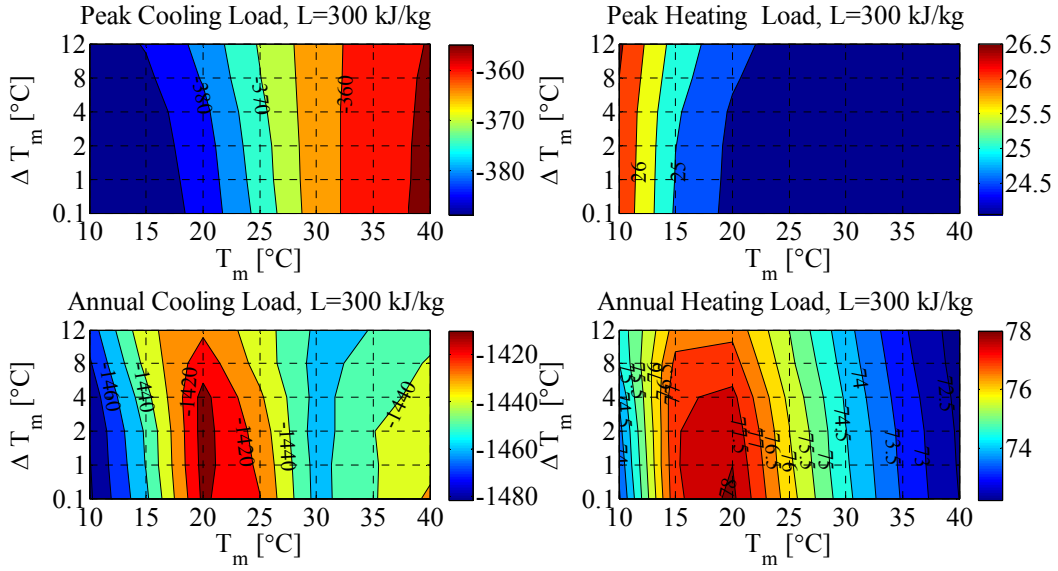

f) A contour plot for the case of 300 kg/kJ showing percentage reduction in cooling and heating loads

Figure B.2 Percentage reductions in cooling and heating loads for south cavity wall when PCM to the exterior, Golden, CO

Appendix B.2 West Wall

Appendix B.2.1 PCM to the interior

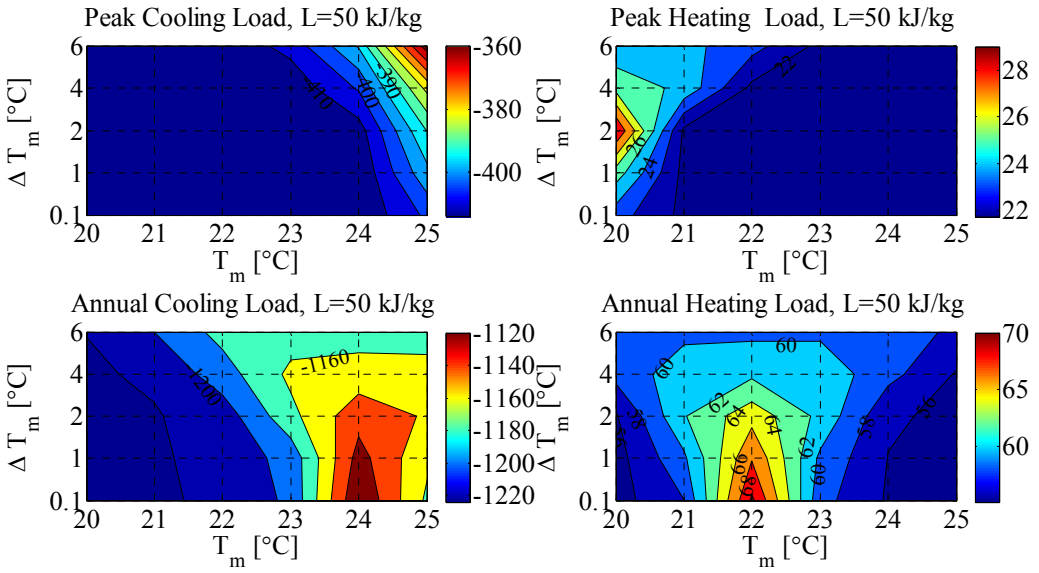

a) A contour plot for the case of 50 kg/kJ showing percentage reduction in cooling and heating loads

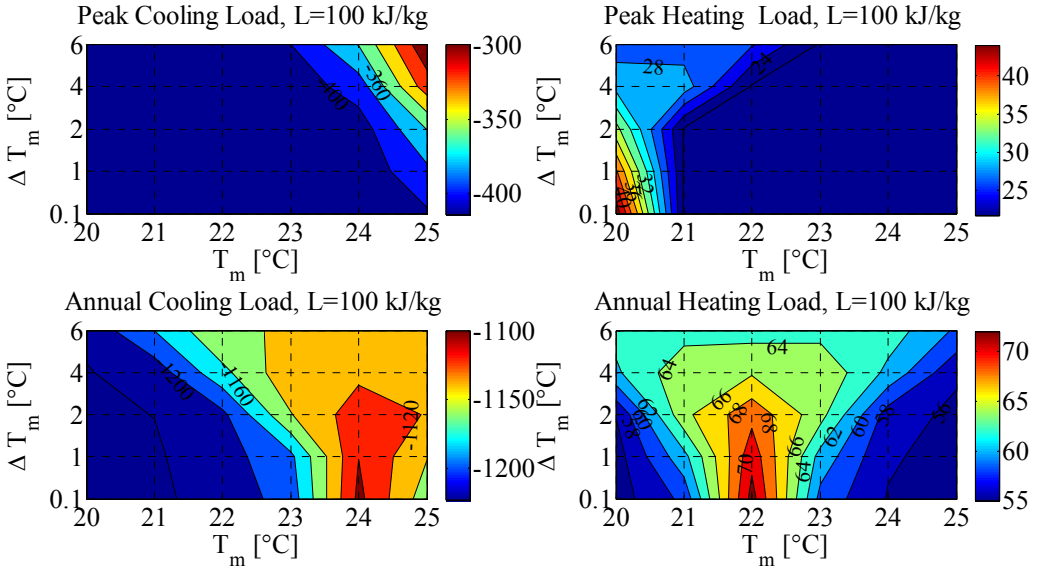

b) A contour plot for the case of 100 kg/kJ showing percentage reduction in cooling and heating loads

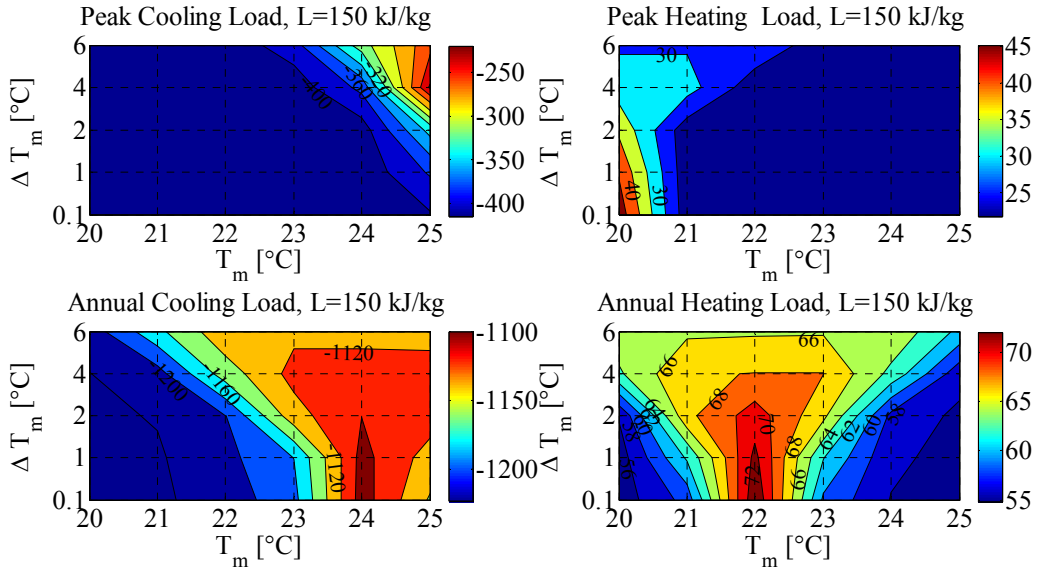

c) A contour plot for the case of 150 kg/kJ showing percentage reduction in cooling and heating loads

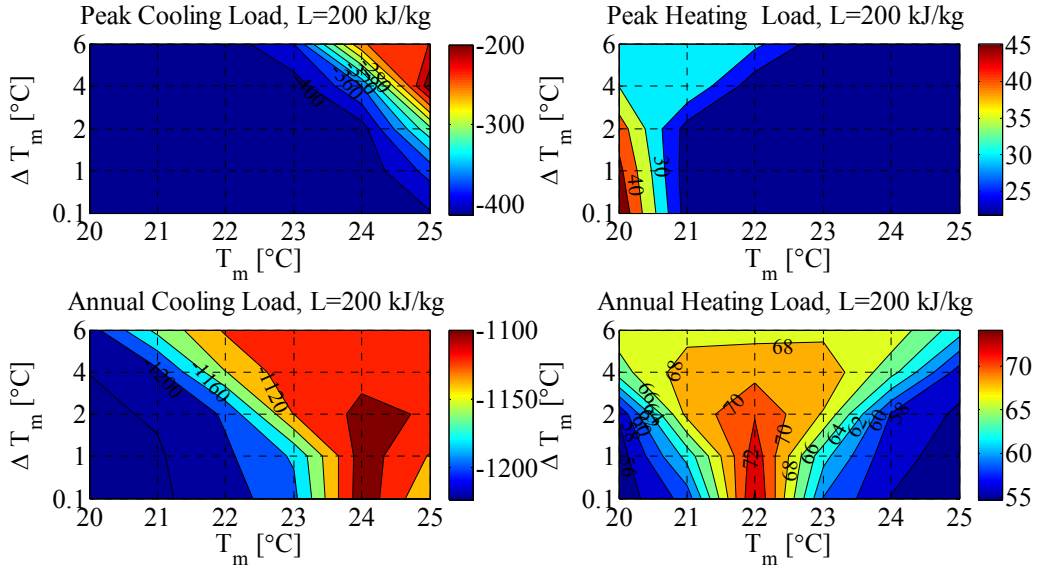

d) A contour plot for the case of 200 kg/kJ showing percentage reduction in cooling and heating loads

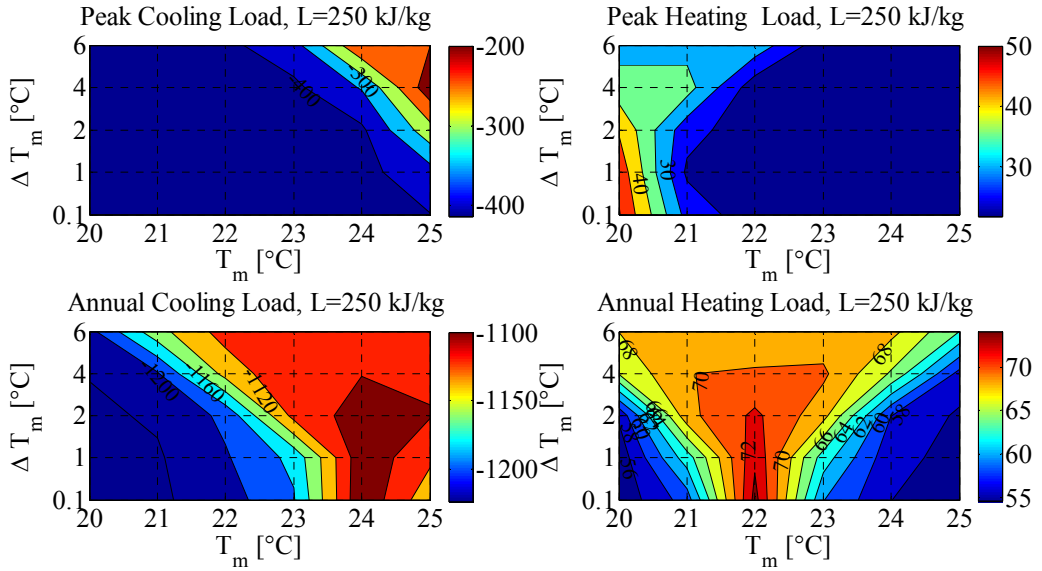

e) A contour plot for the case of 250 kg/kJ showing percentage reduction in cooling and heating loads

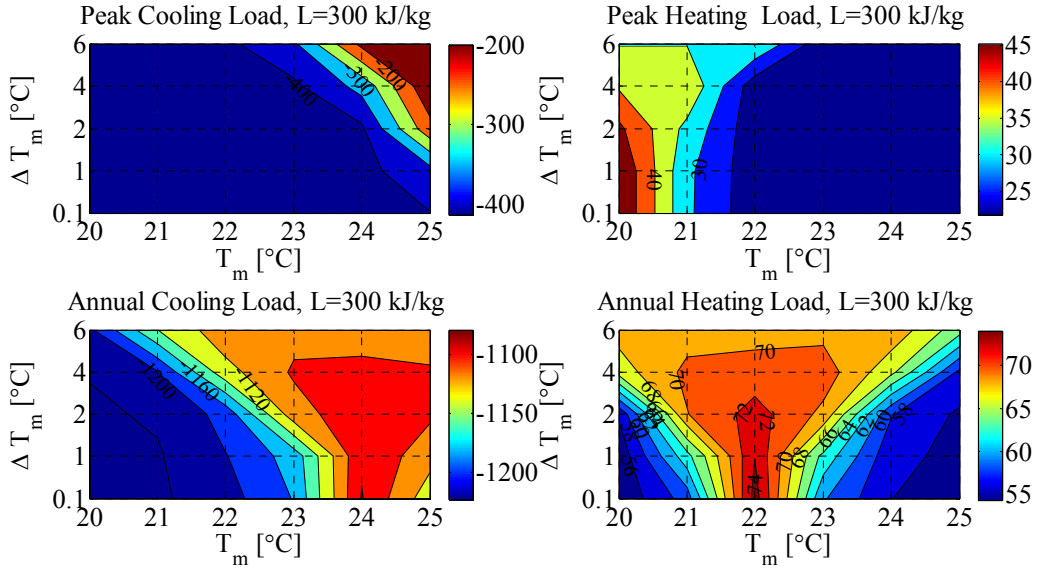

f) A contour plot for the case of 300 kg/kJ showing percentage reduction in cooling and heating loads

Figure B.3 Percentage reductions in cooling and heating loads for West cavity wall when PCM to the interior, Golden, CO

Appendix B.2.2 PCM to the exterior

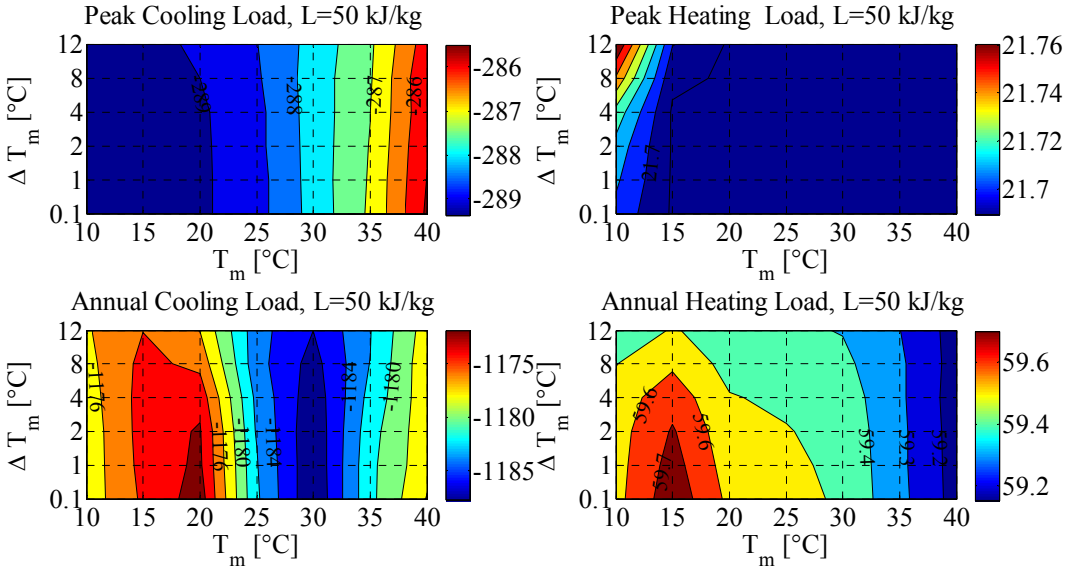

a) A contour plot for the case of 50 kg/kJ showing percentage reduction in cooling and heating loads

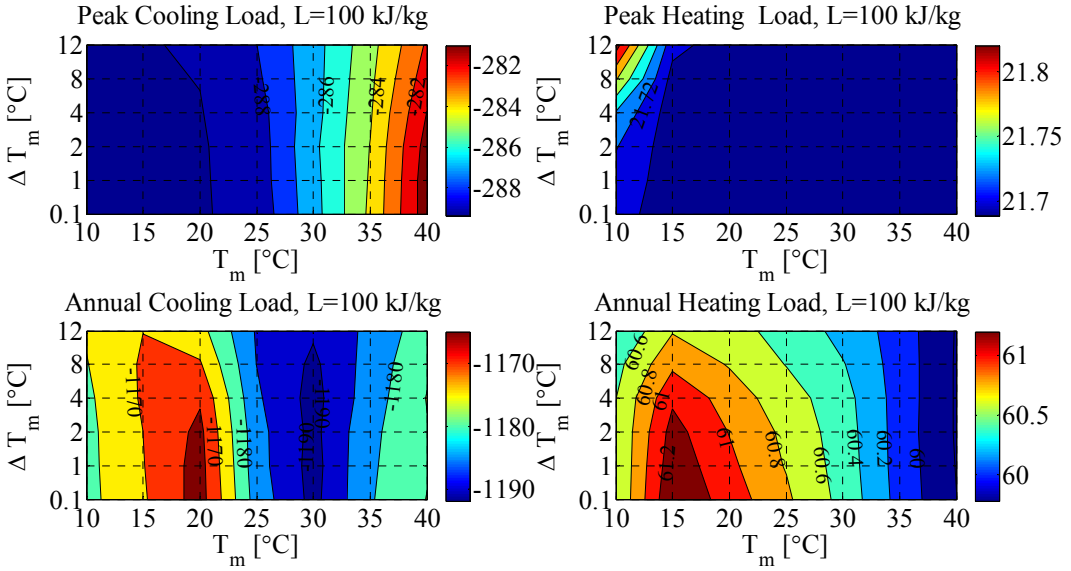

b) A contour plot for the case of 100 kg/kJ showing percentage reduction in cooling and heating loads

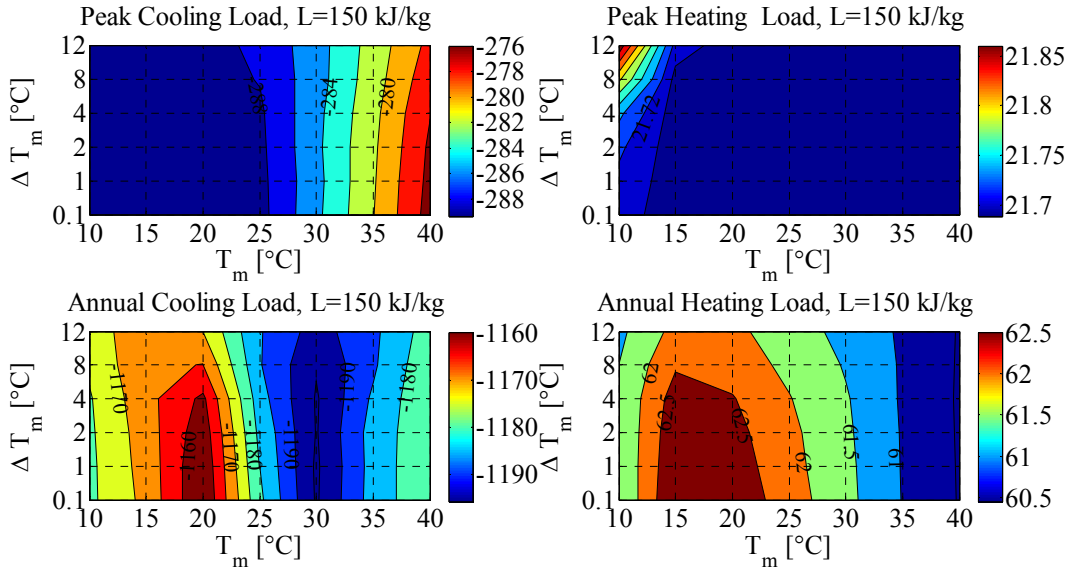

c) A contour plot for the case of 150 kg/kJ showing percentage reduction in cooling and heating loads

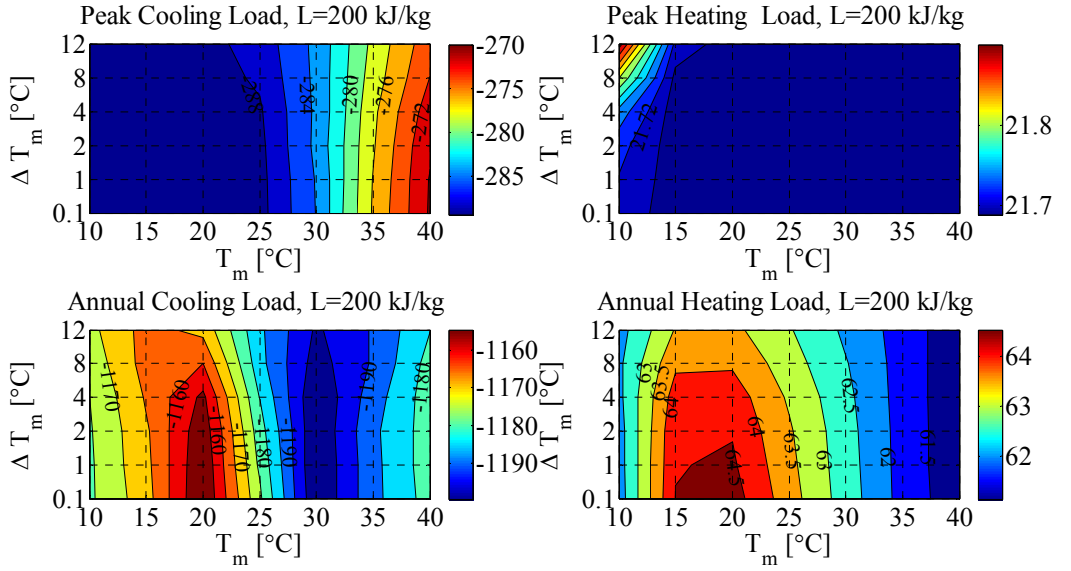

d) A contour plot for the case of 200 kg/kJ showing percentage reduction in cooling and heating loads

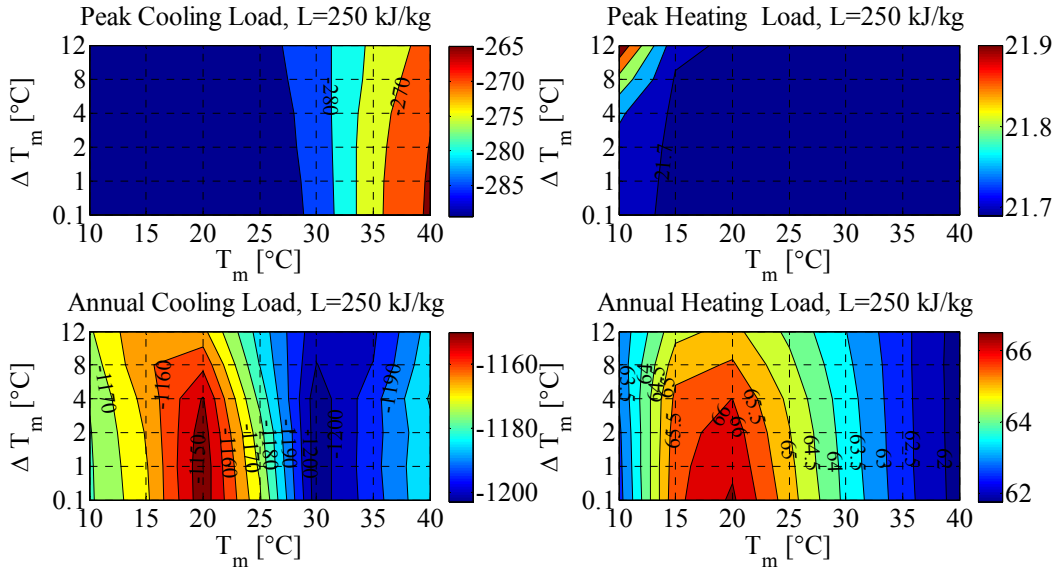

e) A contour plot for the case of 250 kg/kJ showing percentage reduction in cooling and heating loads

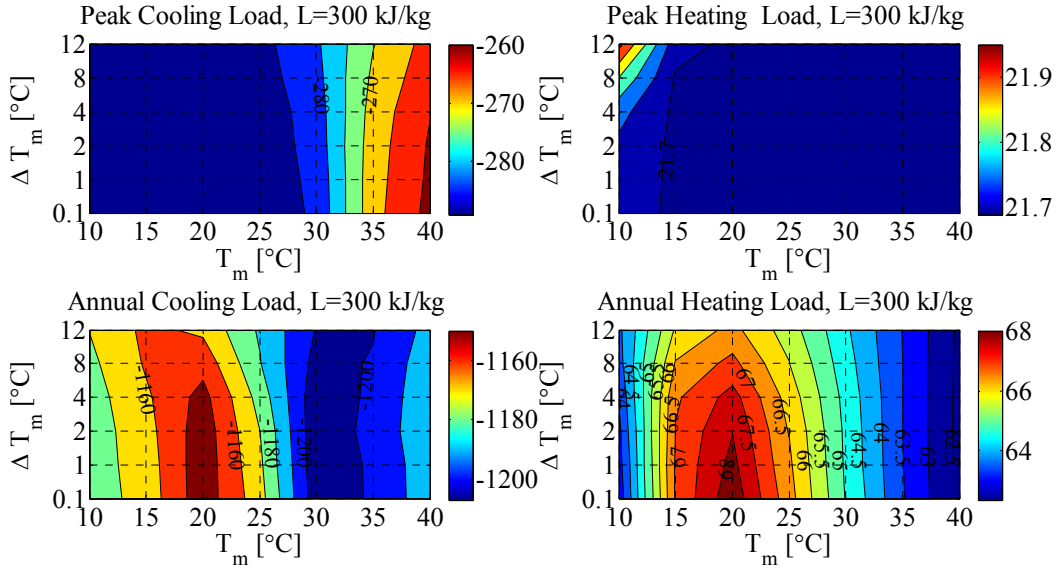

f) A contour plot for the case of 300 kg/kJ showing percentage reduction in cooling and heating loads

Figure B.4 Percentage reductions in cooling and heating loads for West cavity wall when PCM to the exterior, Golden, CO

Appendix B.3 North Wall

Appendix B.3.1 PCM to the interior

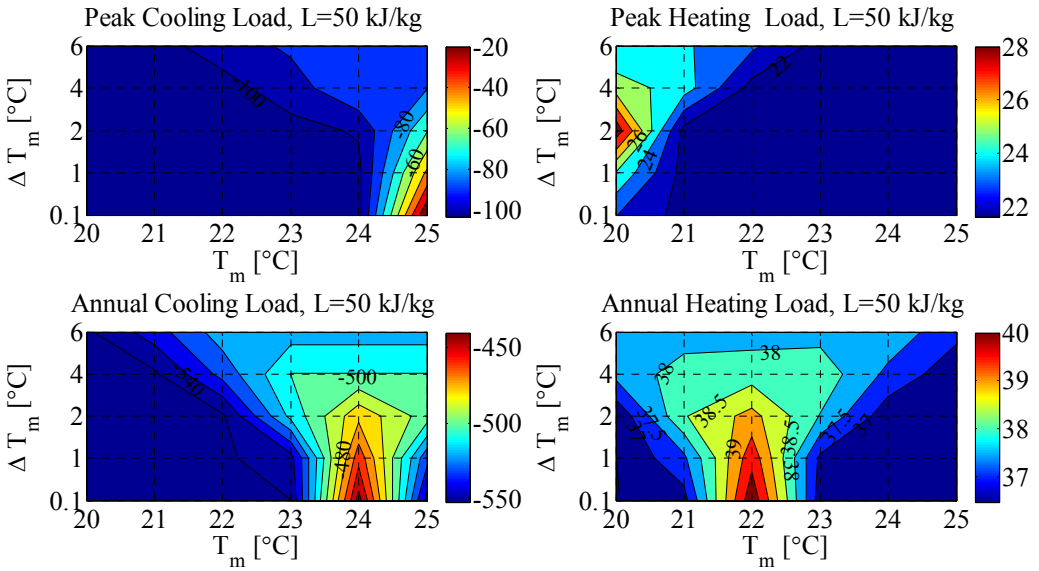

a) A contour plot for the case of 50 kg/kJ showing percentage reduction in cooling and heating loads

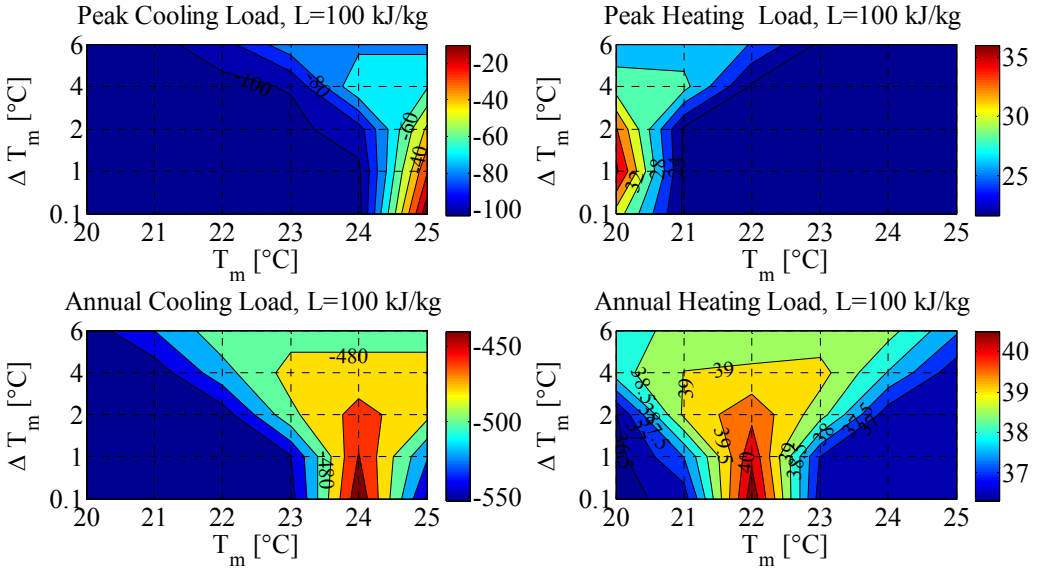

b) A contour plot for the case of 100 kg/kJ showing percentage reduction in cooling and heating loads

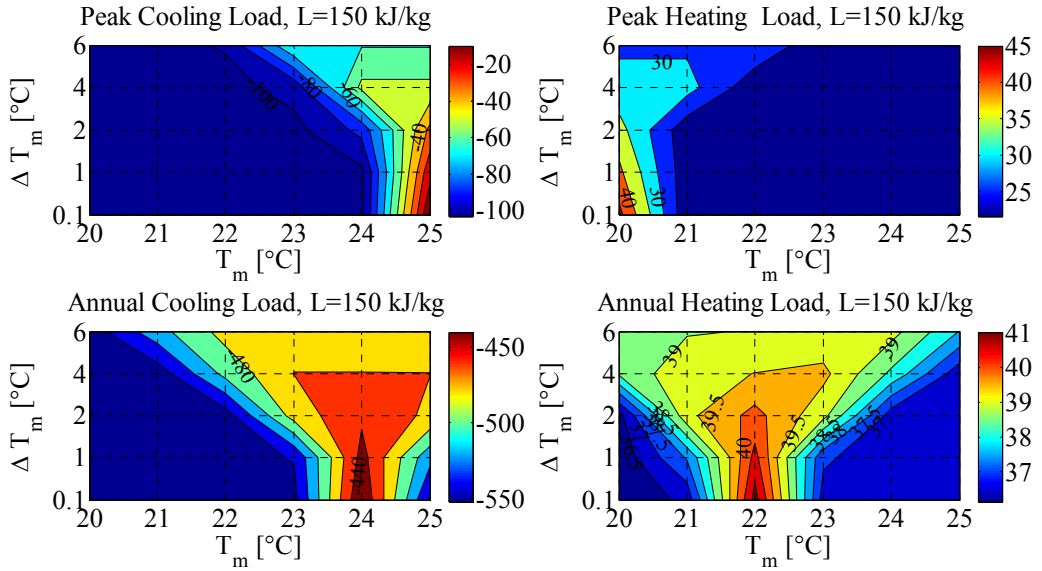

c) A contour plot for the case of 150 kg/kJ showing percentage reduction in cooling and heating loads

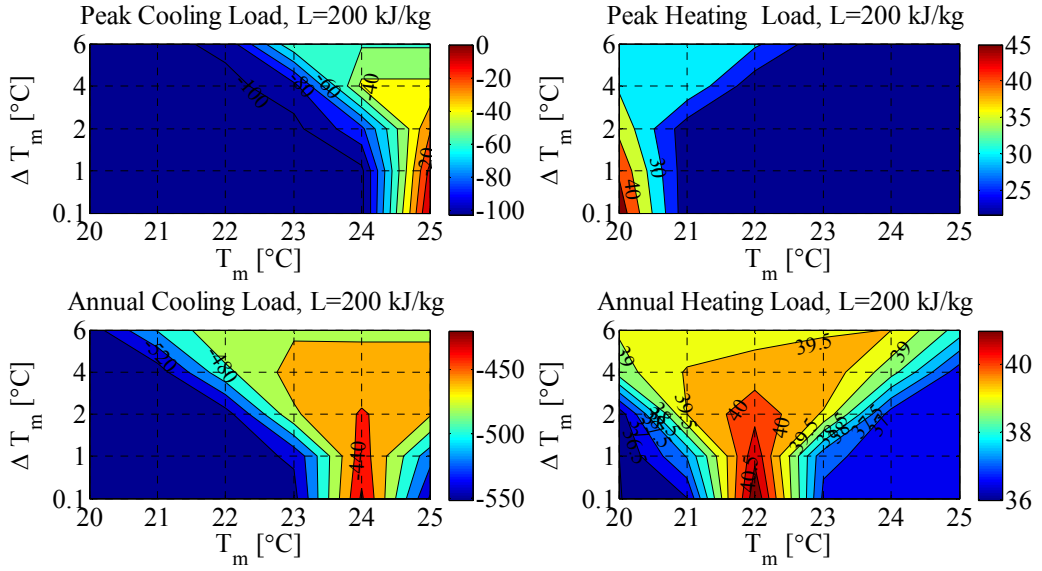

d) A contour plot for the case of 200 kg/kJ showing percentage reduction in cooling and heating loads

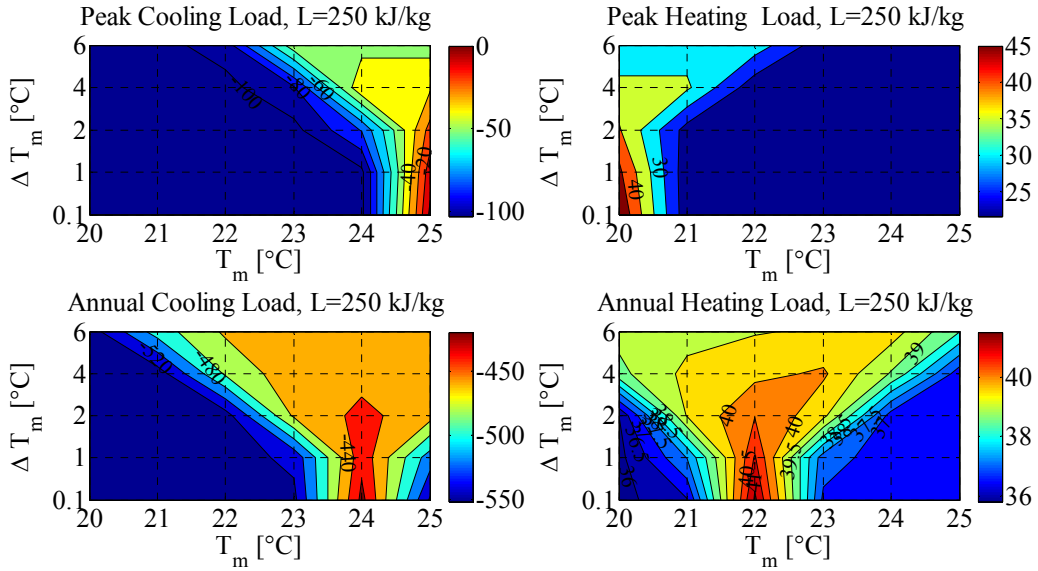

e) A contour plot for the case of 250 kg/kJ showing percentage reduction in cooling and heating loads

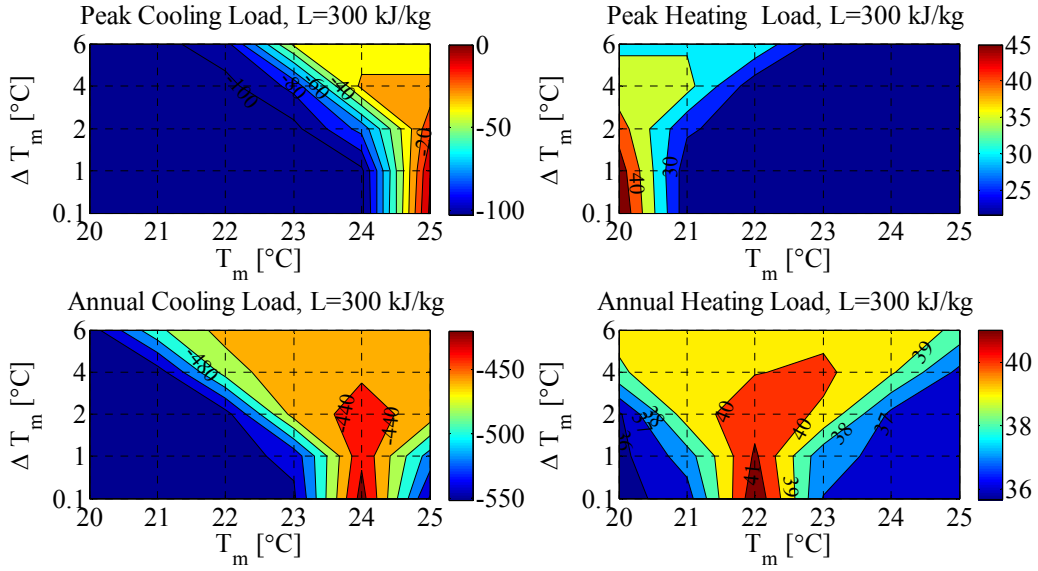

f) A contour plot for the case of 300 kg/kJ showing percentage reduction in cooling and heating loads

Figure B.5 Percentage reductions in cooling and heating loads for North cavity wall when PCM to the interior, Golden, CO

Appendix B.3.2 PCM to the exterior

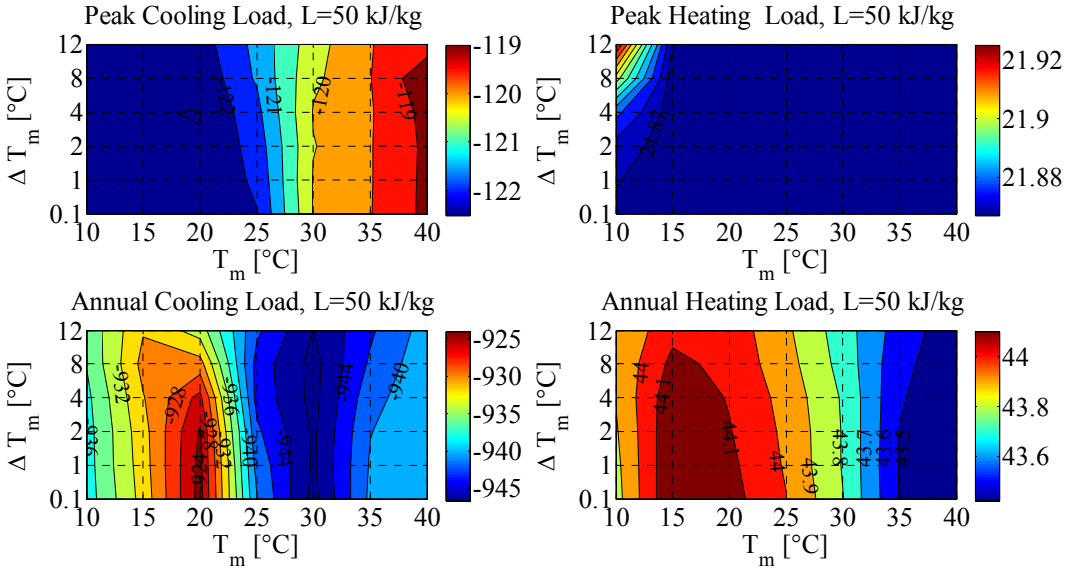

a) A contour plot for the case of 50 kg/kJ showing percentage reduction in cooling and heating loads

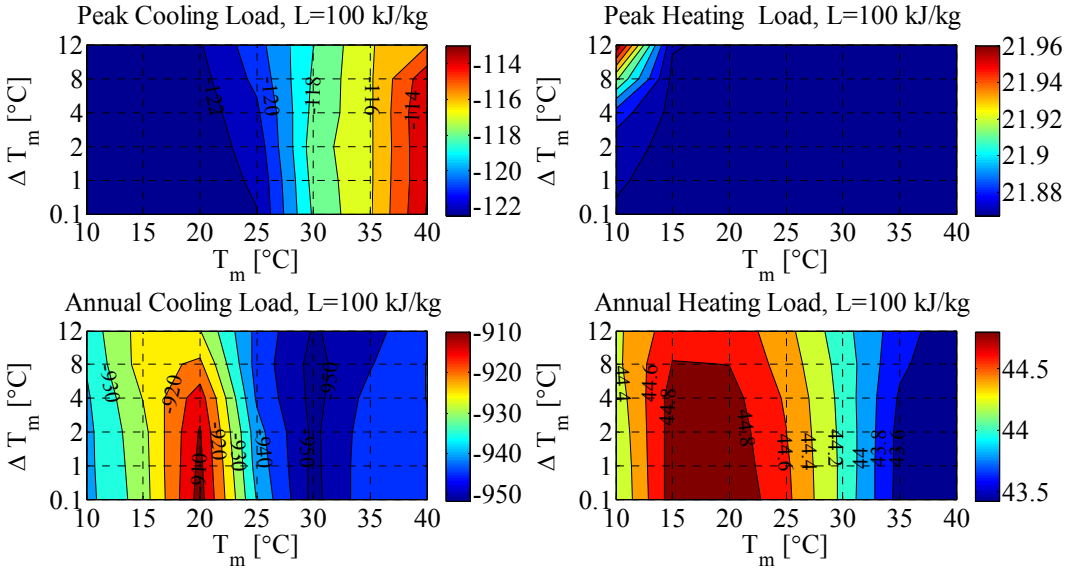

b) A contour plot for the case of 100 kg/kJ showing percentage reduction in cooling and heating loads

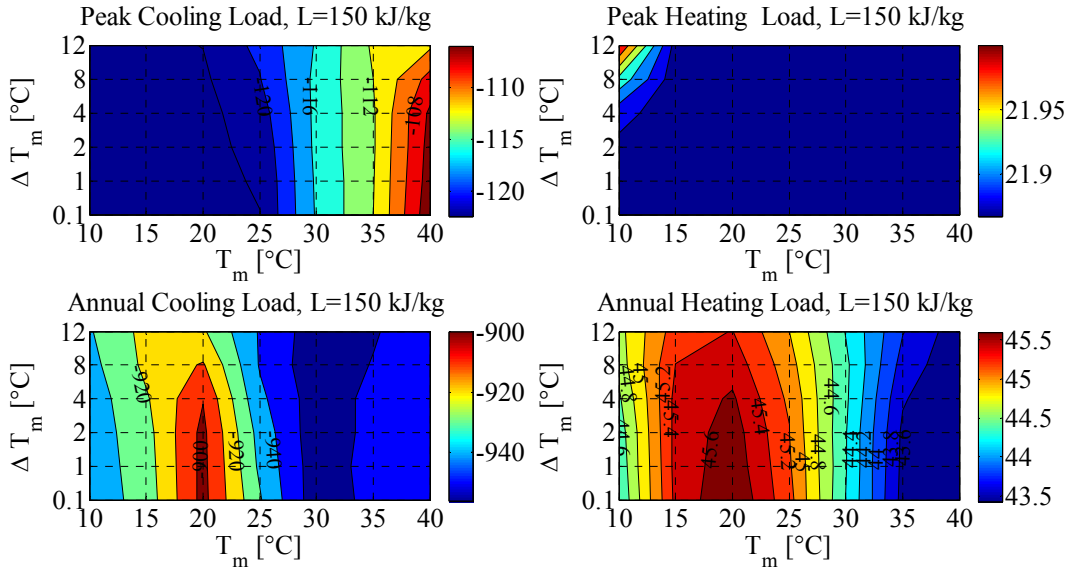

c) A contour plot for the case of 150 kg/kJ showing percentage reduction in cooling and heating loads

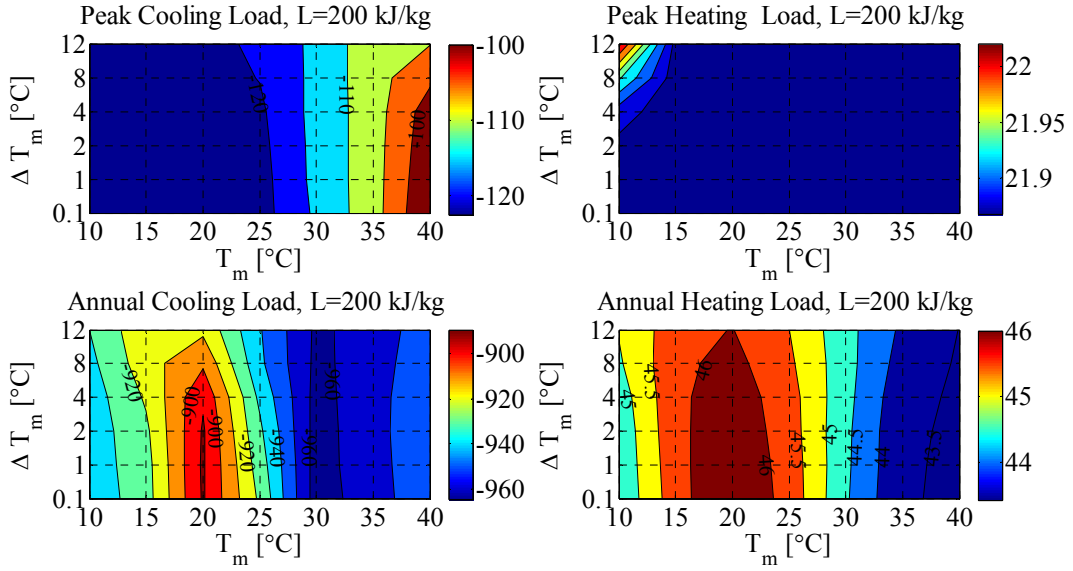

d) A contour plot for the case of 200 kg/kJ showing percentage reduction in cooling and heating loads

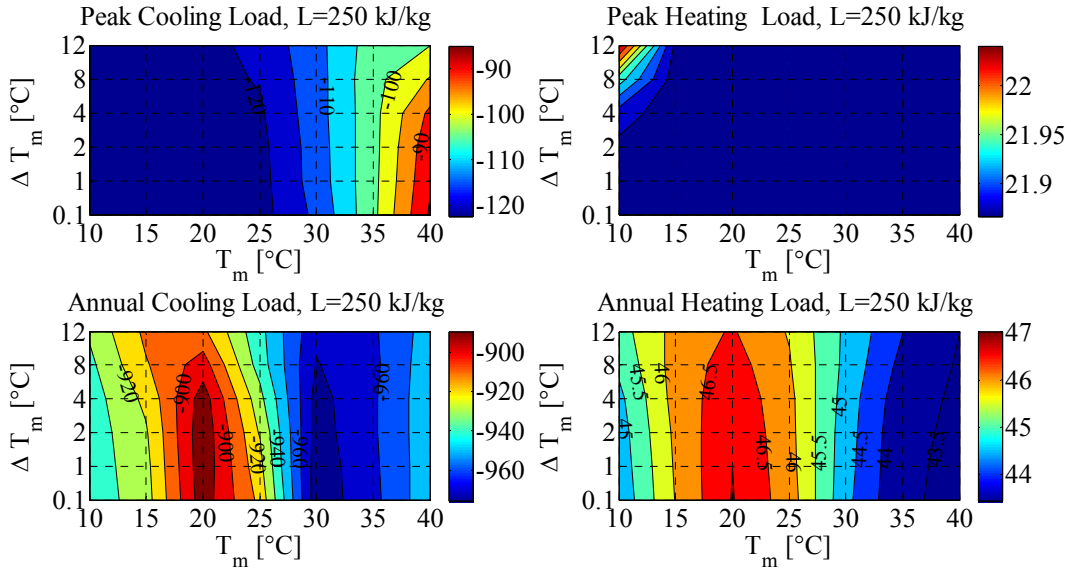

e) A contour plot for the case of 250 kg/kJ showing percentage reduction in cooling and heating loads

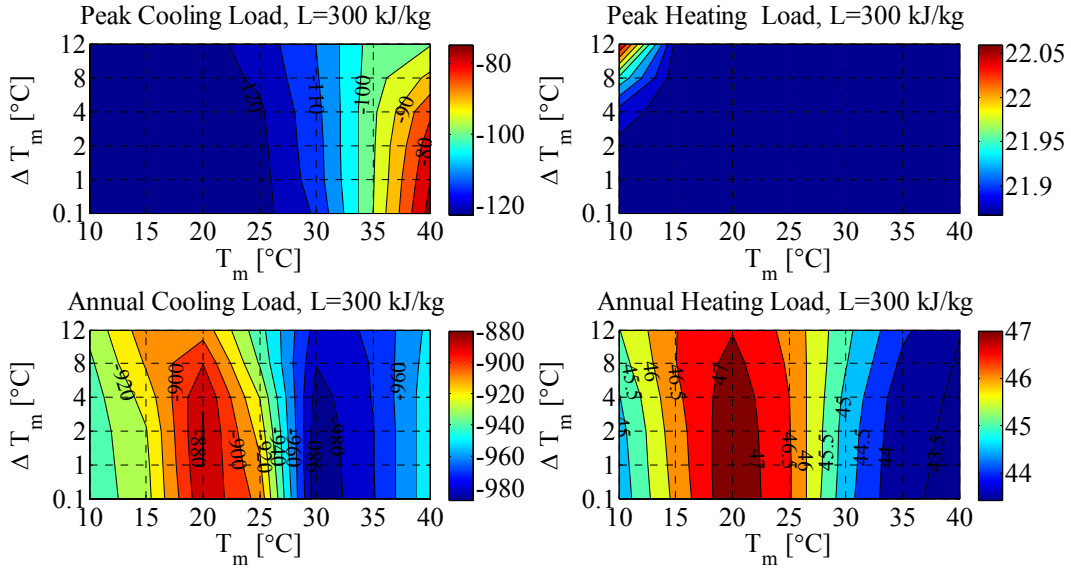

f) A contour plot for the case of 300 kg/kJ showing percentage reduction in cooling and heating loads

Figure B.6 Percentage reductions in cooling and heating loads for North cavity wall when PCM to the exterior, Golden, CO

Appendix B.4 East Wall

Appendix B.4.1 PCM to the interior

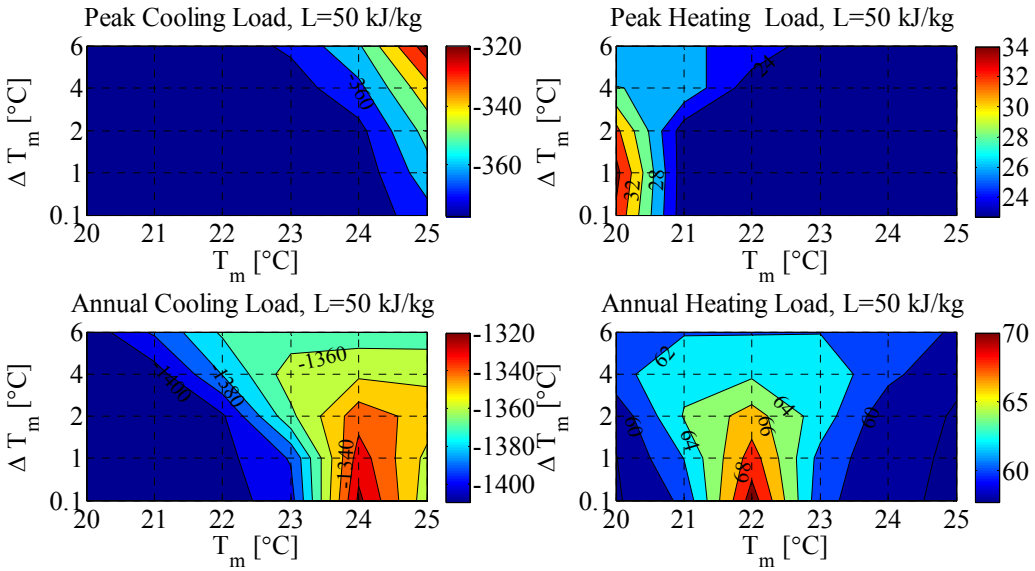

a) A contour plot for the case of 50 kg/kJ showing percentage reduction in cooling and heating loads

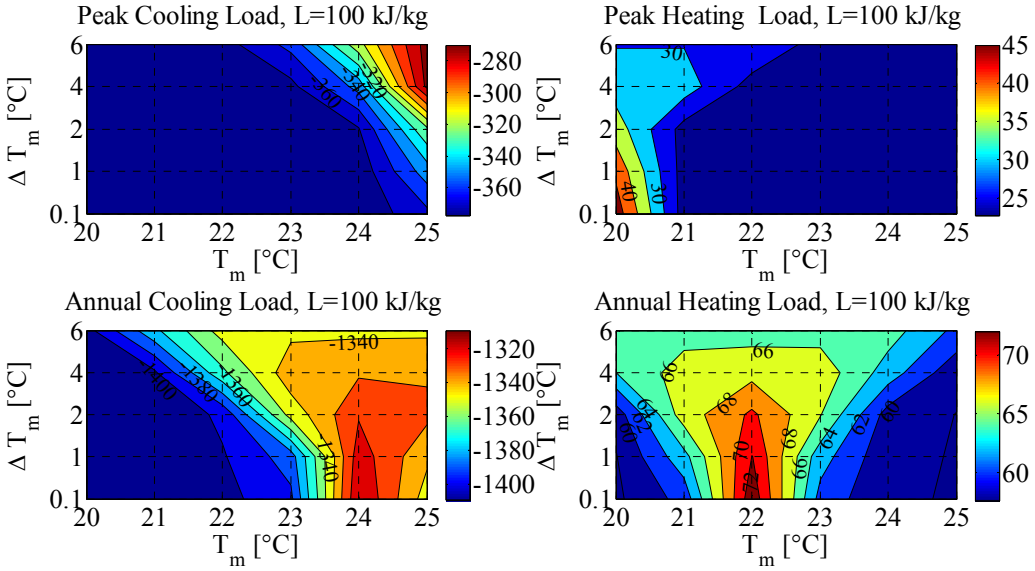

b) A contour plot for the case of 100 kg/kJ showing percentage reduction in cooling and heating loads

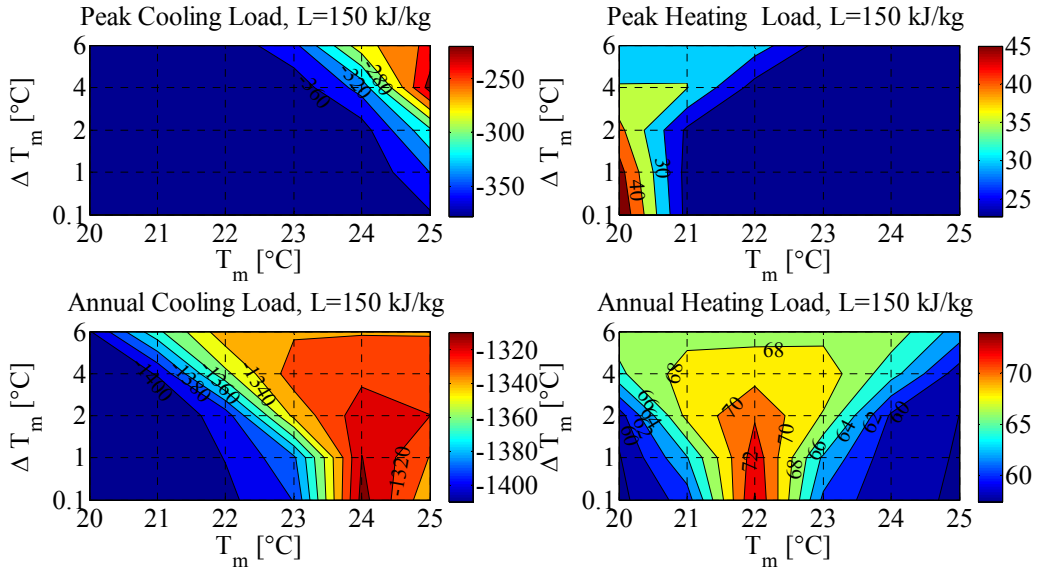

c) A contour plot for the case of 150 kg/kJ showing percentage reduction in cooling and heating loads

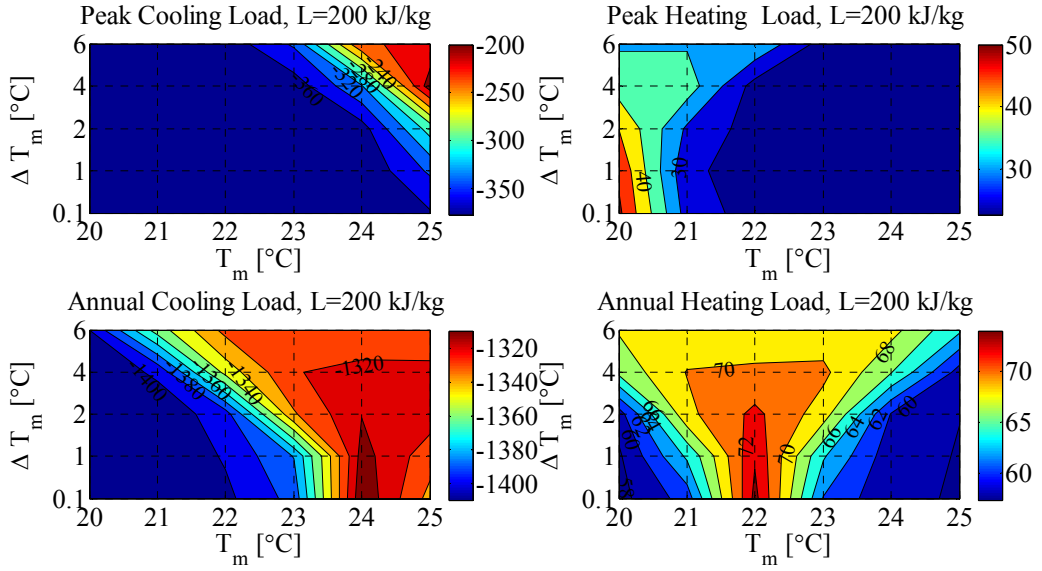

d) A contour plot for the case of 200 kg/kJ showing percentage reduction in cooling and heating loads

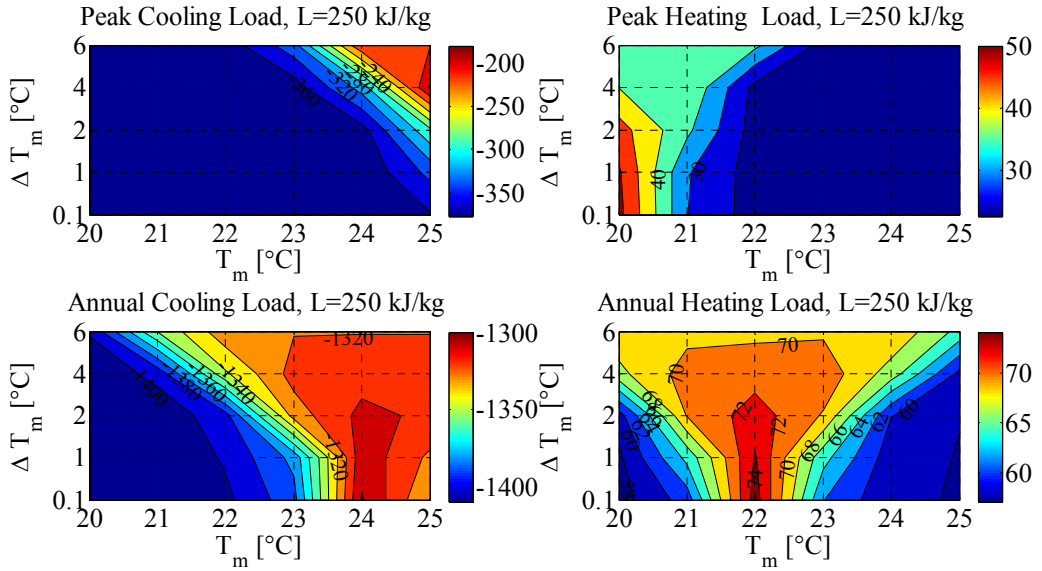

e) A contour plot for the case of 250 kg/kJ showing percentage reduction in cooling and heating loads

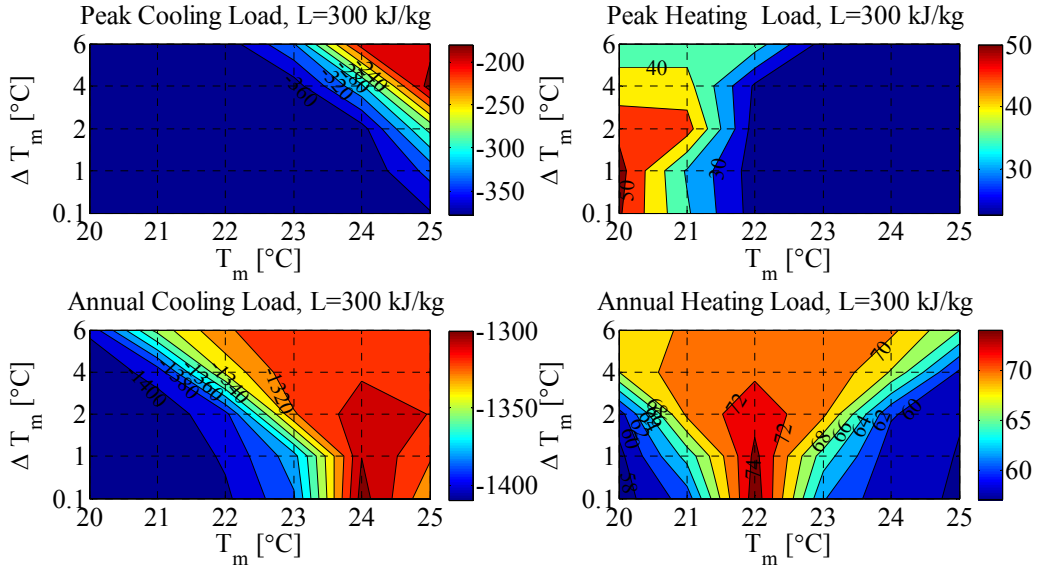

f) A contour plot for the case of 300 kg/kJ showing percentage reduction in cooling and heating loads

Figure B.7 Percentage reductions in cooling and heating loads for East cavity wall when PCM to the interior, Golden, CO

Appendix B.4.2 PCM to the exterior

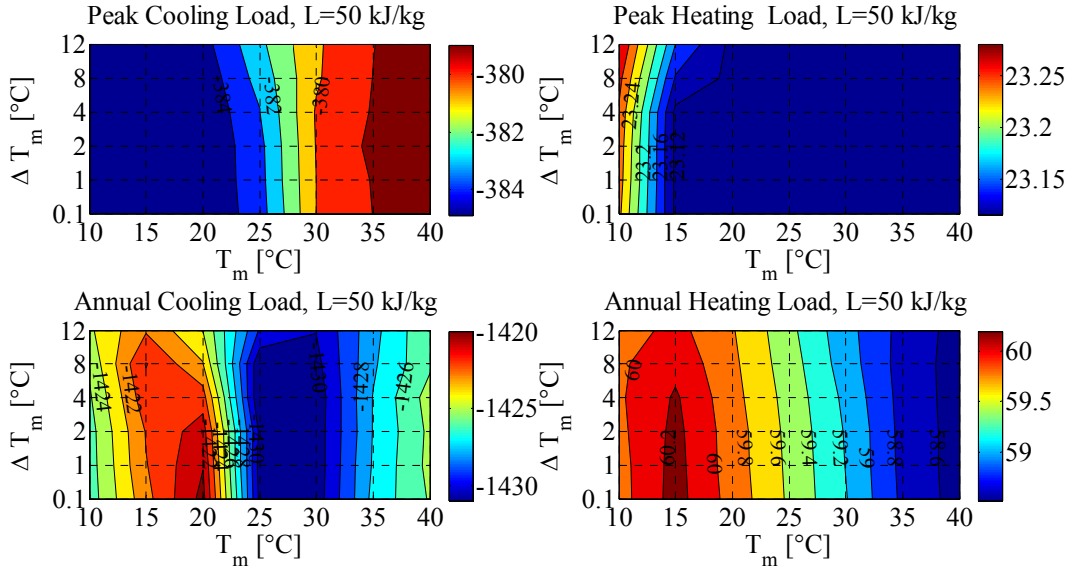

a) A contour plot for the case of 50 kg/kJ showing percentage reduction in cooling and heating loads

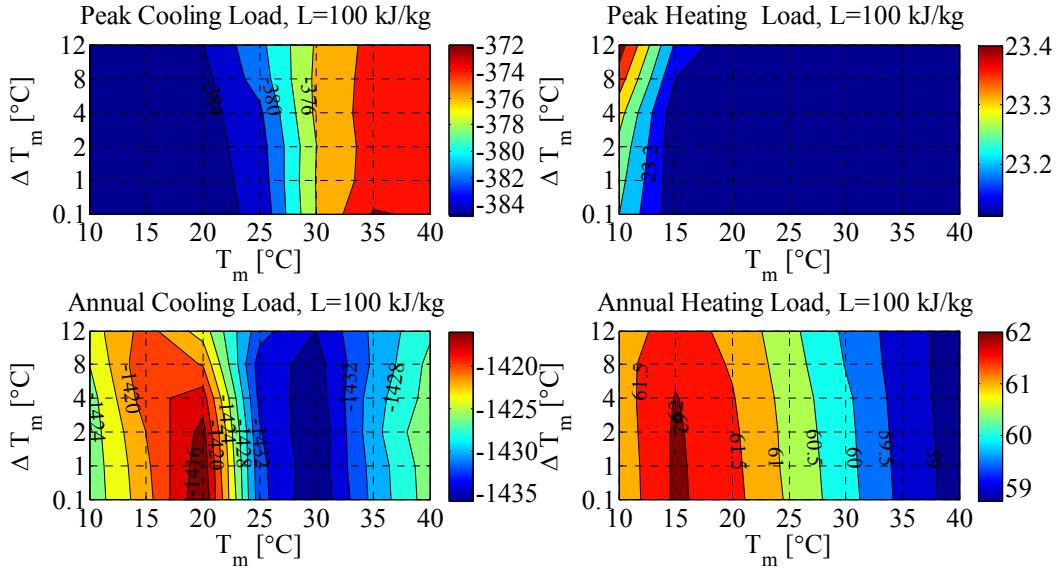

b) A contour plot for the case of 100 kg/kJ showing percentage reduction in cooling and heating loads

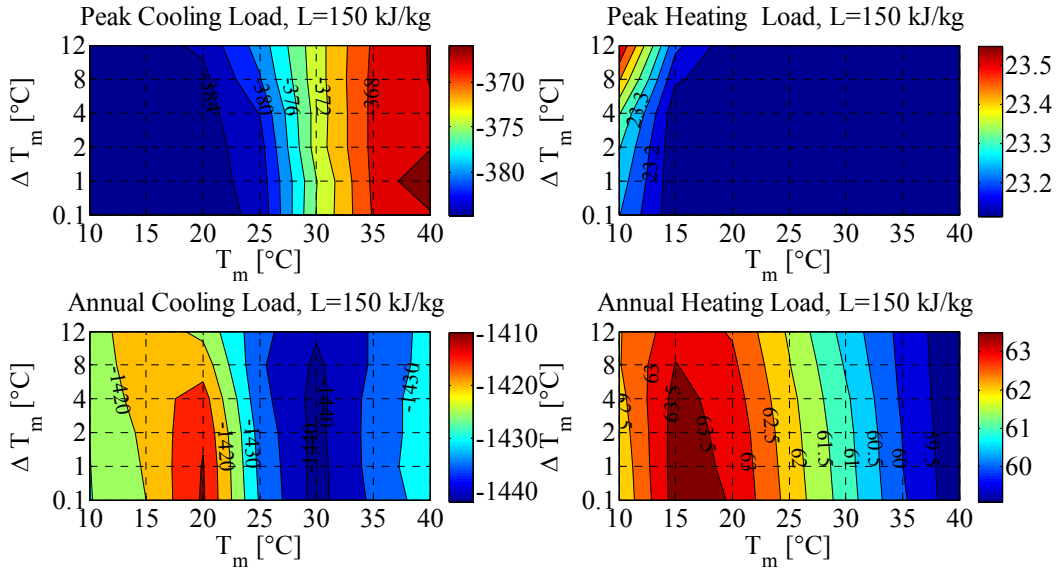

c) A contour plot for the case of 150 kg/kJ showing percentage reduction in cooling and heating loads

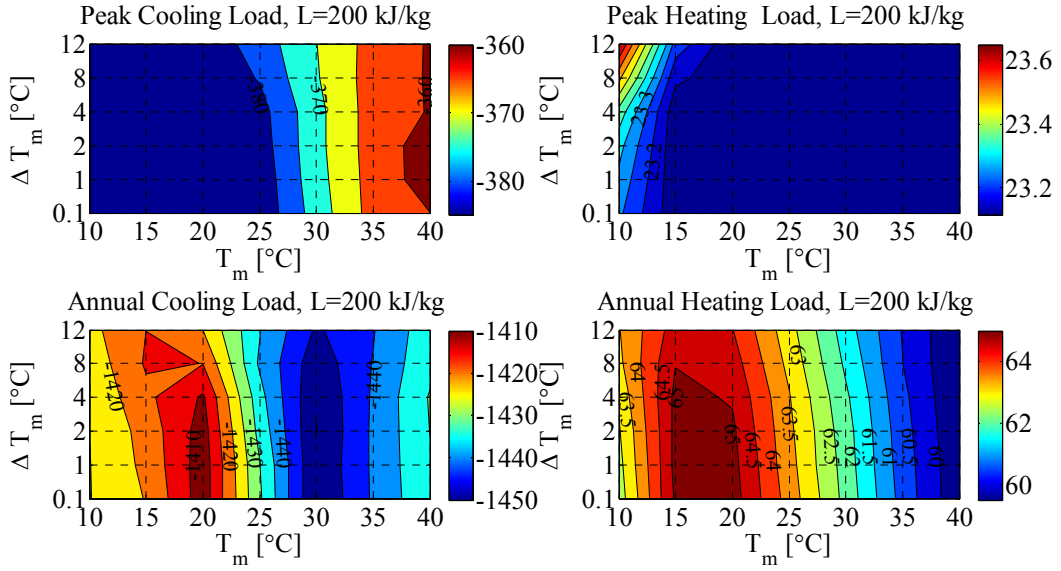

d) A contour plot for the case of 200 kg/kJ showing percentage reduction in cooling and heating loads

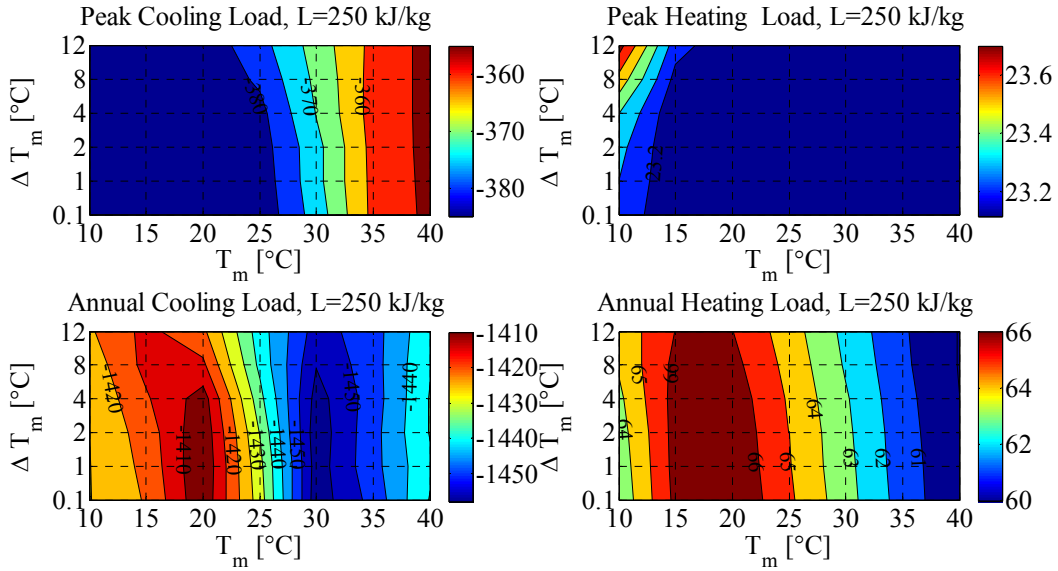

e) A contour plot for the case of 250 kg/kJ showing percentage reduction in cooling and heating loads

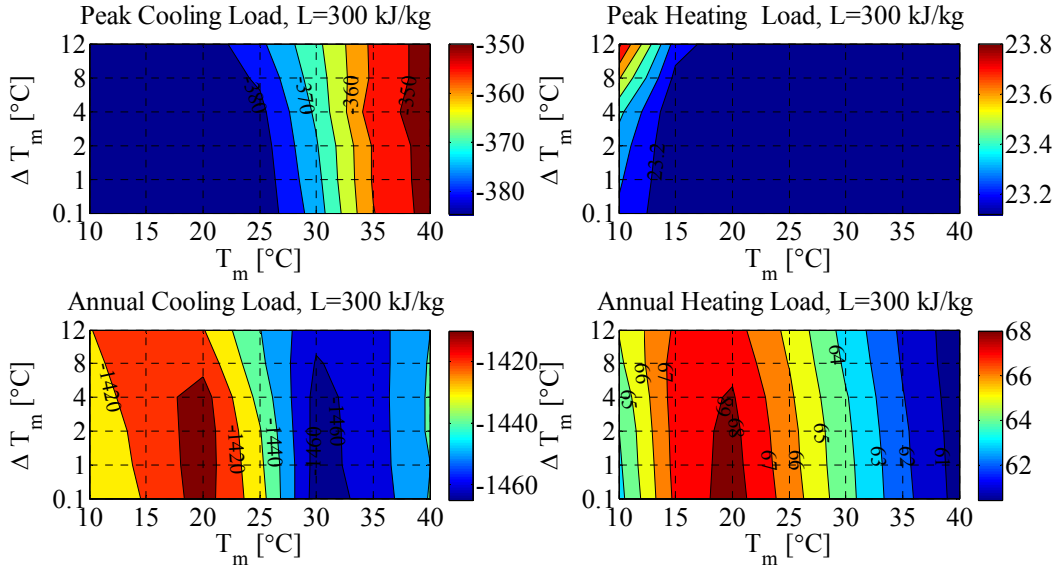

f) A contour plot for the case of 300 kg/kJ showing percentage reduction in cooling and heating loads

Figure B.8 Percentage reductions in cooling and heating loads for East cavity wall when PCM to the exterior, Golden, CO

Appendix C: Compiling SIMULINK project into a DLL TRNSYS Type

1) The first step is to setup the compiler for the MATLAB version. Every MATLAB version is compatible with a different compiler. Consult Mathworks for compatibility issue. For MATLAB R2012b, Microsoft Visual C++ 2010 is a compatible compiler and therefore installed before the setup. The setup is performed as shown in the MATLAB workspace below.

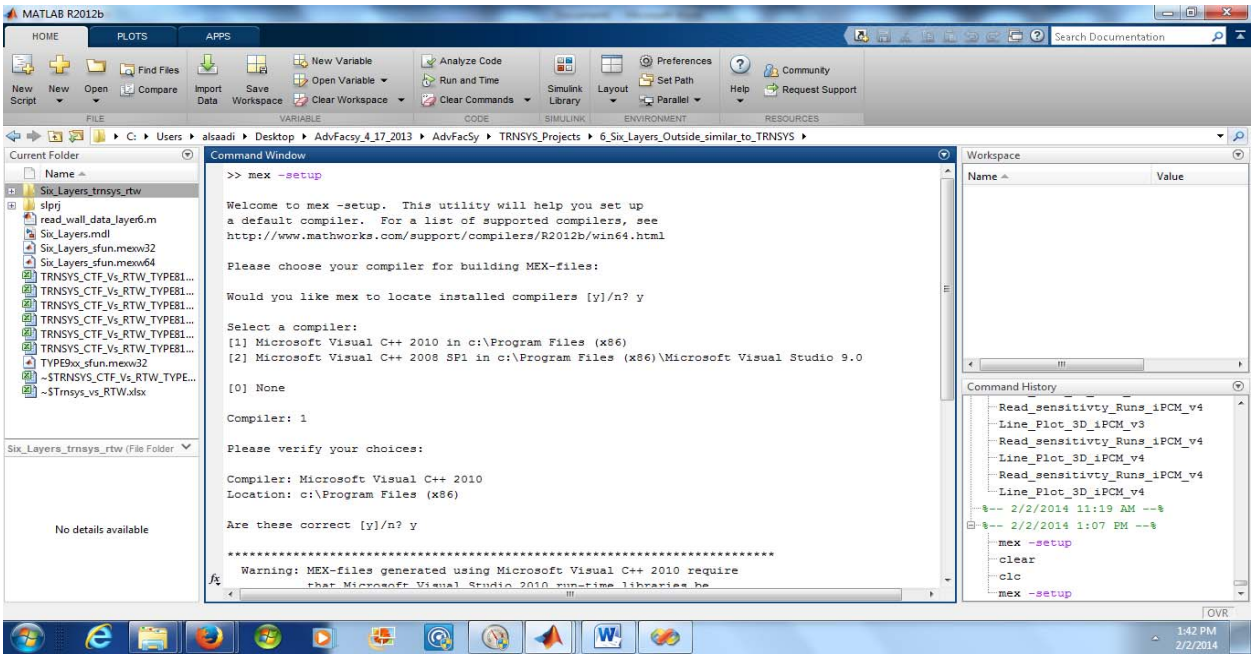

2) Download a zip file that contains codes and files necessary for converting SIMULINK files into TRNSYS Type from the following URL:

ftp://ftp1.cstb.fr/ftp_sop/software/Dynasimul/Matlab2Trnsys/

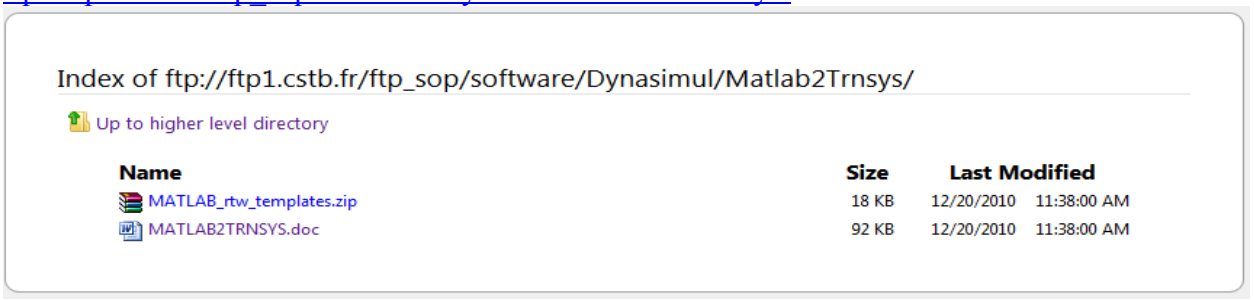

3) Go to C:\Program Files\MATLAB\R2012b\rtw\c and generate a folder called TRNSYS. Unzip the downloaded folder, copy and paste the files inside this folder.

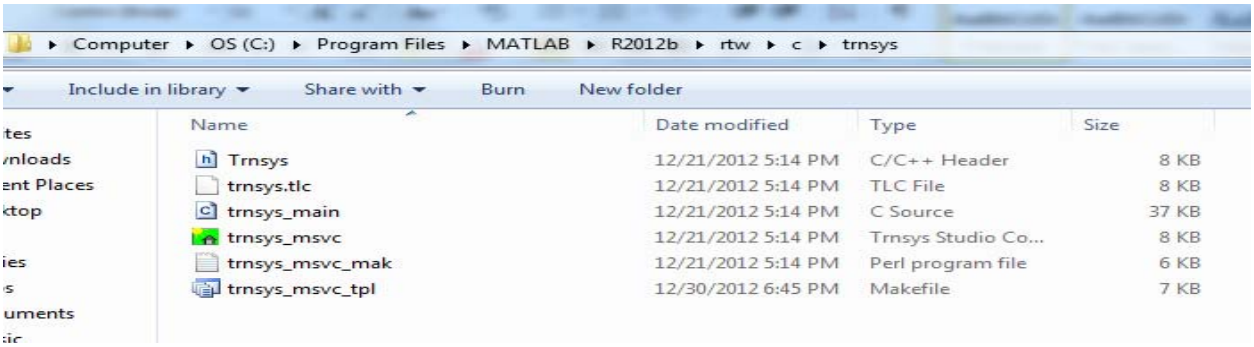

4) Make sure that your SIMULINK project file is contained within a subsystem with inputs and outputs as shown in the screen below. Inside the SIMULINK project file, select the **Model Configuration Parameters from the "Simulation"** tab.

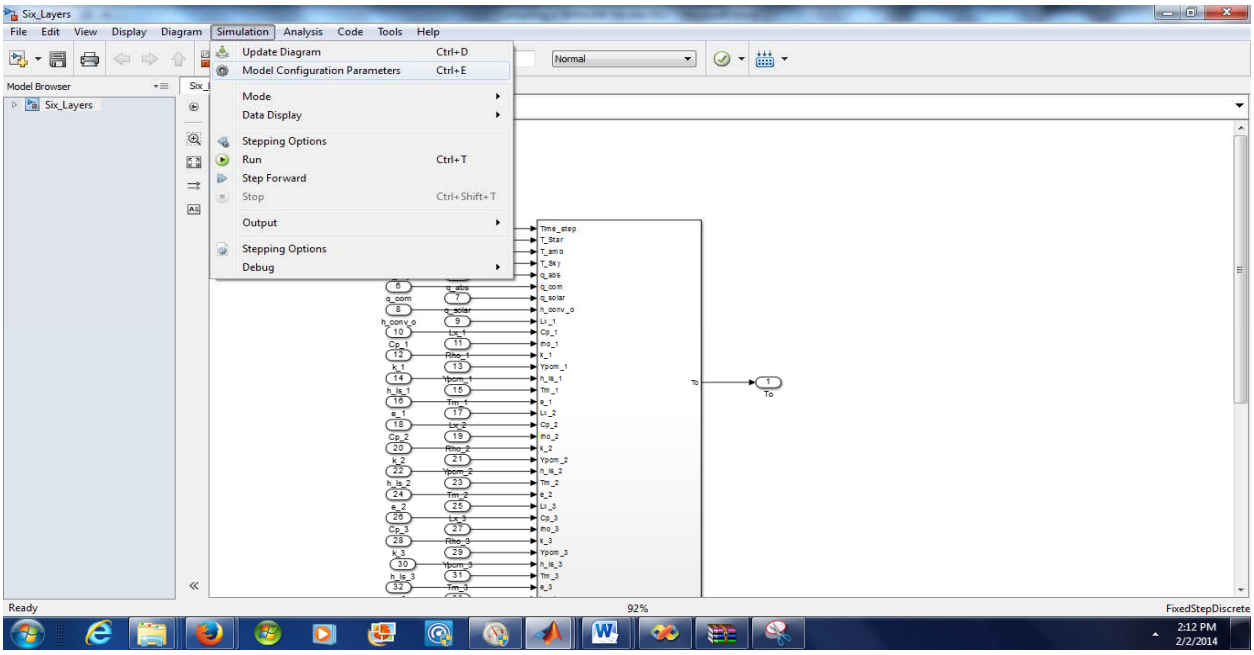

5) Under the configuration Parameters, select **Code Generation** tab.

Once selected, a menu screen appears on your right. Press browse and a dropdown list appears with many target files. Select the trnsys.tlc file "TRNSYS target file" which was

installed in Step 3 above. Then, select the language to C++. Make the following changes if not done automatically:

a. Make command: make_rtw

b. Template makefile: trnsys_msv_tmf

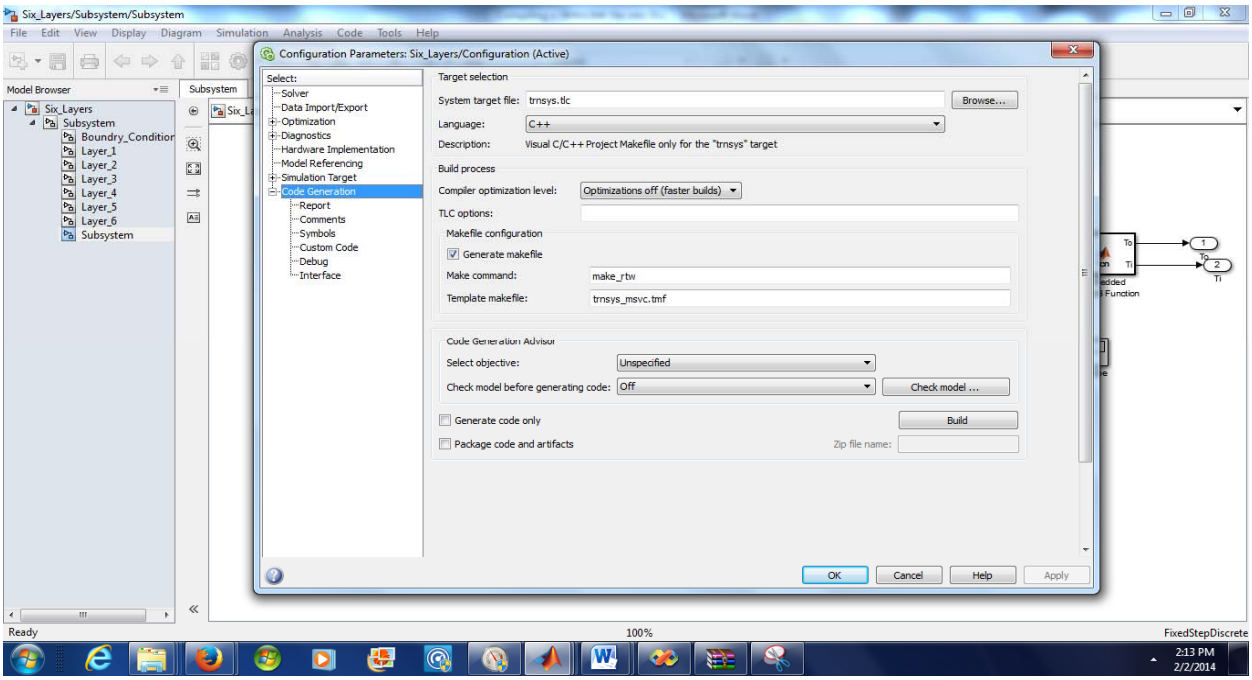

6) Under the Code generation screen, many tabs are available. Select the **custom code**. On your right side, a screen appears. Under the **header file**: write the command that specifies the TRNSYS type number as follows: **#define TRNSYS_TYPE XXX**. "XXX" is a three digits TYPE number. In this case, "**816"** is selected.

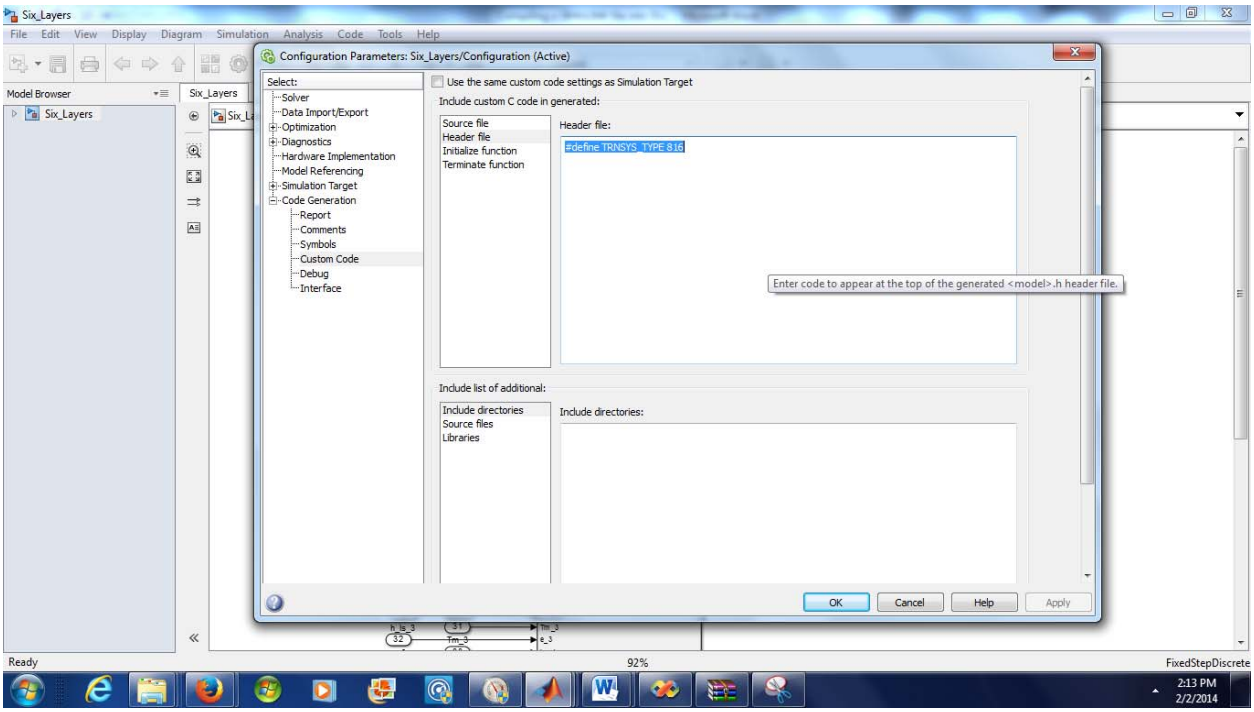

7) Once the TRNSYS Type number is specified, click on **Code menu** and press **C/C++** and **build the model.**

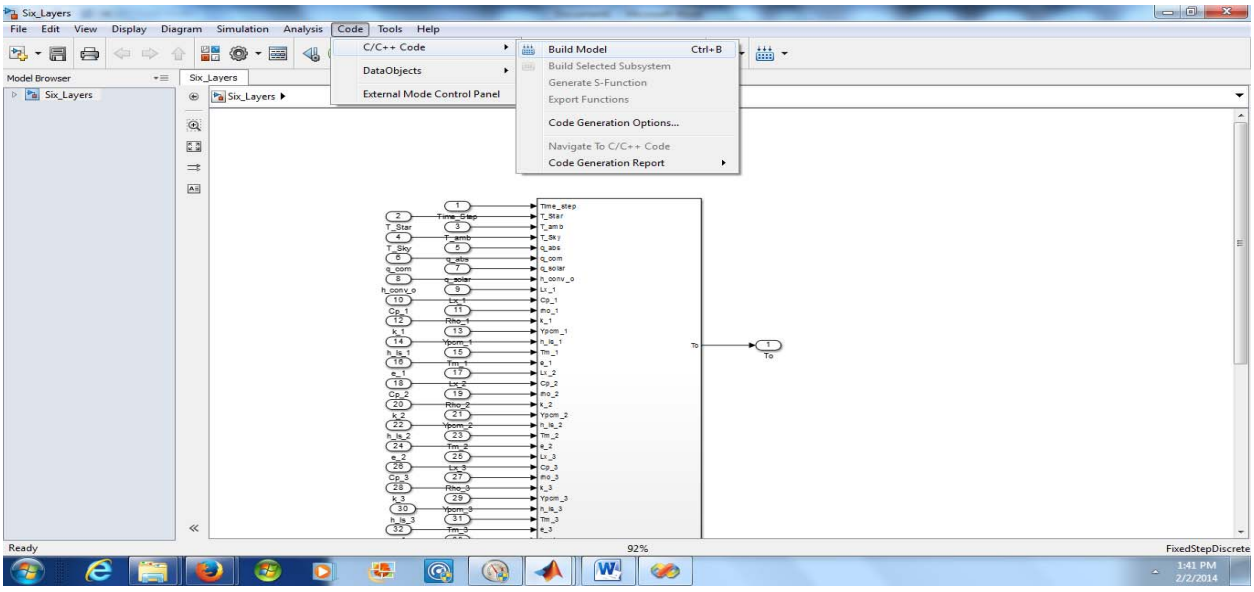

8) The compiling process starts and can be seen in the MATLAB workspace. The screen below shows the successful completion of generating the C++ files. All C++ files are generated under a newly created folder with a name similar to your SIMULINK file name.

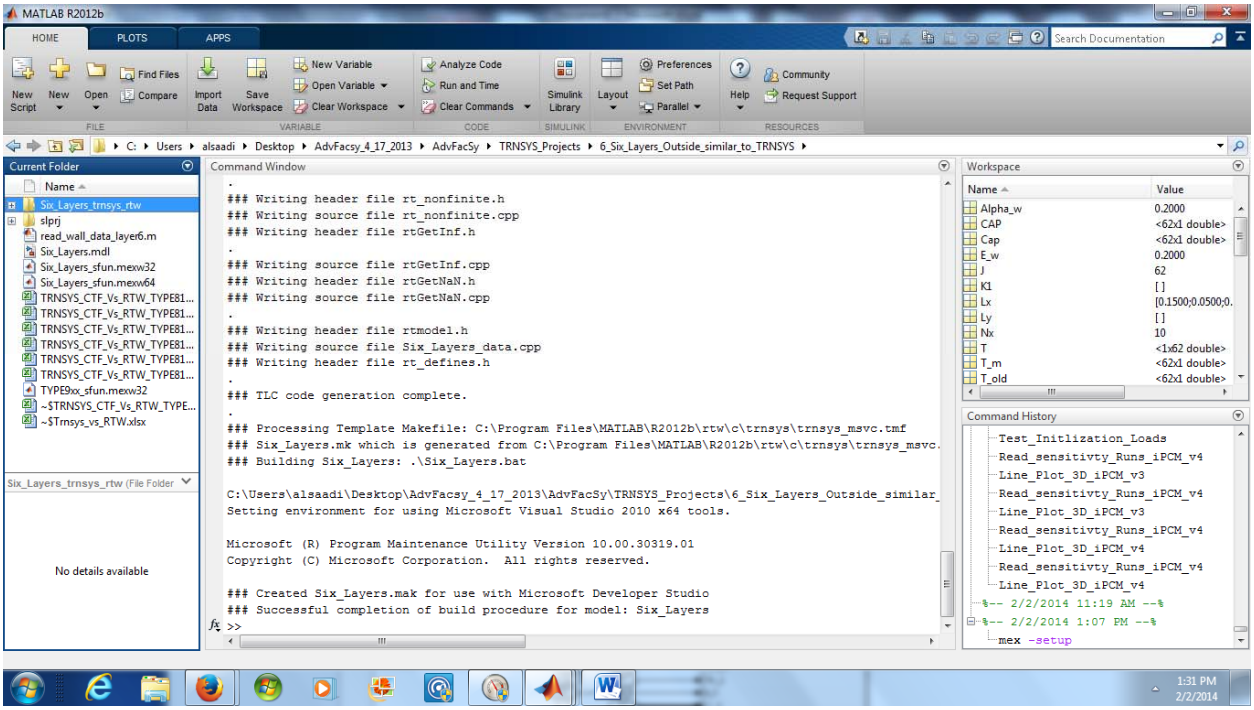

9) Open this folder and open the "**Six_Layers"** file with an extension of "makefile" using Microsoft Visual Studio. For MATLAB 2012b, Microsoft Visual Studio 2008 should be used.

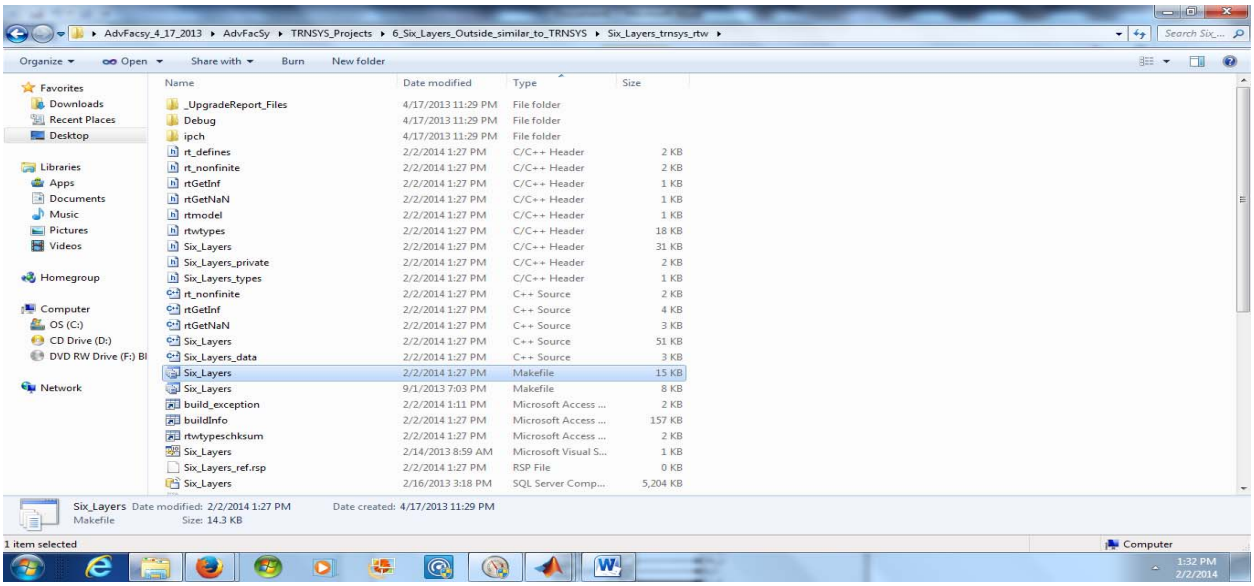

10) Once the "makefile" file is opened using Microsoft Visual Studio 2008, a visual studio project is generated.

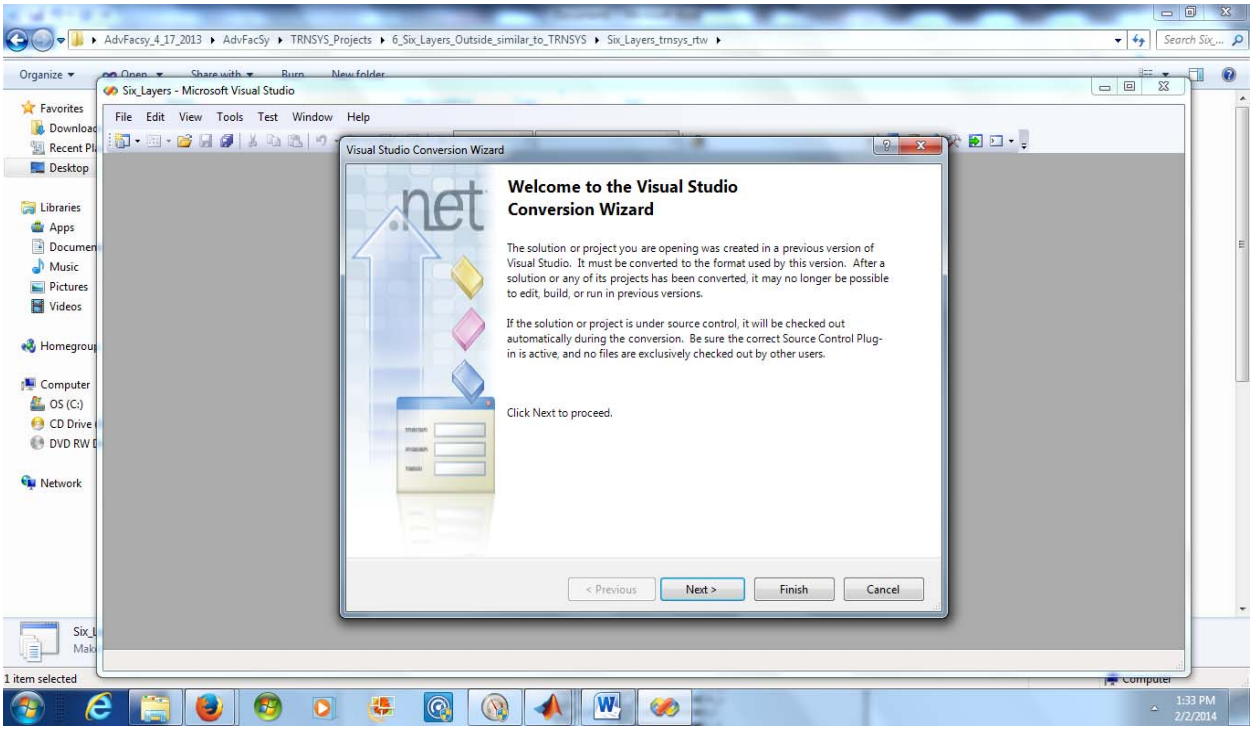

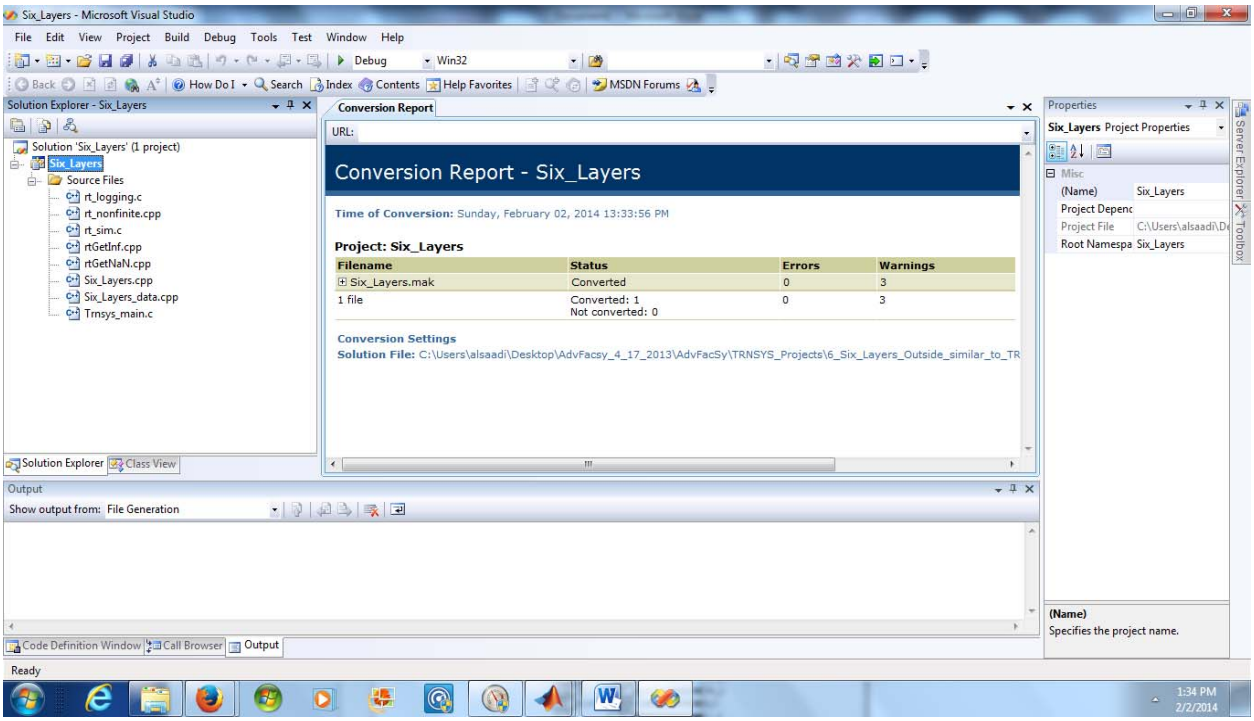

11) From the Microsoft Visual Studio build menu, select **<u>"Build Solution".</u>**

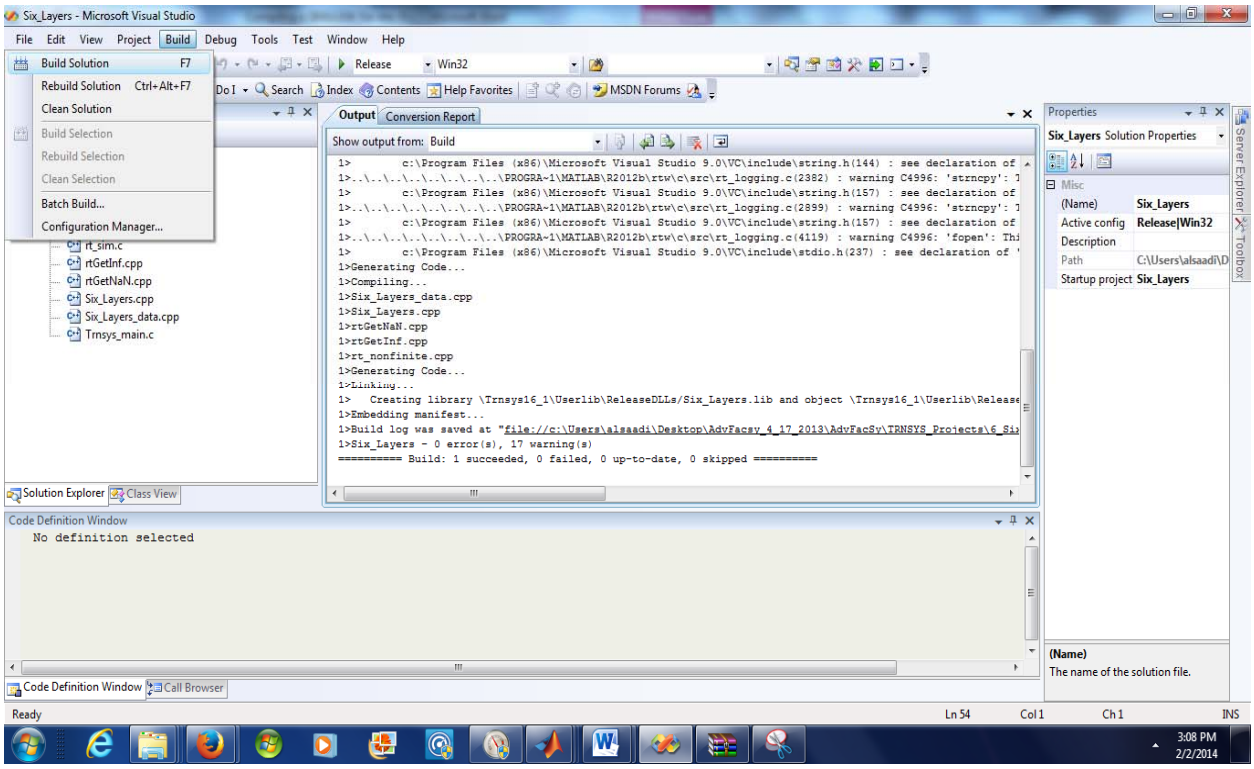

12) As seen below in the screen, a “DLL” file will automatically be generated and copied to the TRNSYS user library folder. The generated DLL file is a TRNSYS_SIMULINK type that is similar to a conventional TRNSYS DLL file generated from C++ or FORTRAN. A Performa for this type should be created as per TRNSYS protocols.

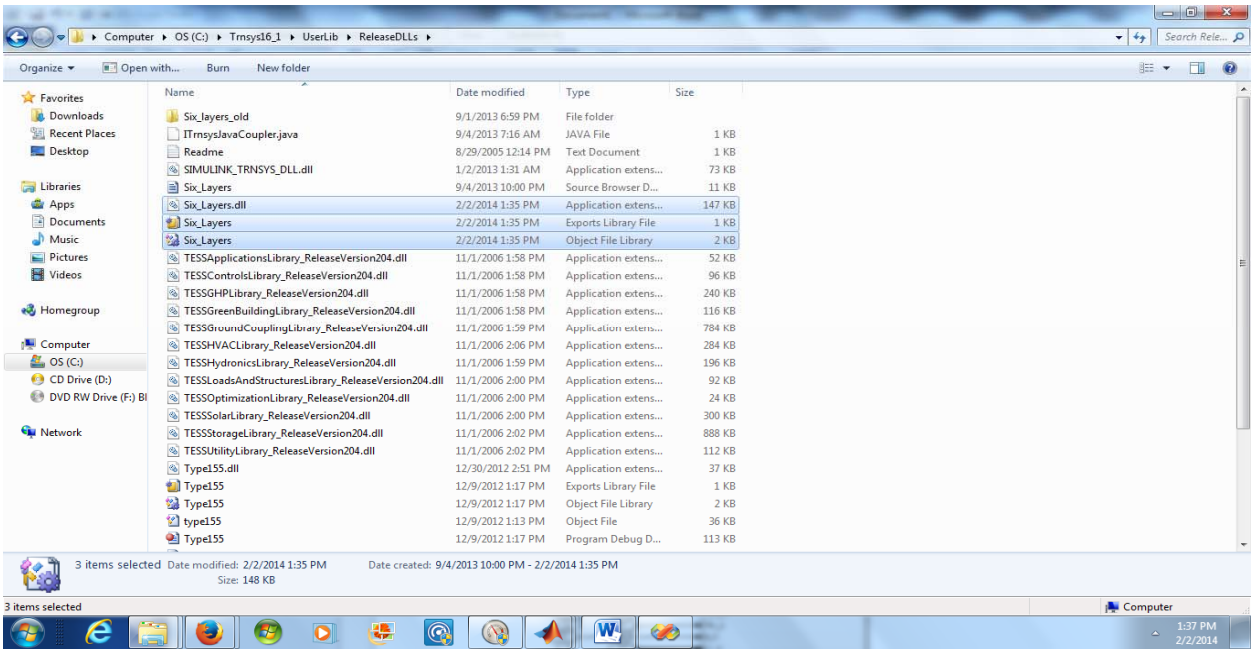

13) Finally for this TYPE to work, a MATLAB Compiler Runtime (MCR) should be installed in your computer. The MCR will be available on computers that already have a MATLAB. MCR is provided free of charge and can be downloaded and installed from the Mathworks website;

http://www.mathworks.com/products/compiler/mcr/

Appendix D: Multilayer wall system, Type-285 Performa

Table D-1 Inputs for Type 285

NTYPE#	Label	Description	Unit	Remarks
NTYPE 21	Qabs_i	Absorbed (or transmitted) at inside surf (includes solar gains, radiative heat, internal radiative gains and wall gains, except long-wave radiation exchange with other walls).	[kJ/h]	This is an output (i.e., surface outputs) from TYPE 56.
NTYPE 19	Qcom_i	Energy from inside surface including the convection to air and long-wave radiation to other surfaces	[kJ/h]	This is an output (i.e., surface outputs) from TYPE 56.
NTYPE 23	Tstar	star node temperature of zone	[°C]	This is an output (i.e., zone outputs) from TYPE 56.
	Tsky	Sky temperature	[°C]	This is an output from TYPE 69 weather file.
	Tamb	Outdoor air temperature	[°C]	This is an output from TYPE 15 weather file.
	qsol	Solar radiation received on the tilted surface	[kJ/(h.m^2)]	This is an output from TYPE 15 weather file.
	hconv_o	Convective heat transfer coefficient at outside surface	[W/(m^2.°C)]	User input (can be constant or based on equation)

Table D-2 Outputs from Type 285

Label	Description	Unit	Remarks
Ts_ext	Exterior surface temperature	[°C]	Exterior node
Ts_int	Interior surface temperature	[°C]	Interior node: this value will be an input to TYPE56 as a boundary temperature for calculating indoor air heat balance.
Iterations	Number of iterations that take the code to converge in each time step	[-]	
T_nodes.txt	Text file that contains the nodes temperature for each time step	[°C]	
h_nodes.txt	Text file that contains the nodes enthalpy for each time step	[kJ/kg]	
F_nodes.txt	Text file that contains the nodes fluid fraction for each time step	[-]	

Table D-3 Parameters of Type 285

Label	Description	Unit	Remarks
Number_of_Layers	Number of layers in the wall	[-]	
Wall_Height	The height of the wall	[m]	
Wall_Width	The width of the wall	[m]	
Surface_Tilt	The slope of the wall	[°]	90° is vertical
Wall_Color	Absorptivity of the wall	[-]	
T_initial	The initialization for nodes temperature	[°C]	The nodes temperature will be updated during the simulation
Logical Unit for the wall descp. file	Logical number assigned by TRNSYS for the text file that includes the wall thermal and physical properties	[-]	
Logical Unit for nodes Temperature file	Logical number assigned by TRNSYS for the text file that includes the nodes Temperatures	[-]	
Logical Unit for nodes Enthalpy file	Logical number assigned by TRNSYS for the text file that includes the nodes enthalpies	[-]	
Logical Unit for nodes Enthalpy file	Logical number assigned by TRNSYS for the text file that includes the nodes fluid fraction	[-]	

```
C This text file has the wall layers information
C ***************************************************
C you have to enter how many layers you have
C***************************************************
C Indx   : wall layer index number
C n      : number of nodes
C Lx     : Wall thickness in x direction [m]
C cp     : Specific heat [J/kg-K]
C rho    : density [kg/m^3]
C k      : conductivity [W/m-K]
C*********PCM Properties*****************************
C Ypcm   : Do we have PCM in this layer? ==> yes=1, no=0;
C h_ls   : latent heat of fusion [J/kg]
C T_m    : Melting Temperature [C];
C e      : Half melting Temperature Range [C];
C***************************************************
4
C *Layer 1: Exterior layer**********"BioPCM"************
1
10
0.0125
1970
235
0.20
1
200000
22
1
C *Layer 2: middle layer**********OSB"*****************
2
10
0.0125
1200
800
0.15
0
0
0
0
C *Layer 3: middle layer**********"Fiberglass Quilt"****
3
10
0.05
840
120
0.065
0
0
0
0
C *Layer 4: Interior layer**********"Gypsum"************
4
10
0.0125
1000
1200
0.21
0
0
0
0
```

Number of layers in the wall

```
C *Layer 1: Exterior layer**********"BioPCM"*********************
1       =======> wall layer index number
10      =======> number of nodes per layer
0.0125  =======> Wall thickness in x direction [m] for this layer
1970    =======> Specific heat [J/kg-K]
235     =======> density [kg/m^3]
0.20    =======> conductivity [W/m-K]
1       =======> Do we have PCM in this layer? ==> yes=1, no=0;
200000  =======> latent heat of fusion [J/kg]
22      =======> Melting Temperature [C]
1       =======> Melting Temperature Range [C]
```

a) Text file for wall description b) Parameters description for one layer

Figure D.1 Example of a text file structure containing a wall with 4 layers, PCM layer to the exterior

Appendix E: Contour plots for multilayer PCM-enhanced walls for whole building model

Appendix E.1 Phoenix, AZ.: PCM to the interior

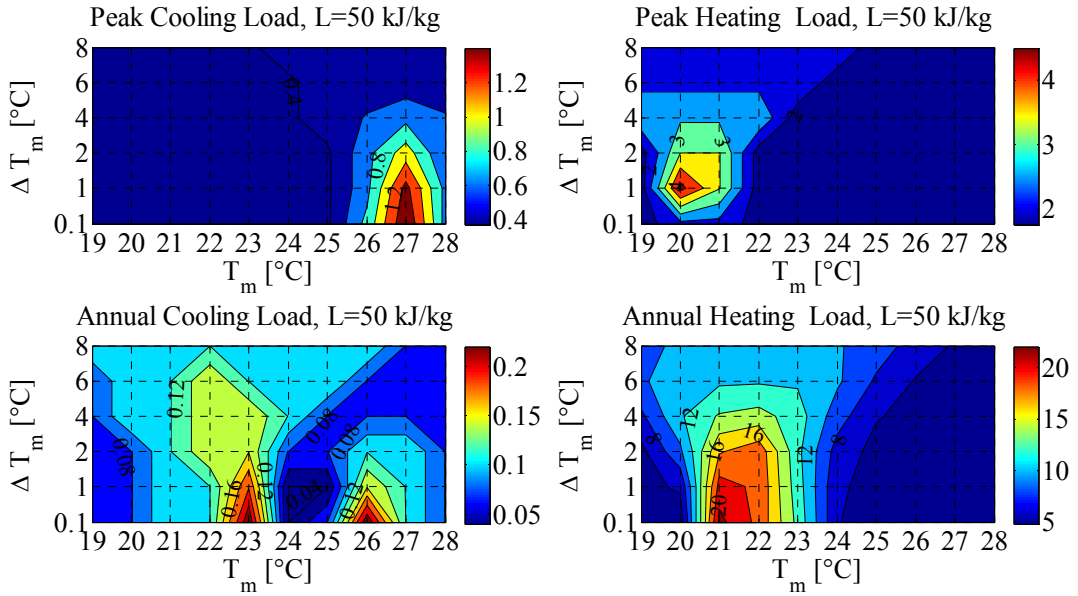

a) A contour plot for the case of 50 kg/kJ showing percentage reduction in cooling and heating loads

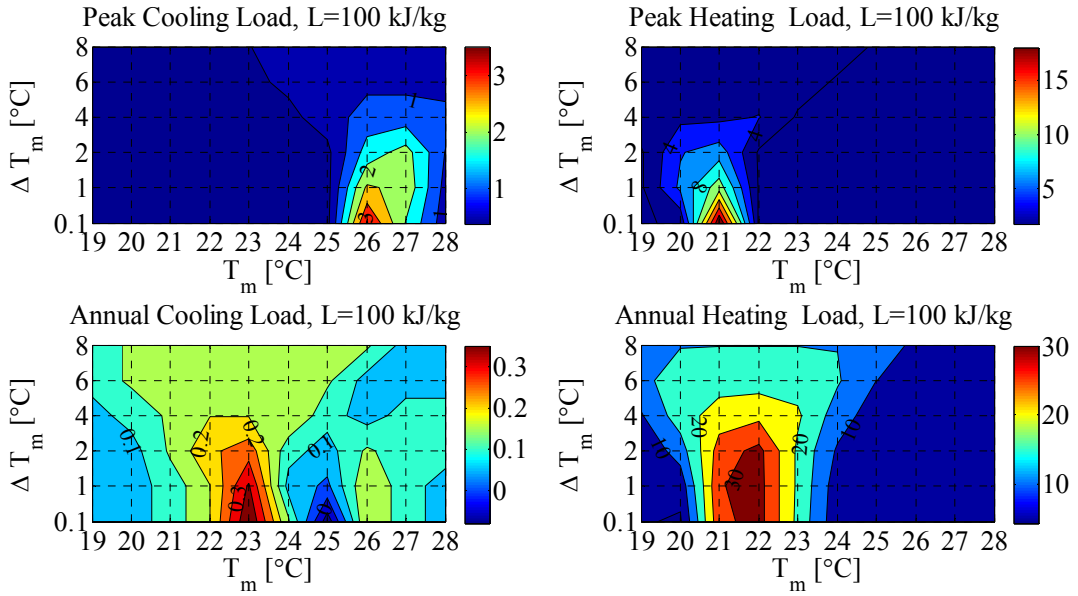

b) A contour plot for the case of 100 kg/kJ showing percentage reduction in cooling and heating loads

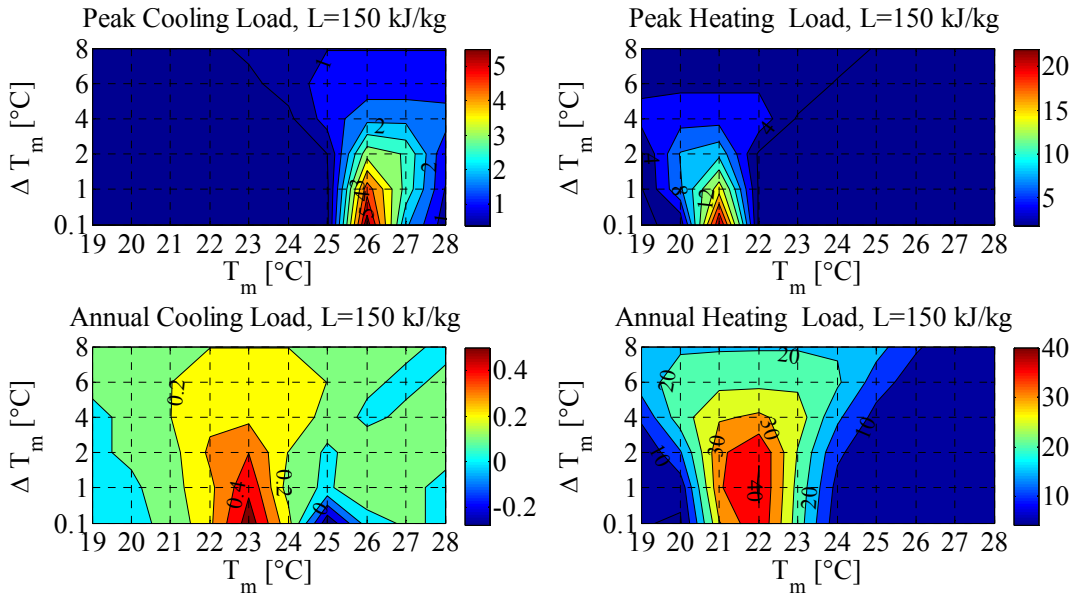

c) A contour plot for the case of 150 kg/kJ showing percentage reduction in cooling and heating loads

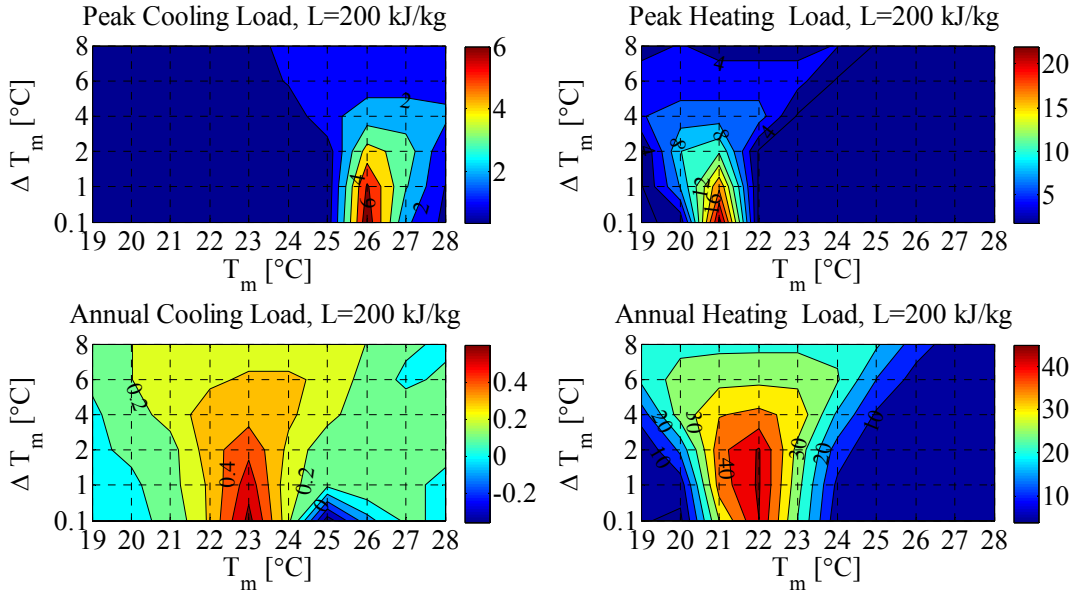

d) A contour plot for the case of 200 kg/kJ showing percentage reduction in cooling and heating loads

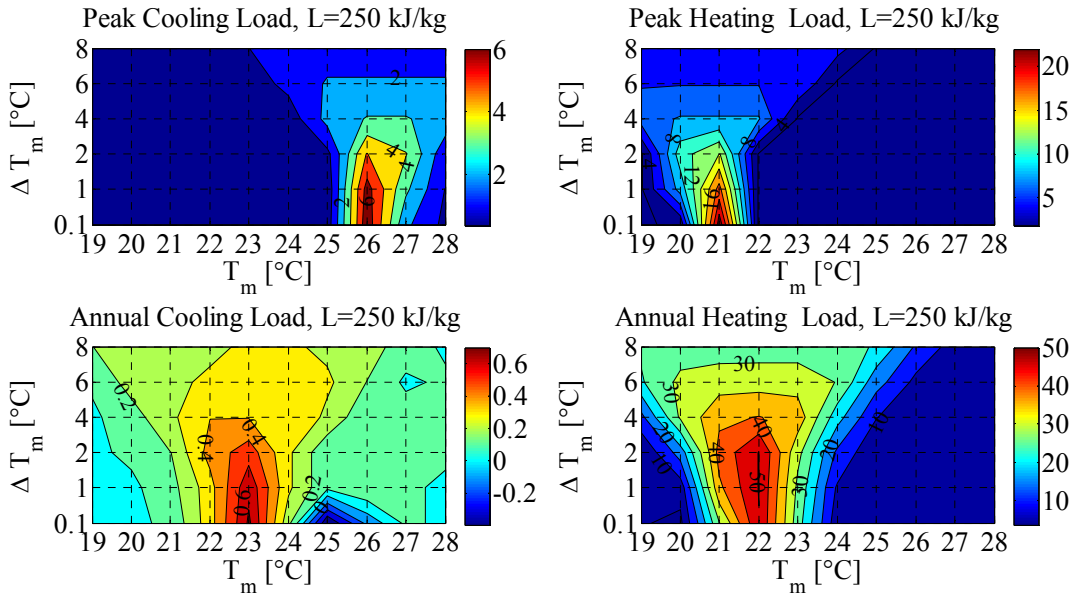

e) A contour plot for the case of 250 kg/kJ showing percentage reduction in cooling and heating loads

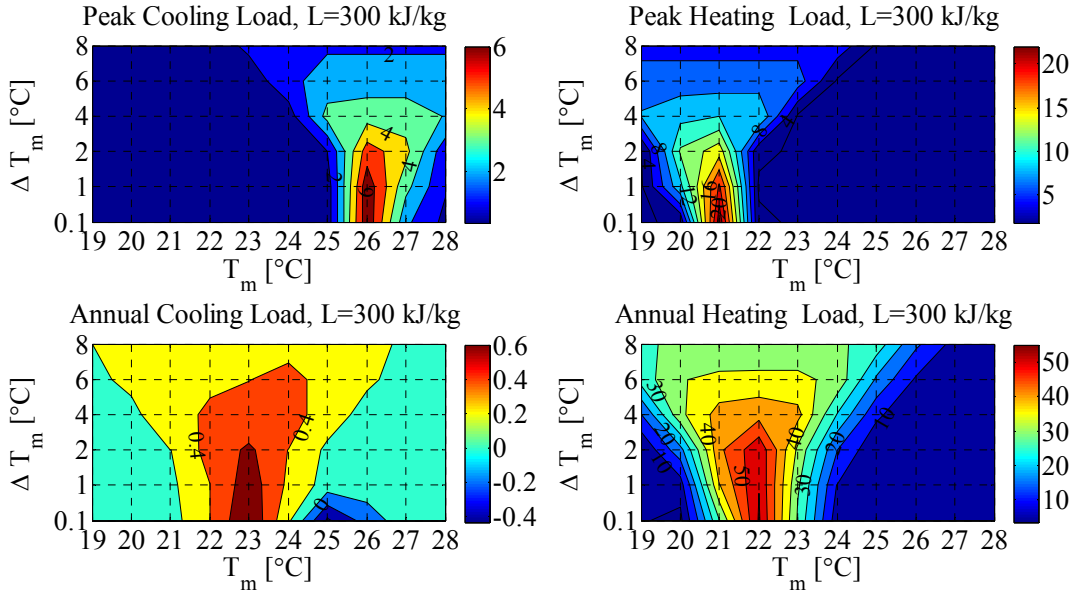

f) A contour plot for the case of 300 kg/kJ showing percentage reduction in cooling and heating loads

Figure E.1 Percentage reductions in cooling and heating loads for whole-house when PCM to the interior for Phoenix, AZ

Appendix E.2 Atlanta , GA: PCM to the interior

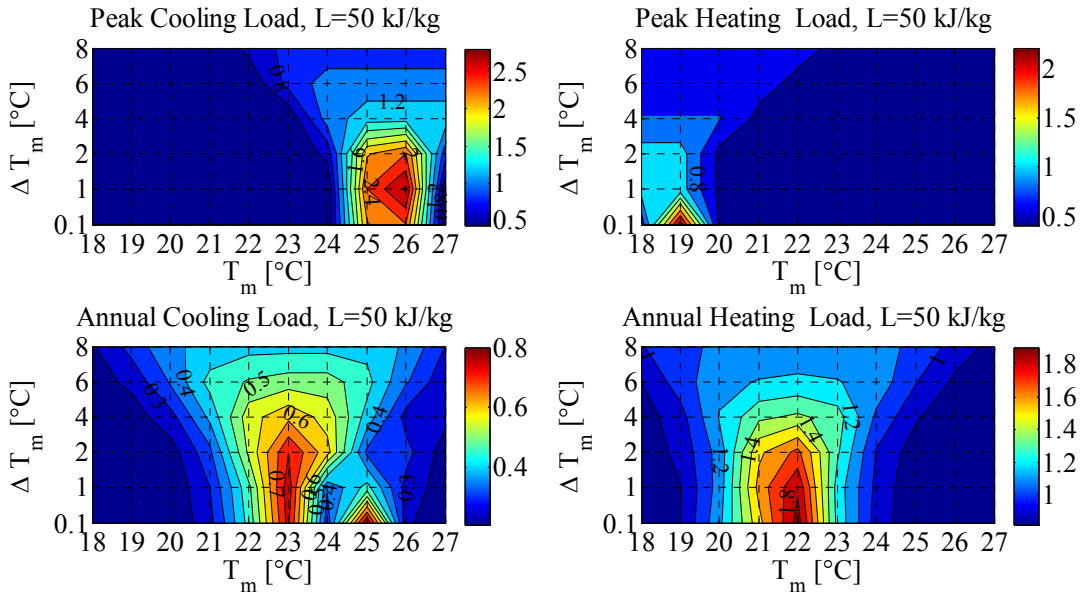

a) A contour plot for the case of 50 kg/kJ showing percentage reduction in cooling and heating loads

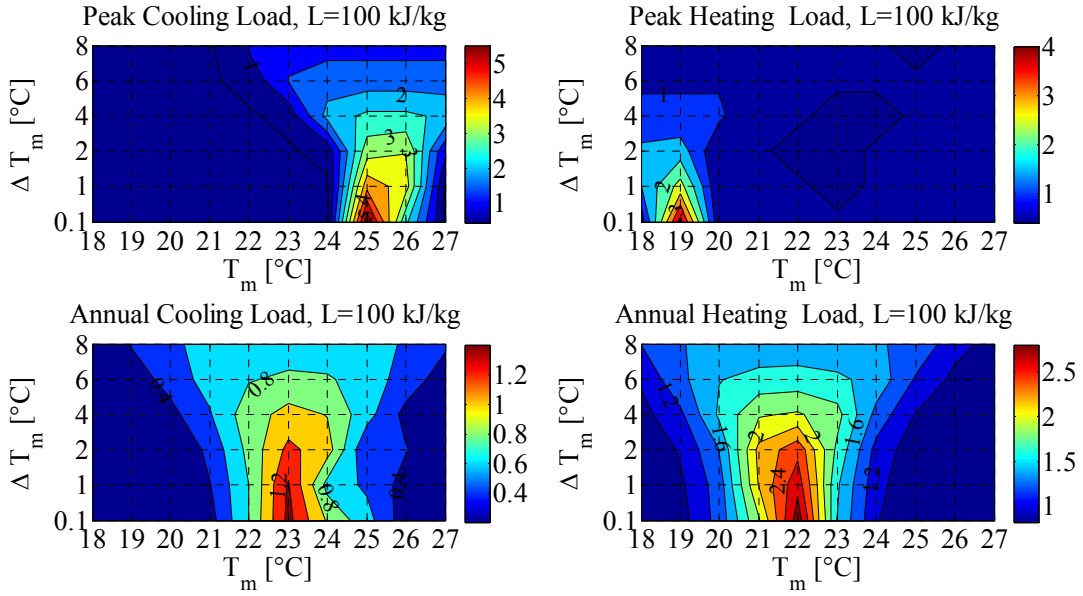

b) A contour plot for the case of 100 kg/kJ showing percentage reduction in cooling and heating loads

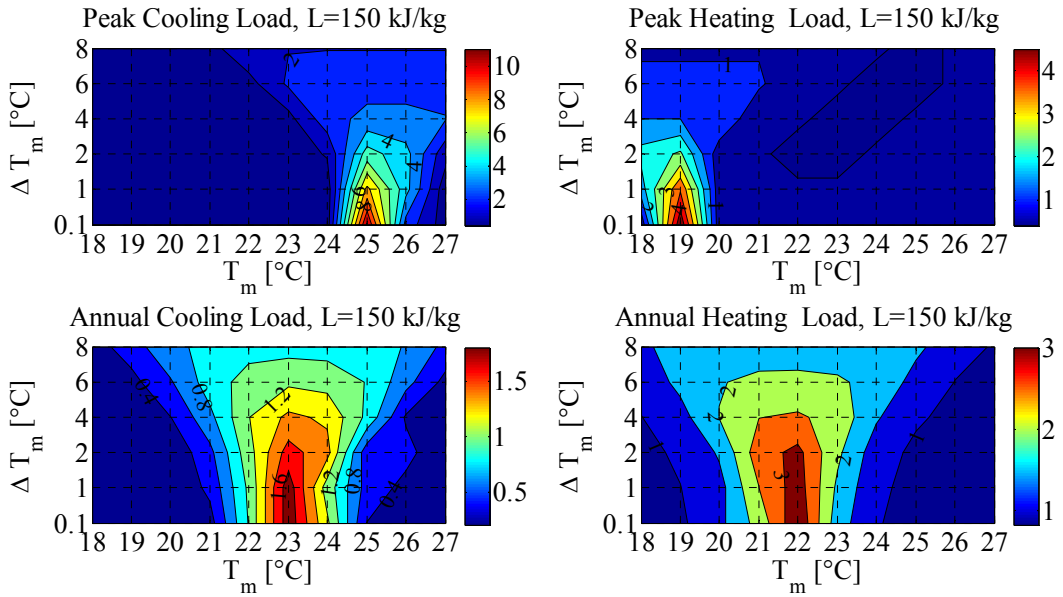

c) A contour plot for the case of 150 kg/kJ showing percentage reduction in cooling and heating loads

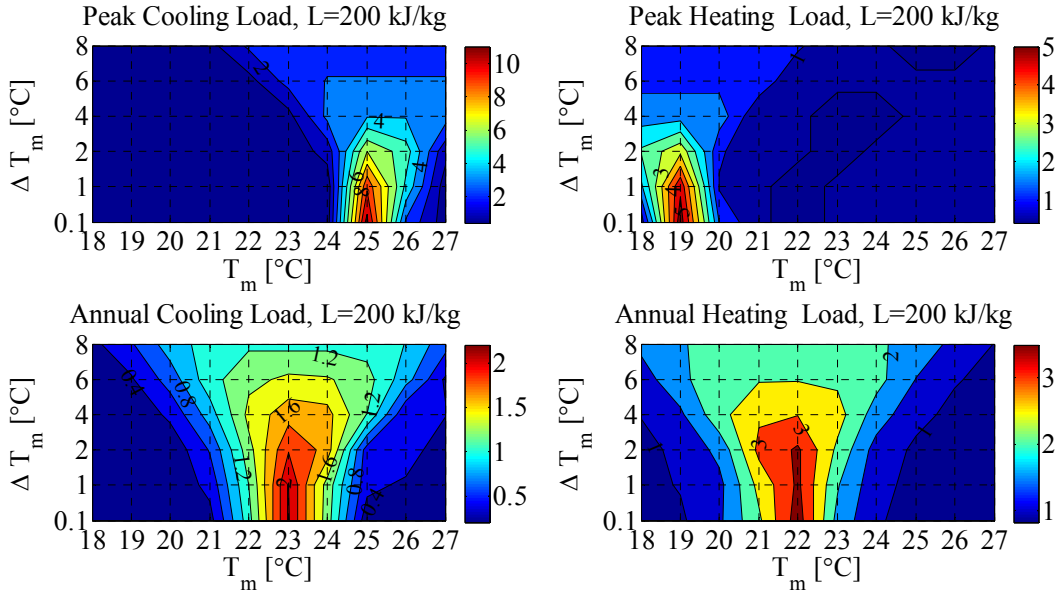

d) A contour plot for the case of 200 kg/kJ showing percentage reduction in cooling and heating loads

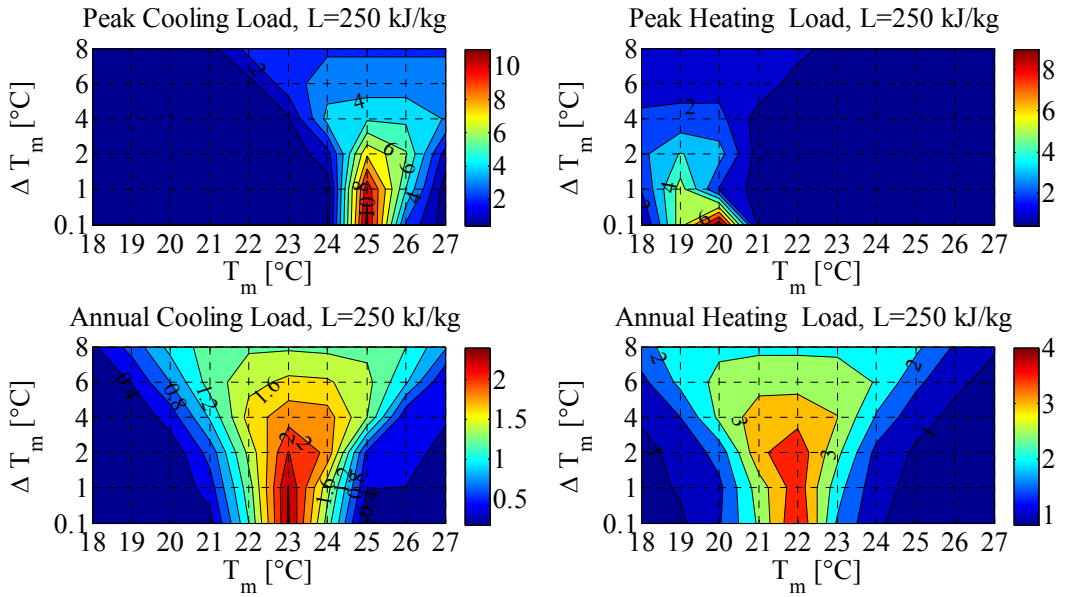

e) A contour plot for the case of 250 kg/kJ showing percentage reduction in cooling and heating loads

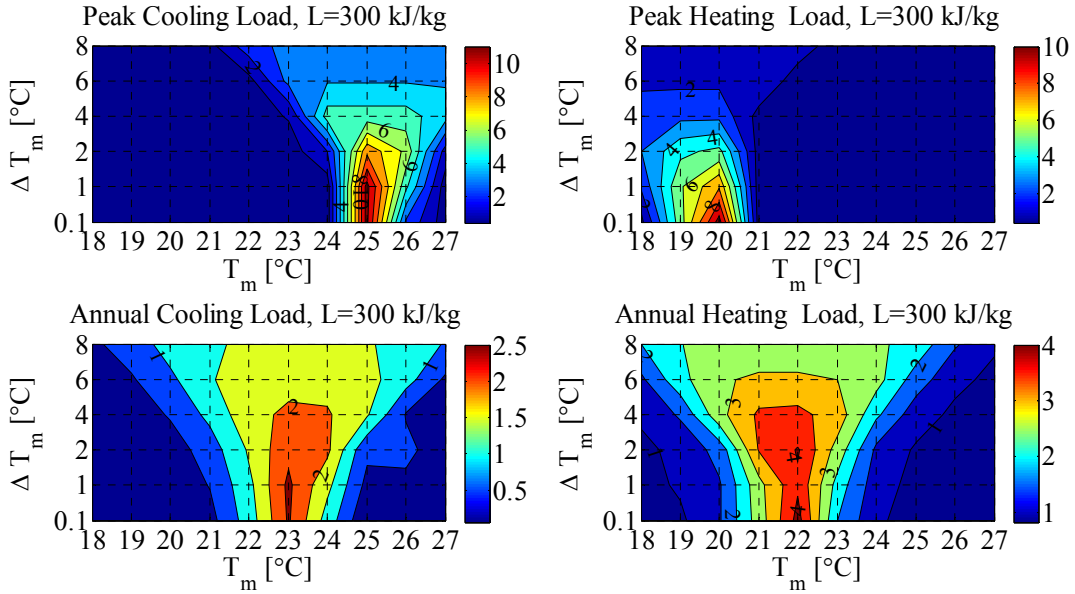

f) A contour plot for the case of 300 kg/kJ showing percentage reduction in cooling and heating loads

Figure E.2 Percentage reductions in cooling and heating loads for whole-house when PCM to the interior for Atlanta, GA

Appendix E.3 Seattle, WA. : PCM to the interior

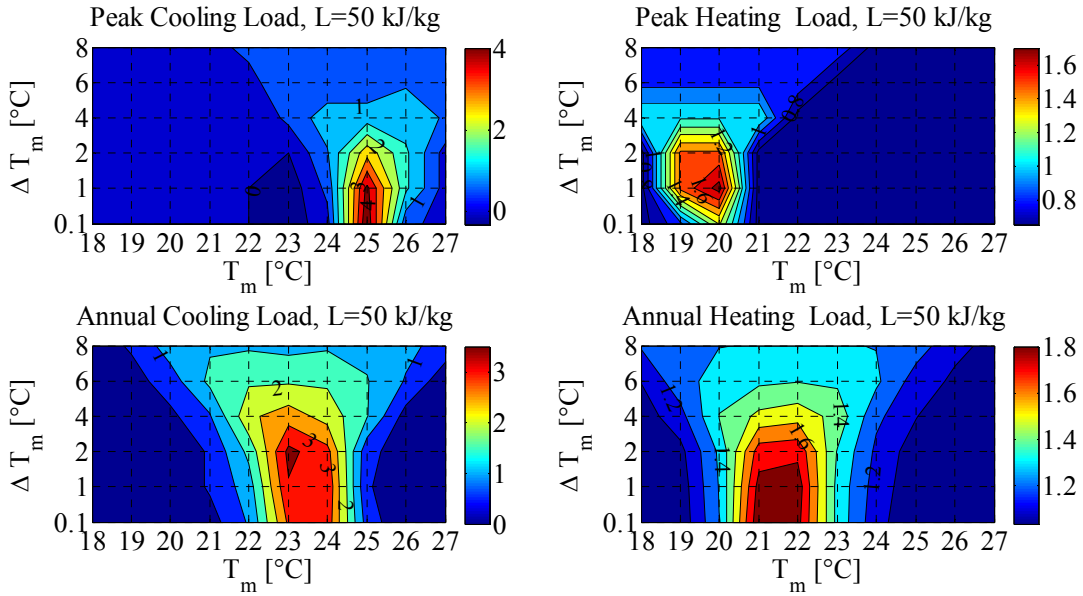

a) A contour plot for the case of 50 kg/kJ showing percentage reduction in cooling and heating loads

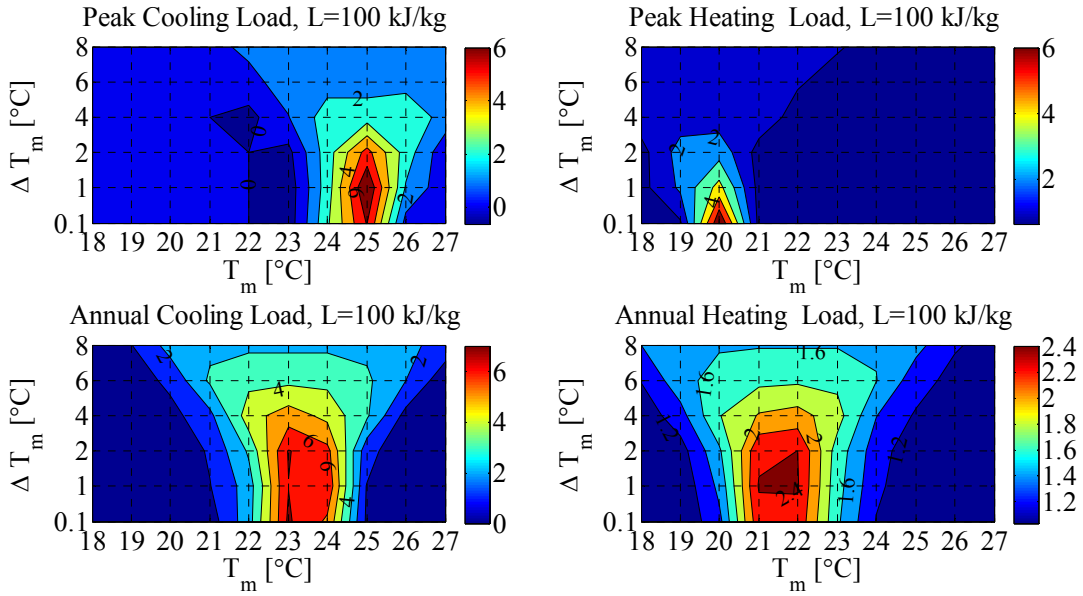

b) A contour plot for the case of 100 kg/kJ showing percentage reduction in cooling and heating loads

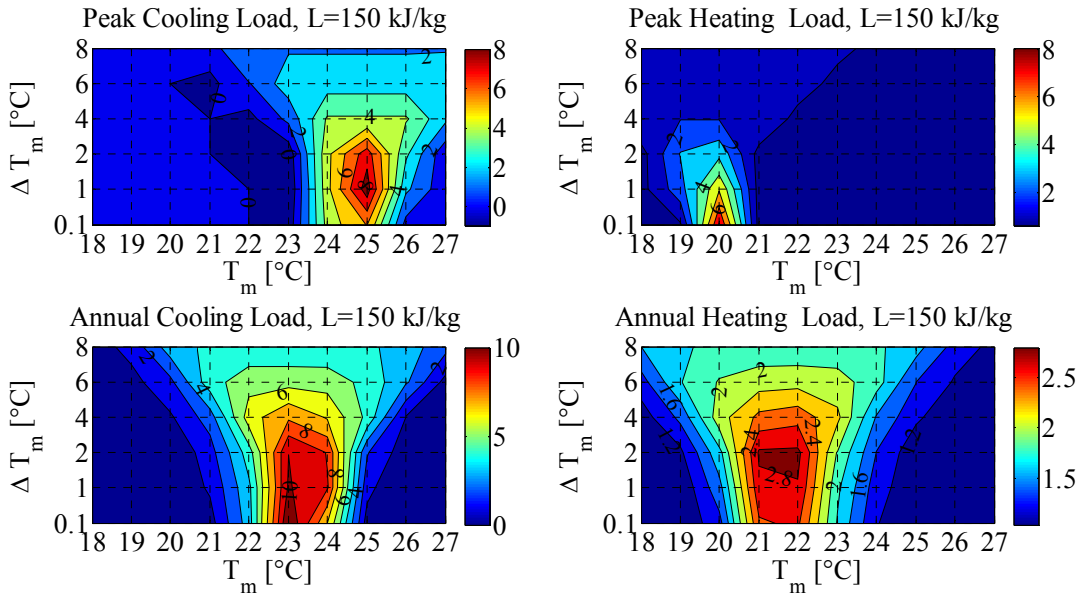

c) A contour plot for the case of 150 kg/kJ showing percentage reduction in cooling and heating loads

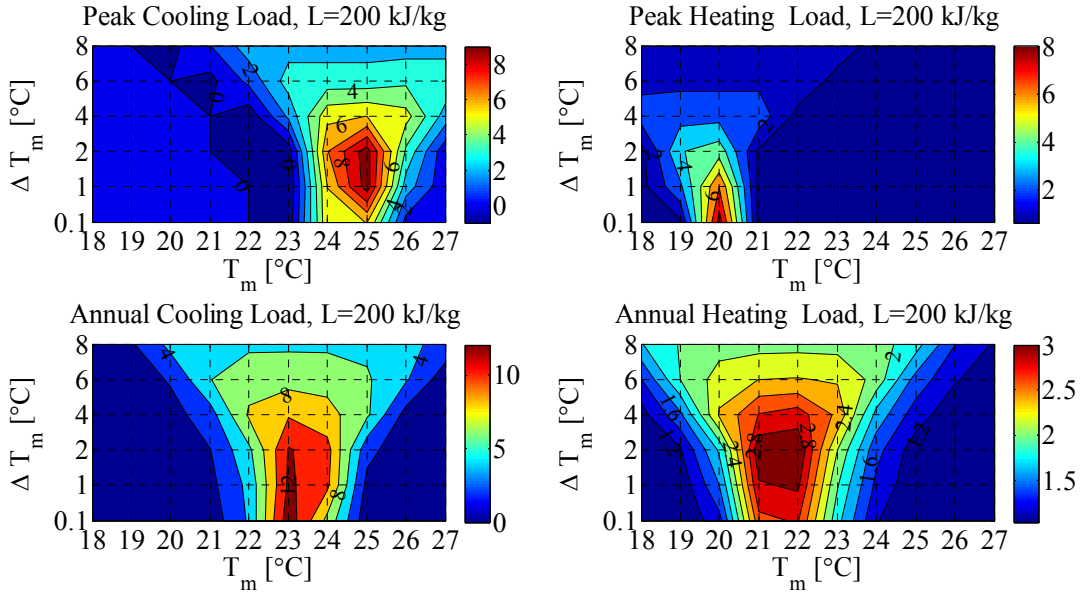

d) A contour plot for the case of 200 kg/kJ showing percentage reduction in cooling and heating loads

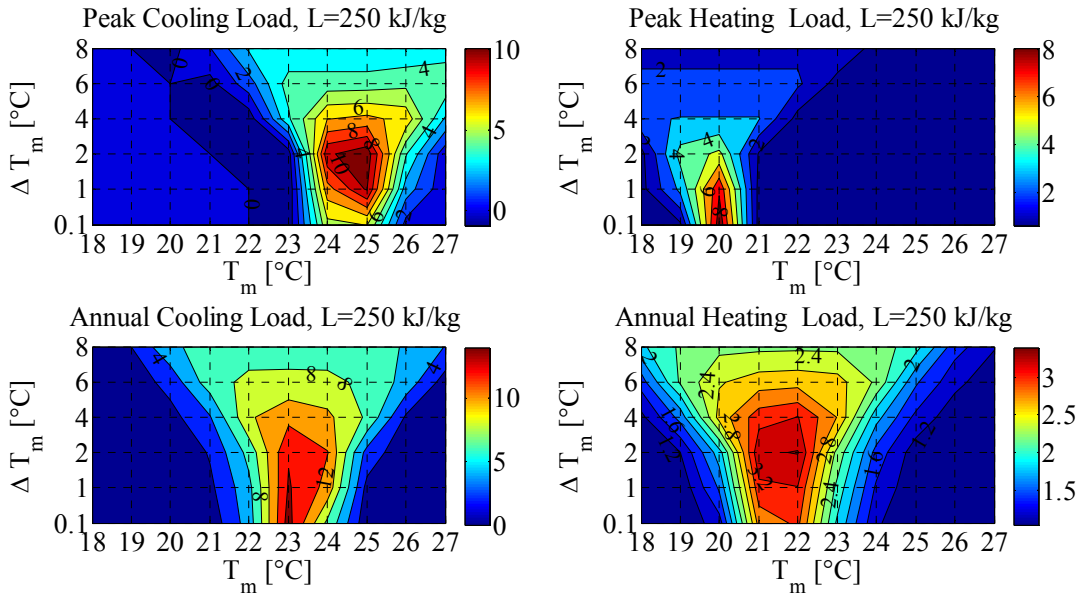

e) A contour plot for the case of 250 kg/kJ showing percentage reduction in cooling and heating loads

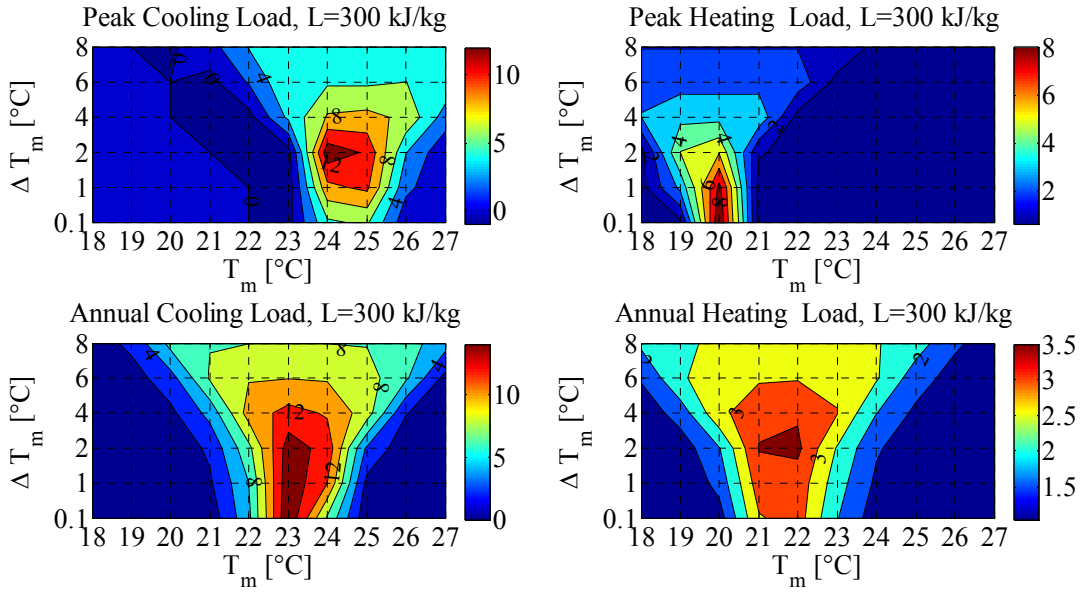

f) A contour plot for the case of 300 kg/kJ showing percentage reduction in cooling and heating loads

Figure E.3 Percentage reductions in cooling and heating loads for whole-house when PCM to the interior for Seattle, WA

Appendix E.4 Golden, CO.: PCM to the interior

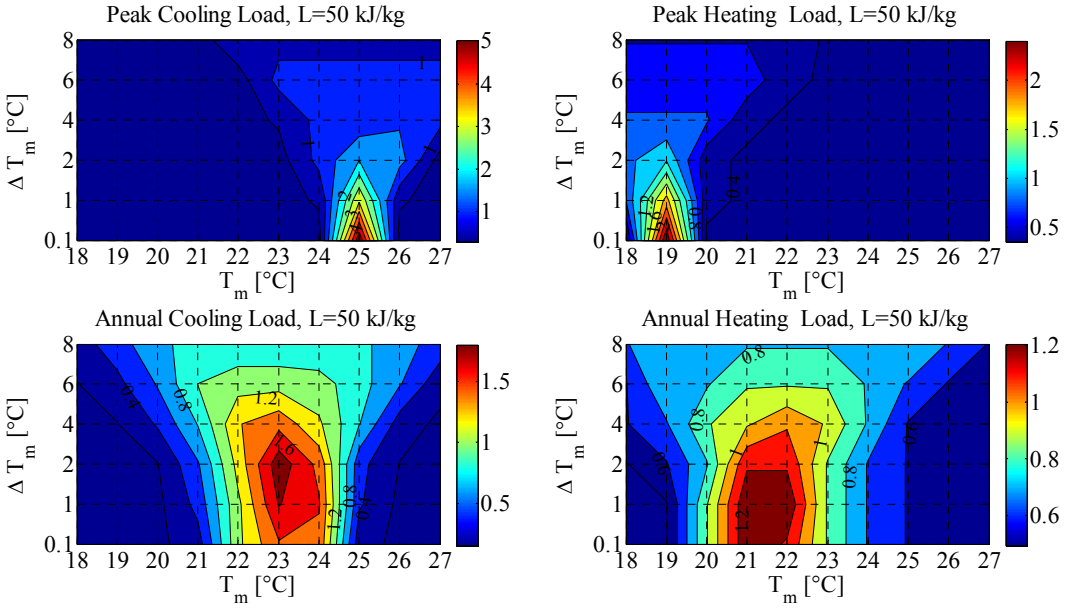

a) A contour plot for the case of 50 kg/kJ showing percentage reduction in cooling and heating loads

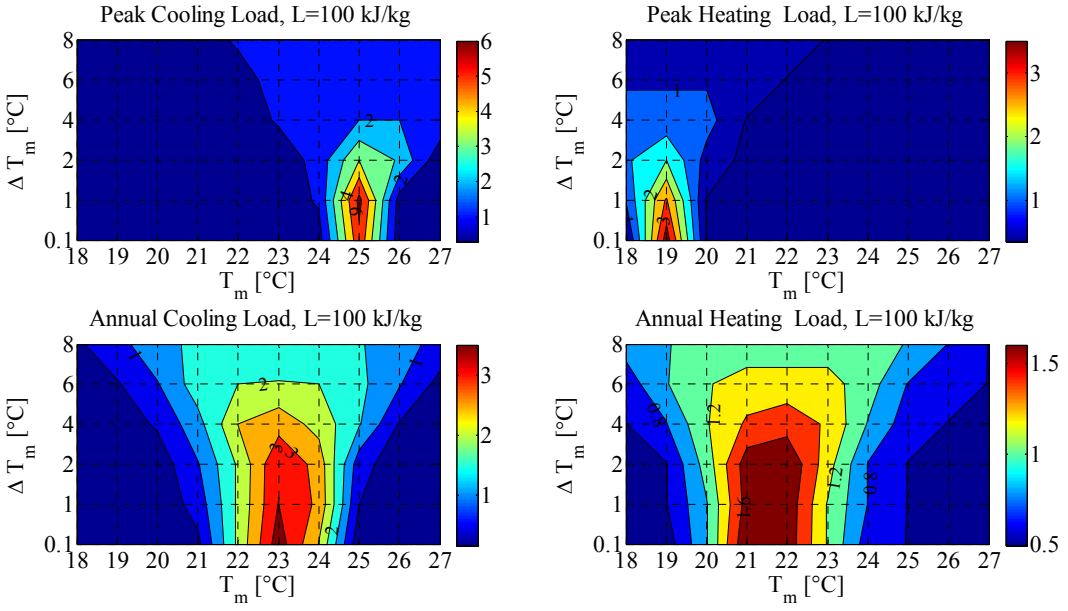

b) A contour plot for the case of 100 kg/kJ showing percentage reduction in cooling and heating loads

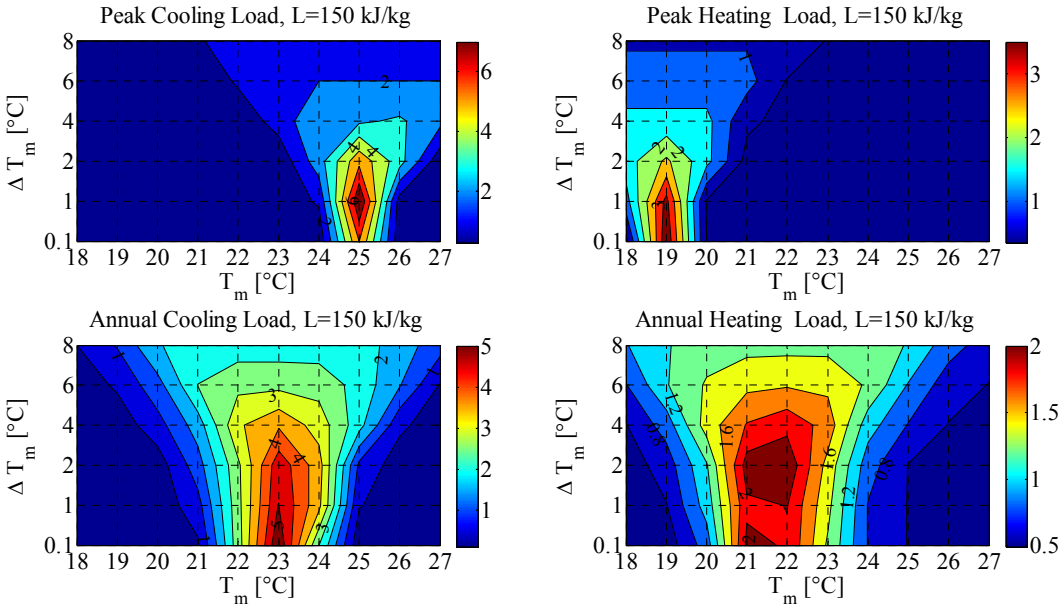

c) A contour plot for the case of 150 kg/kJ showing percentage reduction in cooling and heating loads

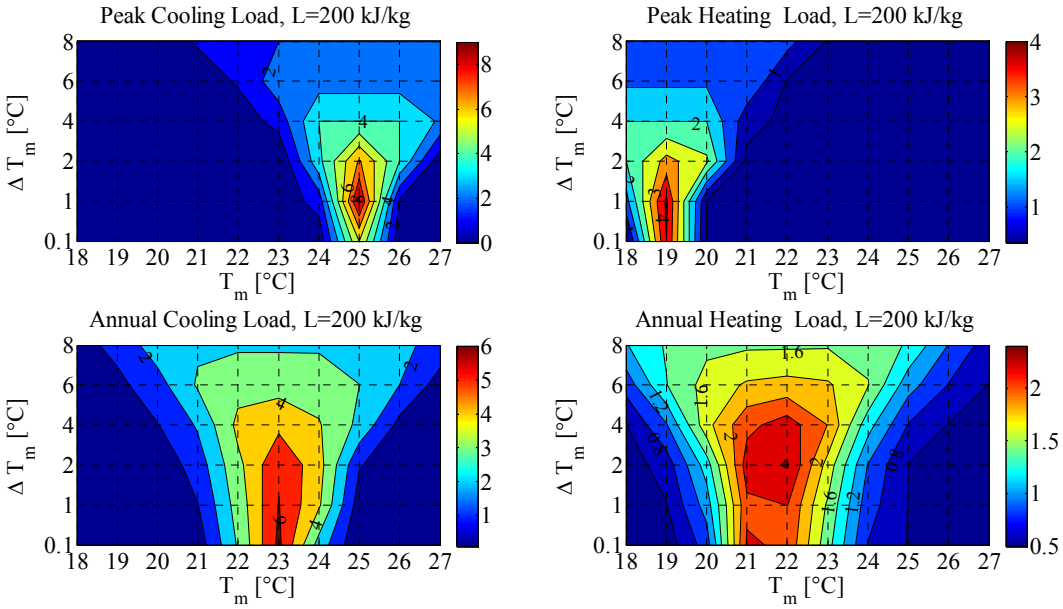

d) A contour plot for the case of 200 kg/kJ showing percentage reduction in cooling and heating loads

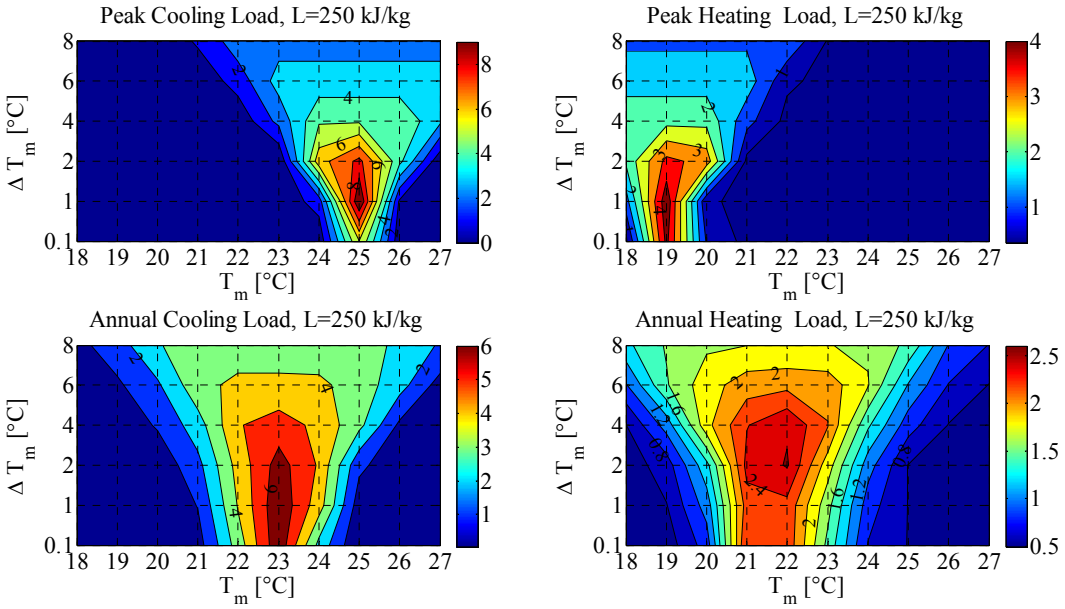

e) A contour plot for the case of 250 kg/kJ showing percentage reduction in cooling and heating loads

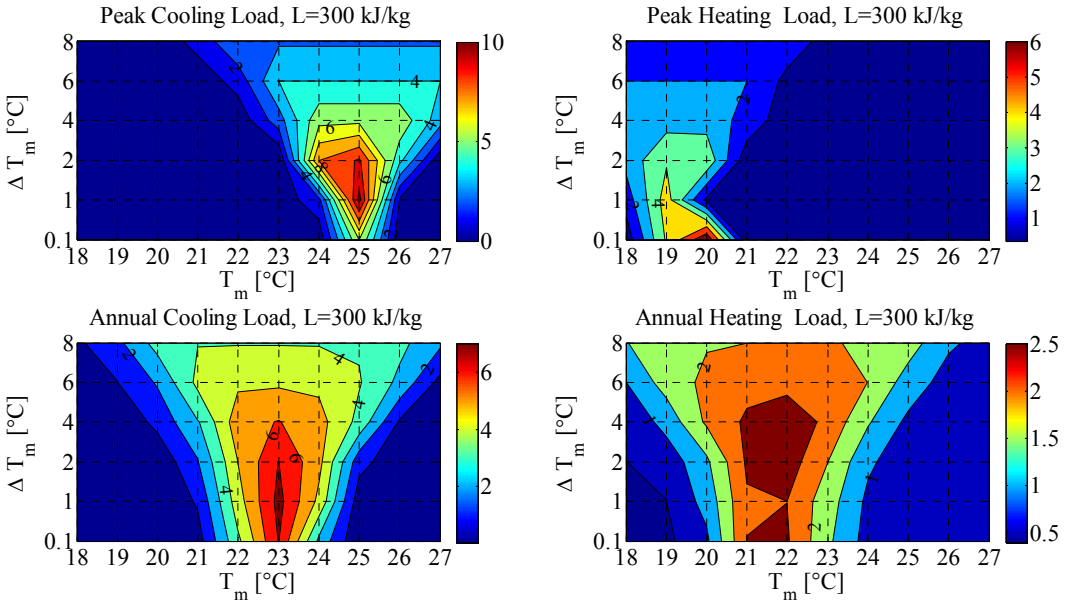

f) A contour plot for the case of 300 kg/kJ showing percentage reduction in cooling and heating loads

Figure E.4 Percentage reductions in cooling and heating loads for whole-house when PCM to the interior for Golden, CO